School of Mechanical Engineering
University of Leeds
Leeds, UK.

Actuation and control for robotic physiotherapy

by

Robert C Richardson,   B.Eng. (Hons)

Submitted in accordance with the requirements of the degree of doctor of philosophy

March 2001

The candidate confirms that the work submitted is his own and that appropriate credit has been given where reference has been made to others

Acknowledgements

I would like to express my gratitude to many people who helped and encouraged me during the course of this work. I would like to thank my research supervisors; Dr M.D.Brown and Prof. J.Fisher for their invaluable support and advice during this work. Furthermore I am especially grateful for the advice provided by Dr M.D.Brown during the write up of this thesis.

I would like to thank my research supervisor for the first year and a half, Dr A.R.Plummer for his input at the early stages of the project and continual advice throughout the project. I would like to express my gratitude to all the members of the School of Mechanical Engineering who aided my course of study, particularly the technical staff and especially Mr M.Martin and Mr D.Readman. I would also like to express my thanks to Dr B.Bhakta for his advice on medical aspects of the project.

Furthermore I would like to thank my parents, Margaret and Geoff Richardson for their continual support and encouragement throughout the period of my studies. Last but not least I would like to thank all my friends for keeping me sane throughout the period of my study.

Abstract

Over the last few years researchers have developed prototype robots that are capable of administering physiotherapy, however, these devices tend to be complex and expensive. The use of modern pneumatic servosystems as actuators would make such devices simpler and cheaper. This thesis assesses the feasibility of a pneumatically actuated robotic physiotherapy device through the implementation of force and position control strategies.

Traditional pneumatic servosystems consist of a pneumatic cylinder prone to stiction effects and a single spool valve. Here the performance of modern pneumatic servosystem, consisting of a low friction pneumatic cylinder and two electro-pneumatic proportional valves has been evaluated. The increased linearity of the modern pneumatic system enabled a self-tuning pole-placement controller to be implemented that would be unsuitable for conventional pneumatic systems. The self-tuning pole-placement controller enabled consistent and accurate position control.

Other researchers have achieved force control of pneumatic systems, however their force models are not applicable on this modern configuration. Accurate control of the servosystem force output, while the position of the cylinder piston is fixed, has been achieved through an open-loop force controller, however applications for fixed position force control are limited. The servosystem force output, during motion, has been found to be a function of the piston velocity and input control signal.

A pneumatic robot has been designed and fabricated with a position workspace that enables the average male to perform upper limb reach and retrieve exercises when attached to the robot. The pneumatically actuated robot, combined with a simple three degree-of-freedom force sensor, form a device capable of administering upper-limb robotic physiotherapy. Impedance control has been identified as the most suitable force and position control strategy for implementing physiotherapy.

Applying the impedance control strategy, to a single link of the robot, resulted in accurate implementation of the desired force and position relationship.

Extending the controller to two and three degrees of freedom has resulted in degradation of the controller performance due to limitations of the three degree-of-freedom force sensor. The controller performance is also found to be dependent upon selection of the impedance characteristics. Low stiffness and high damping, along with high stiffness and high damping have been identified as particular low points in controller performance due to the requirement for the system to provide large forces with little resulting motion.

It was concluded that the pneumatic robot and impedance control strategy have the potential to administer physiotherapy. However, further work incorporating a force sensor with greater accuracy that is robust to torque inputs and a rigorous stability analysis would be required before the device could be clinically evaluated.

Table of contents

List of figures

List of Tables

Nomenclature

a	Orifice area (m^2)
a_{pipe}	Cross sectional pipe area (m^2)
A_1, A_2, A_3	Length of robot links (m)
A_m	Polynomial of closed loop poles
A_a, A_b	Cylinder piston area, chambers A & B (m^2)
A_{cc}	Acceleration (m/s^2)
$A(z^{-1})$	Discrete plant denominator
B	Matrix of offsets (N)
B_m	Coefficient of cylinder force subsystem
B_p	Balance signal (V)
$B(z^{-1})$	Discrete plant numerator
c_i	Coefficient of spool proportionality
C_{mp1}, C_{mp2}	Flow coefficients due to poppet 1 & 2 respectively
c_p	Constant pressure specific heat for air = 1003.5 J kg^{-1} K^{-1}
c_q	Orifice discharge coefficient, 0.9 (poppet valve)
c_v	Constant volume specific heat for air = 718.6 J kg^{-1} K^{-1}
C	Damping (N/ms^{-1})
$Control_{act}$	Input control signal (V)
$Control_{des}$	Linearised control signal (V)
C_1, C_2, C_3	Angle cylinder makes with link (rad)
C_L, C_{BT}, C_Q	Matrix of sensor calibration coefficients
C_f	Proportional voltage coefficient
C_{pop}	Poppet damping = 13 N/ms^{-1}
d	Self-tuning balance coefficient

d_{len}	Length of joints 2 and 3 in y plane (m)
D_{cyl}	Cylinder velocity coefficient (N/ms^{-1})
D	Derivative gain
e	Error between desired and actual response
e_t	Measurement noise and disturbances
E	Proportional valve spool area = 4.5×10^{-4} m^2
E_m	Coefficient of cylinder force subsytem
G_r	Vector of gravitational forces
$G(z^{-1})$	Pole-placement controller polynomial
$H(z^{-1})$	Pole-placement demand filter
I	Integral gain
J_m	Coefficient of cylinder force subsystem
k_a	Closed loop poles gain adjustment
k_c	Poppet circumference = 3×10^{-2} m
k_m	Proportional motor constant (Nm/amp)
k_{of}	Open-loop force gain
k_r	Strain gauge factor = 2
$\underline{k_{st}}$	Self-tuning pole-placement control matrix
K	Stiffness (N/m)
K_p	Proportional gain
K_{pop}	Poppet spring stiffness = 1500 N/m
f_1, f_2, f_3	Externally applied force resolved to joints (N)
f_i	Change to joint torque due to impedance strategy (Nm)
f_t	Force output (N)
f_{c1}, f_{c2}, f_{c3}	Force applied by cylinders 1,2 & 3 respectively (N)
$F(z^{-1})$	Pole-placement controller polynomial
F_{cyl}	Force generated inside the pneumatic cylinder (N)
F_{ext}	Externally applied force (N)
F_i	Impedance change in external force (N)
F_m	Matrix of applied forces (N)
F_p	Perpendicular force (N)
F_{p1}, F_{p2}	Force applied to poppet 1 & 2 respectively (N)

F_s	Force generated on spool (N)
$F_{stiction}$	Stiction force within pneumatic cylinder (N)
F_{xs}, F_{ys}, F_{zs}	Force readings from force sensor (N)
F_{vis}	Force due to cylinder velocity dependent friction (N)
F_x, F_y, F_z	Global force applied in x,y,z respectively (N)
i_s	Spool valve current (amps)
I_m	Motor current (amps)
LF_x, LF_y, LF_z	Perpendicular distance of applied force (m)
m	Degree of discrete numerator
m_a, m_b	Mass of air in chambers A & B respectively (kg)
M_r	Joint inertia matrix
M	Mass (kg)
MSR	Mean square residual
MSS	Mean square signal
n	Degree of discrete denominator
p	Closed loop pole
p_f	Degree of $F(z^{-1})$
P	Proportional gain
P_a, P_b	Chambers A & B pressure (Pa)
P_{ai}	Pressure linearised around an operating point (Pa)
P_d	Pilot pressure (Pa)
P_{eq}	Equilibrium pressure (Pa)
P_r	Valve exhaust pressure $= 1 \times 10^5$ (Pa) (abs.)
P_s	Valve supply pressure $= 7.5 \times 10^5$ (Pa) (abs.)
P_t	Covariance matrix
q_g	Degree of $G(z^{-1})$
Q	Percentage quality (%)
r_t	Demand signal
R	Gas constant for air $= 287$ J kg^{-1} K^{-1}
R_1, R_2, R_3, R_4	Wheatstone bridge resistors (Ω)
t	Time (s)
T	Time period (s)
T_a	Temperature of air in chamber A $= 300$ (K)

T_m	DC motor torque (N/m)
T_s	Temperature of the air supply = 300 (K)
u_1, u_2, u_3	Control signals applied to cylinders 1,2 & 3 respectively (V)
$\underline{u}$	Input vector
u_{eq}	Equilibrium signal (V)
u_t	Input control signal (V)
$u_t{}'$	Input control signal including balance signal (V)
u_{t1}, u_{t2}	Input control signal valve 1 & 2 (V)
u_{tp}	Pole-placement control signal (V)
U_A	Wheatstone bridge strain voltage (V)
U_E	Wheatstone bridge supply voltage (V)
V_a, V_b	Volume of chamber A & B respectively (m^3)
V_{ai}	Volume linearised around an operating point (m^3)
V_r	Coriolis and centrifugal generalised forces
V_{da}, V_{db}	Chamber A & B dead volumes = 5.9x10^{-6}, 5.34x10^{-6} (m^3)
V_i	Voltage applied to valve (V)
V_x, V_y, V_z	Voltages from force sensor (V)
x,y,z	Global task space coordinates
x_{cyl}	Cylinder position (m)
x_d, y_d, z_d	Desired position in x,y & z respectively (m)
x_e	Global position error (m)
x_i, y_i, z_i	Respective impedance position change (m)
x_l	Cylinder stroke length = 0.1 (m)
x_p, y_p, z_p	Respective desired global positions (m)
x_{p1}, x_{p2}	Poppet 1 & 2 displacement respectively (m)
x_s	Proportional valve spool displacement (m)
X_{sp}	Spool orifice area (m^2)
$\underline{y}$	Output vector
y_t	Output
$y_t{}'$	Integrated output
$\varepsilon_1, \varepsilon_2, \varepsilon_3, \varepsilon_4$	Strain on force sensor
$\theta_1, \theta_2, \theta_3$	Joint 1,2 & 3 angle respectively

$\theta_{1d}, \theta_{2d}, \theta_{3d}$	Demand joint 1,2 & 3 angle respectively
θ	Vector of joint angles
$\underline{\theta}$	Parameter estimate
$\underline{\Psi}$	Regressor matrix
ρ	Density of air (kg m^{-3})
γ	specific heat ratio
τ_1, τ_2, τ_3	Torque applied to joints 1,2 & 3 respectively (Nm)
τ'	Torque modified to include impedance force (Nm)
$\tau_{ext1}, \tau_{ext2}, \tau_{ext3}$	Resulting torque on links due to external force (Nm)
$\tau_{cyl1}, \tau_{cyl2}, \tau_{cyl3}$	Required link torque to be exerted by cylinder (Nm)

Abbreviations

ARM	Arm rehabilitation and measurement device
DFT	Discrete Fourier transform
DOF	Degree-of-freedom
FEA	Finite element analysis
LQ	Linear Quadratic
LQI	Linear Quadratic Integral
LVDT	Linear variable differential transducer
MIME	Mirror image motion enabler
MRAC	Model reference adaptive control
MULOS	Motorised upper-limb orthotic system
OT	Occupational Therapist
PI	Proportional and Integral
PID	Proportional, Integral and derivative
PMA	Pneumatic muscle actuator
PWM	Pulse width modulation
RAM	Rubber artificial muscle
ZOH	Zero order hold

Chapter 1

Introduction

This chapter details the background, aims and objectives of this research.

1.1 Background

Modern pneumatic actuators have the potential to accurately control robotic devices. These actuators could enable robots interacting with humans, such as physiotherapy robots, to be cheaper and simpler while 'feeling' less mechanical to the human.

Traditionally, hydraulic systems or electric motors were considered the only options for precision control systems, however these systems cannot be considered ideal. Faults in hydraulic systems can cause leakage, contaminating surrounding objects with hydraulic fluid, moreover the response of hydraulic systems is non-linear, requiring sophisticated control algorithms.

Electric motors have become a standard part of many robotic applications due to their simplicity and ease of control, however, the use of gears to modify speed and torque output, introduces new control problems such as backlash (the amount the gear tooth spacing exceeds the tooth width). In applications that require continual change of direction, backlash increases response time and increases positional error. The use of gearing often prevents the robot from being backdrivable (external forces cannot move the joint against its intended movement direction). Direct drive torque motors can be used without gearing systems, but to achieve the required level of torque they tend to be expensive and heavy.

Until the last decade, pneumatic systems have been largely overlooked, considered only to be suitable for automating simple industrial tasks. They were ideal for these tasks because of their inherent ability to provide a low cost, compact, safe, and simple power source **(Moore et al. 1992)**. The control strategies employed to automate these tasks were limited, with the majority of applications relying upon pre-set mechanical stops ('bang-bang' motion) for their position control. Restricting factors that prevented

wider use of pneumatic cylinders arose from highly non-linear dynamic properties such as air compressibility and friction effects, which combined to severely degrade response time and position accuracy **(Surgenor et al. 1993)**. Recently, with the advent of digital technology, improved electro-pneumatic proportional valves and low friction cylinders these non-linear effects have been reduced, prompting new research initiatives to develop wider applications for pneumatic cylinders. The drive behind this research becomes obvious when considering the cost advantage of pneumatics to hydraulics or electric motors can be as high as 10:1 **(Surgenor et al. 1992)**.

Rehabilitation engineering is one area that could benefit from advances in pneumatic systems. Physiotherapy is a specific form of rehabilitation, which helps to restore the function of limbs after a debilitating medical incident such as a stroke. The annual occurrence rate of stroke alone has been estimated at 2 victims per 1000 population **(Cozens 1995)**. Physiotherapy is normally performed by trained occupational therapists (OT's), who manually assist the patient to perform a series of motions intended to increase muscle strength and re-learn the ability to operate the limb. Each movement the patient is to learn has to be performed correctly and then repeated hundreds of times to become part of the patient's repertoire of well co-ordinated actions stored in their memory. This is a time consuming and labour intensive process. It is a well-known fact that recovery from stroke is based on a dose to response relationship **(Sunderland et al. 1994)**, but due to shortages in staff and funding, patients often do not receive the optimum amount of attention. Recently, technology has progressed to a level where robots are able to provide stimuli while recording patient performance in a way unattainable by human therapists **(Erlandson 1989)**. These robots have the potential to reduce the burden on physiotherapists and improve the patient's degree of recovery through additional therapy. To a limited extent prototype robots are now able to apply physiotherapy exercises, and do so with greater consistency than their human counterparts **(Krebs et al. 1998)**. The high power-to-weight ratio, low cost and direct drive capabilities of pneumatic actuators, however, mean that the potential exists to make such devices simpler and more affordable.

1.2 Motivation for research

The inspiration for this research was taken from conclusions derived by applying physiotherapy on a single degree of freedom robot **(Austin 1999)**. This research developed simple control strategies using a single degree of freedom robot to apply robotic physiotherapy in elbow extension/flexion exercises (figure 1.1).
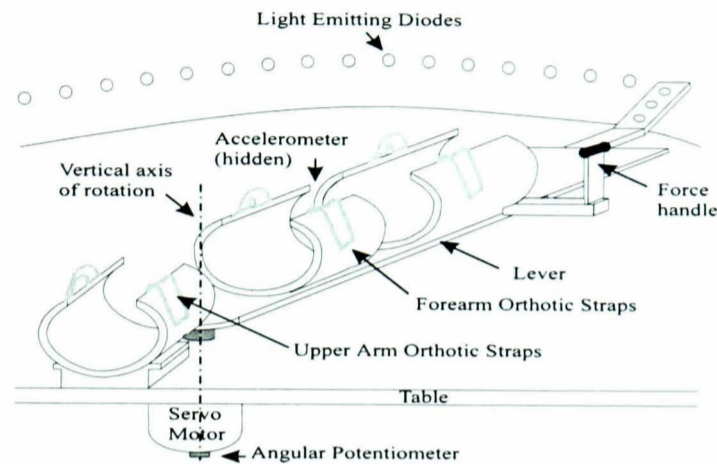
Figure 1.1 *Single degree of freedom robotic physiotherapy device (Austin 1999)*

Torque was used to assist patient movement between points indicated by light emitting diodes. A lead-lag controller was used to control the amount of assistance (torque) provided by the torque motor at low and high frequencies, applying greater assistance at lower frequencies. Empirical methods were used to obtain suitable gains for the controller. A dead-zone was implemented to provide no assistance when the exercise is performed correctly (i.e when position error is within an error band, the patient is performing the exercise correctly, so no assistance is provided). Some of the main conclusions of the study are detailed below.

- The lead lag controller was overly position dependent, not enabling patients to complete a smooth continuous motion in a similar manner as to when they were assisted by a physiotherapist.
- The elbow extension/flexion movement, with gravity removed, required relatively limited ability to complete exercises successfully. Consequently, this limited the patient group who required assistance, as the boundary between 'not enough' and 'too much' assistance was small.

- Development of a reach/retrieve exerciser that is able to assist a more natural movement than the elbow would offer significant improvements over the range of suitable patients and therapeutic values of exercise. **Stranger et al. (1994)** surveyed four robotic rehabilitation groups and found agreement that reach and retrieve actions offer the greatest therapeutic benefits.

From these conclusions, it was decided that development of a three degree-of-freedom robotic device to perform movements related to reach-and-retrieve motions would significantly improve the performance and scope for implementing physiotherapy. Moreover, it is hypothesised that these tasks will instil greater motivation in subjects.

1.3 Pneumatic systems

Over the last century compressed air has been widely used to power pneumatic cylinders that are capable of two-position control (extended or contracted). These cylinders, combined with simple on/off pneumatic control valves enable automation of simple tasks.

1.3.1 Modelling

Shearer (1956) developed a model of pneumatic systems to predict the behaviour of pneumatic cylinders between end stops. The model, developed from thermodynamic principles, describes the behaviour of a directional valve and double ended pneumatic cylinder (rod protruding from both sides of the cylinder casing). This standard arrangement of pneumatic components is illustrated in figure 1.2. Spool movement varies the magnitude and direction of compressed air flow into the cylinder. The pressure difference in either chamber results in piston movement.
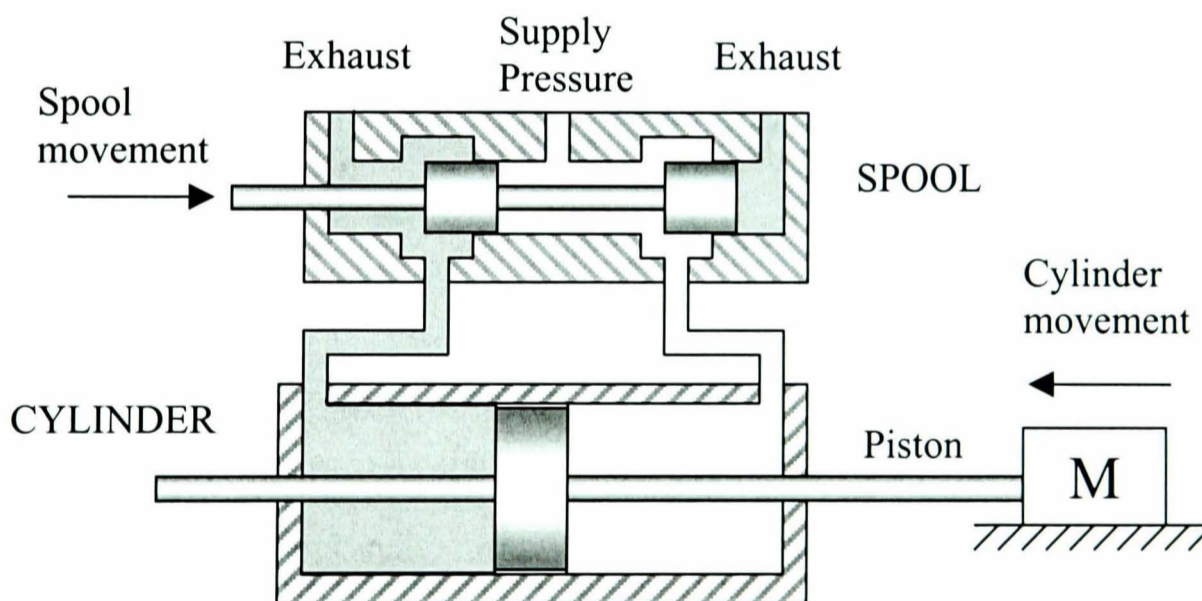
Figure 1.2 Conventional cylinder and spool valve arrangement

Backe and Ohligschlager (1989) applied thermodynamic principles to develop a more detailed description of pressure within a fixed volume pneumatic chamber. Experimental results validated simulation predictions of pressure and temperature. Such a complex analysis of the heat transfer and pressures within a pneumatic

chamber is, however, of little benefit for control design. Moreover, the analysis does not take into account the change in volume that occurs when increased pressure causes piston movement.

Single-ended pneumatic cylinders (rod protrudes from one side only) are the most common form of pneumatic cylinder. Within this arrangement, the single ended cylinder has differences in piston area due to the driving shaft (figure 1.3). **Pu et al. (1996)** highlighted the effect of these differences by examining the extension / retraction acceleration of a single ended cylinder. The larger area was shown to produce significantly higher force and acceleration.
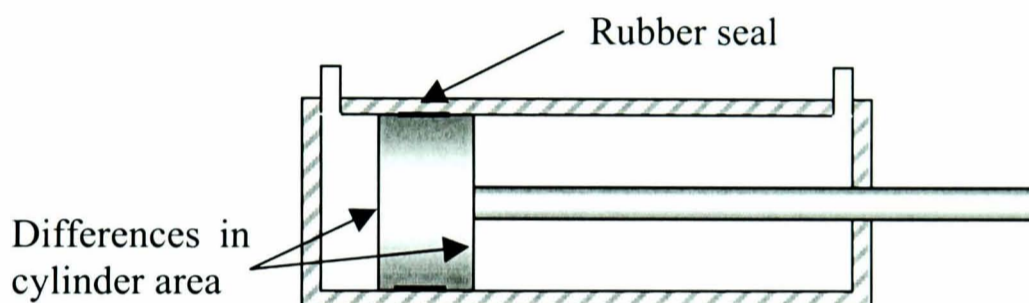
Figure 1.3 Single ended pneumatic cylinder

Richer and Hurmuzlu (2000) modelled in detail the behaviour of a single-ended pneumatic cylinder and spool valve arrangement. The model accounted for valve, cylinder and interconnecting pipes. The complexity of the model required identification of some parameters from experimental results, but the final model was shown to accurately predict the system performance.

The main difference between hydraulic and pneumatic fluid arises from the compressibility of air. Air compressibility significantly effects pneumatic actuator stiffness. **Pu and Weston (1989)** examined the stiffness of pneumatic cylinders, finding the minimum stiffness and natural frequency to occur at the cylinder mid-position.

Models of pneumatic systems simplify what are in essence, multi-degrees of freedom compressible fluid flow problems. **McDonnell and Bobrow (1997)** called into

question the accuracy of the standard model for a spool valve. Their experimental pressure response of a spool valve differed to that predicted by the standard spool model. A model identified from the experimental data was used to accurately predict the valve response.

1.3.2   Friction effects

The rubber seal between the two pneumatic chambers (figure 1.3) is the source of a non-linear friction effect (termed stiction) that degrades the performance of pneumatic systems. The stiction characteristics of pneumatic systems contribute significantly to the overall difficulty in achieving accurate position control. **Nouri et al. (2000)** performed a detailed analysis into the friction characteristics of pneumatic cylinders through experimental analysis. The nature of friction in conventional pneumatic cylinders is illustrated in figure 1.4.
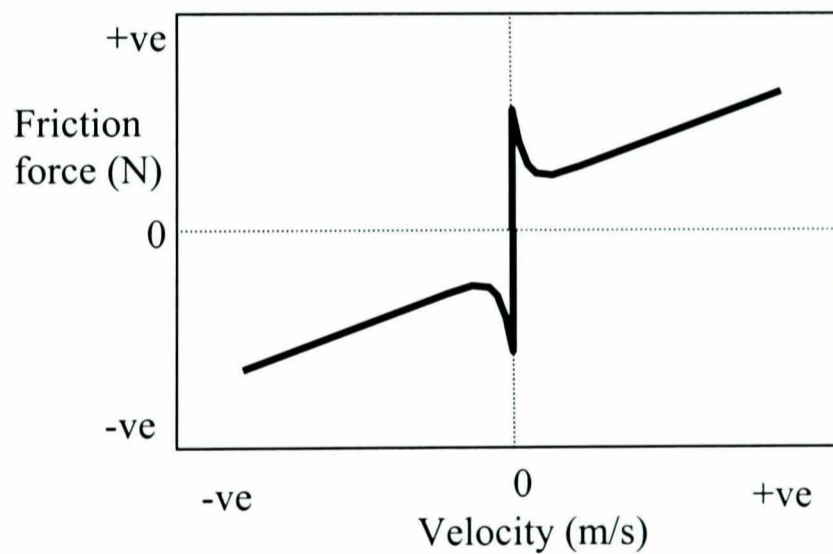
Figure 1.4   Pneumatic cylinder friction characteristics (Nouri et al. 2000)

Before motion can commence, a force to overcome the stiction is required. Once in motion the relationship becomes approximately linear between velocity and friction, until the velocity reduces below a certain level, when increased friction force causes the velocity to become zero. This can result in the pneumatic cylinder exhibiting 'stop/start' motion at low frequencies.

Low friction pneumatic cylinders using a glass lining and air bearing have been developed to greatly reduce stiction effects and enable accurate control. **Gaberman (1995)** details the design of a commercially available cylinder (figure 1.5). The piston floats on an air bearing in a glass lined chamber, reducing the stiction to a minimum. Drawbacks of such a design are sight leakage between chambers and the fragile nature of the glass lining. Low friction pneumatic cylinders have been chosen by several researchers **(Ben-Dov and Salcudean 1995, Fujiwara 1995)** to obtain accurate control of position or force.

AIRPEL CONSTRUCTION

GRAPHITE FILLED
BRONZE PIVOT BUSHING

NICKEL PLATED ALUMINUM
PISTON/ROD COUPLING

SILICONE RUBBER
CYLINDER GASKETS

LOW FRICTION
ROD GUIDE BUSHING

NICKEL PLATED ALUMINUM
CYLINDER HEADS

IMPACT
PROTECTION GAP

PYREX GLASS
CYLINDER LINER

SS SEAL RETAINER

CARBON/GRAPHITE
ROD SEAL

304 SS OUTER TUBE

CARBON/GRAPHITE
PISTON

SILICONE RUBBER
CYLINDER HEAD SEAL

303 SS PISTON ROD

Figure 1.5 Low friction pneumatic actuator, (Gaberman 1995)

1.3.3 Novel actuators

Recent interest in pneumatic systems has spawned a multitude of novel pneumatic actuators. Rodless pneumatic actuators have been developed which have a linear slide on the outside of the cylinder to transmit power **(Hanchin et al. 1992)** and pneumatic motors have been developed that use vanes to generate angular motion **(Pandian et al. 1999)**.

The area of most innovative development involves rubber sacks that expand and contract with variations in pressure. **Tillet et al. (1997)** developed and modelled a rotary actuator based upon flexible inflatable pneumatic bladders. A non-linear model of the system dynamic performance was created and simulated. The actuator

demonstrated lower friction than encountered in conventional pneumatic cylinders. **Caldwell et al. (1995)** developed cylindrical pneumatic muscle actuators (PMA's) using an external nylon interweave to focus the direction of motion (figure 1.6). **Kimura (1997)** analysed and controlled a similar type of pneumatic actuator termed a rubber muscle actuator (RAM). A detailed non-linear model of the system was developed. The non-linear model was used to perform feedback linearisation and improve the system performance.

Although these inflatable rubber actuators remove stiction effects and weigh less than conventional actuators, these advantages come at a price. Non-linearities within the actuator are increased due to hysterisis and heat transfer effects within the rubber, creating additional control problems.
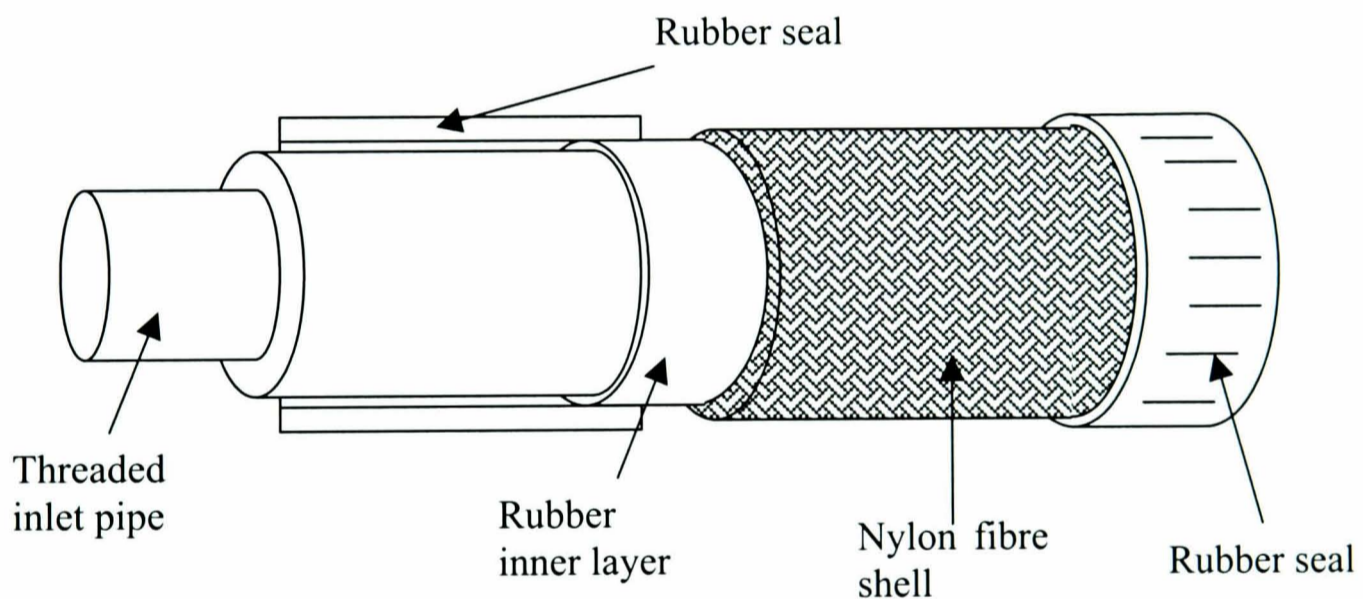
Figure 1.6 Pneumatic muscle actuator

1.3.4 Suitability of modern pneumatics for precision control

Many researchers believe developments in controller design and actuators enable pneumatic systems to perform tasks for which previously only electric motors or hydraulic cylinders would be suitable. **Surgenor and Ioranou (1993)** have demonstrated by examining a gantry crane apparatus with pneumatic and electric actuators that comparable position and velocity tracking can be obtained under appropriate load conditions (constant mass and inertia). Gantry cranes with both

pneumatic and D.C motor actuators (five times more expensive) were constructed and operated using the same control algorithm. It was demonstrated that both actuators produced acceptable results, although the motion of the pneumatic cylinder was less smooth and the response time marginally slower. **Pandian et al. (1999)** proposed an air motor as a potential alternative to electric motors. The performance was demonstrated when using adaptive control, but no experimental comparison to electric motors was performed.

As indicated by the variety of research covered here, the field of pneumatic research is rich and diverse. A large variety of linear and non-linear controllers have been based around the modelling techniques and actuators discussed. The next section details control techniques used by these researchers.

1.4 Position Control Systems

Pneumatic control strategies can be grouped into two distinct categories, linear and non-linear. Generally, pneumatic systems behave with some non-linearity, hence the majority of controllers are non-linear. Some apparently linear controllers use non-linear elements such as spool dither and friction compensation. Controllers in this section are grouped by the primary control technique (i.e. a PID controller with intelligent dither would be classed as a linear controller).

Although pneumatic systems behave in a similar manner to hydraulic, the amount of literature on hydraulic systems is broader and more developed. For this reason some of the reviewed literature relates to hydraulic systems. The compressibility of air causes the behaviour of pneumatic systems to be more complex than hydraulic systems, so the conclusions drawn for hydraulic systems can only be taken as suggestions for improving the performance of pneumatic systems.

1.4.1   Linear position control

A simple example of linear control is proportional integral (PI) control. **Kawanaka and Hanada (1996)** used two electro-pneumatic proportional valves to implement PI control on a single pneumatic cylinder. One valve supplied a fixed pressure while the other was used to control the cylinder. Using two valves in this manner severely limits system performance with the second valve generating a constant return force. **Hamiti et al. (1996)** also implemented a PI controller on a pneumatic system. An inner analogue P controller was used to stabilise the system and reduce non-linearities. The outer PI control loop was then used to control the system. A method of tuning the integrator gain was used to reduce the effect of limit cycles caused by friction within the system. The tuned response greatly reduced servo limit cycling, enabling position tracking to within a few percent.

Liu and Bobrow (1988) developed a detailed model of a pneumatic system, which was used to design a proportional-derivative (PD) controller. It was demonstrated

mathematically and experimentally that including a pressure feedback loop increased the system performance. The main factor limiting the attainable performance was identified as the system response time, which is determined by airflow characteristics and the supply pressure; the control of pressures within the pneumatic system is vital to ensure accurate control. **Noritsugo and Takaiwa (1995)** used a pressure control loop to achieve robust positioning control. A simple proportional controller was used to control the position. Pressure was controlled using a disturbance observer to provide robust performance in the presence of external forces. The performance of the disturbance observer was compared to standard PI control in the pressure feedback loop. The disturbance observer was found to provide superior performance with and without the presence of external force disturbances. **Yin and Araki (1998)** derived a detailed model of pressure within a single pneumatic chamber with spring return (figure 1.7). The model was used to design a pressure feedback control loop and apply force control in one direction. However, the return force is a result of the spring constant of the return spring, limiting applications for this configuration.
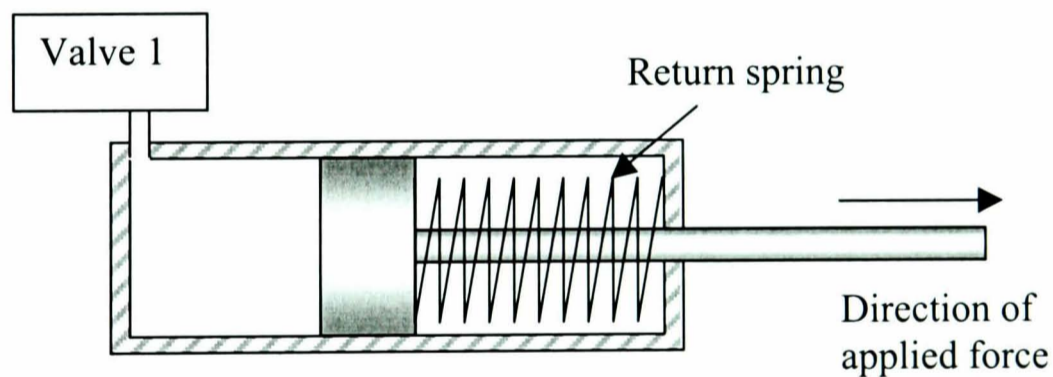
Figure 1.7 *Spring return pneumatic cylinder*

The relationship between pressure and acceleration is well known for pneumatic systems.

$$f_t = P_a.A_a = M.A_{cc} \tag{1.1}$$

where f_t is force, P_a is pressure, A_a is surface area, M is the mass and A_{cc} is the acceleration.

This relationship enables acceleration control to be used as an alternative to pressure regulation. Indeed **Wang et al. (1999)** implemented acceleration feedback to supplement standard PID control. To prevent the cost of a separate accelerometer, the position sensor was differentiated twice to find the acceleration and then digitally filtered to reduce noise. The acceleration feedback was shown to improve the stability of the pneumatic cylinder.

1.4.2 Model based control

Optimum controllers obtain system gains by minimising some measure of the system behaviour. Minimum variance is a form of optimal controller that minimises the effects of disturbances on the system response. **Hua and Yongxiang (1991)** use a form of minimum variance tracking to simulate a pneumatic cylinder required to track an object's position and velocity. They formulated criteria to minimise position and/or velocity.

Linear quadratic (LQ) control minimises the effects of disturbances as well as the control output. **Surgenor et al. (1991)** implemented LQ control for the well-known inverted pendulum problem. Using two 4/3 spool valves driven using a PWM signal, they were able to effectively control a rodless cylinder and inverted pendulum. **Surgenor and Ioranou (1993)** used LQ control to compare the performance of electric DC motors and spool driven pneumatic servo systems for the application of a gantry crane apparatus. Results from the electric and pneumatic systems were comparable under constant load conditions. The presence of external disturbances in the form of additional weight had little noticeable effect on the electric system but caused the pneumatic performance to degrade. They concluded that similar responses could be obtained although the pneumatic system is more sensitive to modelling errors. **Surgenor and Wijesuriya (1992)** applied LQ control to a high friction pneumatic cylinder, electing to use two electro-pneumatic control valves to independently control the pressure in each chamber, simplifying the mathematical model and improving the system performance. LQ control alone was not able to accurately control the cylinder. To improve the response they added an intelligent

dither signal, which increased the driving pressure to the cylinder at locations where the cylinder becomes 'stuck' due to stiction effects. The dither signal was shown to improve the response. **Fujiwara and Ishida (1996)** designed an LQI (Linear quadratic integral) controller for use with electro-pneumatic valves and cylinder system. The integrating element was included to ensure that zero steady state error could be achieved. In addition to the integrating element, a disturbance observer was employed to provide robust performance in the presence of external load disturbances. The disturbance observer was shown to provide superior performance in the presence of large changes in external load.

1.4.3 Self-tuning controllers

All the linear controllers presented up to this point are based upon fixed parameters designed before implementation of the controller. Self-tuning controllers have the ability to alter their gains at the start of a session to cope with plant variations. They can be considered as a one shot attempt to tune linear parameters. This type of controller is particularly suited to pneumatic systems where the response may be approximated as linear, but factors such as changes in ambient air temperature and pressure can change the plant model. **Yamamoto et al. (1995)** developed a self-tuning PID controller for a pneumatic servo that does not require the solution of a diophantine equation. Their self-tuning controller demonstrated superior performance in the presence of additional inertial load when compared to a standard self-tuning PID controller. **Xianwen et al. (1997)** also designed a self-tuning PID control strategy for a chemical plant. Using an initial plant model and a recursive least squares identification technique the gains of the PID controller are tuned on-line. The strategy was shown to accurately control the temperature.

Pole-placement is a popular form of control that can be extended to enable self-tuning (see chapter 3). **Astrom and Wittenmark (1980)** and **Wellstead and Sanoff (1981)** initially developed self-tuning pole-placement controllers. This controller was implemented on an electro-hydraulic actuator by **Vaughan and Plummer (1990)**[1]. Robustness issues were investigated through the choice of closed-loop poles.

Implementation of an input filter was used to attenuate the noise, enabling selection of faster poles. As is apparent from the literature, few linear controllers have been designed and implemented on pneumatic systems, however the linear controller concept is generally unsuitable due to their non-linear nature. Non-linear controllers have the potential for greater flexibility and performance.

1.4.4 Adaptive control

One of the simplest forms of non-linear control is adaptive control. Adaptive control is an extension of self-tuning control, enabling the system parameters to be continually tuned throughout the response. This is achieved by introducing a 'forgetting factor' into the recursive least squares identification technique reducing the weighting of previous data, enabling the controller to adapt to continual parameter variations.

Shih and Huang (1992) used an adaptive pole-placement method to control a pneumatic system. A second order plant model was identified using a PBRS (pseudo random binary sequence) response and system identification techniques. The response of the adaptive controller was compared to a conventional PID controller. The pole-placement strategy demonstrated superior performance before and after changes in plant parameters, so the comparison with a fixed parameter PID controller has little meaning. Indeed, in later work **Shih and Tseng (1994)** modified their previous adaptive pole-placement algorithm to become an adaptive PID controller. The comparison made between adaptive PID and fixed parameter PID clearly demonstrated the adaptive controller's superior performance in the presence of plant parameter variation. **Tanaka et al. (1996)** proposed an adaptive algorithm for pole-placement control of pneumatic systems with constant disturbances. A difference operator was introduced into the identification procedure to eliminate the effect of a constant disturbance. After initial tuning transients, responses to different inertial loads were similar. **Vaughan and Plummer (1990)**[2] extended their pole-placement scheme for an electro-hydraulic actuator to become an adaptive strategy. An integrator was assumed to always be present within the system, enabling it to be

separated from the plant when tuning plant parameters. The adaptive control strategy was shown to respond well for large changes in system parameters.

Guilhard et al. (1995) designed an adaptive controller for a pneumatic quadruped robot. A standard robotic torque equation was combined with a torque model for a pneumatic cylinder to implement the torque controlled robot. The robot parameters were adapted online to maintain the system performance. The torque controller was compared to standard PID control and found to be superior. Adaptive controllers can improve the response of a large range of non-linear systems, however, an adaptive controller takes a finite time to adapt to new parameters. Systems with fast variation of parameters may not, therefore, enable an adaptive controller to perform optimally. Indeed, **Lai et al. (1993)** found an adaptive controller unsuitable to improve the cyclic response of a pneumatic cylinder. Instead a feed-forward learning pressure compensator was implemented, essentially using data from a previous cycle to improve the performance of the current cycle. The learning controller was shown to improve the response after several cycles, but can only be implemented on periodic systems.

Hashimoto and Ishida (2000) implemented a novel form of adaptive PID for pneumatic systems. The system frequency response was identified on-line using a sliding DFT (Discrete Fourier Transform) method. The DFT information was used to adapt the PID gains in order to optimise the performance of the pneumatic cylinder in the presence of time delays. **McDonell and Bobrow (1993)** designed and implemented and adaptive LQ controller. A recursive identification technique was used to identify a plant on-line, from which optimal gains were calculated and implemented. The controller was shown to adapt to changes in external load after an initial tuning transient.

Model reference adaptive control (MRAC) compares the response of a model to that of the actual system. The error between the responses is used to adjust the controller gains and drive the error to zero. **Folk et al. (1995)** developed a simulation of pneumatic cylinder using bond graphs, from which a MRAC controller was developed.

The velocity was controlled under different loading and load orientation conditions, with the position, velocity and acceleration gains tuned adaptively. Again, the requirement for plant parameters to vary slowly with respect to controller adaptation was highlighted as one of the limitations of this approach.

Kurigami et al. (1996) used a MRAC, modified with a delta operator designed to control a non-minimum phase pneumatic system. After an initial transient response the system accurately tracked the reference model.

1.4.5   Fuzzy controllers

Fuzzy logic and neural network controllers are both capable of mapping arbitrary continuous non-linear responses. Several approaches have been taken to implement fuzzy control on pneumatic systems. **Shibata et al. (1999)** used a Takagi-Sugeno fuzzy reference generator to improve the system response. The desired trajectory was modified to become the virtual trajectory as shown in (figure 1.8).
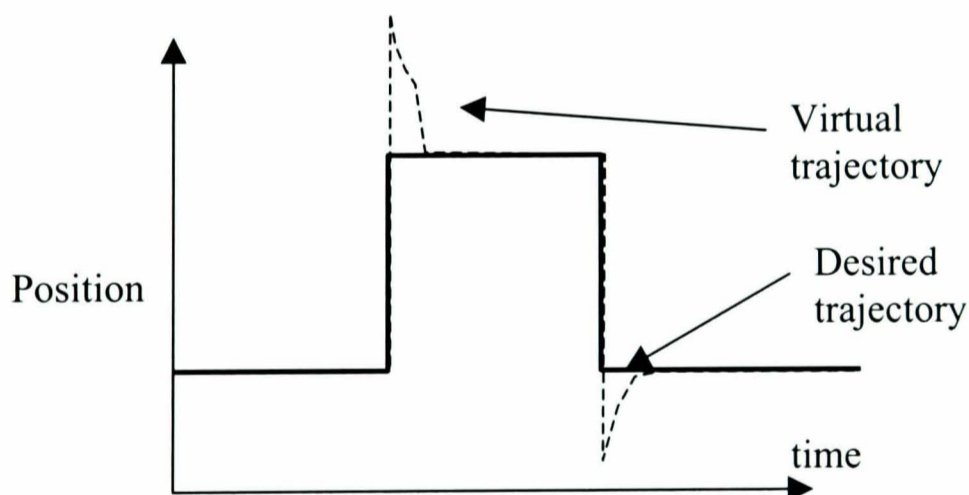
Figure 1.8   Fuzzy virtual trajectory

The virtual trajectory was intended to improve the response time and reduce oscillations. A self-tuning method was employed to alter the defuzzification weights to improve the response. **Shih and Ma (1998)** used a Mamdani fuzzy PD controller on a rodless pneumatic cylinder. The fuzzy controller consisted of fuzzy PD supplemented by a linear integrator. The controller is shown to have good disturbance rejection in

the presence of increased external loads. It is likely that the linear integrator as opposed to the robustness of the fuzzy controller enabled the disturbance rejection properties shown for the controller. The main robustness advantage of this system is its reduced sensitivity to system noise. **Wang and Chang (1999)** implemented fuzzy control on a parallel system consisting of two pneumatic cylinders. The fuzzy controller was used to decouple the motion of the pneumatic cylinders. The controller was shown to be easy to implement and capable of achieving the required tracking. Fuzzy controllers have been designed to solve inverse dynamic problems of robot manipulators. **Graca and Gu (1993)** implemented a learning takagi-sugenor fuzzy controller for a robotic manipulator. A fuzzy regressor was used to enable the manipulator parameters to be tuned on-line. The controller was shown to adapt to the correct manipulator parameters for varied trajectories. The inverse dynamics of robots can be found for all but the most complex robots using conventional techniques (see chapter 5) however, fuzzy systems enable their estimation simply from experimental data. **Bekit et al. (1988)** used a fuzzy controller to adjust PID gains when changes in payload are experienced. Computer simulations show the control scheme to react to sudden changes in payload successfully.

1.4.6 Neural networks

Neural networks use a network of artificial neurones to perform a non-linear mapping. Implementation of these controllers can be complex, with difficulties such as choosing the correct number of neuron. Once the number of neurons has been selected, training the network, using back-propagation for instance, can also be time consuming. These difficulties have not prevented widespread use of neural controllers, largely due to their ability to learn extremely complex non-linear relationships. Several researches have implemented neural networks to control pneumatic systems.

Neural networks have been used to tune the gains of conventional controllers. **Fujiwara et al. (1995)** applied a neural network to self-tune a PID controller implemented on a pneumatic cylinder. The neural network consisted of three inputs, one output and one hidden layer, with the weight of each input representing the PID

gains. These gains were tuned using back-propagation based upon a reference model. In more recent work, **Fujiwara et al. (1997)** used neural networks to improve the LQI control of pneumatic cylinders. Their neural network was used to compensate for non-linear effects in pneumatic systems. The response cost function was significantly reduced for the neural network system. **Song et al. (1997)** implemented a three layer neural network to control a pneumatic cylinder. The controller was shown to quickly improve the response, however, the complexity of the three layer network was not justified. **Gross and Rattan (1997 & 1998)** implemented neural networks for velocity and acceleration control. An adaptive network (continually tuned using back propagation) was implemented and shown to train quickly, improving the response.

1.4.7 Sliding mode controllers

Recently sliding-mode controllers have been implemented on pneumatic actuators. Sliding mode controllers use discontinuities in the system to enable the use of model order reduction and increased robustness to disturbances **(Utkin et al. 1999)**. Pneumatic systems are particularly suitable for sliding mode control due to their non-linear time-variant behaviour. **Pandian et al. (1996)** implemented a sliding mode controller on a pneumatic system. The sliding mode controller was constructed from a state vector containing position, velocity and pressure differential. The third order controller rejected parameter variations. Comparisons with fourth order feedback shows slight improvements in chattering reduction. If the sliding mode controller is designed as second order, the response is severely degraded. **Paul et al. (1994)** highlighted continual switching of the pneumatic valves might cause premature wear when sliding mode is used.

Fuzzy systems can be used to augment sliding mode control. Mathematical models of complex non-linear systems can be difficult to obtain. Some of these systems can be effectively linearised around an operating point. Fuzzy systems enable the combining of several models into a global non-linear model **Yu et al. (1998)**. **Choi and Kim (1997)** detail the use of a fuzzy sliding mode controller for robust tracking of robotic manipulators. Using discontinuous feedback gain from the fuzzy controller, the

performance of the sliding mode controller was improved, resulting in less chattering and improved tracking.

1.5 Force and position control techniques

For industrial tasks, such as picking and placing objects, position control alone is unsuitable. If purely position control were attempted, an exact model of the environment would need to be known. Moreover, any unexpected objects in the robot path would cause collisions, resulting in damage to the robot and/or the object. Conversely, force only controllers have few practical applications.

1.5.1 Force only control

Bobrow and Jabbari (1991) implemented an analogue pressure controller to enable the cylinder pressures to be controlled. Using a dynamic model of the system and the pressure based force controller it was possible to specify position demands. On-line adaptive control was used to ensure the system performance. **Linqi et al. (1994)** implemented a similar force control system. They used a pneumatic cylinder as a force balance to minimise the effects of external forces on a robot arm. Using the pneumatic, cylinder the peak torque on the robot motor actuators was significantly reduced.

1.5.2 Impedance control

Force and position demands cannot be individually specified, however force and position controllers exist that compromise between the two demands. The force and position controller used in the most advanced prototype physiotherapy robot (section 1.6) is *impedance control*. Impedance control is essentially a way of causing the robot's position and force relationship to be specified by mass, spring and damping characteristics. In figure 1.9 the external force (F_{ext}) causes the desired position to change in a predictable manner due to the mass (M), stiffness (K) and damping (C) characteristics. These characteristics, specified at the beginning of a session, enable the robot to behave predictably in an unpredictable environment.
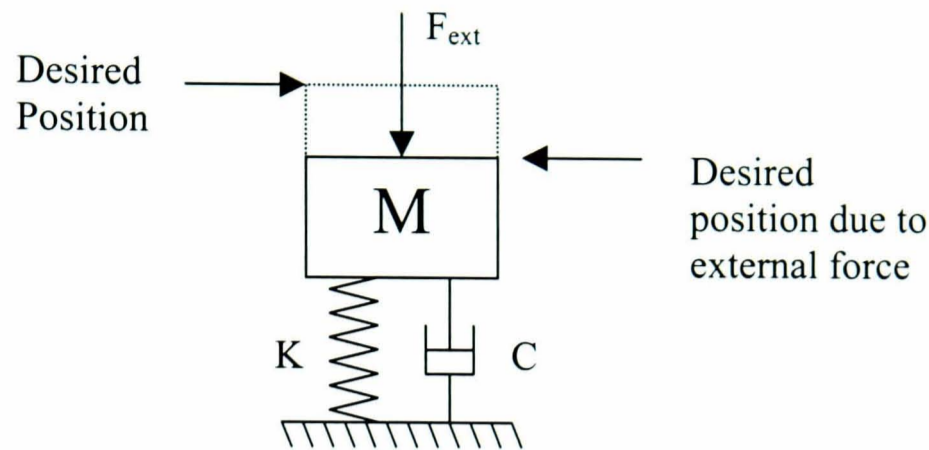
Figure 1.9 *Impedance control strategy*

Hogan (1985) originally developed the concept of impedance control. In a three part study, the concept of impedance control was investigated theoretically, along with possible implementations. Impedance controllers can be based around force controllers (formally termed impedance control, figure 1.10) or position controllers (formally termed admittance control, figure 1.11). **Anderson and Spong (1988)** proposed that different environments required different impedance control approaches. For a purely inertia environment, position based impedance control was suggested. If the environment consists of a mass, damping and stiffness, force based impedance control was proposed. Due to these different requirements they propose a decoupling hybrid impedance controller to switch between controllers. The potential improvements in considering such a system were not demonstrated and the proposed performance advantages are probably outweighed by the increased complexity.

Hogan (1988) performed a mathematical analysis of the stability in impedance control. Greater stability was shown if the appropriate impedance controller was selected (force or position based).

The conventional approach to applying force based impedance control on electric motors has been implemented by **McComuck and Schwartz (1993)**. Electric motors are particularly suitable for torque based impedance control due to their ability to apply torque regardless of position.

Impedance
filter

$$Ms^2 + Cs + K$$

Desired
force

Force
controller

PLANT

Position
error
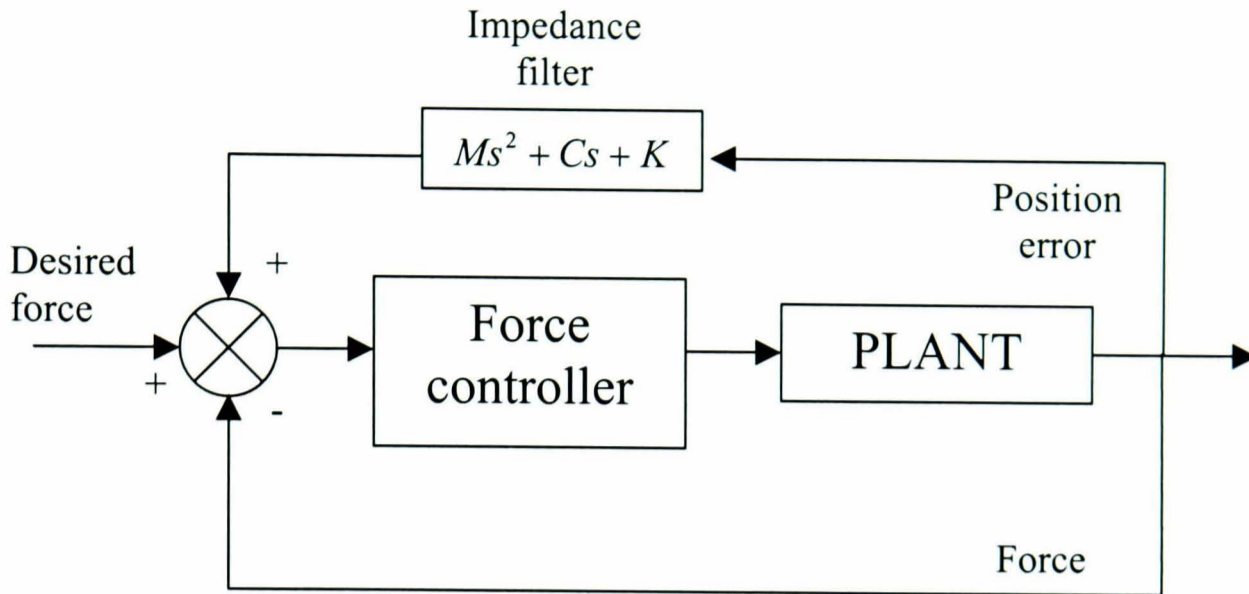
Force

Figure 1.10 *Force based impedance controller*

Impedance
filter

$$\frac{1}{Ms^2 + Cs + K}$$

Desired
Position

Position
controller

PLANT

Force
error
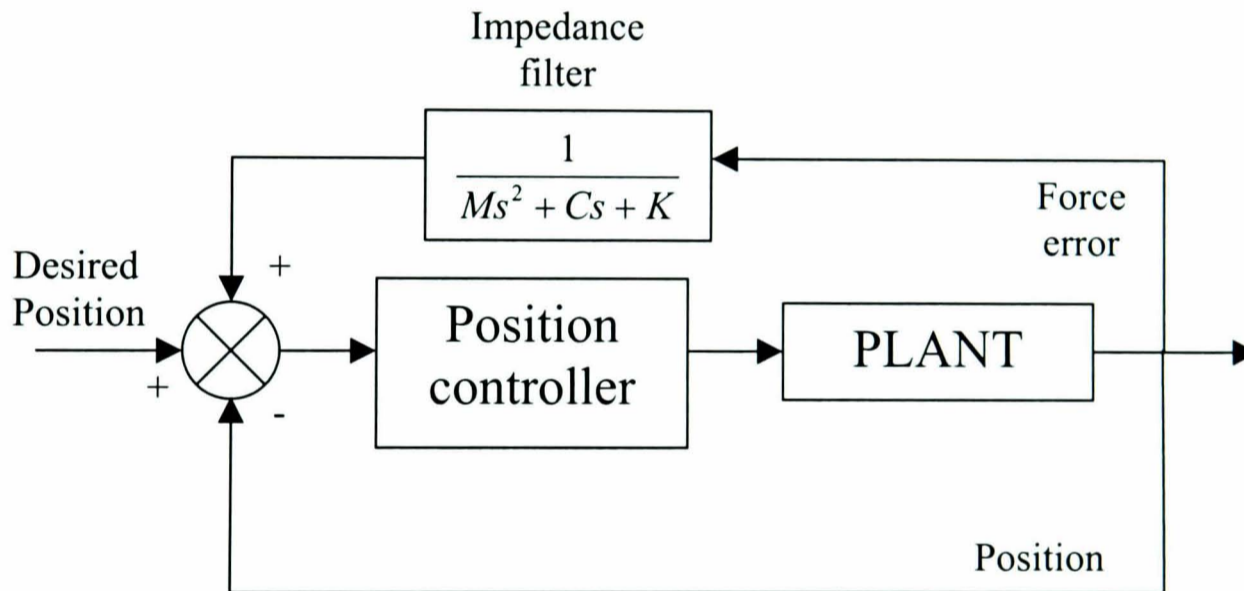
Position

Figure 1.11 *Position based impedance controller*

Position based impedance controllers do not require accurate models of system behaviour or non-linear system dynamics such a friction, simplifying the control. They are particularly suitable for pneumatic and hydraulic systems for which applied torque is affected by motion. **Heinrichs et al. (1997)** designed and implemented a position based impedance control strategy for an industrial hydraulic robot. Force was translated into position demands using an impedance filter. The performance of the proposed controller was demonstrated thorough experimental results. **Bilodeau and Papadopoulos (1998)** designed a similar type of position based impedance controller

for a hydraulic system. Again the applied torque is fed into an impedance filter and used to modify the desired trajectory. A dynamic model of the system was used as a feed-forward signal for the control input. A feedback loop was used to compensate for any errors in the model. Although the feed-forward control signal reduced some of the burden on the position controller, its use complicated the controller and required parameter identification, hence a purely position controller may be more appropriate.

Recently the benefits of position based impedance controllers have been investigated using DC motor based industrial robots **(Matko et al. 1999)**. Industrial robots are in general position controlled with independent joint controllers and kinematics software enabling them to be considered as a single entity. Implementation of position based impedance control on an industrial robot can be achieved by the inclusion of a force sensor at the robot tip. This is a much more simple and less time consuming operation than converting each joint to be force controlled, which is a requirement of force based impedance control.

Shaki et al. (1998) examined three different force controllers, force only, stiffness control and impedance control. Stiffness control is a simplified impedance control approach (figure 1.12).
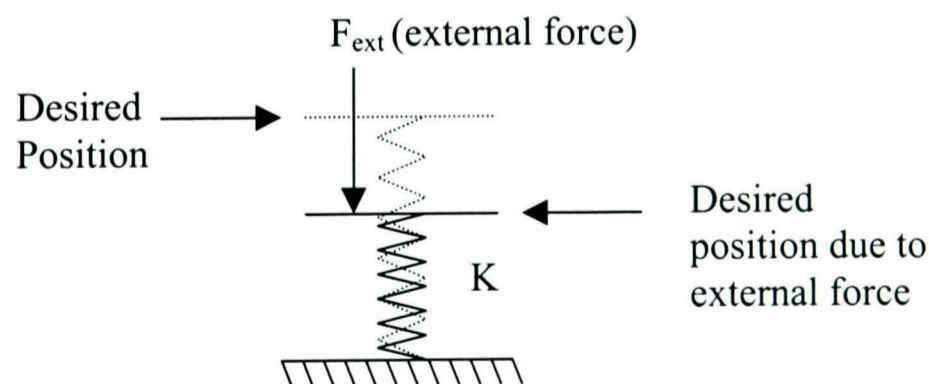
Figure 1.12 *Stiffness control*

Stiffness control causes the robot end point to behave as if it were a spring. This ignores the dynamic behaviour of the system and could result in large contact forces. To compare the three controllers, the performance of each was optimised using criteria

such as number of oscillations and the steady state error. The impedance controller was found to be the one that most satisfied the performance criteria.

One difficulty of impedance control is selection of appropriate mass, stiffness and damping coefficients. These are selected in a heuristic manner depending on the particular application and environment. Several studies have been performed into selection of appropriate impedance characteristics. **Ben-lamine et al. (1997)** used a single degree of freedom robot to assess human emotions when coming into contact with different impedance control parameters. Impedances were assessed on four different scales: reassuring/anxious; light/heavy; pleasant/unpleasant; and human like/mechanical. The results show that high mass, low stiffness and low damping cause humans to feel "threatened" by the robot. High damping reassures humans, even alongside high stiffness and mass. **Lemay et al. (1998)** assessed impedance selection for robotic orthosis devices (robotic devices attached to humans). A device to assist a tetraplegic subject (paralysed in all 4 limbs) enabled subjects to move their paralysed limb using a head driven roller ball. They conclude that a small amount of damping increases the subjective feeling of being in control.

The main drawback of impedance control is due to the accuracy of the force control loop. Impedance control can be considered as proportional force controller when in contact with the environment (**Volpe and Khosla 1995, Heinrichs and Sepehri 1999**). This is a weakness of impedance control as PI force control provides the superior performance.

1.5.3   Hybrid force and position control

Raibert and Craig (1981) developed a force and position control strategy named hybrid force and position control. An example of a pen writing on rough paper can be used to illustrate hybrid force and position control (figure 1.13). For the pen to write, a certain amount of contact force is required between the pen and paper (f_i), also movement of the pen is required across the paper (x). Therefore, force and position controllers are required in orthogonal directions. Essentially, the Raibert and Craig

method involves the use of a 'splitting matrix' to split orthogonal force and position demands. Separate force and position controllers can then be used where appropriate. This controller is only suitable for multiple degree of freedom systems, and requires pre-selection of the directions for which force and position are to be controlled.
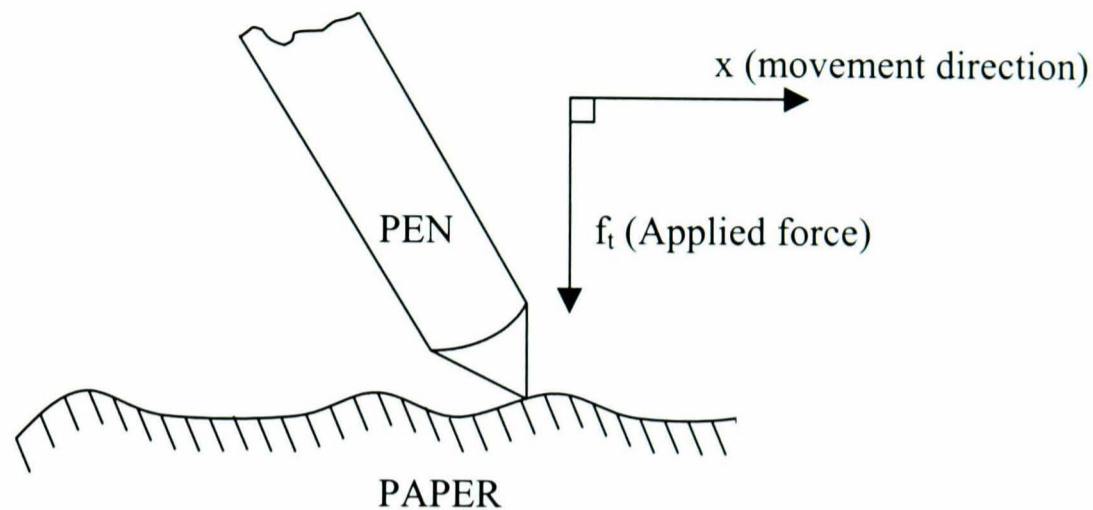
Figure 1.13 *Hybrid control*

Dunnigan et al. (1996) designed and implemented hybrid force/position control on a two degree of freedom hydraulic manipulator for use underwater. The use of the hybrid force and position control system was intended to reduce the difficulty of remotely performed tasks and hence improve the success rate. Implementation of the controller resulted in good force and position tracking.

1.5.4 Parallel force and position control

Siciliano and Villani (2000) compared several force control strategies, grouping them into indirect and direct force control. Indirect force control consists of static force control (stiffness control) and dynamic force control (impedance control). Parallel force and position control is a form of direct force control. **Chiaverini and Sciavicco (1993)** detail the parallel force and position approach in greater depth. A PI force controller (proportional control was identified as a weakness of impedance control) and PD position controller were implemented. Experimental results demonstrate the performance of the parallel controller compared to the impedance controller. When coming into contact with an object, the impedance controller compromises between

force and position demands whereas the parallel force controller sacrifices position regulation to ensure accurate force tracking. This effectively regulates the contact force without explicit information on the constrained and unconstrained environments. **Natale et al. (1999)** demonstrated the performance of parallel force and position control to be superior to hybrid force / position control.

1.5.5 Pneumatic force and position control

Several force and position strategies have been employed on pneumatic systems. **Takaiwa and Noritsugu (1999)** used force and position to design a haptic interface. The system was used to detect applied forces from errors in the position response. Position control was achieved using a standard manipulator dynamics equation enabling force to be the controlled variable. A pressure control system was implemented to reduce actuator and valve dynamics. It was possible to calculate applied forces from the position error by taking the inverse of the system mechanical impedance. Experiments showed the force to be roughly predicted, although the method assumes the impedance characteristics to be constant. It is widely known that pneumatics suffer from non-linear properties, relating to temperature expansion and variations in flow dynamics. This specifically affects identification of damping characteristics, hence ensuring force prediction accuracy for a duration test would be extremely difficult.

Kobayishi et al. (1995) designed and simulated an impedance matching strategy (maintaining system performance in the presence of external forces) for a pneumatic cylinder. Velocity and force feedback was used to make the pneumatic cylinders robust to changes in external loading. Instability was noted if the controller gains were set to be completely robust against the external loads. Experimental results show the impedance matching method to improve the system velocity response to the presence of external forces.

Bobrow and McDonell (1998) designed a torque control subsystem to enable pneumatic cylinders, driven by spool valves, to apply torque on demand during motion. The torque controller was used to implement hybrid force/ position control,

enabling accurate force control without the need for force sensors. The compressibility of pneumatic systems was found to reduce some of the instability problems noted by other researchers using electric motors. **Tzafestas et al. (1997)** implemented a similar torque subsystem to enable torque demands to be specified on a pneumatic cylinder and spool valve arrangement. As well as the torque subsystem, robot dynamics were used to implement an impedance control strategy. The robot dynamics were adapted on-line to ensure controller performance. Simulations demonstrate the controller to accurately track the force and position.

Guilhard and Gorce (1996) implemented an almost identical torque control subsystem for control of a single link of a walking robot. The impedance control strategy enabled the robot to interact in unknown environments. These concepts were extended to multiple degrees of freedom **by Gorce and Guilhard (1999)**. The performance of the single link and the multiple degree of freedom controllers were demonstrated through simulation. **Noritsugu et al. (1996)** used impedance control on a rubber artificial muscle manipulator. A pressure controller was implemented to regulate the pressure in each muscle. Accurate force and position control was demonstrated for a range of damping and stiffness, however, some oscillation is apparent in the response.

It is apparent from studying the literature that little research has been carried out on pneumatic force and position control strategies due the fundamental difficulties of achieving precision control on pneumatic cylinders. Moreover, the majority of studies, particularly into impedance control, have been validated in simulation. However due to the non-linear nature of pneumatic systems with effects such as air compressibility and stick-slip friction it is difficult to ensure that a simulation accurately represents the experimental system.

1.6 Approaches for robotic physiotherapy

A detailed review of current rehabilitation technologies can be found in **Austin (1999)**. Here an overview of the research area is presented to briefly explain current activities in robotic rehabilitation, setting the context for the remainder of the thesis. Focus will be given of the design and control of such devices rather than the underlying medical implications. Currently, several large research groups have applied themselves to designing and developing robotic rehabilitation devices.

Hogan et al. (1995) have made a significant contribution to robotic physiotherapy. They designed and patented a device to provide upper-limb physiotherapy (figure 1.14). The device has two degrees of freedom at the elbow and forearm and three degrees of freedom at the wrist, allowing extension and flexion. Tasks are performed on the robotic physiotherapy device using visual feedback on a computer monitor **(Hogan et al. 1998)**.
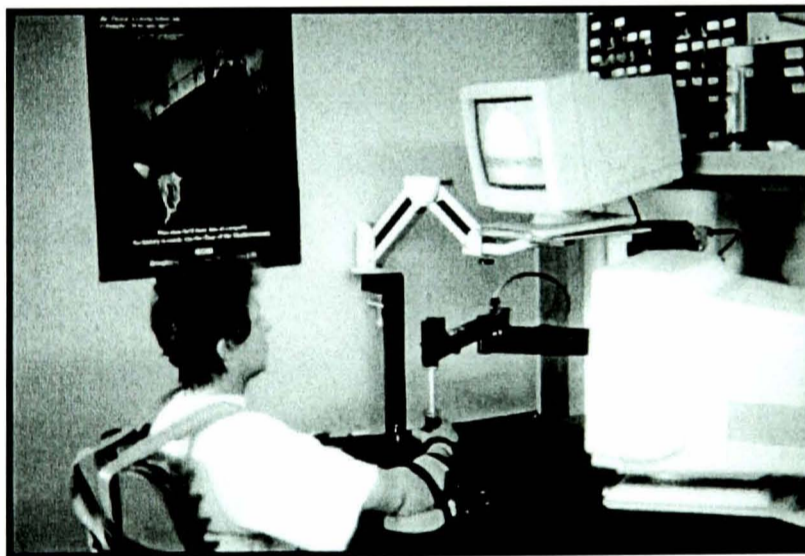
Figure 1.14 MIT-MANUS rehabilitation robot (Hogan et al. 1995)

The robot is designed to be of low inertia and backdrivable, simplifying the control and reducing the feeling of constraint on patients. In order to implement physiotherapy they performed a study of how movement is instigated. They postulated that upper-limb motion was constructed of a series of bell shaped steps merged together. Patients suffering from illnesses such as stroke, loose their ability to merge these bell shaped efforts into smooth motion. A control system based upon a

series of these bell-shaped demands was overlaid and used to implement physiotherapy.

The system is controlled by a three-layer strategy. The higher level controller specifies a desired trajectory as input by a physiotherapist manually moving the device. The trajectory is then broken down to a series of virtual references (task encoding level). These virtual references can be thought of as the point to where the arm was moving at the respective movement stage. Implementation of the virtual reference point is achieved through impedance control (lower level). Sequential virtual reference points are superimposed to achieve a smooth human like motion.

A limited clinical trial demonstrated that patients who received additional robotic physiotherapy, on top of their conventional therapy, showed greater improvement over a control group that only received conventional therapy. Some of the patients were recalled after a 3-year period and their performance re-evaluated **(Krebs et al. 1999)**. Patients that received robotic physiotherapy had improved significantly more than the control group. One of the drawbacks of the device, however, is that it prevents patients from instigating their own motion, which is considered essential if the patient's are to feel in total control, moreover the device supports the patients arm at one point preventing its use on patients with weak shoulders.

Lum et al. (1993) developed a simpler device to perform upper-limb physiotherapy; the bimanual lifting rehabilitator (figure 1.15). The basic idea behind the device is to enable a healthy limb to assist in the rehabilitation of a more damaged limb (strokes normally effect one limb more severely than the other). They base their device on a two-handled tray for which one end has a motor assist device. The patient, using the healthy limb instigates motion. If the patient begins to experience difficulty performing the task the motor provides assistance to the damaged limb ensuring the tilt of the tray does not exceed 1.2^0. Using an error dead-zone, the controller ensured that unwanted assistance was not applied. The bimanual lifting rehabilitator has not been used in clinical trials so the success of the controller has not been proven.

Lum et al. (1999) developed a patient initiated device known as the Mirror-Image Motion Enabler (MIME). The MIME device consists of two commercially available arm supports to limit the range of movement to the horizontal plane. A commercially available robot (PUMA 360) was used to provide motion to the impaired limb. A 6 d.o.f sensor measured forces between the limb and robot. The aim of the device was to provide assessment of patients after initial injury and during the rehabilitation phase.

The robot had two methods of operation; passive and active. In the passive mode patients were asked to relax their limb while the robot moved it through a pre-set series of motions. All forces were measured during this motion, and the abnormal ones noted. In the active assist mode the patients were asked to apply a constant force on the robot while it moves through a series of motions. Patients are provided with visual feedback on the amount of force applied so they can attempt to achieve a constant force. Forces in unintended directions and forces resisting motion are measured to quantify the patient's performance. The results show that the device can be used as an assessment device, but the cost of the industrial robot is prohibitive.
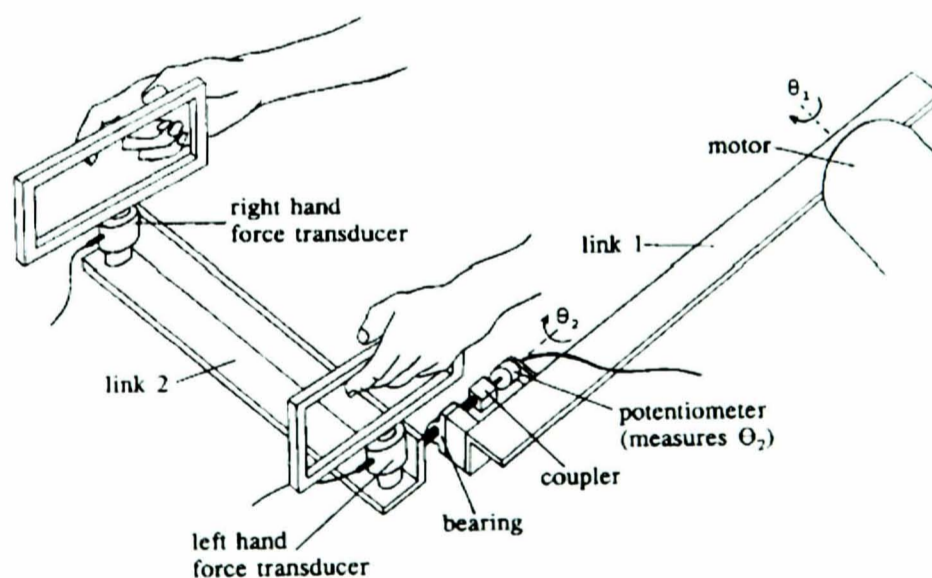
Figure 1.15   Bimanual lifting rehabilitator (Lum et al. 1999)

Reinkensmeyer et al. (1999)[1],[2] developed an arm rehabilitation and measurement device (ARM) (figure 1.16). The device was intended to guide reaching movements across the workspace, recording motion and forces in multiple degrees of freedom. In an early study, the device was used passively to assess patient's movement along the guide. Impaired patients demonstrated smaller movement ranges and large forces in undesired directions. The large forces were significant, resulting from ill co-ordination of motion.

Recently, the ARM has been used actively to assist motion. The patient was asked to relax their limb, while a motor moved their limb up and down the guide. The torque required to move the limb was recorded in a look up table as a function of position. The patient was then asked to move their limb along the guide while a lookup table of the torque assisted their motion. The patient's motion improved when the torque was applied, although the patient's full movement range was not achieved. The authors note a mismatch between the constraints of the ARM guide and the patient's movement, making comparison between patients difficult.
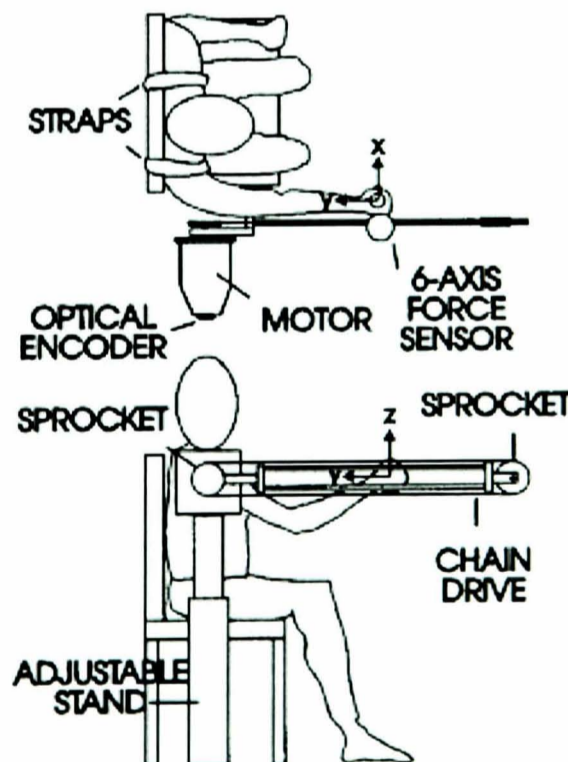
Figure 1.16 A.R.M rehabilitation device (Reinkensmeyer et al. 1999)[1],[2]

A consortium headed by the University of Newcastle upon Tyne has developed a motorised upper-limb orthotic system (MULOS) **(Buckley and Platts 1995)** (figure 1.17). The robot has 5 d.o.f, is wheelchair mounted and was designed primarily for everyday living tasks. **Yardley et al. (1997)** details the approaches to physiotherapy that the device can perform. Presently, it is limited in its ability providing only two exercise modes, percentage assist and percentage resist. These require careful input by the physiotherapist and are not patient responsive. The robot assists shoulder orthosis, which is potentially dangerous requiring considerable attention to prevent damage **(Scattareggia et al. 1997)**. The complexity of design also makes the device expensive.

Figure 1.17   MULOS rehabilitation robot (Buckley and Platts 1995)

Austin et al. (1999) applied physiotherapy to arm extension/flexion using a DC torque motor. The results of a limited patient trial were encouraging, but the small sample of patients meant no definitive conclusions could be drawn. The device was only capable of applying single degree of freedom rehabilitation, thus restricting potential applications.

Limited research has been performed into designing rehabilitation robots using pneumatic actuators. **White et al. (1993)** developed a pneumatic orthosis device that is designed to restore motor function to the elbow joint (figure 1.18). Pressures on either side of the cylinder are measured and this information is used to apply and

monitor forces acting on the patient's limb. With only one joint being exercised, applications for this device are limited.
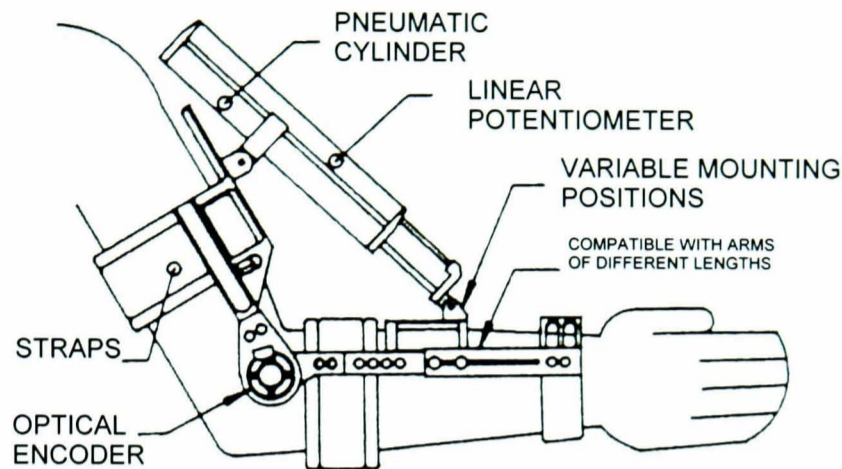
Figure 1.18 *Pneumatic cylinder elbow rehabilitation device (White et al. 1993)*

Noritsugu et al. (1996) used rubber artificial muscle manipulator as actuators for a rehabilitation robot (figure 1.19) in two degrees of freedom. A pressure control system was implemented to control the non-linear pressure response of the muscles. An impedance control strategy was used to implement several physiotherapy techniques. Experimental results showed accurate force and velocity control.
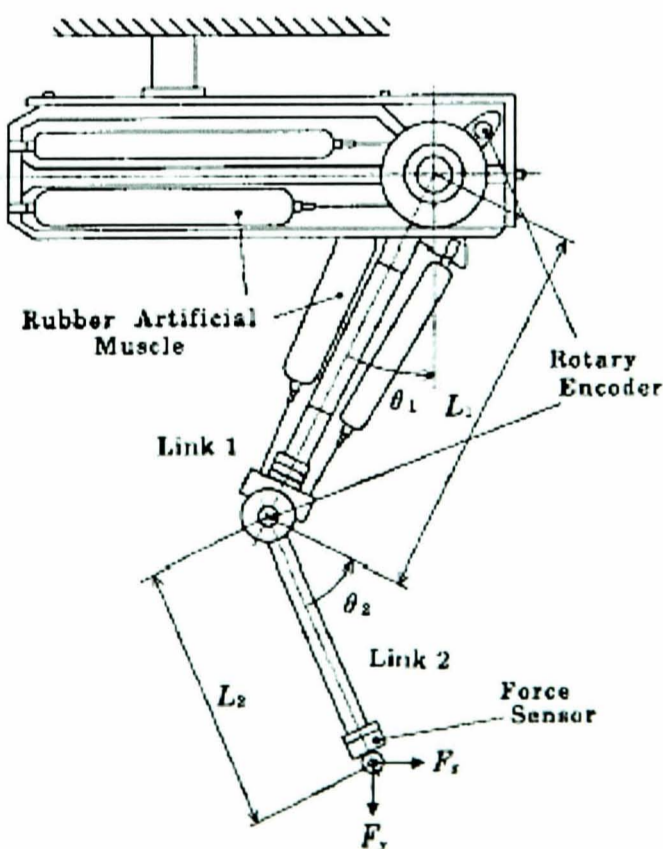
Figure 1.19 *Rubber artificial muscle manipulator (Noritsugu et al. 1996)*

Kawamura et al. (1997) used antagonised rubber actuators for implementation of a motion support device. The robot end point was attached to the human arm and was used to move the patient's limb through motions to facilitate rehabilitation. The maximum force output at the robot end point was 70N. The controller employed on the robot guided the patients arm through the desired trajectory. Slight oscillations were noted in the robot response.

There are a few researchers investigating movement assistance (movement without assisting patient recovery). These would not be suitable for physiotherapy, but the design concepts are similar. **Homma and Arai (1998)** developed a system based on six motors driving the human arm by a series of strings. The motors increase or decrease the length of the strings to move the arm based on position inputs from the user. The device is useful for assisting patients with little voluntary movement. **Nagai et al. (1998)** developed an 8 d.o.f robot to assist human upper limb motion. Experiments were performed on a single degree of freedom, to assist patients lifting a 1kg mass. The device was shown to be able to provide power assistance.

All of the devices reviewed in this section are still in the prototype stage and their clinical effectiveness is still being evaluated. The main limiting factor preventing wider investigation into rehabilitation devices is their cost.

1.7 Summary of literature review

Physiotherapy is normally performed by physiotherapists who apply varying levels of force to guide the subject's limb through a desired trajectory. If robots are to perform physiotherapy in a similar manner, then they too must equate applied force with the subject's ability to follow the desired trajectory. The application of force dependant on the patient's positional accuracy, requires a force and position control strategy.

Three main force and position control strategies enable robots to interact with their environment, hybrid force control **(Raibert and Craig 1981)**, impedance control **(Hogan 1985)** and parallel force and position control **(Chiaverni and Sciavicco 1993)**. During physiotherapy the robot is required to maintain contact with the patient. Hybrid force control behaves solely as a force controller under these conditions and parallel force control is only capable of regulating the maximum force applied.

Impedance control compromises between force and position demands, with the relationship between them specified by mass, stiffness and damping parameters. Modification of the impedance relationship changes how the robot responds to errors in the position, and hence the amount of assistance (force) applied, during the physiotherapy exercise.

The research performed on designing and implementing impedance control has shown it to be suitable for a wide range of robot contact tasks. The majority of these controllers use torque motors as actuators **(McComuck and Schwartz 1993)**, increasing the cost and introducing new control difficulties such as backlash.

Pneumatically driven robots offer increased power to weight ratio, backdrivable characteristics and greatly reduced costs. However, they have not been implemented for such robotic devices due their inherent non-linear behaviour. The major difficulties in applying impedance control on pneumatic systems arise from variations in the torque applied during motion of the cylinder and non-linear friction effects. Electro-pneumatic valves and low friction cylinders reduce these effects.

Little research has been performed to apply impedance control strategies to pneumatic systems. Several researchers have investigated the use of pneumatic cylinder torque models to allow cylinder force to be controlled during motion **(Bobrow and Jabbari 1998, Tzafestas et. al 1997, Guilhard and Gorce 1999)**. Evaluation of these controllers was largely performed in simulation, making it difficult to assess their effectiveness.

Research on hydraulic cylinders has identified position based impedance control to be suitable for non-linear actuators such as pneumatic cylinders **(Heinrichs et al. 1997, Bilodeau and Papadopoulos 1998)**. These controllers do not require accurate models of the system dynamics or torque models. Indeed, these benefits are also being exploited for torque motor based industrial robots **(Matko et al. 1999)**.

During limited clinical trials, robotic physiotherapy devices have been shown to offer clinical benefits to stroke victims **(Krebs 1999, Reinkensmeyer et al. 1999)**. However, such devices (based on electric motors) tend to be complex, expensive, and feel 'mechanical' to the user.

A robotic device based upon pneumatic actuators implementing impedance control would be suitable for a physiotherapy device. Such a device would be cheaper, simpler, while the compressibility of air would remove some of the 'mechanical' feel of the device.

1.8 Research objectives

The overall aim of this study is to design and fabricate a three degree of freedom robot capable of performing robotic physiotherapy. To fulfil the project aim, the following objectives were outlined:

1. To investigate actuation systems that will give acceptable robot movement characteristics for an upper-limb robotic orthosis device.

2. To design and construct an experimental robotic device, allowing forces to be applied to arm segments within the required movement envelope, as well as allowing arm position and motion to be measured.

3. To apply advanced servo and robot control techniques to achieve accurate control over arm force, direction and magnitude at any robot position.

4. If time and ethical approval permits, implement a simple higher-level physiotherapy algorithm, and demonstrate using one or two sample patients.

1.9 Statement of originality

The main areas of original work carried out during this research are highlighted below.

1. A novel self-tuning pole-placement position controller has been designed and implemented to control a pneumatic actuator under the influence of gravity. (Published paper 2)

2. A serial link manipulator has been designed and built from ergonomic data to enable robotic physiotherapy to be performed. (Published paper 1)

3. A PID position based impedance control strategy has been designed in simulation and implemented on a single degree of freedom robot. (Published paper 3)

4. A three degree of freedom force sensor has been designed using FEA analysis and constructed. The single degree of freedom impedance controller has been extended to three degrees of freedom (Paper 4)

5. The PID position based impedance controller has been modified to form a pole-placement position based impedance controller.

Papers published (Appendix B)

1. Richardson R, Austin ME, Plummer AR. Development of a physiotherapy robot. Proceedings of the international Biomechatronics Workshop, Enshede 19-21 April 116-120, 1999.

2. Richardson R, Plummer AR, Brown, MD. Self-tuning control of a low friction pneumatic actuator under the influence of gravity. IEEE Control Systems Technology, March 2001.

3. Richardson R, Brown MD, Plummer AR. Pneumatic impedance control for physiotherapy. Proceedings of the EUREL int. conf. Robotics. Vol. 2. March 2000.

Papers pending publication

4. Richardson R, Brown MD, Plummer AR. Design and control of a three degree of freedom pneumatic physiotherapy robot. To be submitted to Journal Mechatronics.

5. Richardson R, Bhakta B, Brown MD, Plummer AR. A three degree of freedom physiotherapy robot. To be submitted to IEEE Transactions On Rehabilitation Engineering.

1.10 Thesis overview

The main body of this thesis consists of seven chapters. A breakdown of the content of each chapter is given below.

Chapter 2: Experimental equipment

This chapter details the design, development and specification of experimental equipment used throughout this study. The design and development of the robot from design specification to fabrication is presented (section 2.1). A three degree of freedom force sensor is also produced using FEA analysis and calibration methods are discussed (section 2.2).

Chapter 3: Position control

This chapter details position control techniques implemented on the test rig to assess the potential performance of pneumatic systems. Proportional control was used to identify a plant model (section 3.3), enabling pole-placement control to be performed (section 3.4). The pole-placement controller is then modified to include a self-tuning element. The self-tuning controller is then modified to include a term to compensate against external forces when the cylinder acts against gravity.

Chapter 4: Force control

This chapter details experiments performed to control the force applied by the pneumatic cylinder. Open-loop force control while the cylinder position is fixed has been performed. The desired force is accurately tracked (section 4.2). With the position no longer fixed, open-loop force control was performed. The performance of the force controller was shown to degrade with force being a function of velocity (section 4.3).

Chapter 5: Modelling and simulation

This chapter develops mathematical models and simulations of the experimental equipment detailed in chapter 2. A computer model and Matlab simulation of a single degree of the three degree of freedom pneumatic robot is developed. A detailed

analysis of the behaviour of the electro-pneumatic valves has been performed (section 5.2). The valve model is then combined with a standard pneumatic cylinder model (section 5.3). The simulated response was compared to experimental results and found to accurately represent the system (section 5.5).

Chapter 6: Force and position control:

This chapter develops a force and position control strategy (termed impedance control) on a single link in simulation. Experimental results applying the impedance controller on a single link show that the performance predicted by the simulation has been experimentally verified (section 6.3). The impedance controller is extended to three degrees of freedom, through forward and inverse kinematics (section 6.6).

Chapter 7 Pole-placement impedance control

This chapter details modifications to the impedance control strategy. A pole-placement position control strategy was used in place of the PID control strategy to implement position based impedance control (section 7.3).

A flow chart of the overall design and development process is shown in figure 1.20 and a flow chart of the controller design process is shown in figure 1.21.

```
                    ┌─────────────────────┐
                    │   DESIGN PROCESS    │
                    └─────────────────────┘
                              │
                              ▼
              ┌───────────────────────────────────┐
              │  EXPERIMENTS ON PNEUMATIC         │
              │  CYLINDERS TO ASSESS PERFORMANCE  │
              │         (CHAPTER 3)               │
              └───────────────────────────────────┘
```

DESIGN PROCESS

EXPERIMENTS ON PNEUMATIC CYLINDERS TO ASSESS PERFORMANCE (CHAPTER 3)

INVESTIGATION INTO PHYSIOTHERAPY TECHNIQUES (CHAPTER 1)

INVESTIGATION INTO HUMAN ERGONOMICS (CHAPTER 2)

DESIGN OF THREE DEGREE OF FREEDOM PHYSIOTHERAPY DEVICE (CHAPTER 2)

DESIGN AND DEVELOPMENT OF THREE DEGREE OF FREEDOM FORCE SENSOR (CHAPTER 2)

COMBINING FORCE SENSOR AND ROBOT TO IMPLEMENT 3 D.O.F IMPEDANCE CONTROL (CHAPTER 6)

POLE-PLACEMENT IMPEDANCE CONTROL (CHAPTER 7)

Figure 1.20   *Design and development process*
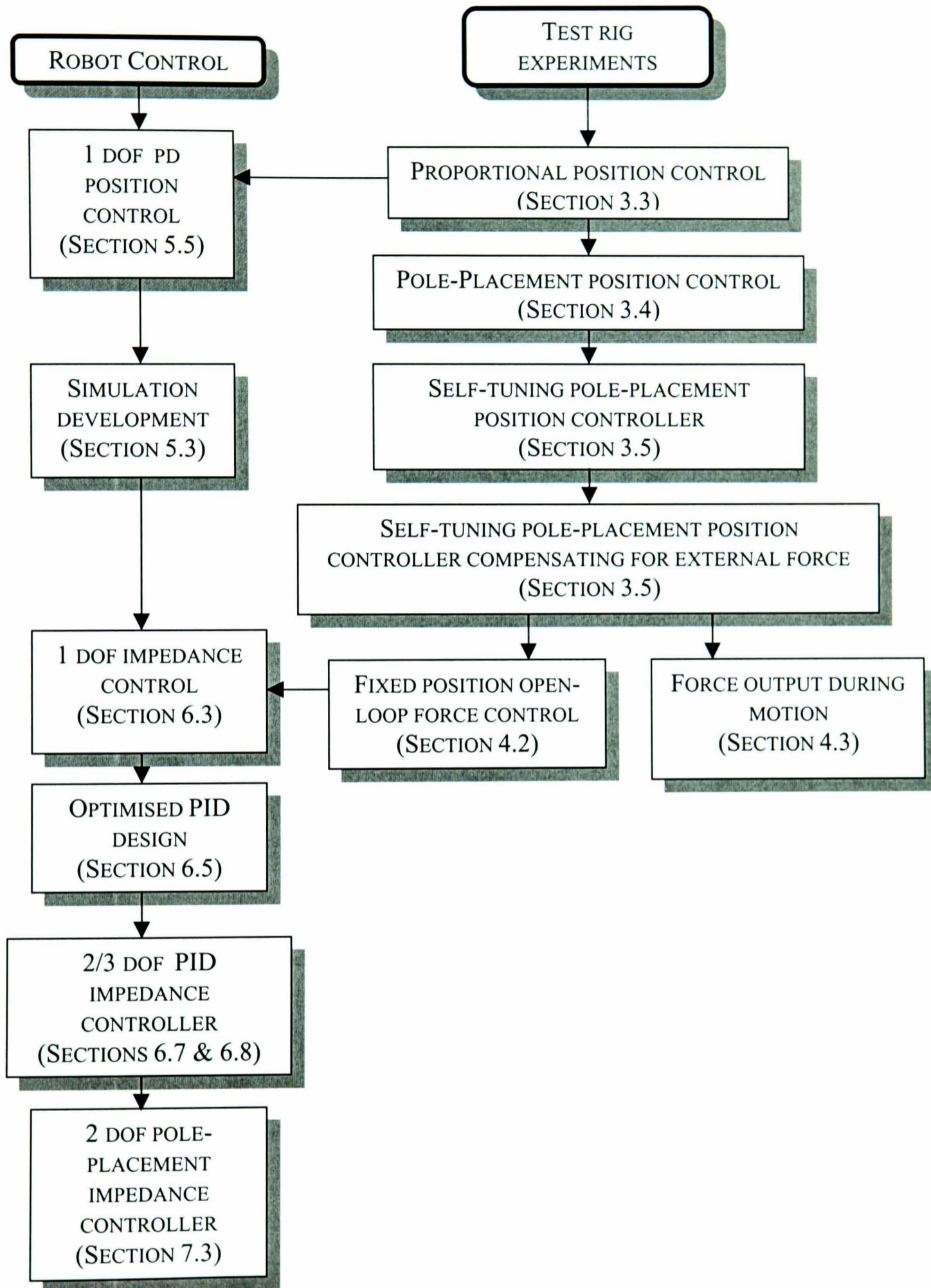
Figure 1.21 *Controller design and development process*

Chapter 2

Experimental Equipment Development

This chapter details the experimental equipment used to implement and validate the controllers developed throughout this thesis.

2.1 Experimental assessment of controllers

Two sets of experimental equipment were used during this research to develop and validate control strategies applied to pneumatic systems;

1. A test rig constructed from steel channel was used to assess, in a single degree of freedom (one pneumatic cylinder), the performance obtainable from low friction pneumatic cylinders.

2. A three degree of freedom prototype physiotherapy robot was designed and fabricated to implement controllers in multiple degrees of freedom.

All the components used in the prototype robot and test rig are detailed in table 2.1.

2.1.1 Test rig

A test rig was developed to assess the performance of a single pneumatic cylinder. Two alternative configurations of the test rig were used to perform position control and fixed position force control (figures 2.1 & 2.2)

Position control configuration

The position control rig allows movement of the pneumatic cylinder while collecting performance data. Pressures in the cylinder chambers (measured by pressure transducers) generate forces to overcome any stiction, friction and external forces acting upon the cylinder, resulting in movement of the cylinder piston. A force sensor measures the output force of the cylinder and an LVDT (linear variable differential transducer) measures the cylinder position. Experiments performed on the position test rig are detailed in chapter 3.

COMPONENT	PROPERTIES	USE
Low Friction pneumatic cylinder - Airpot Airpel – Air bearing design	Bore 0.627 inch Stroke: 4 inch	Test rig
Low Friction pneumatic cylinder - Airpot Airpel – Air bearing design	Bore 0.627 inch Stroke: 6 inch	Robot
Conventional seal cylinder – Lip seal	Bore dia: 20mm Stroke: 80mm	Test rig friction comparison
Electro-pneumatic pressure control valves – SMC E– P Hyreg VY1100	Pressure range:0 – 8.8 bar Voltage Range: 1 – 5V	Test rig and robot
Pressure Transducer RS 249-3959	Pressure Range: 0 – 6 bar Accuracy (%FS) ± 0.1%	Modelling validation
Force Transducer RDP 51/1117 - 01	Capacity: 890 N Accuracy (%FS) ± 0.5%	Test rig and robot
Mass (M)	4.5 kg	Test rig
Linear rotary potentiometer Novotechnik P2701	Mechanical travel: 360^0 continuous Nominal resistance :5kΩ	Robot
PC-Labcard PCL-727 12 channel D/A output card	12 D/A channels 12-bit resolution	Robot
PC-Labcard PCL 816/814B 16 A/D channels	16 A/D channels 16-bit resolution	Robot
Amplicon PC-30 I/O board	8 A/D channels 12-bit resolution, 2 D/A channels 12-bit resolution	Test Rig
LDVT RDP D5/6000	Linear Range: ± 150mm Linearity (%FS) ± 0.2%	Test rig

Table 2.1   *Equipment Specifications*
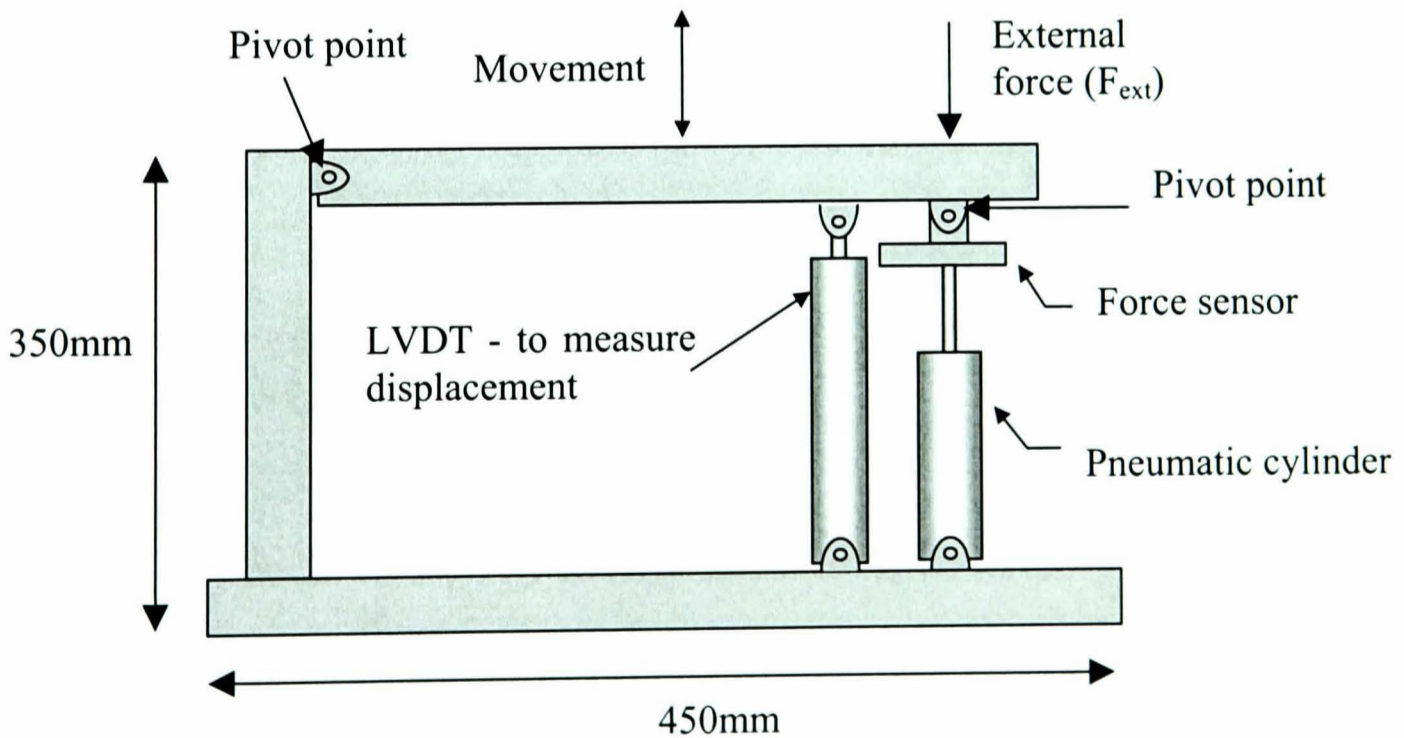
Figure 2.1   *Test rig to perform position control*

<u>Fixed position force control configuration</u>

The fixed position force rig enables measurement of cylinder output force while cylinder piston movement is prevented. Pressures in both cylinder chambers generate forces on the piston, which are measured by the force sensor. A screwed bar prevents movement of the cylinder and insulates the cylinder from any external forces. Experiments performed on the force rig are detailed in chapter 4.
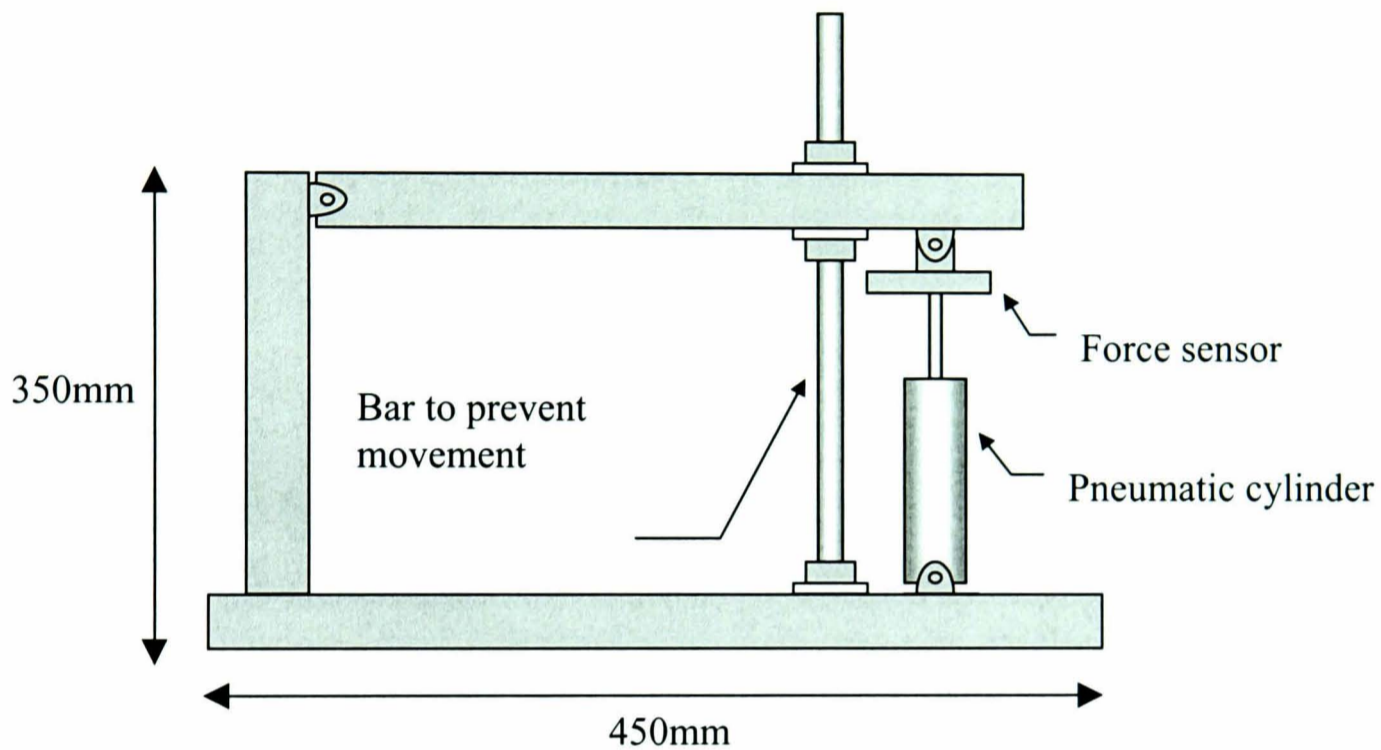
Figure 2.2   Test rig to perform fixed position force control

2.1.2 Three degree of freedom physiotherapy robot

A three degree of freedom robot has been designed and built which is capable of imposing force demands and measuring position in three degrees of freedom (figure 2.3). The design specification for the prototype physiotherapy is given in table 2.2.

<u>Robot design and fabrication</u>

The main body of the robot was constructed from aluminium U channel. Three degrees of freedom were achieved using revolute joints, with joints two and three implemented through bearings in the aluminium U-channel. The first joint was constructed from two angular contact bearings situated in a steel housing (figure 2.4). The two halves of the bearing arrangement close around the pivot point of the first link. To ensure alignment of bearings the two halves fit together using a location edge

around the casing and a single locating pin. Rotation of the joint is measured using an angular potentiometer coupled to the pivot point. Production drawings for the robot are shown in appendix A. Photographs of the assembled robot are shown in figures 2.5 & 2.6.
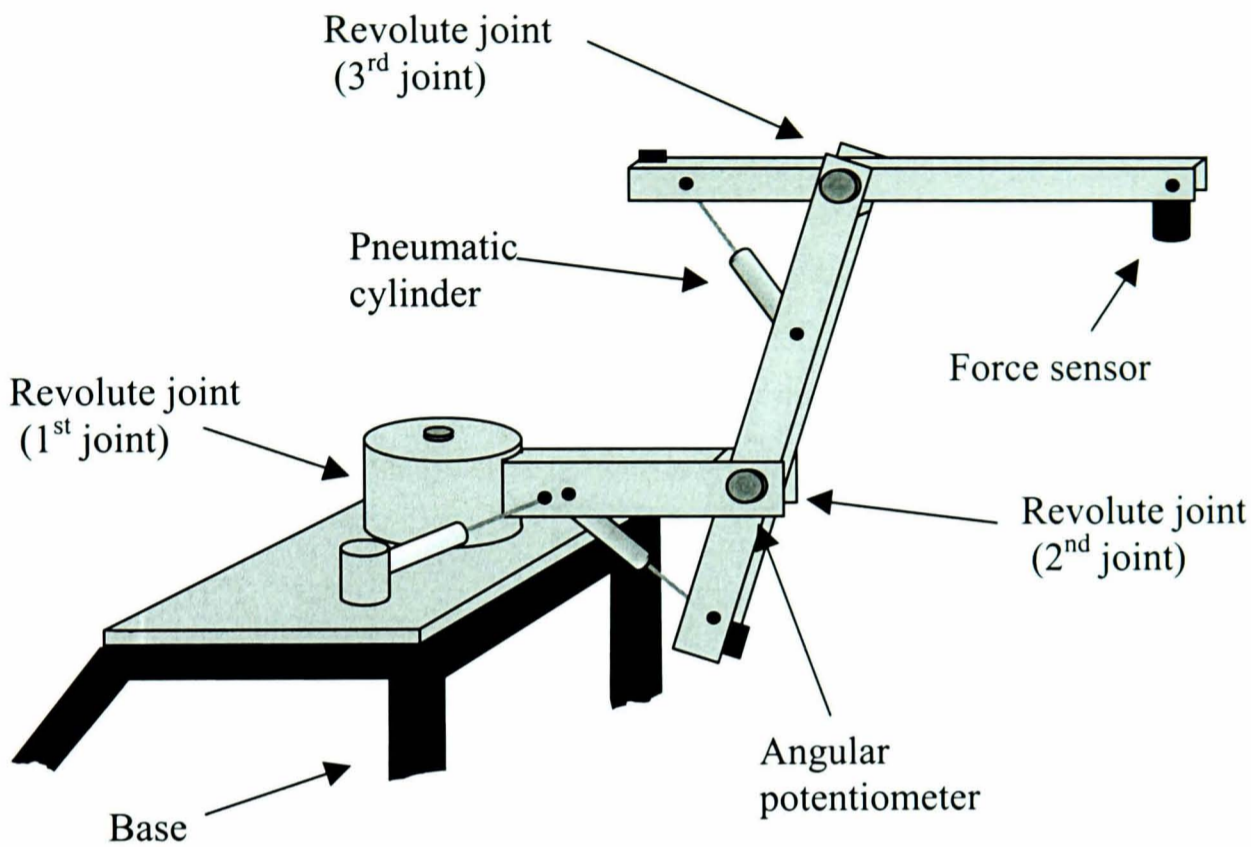
Figure 2.3 *Three degree of freedom robot*
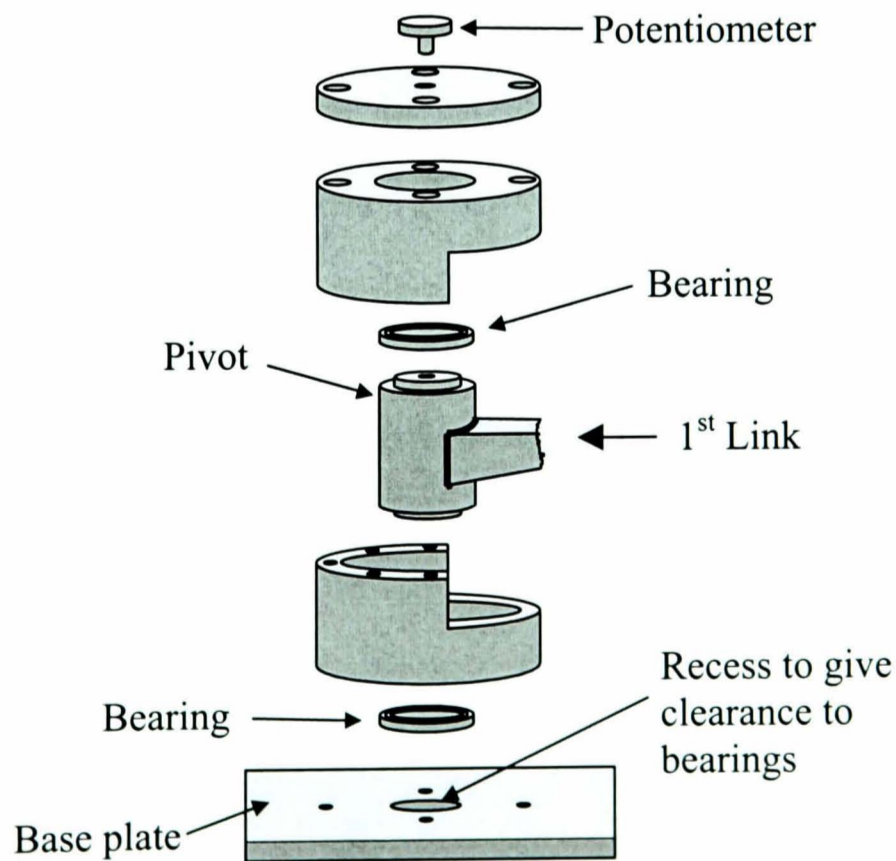
Figure 2.4 *Exploded view of 1ˢᵗ joint bearing arrangement*

DESIGN SPECIFICATION		**DATE:**	10 July 1998	
TITLE:		Three degree of freedom robot for physiotherapy		
DESCRIPTION:		A three degree of freedom robot is to be designed and fabricated that is capable of applying forces to arm segments within the required movement envelope as well as implementing position demands.		
WEIGHT:		The overall weight of the device is not critical. The weight of individual links is important. Lighter joints will reduce the joint inertia and reduce the force required from the actuators under no external load conditions. Aluminium channel has been identified as an appropriate choice for construction of links.		
SIZE AND ERGONOMICS:		The robot is required to move in a workspace based upon the optimum reach ability of the average human. Ergonomic data has been examined to ensure the range of motion is sufficient **(McCormick 1970)**. An oval approximately 0.25m (x)*0.15m (y) *0.400m (z) diameter will allow sufficient movement range. Ergonomic data identified the height of the robot at mid range to be 1m from the ground to enable an average seated human to attach their arm to the device **(Kantowitz and Sorkin 1983)**.		
SAFETY:		Safety issues are of critical concern when robots are interacting directly with humans. It is important that the range of motion can be reduced through mechanical end-stops to ensure the robot is not capable of causing damage through its movement. An emergency stop button is required to remove power to the actuators. Use of an electrically powered shut off valve would remove pneumatic power. A 'force fuse' could be used to prevent large forces being applied to the human **(Salganicoff and Hersh 1996)**.		
POWER SOURCES:		The power source must be suitable for medical environments. Pneumatic power has been selected as an appropriate power source.		
MECHANICAL LOADING:		Mechanical loading will result from interaction with the human. The loading will be small and variable. The pneumatic cylinders are capable of supplying 100N of force. The weight of a human arm has been identified as around 5kg **(Dolan et al. 1993)**. 20N has been selected as the maximum loading.		
OPTIMUM METHOD OF CONTROL:		Robotic physiotherapy requires robots to interact with humans requiring consideration of both force and position. Position only control is insufficient, and would result in the patient's limb being dragged along a trajectory. Force only control would neglect the control of position with the potential for the robot to attempt to force the patient's limb outside the desired range of motion. From the available force and position control strategies, impedance control is the most suitable, allowing direct interaction between the human and robot. Indeed, impedance control has been used in a prototype physiotherapy robot with promising initial results **(Hogan et al. 1995)**		
DESIRED CONTROL PERFORMANCE:		Few researchers have implemented impedance control using pneumatic systems so it is difficult to quantify the performance expected, moreover, robot rehabilitation is at an early stage of development so the required performance of the robot is not known. The position accuracy of the controller is not critical, as exact positioning would have little beneficial effect on patient's recovery. The specification of the impedance characteristics does not need to be exact, but is required to be as consistent as possible. Stability is critical.		

Table 2.2 *Design and control specification*
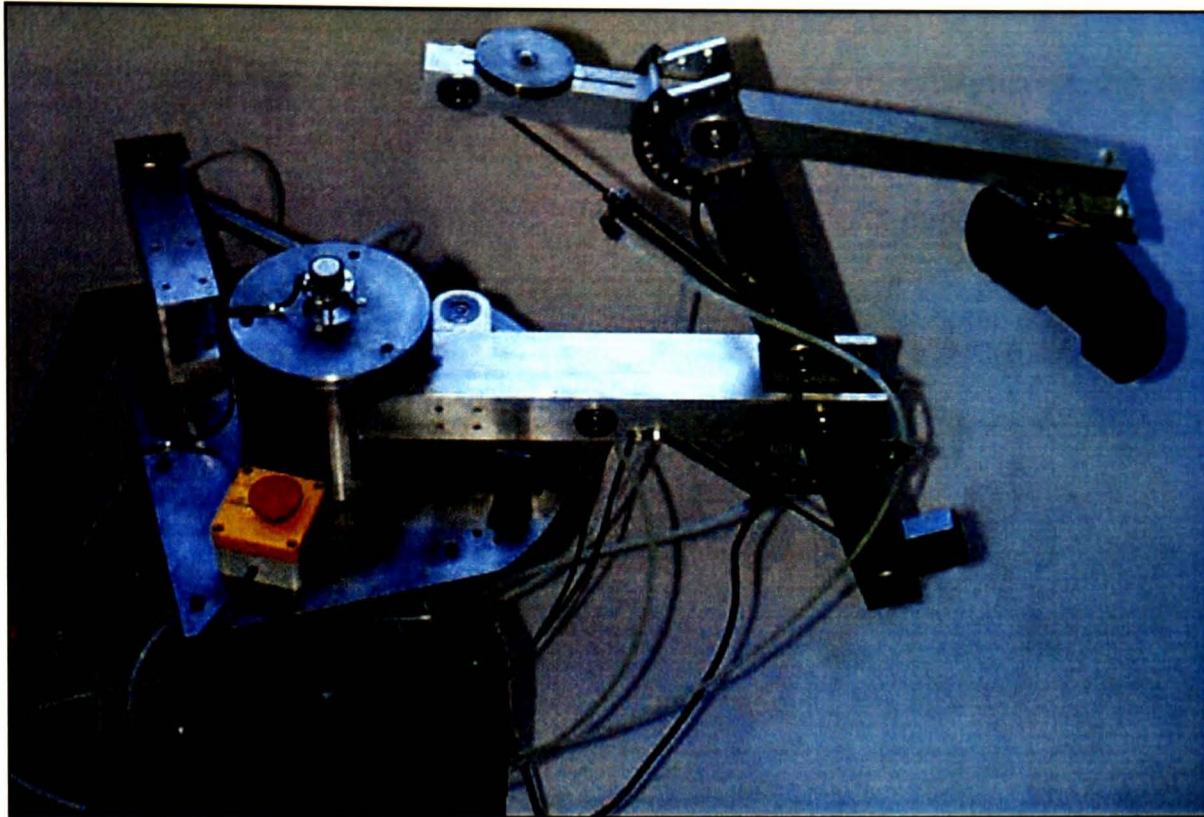
Figure 2.5 *Photograph of pneumatic physiotherapy robot*
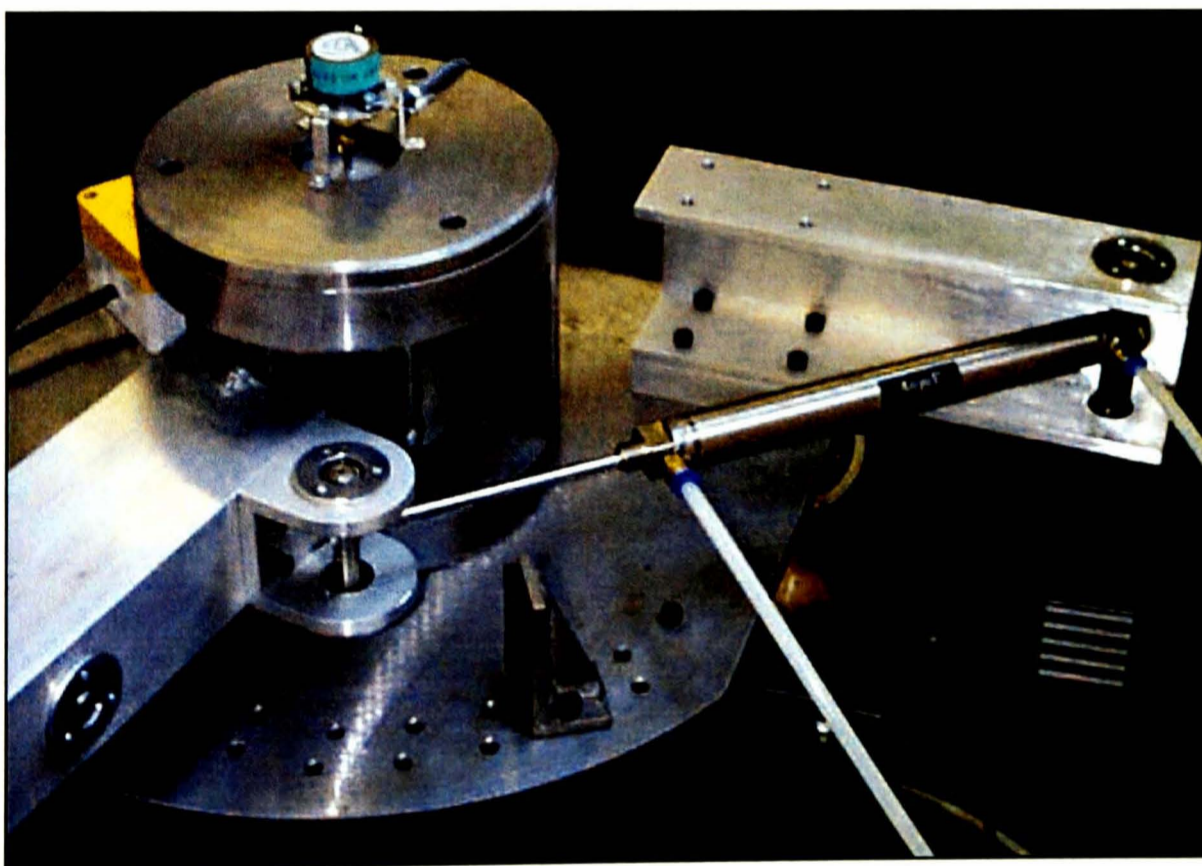
Figure 2.6 *Photograph of robot's first link*

Position criteria

The operational range of the robot has been designed to encompass the movement range of the average human. Ergonomic data was used to quantify this required movement range **(McCormick 1970)**. The average male is capable of movement over a large region, however, within this region is an area where the majority of every day reach and retrieve operations are performed (the 'optimum reach' area). This optimum reach area has been approximated as a sphere with dimensions 0.3m x 0.4m x 0.2m (figure 2.7). The robot has been designed so that the movement range of its end point encompasses this sphere.

Approximated workspace that the hand is
required to be moved through
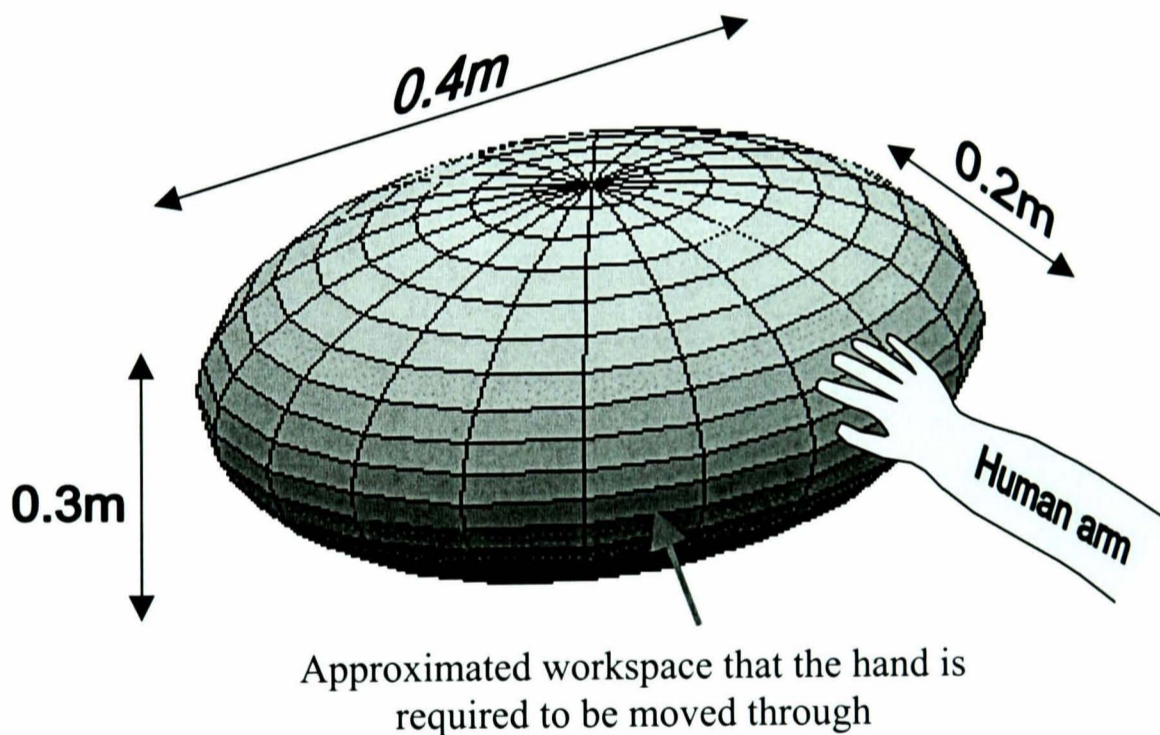
Figure 2.7   Ergonomic operational range

Each of the revolute joints has a movement range of +/- 20 degrees, resulting in the robot's operational range (workspace) as is shown in figure 2.8. The ergonomic workspace (figure 2.7) is shown to be within the overall workspace of the robot. This movement region should be sufficient to enable humans to perform reach/and retrieve operations when attached to the device.
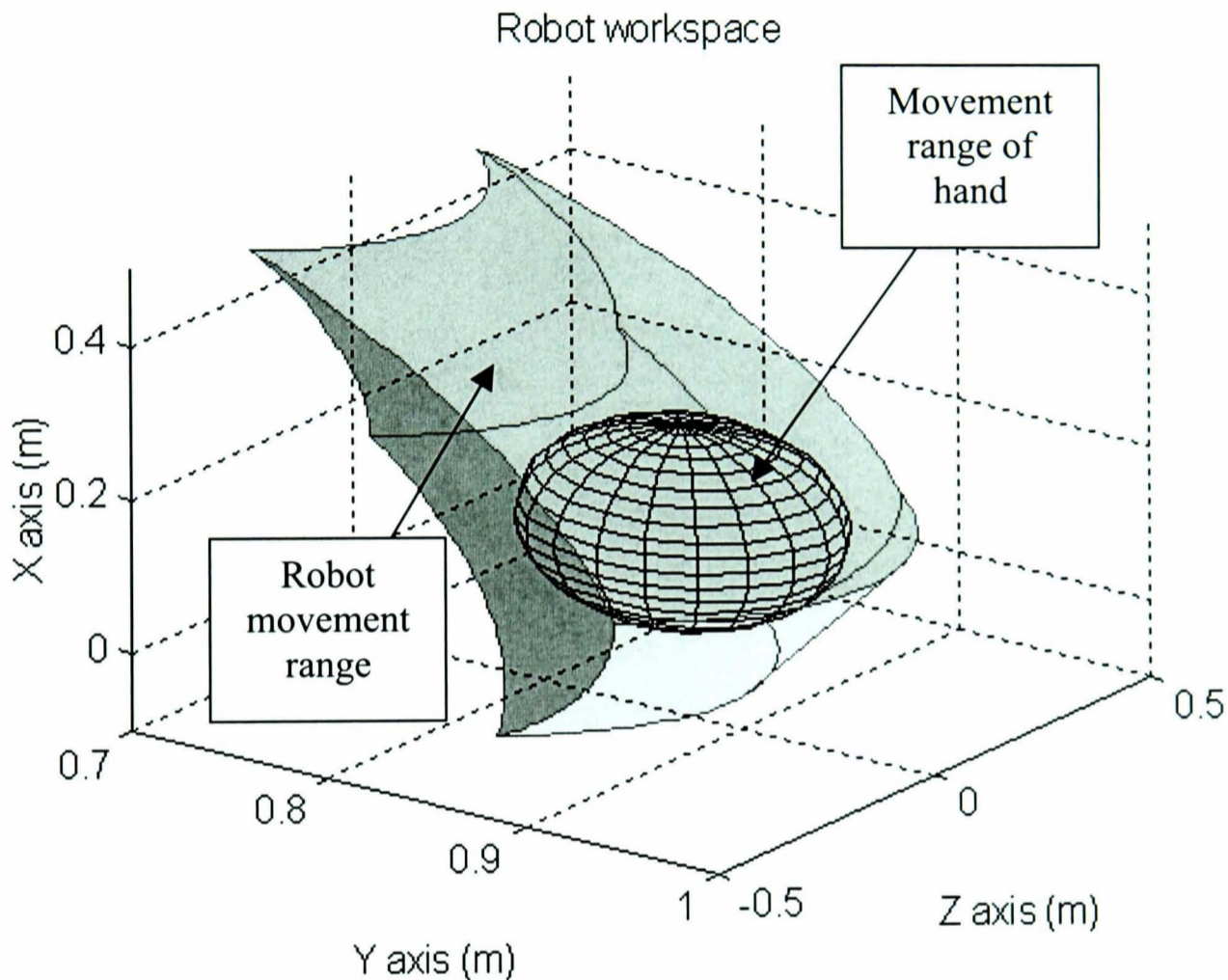
Figure 2.8   *Robot workspace*

Force criteria

One of the important aspects of the robot design is its ability to provide forces to the patient's limb. The maximum force output of an individual Airpel low friction pneumatic cylinder at 6.5 bar can be calculated to be approximately 100N.

The maximum force applied to the robot has been specified to 20N. Supporting this force in the x direction is most critical, where the robot is required to support the patient's limb against gravity. The required actuator force to support this external

force can be calculated by considering moments at that joint (figure 2.9). The counterbalance reduces link torque generated by an imbalance in link length.
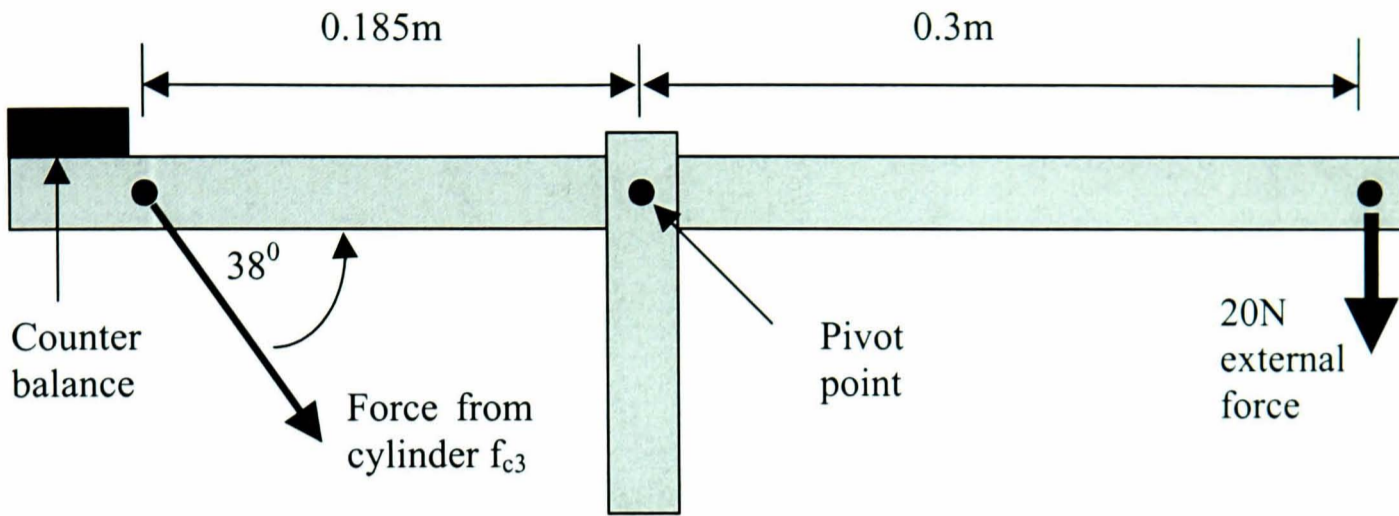
Figure 2.9 *Joint 3 cylinder force requirement*

Taking moments about the pivot point in joint 3 gives:

$$\Sigma M = 0 = 20*0.3 - 0.185*f_{c3}*\sin 38^0 \Rightarrow f_{c3} = 53N \tag{2.1}$$

The approximate cylinder force (f_{c3}) of 53N is well within the available cylinder force of 100N.

The force required to drive the second joint, to support the 20N load in the x direction can be calculated assuming the first joint to be fixed. The greatest torque required to drive the link occurs when the robot is fully outstretched (figure 2.10)

Examining clockwise moments for the two-link robot with the counterbalance removing all gravity loads gives

$$\Sigma M = 0 = 0.4*20 - f_{c2}*\sin 45^0*(0.232/\cos 20^0) \Rightarrow f_{c2} = 45.8N \tag{2.2}$$

The 45.8N force required to balance the force at the end of the link can be provided by one actuator.

Gravitational load from the patient's limb is exerted solely in the x plane, therefore the required robotic forces applied in the (y,z) directions are smaller, hence less critical. Detailed analysis of the forces applied in the y and z directions is not presented here for brevity.
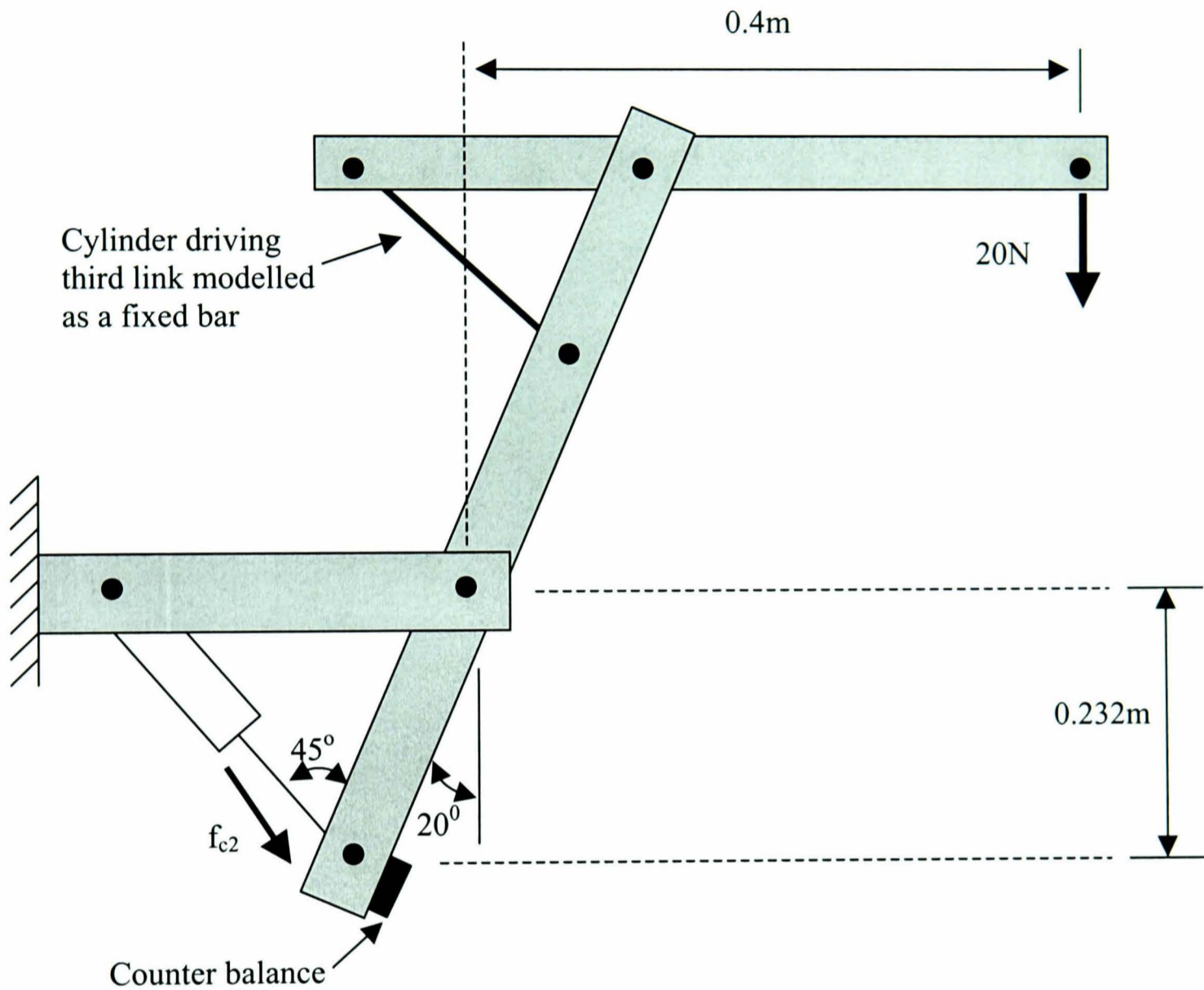
Figure 2.10 *Joint 2 cylinder force requirement*

The robot operates in direct contact with humans. A requirement for safe operation is knowledge of the interaction forces between the robot and the human. A three-degree of freedom force sensor has been designed and developed for this purpose.

2.2 Three degree of freedom force sensor

For safe operation it is important to measure the interaction forces between the robot and human in multiple degrees of freedom. To measure these interaction forces a force sensor is mounted at the robot endpoint, becoming the connection between the robot and human (figure 2.11).
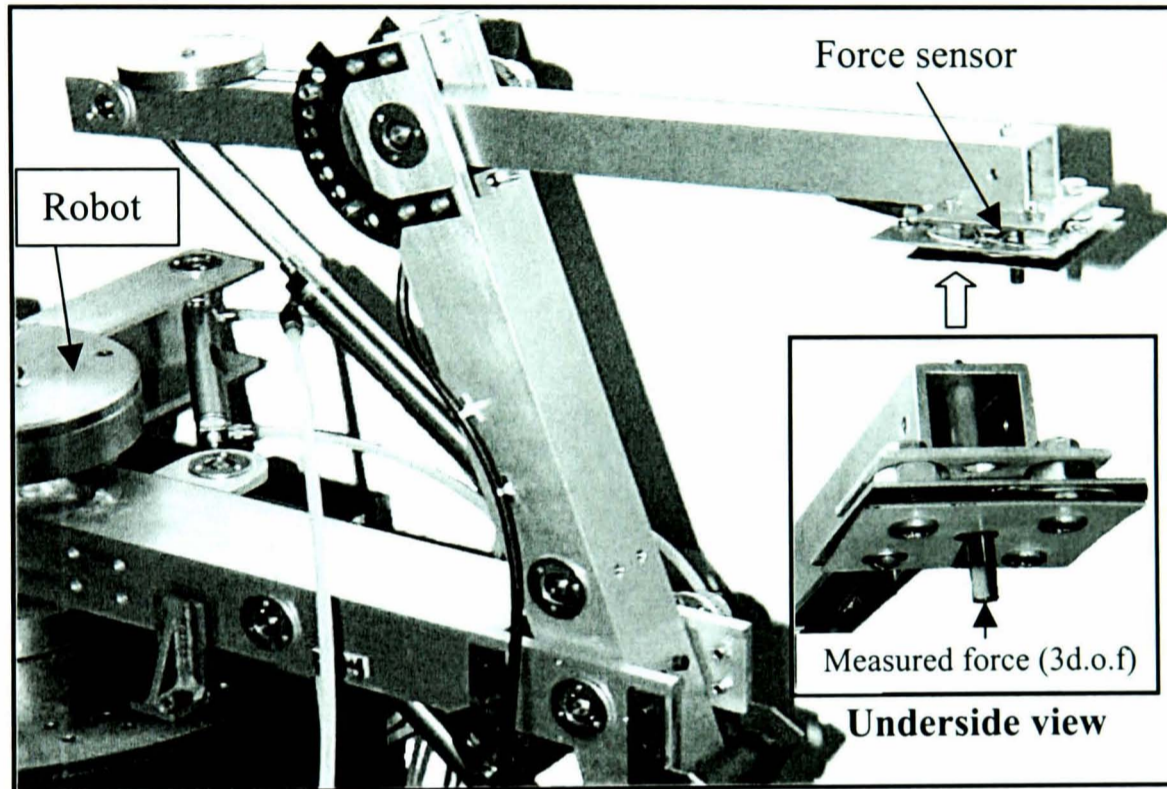
Figure 2.11 Location of force sensor

Commercial multi-degree of freedom force sensors are available, however they are expensive, retailing at several thousand pounds. Research has been performed into the design and development of multiple degree of freedom force sensors. **Kim et al. (1999)** designed and fabricated a six-degree of freedom force and moment sensor. Analysis of the design was performed using FEA (Finite element analysis) and analytical techniques. The force/torque sensor was constructed using more than 50 strain gauges and was shown to be accurate, with little cross coupling. **Chao and Yin (1999)** designed a six component force and moment sensor for measuring the loading of human feet in locomotion. The force sensor was calibrated by collecting data while applying forces in single degrees of freedom. The sensor cross coupling was shown to be small. Both these designs operate well as multi-degree of freedom force sensors, however the complexity of the devices mean they are expensive to produce and

require advanced manufacturing techniques. A simple force sensor has been designed to measure forces in three degrees of freedom for the prototype physiotherapy robot.

2.2.1 Finite element sensor design

The force sensor was designed based upon a simplified version of Choa and Yin's (1999) force and torque sensor. Design of the sensor was performed using FEA (finite element analysis) software. Finite element analysis provides a method of predicting the stress and strain within a component under specific loading conditions **(Fagan 1992)**. The region for which stress and strain is unknown is first divided into an assembly of subdivisions called elements, which are considered to be interconnected at joints, known as nodes. Stress and strain is assumed to act over each element in a predetermined manner, with the number and type of elements chosen so that the distribution can be approximated (i.e fine mesh allows rapid changes in gradient to be predicted). The finite element model constructed to develop the force sensor is shown in figure 2.12. The overall FEA model is coarsely meshed with trahedral elements as they are more adaptive around corners and curves. The mesh around the areas of interest (location of the strain gauges) is refined to contain smaller elements resulting in a more accurate prediction of strain gradients. Overall 9224 nodes and 4699 elements form the FEA mesh. The maximum required loading between the robot and force sensor was specified to be 20N. After several design iterations the final sensor configurations was reached (figure 2.13).
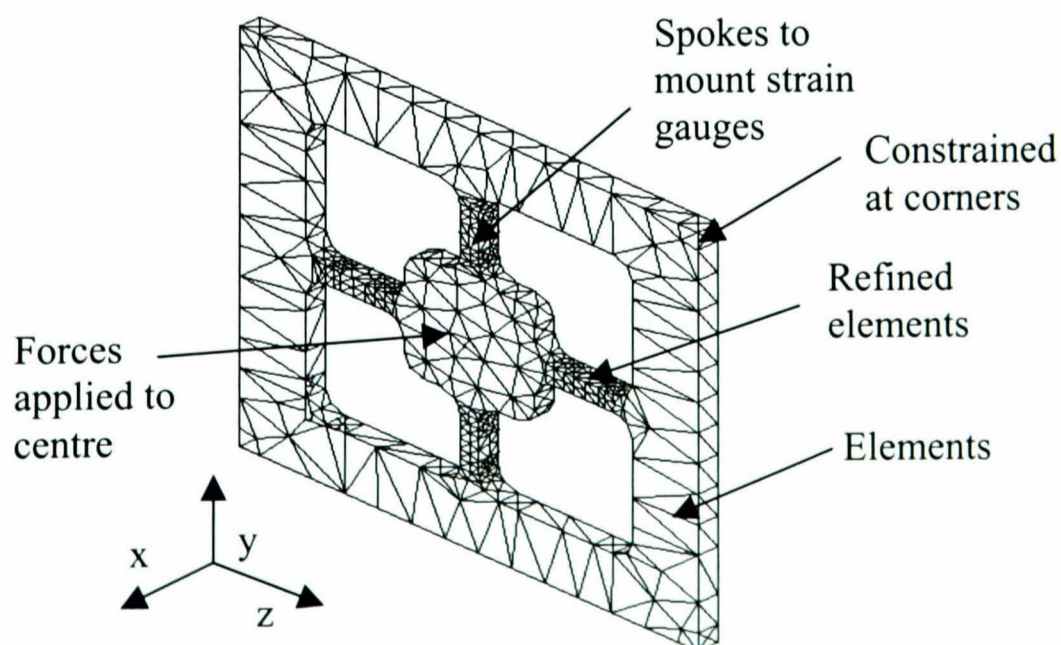
Figure 2.12 Finite element representation of force sensor
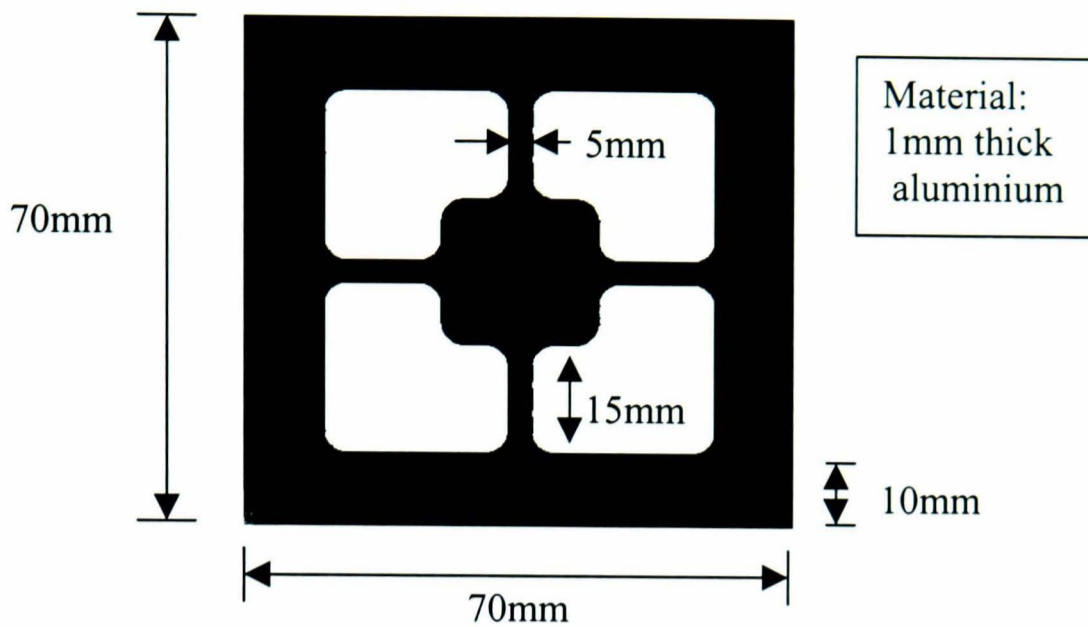
Figure 2.13 *Dimensions of force sensor*

The respective y & z FEA strain predictions when applying 20N of force in the z direction is shown in figure 2.14. Measurement of strain in the z direction requires strain gauges to be mounted on a spoke aligned with the z plane and strain in the y direction would be measured by placing strain gauges on a spoke in the y plane. Due to symmetry strain predictions in the z direction, when rotated through 90^0, will be valid predictions of the strain in the y direction. The FE predications of strains produced by applying 20N in the x direction are shown in figure 2.15.

The finite element analysis demonstrates that by comparing the magnitude and respective phase of strain, forces can be measured in three degrees of freedom. The design of the force sensor allows two strain gauges to be attached to each spoke, allowing the use of eight strain gauges. One full wheatstone bridge was formed to measure forces in the x direction and two half wheatstone bridges measure the y and z forces. The positions of the strain gauges are shown in figure 2.16. Each wheatstone bridge was attached to a separate strain gauge amplifier, resulting in three voltage outputs for any applied force. The strain gauge amplifiers scale up the change in voltage for each wheatstone bridge by a factor of 1000.

In the real force sensor external forces are applied to a spindle attached to the centre of the sensor. The sensor is secured in position by four bolts, one at each corner.
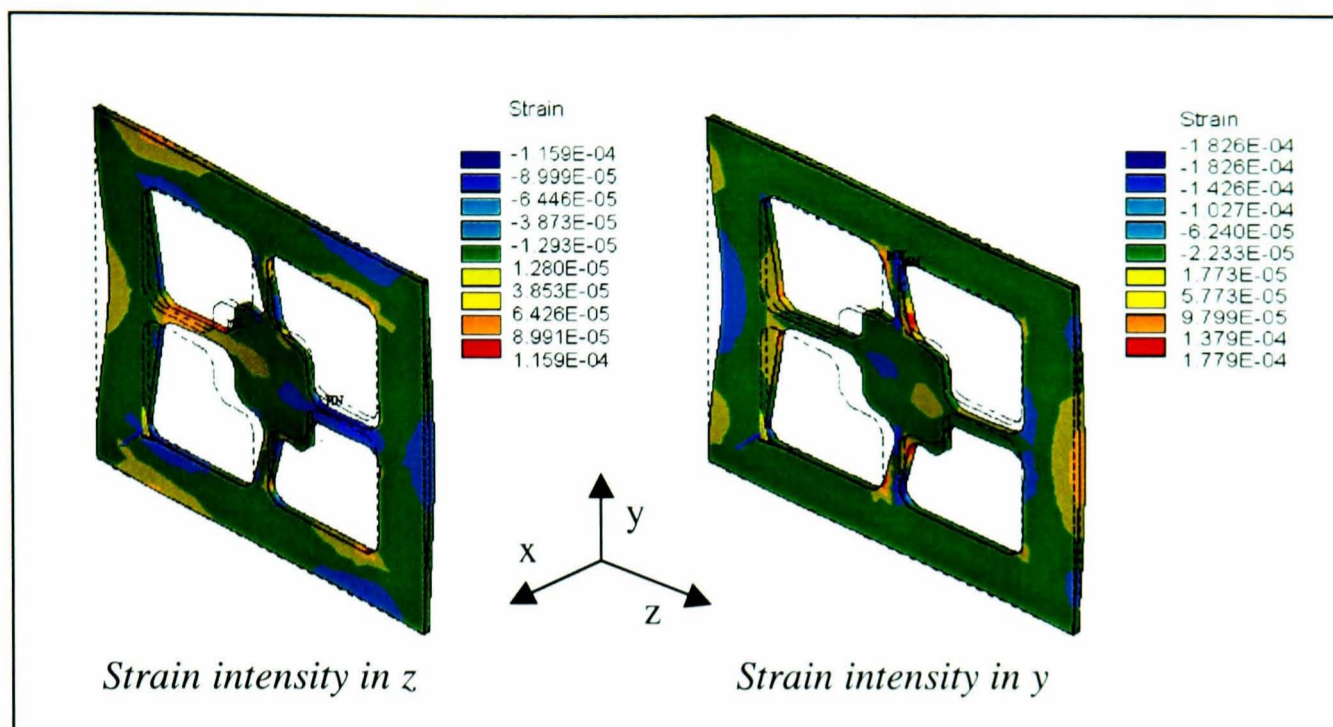
Figure 2.14 *Strain intensity for 20N applied in z direction*
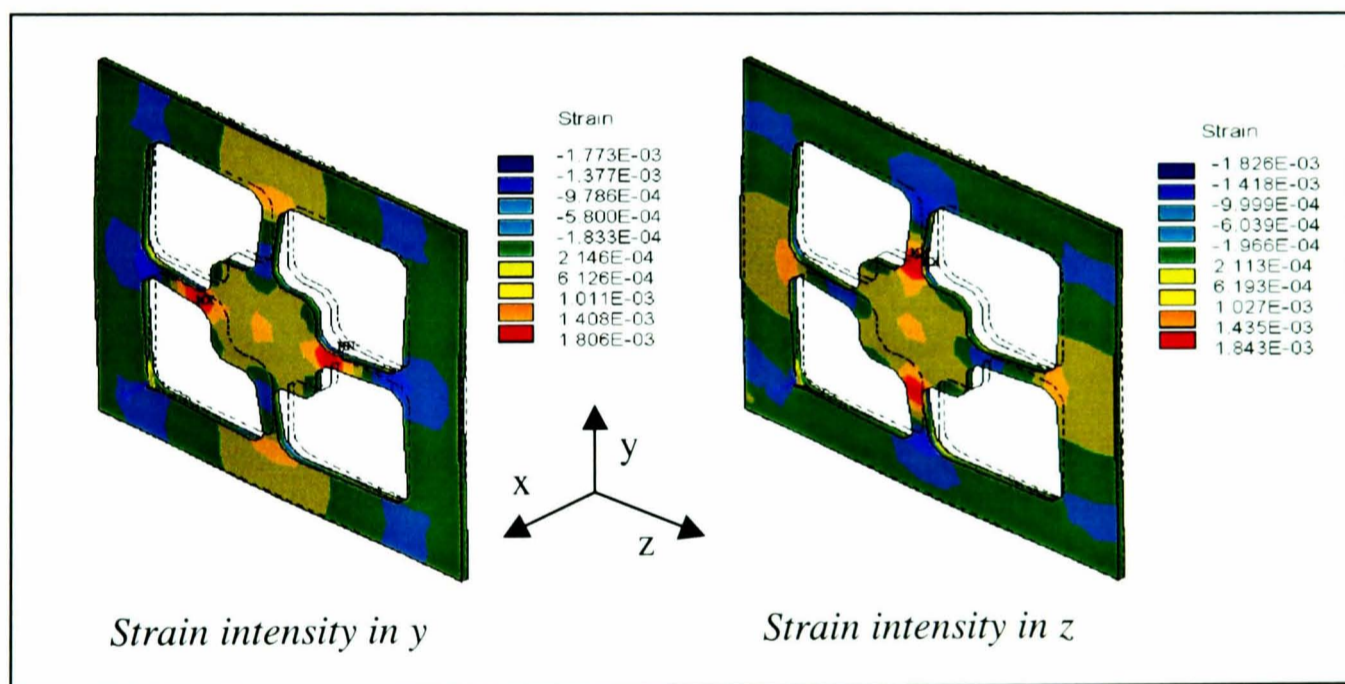
Figure 2.15 *Strain intensity for 20N applied in x direction*

2.2.2 Calibration of the force sensor

Calibration of the force sensor voltages was required to reduce cross coupling between directions (force in one direction causing force errors in other directions) and correlate measured voltages to applied forces. Ideally, to calibrate the force sensor a multiple degree-of-freedom force sensor, with resolution ten times the resolution of the sensor to be calibrated, would be used. However, it is possible to use a commercial single degree-of-freedom force sensor to calibrate the sensor. Three experiments, applying

force in single degrees of freedom in the x,y and z plane were used to obtain calibration data. Figure 2.17 illustrates calibration forces applied in the x and y planes.

TOP   BOTTOM

Y strain
gauges

Z strain
gauges
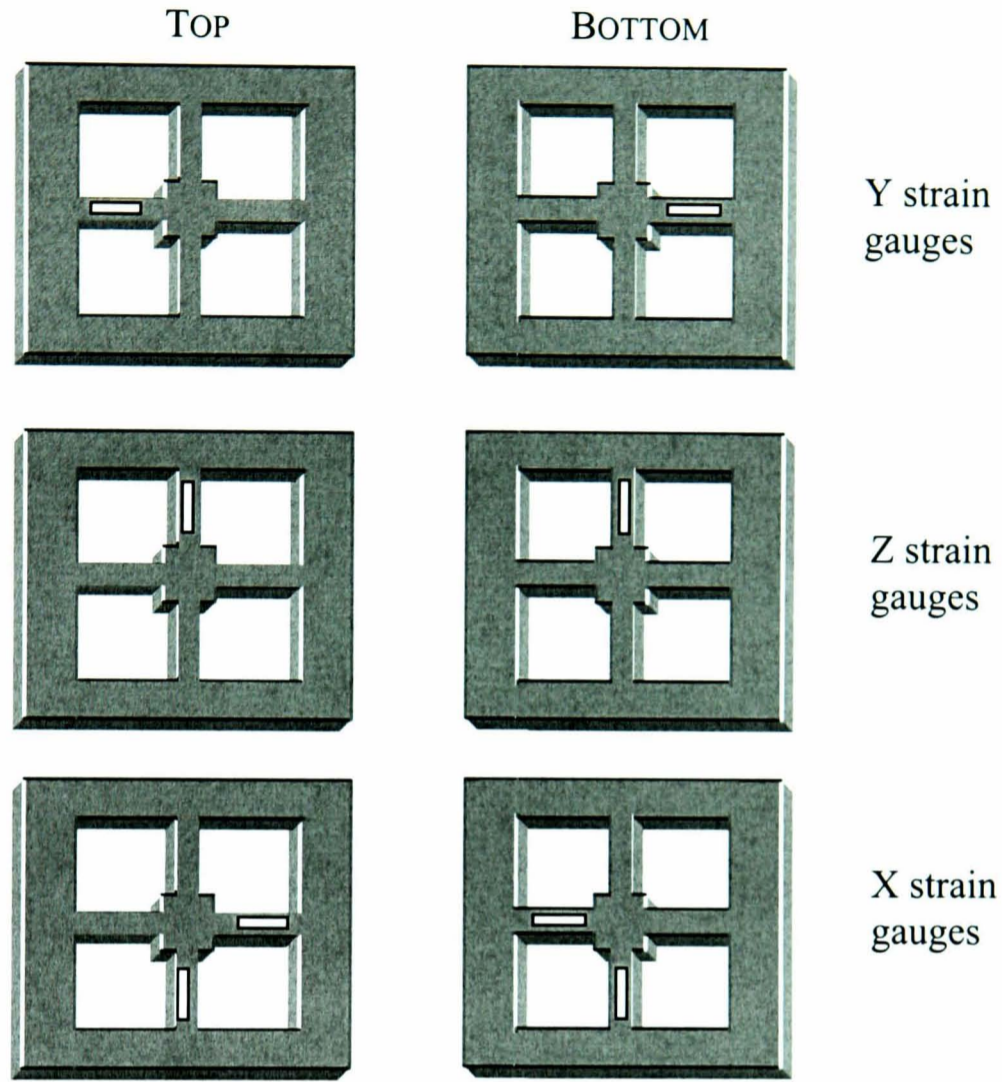
X strain
gauges

Figure 2.16 *Position of strain gauges*

Clamp

Multi-degree of
freedom force
sensor

Clamp

Multi-degree of
freedom force
sensor

Applied
force (y)

Commercial
force sensor

Commercial
force sensor

Applied
force (x)

Forces applied in x   **Forces applied in y**
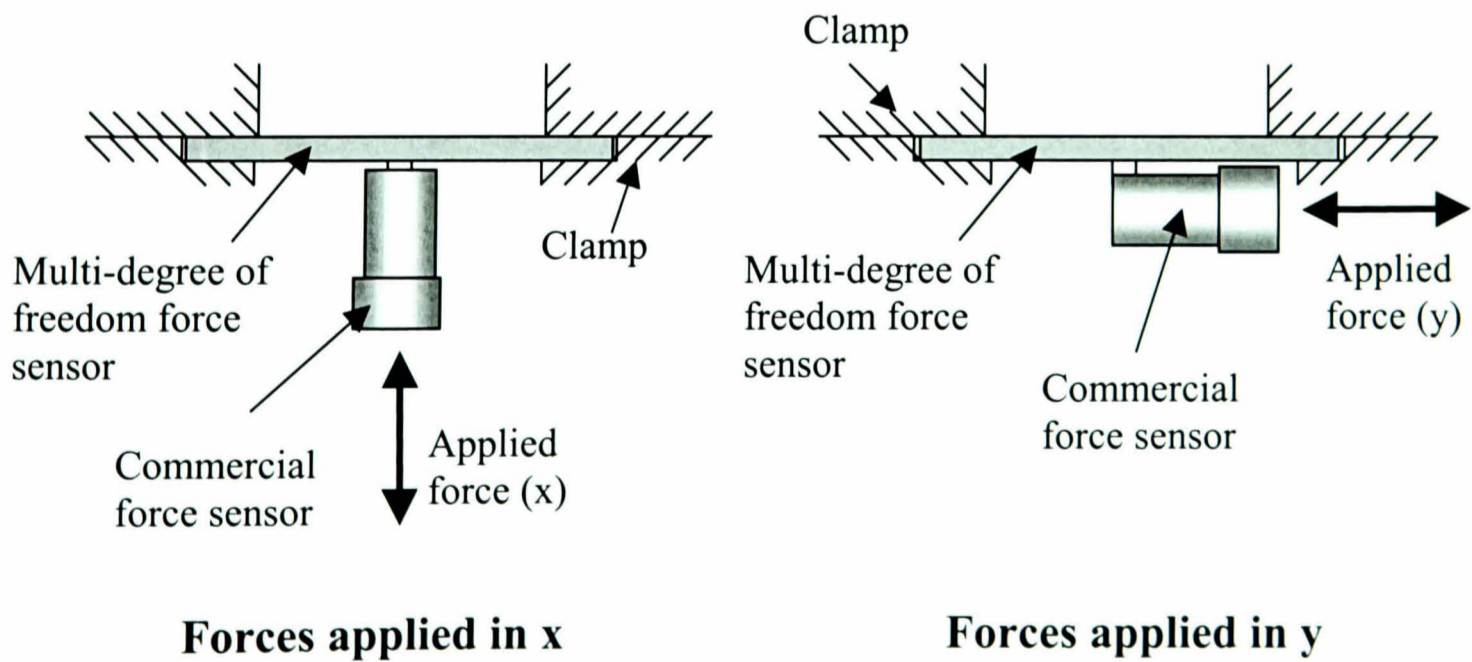
Figure 2.17 *Obtaining force sensor calibration data*

The calibration voltages, when applying force in the z plane, are shown in figure 2.18. The magnitude of the z voltage trace is significantly larger than the other directions indicating the sensors exhibits little inherent cross coupling. Combining the calibration data, enables a single calibration to be performed on the sensor. The standard calibration matrix as implemented by **Chao and Yin (1999)** uses a matrix of gains, as:

$$F_m = C_L.V \tag{2.4}$$

where C_L is a matrix of linear calibration coefficients, F_m is a matrix of forces in three degrees of freedom and V is a matrix of voltages.
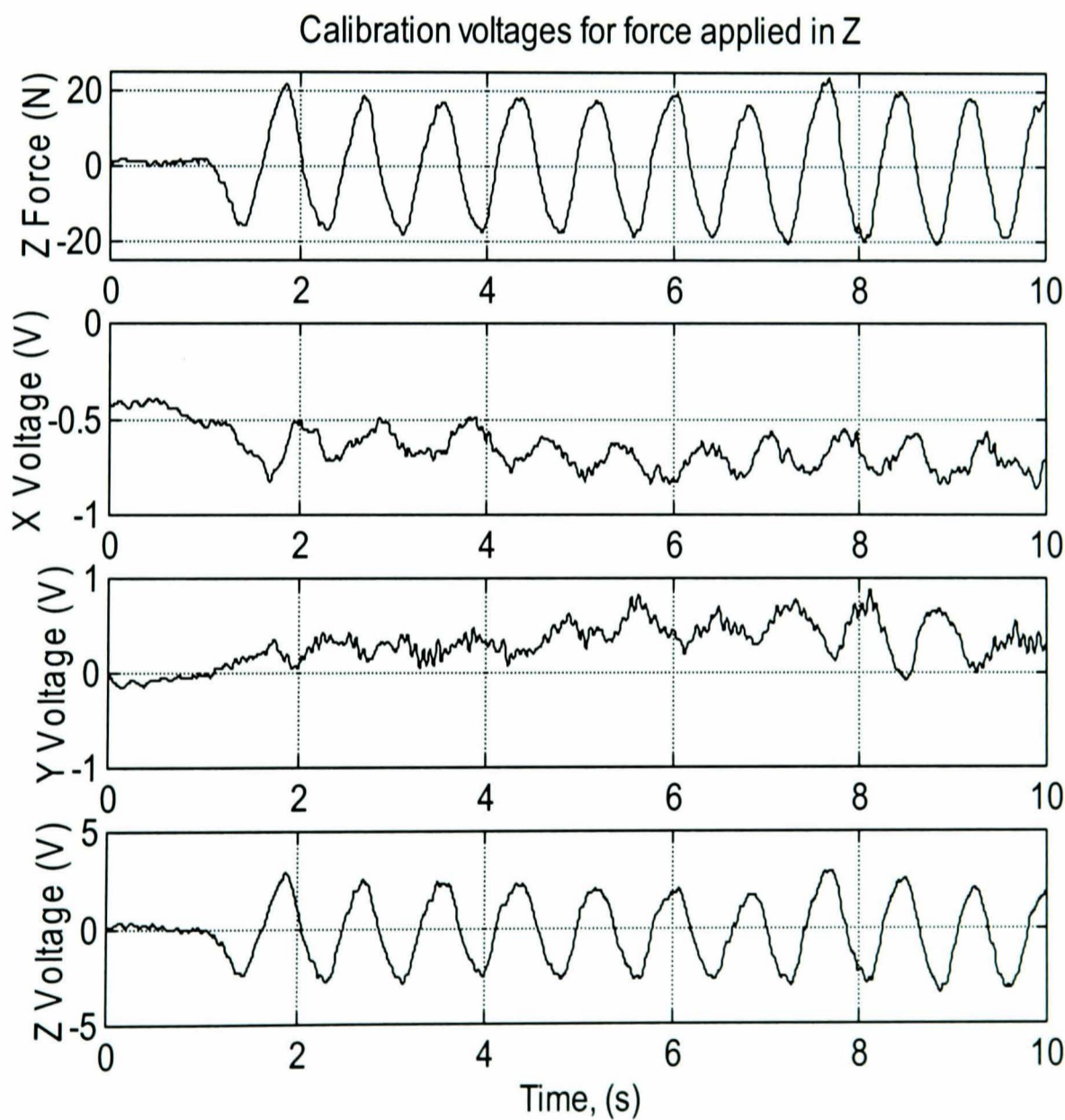
Figure 2.18 *Calibration voltages for forces applied in Z direction*

Voltage offsets can exist from the output of strain gauge amplifiers, and these can be tuned to small values, however they are always present. A constant offset term was included to account for this as follows.

$$F_m = C_L.V + B \qquad (2.5)$$

where B is a matrix of offsets.

A least squares estimate results in a prediction of the gain matrix (C_L) and offset matrix (B). The calibrated force results are shown in figures 2.19, 2.20 & 2.21. It is important to note that errors exist in the measurement of forces in all directions, but most importantly small forces are measured in directions where no force is applied. These false readings indicate the calibration has not completely removed coupling between directions, degrading the performance of any control strategy based upon these measured forces.

Calibration coefficients are shown below:

$$\begin{bmatrix} F_x \\ F_y \\ F_z \end{bmatrix} = \begin{bmatrix} -9.36 & 1.47 & 0.02 \\ -0.34 & 6.17 & -0.19 \\ 0.05 & 0.38 & 7.06 \end{bmatrix} . \begin{bmatrix} V_x \\ V_y \\ V_z \end{bmatrix} + \begin{bmatrix} -3.35 \\ 0.33 \\ 1.35 \end{bmatrix} \qquad (2.6)$$

where F_x, F_y, F_z are forces in orthogonal directions. V_x, V_y, V_z are voltages from the strain gauges intended to read the respective direction of force.

It can be seen from equation (2.6) that the cross coupling of the calibration (off diagonal elements) between strain gauges is small. Estimations of greater complexity are able to improve the force sensor calibration. A Bilinear and Tri-linear estimation can be used to calibrate the force sensor.

Performing a bilinear/tri-linear estimation we have:

$$\begin{bmatrix} F_x \\ F_y \\ F_z \end{bmatrix} = [C_{BT}][Vx \quad Vy \quad Vz \quad Vx*Vy \quad Vx*Vz \quad Vy*Vz \quad Vx*Vy*Vz \quad 1]^T \qquad (2.7)$$

where C_{BT} is a matrix of bilinear and tri-linear calibration coefficients, estimated as:

$$[C_{BT}] = \begin{bmatrix} -7.5667 & -0.0265 & 0.2585 & 0.4658 & 1.8845 & -1.5112 & -10.9255 & -0.6366 \\ 1.2709 & 6.3715 & 0.1597 & -0.2699 & -0.5180 & -1.0174 & -2.1018 & -0.3727 \\ -0.0016 & -0.4551 & -6.9298 & 0.9267 & -1.7521 & 3.1285 & 9.8509 & 0.5152 \end{bmatrix} \quad (2.8)$$
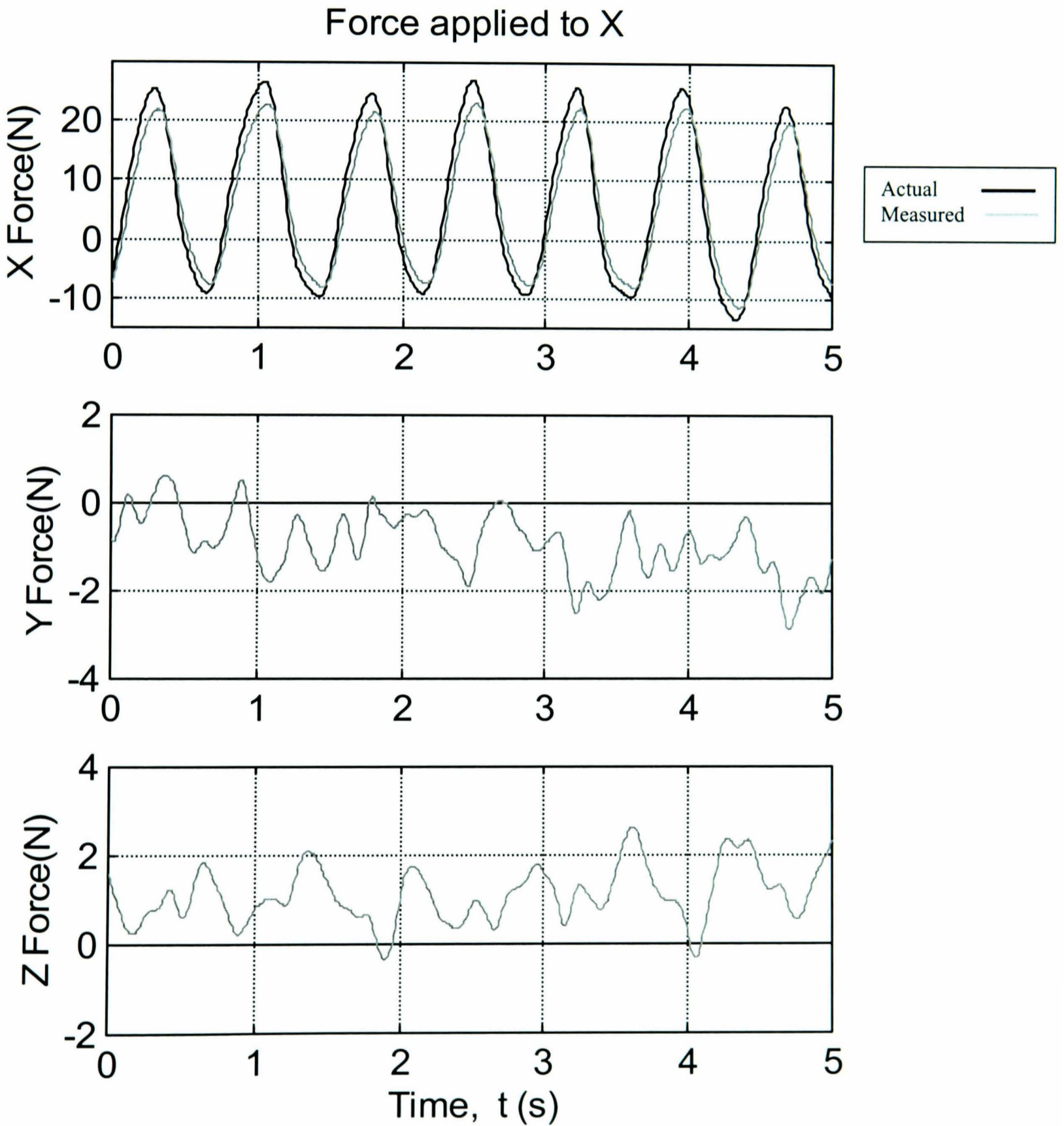
Figure 2.19 *Linear with offset force calibration (X)*
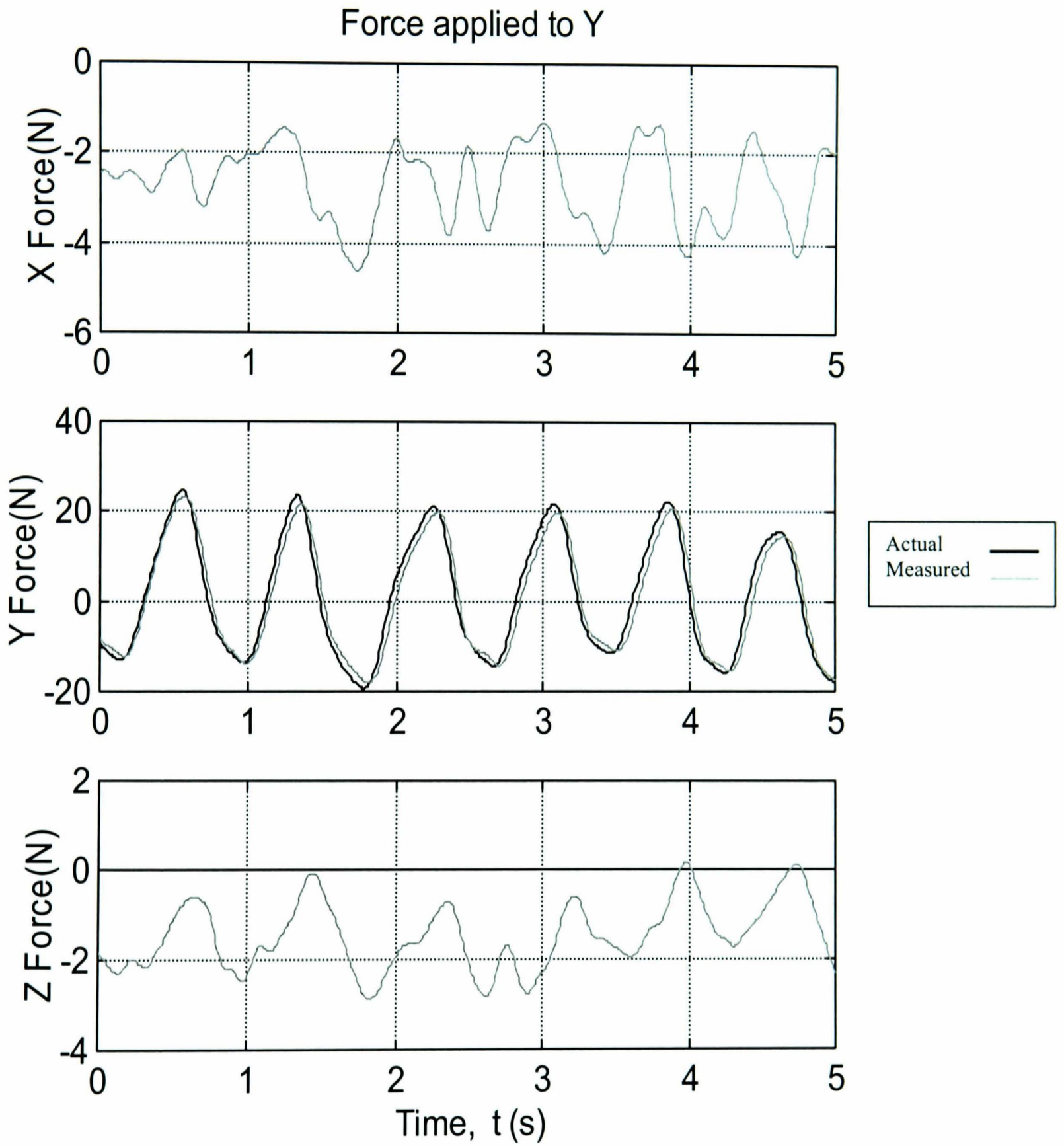
Figure 2.20 *Linear with offset force calibration (Y)*
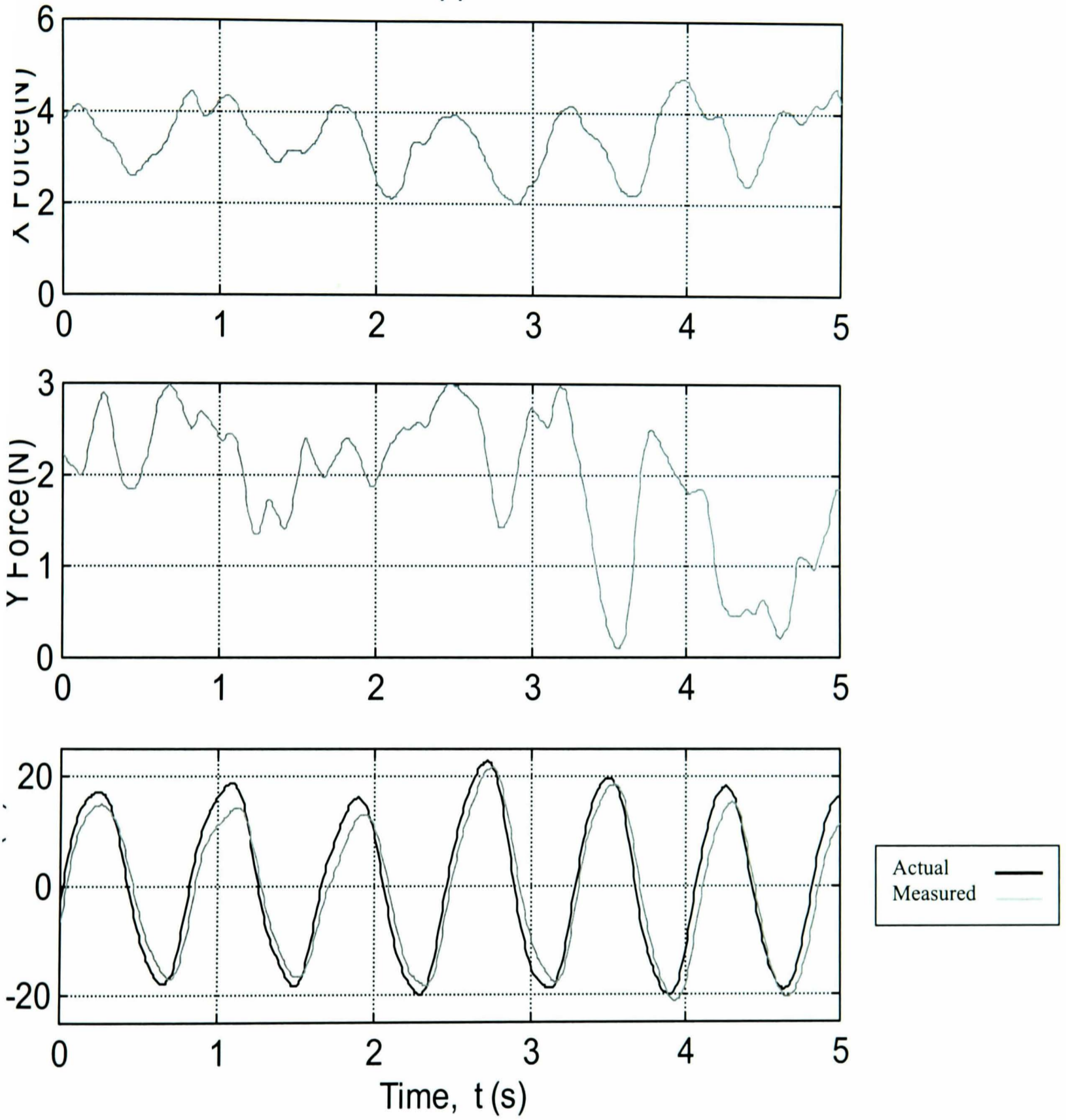
Figure 2.21 *Linear with offset force calibration (Z)*

A quadratic estimate can also be used to calibrate the sensor as:

$$\begin{bmatrix} F_x \\ F_y \\ F_z \end{bmatrix} = [C_Q]\begin{bmatrix} V_x & V_y & V_z & V_x^2 & V_y^2 & V_z^2 & 1 \end{bmatrix}^T \tag{2.9}$$

where C_Q is a matrix of quadratic calibration coefficients, estimated as:

$$[C_Q] = \begin{bmatrix} -8.51 & -1.03 & -0.28 & 0.98 & 0.27 & -0.57 & -3.19 \\ 1.30 & 5.53 & 0.21 & 0.21 & 0.23 & -0.28 & 0.23 \\ -0.43 & -0.45 & 7.126 & -0.26 & 0.09 & 0.13 & 1.11 \end{bmatrix} \tag{2.10}$$

The percentage quality of the calibration can be used to compare the different estimation methods, and is given as:

$$Q = \left(1 - \frac{MSR}{MSS}\right)*100 \tag{2.11}$$

$$MSR = \frac{1}{N}\sum_{1}^{N}(y_i - y_{mi})^2 \tag{2.12}$$

$$MSS = \frac{1}{N}\sum_{1}^{N}y_i^2 \tag{2.13}$$

where Q is percentage quality (%), MSR is the mean square residual, MSS is the mean square signal, y_i is the plant output (i.e actual force) and y_{mi} is the model output (i.e estimated force).

The percentage quality of each calibration is shown in table 2.3.

Direction of applied force	Quality of estimate (%)								
	Linear with offset			Bilinear / Tri-linear			Quadratic		
	X	Y	Z	X	Y	Z	X	Y	Z
X	95.6	99.3	99.2	94.4	99.5	99.5	95.8	99.6	99.7
Y	95.5	95.8	98.7	99.3	95.8	99.2	98.2	95.8	99.1
Z	93.3	99.1	90.8	97.6	99.3	90.7	98.0	99.1	91.3

Table 2.3 *Percentage quality of force sensor calibration*

As can be seen from the table, the quadratic estimation produces the best overall prediction of the forces applied to the sensor, and hence was chosen for the sensor calibration. Results from the quadratic calibration are shown in figures 2.22, 2.23 & 2.24.
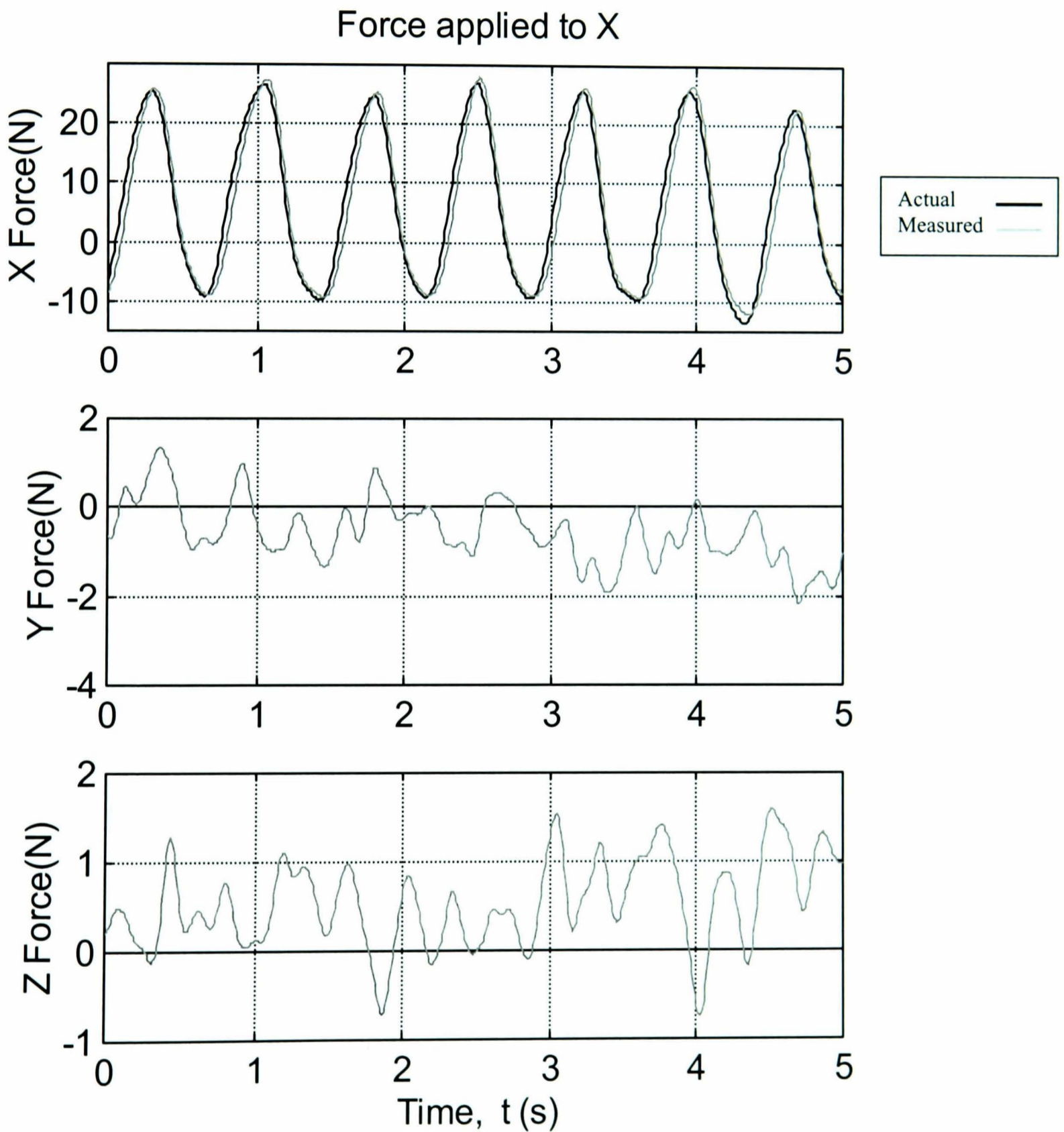
Figure 2.22 *Quadratic force calibration (X)*
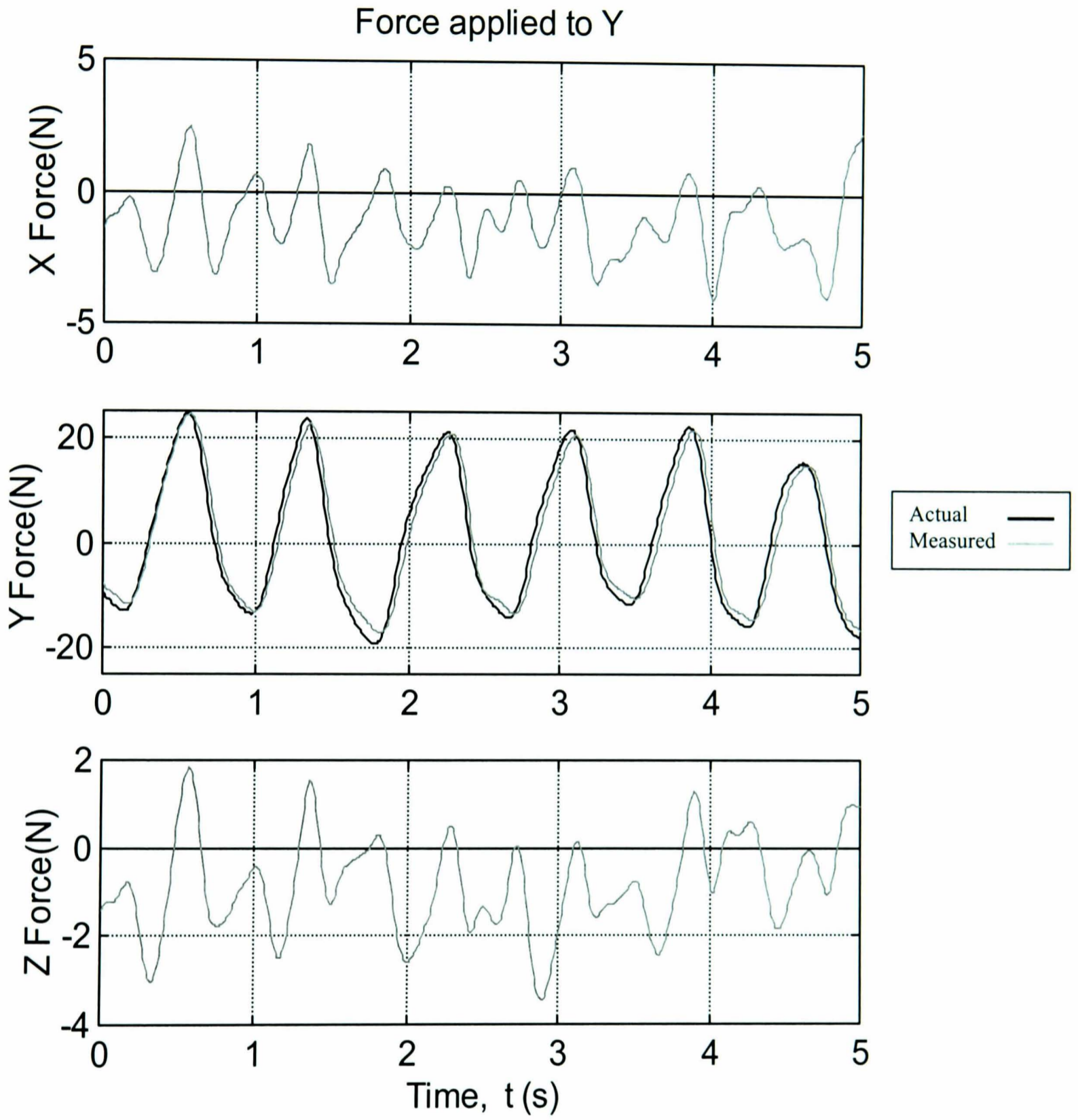
Figure 2.23 *Quadratic force calibration (Y)*
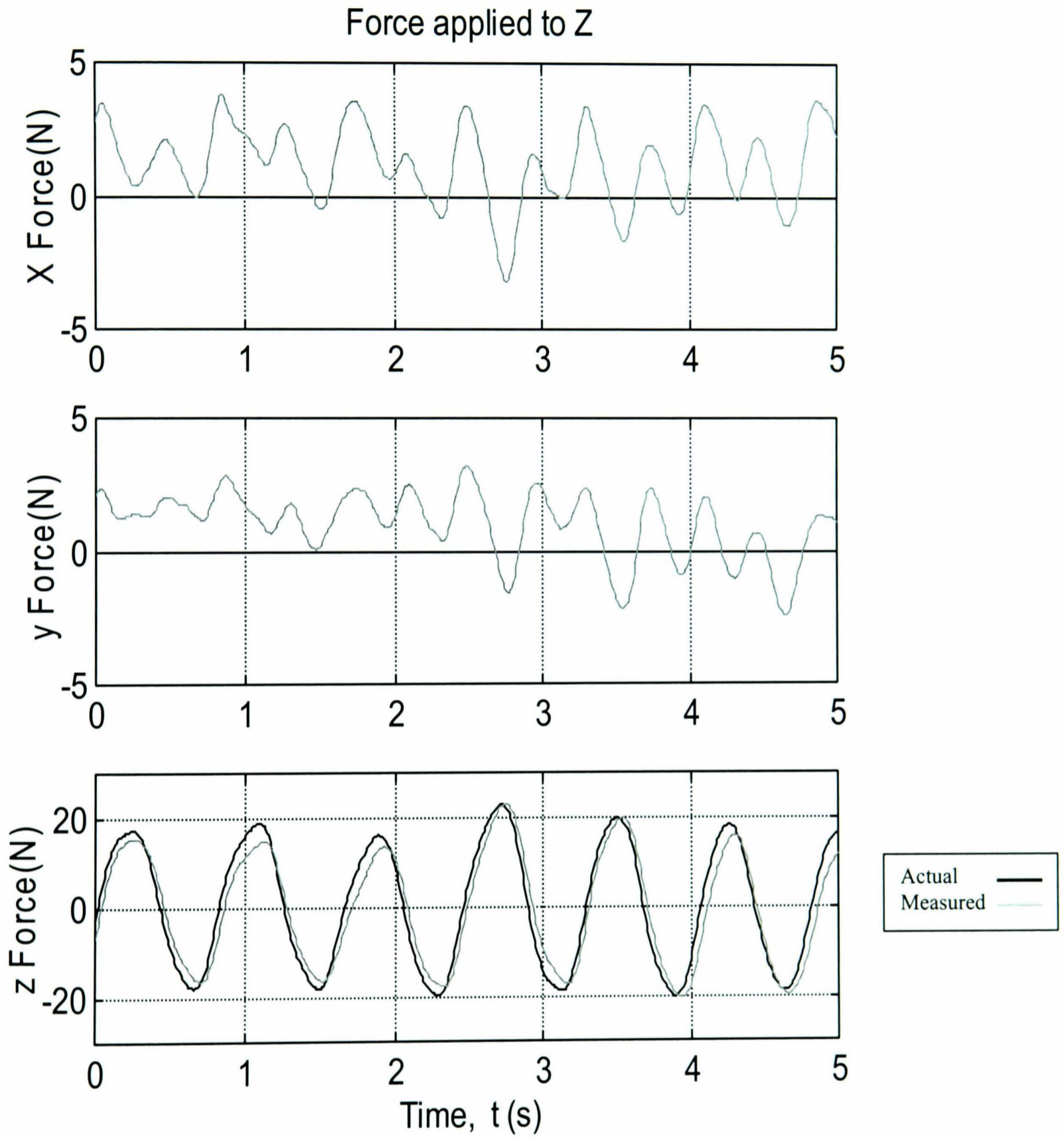
Figure 2.24 *Quadratic force calibration (Z)*

2.2.3 Validation of finite element analysis

The experimental voltages of the force sensor can be used to compare the actual strain with that predicted by the finite element analysis. The strain gauge resistor configuration (figure 2.25) is analysed in this section.
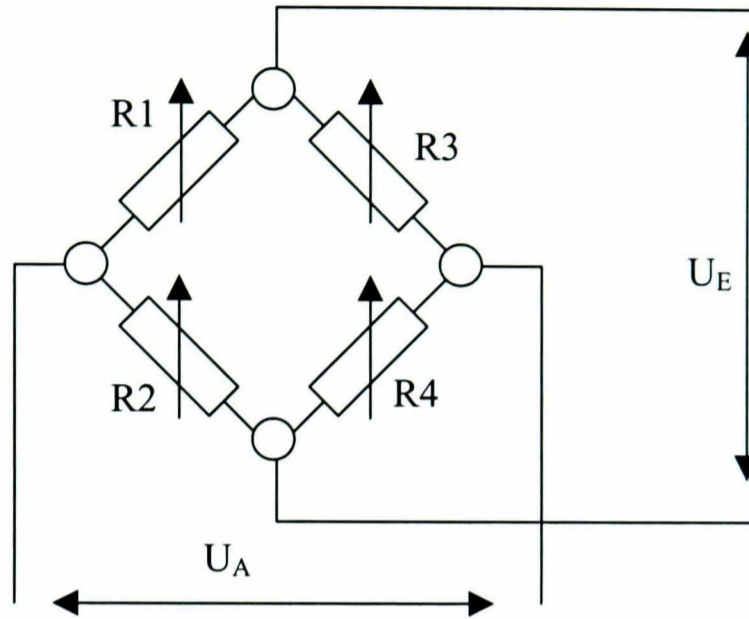
Figure 2.25 *Standard wheatstone bridge configuration*

The change in resistance caused by strain, affects the wheatstone bridge voltages as

$$\frac{U_A}{U_E} = \frac{1}{4}\left(\frac{\Delta R_1}{R_1} - \frac{\Delta R_2}{R_2} + \frac{\Delta R_3}{R_3} - \frac{\Delta R_4}{R_4}\right) \qquad (2.14)$$

Where U_E is the supply voltage, U_A is the strain voltage, R_1 to R_4 are the initial resistance values and ΔR_i the respective change in resistance due to strain.

Strain gauges respond to strain as

$$k_r \varepsilon_i = \frac{\Delta R_i}{R_i} \qquad (2.15)$$

where k_r = strain gauge factor, and ε is the strain

Substituting equation (2.15) into (2.14) gives:

$$\frac{U_A}{U_E} = \frac{k_r}{4}\cdot(\varepsilon_1 - \varepsilon_2 + \varepsilon_3 - \varepsilon_4) \qquad (2.16)$$

From the experimental calibration voltages (figure 2.17) 20N, applied in the z direction, corresponds to approximately 2.5×10^{-3} V (the strain gauge amplifier has a

gain of approximately 1000). The supply voltage to the strain gauges is 15V. In the Z direction a half wheatstone bridge is implemented so the strains ε_3 and ε_4 are zero.

The strain gauges used have a strain gauge factor of 2, so the overall strain, ε, detected by the force sensor is:

$$\frac{2.5 \times 10^{-3} * 4}{15 * 2} = \varepsilon = 3.33 \times 10^{-4} \qquad (2.17)$$

Equation 2.17 gives the strain measured by two strain gauges, halving this value results in the strain measured by a single strain gauge (1.66×10^{-4}). From figure 2.14 the strain predicted by the FE analysis on an individual strain gauge is approximately 7×10^{-5}. The actual strain is larger than the strain predicted by the FE analysis, but is a reasonable estimate considering the approximations used in the calculations.

2.3 Pneumatic systems

The pneumatic system consists of several components to prepare and control air. The arrangement of the pneumatic components is shown in figure 2.26. A standard compressor and storage tank arrangement is used to supply compressed air to the system. The air is then passed through a water trap and dust filter. The filter has particular importance when using low friction cylinders as the air bearing inside the low friction cylinder can become blocked by dust particles. In a conventional pneumatic system, oil droplets would be added to the air to lubricate the components. Air bearing cylinders however, do not require lubrication, indeed lubrication can cause blockage of the air bearing. Two electro-pneumatic proportional valves are used to control the flow of air into and out of the pneumatic cylinder. The use of two electro-pneumatic valves enables accurate control of the pressures within each chamber without the requirement for additional pressure regulation, moreover the pressures in both chambers can be modified by software changes alone. Further explanation on the use of the electro-pneumatic valves to control the pneumatic cylinder is given in chapter 3.
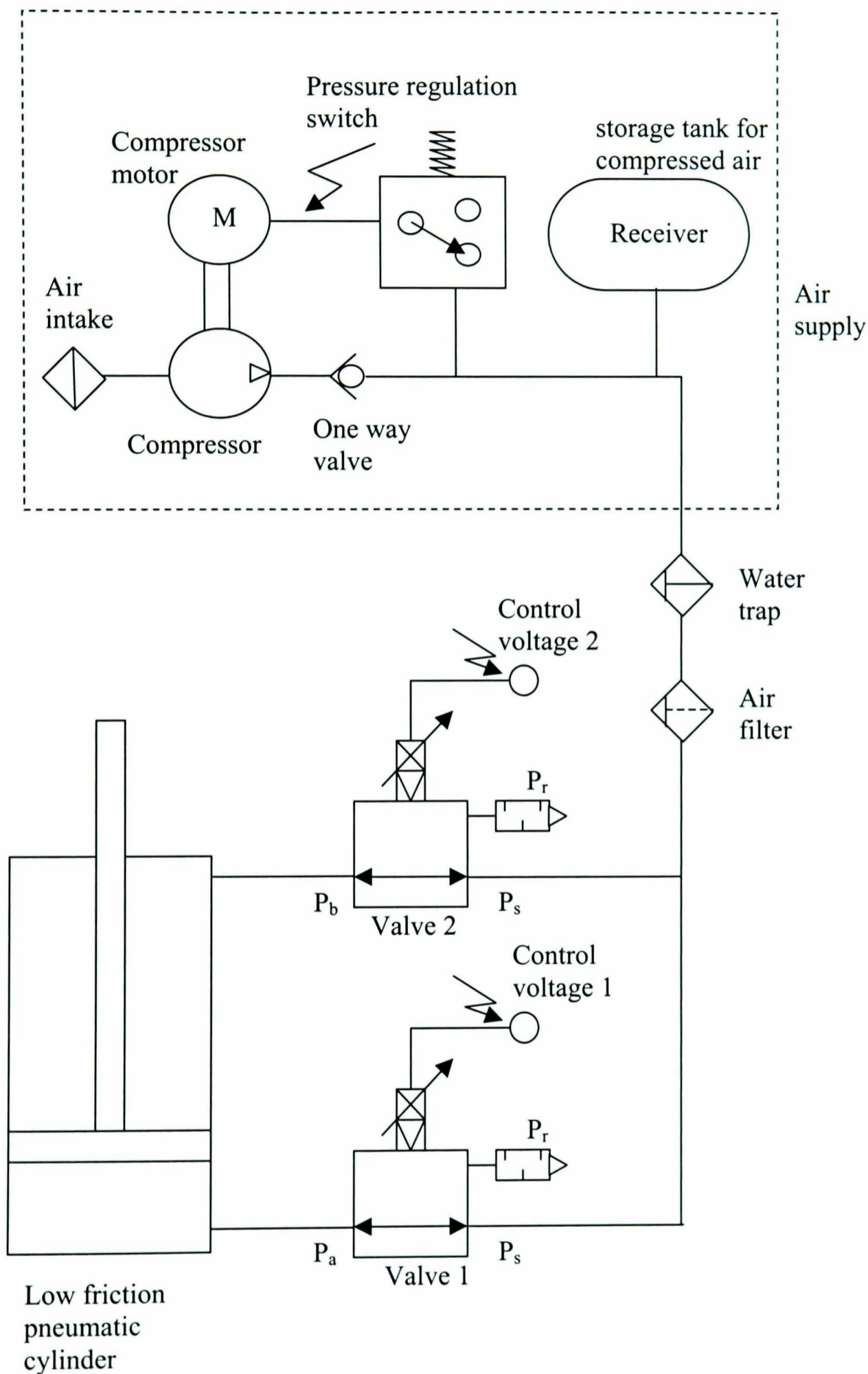
Figure 2.26 *Pneumatic circuit*

Before any computer control of the components detailed so far can be performed it is necessary to decide upon an appropriate sampling interval. This is the topic of the next section.

2.4 Selection of Sampling Interval

Selection of the sampling interval for control of discrete time systems is one of the most important issues. In the process of sampling, high frequencies in the analogue signal may be misrepresented as low frequencies in the discrete signal. This misrepresentation of frequencies is called aliasing. To prevent aliasing of the signal, an analogue lowpass filter reduces the high frequency components before the signal is sampled, preventing these high frequency components from being 'folded' into the low frequency spectrum. Sampling the system too quickly to prevent aliasing, however, can result in large computational burden and can lead to numerical instability. It has been suggested that an optimal sampling interval exists **Xin et. al (1995)** and can be found by decimation and interpolation of a quickly sampled impulse response. However, the performance advantage of optimising the sample interval for digital control was not demonstrated. As a general rule of thumb the sampling interval should be 4-10 times the bandwidth of the system. For a first order system the bandwidth is equal to the inverse of the time constant and for a second order system the bandwidth can be approximated to the natural frequency.

Several techniques can be used to obtain the system bandwidth. A pseudo-random binary sequence can be used to excite the system at all frequencies, enabling selection of a sample interval. However this technique can result in large unpredictable changes in position and is not suitable for large robotic devices. A more controlled approach is to estimate the desired parameters from system step responses.

The three degree of freedom robot is required to respond to both force and position demands. Examining a digital proportional control position control step response (see chapter 3), for the third link (figure 2.27) and using data sheets of second order responses, the natural frequency and hence the bandwidth can be approximated to 2.4

H$_z$. Using 8 times the bandwidth a sampling interval of 50ms was selected. Examining the force step response for open loop discrete control (see chapter 4) at the third joint (figure 2.28) and approximating the response as first order, the bandwidth can be found to be approximately 4 H$_z$, hence using 8 times the bandwidth, a sample interval of 30ms was selected. Due to the varying inertial loads on each joint of the robot, their respective response time will differ, potentially requiring a mixed or distributed sampling interval controller. Distributed sampling systems control MIMO systems at different sampling intervals for each input/output pair **(Smiarowski and Anderson 1990)**. But this was not deemed necessary for the current application since the joint response times are similar and the sample interval has been approximated, however it should be noted that the sample interval selected was based upon the joint with the highest bandwidth to prevent aliasing.
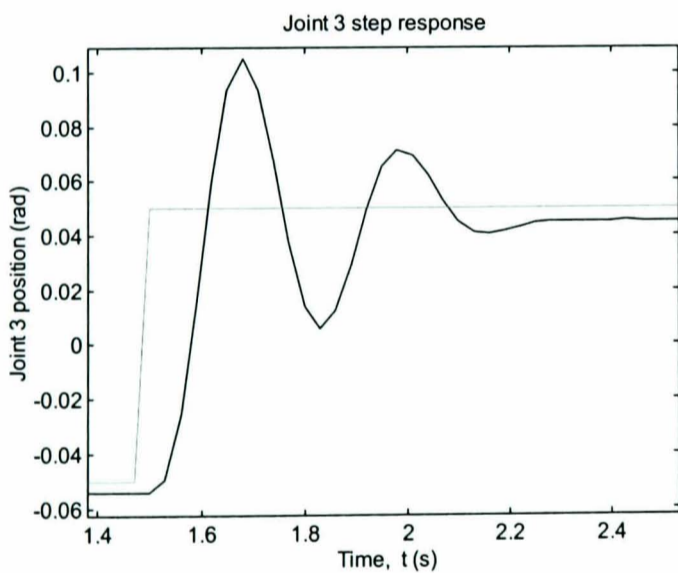
Figure 2.27 Step response
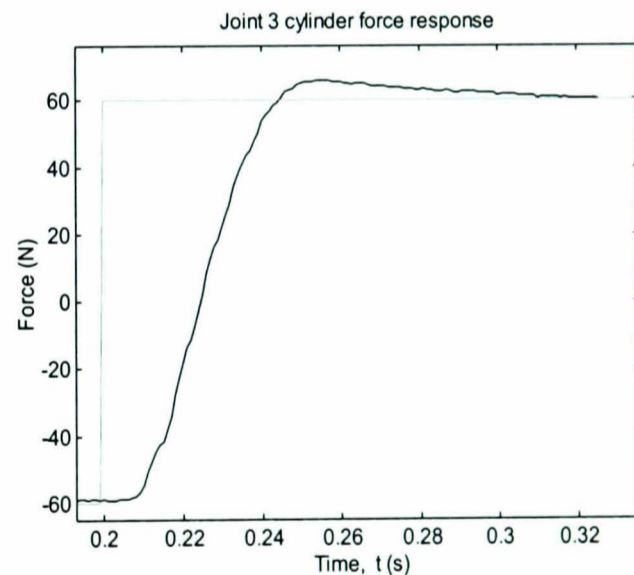
Figure 2.28 Force step response

2.5 Low friction pneumatic actuators

To demonstrate the benefits of low friction pneumatic cylinders they were compared to conventional cylinders. Using the position control test rig it was possible to calculate the stiction within the cylinder (figure 2.29).
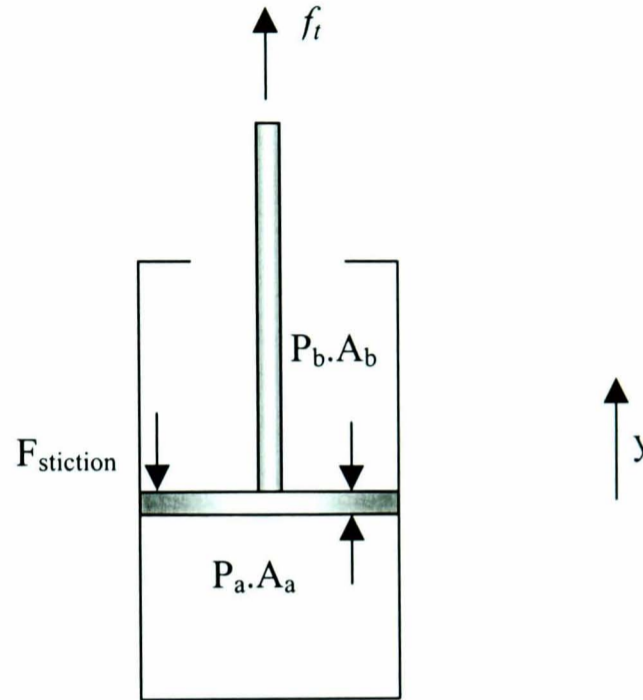
Figure 2.29 *Calculating friction within the pneumatic cylinder*

Summating the forces in figure 2.29.

$$\sum F = f_t + P_a A_a - P_b A_b - F_{stiction} = 0 \tag{2.18}$$

Where $F_{stiction}$ is the force acting on the piston due to stiction and friction.

Therefore

$$F_{stiction} = f_t + P_a A_a - P_b A_b \tag{2.19}$$

The performances of two cylinders were compared using pole-placement control (Chapter 3). The respective discrete plant models were identified using least squares identification, to give the following transfer functions:

Conventional cylinder

$$y_t = \frac{0.02z^{-2}}{1 - 1.63z^{-1} + 0.63z^{-2}} . u_t \tag{2.20}$$

Low friction cylinder (Airpel)

$$y_t = \frac{0.06z^{-2}}{1 - 1.71z^{-1} + 0.7z^{-2}} . u_t \tag{2.21}$$

where y is the position output and u_t is the command signal

The results from the pole-placement tests are shown in figure 2.30. The low friction cylinder exhibits smaller internal friction characteristics enabling smoother, more accurate position control.

It is interesting to note that the airpel response drops below the desired position. This is due to the balance signal (Section 3.2) not fully compensating for the external force. With the airpel cylinder exhibiting low friction and stiction, its response is more sensitive to external forces. Self-tuning of the plant and balance signal (Section 3.5.3) would remove this effect.
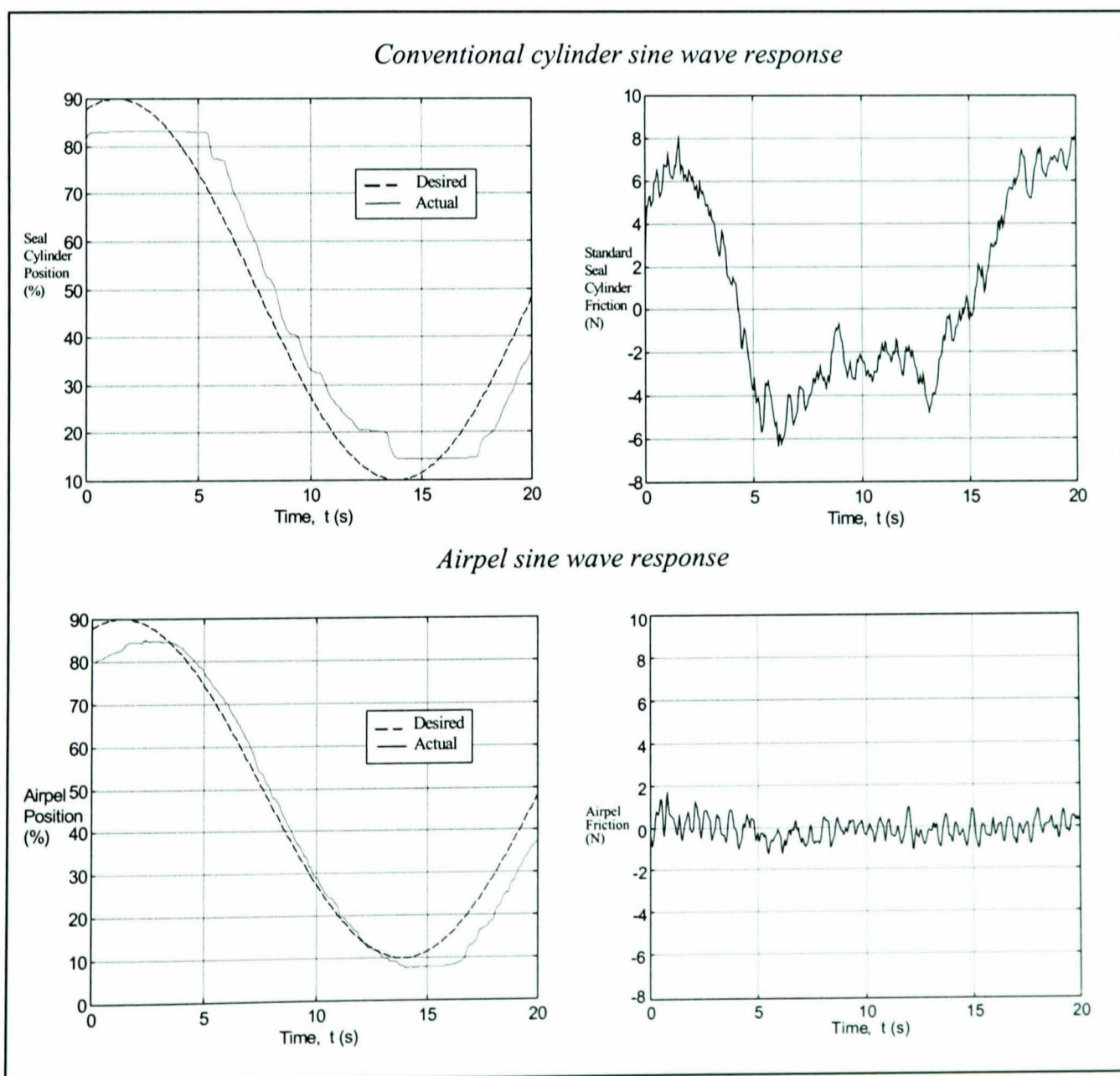
Figure 2.30 Response of low friction and conventional cylinders

2.6 Discussion and conclusions

This chapter details the experimental equipment used throughout this thesis. The test rig enables position and force control to be performed on a single pneumatic cylinder. Assessment of the controller performance on a single actuator allows the controller performance to be assessed without the added complexity of multiple degrees of freedom.

The three degree-of-freedom robot has been designed to extend the controllers developed on the test rig. The primary aim of the robot is to enable the testing of pneumatic controllers in multiple degrees of freedom. These controllers, if successfully implemented, would enable the robot to interact with humans performing tasks such as robotic physiotherapy. Indeed the robot workspace and configuration has been developed with this application in mind, with the robot movement range encapsulating the optimum reach area of the average adult. This optimum reach area is a realistic representation of everyday limb movement, indeed we often go out of our way to prevent movement beyond normal motion patterns (stretching to reach objects).

The three degree of freedom force sensor that has been developed can measure forces applied to the robot. A variety of techniques are capable of calibrating this force sensor, however, the quadratic estimation calibrates the forces with the greatest degree of accuracy.

Preliminary experiments have shown that the low friction pneumatic cylinder exhibits much smaller friction characteristics than traditional pneumatic cylinders. When the performance of these two cylinders were compared using identical control techniques, the low friction cylinder exhibited smoother motion. This smoother motion enables pneumatic cylinders to be considered for control applications where they would previously be discounted.

The single degree of freedom test rig and three degree of freedom robot, combined with force sensors enable assessment of a wide variety of controllers for not only position control, but also position and force interaction. Implementing controllers that consider both applied force and position enables robots to interact safely in unknown environments, such as that encountered when performing physiotherapy.

Chapter 3

Position control

This chapter investigates the performance obtainable from modern low friction pneumatic cylinders and proportional electro-pneumatic valves for position control in the presence of external loads.

3.1 Introduction

Traditionally, position control of pneumatic systems has proven difficult. Non-linear friction effects such as stiction and air compressibility combine to degrade servo performance. Some researchers have opted to use add-ons to improve the response of standard linear controllers. Examples of these additional elements include intelligent dither (rapidly oscillating signal), which is turned on when the cylinder is judged to be under the influence of stiction **(Surgenor and Wijesuriya 1992)** and an analogue inner control loop to help linearise the system **(Hamiti et al. 1996)**.

A more common approach has been to implement adaptive controllers such as the adaptive pole-placement controllers designed by **Shih and Huang (1992)** and **Tanaka et al. (1996)**. These controllers vary their internal structure to cope with variations in system response.

Some researchers have found it necessary to implement non-linear controllers such as neural networks **(Gross and Rattan 1997)**, fuzzy logic **(Shibata et al. 1999)**, and sliding mode control **(Pandian et al. 1996)** to obtain adequate performance from pneumatic systems.

Low friction pneumatic actuators have greatly reduced stiction effects, and electro-pneumatic valves are capable of accurately controlling the pressure within each chamber of the pneumatic cylinder. It is hypothesised that combining these components will produce a pneumatic system that exhibits greater linearity than traditional pneumatic systems, suggesting conventional linear controllers may now

be appropriate. This chapter details the design and implementation of linear controllers to control the position of a pneumatic cylinder, under the influence of external gravity loads.

3.1 Controlling the electro-pneumatic valves

Traditionally, one spool valve controls the flow of air into both chambers of a pneumatic cylinder. One of the drawbacks of this arrangement is that the relationship between the pressures within the two chambers remains fixed, moreover regulating these pressures is difficult, often requiring a pressure control loop.

Electro-pneumatic valves regulate the pressures within a volume through analogue pressure control circuitry. Two electro-pneumatic valves can independently control the pressure within each chamber of the pneumatic cylinder enabling the relationship between the chamber pressures to be set by software changes alone. The configuration of two electro-pneumatic valves to control a single cylinder is shown in figure 3.1.
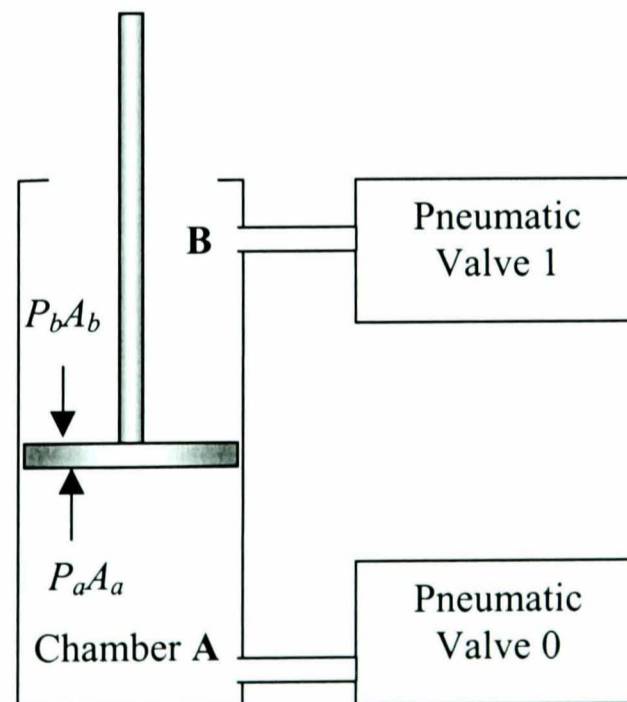
Figure 3.1 *Two valves controlling one cylinder*

It is desirable to control the force generated within the pneumatic cylinder from one control signal, however, this requires one control signal to control two electro-pneumatic valves.

Several researchers have devised strategies for controlling two valves from one control signal. **Kawanaka and Hanada (1996)** proposed that valve 1 should supply a fixed pressure to chamber B while valve 0 varies the pressure in chamber A to control the position of the cylinder piston. This restricts the maximum force output of the pneumatic cylinder and limits the maximum rate of change of force. **Ben-Dov and Salcudean (1995)** devised a strategy to increase the pressure in one chamber while decreasing the pressure in the other chamber. In order for a pneumatic valve to reduce the pressure within a pneumatic chamber, the chamber must initially contain pressure higher than atmospheric pressure. So a default pressure is required in each pneumatic chamber. This pressure, termed 'equilibrium pressure', is present in both chambers of the pneumatic cylinder for a zero control signal. The strategy requires the control signal to be split, increasing the pressure in one chamber while decreasing that in the other. The control signal (u_t) is halved, added to the equilibrium signal (u_{eq}) for valve 0 and subtracted from the equilibrium signal for valve 1 (figure 3.2).
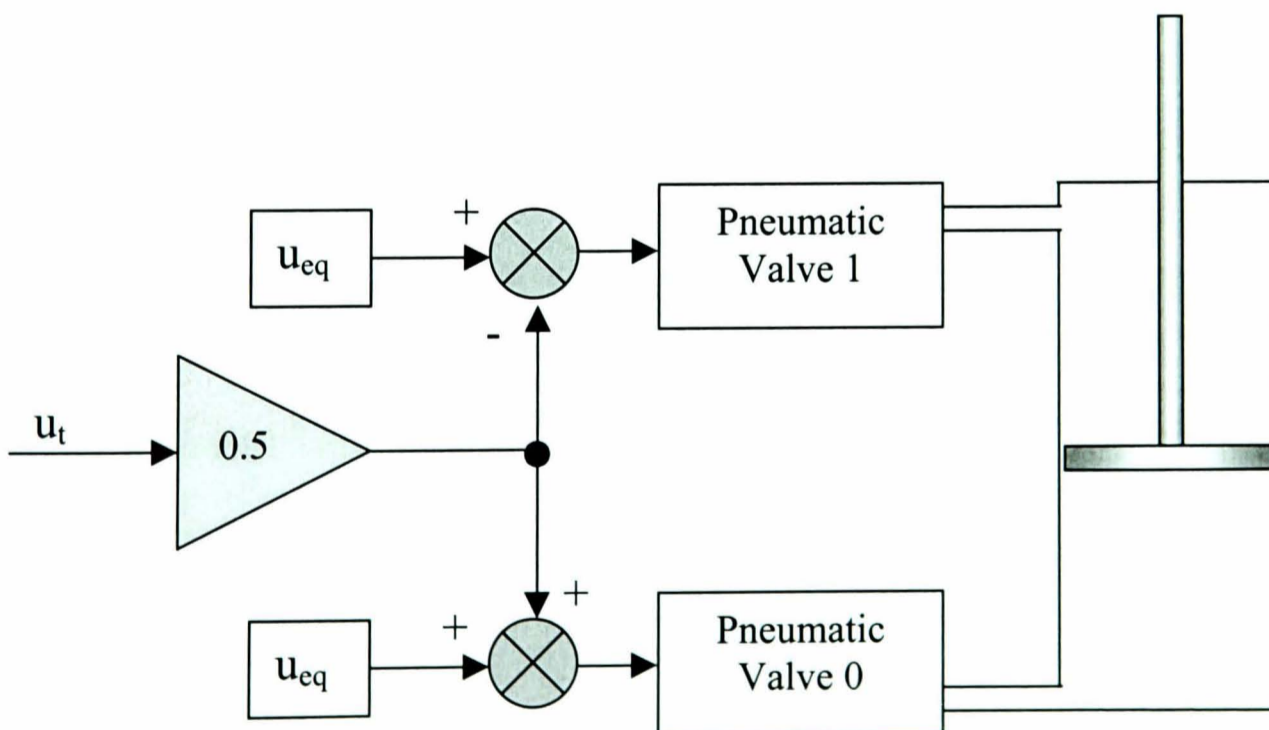
Figure 3.2 Splitting the control signal

The selection of this equilibrium pressure affects the performance of the pneumatic system, two methods can be considered for selection of this:

Mid-point between supply and exhaust pressure

The equilibrium pressures can be set to the mid-point between the supply and exhaust pressures. Due to the symmetry of the control strategy this method enables the maximum force to be applied by the pneumatic cylinder (i.e. 1 bar (abs) in one chamber and 7.5 bar (abs) in the other chamber).

With the equilibrium pressure set to 4.25 bar (abs) the cylinder can apply approximately 100N.

Maximum region of sonic flow

The pressure ratios when supplying and exhausting from the cylinder can be inspected to select an equilibrium pressure for which sonic flow occurs in both chambers for the largest pressure range. During sonic flow the maximum mass flow rate is maintained.

From chapter 5 sonic airflow occurs for a pressure ratio smaller than 0.528:

Supplying sonic flow: $\dfrac{P_a}{P_s} < 0.528 \Rightarrow P_a < 4$ bar (abs) $\qquad$ (3.2)

Exhausting sonic flow: $\dfrac{P_r}{P_a} < 0.528 \Rightarrow P_a > 1.9$ bar (abs) $\qquad$ (3.3)

where P_a is the chamber pressure, P_r is the atmospheric pressure and P_s is the supply pressure.

The mid-point between the pressures (obtained by equations 3.2 and 3.3) is approximately 3 bar (abs). This equilibrium pressure creates the greatest region of choked flow when supplying and exhausting air. Selecting this equilibrium pressure,

however, restricts the maximum force that can be applied to 80N (the pressure can only be reduced by 2 bar before atmospheric pressure is reached).

The initial tests to ascertain the performance of pneumatic systems require the equilibrium pressure to be set for the largest region of sonic flow (Sections 3.3 – 3.5). This creates a servosystem with the greatest possible linearity. The three degree-of-freedom robot does not require fast changes in position so the need to maintain sonic mass flow lessens, however, increased non-linearity occurs within the sub-sonic flow region. Inspite of these increased non-linearities, the equilibrium pressure was selected as the mid-point pressure to enable the maximum force to be applied.

Note that due to the difference in piston area between the two chambers, chamber B requires a pressure increase by approximately 10% for the force generated by each chamber to be balanced. This is included in the controller but will not be shown in controller diagrams for brevity.

3.2 External gravity loads

Under real operating conditions the pneumatic actuator will be required to operate against gravity loads, resulting in constant external forces acting upon the pneumatic system. These external forces have a considerable effect on the actuator positioning due to the low stiffness and back-driveable nature of pneumatic actuators.

To achieve accurate position control under the influence of these external forces, an equal but opposite force needs to be generated from within the cylinder. This internal force, termed the balance force, will be constant for a fixed gravity load acting vertically upon the pneumatic cylinder. A constant control signal creates a constant pressure difference between the pneumatic cylinder chambers, hence a constant force to balance the gravity load.

The balance force was incorporated into the two-valve control strategy by the inclusion of a balance signal (B_p), which is added to the input control signal. The two valve control strategy with balance signal is shown in figure 3.3. For ease of controller design the two valve strategy and balance signal was considered part of the plant (figure 3.4).
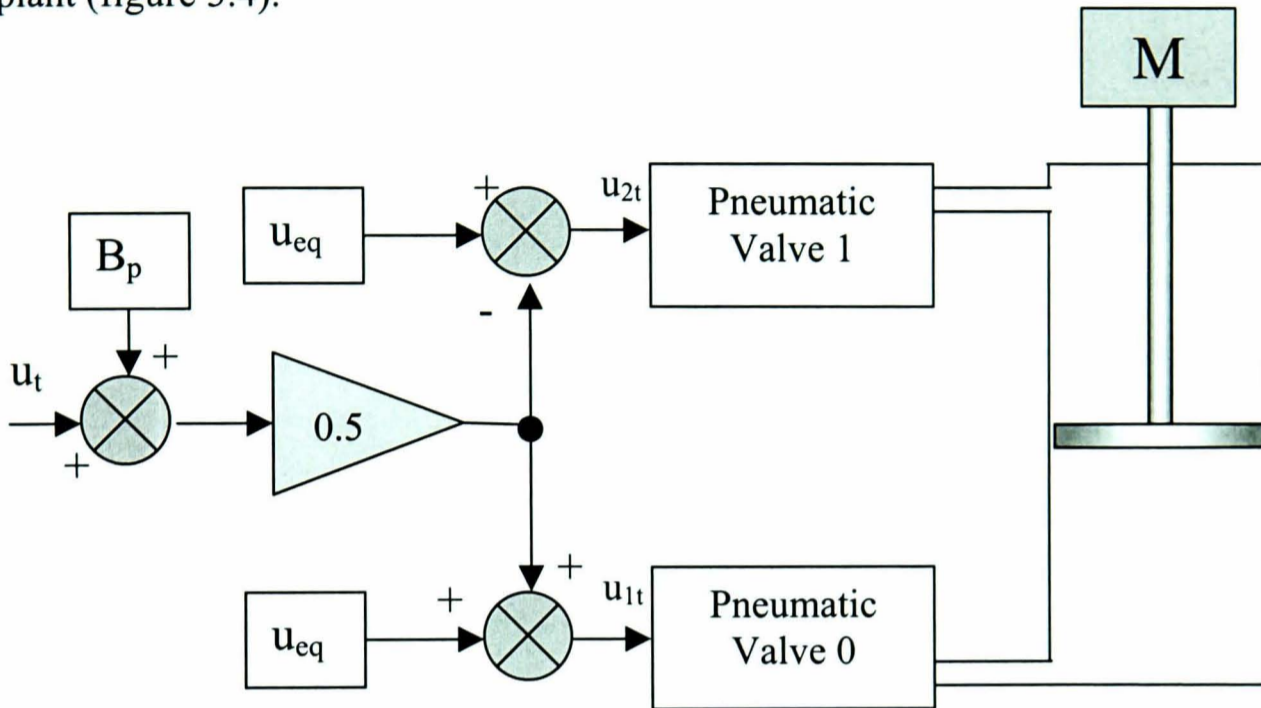
Figure 3.3   Inclusion of balance signal
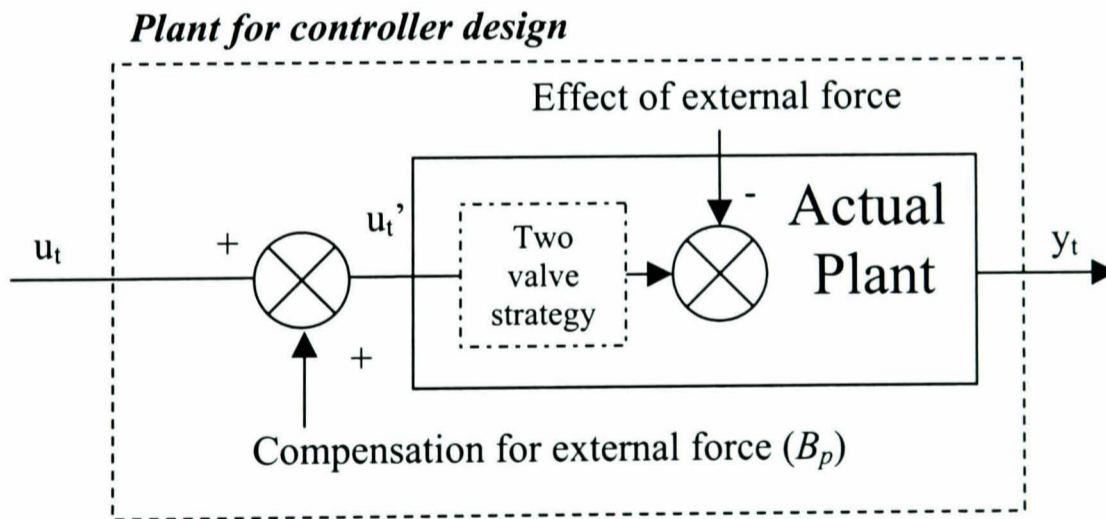
Figure 3.4   Considering balance pressure as part of plant

Expressing the two valve control strategy in mathematical terms:

The control signal applied to valve 0 is given by:

$$u_{1t} = P_{eq} + \frac{u_t{}'}{2} \qquad (3.4)$$

The control signal applied to valve 1 is given by:

$$u_{2t} = P_{eq} - \frac{u_t{'}}{2} \qquad (3.5)$$

Where the signal $u_t{'}$ includes the balance signal, i.e.:

$$u_t{'} = u_t + B_p \qquad (3.6)$$

Here u_{1t} is the control voltage into valve 0, u_{2t} is the control voltage into valve 1, P_{eq} is the equilibrium control signal, u_t is the input control signal, $u_t{'}$ is the control signal and balance signal.

To summarise, the equilibrium pressure enables the pressures within each chamber to be reduced on demand. External gravity loads exert constant forces upon cylinders acting vertically. A constant control signal is required to produce a force to balance these external forces. Including this constant control signal as part of the equilibrium pressure causes a zero control signal to result in no change in position in the presence of constant external force. This strategy of controlling the two valves and cylinder forms the basis of all the controllers implemented throughout this thesis. The next section implements proportional position control on the pneumatic cylinder.

3.3 Proportional control

Proportional control is one of the simplest forms of control, utilising one feed-forward gain and negative feedback (figure 3.5). Few devices are controlled by solely proportional control due to the limited response normally obtained. This is reflected in the lack of published literature. Indeed, proportional control is usually augmented with integral and derivative elements to improve the performance. However, proportional control provides a means of obtaining an idea of the system performance and linearity with its simplicity revealing the underlying system dynamics. Proportional control was implemented on the position control test rig with a proportional gain (K_p) of 2.5 identified through empirical methods. The position response is shown in figure 3.6.
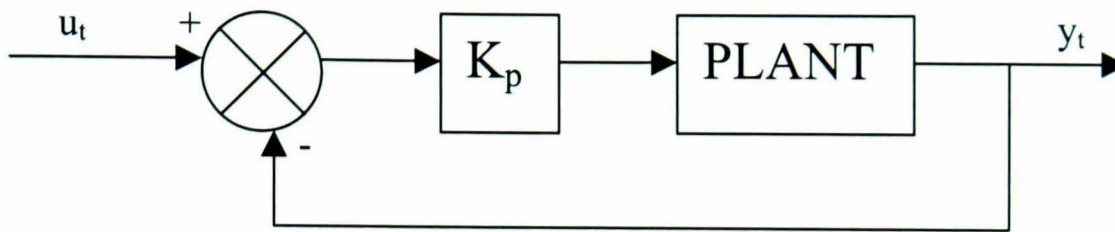
Figure 3.5 *Proportional control block diagram*
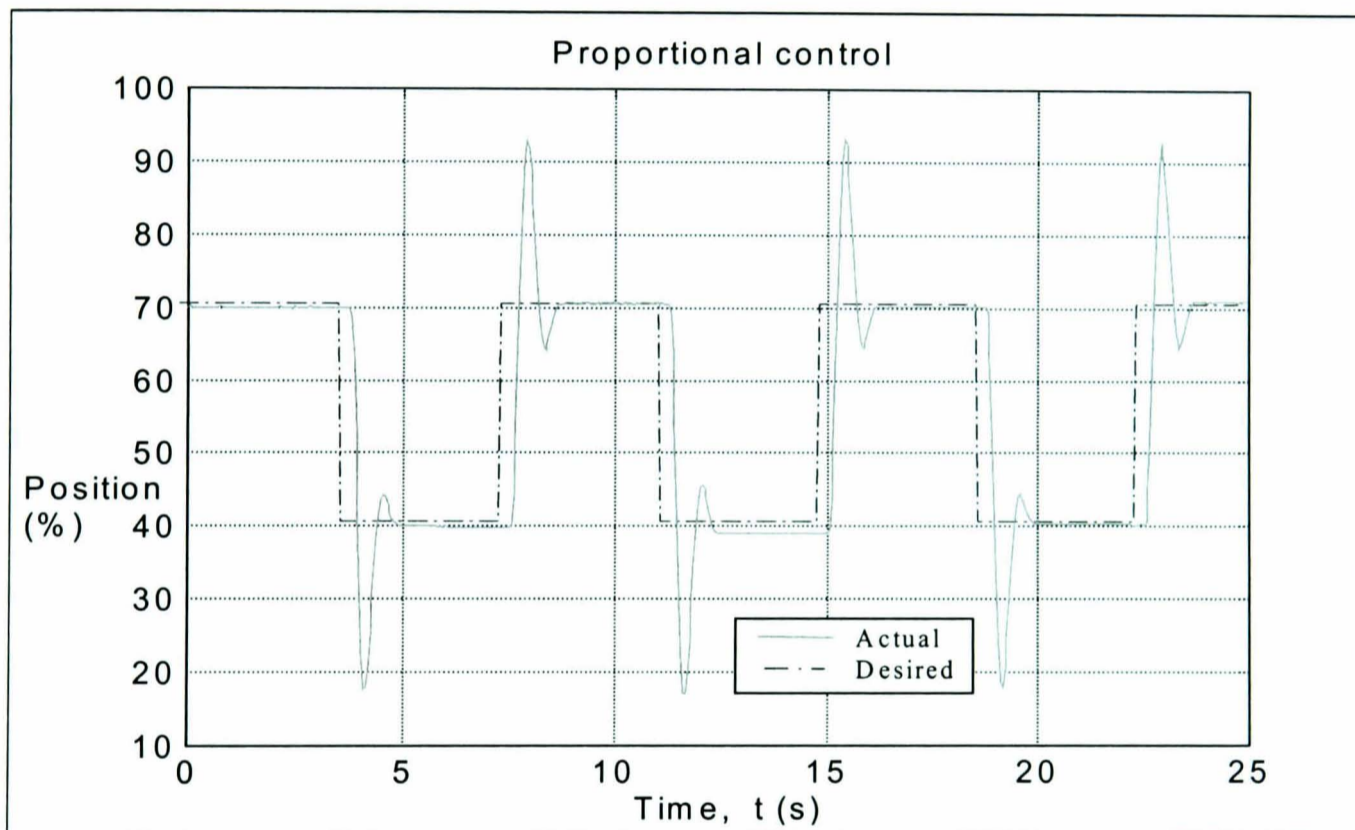
Figure 3.6 *Proportional control response*

The experimental proportional control response undergoes large overshoot before settling close to the desired steady state value. The steady state error is a result of friction within the experimental equipment and hysterisis within the electro-pneumatic valves.

The overshoot and oscillation for a step response around the cylinder mid-position are almost identical, which is important for design of a linear controller and is as a

result of the increased pressure in chamber B compensating for the piston area difference of single ended pneumatic cylinders.

It is apparent that the optimum performance obtainable from proportional control results in large overshoot, which is unacceptable. Proportional, integral and derivative (PID) control has therefore been implemented on the 3 degree of freedom robot (chapter 6).

The proportional control response of the low friction pneumatic cylinders and electro-pneumatic valves demonstrates that the response is approximately linear, therefore pole-placement control can be considered to improve the system performance.

3.4 Pole-Placement Control

Pole-placement control is a model-based approach that enables the design of a controller to meet specified goals. These goals can be achieved by the manipulation of the desired pole-positions for the system closed-loop response. **Astrom and Wittenmark (1997)** describe the pole placement approach in detail.

3.4.1 Controller Design

The pole placement controller structure is shown in figure 3.7 (where r_t is the demand, e_t is the measurement noise and y_t is the output). The controller consists of a feedforward $F(z^{-1})$ and feedback $G(z^{-1})$ polynomial.

These polynomials are of the form;

$$F(z^{-p}) = f_0 + f_1 z^{-1} + f_2 z^{-2} + ... + f_p z^{-p} \tag{3.7}$$

$$G(z^{-q}) = g_0 + g_1 z^{-1} + g_2 z^{-2} + ... + g_q z^{-q} \tag{3.8}$$
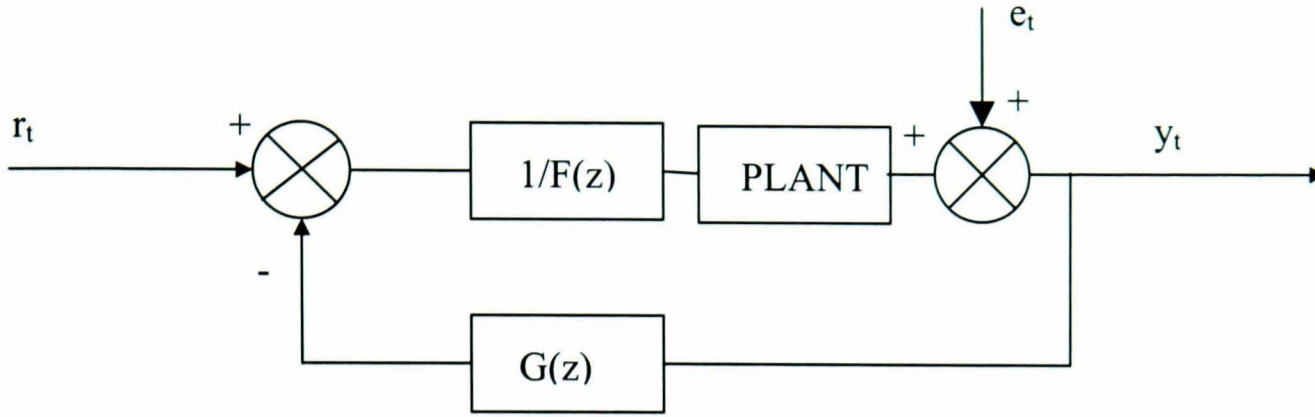
Figure 3.7 *Pole-placement control*

For the controller polynomials to be designed appropriately an accurate discrete model of the system behaviour (plant) is required.   A plant model is a linear approximation of the input/output relationship of the system. Digital control system plant models (for single input single output) are of the form;

$$y_t = \frac{B(z^{-m})}{A(z^{-n})} . u_t \tag{3.9}$$

where the plant polynomials are of the form;

$$A(z^{-n}) = 1 + a_1 z^{-1} + a_2 z^{-2} + a_3 z^{-3} + ... + a_n z^{-n} \tag{3.10}$$

$$B(z^{-m}) = b_0 + b_1 z^{-1} + b_2 z^{-2} + b_3 z^{-3} + ... + b_m z^{-m} \tag{3.11}$$

3.4.2   Identifying the plant model

Two common methods can be used to obtain a discrete-time plant model;

Physical modelling

The mathematical relationship between input and output can be derived from the physical relationships of system components in the s-domain. This model can then be discretised using the *zero order hold (ZOH)* method or equivalent. Physical modelling can be time consuming, moreover some parameters can only be accurately obtained through inspection of the experimental behaviour.

System identification

A plant model can be obtained by performing system identification from a set of data relating inputs to outputs (this approach cannot be used unless physical experiments can be performed on the system).

If $\underline{y}$ is an output vector and $\underline{u}$ is an input vector then the system including the plant model can be written in matrix form;

$$
\begin{bmatrix} y_i \\ y_{i+1} \\ y_{i+2} \\ \dots \\ y_{i+d-1} \end{bmatrix} = \begin{bmatrix} y_{i-1} & y_{i-2} & \cdots & y_{i-n} & u_{i-1} & u_{i-2} & \cdots & u_{i-m} \\ y_i & y_{i-1} & \cdots & y_{i+1-n} & u_i & u_{i-1} & \cdots & u_{i+1-m} \\ y_{i+1} & y_i & \cdots & y_{i+2-n} & u_{i+1} & u_i & \cdots & u_{i+2-m} \\ \vdots & \vdots & & \vdots & \vdots & \vdots & & \vdots \\ y_{i+d-2} & y_{i+d-3} & \cdots & y_{i+d-1-n} & u_{i+d-2} & u_{i+d-3} & \cdots & u_{i+d-1-m} \end{bmatrix} \begin{bmatrix} -a_1 \\ -a_2 \\ \vdots \\ -a_n \\ b_1 \\ b_2 \\ \vdots \\ b_m \end{bmatrix} \qquad (3.12)
$$

where

$$
\underline{y} = \begin{bmatrix} y_i \\ y_{i+1} \\ y_{i+2} \\ \vdots \\ y_{i+d-1} \end{bmatrix} \quad \text{and} \quad \underline{\theta} = \begin{bmatrix} -a_1 \\ -a_2 \\ \vdots \\ -a_n \\ b_1 \\ b_2 \\ \vdots \\ b_m \end{bmatrix} \qquad (3.13)
$$

The vector $\underline{\theta}$ is known as the parameter estimate and the matrix containing input and output values ($\underline{\Psi}$) is called the *regressor* matrix.

Rearranging equation 3.12 to obtain an estimate of the plant model coefficients, gives:

$$
\underline{\theta} = \underline{\Psi}^{-1} \underline{y} \qquad (3.14)
$$

Note that inversion of the regressor matrix is possible as it is a square matrix.

It is desirable to include more equations than parameters in equation 3.14 to improve the estimate of the plant model, however the regressor matrix is no longer square and cannot be inverted. The least squares technique provides a method of inverting a matrix that is not square (**Astrom and Wittenmark 1997**).

The *least squares* estimate of the parameters is obtained from the following equation.

$$\hat{\underline{\theta}} = (\underline{\Psi}^T \underline{\Psi})^{-1} \underline{\Psi}^T \underline{y} \tag{3.15}$$

It can be shown that the least squares parameters estimate gives the minimum possible sum square of the error when the plant model output and experimental response are compared. It also has the added benefit of lending itself easily to self-tuning system identification (section 3.5).

The data collected for the least squares estimate must contain sufficient information for an accurate plant model to be obtained. A pseudo random binary sequence (PBRS) has been proven to be the optimal input signal for the parameter estimation of dynamic systems (**Hsia 1977**), however the system output for such a signal can be erratic and potentially destructive for large robotic devices. Experimental data, obtained over the operational frequency range, can be used to identify an accurate model. The proportional control step response contains suitable information for system identification.

One of difficulties of plant model identification is selection of the model order. If the model order is too small it will not contain the necessary information to accurately model the system response. Conversely if the model were over parameterised (the model order too large) there would be a tendency for the extra zeros to cancel out the extra poles so the equations become ill-conditioned.

Modelling of the pneumatic cylinder and electro-pneumatic valve (Sections 5.2 & 5.4) have shown the valves to approximate to a gain and the cylinder and load configuration to be second order. Therefore a second order model was chosen to represent the overall valve and cylinder configuration. The input and output signals

from the proportional response were filtered by a first order, low pass digital filter off-line to remove any noise which might affect the plant estimation. The plant model obtained from the least squares estimate becomes:

$$y_t = \frac{0.059z^{-2}}{1 - 1.75z^{-1} + 0.75z^{-2}}.u_t$$ (3.14)

where y_t is position and u_t is the input control signal

Examining the plant denominator reveals the presence of an integrator. An integrator within the plant model results in constant, non-zero control voltage input producing a constant change of the cylinder's position. Once an accurate plant model has been identified it is possible to calculate the controller polynomials.

3.4.3 Calculation of F(z) and G(z) coefficients

The controller aim is to impose the poles of the system closed loop response. So the desired closed-loop transfer function is given by:

$$y_t = \frac{B(z)}{A_m(z)}.r_t$$ (3.17)

where

$$A_m(z^{-1}) = (1 - p_1 z^{-1})(1 - p_2 z^{-1})(1 - p_3 z^{-1})...(1 - p_r z^{-1})$$ (3.18)

The polynomial A_m contains poles specified by the control system designer. Selection of these poles is an important part of the controller design procedure, altering the speed and damping of the response.

The closed-loop transfer function requires unity steady state gain for any poles that the system designer may specify. So

$$\frac{B(1)}{A_m(1)} = 1 \Rightarrow \frac{B(1)}{k_a(1 + am_1' + am_2' + am_3' + ... + am_r')} = 1$$ (3.19)

Hence the polynomial A_m is required to be scaled by a factor (k_a) to maintain the system steady state gain.

From the controller block diagram (figure 3.7) it can be shown that the controller polynomials are related to A_m by the following equation, known as the diophantine equation:

$$F(z)A(z) + B(z)G(z) = A_m(z) \tag{3.20}$$

The degree of the $F(z^{-1})$ and $G(z^{-1})$ polynomials can be found by the following equations (Astrom and Wittenmark 1980).

$$p_f = deg\ F(z) = deg\ B(z) - 1 \tag{3.21}$$

$$q_g = deg\ G(z) = deg\ A(z) - 1 \tag{3.22}$$

Therefore, the diophantine equation for this second order plant model can be expressed in matrix form thus;

$$\begin{bmatrix} 1 & 0 & b_0 & 0 \\ a_1 & 1 & b_1 & b_0 \\ a_2 & a_1 & b_2 & b_1 \\ 0 & a_2 & 0 & b_2 \end{bmatrix} \cdot \begin{bmatrix} f_0 \\ f_1 \\ g_0 \\ g_1 \end{bmatrix} = \begin{bmatrix} a_{m0} \\ a_{m1} \\ a_{m2} \\ a_{m3} \end{bmatrix} \tag{3.23}$$

The coefficients of $F(z^{-1})$ and $G(z^{-1})$ can be obtained by inversion of the parameters matrix. Inverting a large matrix is a computationally intensive task, with small increases in the size of the matrix resulting in large increases in computation time. A quicker and more computer friendly method is *Gaussian elimination* **(James et al. 1994)**. This involves reducing the matrix to a form where it can be solved recursively.

3.4.4 Selection of closed-loop poles

Selection of correct closed-loop poles is essential to achieve the desired controller performance. Analysis of the system behaviour for specific poles can be performed in the frequency domain. **Plummer (1997)** has shown that the transfer functions relating the control signal and system output to noise and disturbances are given by:

Control sensitivity function

$$U(z^{-1}) = \frac{G(z^{-1})A(z^{-1})}{F(z^{-1})A(z^{-1}) + G(z^{-1})B(z^{-1})}$$ (3.24)

Output sensitivity function

$$S(z^{-1}) = \frac{F(z^{-1})A(z^{-1})}{F(z^{-1})A(z^{-1}) + G(z^{-1})B(z^{-1})}$$ (3.25)

Bode plots for the control sensitivity and output sensitivity of the plant and controller are shown in figures 3.8 and 3.9 for closed-loop poles of $0.2\pm0.1i$, $0.4\pm0.1i$, $0.6\pm0.1i$, $0.8\pm0.1i$. The control sensitivity shows the faster poles ($0.2\pm0.1i$) to have increased gain at higher frequencies enabling the controller to quickly respond to disturbances, however noise is prevalent at these high frequencies so a trade-off between speed of response and noise rejection is required.

Examining the output sensitivity frequency response, the gain for the low frequency response for slow poles ($0.8\pm0.1i$) is large, causing the controller to become sensitive to modelling errors at low frequencies, indicating poor robustness.

Poles were selected at $0.4\pm0.1i$ as a trade-off between noise rejection and performance robustness. The complex part of the poles was selected at 0.1 to give the response a small amount of damping.
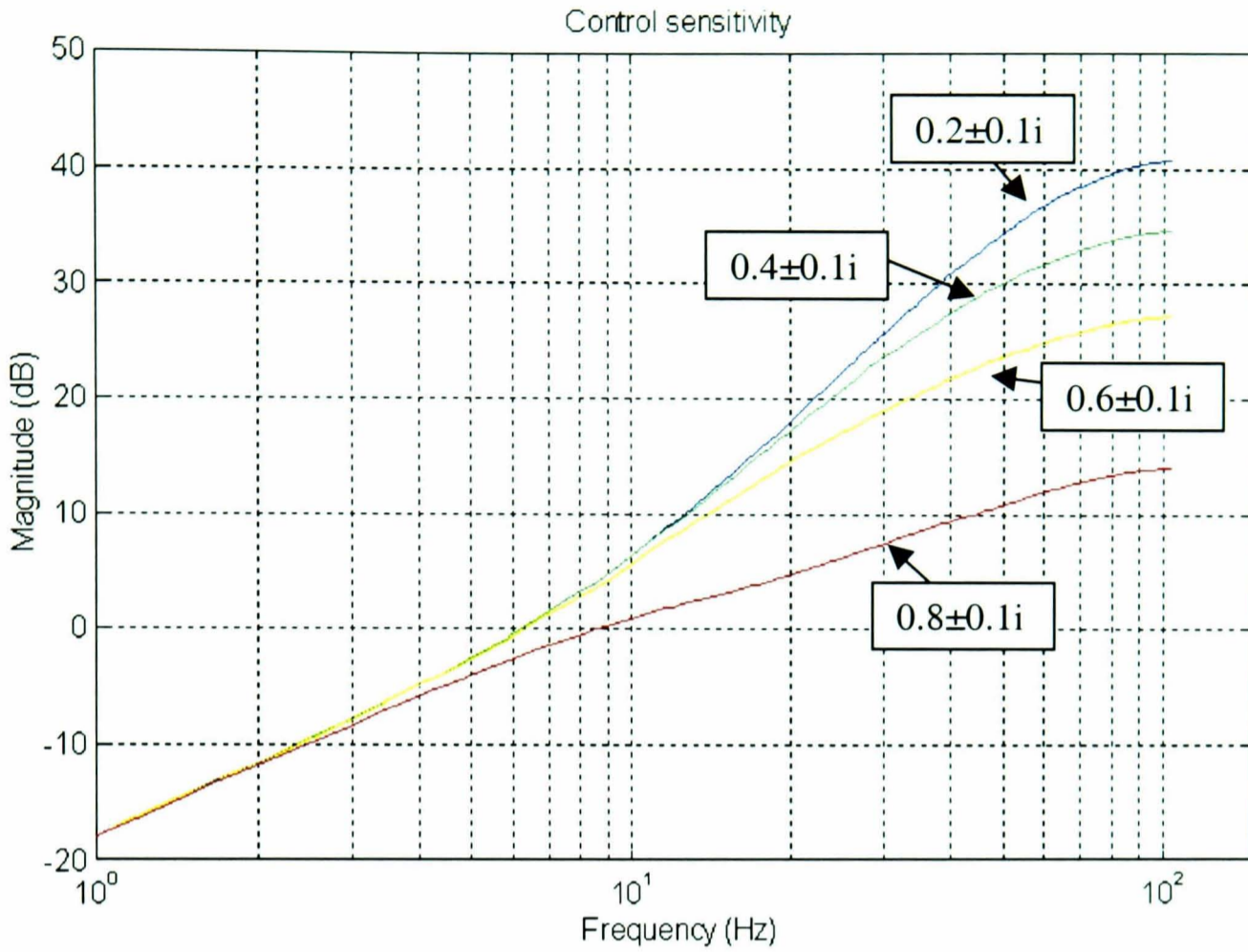
Figure 3.8 *Response of control signal to disturbances*
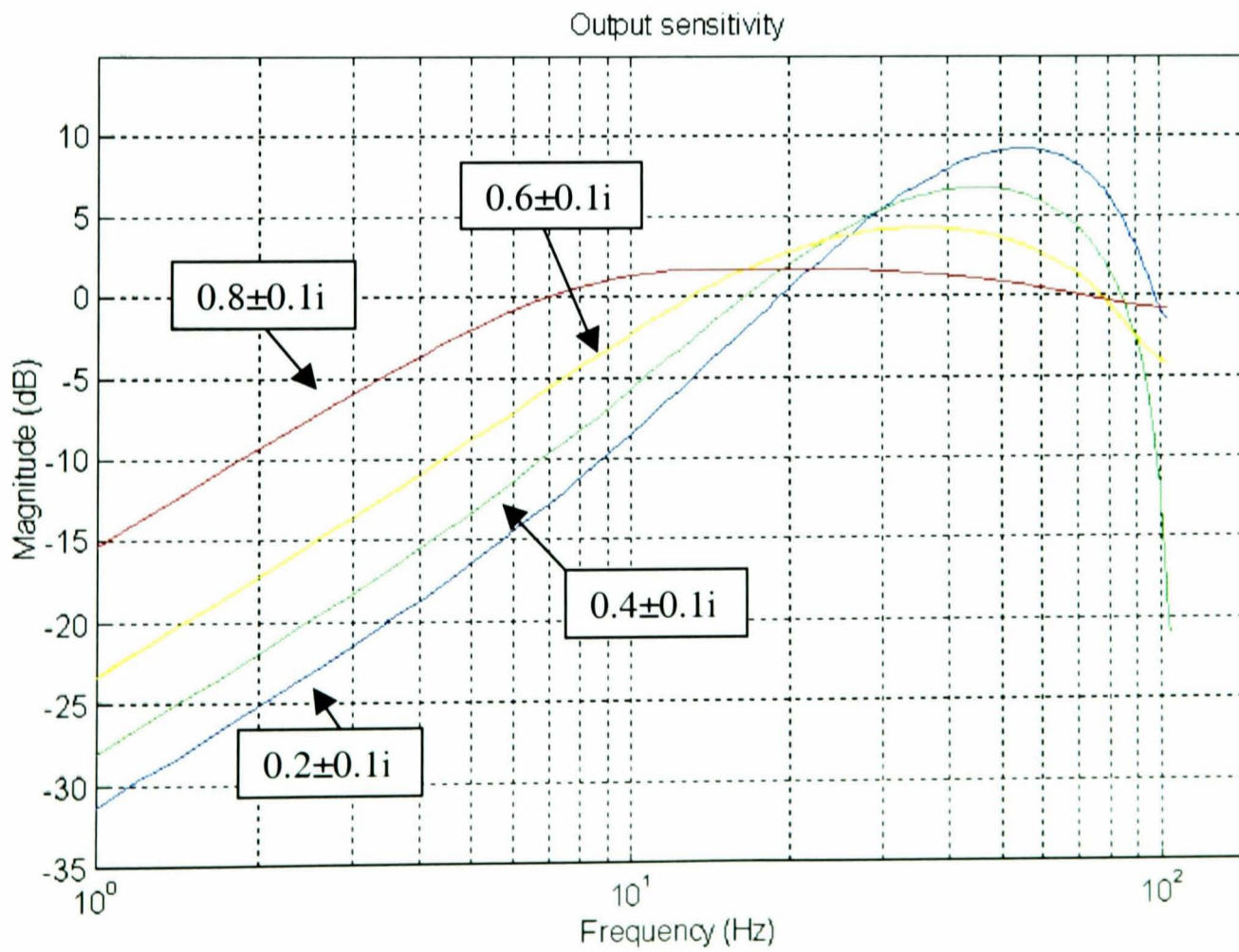
Figure 3.9 *Response of output to disturbances*

3.4.5 Experimental response

The pole-placement controller was implemented on the position control test rig. The position response (figure 3.10) experienced slight overshoot and steady state error. The slight oscillation of the position during steady state is due to the controller responding to measurement noise. The control signal for this response is shown in figure 3.11.

Applying the pole-placement controller with closed-loop poles at $0.4 \pm 0.1i$ has greatly improved the response compared to the proportional controller. However these results to do not demonstrate the changeable nature of the plant requiring identification of plant parameters at commencement of testing to produce an optimal response. It was decided that a self-tuning strategy should be employed so these parameters could be automatically tuned at the start of each session.
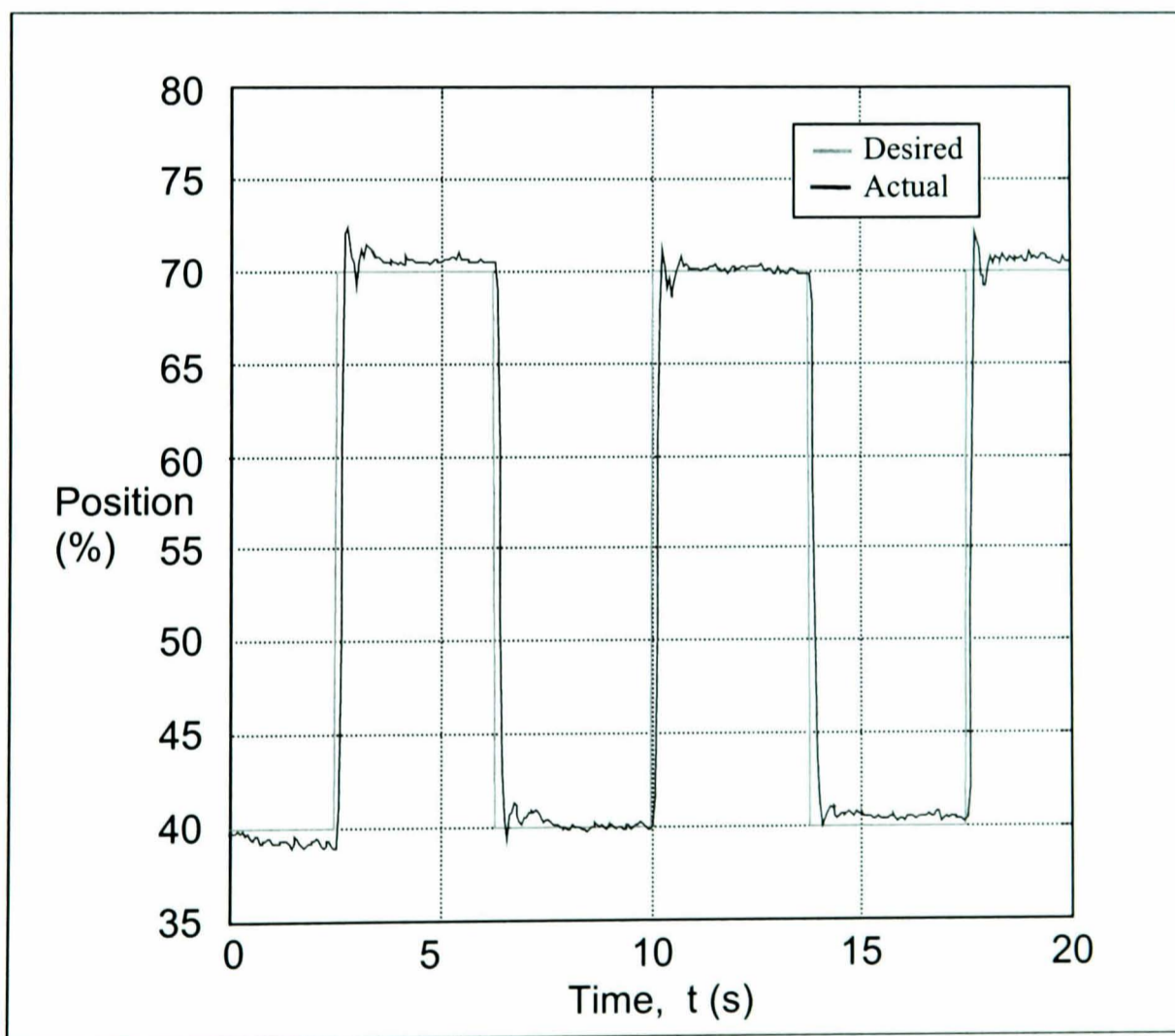
Figure 3.10   Pole-placement control performed with one pole pair at (0.4±0.1i)
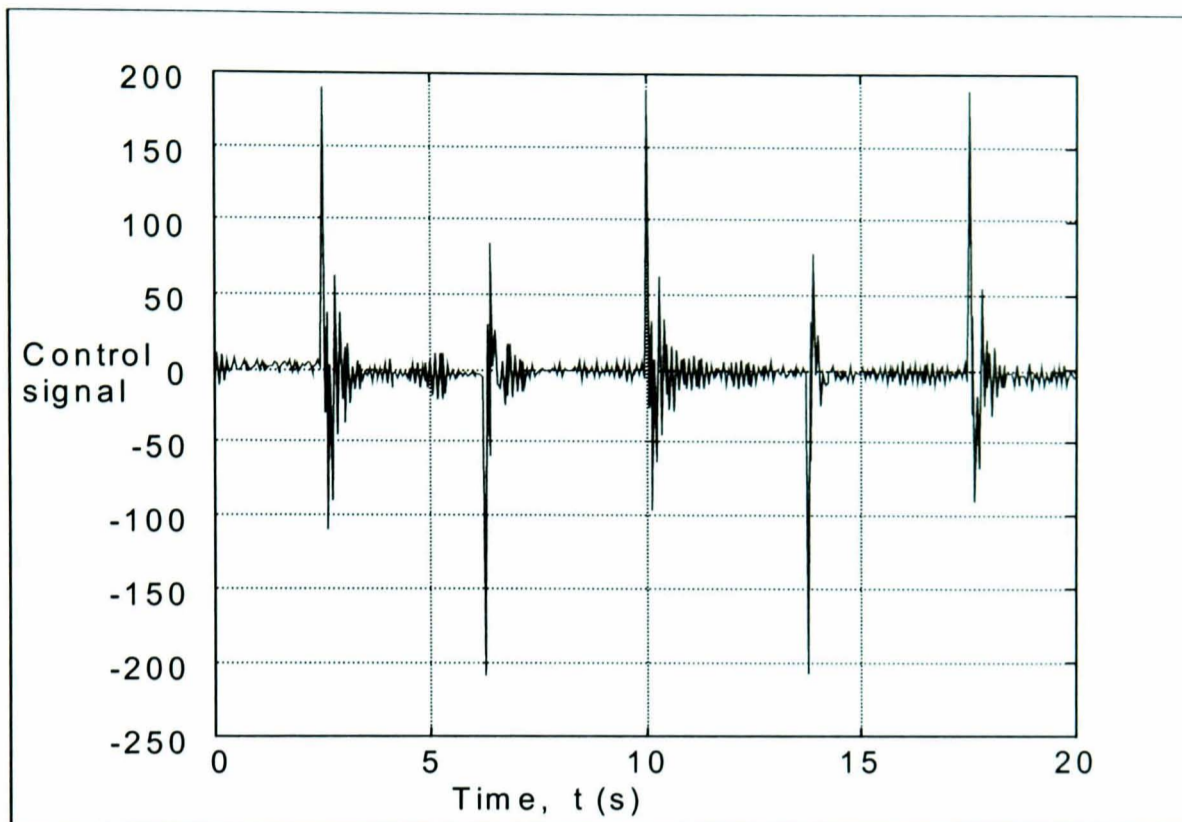
Figure 3.11 *Control signal for pole-placement with poles at (0.4±0.1i)*

3.5 Self-tuning pole-placement control

Self-tuning pole-placement control can be considered a one-shot method of tuning a plant model. The recursive least squares technique is used to update the estimate of the plant model on-line **(Astrom and Wittenmark 1997)**. This technique enables each new input/output data set to alter the plant model and hence the controller polynomials.

3.5.1 Self-tuning strategy

Recursive least squares self-tuning control requires an initial estimate of the parameters vector ($\underline{\theta}$). The previously identified pole-placement plant model is used in this instance.

$$\underline{\theta} = \begin{bmatrix} -a_1 \\ -a_2 \\ \vdots \\ -a_n \\ b_1 \\ b_2 \\ \vdots \\ b_m \end{bmatrix} \qquad (3.26)$$

Previous input and output values are entered into the regressor vector ($\underline{\psi}$):

$$\underline{\psi} = \begin{bmatrix} y_{t-1} & y_{t-2} & \cdots & y_{t-n} & u_{t-1} & u_{t-2} & \cdots & u_{t-m} \end{bmatrix} \qquad (3.27)$$

Note that the regressor vector contains only a single set of input/output data.

Assuming the system to be in steady state when implementing the controller, results in all the inputs to be zero and all the outputs constant. With the parameters vector and regressor vector formed, self-tuning control can be performed as follows;

1. Perform pole-placement control with initial plant model, obtaining input and output data points.

2. Form the regressor vector ($\underline{\psi}$) for the current sample period.

3. Calculate $\underline{k_{st}}$ using:

$$\underline{k_{st}} = \frac{\underline{P}_{t-1}\underline{\psi}_t}{1 + \underline{\psi}_t^{T}\underline{P}_{t-1}\underline{\psi}_t} ; \qquad (3.28)$$

Note that, initially, the leading diagonal of the P_t matrix should be set to a value that reflects the amount of tuning (a larger value causes more rapid tuning)

4. Produce new plant parameters:

$$\hat{\underline{\theta}}_t = \hat{\underline{\theta}}_{t-1} + \underline{k}_{st}(y_t - \underline{\psi}_t^T \hat{\underline{\theta}}_{t-1}) \tag{3.29}$$

(where $\hat{\underline{\theta}}$ is an estimate of the plant parameters)

5. Update the $\underline{P}_t$ matrix to reflect current conditions:

$$\underline{P}_t = \underline{P}_{t-1} - \underline{k}_{st}\underline{\psi}_t^T \underline{P}_{t-1}; \tag{3.30}$$

6. Calculate new $F(z^{-1})$ & $G(z^{-1})$ coefficients

7. This process is then repeated for the next sample instance

(It is important to note that in changing the plant parameters, unity steady state gain may not be maintained. In order to maintain steady state gain the magnitude of the controller-specified polynomial (A_m) needs to be adjusted at each sample instance)

3.5.2 Reduced order self-tuning strategy

To self-tune the plant identified earlier, the parameter vector would take the form:

$$\underline{\theta}_t = \begin{bmatrix} -a_1 \\ -a_2 \\ b_2 \end{bmatrix} = \begin{bmatrix} 1.75 \\ -0.75 \\ 0.0591 \end{bmatrix} \tag{3.31}$$

Therefore, three parameters are to be identified. However, it was noted earlier that the plant model contains an integrator. This integrator can be assumed constant in the plant model enabling it to be removed from the estimate **(Vaughan and Plummer[2] 1990).**

The reduced parameter plant model is shown below:

$$y_t(1 - z^{-1}) = \frac{0.0591z^{-2}}{1 + 0.6751z^{-1}}.u_t = \frac{b_2 z^{-2}}{1 + a_1 z^{-1}}; \tag{3.32}$$

On identification of each reduced order plant model, the integrator is required to be reassembled into the plant model for calculation of the new $F(z^{-1})$ and $G(z^{-1})$ controller polynomials. The reduced parameters vector, therefore takes the form:

$$\underline{\theta}_t = \begin{bmatrix} -a_1 \\ b_2 \end{bmatrix} = \begin{bmatrix} -0.75 \\ 0.0591 \end{bmatrix} \tag{3.33}$$

The reduced parameter self-tuning pole-placement control was implemented on the position control test rig. After the initial tuning transient the positional self-tuning response (figure 3.12) demonstrates fast rise time, slight overshoot and small steady state error. To demonstrate the system self-tuning transient response, the leading diagonal of the covariance matrix (P_g) was set to 1000, however during normal operation this tuning coefficient would be smaller preventing the vigorous tuning transient shown here. Initial rapid tuning of the coefficients a_1 and b_2, during self-tuning, is shown in figures 3.13 & 3.14. Both coefficients have settled to approximately constant values within 10 seconds.
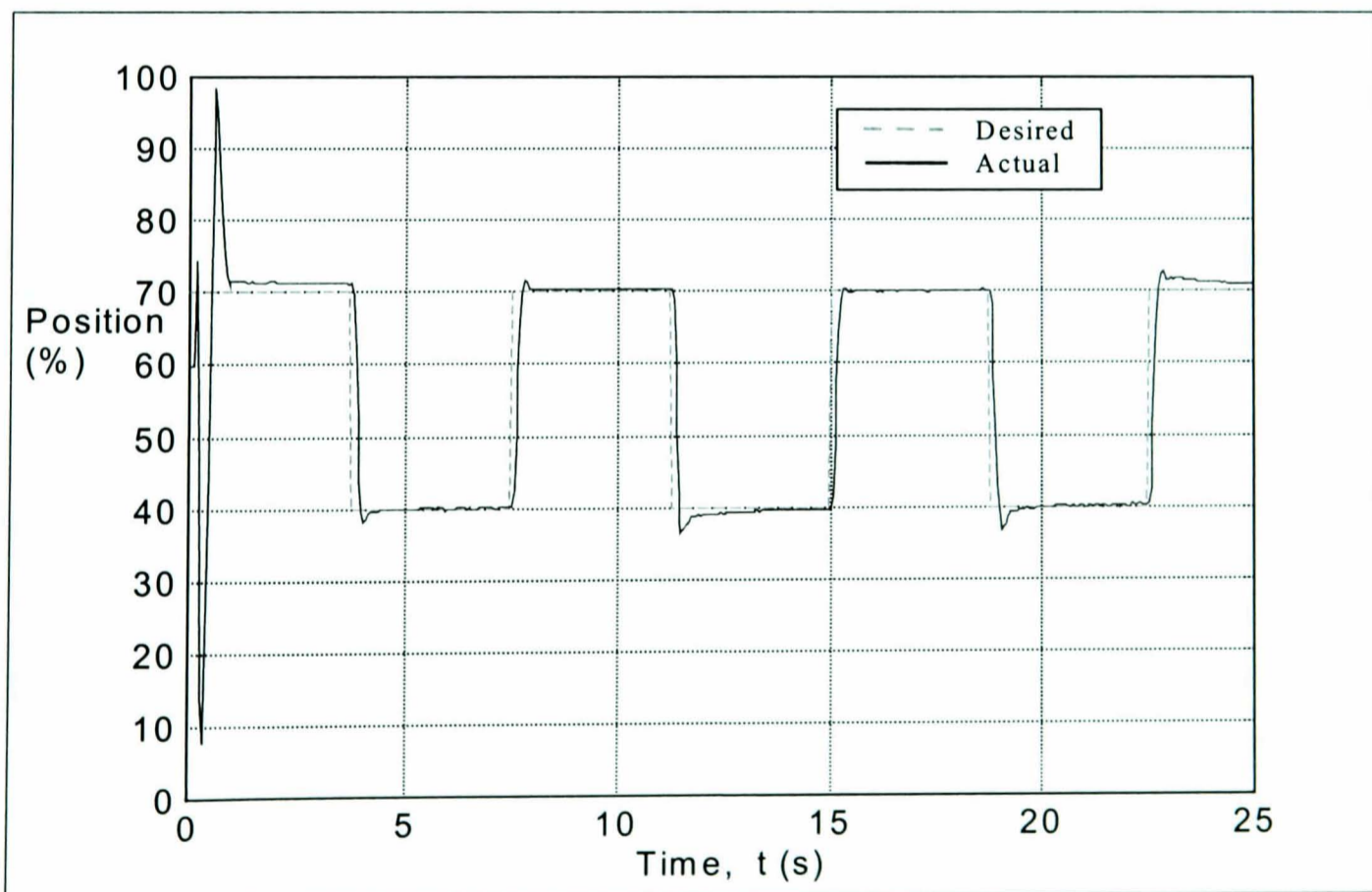
Figure 3.12 *Reduced parameter self-tuning position response*

Although self-tuning pole-placement control showed improvements in the overall response, it was still necessary to manually tune the balance signal. Self-tuning the gravity balance signal along with the parameters a_1 & b_2 would enable all controller parameters to be correctly identified at the start of each session.
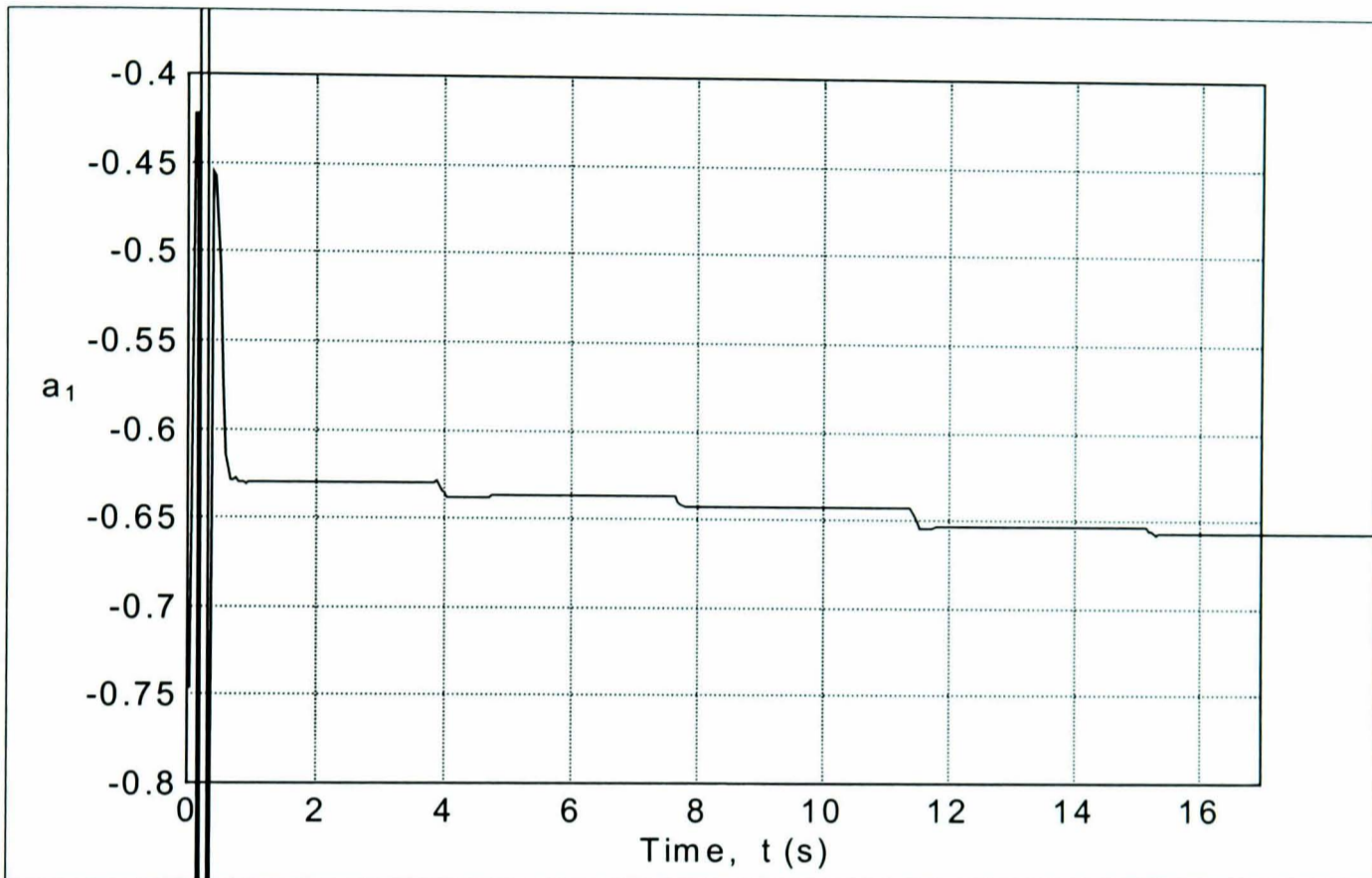
Figure 3.13   *Tuning parameter a_1*
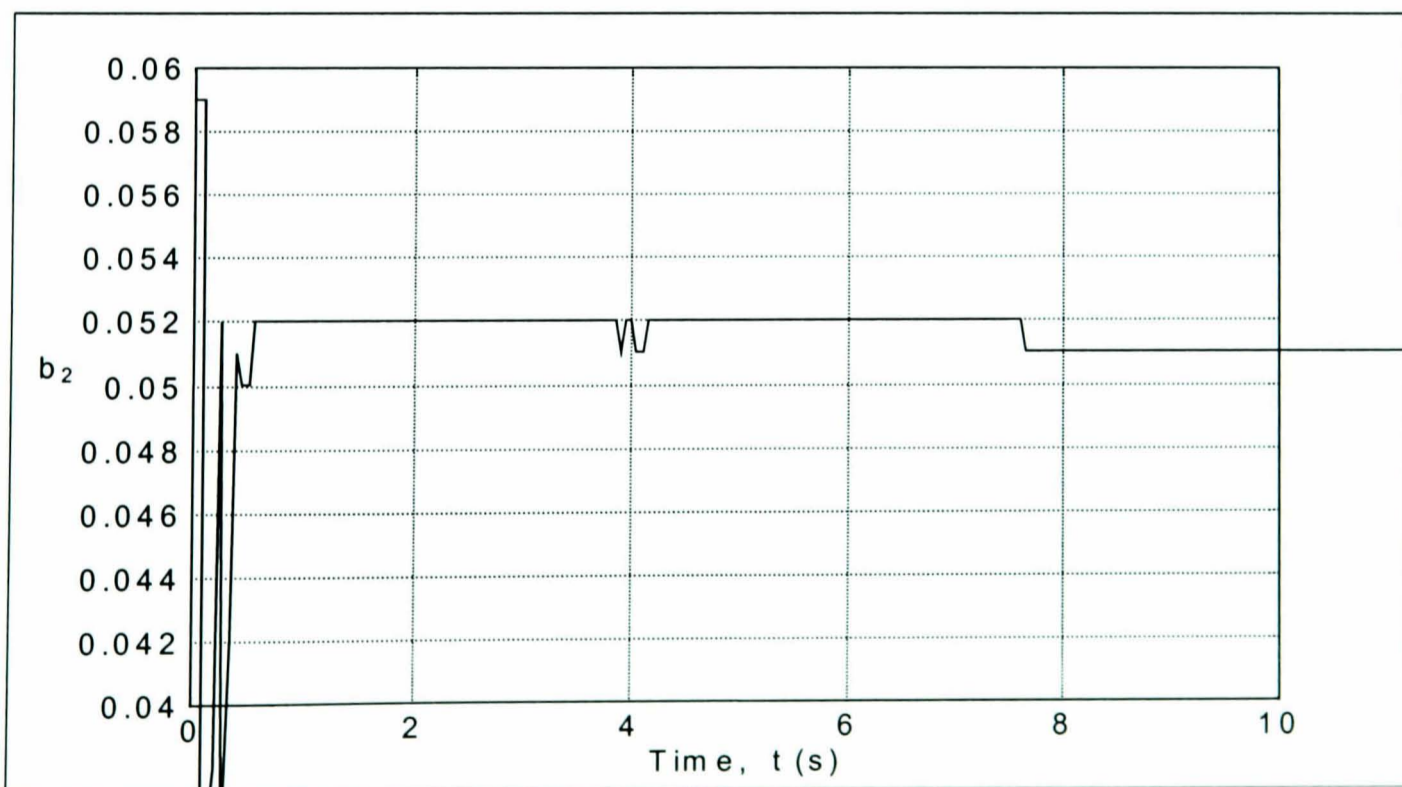
Figure 3.14   *Tuning parameter b_2*

5.6.5 Self-tuning balance

To include the balance signal as part of the self-tuning strategy it can no longer be considered part of the plant (figure 3.15).

Analysing the plant to obtain a method of self-tuning the balance signal gives:

$$y_t(1-z^{-1}) = \frac{b_2 z^{-2}}{1+a_1 z^{-1}} . u_t \tag{3.34}$$

For ease of notation

$$y_t' = y_t(1-z^{-1}) \tag{3.35}$$

$$\Rightarrow y_t' = \frac{b_2 z^{-2}}{1+a_1 z^{-1}} . u_t \tag{3.36}$$

Substituting for u_t in (3.34) using (3.6):

$$\Rightarrow y_t'(1+a_1 z^{-1}) = b_2 z^{-2} u_t' - b_2 B_p z^{-2} \tag{3.37}$$

A parameter d can be estimated on-line as:

$$d = -b_2 B_p \tag{3.38}$$
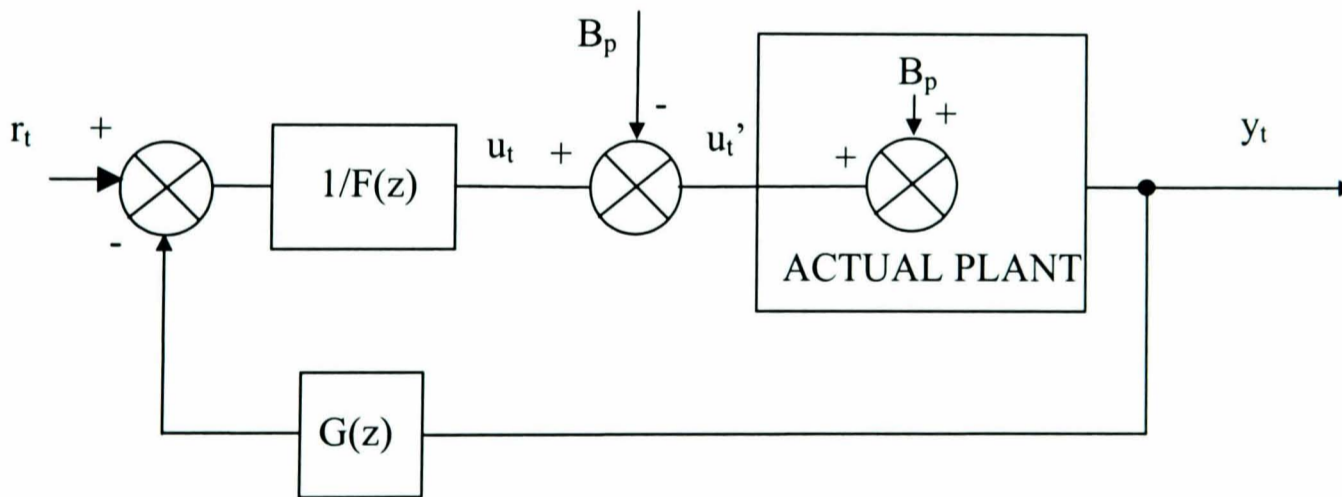
Figure 3.15 *Pole-placement control with balance signal block diagram*

The time delay (z^{-2}) of d can be ignored since B_p is a constant. Forming the regressor and parameter vectors necessary for recursive least squares self-tuning leads to:

The regressor vector:

$$\underline{\psi} = \begin{bmatrix} y_{t-1}{'} & u_{t-2}{'} & 1 \end{bmatrix}^{\mathrm{T}}$$

(3.39)

And the parameter vector:

$$\underline{\hat{\theta}}_t = \begin{bmatrix} -a_1 & b_2 & d \end{bmatrix}^{\mathrm{T}}$$

(3.38)

The parameter vector is calculated online using standard recursive least squares identification equations. The balance value is then reconstructed from (3.38) and the plant model from (3.36). The coefficients $F(z^{-1})$ and $G(z^{-1})$ are recalculated using the diophantine equation. Pole placement control can then be performed for the next sample interval using the new $F(z^{-1})$ and $G(z^{-1})$ coefficients.

Implementing the self-tuning balance to the test rig results in the positional response shown in figure 3.16. After the initial tuning transient the position demand is accurately tracked. The convergence of parameters a_1, b_2 and B_p during this response is shown in figures 3.17, 3.18 and 3.19. The self-tuning controller with balance signal accurately tunes the pole-placement controller. With the controller parameters tuned on-line an optimised pole-placement controller can be implemented at the start of each session.

Figure 3.16 *Self-tuning balance position response*

Figure 3.17 *Evolution of parameter a_1*

Figure 3.18 *Evolution of parameter b_2*
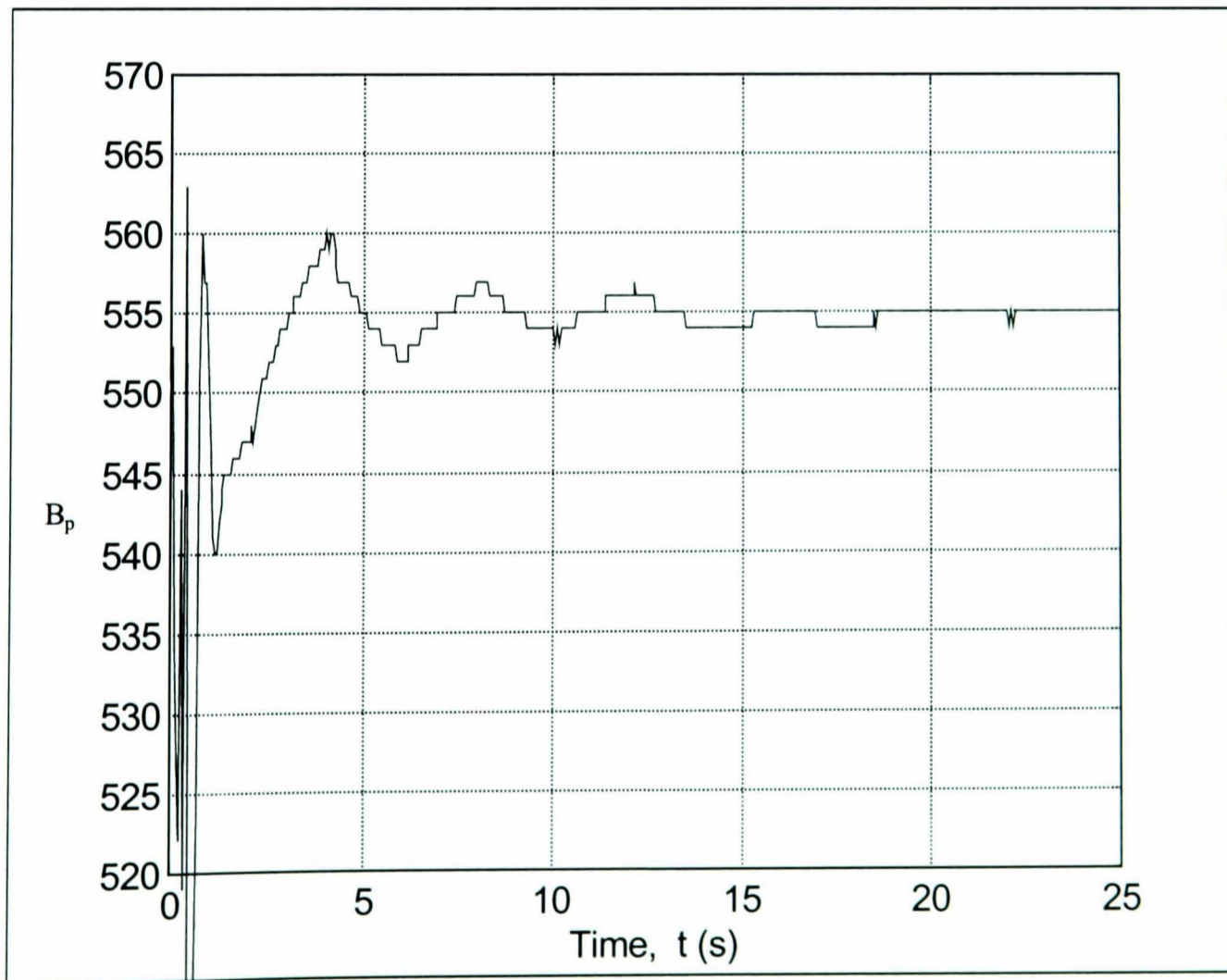
Figure 3.19 *Evolution of balance parameter, B_p*
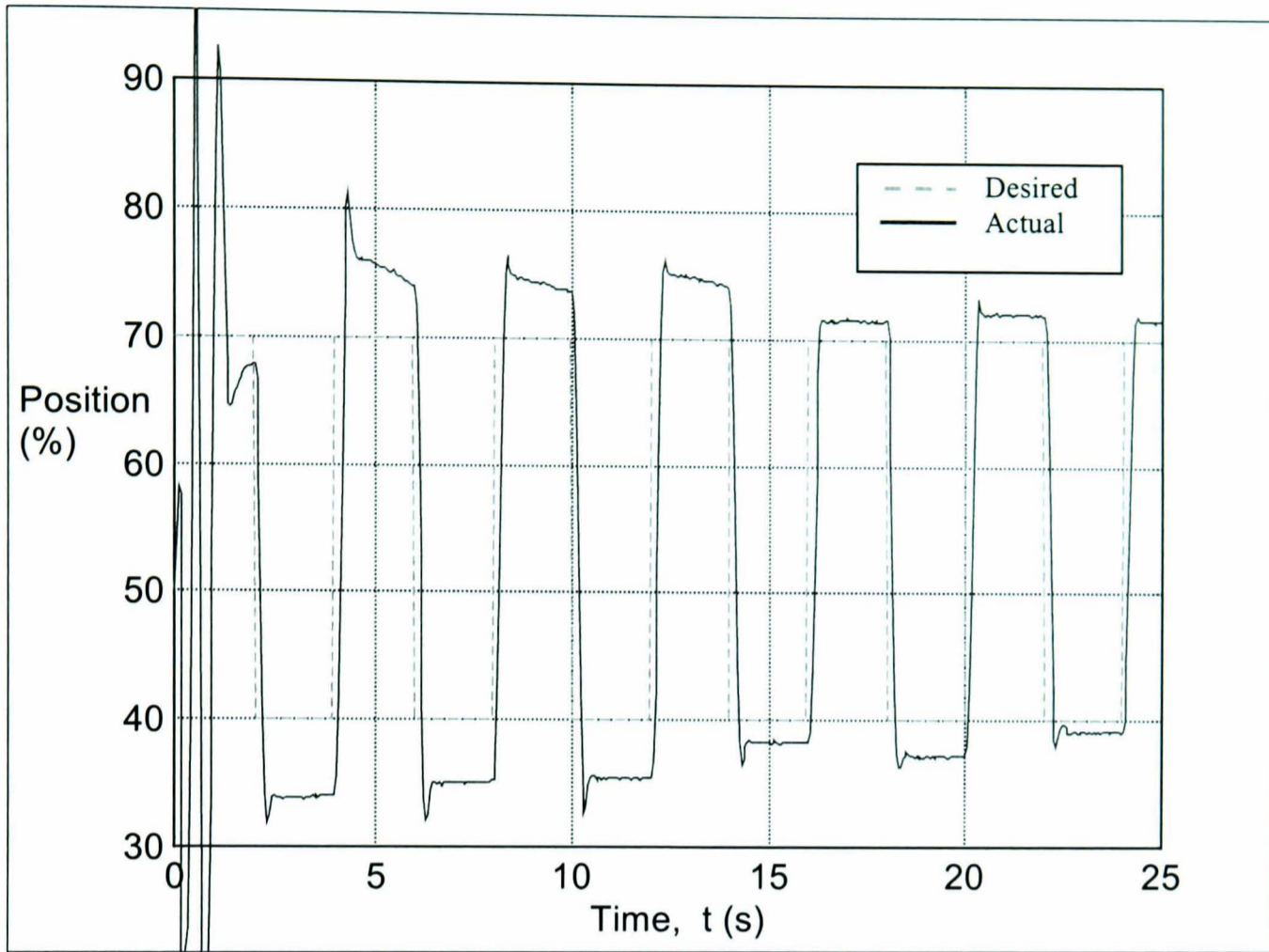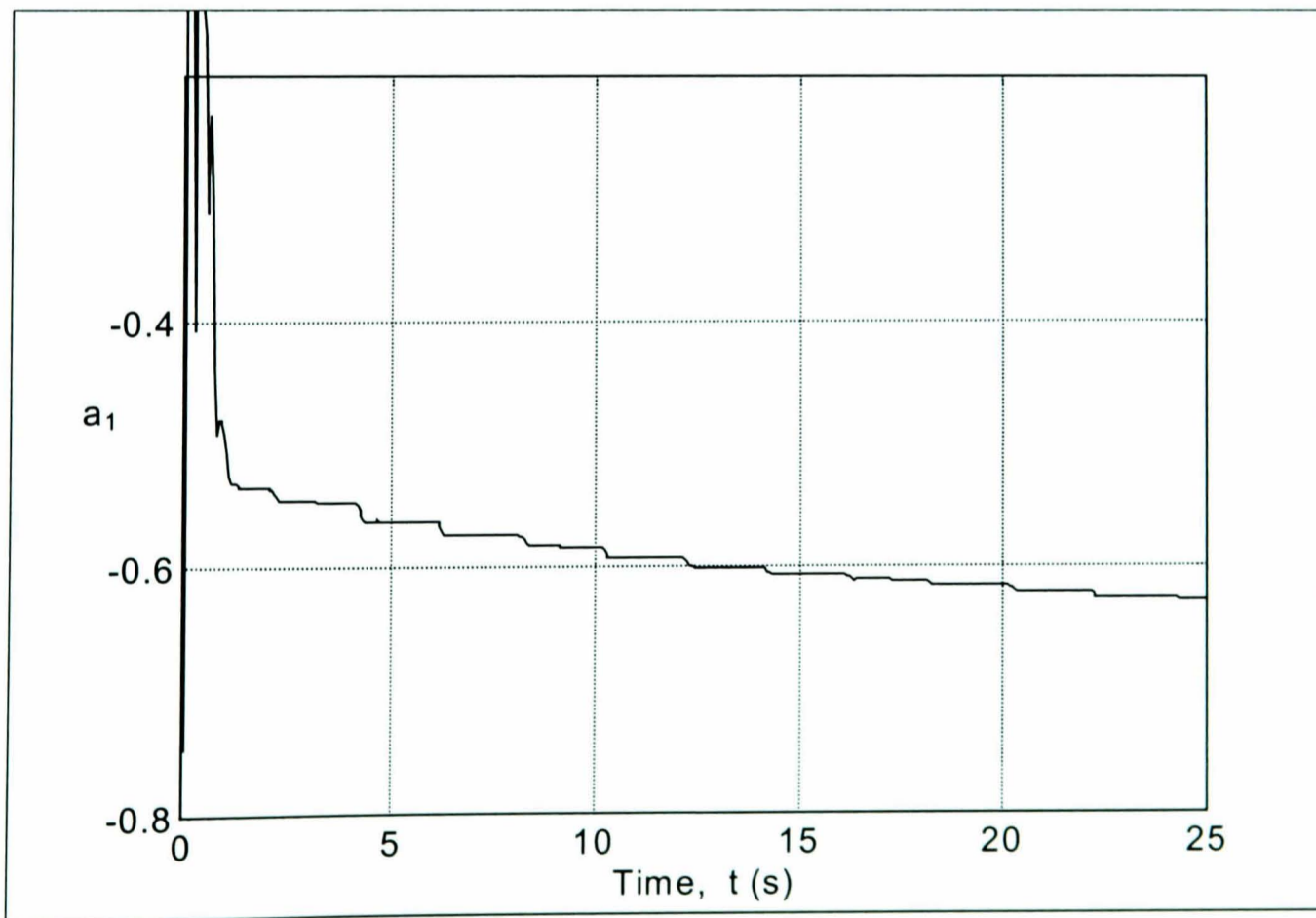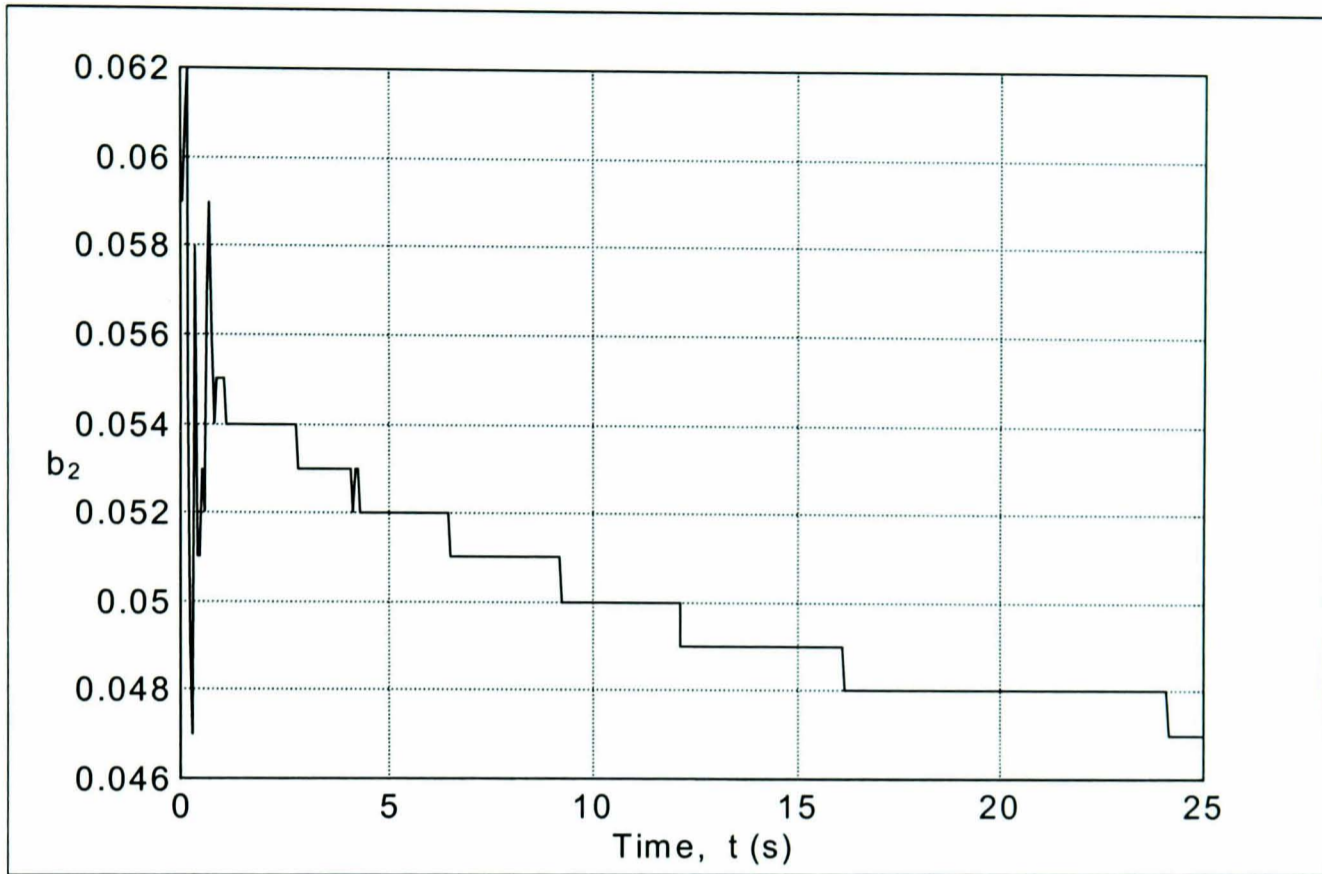
3.4 Discussion and Conclusions

Traditional pneumatic servo systems consist of one spool valve and pneumatic cylinder which are prone to stop-start motion due to internal stiction effects. Non-linear fluid dynamics and air compressibility add to the stiction to compound the problem of accurate position control.

The combination of low friction pneumatic actuators and electro-pneumatic valves creates a pneumatic system that behaves with much greater linearity, however air compressibility and non-linear fluid flow dynamics still make accurate position control challenging.

Replacing the traditional spool valve with electro-pneumatic valves presents problems within itself. A single valve is required to regulate the pressure within a single chamber of the pneumatic cylinder, therefore two independent valves are required to control the twin chambers of a pneumatic cylinder. These two valves require a control strategy that enables them to operate simultaneously. A proven method of controlling these two valves involves reducing the pressure in one chamber of the pneumatic cylinder while simultaneously increasing the pressure within the other chamber. Assuming the valves to behave identically, this strategy provides the greatest linearity in the cylinder response.

In order for the two-valve control strategy to be successful it is necessary that a raised pressure is present in both chambers of the pneumatic cylinder, which can be reduced when required. Two strategies have been identified for selection of this 'equilibrium pressure': the maximum region of sonic flow and the maximum force output. The maximum region of sonic flow allows the fastest response of the pneumatic cylinder and the greatest linearity when supplying and exhausting fluid, however the maximum force output is restricted. Setting the equilibrium pressure to the mid-point between supply and exhaust pressures allows the maximum cylinder force output. To demonstrate the best performance obtainable from the pneumatic servosystem the equilibrium pressure is set for the greatest region of sonic flow on

the test rig. However, the equilibrium pressure was set to allow the maximum force output for the three degree of freedom robot.

Since two pressure control valves were used instead of a conventional servovalve, the natural integrating action of the servovalve which counteracts constant external forces was eliminated. This gives rises for the need of a bias command, termed the 'balance signal', to balance external forces. This balance signal takes the form of a constant input signal.

The pressure control valves allow a pressure increase to be incorporated into chamber B to compensate for differences in piston area. Without this pressure increase, greater force would be applied in chamber A causing motion for a zero control signal and producing significant differences in the extension and retraction of the piston. The proportional control results show that the cylinder responds almost identically for extension and retraction motions indicating that this area difference has been successfully compensated.

Implementation of pole-placement control improved the response of the pneumatic servosystem through increased response time and reduced overshoot when compared to proportional control. However, pole-placement control is a model-based approach requiring an accurate system model to obtain the correct controller polynomials. The changeable nature of pneumatic systems due to factors such as air temperature and humidity results in changes of the system behaviour, all of which alter the plant model. Self-tuning control therefore provides a means of obtaining an accurate plant model whenever the controller is implemented.

Identifying the plant as second order accurately represents the system behaviour requiring the identification of three plant coefficients. Most pneumatic and hydraulic servosystems contain an integrating element within the plant model. Assuming the integrator to be an inherent element of the plant model removes the need for its identification and reduces the number of coefficients to be identified.

Implementation of the self-tuning controller demonstrated accurate tuning of the plant model. An empirical selection of the balance signal is, however, required to compensate for the external forces.

Including this balance signal within the self-tuning algorithm removed the need for empirical tuning, indeed the self-tuning strategy proves a means of identifying the optimum balance signal that would otherwise be difficult to obtain.

Pole-placement control provides a means of performing accurate position control on modern low friction pneumatic actuators and pressure control valves. When combined with a self-tuning strategy, the controller provides consistent performance in the presence of a time varying plant under the influence of a gravity load.

Chapter 4

Force Control

This chapter examines force control techniques applied to pneumatic systems. Force control of the pneumatic servosystem is investigated when the cylinder piston position is fixed, and when it is free to move.

4.1   Introduction

Actuator force control is a fundamental part of robotic control techniques and when combined with dynamic equations of motion for the robot enables accurate position control. These robotic dynamic equations of motion can be formulated by several methods, the two most common methods are the application *of Newton and Euler laws* and formulation of *Lagrange's equations of motion* (**Tsai 1999**).

The Newton and Euler method creates equations for each body of a mechanical system, detailing both applied and constrained forces. The constrained forces can be eliminated through consideration of the robot geometry, revealing the equations of motion.

Lagrange's equations of motion eliminate the forces of constraint at the outset, although reconstruction of these forces may be required (in situations such as robot design). This method has been employed by many authors e.g. (**Sicilano 2000, McCormick and Schwartz 1993, Anderson and Spong 1988**). The Lagrangian approach will be considered here on the assumption that the applied forces are well within the robot's operating range. These dynamic equations of motion take the form:

$$M_r(\theta)\ddot{\theta} + V_r(\theta,\dot{\theta}) + G_r(\theta) = \tau - \tau_{ext} \tag{4.1}$$

where M_r = inertial matrix, which is a function of position, V_r = vector of Coriolis and centrifugal generalised forces, G_r = vector of gravitational forces, θ = vector of

joint positions, τ = vector of actuator torque, τ_{ext} = vector of externally applied link torque.

This equation describes how the robot position can be controlled through manipulation of the actuator force, however, difficulties arise generating the desired force during actuator motion. The majority of robots are based upon DC motor actuators, for which torque output is proportional to current (**Bradley 1994**), i.e. :

$$T_m = k_m I_m \tag{4.2}$$

where T_m = torque from motor, k_m = proportional constant, I_m = motor current.

During motion, the motor coils are moving relative to the magnetic field inducing a voltage within them (back EMF). The back EMF reduces the overall voltage supplied to the motor, reducing the current, and hence decreasing the torque supplied by the motor. Control of the applied current through manipulation of supplied voltage allows accurate torque to be supplied by the motor during motion. Many researchers control DC motor based robotic systems using this torque control method (**Chang and Lee 1999, Guldner 1992**).

Controlling the torque supplied by pneumatic actuators is more complex as a result of non-linear fluid flow effects, stiction, and changes in the pneumatic chamber volume during motion. Fixing the position of the pneumatic actuator removes a large proportion of the non-linear effects, simplifying force control.

4.2   Fixed position force control

With the cylinder piston position fixed, the electro-pneumatic valves supply a constant volume with air. The electro-pneumatic valves have within them analogue circuitry that regulates the output pressure to be proportional to input voltage. Analysis of these valves (Chapter 5) results in an accurate model of the valve behaviour. If the bandwidth of the transient response is considered to be large, then the valves can be considered to behave as a single gain (a conversion factor between voltage input and pressure output). When combined with a pneumatic cylinder, the voltage input can be considered proportional to the cylinder piston force output, thus enabling force control without feedback (open-loop control).

Open-loop control is the simplest way to control any device utilising no feedback paths, relying on an accurate prediction of the output response for any given input (figure 4.1).   In many situations, such as pneumatic position control, applying accurate open-loop control is practically impossible due to the difficulty predicting the system behaviour.
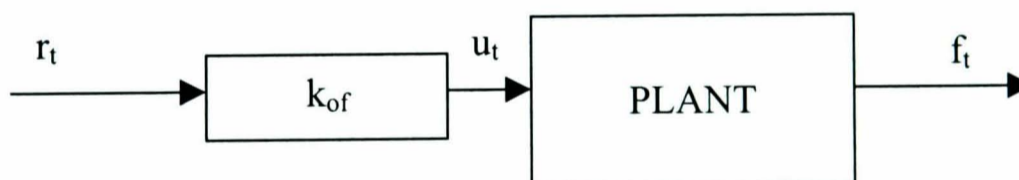
Figure 4.1 Open-loop force control block diagram

where r_t is the demand force, u_t is the control signal, f_t is the output force and k_{of} is the open loop controller gain.

The analysis of the twin electro-pneumatic valves and pneumatic cylinder system has shown them to produce 43.56N when 1V is applied (Chapter 5). Therefore, the required open loop gain (k_{of}) can be calculated to be 1/43.56 = 0.023 V/N. (Note that although open-loop demand signals are applied to the valve, the system cannot be considered completely open-loop due to analogue pressure regulation within the valves themselves).

The fixed position test rig (Chapter 2) enables pressures to be supplied to the pneumatic cylinder without cylinder movement. A force sensor measures the force output from the cylinder. Open-loop force control for a step response between 20N and 40N demonstrates that the desired force is accurately tracked (figure 4.2). Pressure sensors for both chambers, measure the respective chamber pressure from which the force generated within the cylinder can be reconstructed (see section 2.5). The force generated within the cylinder (the calculated force in figure 4.2) closely matches the measured output force. The control signal to generate this response is also shown in figure 4.2. Note that the output force does not influence the open-loop control signal.
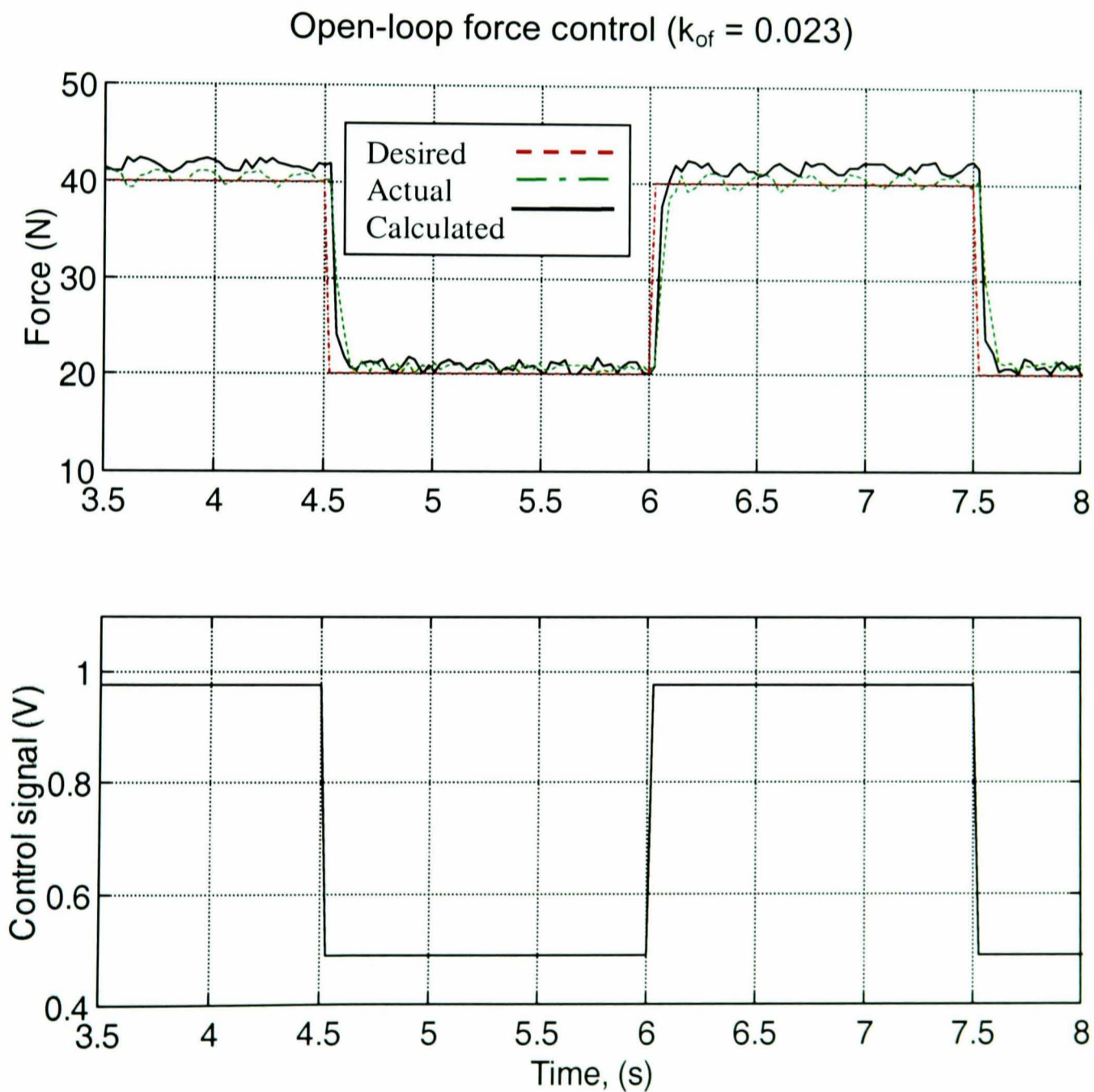
Figure 4.2 *Open loop force control experimental response*

One of the limiting factors when controlling pneumatic cylinder has been identified as airflow saturation (**Lui and Bobrow 1988**). Airflow is dependent on pressures either side of an orifice, and at a certain pressure differential the flow of air saturates (see chapter 5). This saturation of airflow severely limits the available performance of pneumatic systems. Indeed, it is the saturation of the airflow that limits the rise time of the open-loop force controller.

Applications for fixed position force control are extremely limited, indeed this is reflected in the lack of published literature, on the other hand force control during motion is used widely for controlling robotic systems. During motion the force output of pneumatic cylinders is more complex as a result of a variety of effects, such as changes in cylinder volume. The next section examines force control of a pneumatic cylinder during piston motion.

4.3 Force control during cylinder motion

Several researchers have developed models of pneumatic cylinder force output, during piston motion, for conventional cylinder and spool valve configurations. This knowledge of actuator torque during motion is necessary for any robotic force control operation and bridges the gap between standard torque input controllers (as mentioned in the introduction) and pneumatic robots.

4.3.1 Spool valve torque subsystem

A mathematical model can be developed to predict the pressure, in a pneumatic cylinder chamber, for a spool valve and conventional pneumatic cylinder configuration (**Wang et al. 1999 & Gross and Rattan 1998**).

For chamber A:

$$\dot{P}_a = \frac{\gamma R T_s}{V_{ai}} \left(-\frac{A_a P_{ai}}{R T_s} \dot{x}_{cyl} + \dot{m}_a \right) \qquad (4.3)$$

where P_{ai} is the pressure linearised around an operating point, V_{ai} is the volume linearised around an operating point and x_{cyl} is the cylinder position.

If the spool orifice area is X_{sp}, then the standard equation for mass flow through an orifice (chapter 5 equation 5.2) becomes

$$\dot{m}_a = c_q c_{mp} X_{sp} \frac{P_s}{\sqrt{T_s}} \qquad (4.4)$$

Many researchers assume current input into a spool valve is proportional to orifice opening (**Wang et al. 1999, Noritsugu & Takaiwa 1995, Bobrow and Jabbari 1991**)

If the spool valve is linearised around an operating point, spool current can be assumed to be proportional to orifice area[1]. Assuming the supply pressure and temperature to be constant, and sonic airflow, the mass flow rate becomes proportional to current:

$$\dot{m}_a = c_i . i_s \qquad (4.5)$$

where c_i is the coefficient of proportionality and i_s is the spool current.

Combining equation 4.5 with equation 4.3, results in an equation for change in pressure with the cylinder chamber, as:

$$\dot{P}_a = \frac{\gamma R T_s}{V_{ai}} \left(-\frac{A_a P_{ai}}{R T_s} \dot{x} + c_i i_s \right) \qquad (4.6)$$

---

[1] **Bobrow and McDonell (1998)** are critical of the assumption that spool current can be assumed proportional to mass flow rate. They state that the assumption of perfect orifice flow (eq[n] 5.14) is incorrect, preferring to identify quadratic non-linear relationships between current and mass flow for supplying and exhausting fluid.

This simplified equation, combined with a similar equation for chamber B, are the basis for a pneumatic torque model (**Bobrow and McDonell 1998, Tzafestas 1997, Guilhard and Gorce 1999**), given by:

$$\dot{f}_c = J_m.i_s - B_m.f_c - E_m.\dot{x}_{cyl} \tag{4.7}$$

where f_c is the cylinder output force, J_m, B_m and E_m are all coefficients to be identified experimentally.

4.3.2 Electro-pneumatic valve force subsystem

A similar derivation can be performed using the two pressure proportional valves and cylinder arrangement used within this research.

Equation 4.3 remains the same, however the mass flow rate is now controlled by the electro–pneumatic proportional valves. These valves have analogue circuitry to regulate the pressure within each cylinder chamber. If these valves behaved ideally, they would maintain constant pressure within each chamber, through control of the mass flow rate, during changes in chamber volume. The constant pressure results in constant force output, hence, movement of the cylinder would have no effect on force output.

A model can be experimentally identified to predict the cylinder force output during motion. The position control test rig (chapter 2) enables cylinder output force to be measured during pneumatic cylinder motion. Applying the open-loop force controller to apply a sinusoidal force while external forces move the cylinder, enables the force and position relationship of the pneumatic actuator to be identified.

Figure 4.3 shows force output of the pneumatic cylinder piston while undergoing the velocity shown in figure 4.4. Upon examining these graphs a proportional relationship between errors in actuator force output and actuator velocity is apparent.

Cylinder force output during motion

Actuator force (N)

Desired force output - - - - - - -
Experimental force output —

Time, t (s)
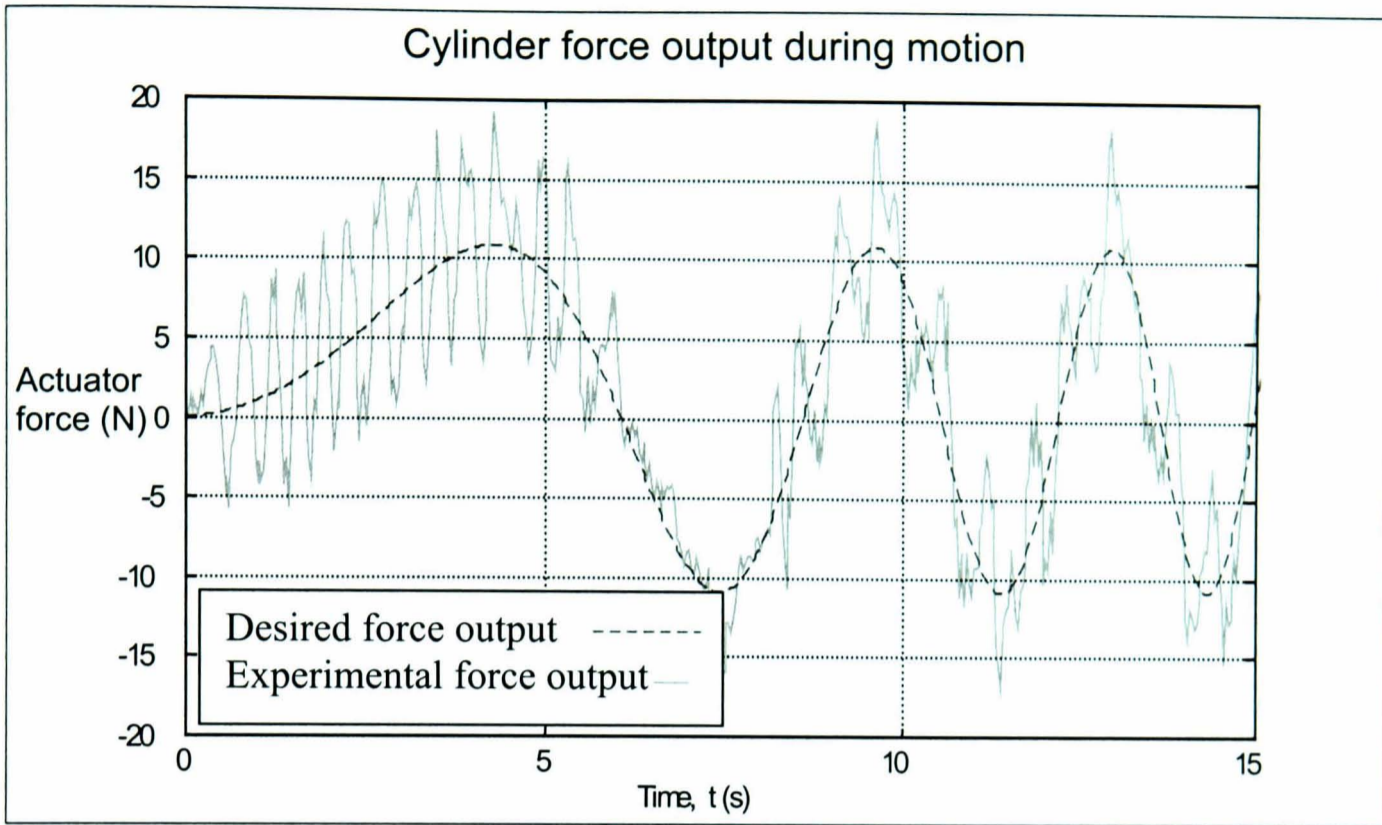
Figure 4.3 *Experimental force output during cylinder motion*
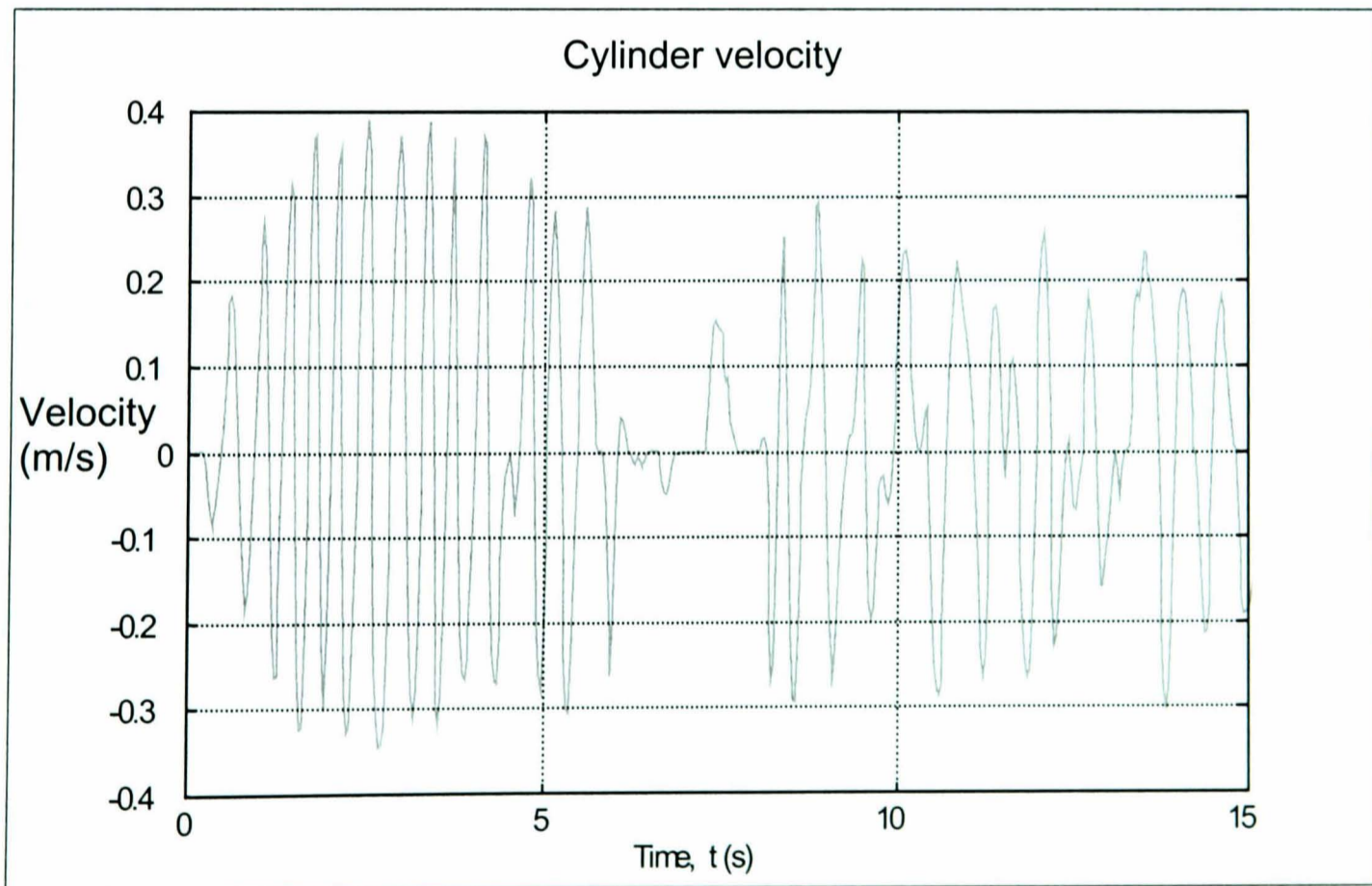
Cylinder velocity

Velocity (m/s)

Time, t (s)

Figure 4.4 *Cylinder velocity*

So the cylinder force model takes the form:

$$f_c = 1/k_{of} .u_t - D_{cyl} .\dot{x}_{cyl} \tag{4.8}$$

where u_t is the desired force and D_{cyl} is the piston velocity coefficient.

4.3.3 Identification of force subsystem

Applying the least squares identification technique, an estimate of the velocity gain can be obtained. The estimated gain was found to be approximately 23.

So the actuator force model is given by:

$$f_c = 43.56.u_t + 23\dot{x}_{cyl} \tag{4.9}$$

Figure 4.5 shows the force output from this model, alongside the actual force output and the predicted force output reconstructed from pressure readings. The forces applied to the piston caused movement of approximately 50mm.
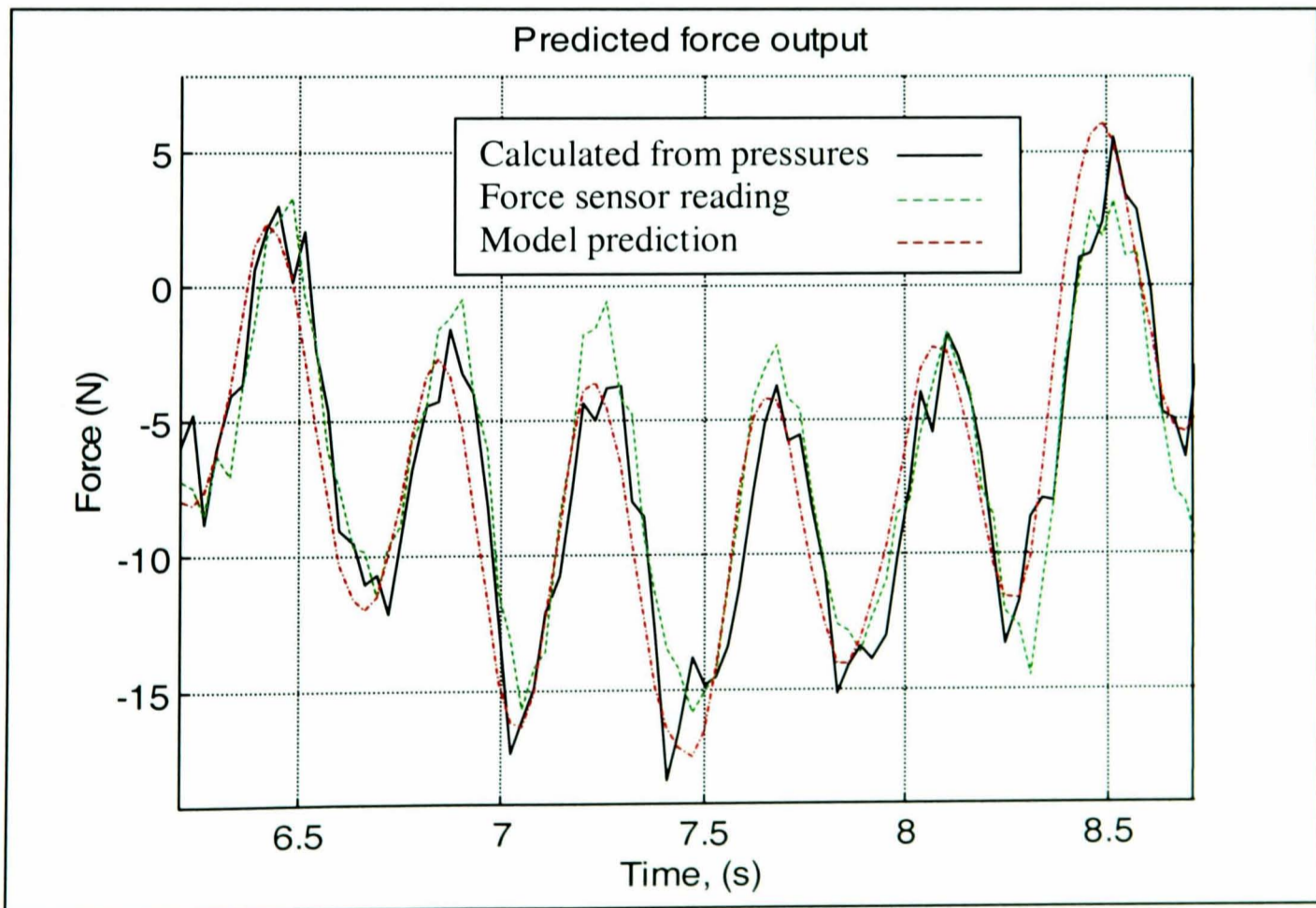

Figure 4.5 Force output

The model accurately predicts the force output of the pneumatic cylinder, however, the velocity coefficient varies between sessions and would need to be identified at the commencement of each session to ensure accurate force prediction.

4.4 Discussion and conclusions

Force control of a pneumatic cylinder has been investigated when the cylinder piston is fully constrained (fixed position) and during piston motion.

With the position fixed, the volume of the pneumatic cylinder chambers remains constant for any pressure difference across the cylinder. Under these constant volume conditions, an open-loop force controller has been demonstrated to provide accurate force control.

Several researchers, using conventional spool valve and cylinder configurations, have examined the force output of pneumatic cylinders during motion. They derived a 'torque subsystem' which is a mathematical connection between factors such as velocity and change in force. This torque subsystem enables the use of force based controllers which have been well developed for use with electric motors.

Modifying the open-loop force model with an experimentally identified velocity coefficient provides an accurate prediction of cylinder force output during motion. This 'torque subsystem' could be used to implement standard robotic torque control systems. Experimentally implementing the pneumatic torque subsystem would enable assessment of low friction pneumatic actuators and electro-pneumatic valves for general robotic applications.

Chapter 5

Modelling and simulation

This chapter develops mathematical models of the robot and actuator configuration.
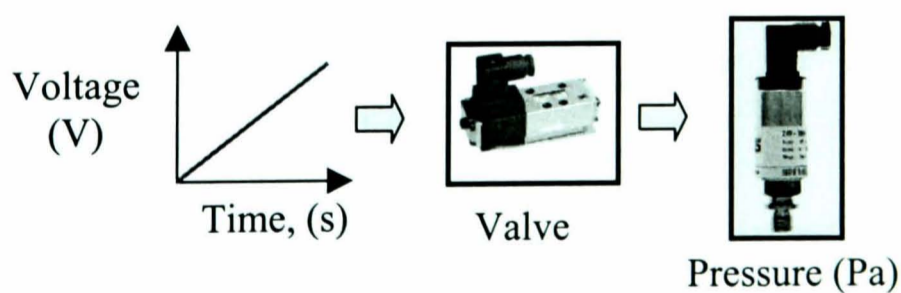
5.1   Introduction

The robot and actuator system can be modelled by three main elements: the pneumatic valves; pneumatic cylinders; and the robot (figure 5.1). The analysis of the overall system will begin by analysing the electro-pneumatic valve (section 5.2) from which models of the valve, cylinder (section 5.3) and entire robot (section 5.3) will be developed.

5.2   Electro-pneumatic valves

The electro-pneumatic valves convert control voltages into pressure outputs. The manufactures literature states that pressure output is proportional to the input voltage. Several tests were performed to assess the performance of the valves.

5.2.1   Proportional test

To evaluate the valves proportional response, a ramp voltage input was applied while measuring the pressure output using a pressure transducer (figure 5.2).

Figure 5.2 *Measuring pneumatic valve proportionality*

Control signal (V)

Electro-pneumatic
proportional valves
(section 5.2)

Pressure (Pa)

Low   friction
pneumatic
cylinder
(section 5.3)

Force (N)

Prototype
robot
(section 5.3)

Force (N) &
Position (m)
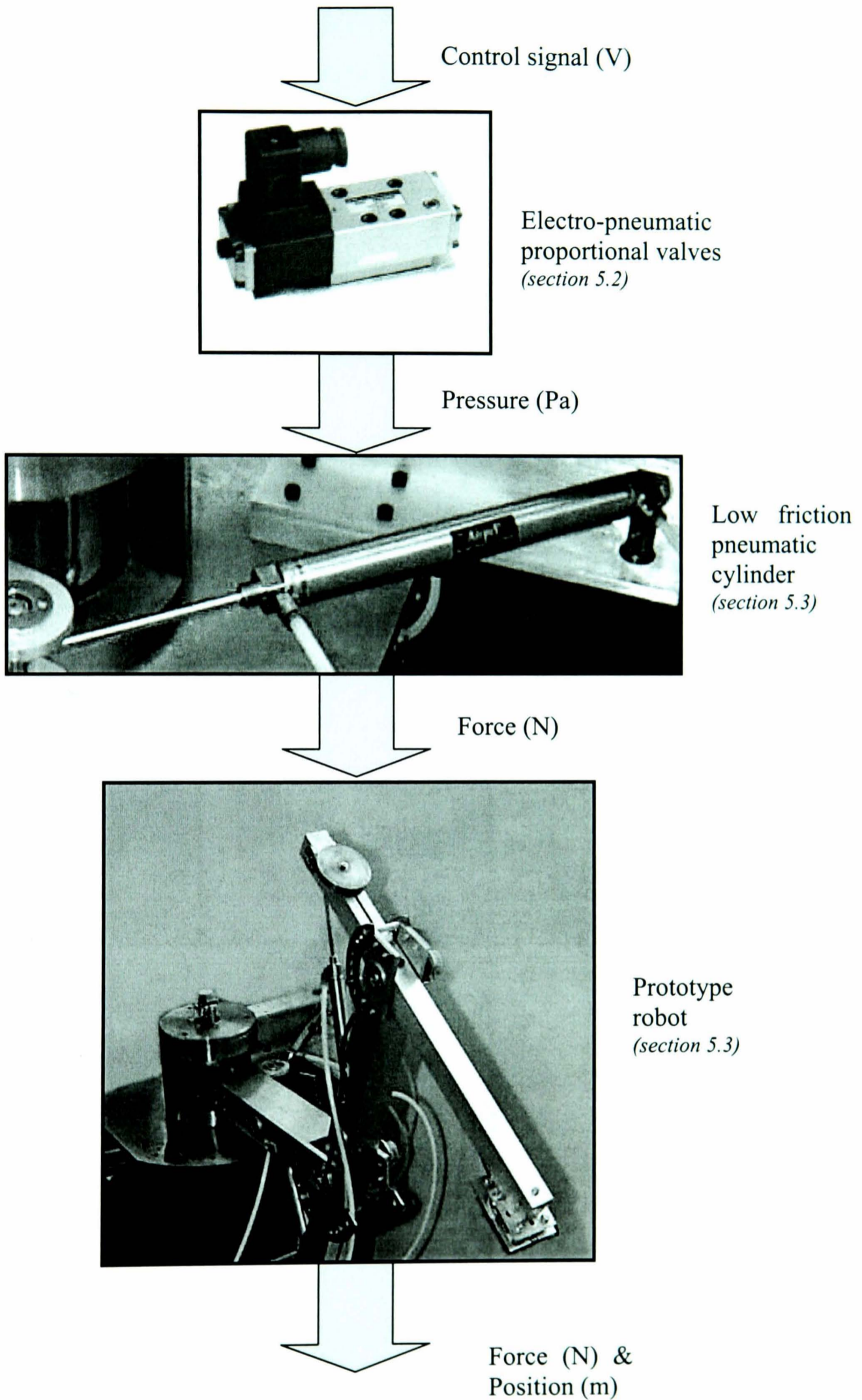
Figure 5.1 *Components of the pneumatic robot*

The experimental results of the proportional test (figure 5.3) show that shortly after the 1V valve turn on voltage, changes in input voltage are proportional to changes in the pressure output. The proportional relationship is maintained until approximately 4 bar (the supply pressure at time of testing).
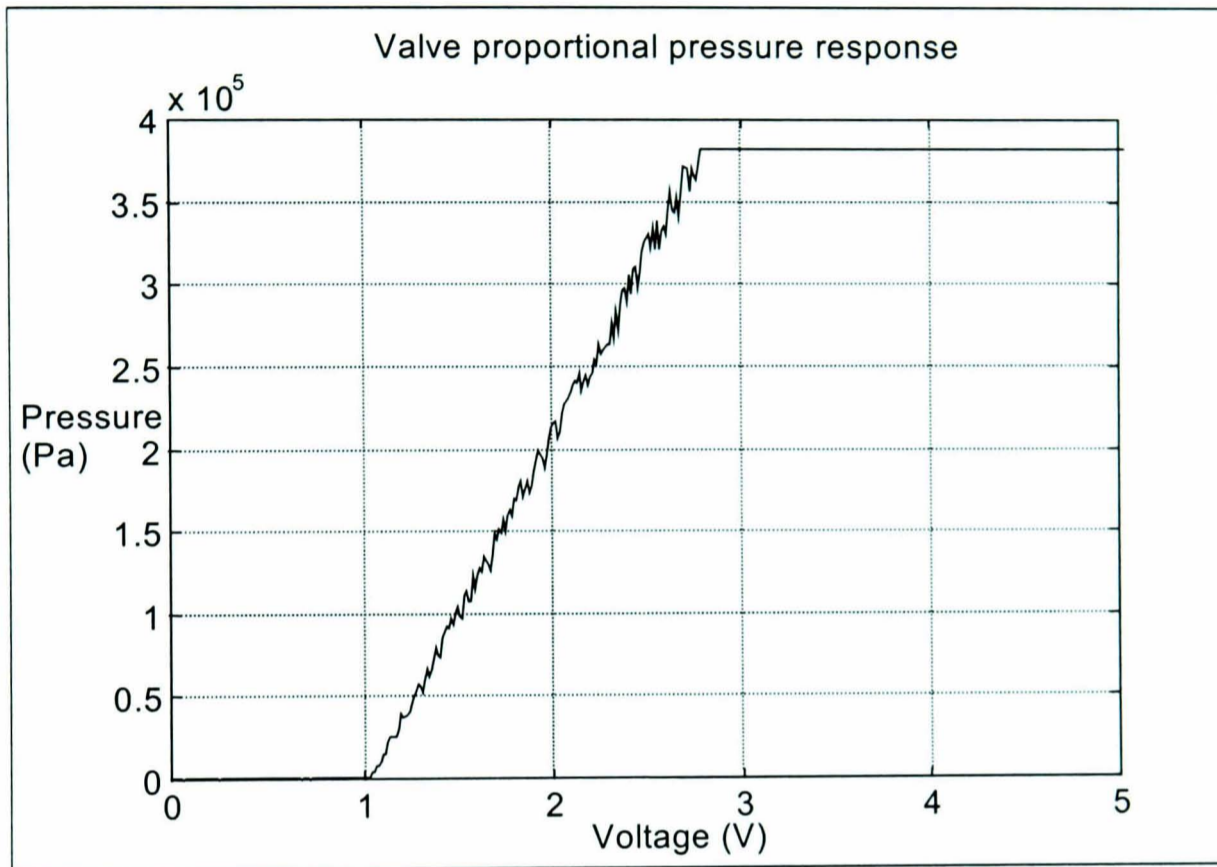
Figure 5.3   Valve proportional pressure response

The valve pressure response was found to be described by the following equation:

$$P_d = (V_i - 1) * 2.2 \times 10^5 + 1 \times 10^5 \qquad\qquad (5.1)$$

where P_d is the pressure output (abs[1]) and V_i is the voltage input.

5.2.2   Step test

Underlying non-linearities within the pressure response are revealed by the valve step response. The valve pressure output was directly connected to one chamber of the pneumatic cylinder (figure 5.4). Movement of the cylinder piston was prevented by

---

[1] Absolute (abs) air pressure includes the atmospheric air pressure (1×10^5 Pa) in the pressure reading.

the screwed bar of the force control test rig (chapter 2). The cylinder chamber provides a volume into which air is to be supplied, enabling an accurate assessment of the valve response under normal operating conditions.

A voltage step between 2.25V and 2.75V was applied to the pneumatic valves. The step response was compared to the response predicted by equation (5.1) is shown in figure 5.5, revealing non-linearities and dynamic behaviour in the response.
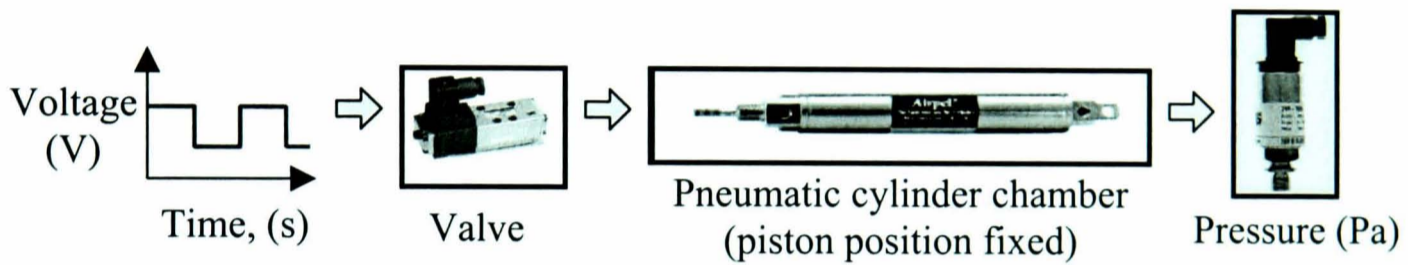
Figure 5.4 *Measuring pneumatic valve step response*
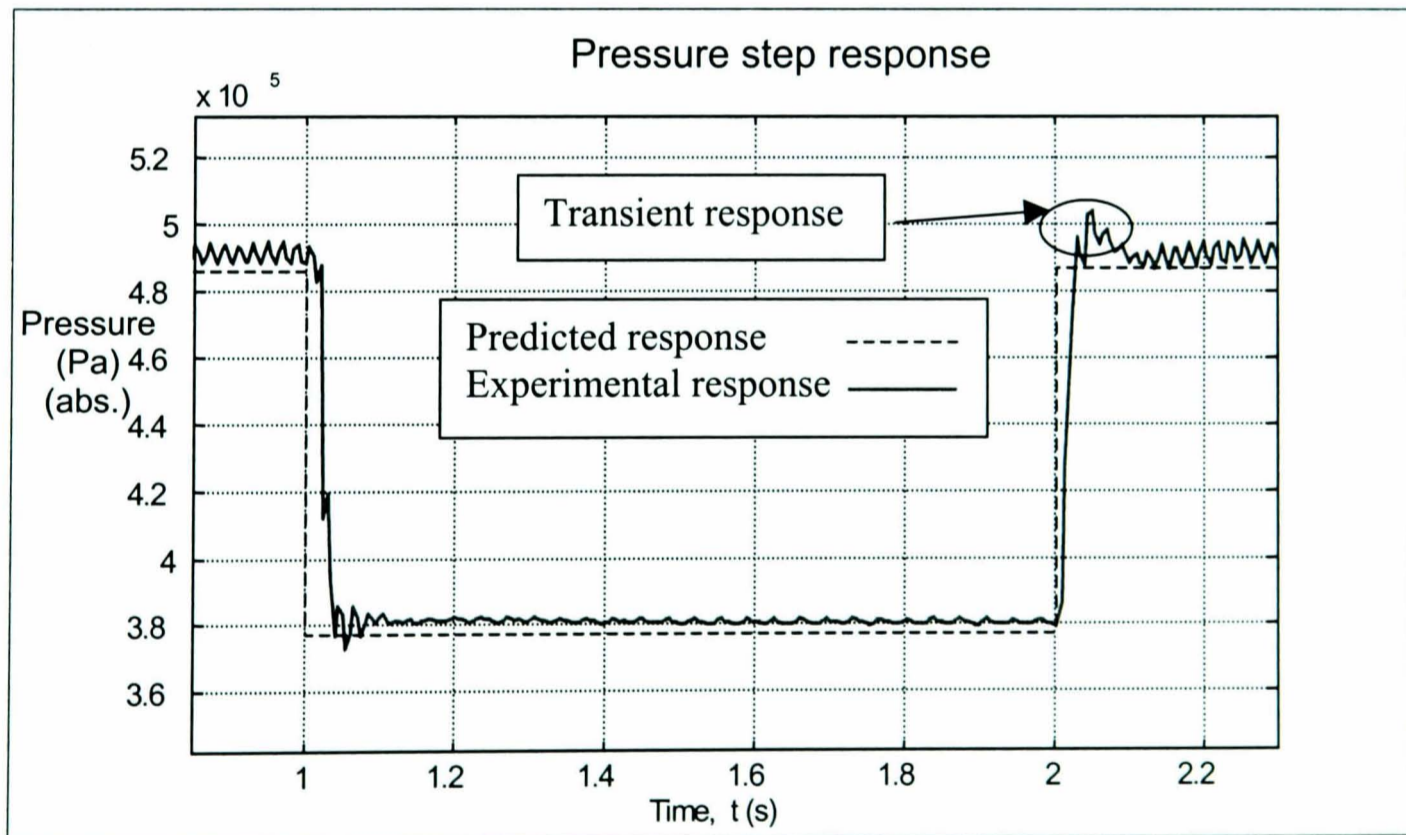
**Figure 5.5** *Experimental pressure step response*

Slight overshoot and a delay in response degrade the performance of the valves. A mathematical model of the valves was therefore constructed to ensure that these effects can be predicted.

5.2.3   Modelling of pneumatic valves

Examining the structure of the valve (figure 5.6), a controlled pilot stage supplies pressure proportional to voltage into a small volume. The pressure differential between the pilot or desired pressure (P_d) and output pressure (P_a) moves the spool, which in turn operates the poppet valves.

where F_s is the force on spool, P_r is the exhaust pressure (abs), x_s is the displacement of spool and P_s is the supply pressure.

This structure can be illustrated by examining a photograph of the valve cross section (figure 5.7).
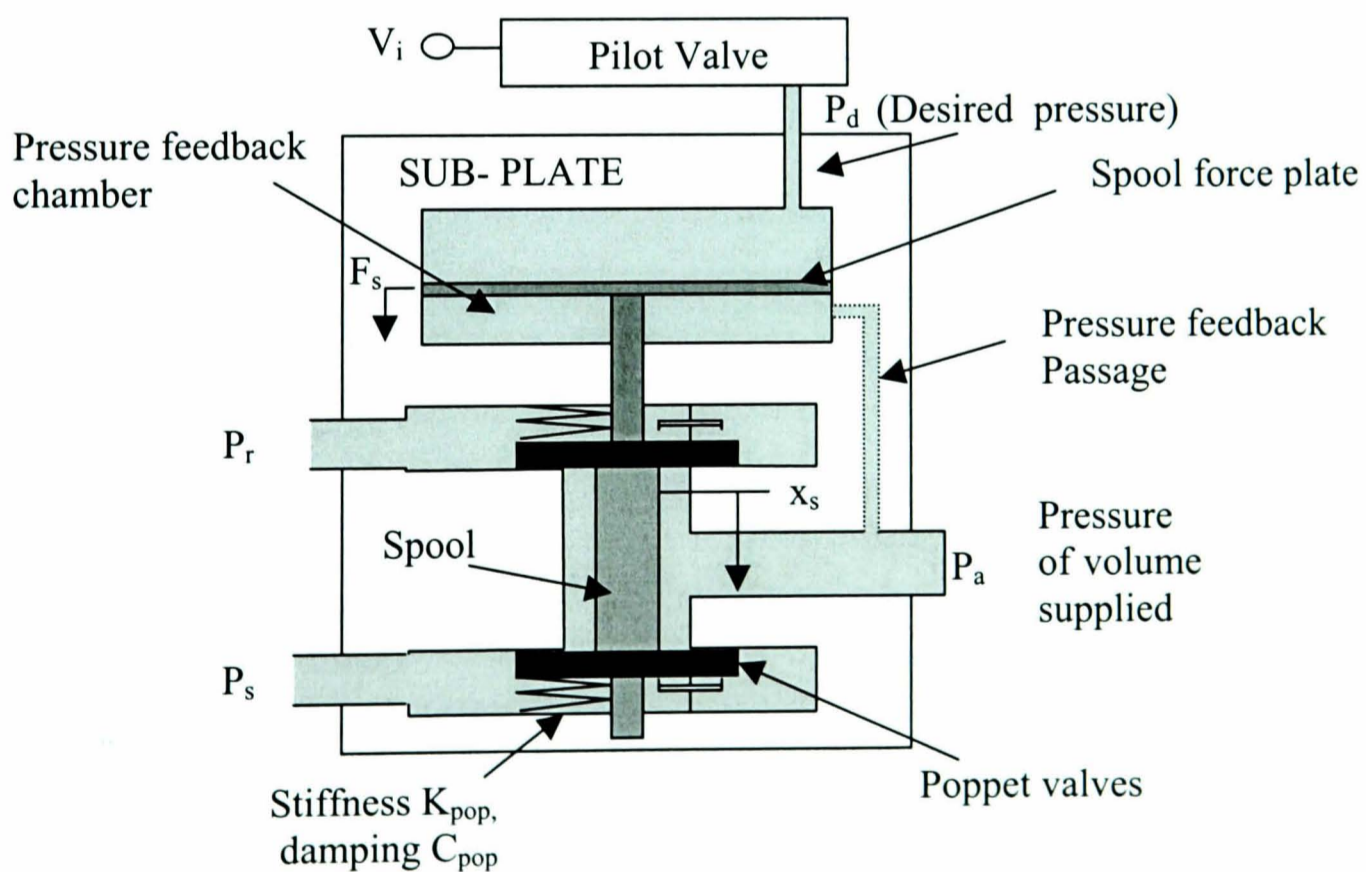
Figure 5.6 *Operation of pneumatic valve*
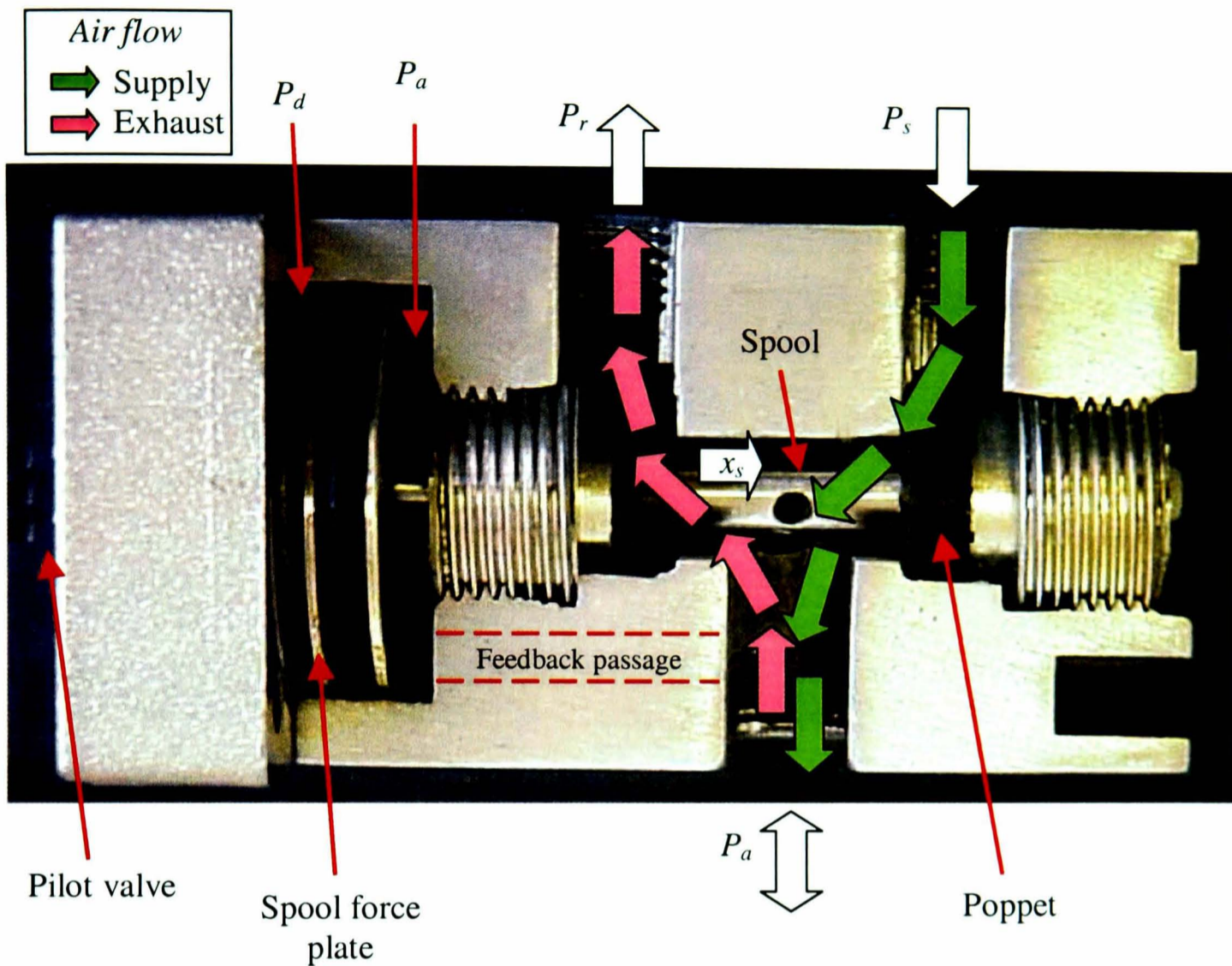
Figure 5.7 *Cross section of pneumatic valve*

Several assumptions were made to simplify the mathematical model:

- The pressure feedback passage and chamber are always at the same pressure as the output pressure (P_a)

- The desired pilot pressure (P_d) can be generated instantly on specific demand voltage, behaving as predicted by equation (5.1).

- The air has the properties of an ideal gas

- Adiabatic conditions [2]

---

[2] Adiabatic conditions assume that no energy exchange occurs from the fluid to the surroundings. An alternative would be to assume isothermal conditions, where changes in pressure and volume incur no change in temperature. The actual system behaviour is a combination of both these behaviours (**Backe and Ohligschlager 1989**).

The pneumatic valve controls the flow of air by varying the gap between the poppets and subplate, effectively varying the area of an orifice. The equation for mass flow through an orifice is well known:

$$\dot{m}_a = c_q c_{mp1} a \frac{P_s}{\sqrt{T_s}}$$ (5.2)

where c_q is based upon the valve type, in this case $c_q = 0.9$ (Poppet valve), T_s is the supply pressure temperature, a is orifice area and c_{mp1} is a non-linear term based upon pressures either side of the orifice. The coefficient c_{mp1} can be calculated using the complex equation:

$$c_{mp1} = \sqrt{\frac{2.8}{R(\gamma - 1)} \left(\left(\frac{P_a}{P_s} \right)^{\frac{2}{\gamma}} - \left(\frac{P_a}{P_s} \right)^{\left(\frac{\gamma+1}{\gamma} \right)} \right)}$$ (5.3)

where R is the gas constant for air, P_a is the down stream and γ is the specific heat ratio.

An easier way to understand this equation is to draw a graph of c_{mp1} against the pressure difference across the orifice (P_a/P_s) (figure 5.8).
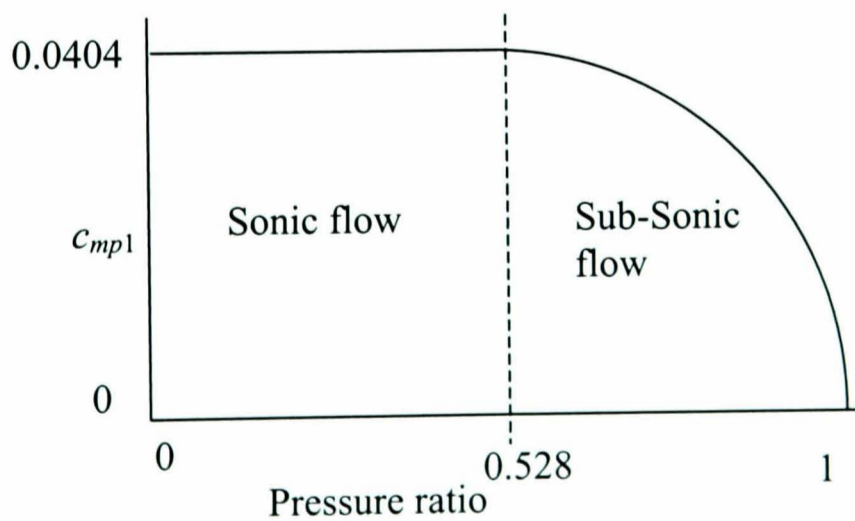
Figure 5.8 *Variation of c_{mp1} with pressure ratio*

Two distinct regions of airflow exist: sonic and sub-sonic. The maximum mass flow rate occurs during sonic airflow, for which increases in pressure difference offer no increase in the mass flow rate. During subsonic flow the mass flow rate is a function of the pressure differential.

Examining the air flow for one of the poppets:

The orifice area, a, is given as:

$$a = k_c x_{p1}$$

(5.4)

where k_c is the poppet circumference and x_{p1} is the poppet displacement. Combining (5.2) & (5.4) gives:

$$\dot{m}_a = c_q c_{mp1} k_c x_{p1} \frac{P_s}{\sqrt{T_s}}$$

(5.5)

Equation (5.5) predicts the mass flow rate as a function of poppet displacement. This displacement is dependent upon the force applied by the spool.

The force generated on the spool is given by:

$$(P_d - P_a)E = F_s$$

(5.6)

where E is the spool force plate area and F_s is the force applied to the spool. Note that poppet and spool inertia is assumed to be negligible along with differences in spool force plate area.

Predicting the behaviour of the poppets from knowledge of the spool position is not as simple as at first it may seem. The spool does not necessarily maintain contact with the poppet, so their displacements cannot be assumed equal. A simplified model of the poppet and spool arrangement develops this idea further (figure 5.9). It can be seen that it is the spool force, rather than position, that effects poppet behaviour.
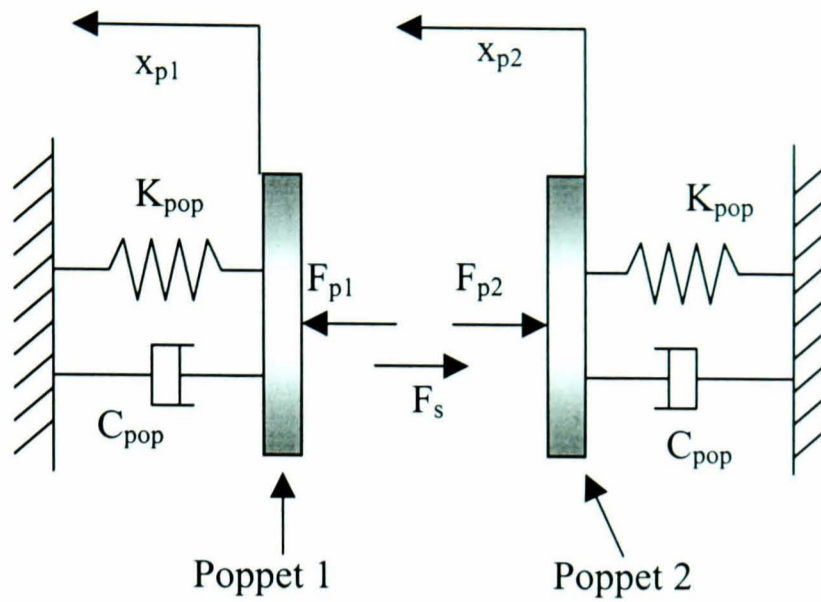
Figure 5.9 *Simplified valve arrangement*

Due to small amounts of stiction and spring pre-load, small forces are not sufficient to cause poppet motion. The force required to move each poppet was experimentally approximated to be 1N.

Since the spool is never in contact with both poppets at the same time, the force transmitted by the spool to the poppets can be obtained from a simple set of rules:

if $|F_s| < 1$ then $F_{p1} = 0$ and $F_{p2} = 0$ \hfill (5.7)

if $F_s \leq -1$ then $F_{p1} = F_s$ and $F_{p2} = 0$ \hfill (5.8)

if $F_s \geq 1$ then $F_{p1} = 0$ and $F_{p2} = F_s$ \hfill (5.9)

where F_{p1} & F_{p2} are the forces applied to poppets 1 & 2 respectively.

Hence from figure 5.8 the motion of, for example, poppet 2 is given by:

if $F_s \geq 1$ $\qquad x_{p2} = \dfrac{F_s}{C_{pop}s + K_{pop}}$ \hfill (5.10)

if $F_s \leq 1$ $\qquad x_{p2}(C_{pop}s + K_{pop}) = 0$ \hfill (5.11)

where C_{pop} is the poppet damping coefficient and K_{pop} is the poppet stiffness.

The pressure within the pneumatic cylinder chamber is dependent on factors such as temperature and volume.

Assuming adiabatic conditions the change in energy due to mass transport, as detailed by **Ben-Dov and Salcudean (1995)**, takes the form:

$$\frac{d}{dt}(c_v.\rho.V_a.T_a) = \dot{m}_a.c_p.T_a - P_a.\dot{V}_a \tag{5.12}$$

where ρ is the density of air and T_a is the temperature of air in chamber A, c_p is the specific heat of air at constant pressure, c_v is the specific heat of air at constant volume and V_a is the volume of chamber A.

Assuming an ideal gas, the density of air in the chamber is given by:

$$\rho = \frac{P_a}{RT_a} \tag{5.13}$$

Remember that the actuator is fixed at this modelling stage, so V_a is constant. Combining equation 5.13 with equation 5.12 and reducing, results in an equation relating the mass flow rate and change in pressure, thus:

$$\dot{m}_a = \frac{V_a}{\gamma RT_a} \dot{P}_a \tag{5.14}$$

We now have an equation to predict the change in pressure for any given mass flow rate. The total mass flow rate into the chamber is the sum of the mass flow rates from both poppets (mass leaving chamber is considered as negative mass flow rate).

From equation (5.5) we then have:

$$\dot{m}_a = \frac{c_q k_c}{\sqrt{T_s}}(x_{p1}P_s c_{mp1} - x_{p2}P_a c_{mp2}) \tag{5.15}$$

where c_{mp2} is the mass flow rate coefficient for poppet 2.

Hence, by combining equations (5.14) & (5.15) and rearranging (assuming $T_a = T_s$) we have a model for $\dot{P}_a$ given by:

$$\dot{P}_a = \frac{\gamma R c_q k_c \sqrt{T_s}}{V_a}(x_{p1} P_s c_{mp1} - x_{p2} P_a c_{mp2})$$
(5.16)

To summarise, the pilot valve pressure responds to the input voltage (eq^n 5.1). The pressure differential between the pilot pressure (desired) and the actual pressure creates forces on the spool valve plate (eq^n 5.8). This force is applied to the one of the poppet valves (eq^n 5.7, 5.8, 5.9, 5.10, 5.11) depending upon whether the valve is to exhaust or supply air. The flow of air into the volume dictates the pressure within the volume and is dependent on the orifice areas as a result of the poppet displacements (eq^n 5.16).

One more factor needs to be considered before the model is complete. The maximum mass flow through the valves is dictated by saturation at maximum orifice opening. In the experimental rig, this saturation effect is more severe as a result of the area of the interconnecting pipes, which is less than the maximum valve area. The resulting saturation equation becomes:

$$a = \begin{cases} a & a < a_{pipe} \\ a_{pipe} & a \geq a_{pipe} \end{cases}$$
(5.17)

i.e the orifice opening area (5.17) is restricted to the pipe area a_{pipe}

5.2.4 Pneumatic valve simulation

Using the mathematical equations derived earlier, a simulation of the valve response was created using Matlab/ simulink and is shown in figures 5.10 and 5.11. The simulation enabled comparison of the results obtained experimentally and those predicted by the mathematical analysis. The step response obtained from the valve was compared with the simulated response as shown in figure 5.12.
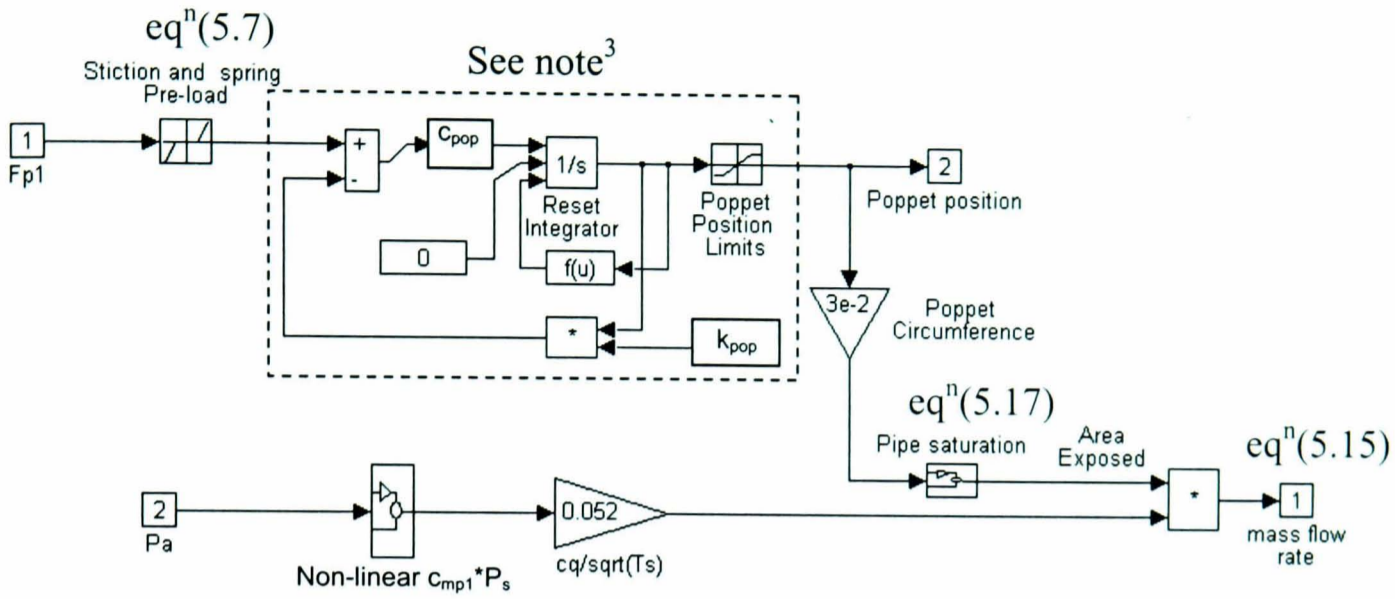
$$eq^n(5.7)$$

Stiction and spring Pre-load

See note[3]

$$eq^n(5.17)$$

Pipe saturation

$$eq^n(5.15)$$

Figure 5.10 Poppet simulation

$$eq^n(5.15)$$

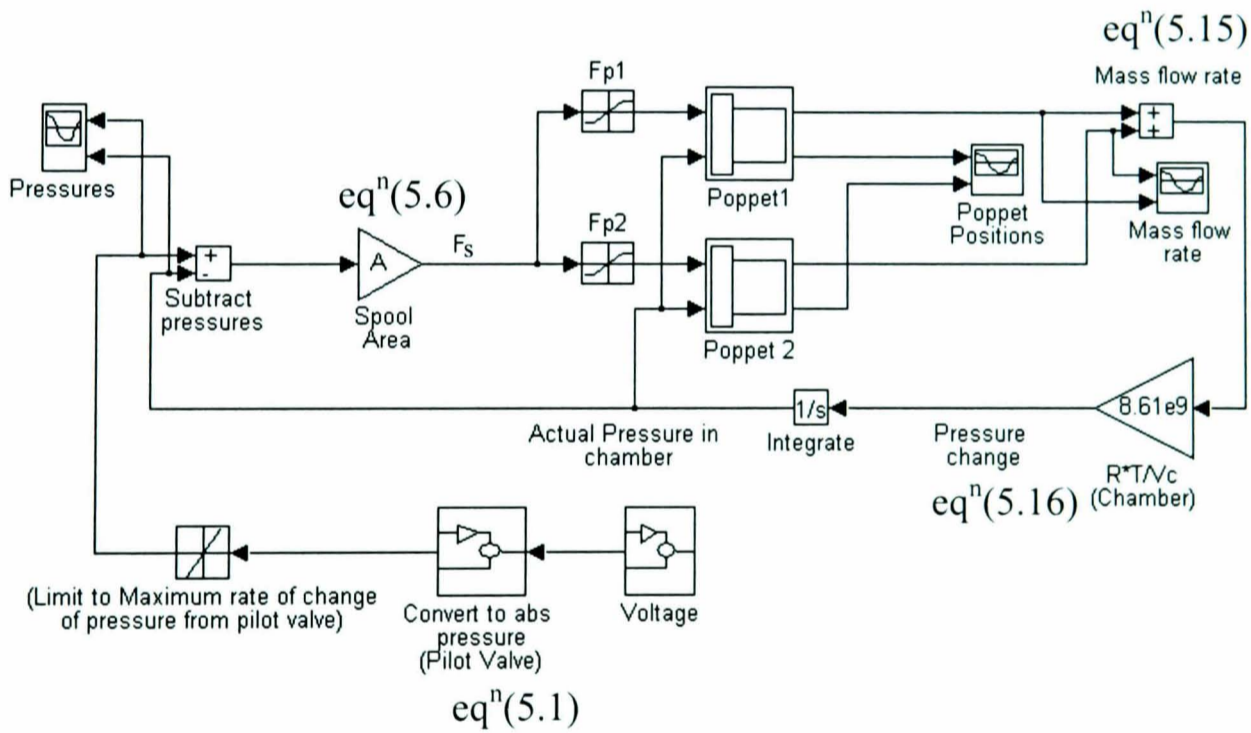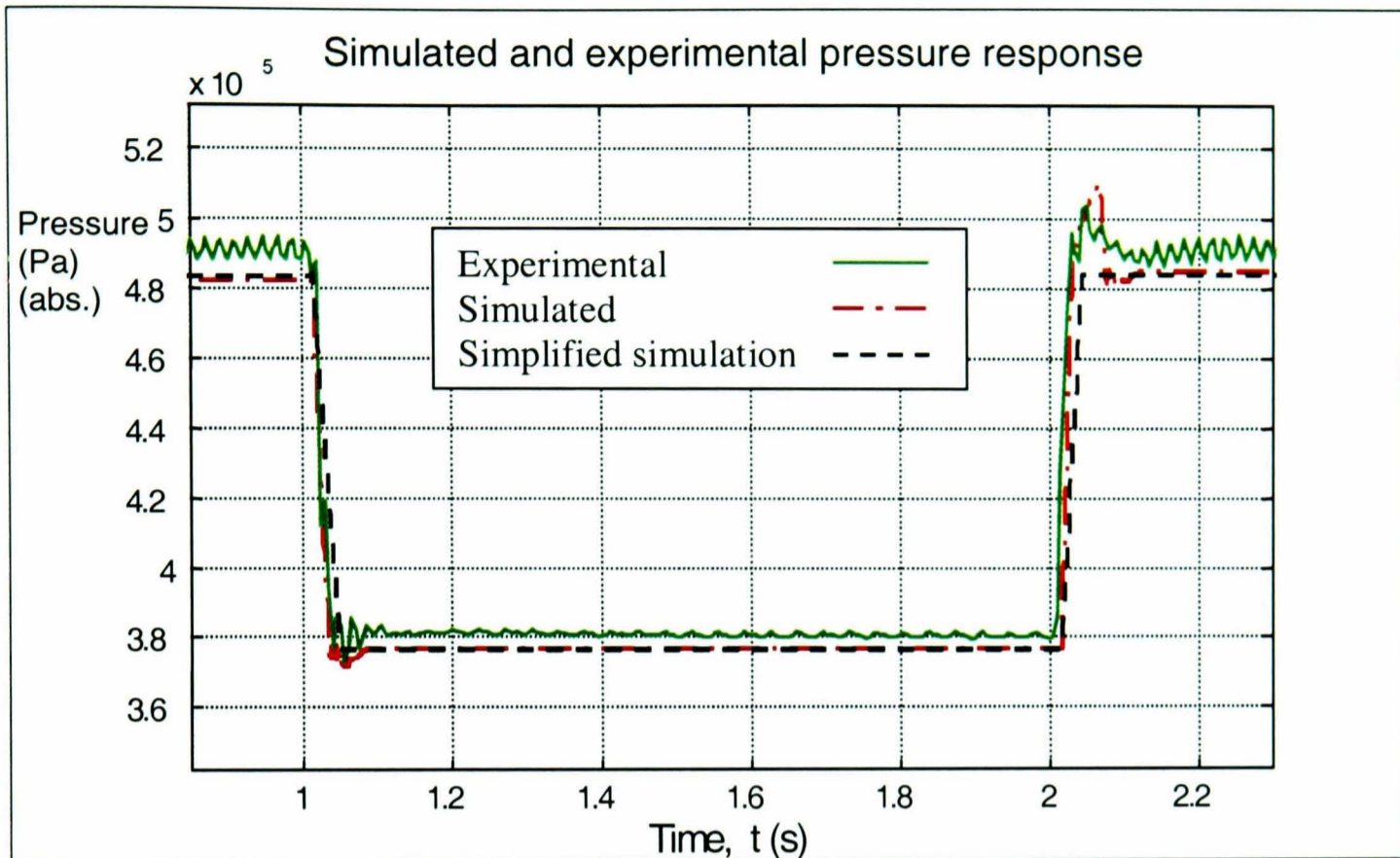$$eq^n(5.6)$$

$$eq^n(5.16)$$

$$eq^n(5.1)$$

Figure 5.11 Valve simulation

---

[3] The dashed region represents the poppet damping and stiffness. The complexity of this block is as a result of the poppet striking its endstop. Use of a saturation block alone to restrict the motion would not prevent force integration. The reset integrator resets upon striking an endstop.

Figure 5.12 *Simulated and experimental pressure response*

The simulated response closely matches the response time, and general shape of the experimental response. It is apparent from inspection that the pressure overshoot for supply is greater than exhaust. This is due to the difference in supply pressure and chamber pressure (P_s and P_a). For example, with the chamber pressure P_a = 4.5 bar (abs.) the maximum mass flow rate for supplying air is 1.5 times larger than the mass flow rate for exhausting air. As both poppets have the same delay in closing, a larger pressure overshoot is created when supplying pressure. Examining the simulated poppet displacements (figure 5.13) at approximately 2s, for a pressure increase, illustrates the valves operation:

1) Poppet 1 opens due to desired pressure being greater than actual pressure
2) Due to overshoot in pressure, poppet 2 opens
3) Poppet 1 closes (lag due to damping)
4) Then poppet 2 closes (again with lag)

(Note that the delay in poppet closing allows both poppets to be open simultaneously).
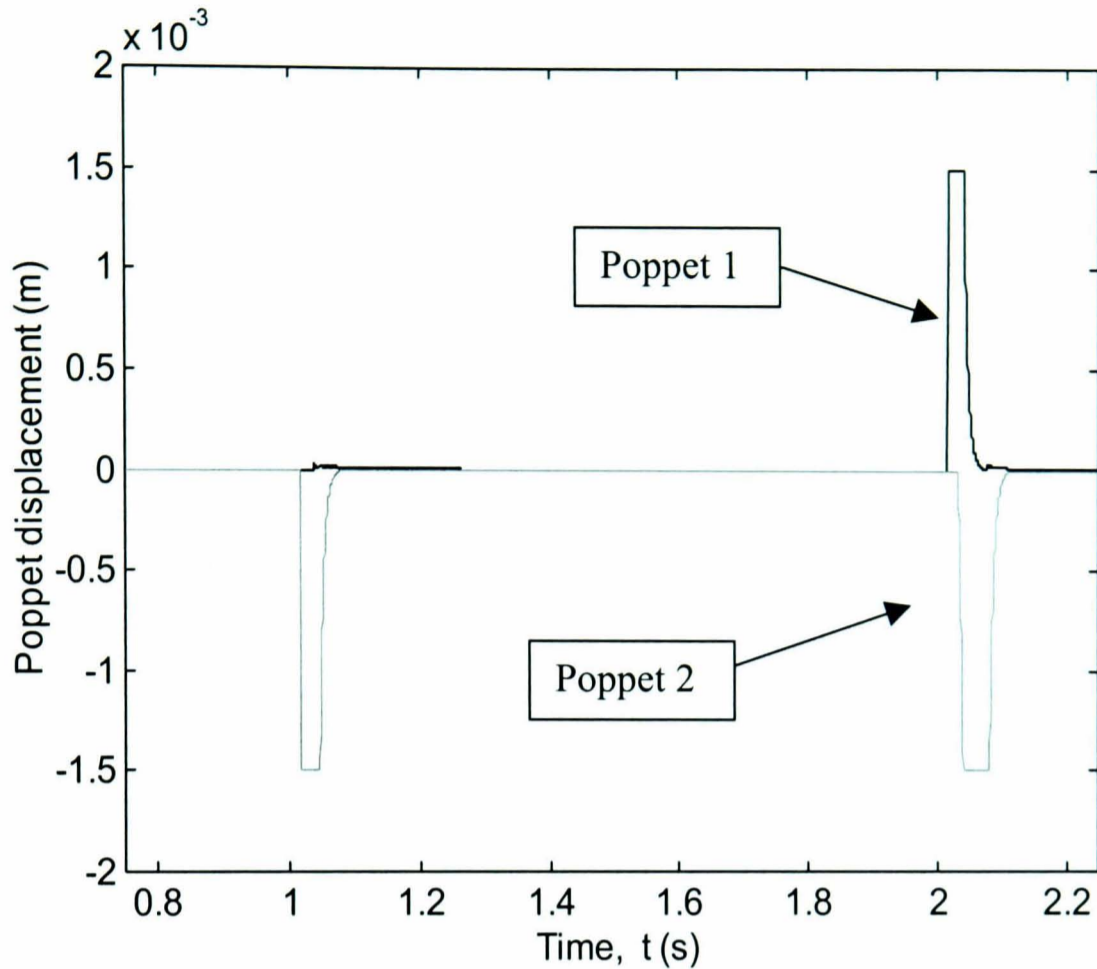
Figure 5.13 *Displacements of poppets*

5.2.5   Simplified valve model

The small pressure overshoot would not have any significant effect when controlling the cylinder due to its bandwidth being much larger than that of the cylinder. This assumption enables the valve model to be simplified by ignoring the poppet damping. For poppet 2, equations (5.10) and (5.11) then become:

if $F_s \geq 1$ $\qquad\qquad x_{p2} = \dfrac{F_s}{K_{pop}}$ $\qquad\qquad\qquad\qquad\qquad$ (5.18)

if $F_s \leq 1$ $\qquad\qquad x_{p2}.K_{pop} = 0$ $\qquad\qquad\qquad\qquad\qquad$ (5.19)

This simplified model was simulated using Matlab (figure 5.14). The steady-state and response times of the simplified model (figure 5.12) are similar to the experimental but the transient peaks have not been modelled.
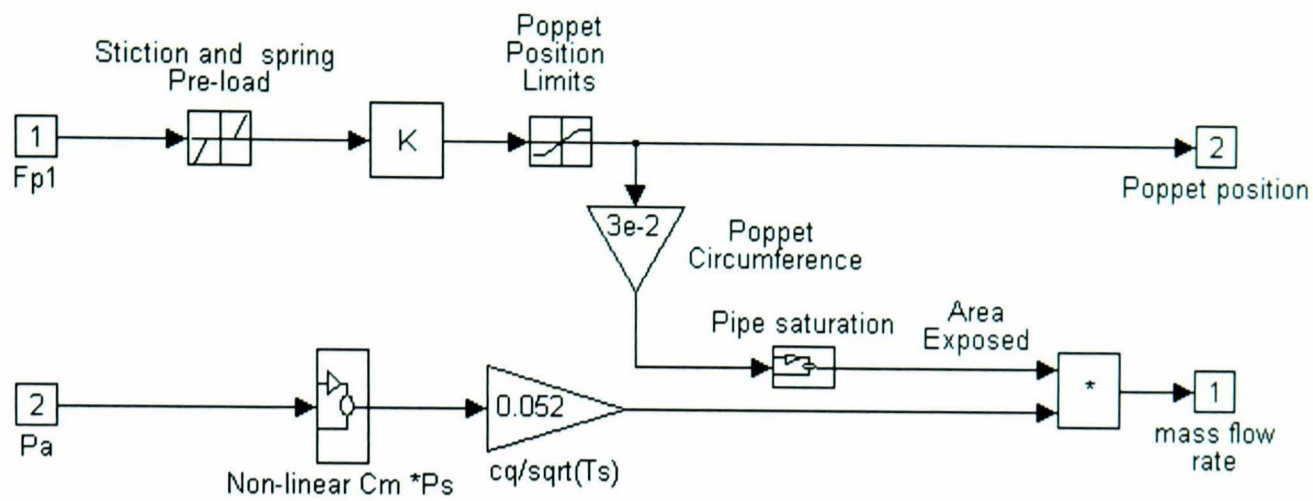
Figure 5.14 *Simplified poppet model*

The simplified model is suitable for inclusion in the overall valve/cylinder model as the bandwidth of the transient peaks is larger than that of the pneumatic cylinder. The simulation of valves and cylinder is the topic of the next section.

5.3 Simulation of valve and cylinder

A mathematical model was constructed for two valves supplying air to both chambers of a pneumatic cylinder based on the work of **Shearer (1956)** and **Lui et al. (1988)**. The difference between modelling the pressures within a fixed volume (as modelled in the previous section) and the pressures within a free-to-move pneumatic cylinder chamber occur as a result of changes in volume.

This analysis is performed on a single-ended pneumatic cylinder. Differences in piston area and chamber volume require each chamber to be considered independently. The arrangement of two pneumatic valves supplying air to one of the pneumatic cylinders is detailed in chapter 2.

The layout of the valves and cylinder are shown in figure 5.15. The dead volumes of the cylinder result from volume that is not affected by piston movement (this also includes the volume of air in any connecting pipes).
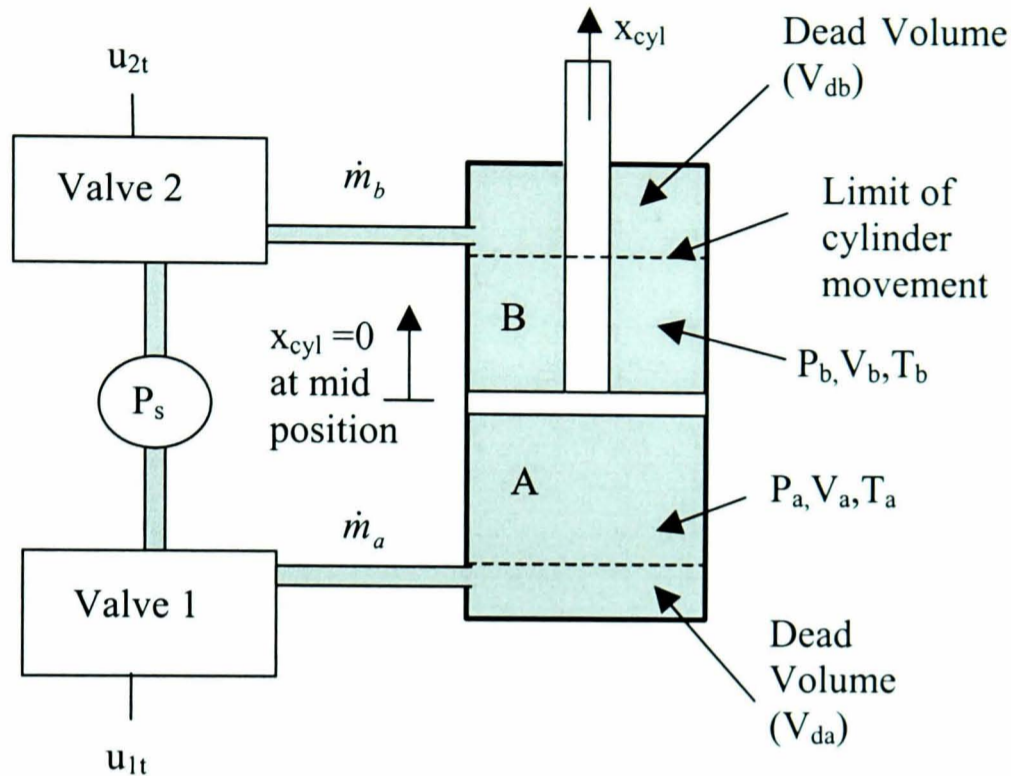
Figure 5.15 *Valve and cylinder model*

<u>For chamber A</u>

The conservation of energy equation (5.12) is again combined with equation (5.13). However, the piston is now free to move, so V_a is no longer a constant:

$$\dot{m}_a = \frac{P_a}{c_p.T_a}\dot{V}_a + \frac{1}{\gamma.R.T_a}.\frac{d}{dt}(P_a.V_a) \tag{5.20}$$

Using the fact that for a perfect gas, $R = c_p-c_v$, equation 5.20 can be reduced to:

$$\dot{m}_a = \frac{P_a}{R.T_a}\dot{V}_a + \frac{V_a}{\gamma.R.T_a}\dot{P}_a \tag{5.21}$$

Say the temperature of the air supply (T_s) is equal to the chamber temperature (T_a), and using the knowledge that the change in chamber volume is a result of the piston movement, equation 5.21 becomes:

$$\dot{m}_a = \frac{P_a}{R.T_s} A \dot{x}_{cyl} + \frac{V_a}{\gamma.R.T_s} \dot{P}_a \qquad (5.22)$$

where $T_a = T_s$ and $\dot{x}_{cyl}$ is the cylinder piston velocity.

The volume to be supplied with air consists of the chamber volume and the volume of interconnecting pipes:

$$V_a = V_{da} + (x_{cyl} + \frac{x_l}{2})A_a \qquad (5.23)$$

(where V_{da} is the cylinder dead volume (volume unaffected by piston movement), and x_l is the cylinder stroke.

Rearranging (5.22) and combining with (5.23) gives:

$$\left(\dot{m}_a - \frac{P_a.A_a}{R.T_s} \dot{x}_{cyl} \right) \frac{c_p RT_s}{c_v (V_{da} + (\frac{x_l}{2} + x_{cyl})A_a)} = \dot{P}_a \qquad (5.24)$$

Equation 5.24 represents the change within pressure for chamber A, taking into account both the air mass transfer and piston movement. It is similar to that derived by **Lui et al. (1988)**, but there are differences in the calculation of the chamber volume.

Chamber B

The analysis for chamber A can be repeated for chamber B to give:

$$\left(\dot{m}_b + \frac{P_b.A_b}{R.T_s} \dot{x}_{cyl} \right) \frac{c_p RT_s}{c_v (V_{db} + (\frac{x_l}{2} - x_{cyl})A_b)} = \dot{P}_b \qquad (5.25)$$

where all b subscripts refer to chamber B variables.

Equations 5.24 & 5.25 detail the pressure within the pneumatic cylinder. This pressure acts against the cylinder piston, generating a force.

Small amounts of stiction exist even within the low friction cylinder chosen for this design. A dead band approximated at ±1N from the experimental friction response of the low friction cylinder (chapter 2) was included in the cylinder model to take this into account.

The difference in the chamber pressures P_a and P_b produces a force (f_c) acting on the cylinder piston given by:

$$P_a A_a - P_b A_b = f_c - F_{vis} \qquad (5.26)$$

Viscous and coulomb friction results in a force opposing the pressure generated force (F_{vis}) (**Gross and Ratan 1997, Wang and Lin-Chen 2000, Drakunov 1997**). These friction effects depend on the operating temperature, which varies during cylinder motion.

The friction effects are grouped together to form one linear friction coefficient (D_{cyl}), (in reality this coefficient would be non-linear but the determination of its form is non-trivial):

$$F_{vis} = D_{cyl} . \dot{x}_{cyl} \qquad (5.27)$$

This equation is used in the simulation (viscous friction block).

5.4   Robot dynamics

The simulation incorporates the pneumatic cylinder and joint 3 of the physiotherapy robot (figure 5.16). Linear movement of the pneumatic cylinder results in angular rotation of the joint.

As the joint angle varies, the angle at which the cylinder acts upon the link alters, therefore the simulation resolves cylinder torque perpendicular to the link. The equation of motion for the link, including the velocity term and resolving the cylinder perpendicular to the link is given by:

$$M\ddot{\theta}_3 = (f_c - D_{cyl} . \dot{x}_{cyl}).f(\theta_3) \qquad (5.29)$$

where M is link moment of inertia and $f(\theta_3)$ is a function resolving the cylinder force to angular torque. The value of the velocity coefficient (D_{cyl}) has been obtained experimentally in chapter 4.
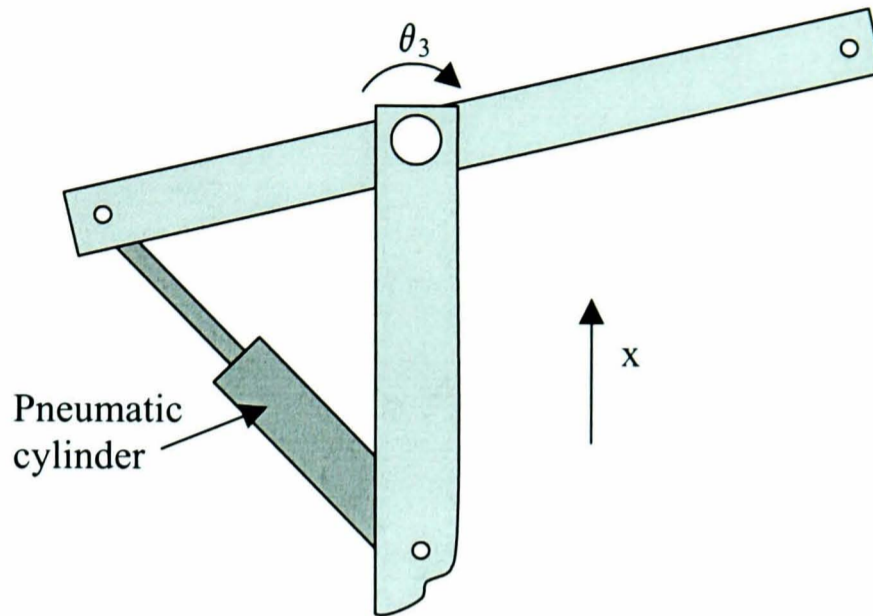

Figure 5.16 *Link 3 configuration*

5.5 Model Validation

Using the simplified model of the valves, the cylinder model, and a model of joint 3, a simulation of the valves and cylinder was constructed (figure 5.17). Experimental results were obtained using proportional control. Proportional control is a simple control method utilising one forward path (K_p) and unity negative feedback (see chapter 3). This control method was chosen as its simplicity masks very few of the underlying system dynamics, the purpose being to verify the model rather than achieve optimum control. The experimental results were obtained with $K_p = 3 \times 10^{-2}$. These were then compared to the simulation.

The simulation position response (figure 5.18) is similar to the experimental, although approximating the non-linear velocity coefficient (D_{cyl}) as linear and using a simplified stiction model can account for some of the differences in the responses. (Note the position response is not symmetrical due to a non-linear relationship between cylinder position and angle). The simulated and experimental pressure responses (figure 5.19) are very similar. The torque response due to pressures either side of the cylinder (figure 5.20) and the control signal (figure 5.21) are both similar to the experimental.
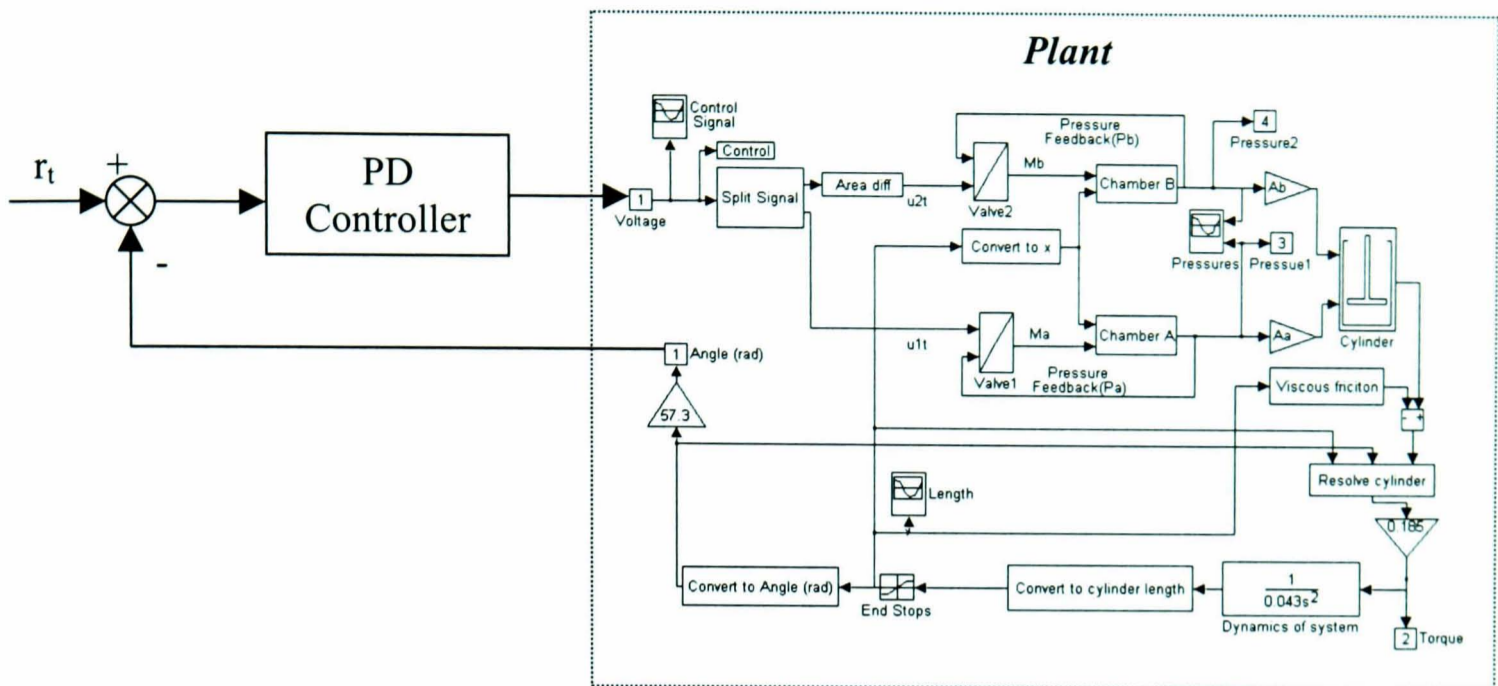
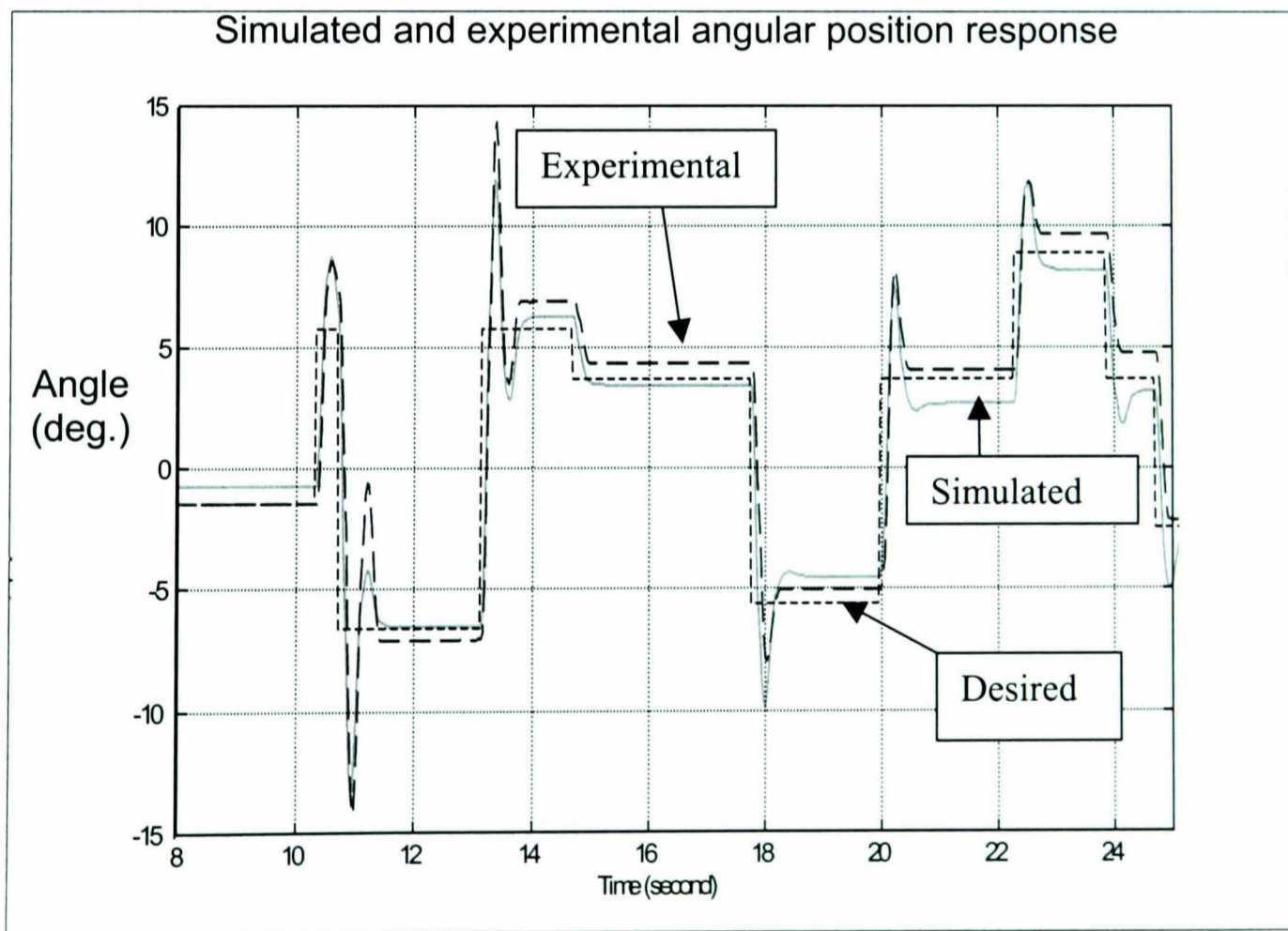**Figure 5.17** *Simulation of cylinder, valves and robot*

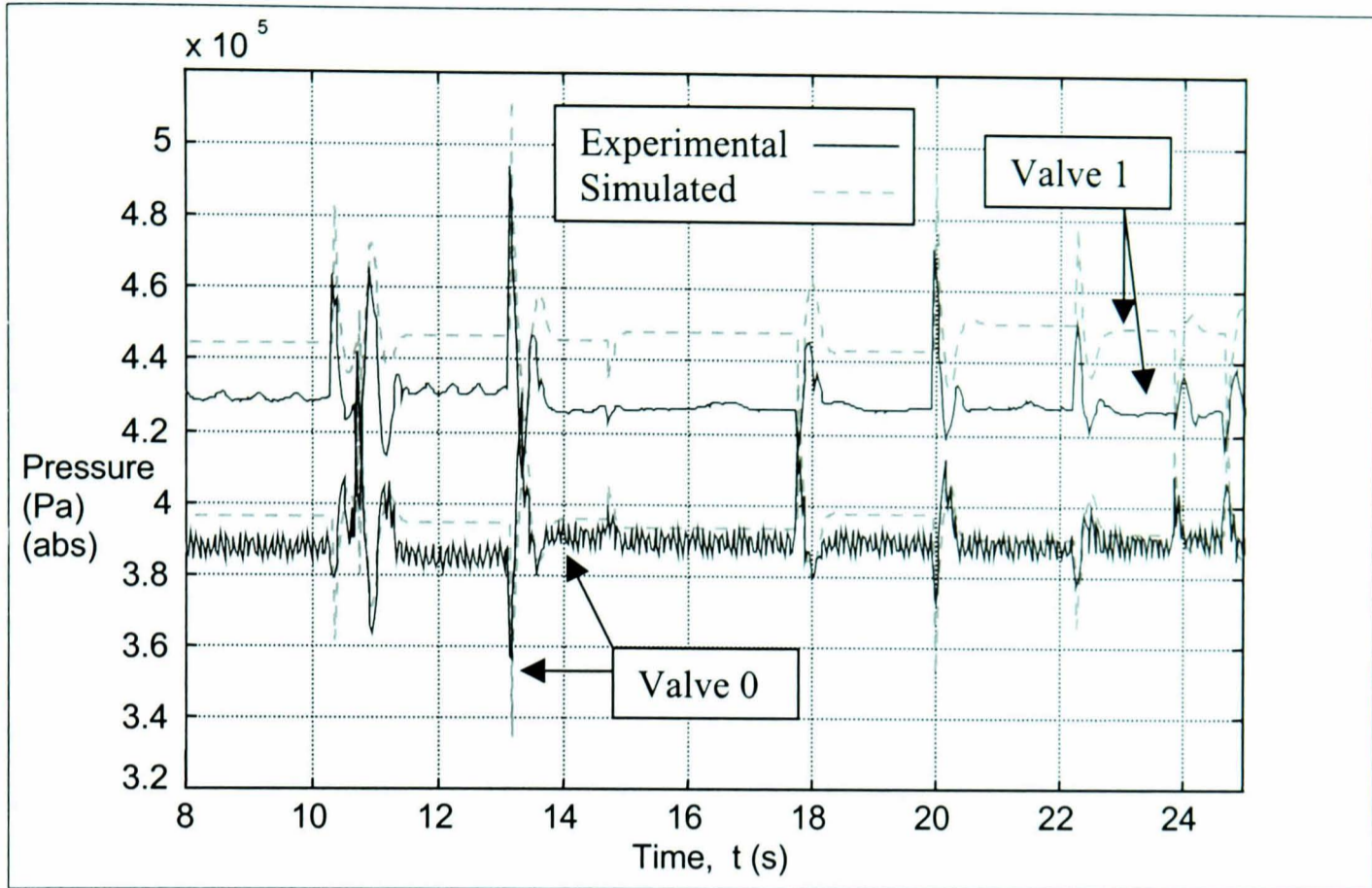**Figure 5.18** *Simulated and experimental angular position response*

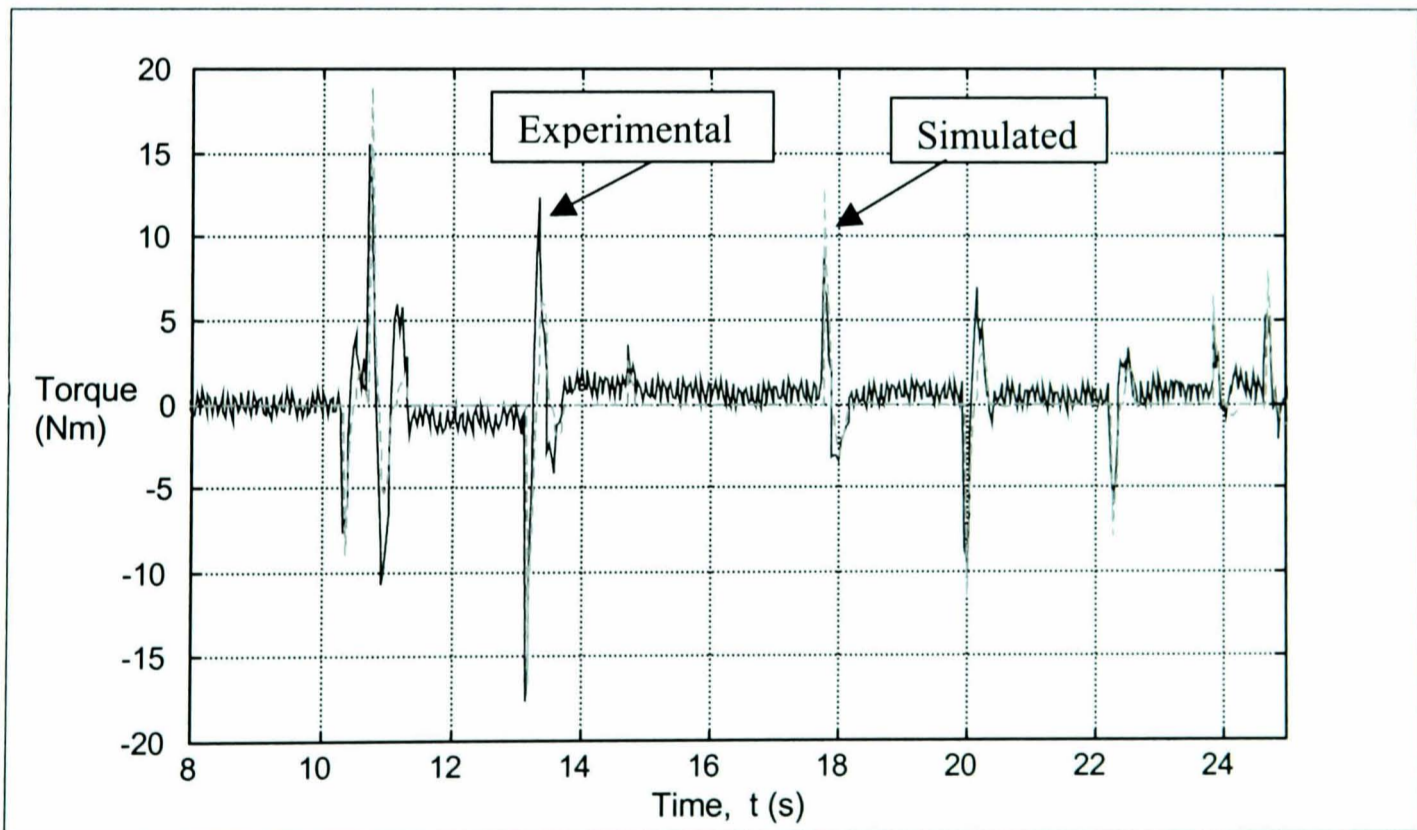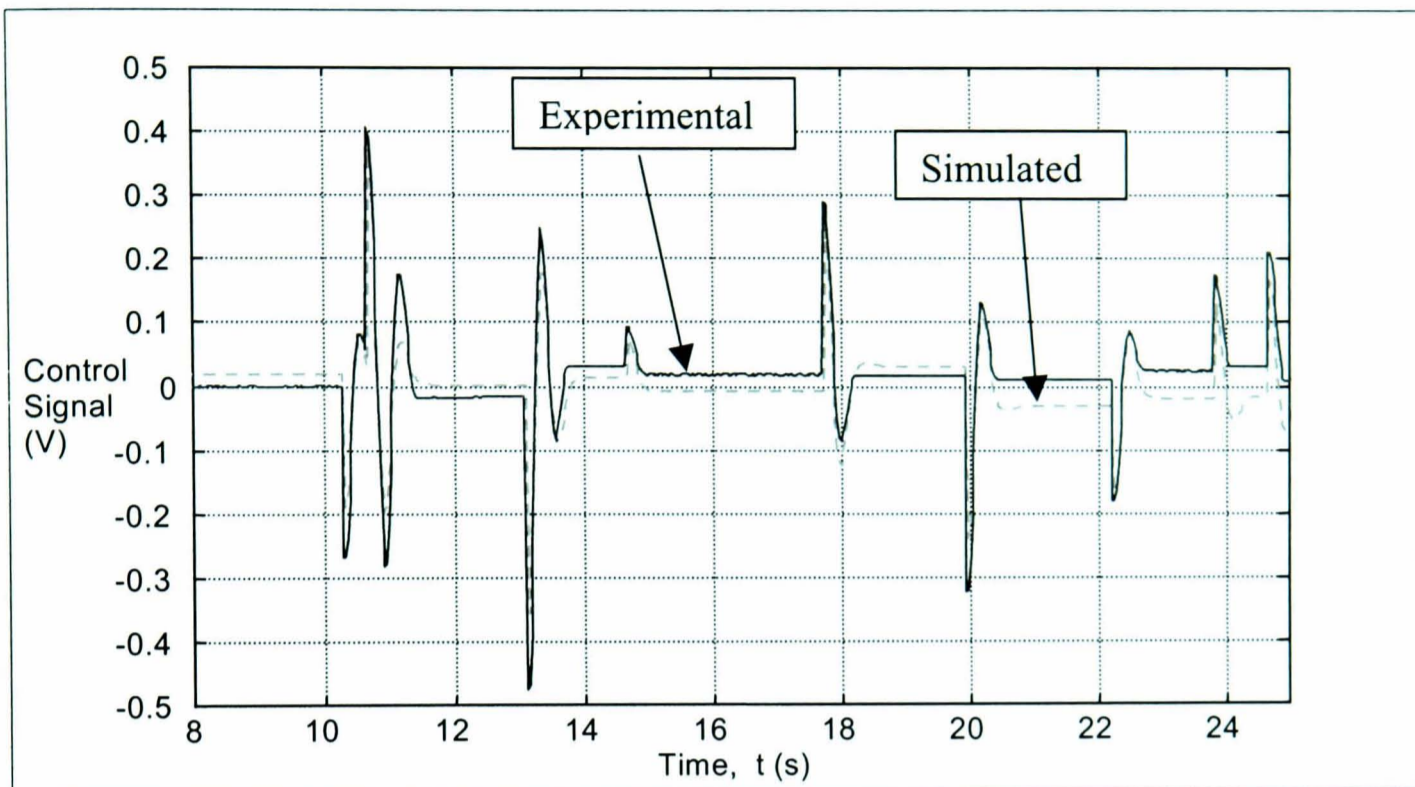**Figure 5.19** *Simulated and experimental pressure response results*

Figure 5.20 *Simulated and experimental torque*

Figure 5.21 *Simulated and experimental control signal*

5.6 Discussion and Conclusions

A mathematical model of the electro-pneumatic valves, pneumatic cylinder, and one link of a robot has been derived. When combined, these equations approximate the system behaviour.

Constructing a simulation from these equations enables the experimental results to be compared to that predicted by the mathematical model. Comparison of these results has shown that the mathematical model accurately predicts the behaviour the position, pressures and torque of the pneumatic cylinder, however a velocity coefficient was identified experimentally.

The model of the electro-pneumatic valves was simplified to a single gain due to the bandwidth of the transient response being much larger than the cylinder response. This is apparent from examining the response time of the overall system when compared to the decay time of the valve transient response. If the experimental

equipment were modified with smaller actuators or reduced inertia then these discarded transient elements could influence system behaviour.

The stiction within the pneumatic cylinder, although small, was incorporated into the mathematical model as a dead band around the applied force. In reality this friction effect would be much more complex. Improving the prediction of these stiction effects should improve the model accuracy at low forces.

Measurement of mass flow rate to and from the cylinder, during motion, would enable validation of the performance of the valves responding to pressure changes. Time delays and pressure drops within the interconnecting links could also be examined to improve the simulation (**Richer and Hurmuzlu 2000**).

The model presented only describes the behaviour of one link of the three degree of freedom pneumatic cylinder. The model could be extended to incorporate additional degrees of freedom, describing the behaviour of the entire robot. Accurate equations of motion for all links of the robot would be required to incorporate these additional degrees of freedom, moreover the complexity of predicting and validating the dynamic behaviour of three pneumatic cylinders simultaneously would limit the insight that could be obtained from the simulation. The simulation model will be used to develop a force and position control strategy in chapter 6.

Chapter 6

Force and position control

Many applications, such as robotic physiotherapy, require consideration of both applied force and position. Specifying arbitrary force and position demands is impossible, but, control strategies exist that compromise between force and position demands. Force and position control of a pneumatic robot will be examined in this chapter.

6.1 Introduction

Control of force and position is fundamental in all aspects of life. To drink a cup of coffee we are required to provide sufficient force to grasp the mug, while changing its position to bring it into contact with our lips. Purely position control may result in the cup being dropped, while purely force control would be incapable of accurately moving the cup.

To enable robots to behave predictably with unknown environments consideration of force and position is essential. Over the last couple of decades researchers have begun to develop methods of force and position control. An outcome of this research is three main force and position control strategies: hybrid force control, parallel force and position control and impedance control.

Of these control strategies, hybrid (**Raibert and craig (1981)**) can only control force and position in orthogonal directions on multi-degree of freedom systems. Parallel force and position control (**Chiaverini and Sciavicco (1993)**) implements force and position demands, however position is sacrificed to regulate force. Impedance control (**Hogan 1985**), however, controls neither force or position, but rather the dynamic relationship between the two. This is the strategy adopted for control in the present study.

Impedance control utilises a mass, spring and damping relationship between force and position (figure 6.1, repeated from figure 1.9 for clarity).
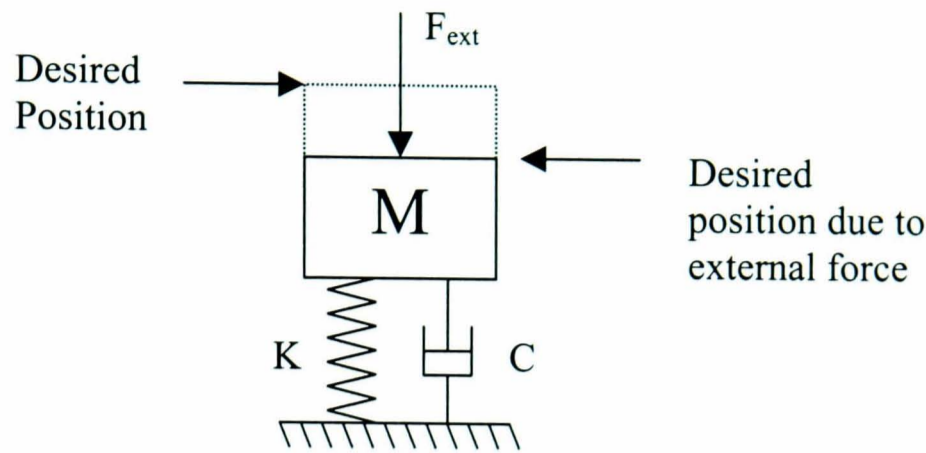
Figure 6.1 *Impedance control free body diagram*

The transfer function connecting force and position demands can be specified in the s-domain as:

$$\frac{x_i}{F_{ext}} = \frac{1}{Ms^2 + Cs + K}$$

(6.1)

where x_i is the change in position due to external force (F_{ext}), M is the inertial component, C is the damping component and K is the stiffness component.

Rearranging equation 6.1 so that position becomes the input gives:
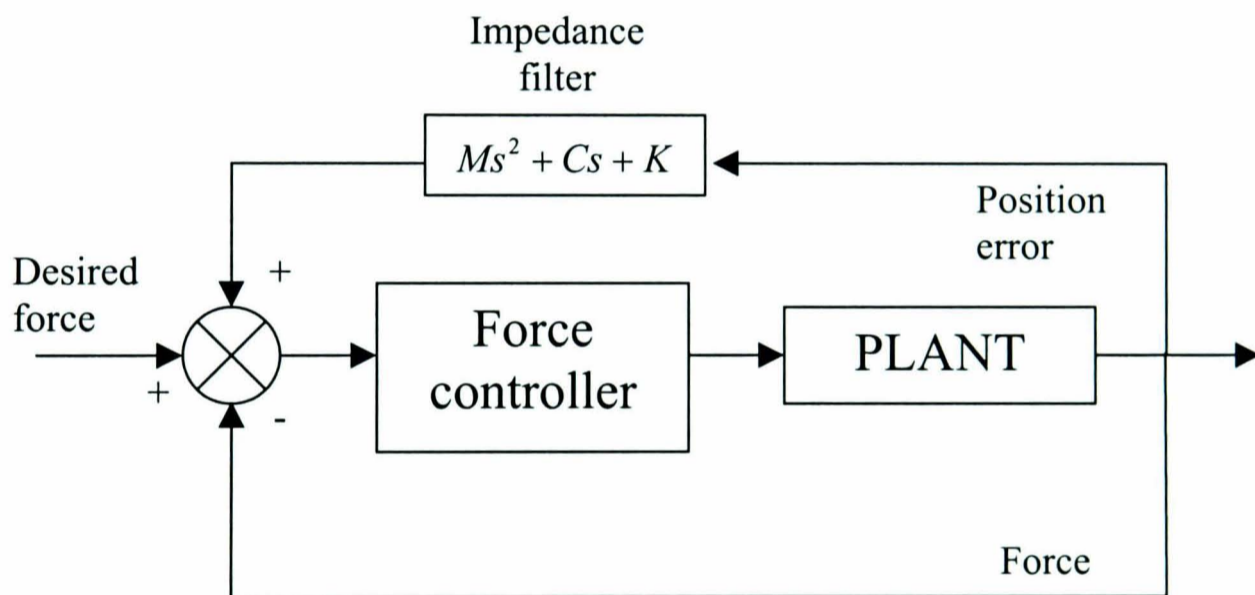
$$\frac{F_{ext}}{x_i} = Ms^2 + Cs + K$$

(6.2)

Equations 6.1 & 6.2 are known as the duality of impedance control (i.e either force can be considered the input and position the output or position can be considered the input and force the output)[1]. These two subtly different approaches require different controller structures. To explain this duality further, consider the simple controller implementations of equations 6.1 and 6.2 (figures 6.2 and 6.3 respectively, repeated from figures 1.11 and 1.12 for clarity).

---

[1] Note that the force based controller is formally termed *impedance control* and the position based controller is formally termed *admittance control*, however both controllers tend to be termed impedance controllers **(Heinrichs et al. 1997, Carignan and Smith 1994)**.

Impedance
filter

$$\frac{1}{Ms^2 + Cs + K}$$

Position
controller

PLANT

Desired
Position

Force
error
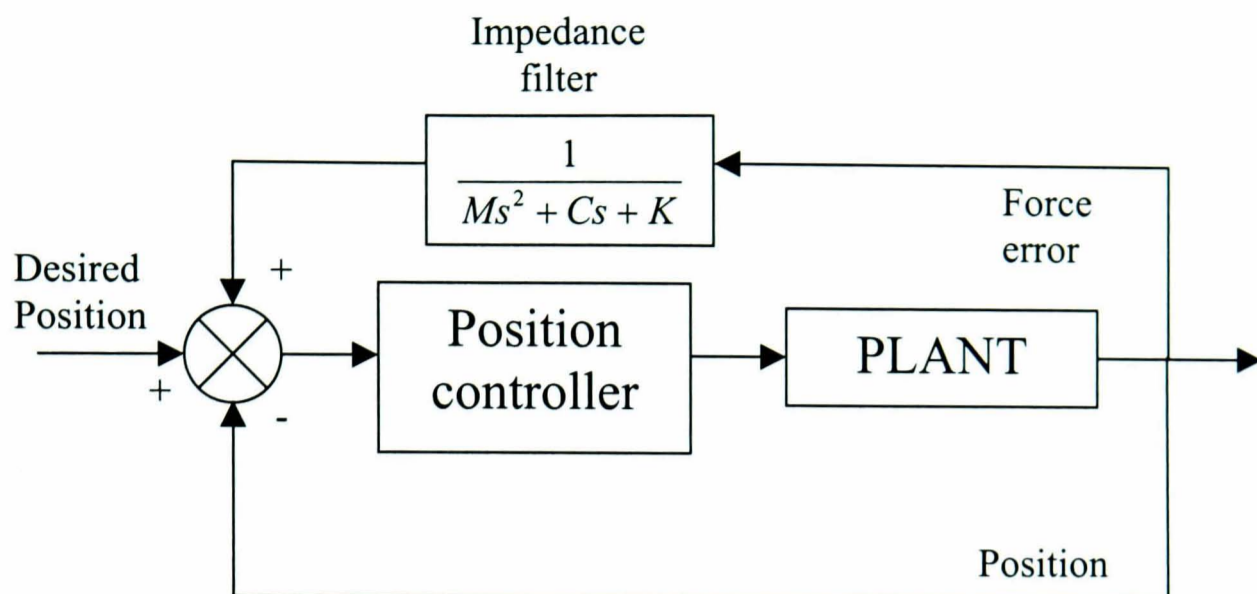
Position

Figure 6.2 *Position based impedance controller block diagram*

Impedance
filter

$$Ms^2 + Cs + K$$

Force
controller

PLANT

Desired
force

Position
error

Force

Figure 6.3 *Force based impedance controller block diagram*

The position based impedance controller (figure 6.2) behaves purely as a position controller in free space. When in contact with the environment, the error in force (if no contact force is required this would be the force itself) is translated into a change in position set-point. Conversely the force based impedance controller controls force, with position errors modifying the output force. Selection of the most appropriate impedance control strategy is considered in the next section.

6.2 Force or position based impedance control

6.2.1 Force based control

Force based impedance control is the most widely used impedance controller, as a result of the ease at which torque can be controlled during motion for DC motors.

A force based impedance controller (figure 6.2) can be implemented through modification of the position control strategy based upon a manipulator's dynamic equation of motion (see chapter 4). Indeed, the only difference between Lagrange's equations of motion and force based impedance control is in the calculation of joint forces.

Using equation 4.1 it is possible to predict the manipulator motion for a specific joint torque. To recap, the dynamic relationship between force and position for a specific joint is:

$$M_r(\theta)\ddot{\theta} + V_r(\theta,\dot{\theta}) + G_r(\theta) = \tau - \tau_{ext} \qquad (6.3)$$

where M_r is the inertia matrix, V_r is the coriolis/ centrifugal force, G_r is the gravitational force, τ is the actuator joint torque and τ_{ext} is the external force resolved to the torque applied to individual joints.

So, the torque acting upon the individual link dictates the acceleration of that link. Assuming slow manipulator motion, the coriolis and centrifugal forces can be assumed negligible. Equation 6.3 then becomes:

$$M_r(\theta)\ddot{\theta} + G_r(\theta) = \tau - \tau_{ext} \qquad (6.4)$$

Forward kinematics (section 6.4) translate these joint angles (θ) into global positions (x). For solely position control, the aim would be to generate the required actuator torque to achieve the desired global position (x_p). Force based impedance control uses the error between desired position and actual position to modify the joint torque, hence the force output of the entire robot. If the global position error (x_e) is defined as:

$$x_e = x_p - x \tag{6.5}$$

where x is the actual position in the global co-ordinate frame.

then the resulting change in global output force (F_i) at the robot end point, due to the impedance strategy is:

$$F_i = x_e(Ms^2 + Cs + K) \tag{6.6}$$

The change in this global force is achieved by altering the joint torque (τ) on individual links of the robot. So a force now exists between the robot end-point and the environment dependant on the global position error of the robot.

It is apparent that accurate control of actuator torque is essential for successful implementation of this control strategy. As discussed in chapter 4, torque control of a pneumatic actuator during motion is not a simple task, with stiction, and fluid flow dynamics combining to degrade the response.

Similar difficulties exist for hydraulic systems, involving stiction and fluid flow dynamics when attempting to control torque output during motion. **Heinrechs et al. (1997)** implemented a position based impedance control strategy on a hydraulic actuator to remove a large proportion of the difficulties regulating hydraulic force output during motion. Indeed, stiction and viscous friction effects are velocity dependant, so it makes sense to implement a controller to accurately control the velocity.

6.2.2 Position based control

Position based impedance control has the added advantage of not requiring an accurate model of the manipulator dynamics (the exact valve of the inertial matrix (M_r) etc) which can be difficult to obtain. The drawback of position based impedance control is the requirement for a high gain position controller that is robust to external forces.

To implement position based impedance control, the external force applied to the robot manipulator (F_{ext}) creates a desired change in global desired position (x_i) thus:

$$x_i = \frac{F_{ext}}{Ms^2 + Cs + K} \qquad (6.7)$$

These external forces are measured through a force sensor mounted at the manipulator end-point. Note that in this particular situation the desired force is zero, therefore, the external force itself becomes the force error.

So the resulting demand for the position controller (x_d) becomes

$$x_d = x_i + x_p \qquad (6.8)$$

where x_p = desired position without any external forces

To implement this demand position, the appropriate individual joint angles are required. These joint angles can be found from the robot inverse kinematics (see section 6.4).

The approach taken here uses the position based impedance controller for the above mentioned advantages, however, the difficulty of designing a position controller that is robust to external forces in the presence of air compressibility is not straightforward. The next section develops the position based impedance controller.

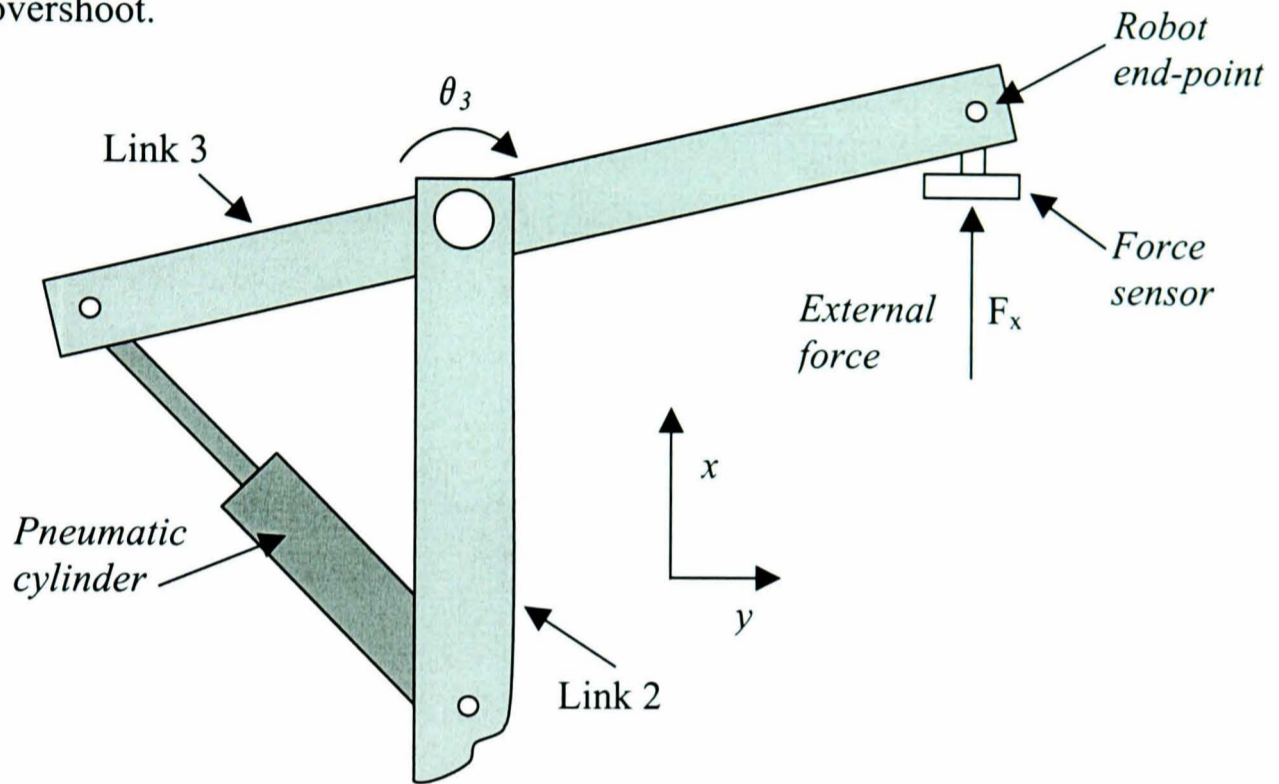## 6.3   Single degree of freedom impedance control

The impedance controller was developed on a single joint of the three degree-of-freedom robot (figure 6.4). The single degree of freedom force sensor measures forces applied in the x direction[2]. The controller objective is to cause the point at which these forces are applied, the robot end point, to behave with specified inertia, damping and stiffness while tracking a desired trajectory (x_p).

---

[2] Note that movement of the joint results in motion in the x & y direction. If link 3 is assumed to vary only slightly from being perpendicular to link 2 then movement in the y direction can be assumed negligible.

6.3.1 Design

With no external forces applied to the joint, it is required to respond to purely position demands, following the desired trajectory (x_p). A PD position controller was designed to achieve this joint motion. Using empirical methods, the PD gains were selected to be 2.5 and 0.25 respectively. The performance of this controller for a step demand is demonstrated in figure 6.5. The PD controller rapidly reaches the desired set-point with little overshoot.

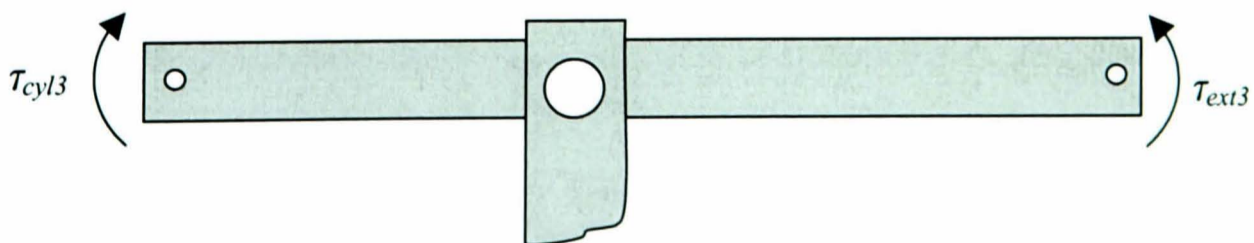**Figure 6.4** *Single degree of freedom impedance control*
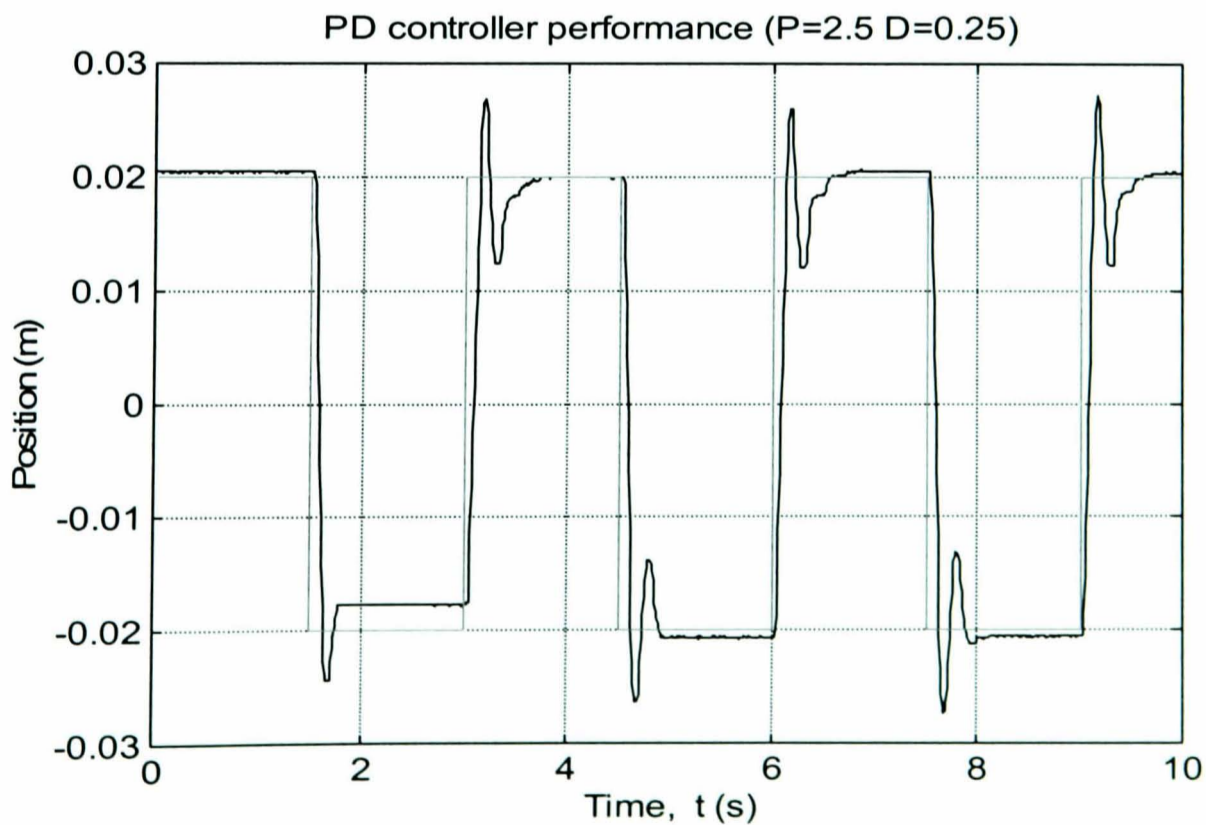
**Figure 6.5** *Link 3 PD position step response*

If the PD controller were able to reject all force disturbances it would be possible to use a PD position only strategy to implement the desired impedance trajectory (x_d) given by equation 6.8. However, external forces on the link have considerable effect on the PD controller performance due to the low actuator stiffness and back-drivable nature of the pneumatic cylinder.

Position control of pneumatic cylinders under the influence of an unknown constant external force has been achieved in chapter 3. A self-tuning, constant control signal was used to produce a force to counteract the external force and enable accurate control. When an unpredictable and rapidly varying external force is applied, tuning of a constant balance force cannot be achieved. Modifying this strategy to be adaptive would not be successful due to the external force varying quicker than the controller would be able to adapt.

The open-loop force controller developed in chapter 4 is capable of counteracting the influence of the external force. For the external force to have no influence on the link, an equal but opposite force needs to be applied. Since the impedance control strategy requires a force sensor to measure the external forces acting upon the link, the reading from this force sensor can also be used to generate a balancing force from the open-loop force controller. The external force and the force generated by the force controller cancel each other out (i.e. link torque resulting from the external force (τ_{ext3}) is equal, but opposite to the torque applied by the cylinder (τ_{cyl3}) due to the open-loop force element (figure 6.6)). So the PD position controller and force controller forms the impedance control strategy shown in figure 6.7. Remember that the open-loop force controller is influenced by cylinder velocity. With the force and position controllers combined the PD position controller would reduce the influence of this effect.

Figure 6.6 *Counteracting the external force*
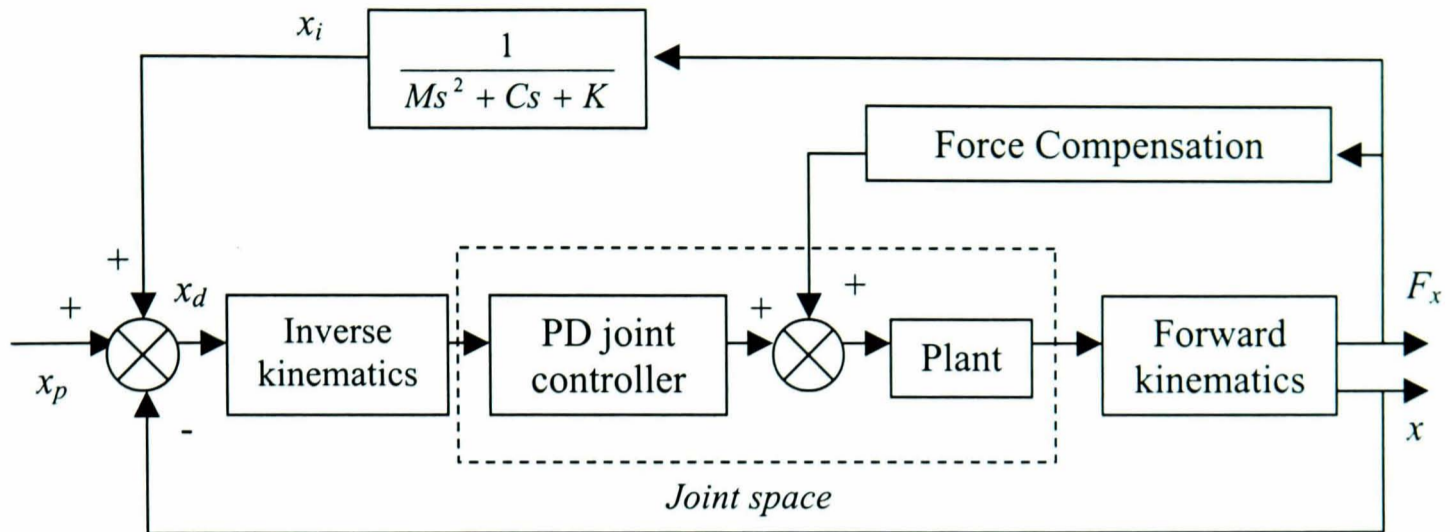
**Figure 6.7** *Impedance controller strategy*

Implementing the controller in multiple degrees of freedom requires the manipulator inverse kinematics to be known. In a single degree of freedom, the calculation of the relationship between joint angle and global position is straightforward (figure 6.8).

So the robot end point position, in the x plane, is given by:

$$x = -0.3\sin\theta_3 \tag{6.9}$$

The external force (F_x) is resolved perpendicular to the link and multiplied by the link length to obtain the external torque applied to the link (τ_{ext3}).

$$\tau_{ext3} = 0.3 * F_x * \cos\theta_3 \tag{6.10}$$
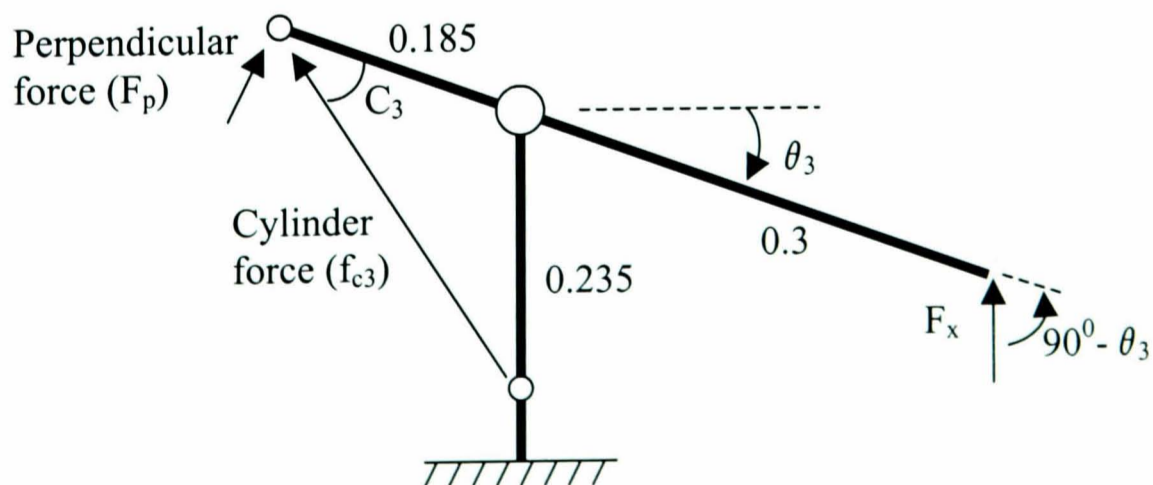
Figure 6.8 *Resolving joint 3*

Due to the positioning of the pneumatic cylinders, the actuator torque at each joint is a function of joint angles and control signal. Earlier analysis of the valve and cylinder combination (chapter 5) identified the relationship between control signal and cylinder force ($0.023V \equiv 1N$). This force needs to be resolved perpendicular to the link and then multiplied by the length to the pivot point to obtain cylinder torque.

Obtaining link torque (τ_{cyl3}) due to actuator force gives:

$$\tau_{cyl3} = f_{c3} * \sin C_3 * 0.185 \qquad (6.11)$$

The angle C_3 can be found using both the sine and cosine rule:

$$C_3 = a\sin\left(\frac{0.235 * \sin(\theta_3 + \pi/2)}{\sqrt{0.185^2 + 0.235^2 - 2*0.185*0.235*\cos(\theta_3 + \pi/2)}}\right) \qquad (6.12)$$

For the link to balance, the externally applied torque has to equal the torque applied by the pneumatic cylinder. Combining equations 6.10 & 6.11:

$$\tau_{ext} = \tau_{cyl} = f_{c3} * \sin C_3 * 0.185 = 0.3 * F_x * \sin \theta_3 \qquad (6.13)$$

Rearranging equation 6.13 gives:

$$f_{c3} = \frac{0.3 * F_x * \cos \theta_3}{\sin C_3 * 0.185} \qquad (6.14)$$

So the cylinder force of f_{c3} will balance the external force. The open-loop force controller developed in chapter 4 can be used to generate the force required to balance the external force.

6.3.2 Simulation

The simulation developed in chapter 5 can be augmented to test the impedance controller concept (figure 6.9).

The cylinder and valve model from the previous simulation forms the plant. The inputs to this plant are the voltage supplied to the valve and cylinder system and the external
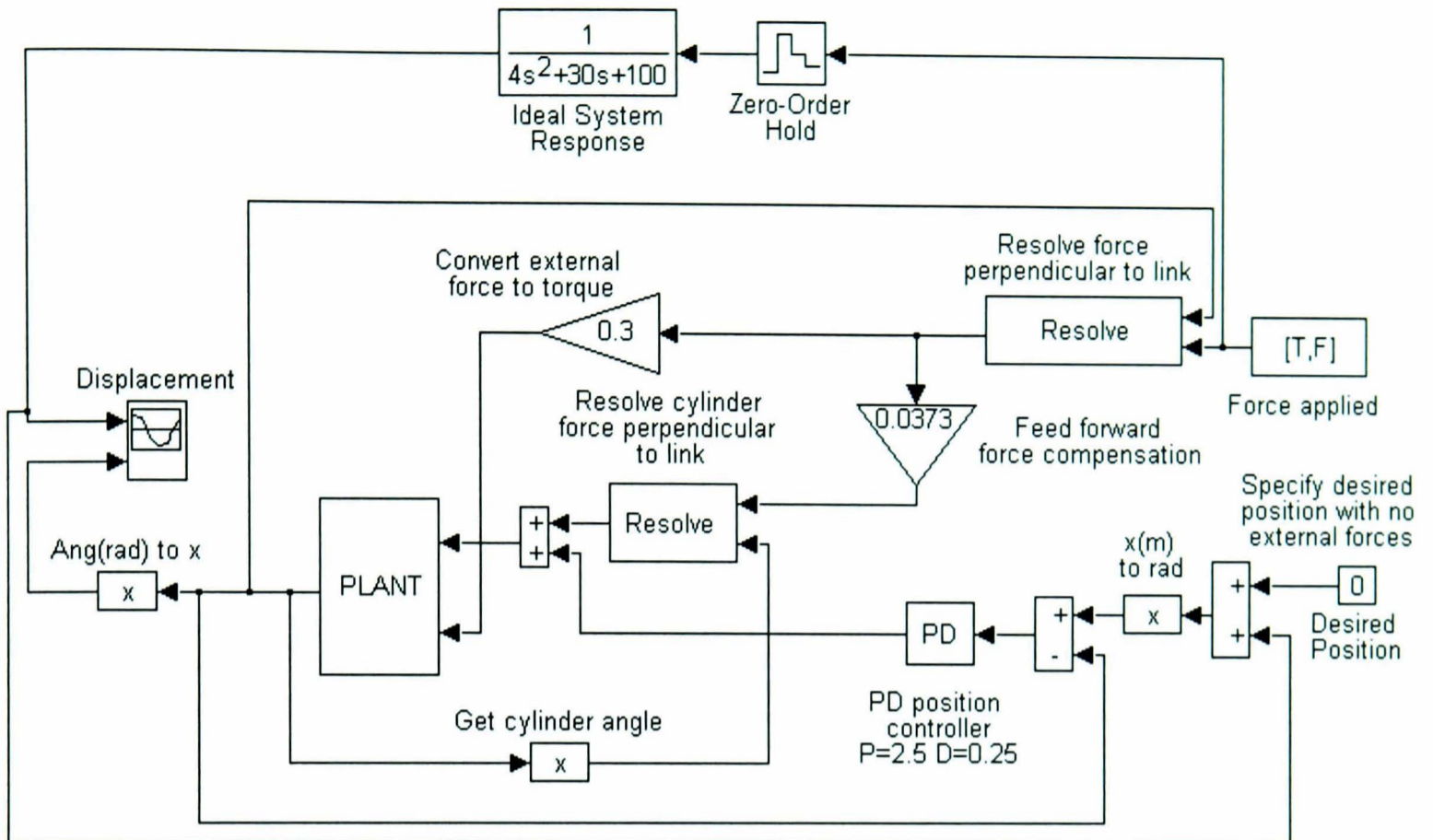
Figure 6.9 *Impedance controller simulation*

torque that is directly coupled to the link. The output of the plant is the joint angle which is later resolved into a global position. The simulations demonstrated the impedance controller to behave as designed. Results of the simulation are shown alongside the experimentally obtained results in the next section.

6.3.3 Results

In order to assess controller performance a mass of approximately 1.8kg was applied and removed from the end of the robot. With the mass attached, an approximately constant force is applied, regardless of position. This is not representative of physiotherapy, where force would be applied gradually, but is an extreme test of controller performance. Note the experimental forces were input into the simulation to enable a direct comparison with the experimental response.

The constant force combined with zero desired position ($x_p=0$) enables the controller performance to be easily assessed. The experimental results were compared to those produced from the simulation (figures 6.10, 6.11, 6.13, 6.14). The results obtained with

inertia, damping and stiffness (figures 6.10 & 6.11), show the experimental and simulated response to closely follow the desired trajectory. For small oscillations the experimental tracking is poor, mainly due to friction within the system. Examining the voltage output from the PD controller and open-loop force controller (figure 6.12) for the response shown in figure 6.10, illustrates the operation of each element of the impedance controller. The open-loop force controller provides a compensation force to oppose link movement due to the external force. The PD controller's output moves the link along the desired trajectory providing little compensation for the external force, as such its output is much smaller than the force controller.

Although impedance control can be performed with inertia, damping and stiffness, the inertial element is considered to offer little therapeutic value for physiotherapy. Damping and stiffness alone can be specified for impedance control, requiring the controller to mask the physical inertia within the link. Examining the results obtained with only damping and stiffness (figures 6.13 & 6.14), both the simulated and experiment results accurately track the desired trajectory. Some steady state offset is present within the system due to modelling errors when resolving forces.
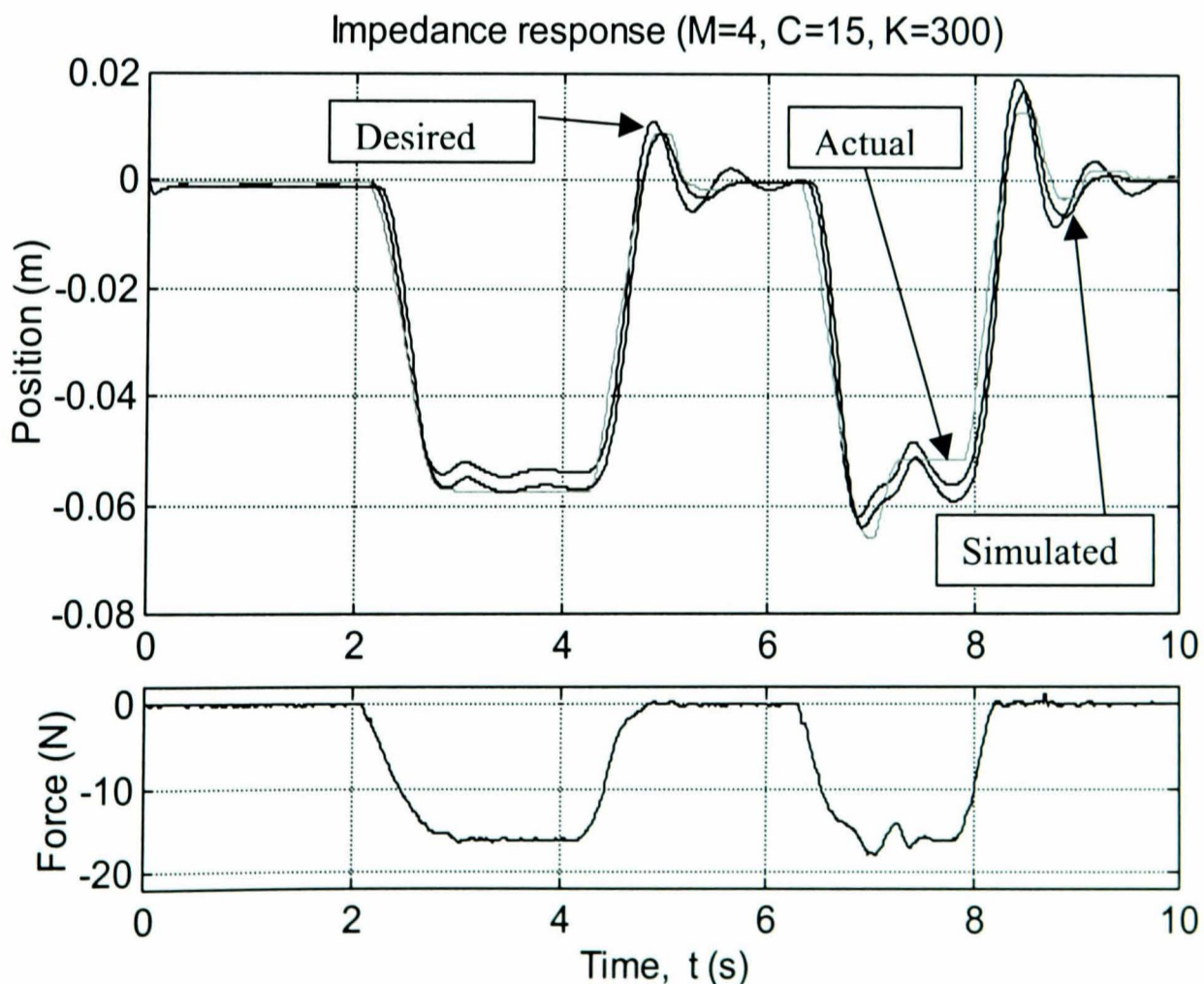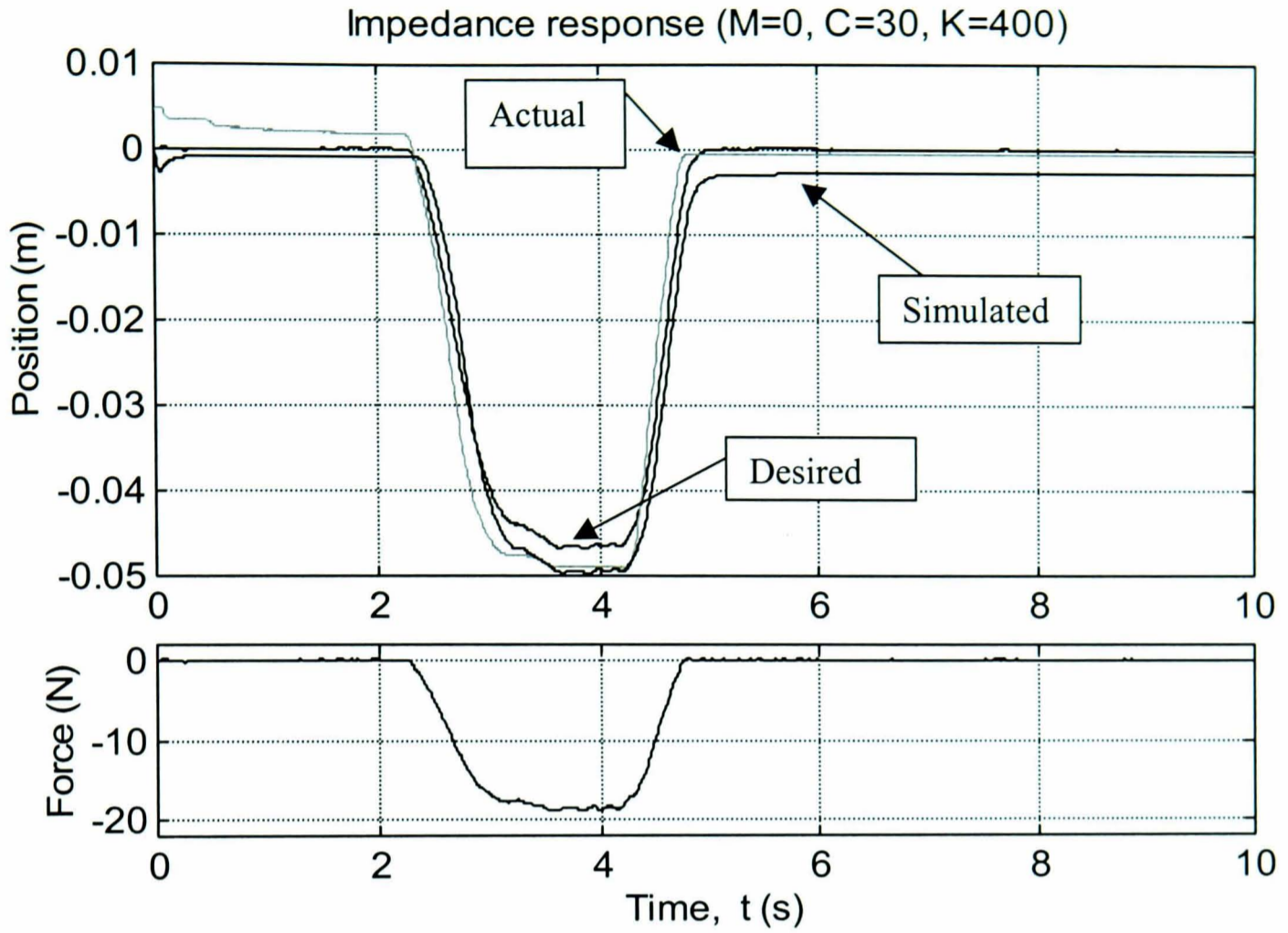

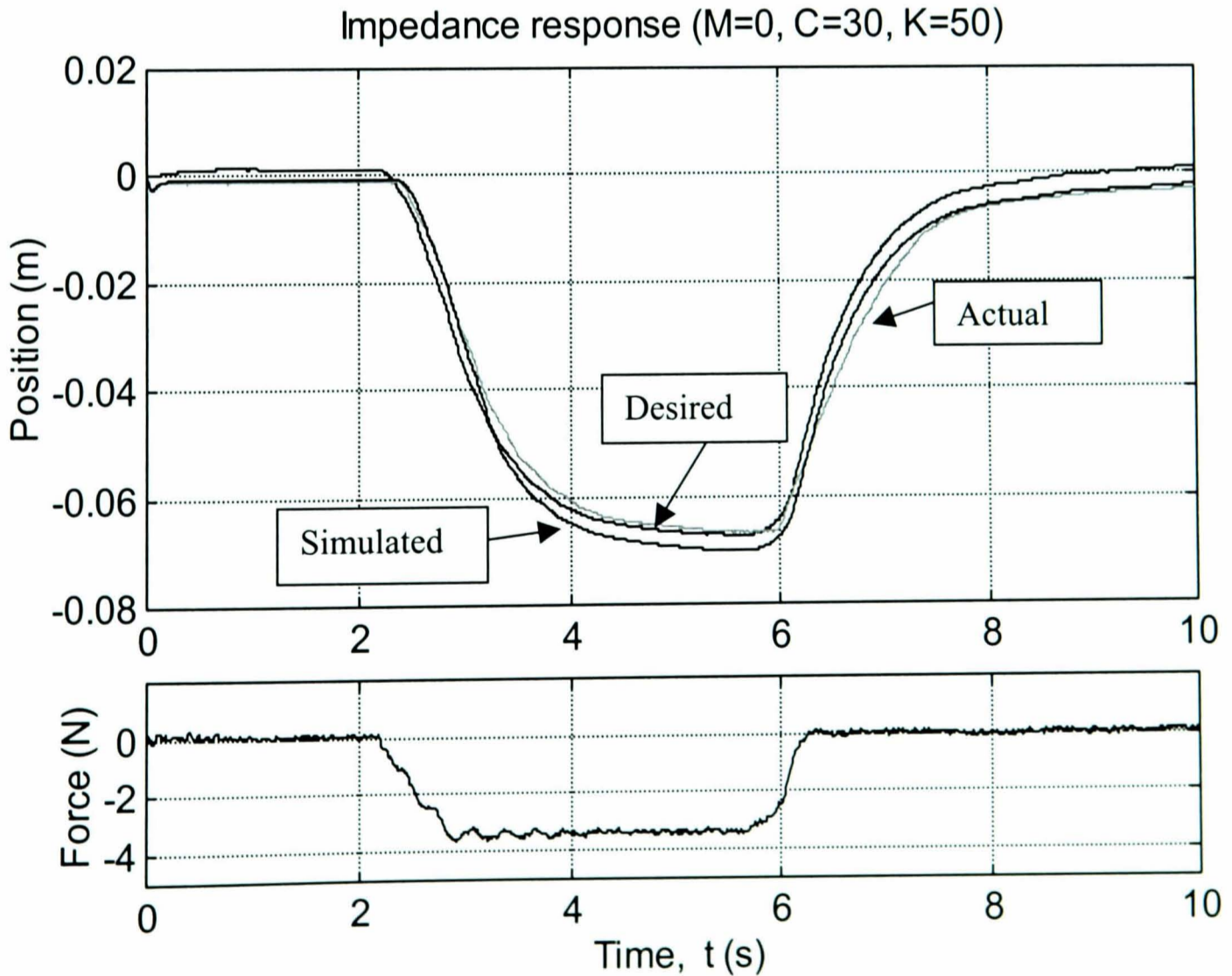**Figure 6.10** *Simulated and experimental impedance controller results (M=4,C=15,K=300)*
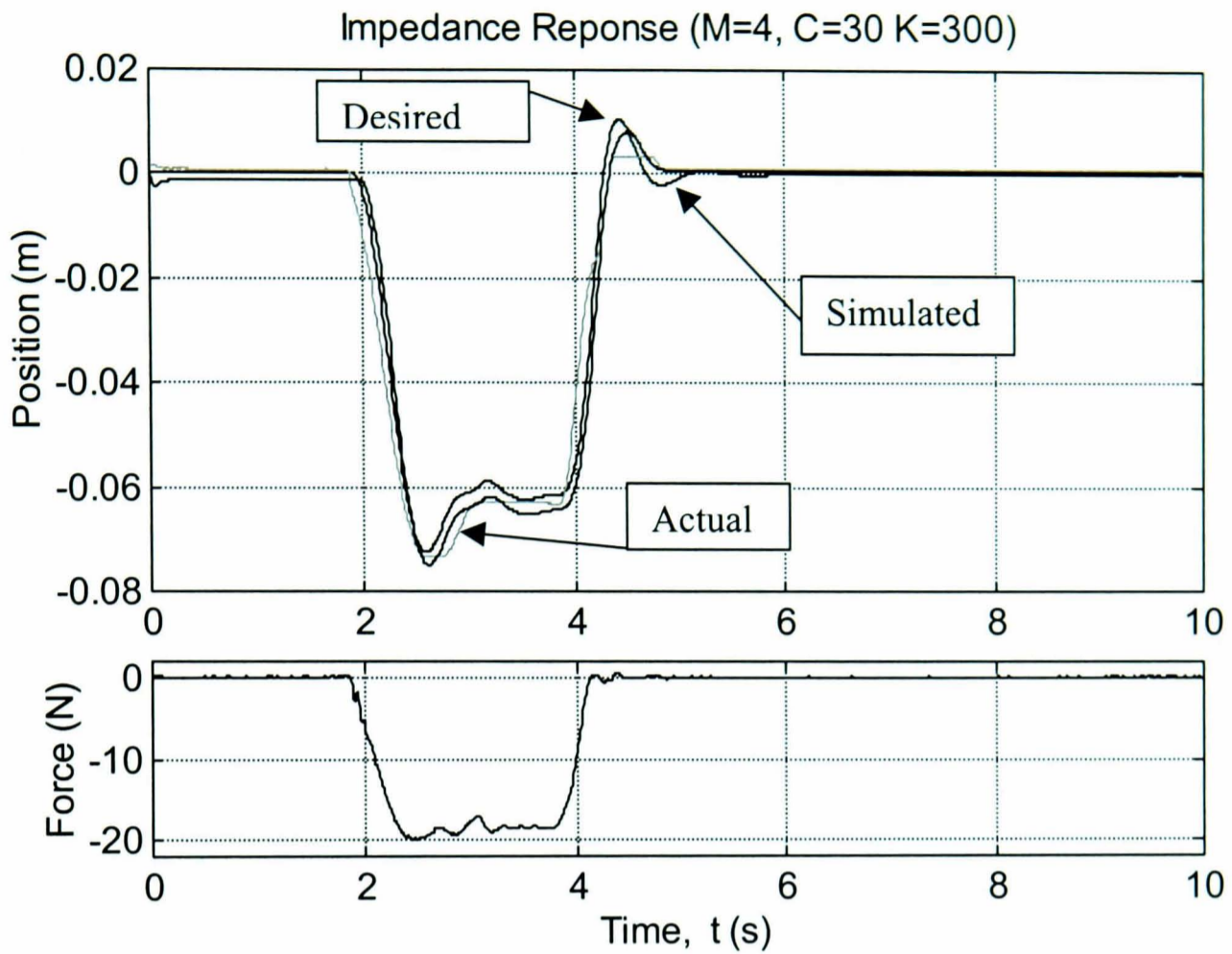
Figure 6.11 Simulated and experimental impedance controller results (M=4,C=30,K=300)
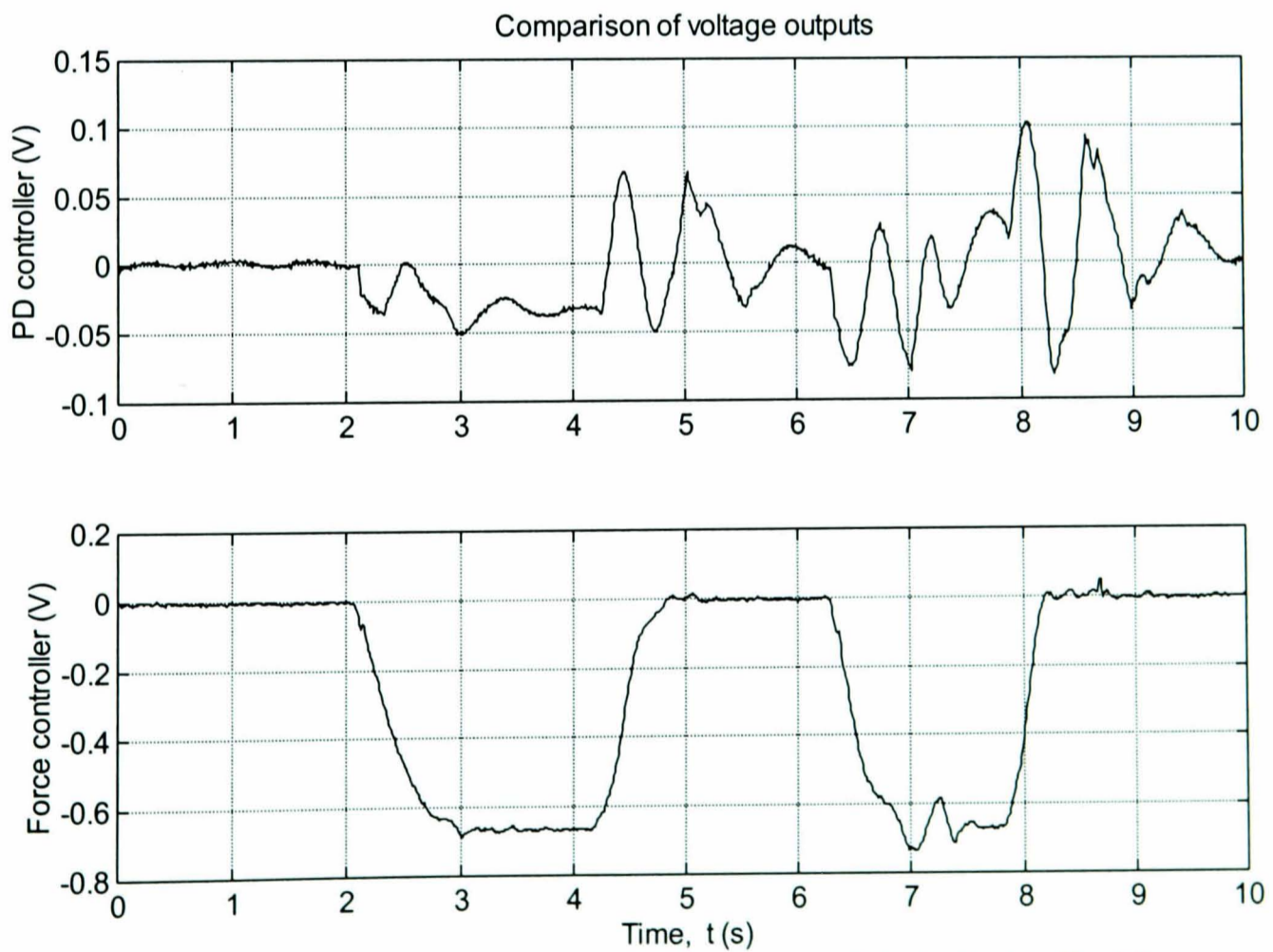
Figure 6.12 Voltage outputs for response (M=4, C=15, K=30)

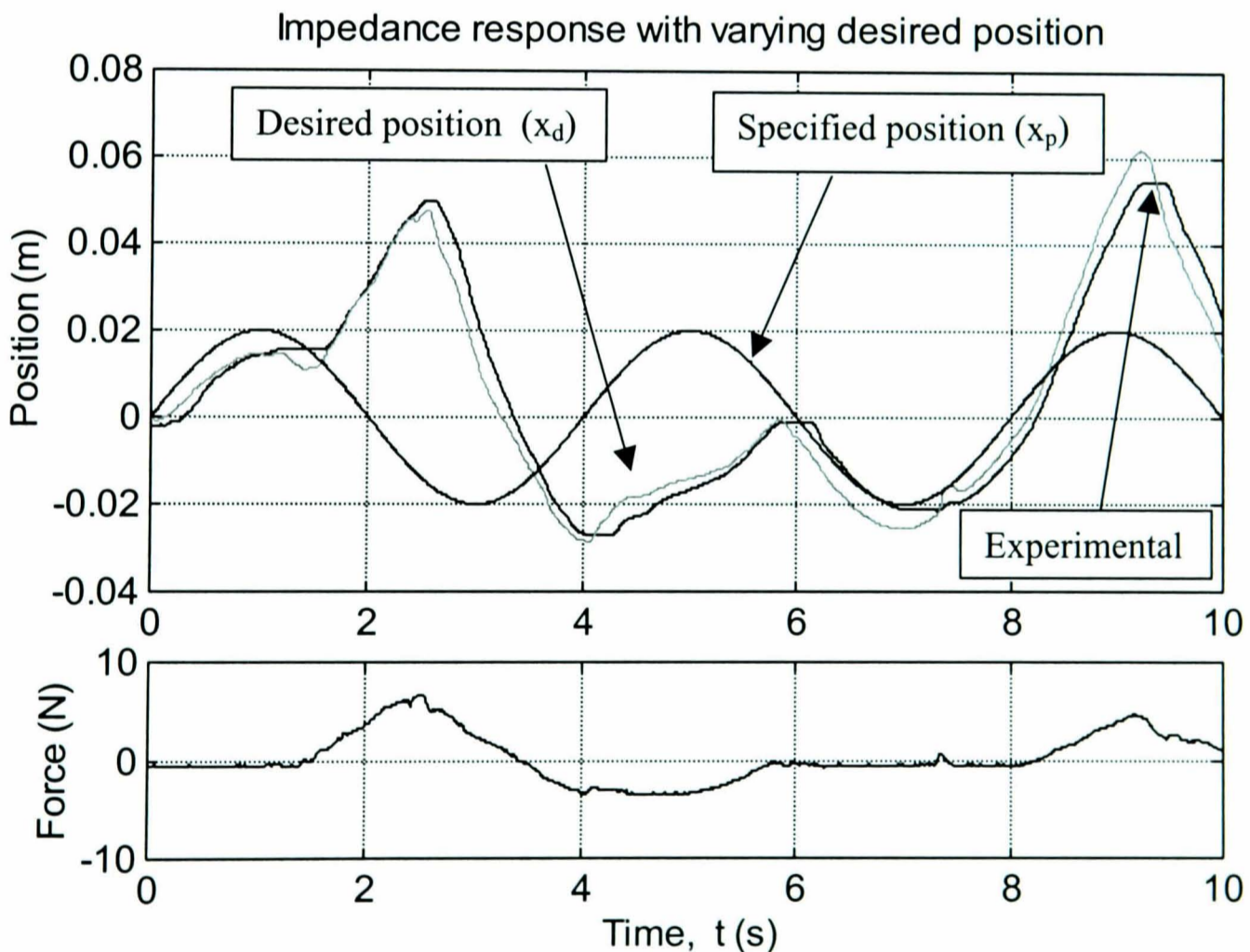**Figure 6.13** *C=30, K=400 Impedance response*

Figure 6.14 *C=30, K=50 Impedance responses*

Implementing the impedance controller with varying external forces (F_x) and desired position (x_p) illustrates the behaviour of the controller under normal conditions. Examining the response with M=0, C=10, K=100 (figure 6.15):

1   From 0 until 1.5s (approx.) the controller tracks the desired position with a small constant external force resulting in slight position offset.

2   Between 1.5s and 6s external forces are gradually applied to the link resulting in movement away from the specified position (x_p) .

3   Between 6s and 8s the external force becomes small allowing the impedance controller to behave mainly as a position controller.

4   Finally, between 8s and 10s an external force is applied again causing deviation from the specified position.

Figure 6.15 *Impedance response with varying desired position, M=0, C=10, K=100*

In a physiotherapy scenario the external force is representative of patients experiencing difficulty tracking the desired trajectory. The force would assist the patient movement towards the specified position while the change in robot position prevents the patient's limb being dragged (moved without input from patient). The next section extends the controller to three degrees of freedom.

6.4 Robot kinematics

The impedance controller can be extended to multiple degrees of freedom. For a robot to implement positions in multiple degrees of freedom, it is necessary to understand the relationship between joint angles and global positions. Each joint requires a separate co-ordinate frame as a first step to defining the relationship between joint angles and global positions. *Denavit-Hartenburg* notation consists of a set of rules designed to enable joint axis frames to be systematically assigned to varied robot configurations. These joint axis frames enable the forward kinematics (global position from joint angles) to be derived. The converse of the forward kinematics is inverse kinematics, enabling joint space angles to be found from global co-ordinates. The following section applies these techniques to the prototype robot.

6.4.1 Denavit-Hartenburg Notation

Denavit-Hartenburg Notation consists of a set of rules to enable joint frames to be systematically attached to any configuration of robotic manipulator, as described in detail by **Tsai (1999)**. Using this notation, joint frames can be attached to the prototype physiotherapy robot (figure 6.16). As all joints are revolute, the joint angle (θ) at each axis effects the manipulator configuration. Note that joint (0) is mapped onto a base frame (b) to enable consistent global co-ordinates for the one and three degree-of-freedom controllers (x direction points upwards). Mapping these joint frames together enables the orientation and global position of the robot end-point to be found. This is known as the robot's forward kinematics.
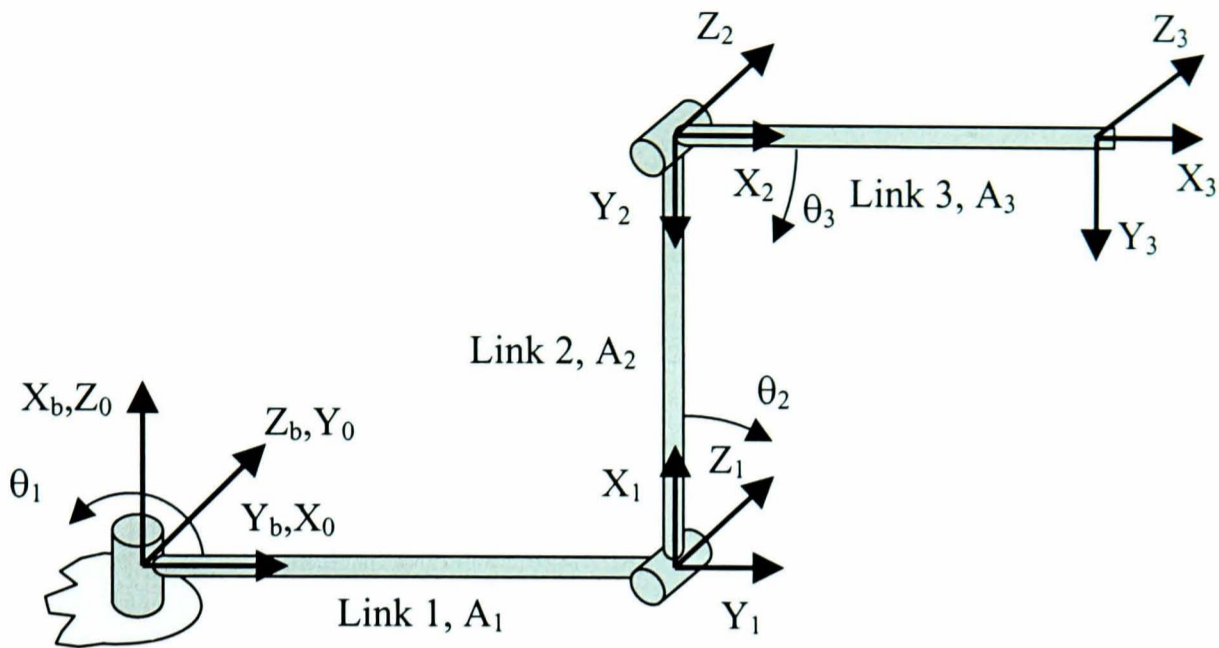
Figure 6.16 *Attaching joint space axes*

6.4.2 Forward Kinematics

Combining the rotations and translations shown in figure 6.16 enables a single matrix of rotation and translation to be produced. To simplify the derivation, say $\alpha_k = \theta_1$, $\beta_k = \theta_2 - 90^0$, $\gamma_k = \theta_3 + 90^0$. The robots forward kinematics can be found to be:

$$\begin{bmatrix} \cos(\beta_k + \gamma_k) & -\sin(\beta_k + \gamma_k) & 0 & -0.3\sin(\beta_k + \gamma_k) - 0.3\sin(\beta_k) \\ \cos(\alpha_k).\sin(\beta_k + \gamma_k) & \cos(\alpha_k).\cos(\beta_k + \gamma_k) & -\sin(\alpha_k) & 0.3\cos(\alpha_k).\left(\cos(\beta_k + \gamma_k) + \dfrac{0.395}{0.3} + \cos(\beta_k)\right) \\ \sin(\alpha_k).\cos(\beta_k + \gamma_k) & \sin(\alpha_k).\sin(\beta_k + \gamma_k) & \cos(\alpha_k) & 0.3\sin(\alpha_k).\left(\cos(\beta_k + \gamma_k) + \dfrac{0.395}{0.3} + \cos(\beta_k)\right) \\ 0 & 0 & 0 & 1 \end{bmatrix} \quad (6.15)$$

Equation 6.15 is known as the homogeneous transformation matrix, containing end point orientation and translation. Columns 1:3 identify the end point orientation, and column 4 identifies end point translation (the robot kinematics)
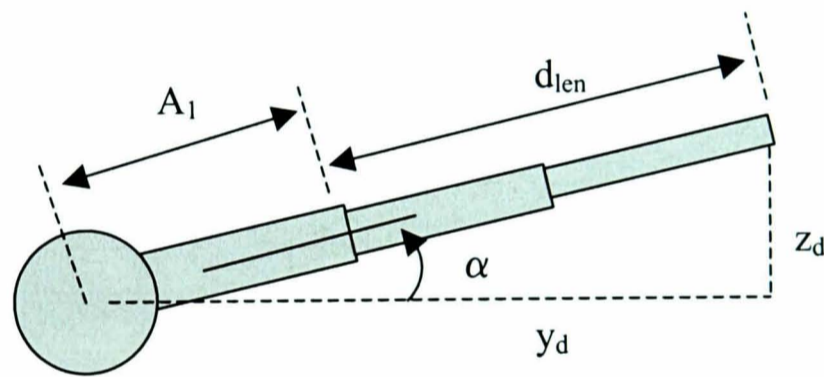
6.4.3 Inverse Kinematics

In order to implement any desired trajectory in task space it is necessary to know the joint space angles corresponding to the required end point position (the opposite to the

robot forward kinematics). Obtaining these joint space angles from specified task space co-ordinates is known as inverse kinematics. Two solution approaches can be used, numerical solution and specific closed-form solution. The numerical approach uses iterative techniques, which can be computationally intensive and time consuming. Many manipulator configurations enable a specific closed-form solution to be obtained from examining the manipulator configuration. This technique is particularly suited to simpler robot configurations. The closed-form solution technique was adopted here.

To find α_k (see figure 6.17) we have:

$$a \tan 2 \left(\frac{z_d}{y_d} \right) = \alpha_k \tag{6.16}$$

where z_d, y_d are desired task space co-ordinates.

**Figure 6.17** *Inverse kinematics of the first joint (robot top view)*

A rotation of α_k affects the y positioning. For given y_d & z_d co-ordinates the required manipulator length due to joints 2 & 3:

$$d_{len} = (\sqrt{y_d{}^2 + z_d{}^2}) - A_1 \tag{6.17}$$

Note that A_1 is a fixed length and cannot be altered by changes in joint angles.
Initially we consider a simplified two degree of freedom solution (see figure 6.18) to find the α_k and γ_k angles.
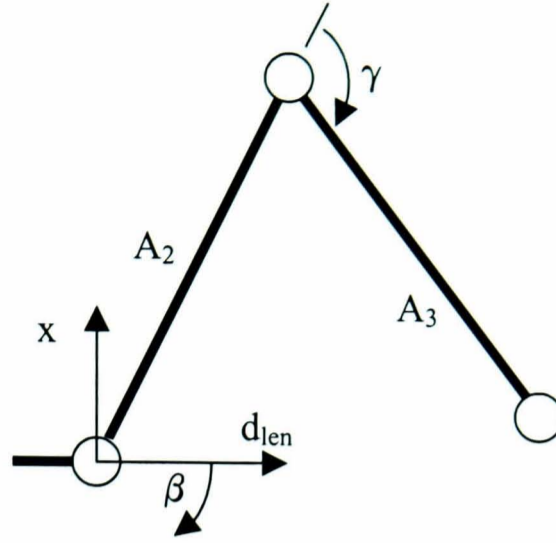
Figure 6.18 *Two degree of freedom inverse kinematics*

So,

$$x_d = -A_2 \sin(\beta_k) - A_3 \sin(\beta_k + \gamma_k) \tag{6.18}$$

$$d_{len} = A_2 \cos(\beta_k) + A_3 \cos(\beta_k + \gamma_k) \tag{6.19}$$

$$x_d{}^2 + d_{len}{}^2 = A_2{}^2 + A_3{}^2 + 2A_2 A_3.(\cos(\beta_k).\cos(\beta_k + \gamma_k) + \sin(\beta_k).\sin(\beta_k + \gamma_k)) \tag{6.20}$$

Reducing (6.20) gives:

$$x_d{}^2 + d_{len}{}^2 = A_2{}^2 + A_3{}^2 + 2A_2 A_3.\cos(\gamma_k) \tag{6.21}$$

$$\gamma_k = a\cos\left(\frac{x_d{}^2 + d_{len}{}^2 - A_2{}^2 - A_3{}^2}{2A_2 A_3}\right) \tag{6.22}$$

Expanding (6.22) and collecting terms:

$$d_{len} = \cos(\beta_k)(A_1 + A_2.\cos(\gamma_k)) - A_2 \sin(\beta_k).\sin(\gamma_k) \tag{6.23}$$

As angle γ_k is already known say,

$$d_{len} = \cos(\beta_k) * k_1 - k_2.\sin(\gamma_k) \tag{6.24}$$

$$x_d = -\sin(\beta_k) * k_1 - k_2.\cos(\gamma_k) \tag{6.25}$$

Let $k_1 = r.\cos(\lambda_k)$ & $k_2 = r.\sin(\lambda_k)$ $\tag{6.26}$

Then,

$$\lambda_k = \text{atan2}(k_2, k_1) \tag{6.27}$$

(6.24) & (6.25) then become:

$$\frac{x_d}{r} = -\sin(\lambda_k + \beta_k) \tag{6.28}$$

$$\frac{d_{len}}{r} = \cos(\lambda_k + \beta_k) \tag{6.29}$$

Dividing (6.32) by (6.33) gives:

$$\frac{x_d}{d_{len}} = -\tan(\lambda_k + \beta_k) \tag{6.30}$$

Finally, rearranging (6.30) and combining with (6.27) gives the solution β_k as:

$$\beta_k = -a\tan 2(x_d, d_{len}) - a\tan 2(A_3 \sin(\gamma_k), A_2 + A_3 \cos(\gamma_k)) \tag{6.31}$$

Equations 6.31, 6.27, 6.16 specify the joint angles required to achieve any global position within the robot workspace. To implement these joint space angles the joint position controller performance is crucial. To ensure these controllers are tuned appropriately, an optimising tuning strategy has been developed. This is detailed in the next section.

6.5 Optimisation of PID controller

Selection of controller gains is important to ensure that the best (optimum) response is obtained. The PD gains for the single degree of freedom controller were selected using empirical methods, however, these may not result in the optimum response. Many researchers have investigated the selection and tuning of PID gains, their methods can be broken down into two distinct subgroups, model based and results orientated. PID gain selection through generation of plant models (as long as the plant can be represented as second order) is common, however, the main drawback of this method is the requirement for an accurate system model **(Astrom and Wittenmark 1997)**.

6.5.1 Experimentally tuning PID gains

The tuning of PID controllers based on experimental results is the most common form of PID tuning. The Ziegler-Nichols step-response method and ultimate sensitivity method are two variations of this tuning strategy designed for continuous time PID controllers, however, if the sampling interval is short they can be used for discrete systems **(Astrom and Wittenmark 1997)**.

The Ziegler and Nichols step response method utilises the time delay and response time, which can be obtained from the system experimental step or impulse response. PID gains are then selected from a table. The ultimate sensitivity method requires the experimental system to be controlled purely by proportional control. This proportional gain is then increased until the controller stability limit. The proportional gain at this stability limit is used to select appropriate PID gains.

These tuning rules can provide a rough approximation of the optimum controller gains, but the tuning can often be improved.

6.5.2 Optimisation of PID gains

Here, the controller gains will be optimised on-line by assessing the quality of the previous response and adjusting the gains appropriately. This method requires the optimisation of the response by tuning the three PID gains. The *downhill simplex*

method enables the minimisation of functions in multiple degrees of freedom (**Press et al. (1991)**), and was used in this study.

This method summarises the quality of a response (cost) as a single number (the lower the cost function the better tuned the system). At the commencement of tuning four responses are required, that are then summarised as four costs, dependent upon the quality of the response. The strategy tests PID gains around the four best responses (lowest costs) in an attempt to improve the response. A set of rules dictates the variations to the PID gains to be attempted. If an improvement in response is obtained for these new PID parameters then the response replaces one of four the previously stored data points. This method of trial and error systematically encloses the optimum controller gains.

The performance of any optimisation strategy is completely dependent upon selection of the cost function (assessment of the quality of the current response). The cost function selected for the PID gain optimisation used the ISTE criterion for quality of response (**Astrom and Hagglund (1994)**):

$$\int_0^\infty T^2 e^2(t)dt \tag{6.32}$$

where T is the time period and e is the error between desired and actual response.

Equation 6.32 results in a reasonable representation of the quality of the system response, however, slight steady state error can result in the response being considered worse than an oscillatory response. Indeed, this effect is evident for the second joint of the robot, where slight gravity imbalance results in a small amount of steady state error. Optimising the PID gains of this joint using solely the ISTE performance criterion results in an oscillatory response.

To bias the cost function against the transient response, the demand and actual responses were passed through a high pass filter before assessment by the ISTE criterion. With the high-pass filter included no movement of the joint results in an

optimum response. To prevent the controller tuning to obtain this effect, the controller gains were restricted to a minimum bound. This is not a large consideration as gain limits are required at extreme low and high gains to prevent instability, especially preventing the potentially damaging assessment of negative gains on controller performance.

The optimum PID tuning transients for joints 1,2 and 3 are shown in figures 6.19, 6.20 and 6.21 respectively. The PID optimisation was performed twice for each joint, with the gains converging to similar values. Step responses for each joint are shown in figures 6.22, 6.23 and 6.24. The identified PID gains for each joint are shown in table 6.2.

	Proportional (P)	Derivative (D)	Integral (I)
Joint 1	18	2.5	0.04
Joint 2	5.5	0.45	0.5
Joint 3	2.2	0.065	0.7

Table 6.1 Optimised PID gains

Note the steady state error present in the second joint, with the high-pass filter enabling optimisation of the transient element of the response. All three joints exhibit fast response time and little overshoot.
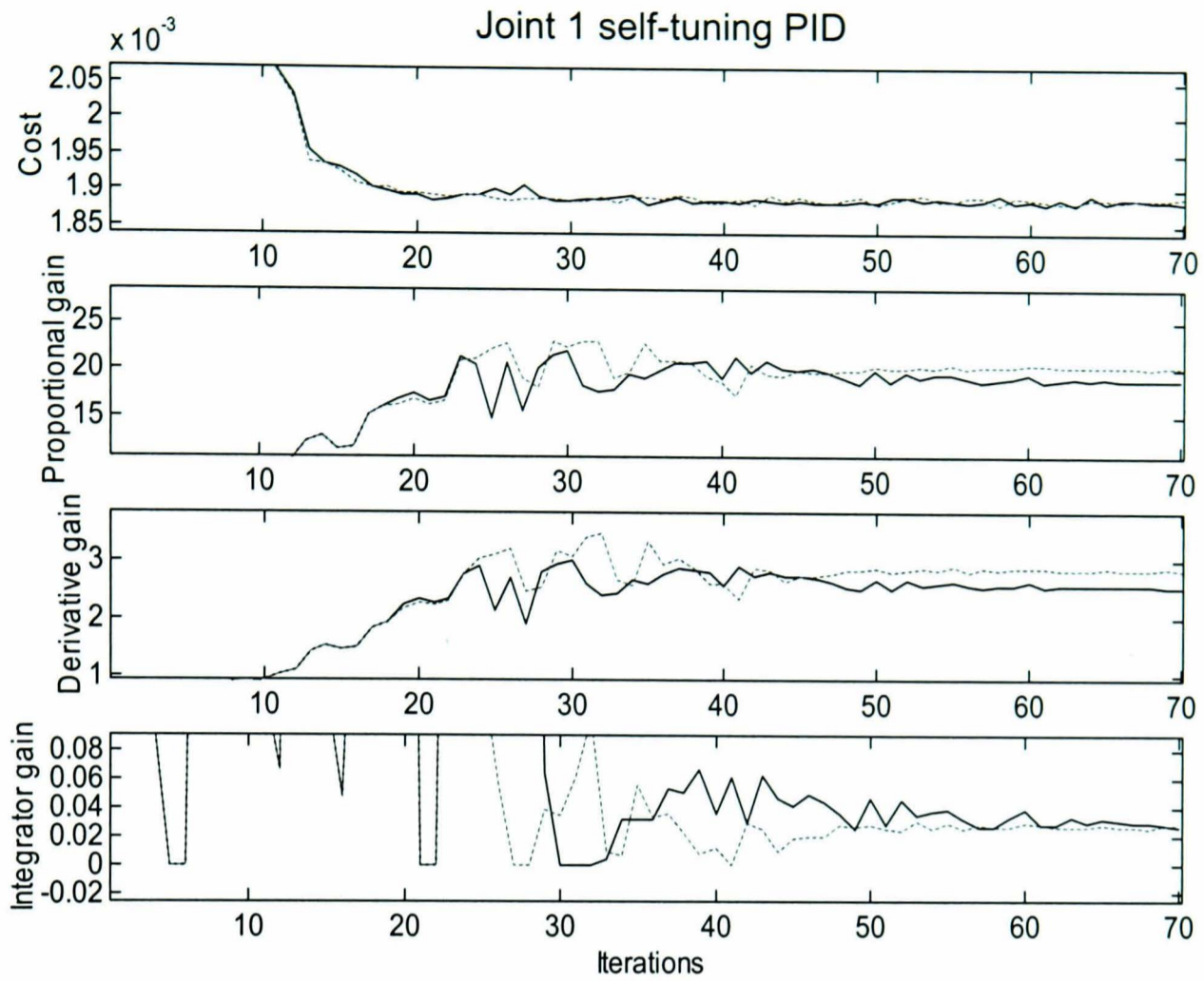
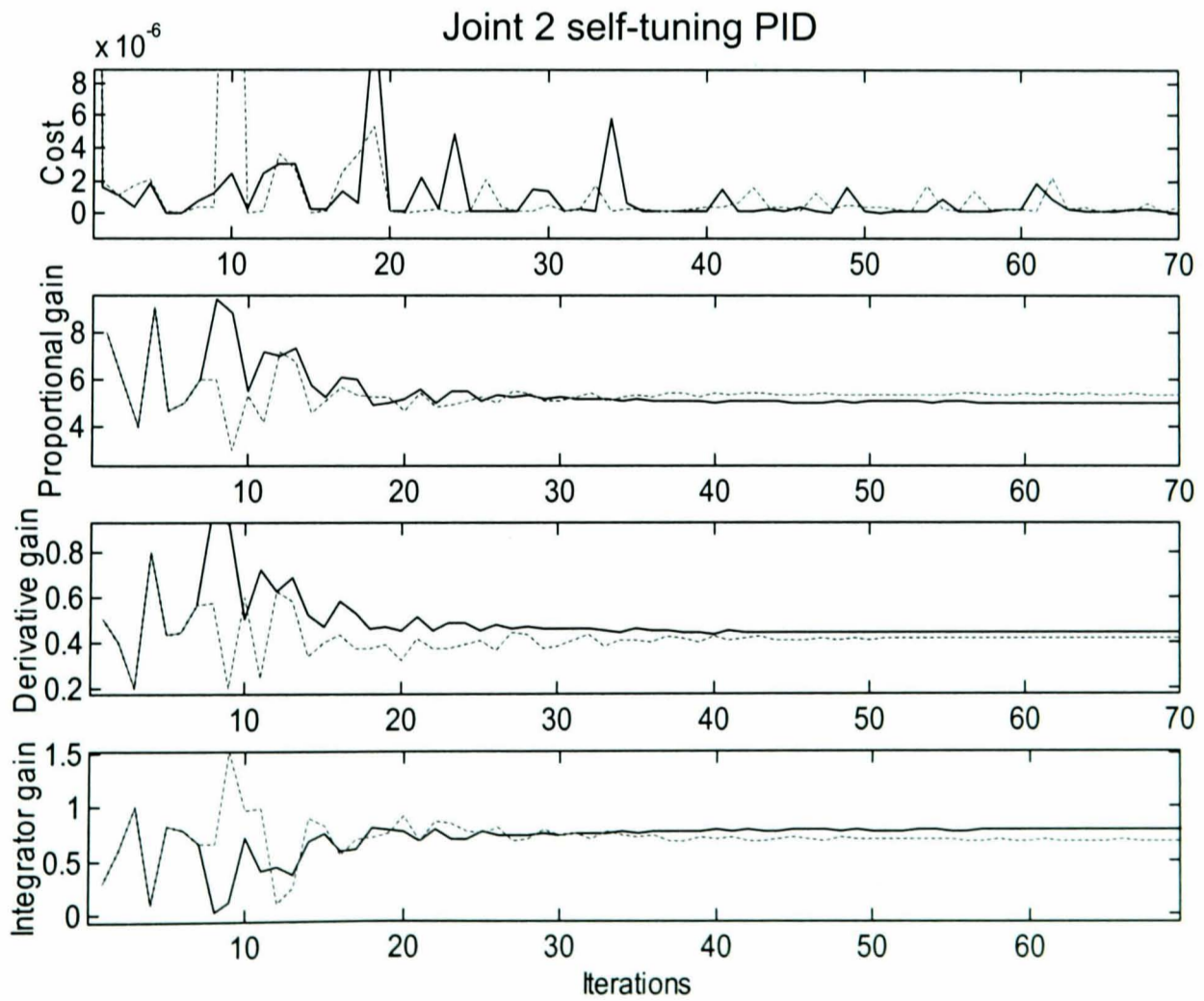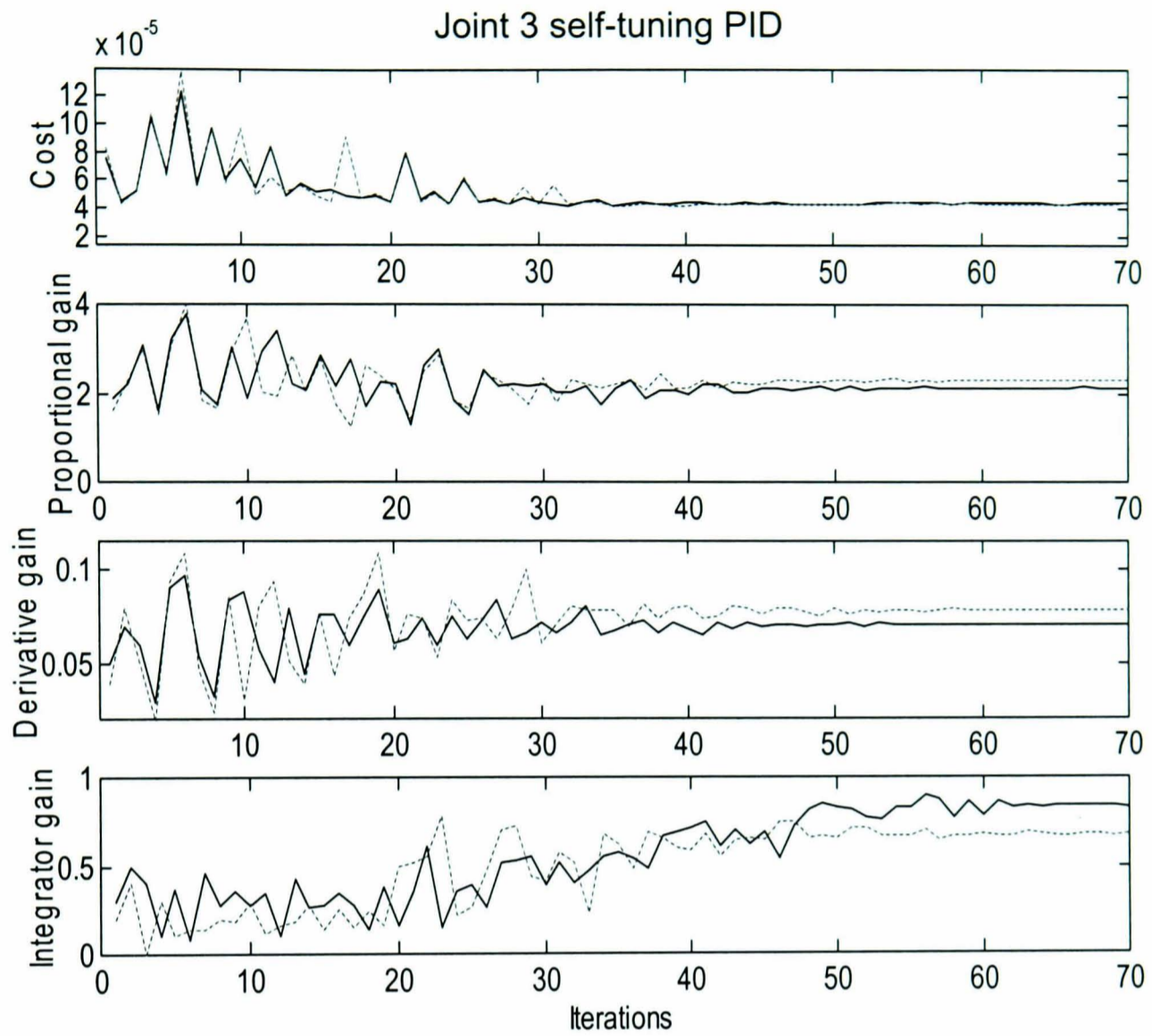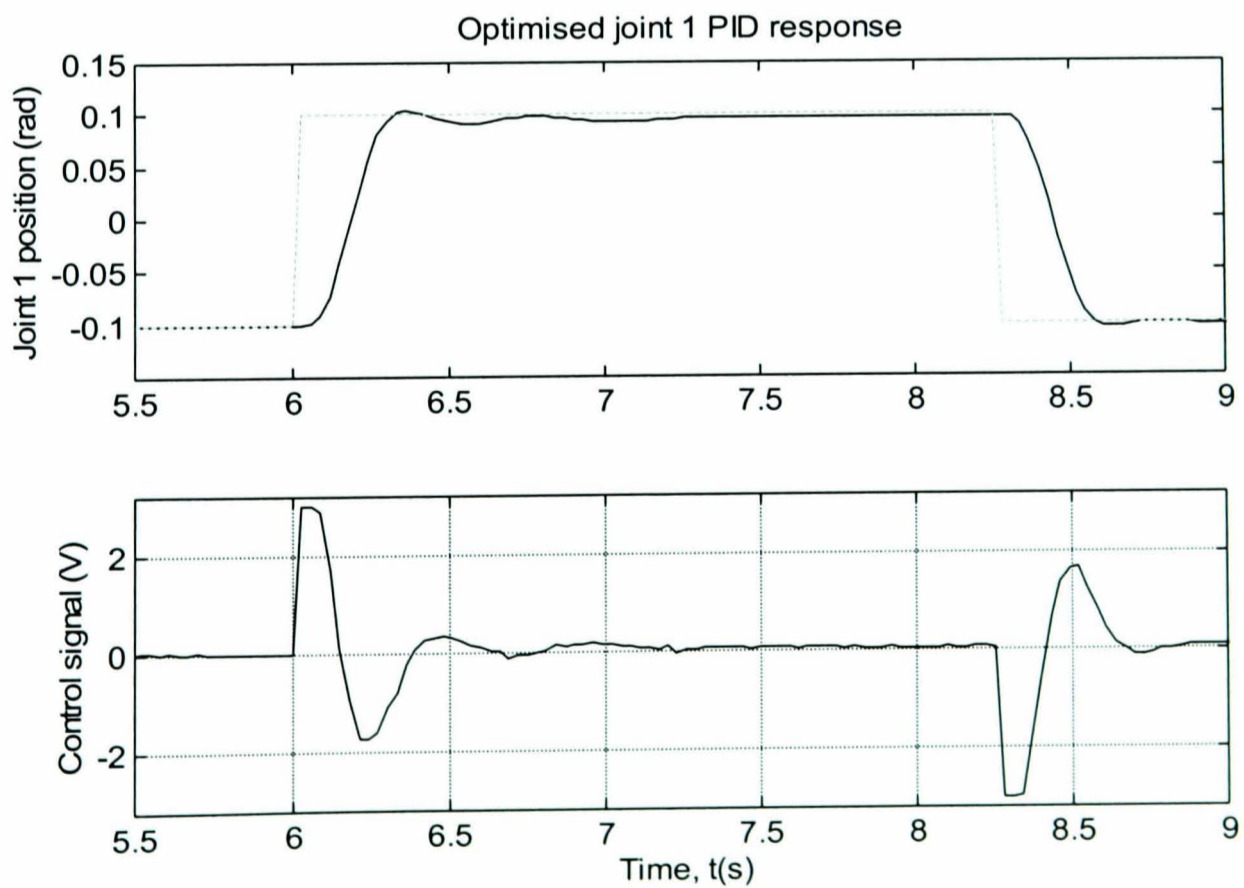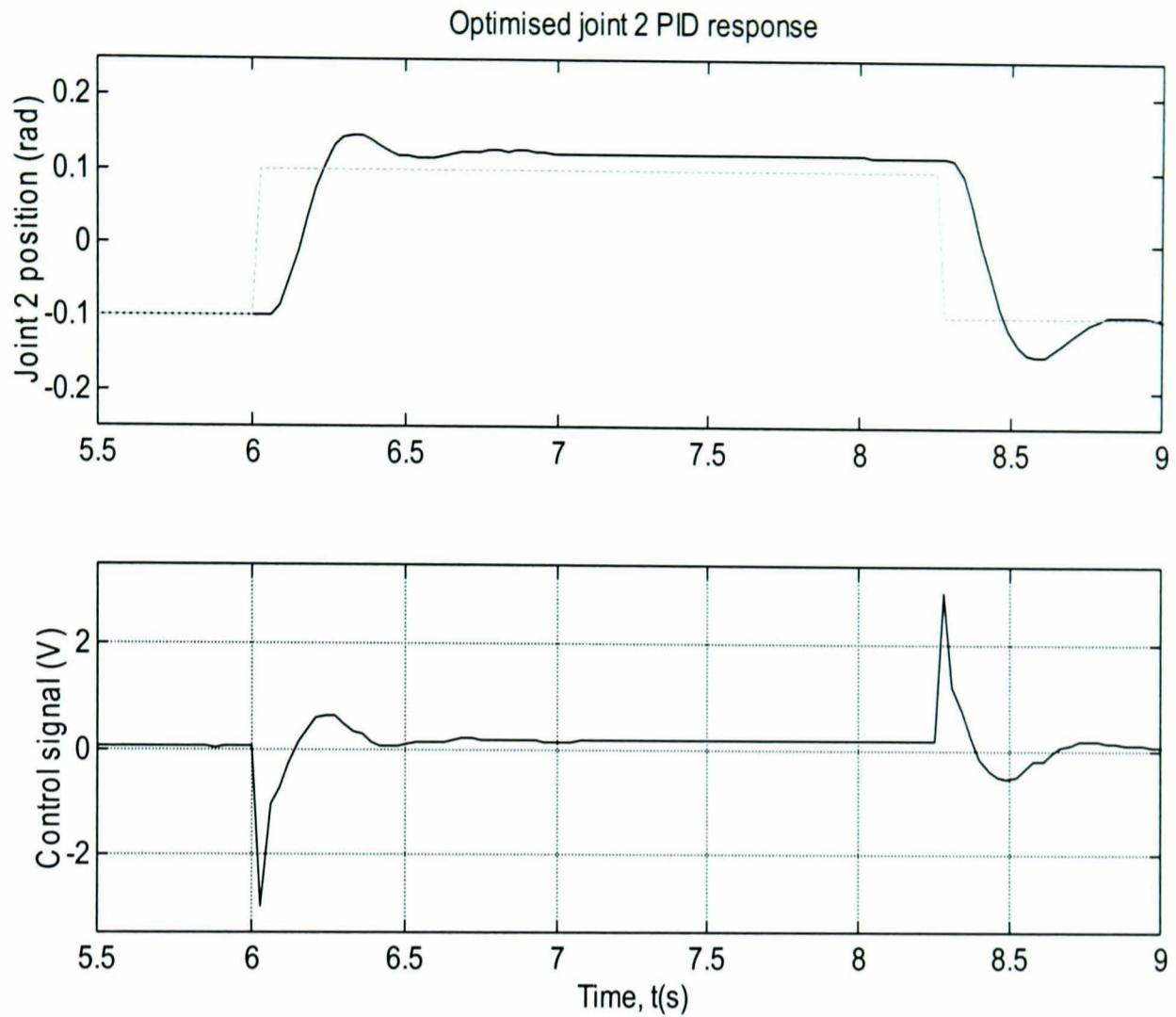**Figure 6.19** *Tuning joint 1 optimum PID response*
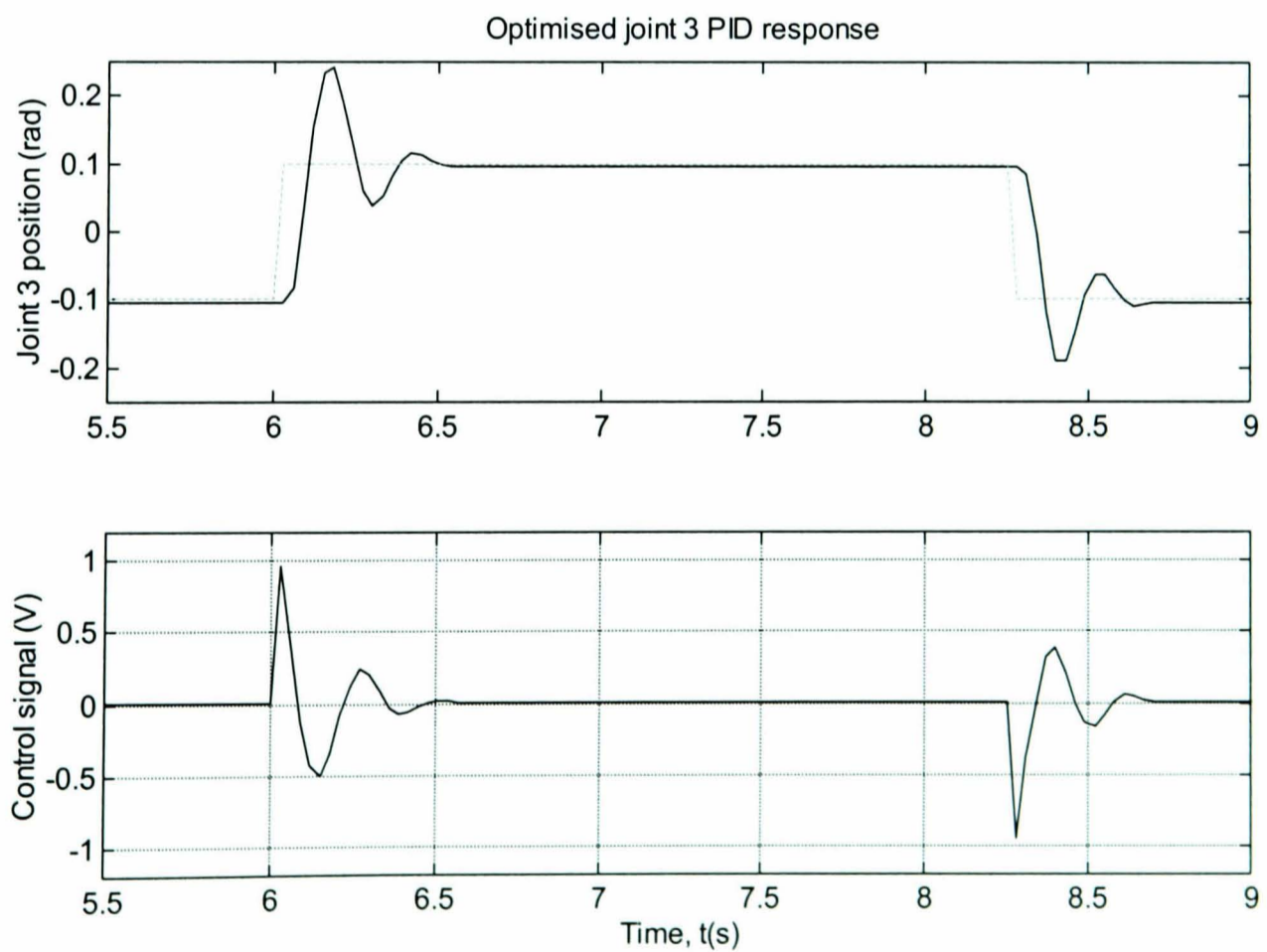

Figure 6.20 *Tuning joint 2 optimum PID response*

Figure 6.21 *Tuning joint 3 optimum PID response*

Figure 6.22 *Optimised joint 1 PID response*

Optimised joint 2 PID response

Figure 6.23 *Optimised joint 2 PID response*

Optimised joint 3 PID response

Figure 6.24 *Optimised joint 3 PID response*

6.6   Extension to multiple degrees of freedom

The optimised PID joint space controllers and inverse kinematics enable, the impedance controller to be extended to multiple degrees of freedom. The controller implementation takes the form shown in figure 6.25.

The desired end point trajectory is specified before implementing the controller, in the form of global position co-ordinates (x_p, y_p, z_p). These co-ordinates when added to the desired change in position due to external forces (as a result of the impedance filter) (x_i, y_i, z_i), form the desired robot position at any instant. The desired global positions are converted into joint space demands $(\theta_{1d}, \theta_{2d}, \theta_{3d})$, using the robot inverse kinematics. Three independent controllers implement the desired joint space positions.

External forces are resolved through the robot to obtain their influence on each joint $(\tau_{ex1}, \tau_{ex2}, \tau_{ex3})$. An equal, but opposite force is generated by the joint space open-loop force controllers, to reduce the effects of these external forces on link position.

The forward kinematics of the joint positions reveals the robot end position in task space co-ordinates (x, y, z). External forces are measured at the robot end-point using the three degree-of-freedom force sensor. Three separate impedance filters convert the global external forces F_x, F_y and F_z into changes of the x,y & z desired task space co-ordinates respectively. Note that it is possible to implement different impedance filters for different degrees of freedom.

So the implementation of the impedance controller in multiple degrees of freedom requires knowledge of the kinematic relationship between global end-points, external forces and actuator forces. The forward and inverse kinematics have been detailed in section 6.4, however the global forces, the influence of the external force on individual links, and resolution of the actuator line of action are required to implement the impedance controller. For brevity these are detailed in appendix C.
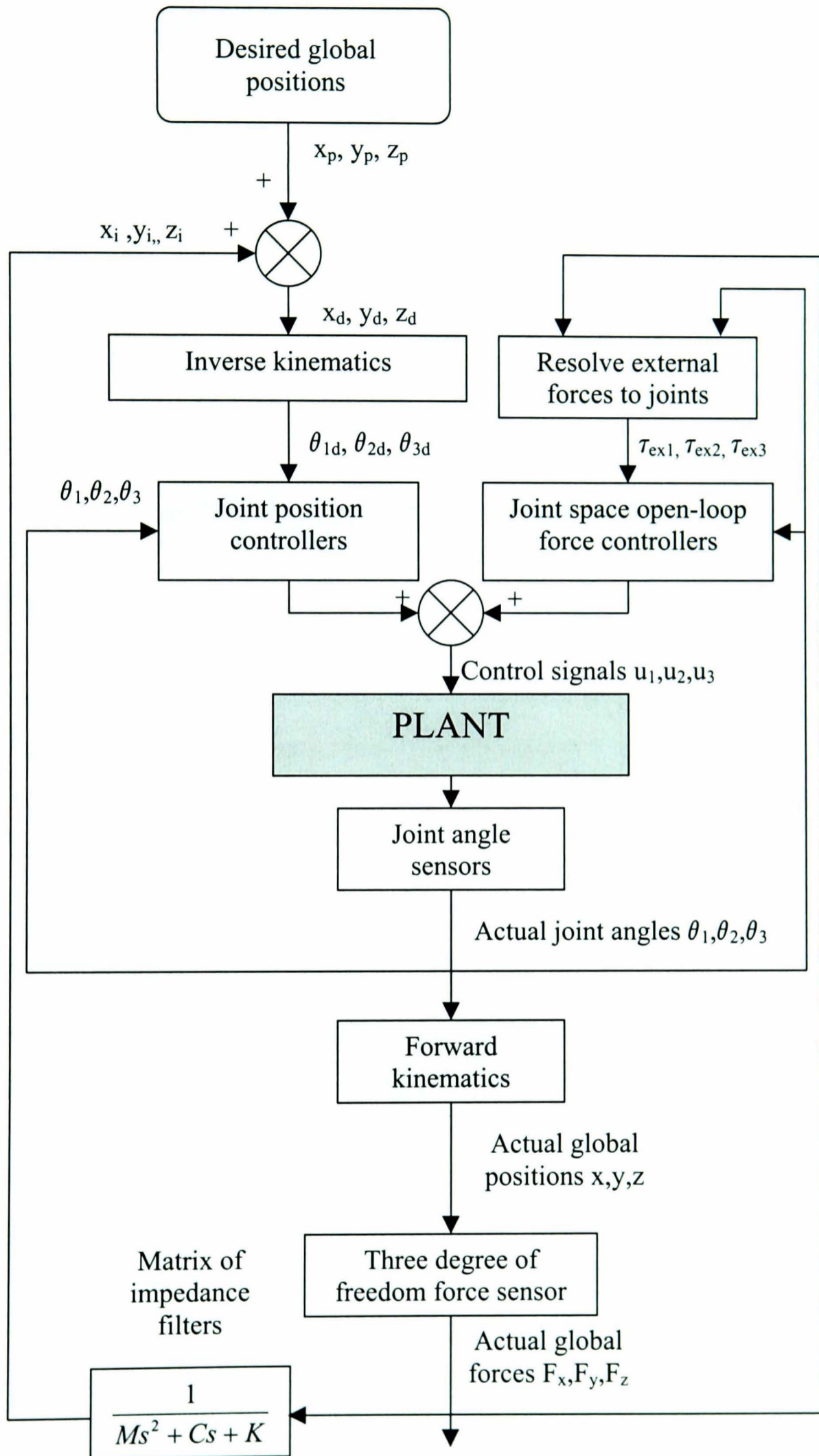
Figure 6.25 *Implementing impedance control in multiple degrees of freedom*

6.7 Two degree of freedom impedance control

The multiple degree-of-freedom impedance controller developed in the previous section has been implemented in two degrees-of-freedom (three degrees of freedom is in section 6.8). Joint 1 was fixed at zero degrees, with the two degrees-of-freedom achieved through manipulation of joints 2 and 3.

To assess the performance of purely the two degree-of-freedom position controller, no external forces were applied to the robot and the readings from the force sensor were set to zero. The position tracking of the robot was tested using a motion (in x,y co-ordinates) commencing at (0.29,0.68) moving to (0.28,0.71) then returning to (0.29,0.68). The experimental results of this movement are shown in figures 6.26 and 6.27. The desired response is tracked, however, errors exist between the desired position and actual position. To examine the position error further, the actual position has been subtracted from the experimental response figures 6.28 and 6.29. The greater position error is present in the x direction with the error negative in the first half of the response and positive in the second half of the response.

The two degree-of-freedom position controller has been extended to the full impedance controller. To assess the performance of the controller, varying forces were applied simultaneously in two degrees of freedom. Ideally, force would be applied across a broad frequency range in multiple degrees-of-freedom. Experimental equipment capable of applying these variable forces in multiple degrees-of-freedom would be extremely difficult to obtain. The forces were applied through human input and were intended to be as consistent as possible. The use of a human to apply the forces tests the controller under actual operating conditions. When visually assessing the performance of these results it is important to take into account the applied force. Five sets of impedance characteristics have been selected to assess the controller performance. In reality, an infinite number of damping and stiffness parameters can be specified.

The impedance characteristics chosen were intended to demonstrate the controller over a broad range. Low values of damping and stiffness values (K=50, C=50) were used to assess the controller performance applying little assistance (figure 6.30). Low stiffness

and damping causes a small amount of force to result in large displacement. The experimental tracking with these parameters is good, with both the desired x and y trajectory accurately followed. Due to the low stiffness, the maximum applied force is approximately 5N.

The second response implements a large difference between the stiffness and damping coefficients (K=170, C=50). These parameters enable the assessment of the controller performance for predominantly stiffness characteristics. The experimental response for these parameters (figure 6.31) accurately tracks the desired, although the amplitude of the experimental response is slightly larger than the desired. It is likely this is a result of errors in force measurement.

The third response implements large damping and low stiffness (K=50, C=170). One of the previously identified problems of pneumatic systems is the rate of change of mass, since this causes delays in system response. A response with high damping and low stiffness becomes a predominantly velocity controller, for which delays in response are significant. The experimental response for these impedance parameters (figure 6.32) illustrates that the response has degraded. The x response, in particular, demonstrates poor amplitude tracking alongside poor velocity tracking.

The fourth response implements large stiffness and damping parameters (K=250, C=250). These parameters result in a large force required to produce any motion. The experimental response for these parameters (figure 6.33) illustrates significantly reduced performance when compared to the low stiffness and damping response. It is important to note that the applied force is now approximately 15N to achieve a similar magnitude of motion. The reduction in performance is possibly due to the increased force highlighting any deficiencies in force measurement. Finally, the fifth response implements stiffness and damping parameters between the previously examined low and high impedance sets (C=130, K=130). The experimental response (figure 6.34) accurately tracks the desired trajectory with little degradation in response noticeable when compared to the low stiffness and damping.
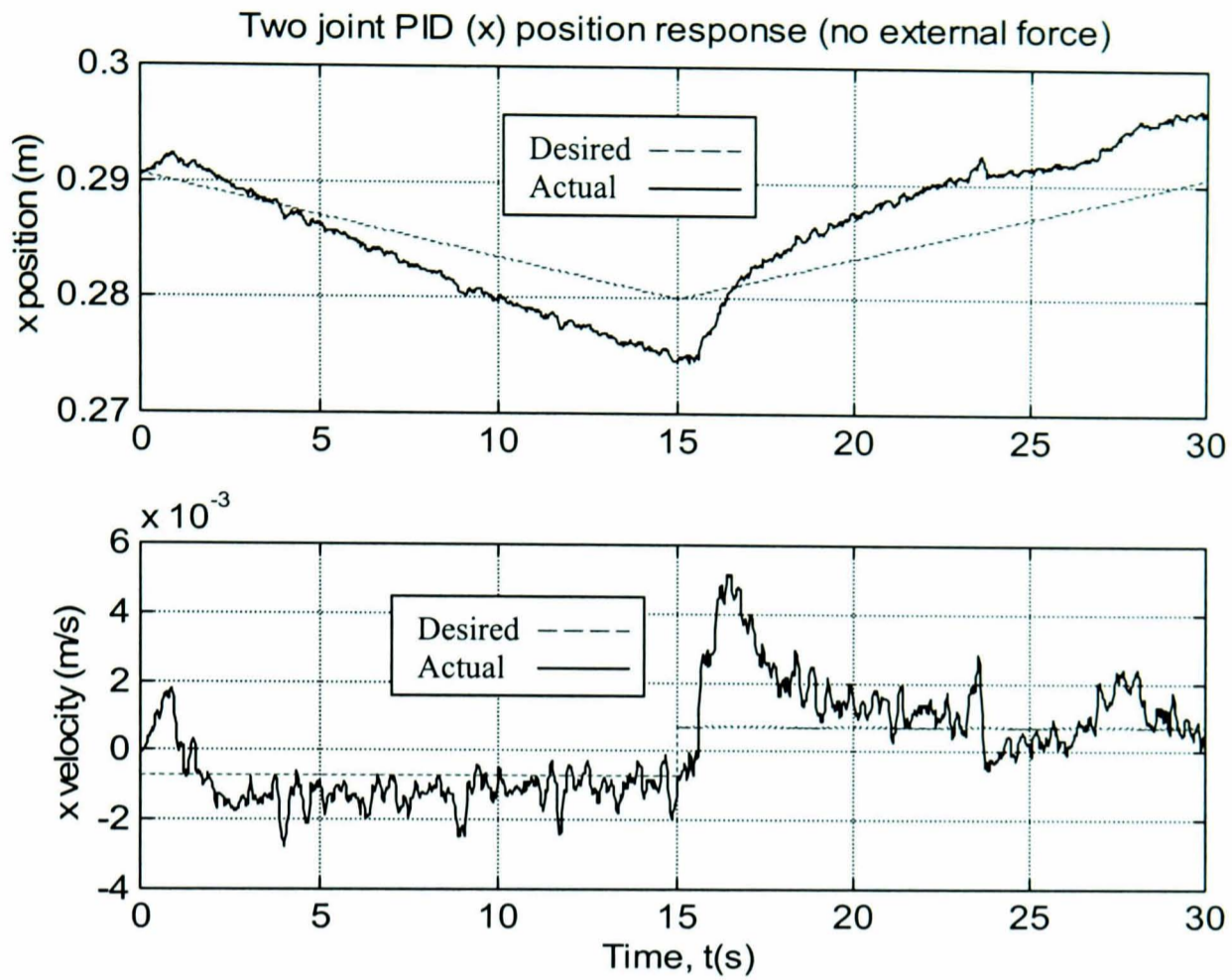
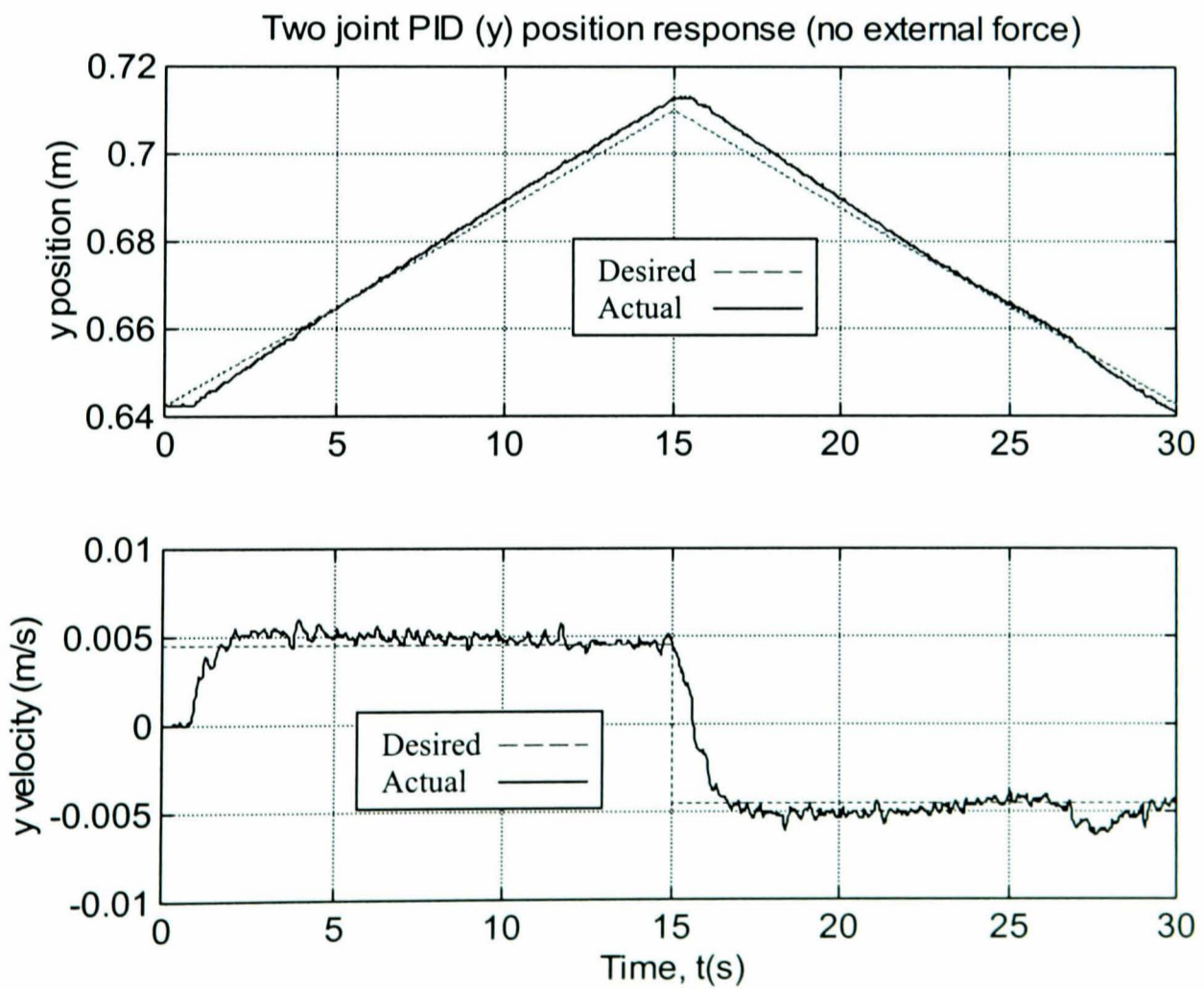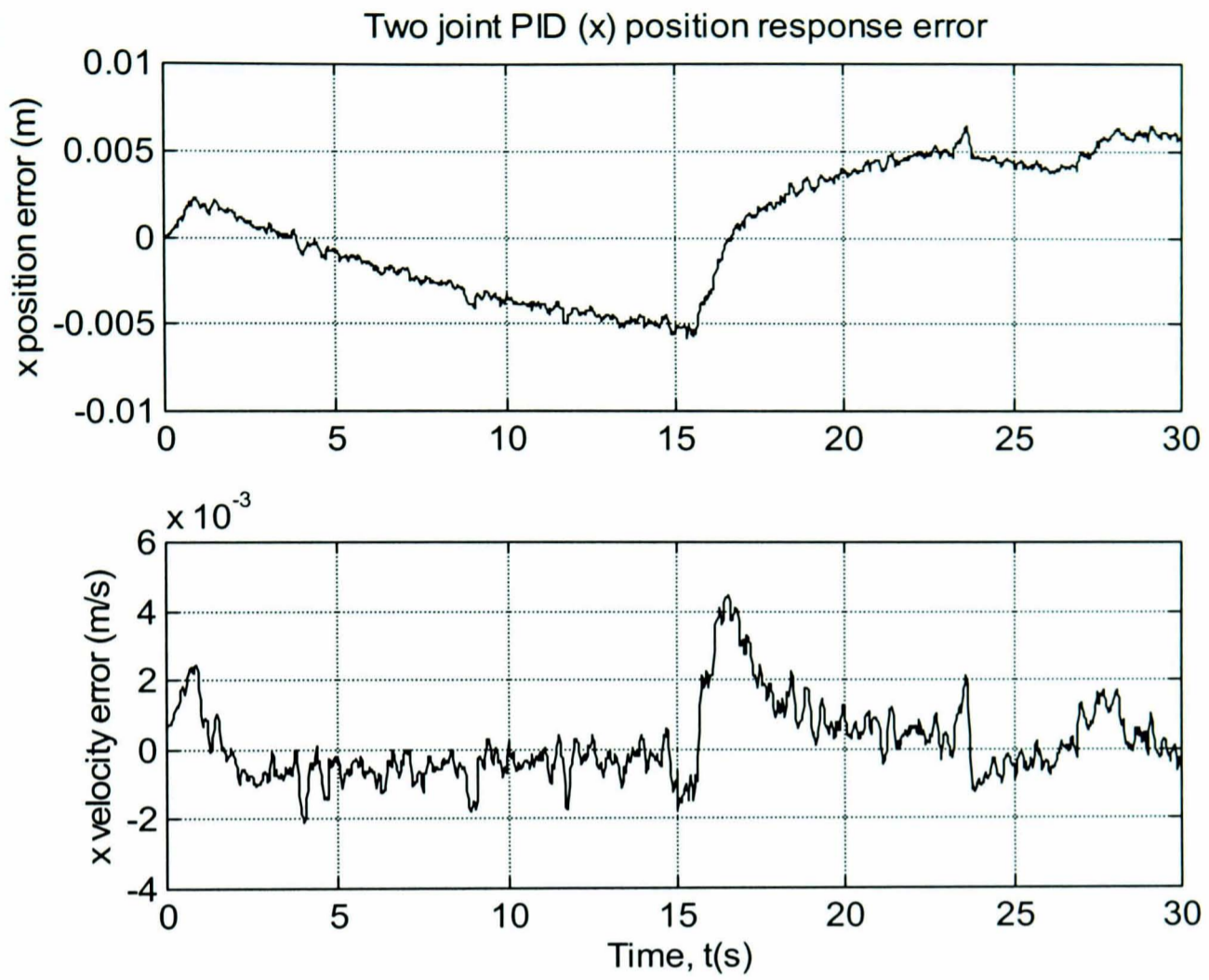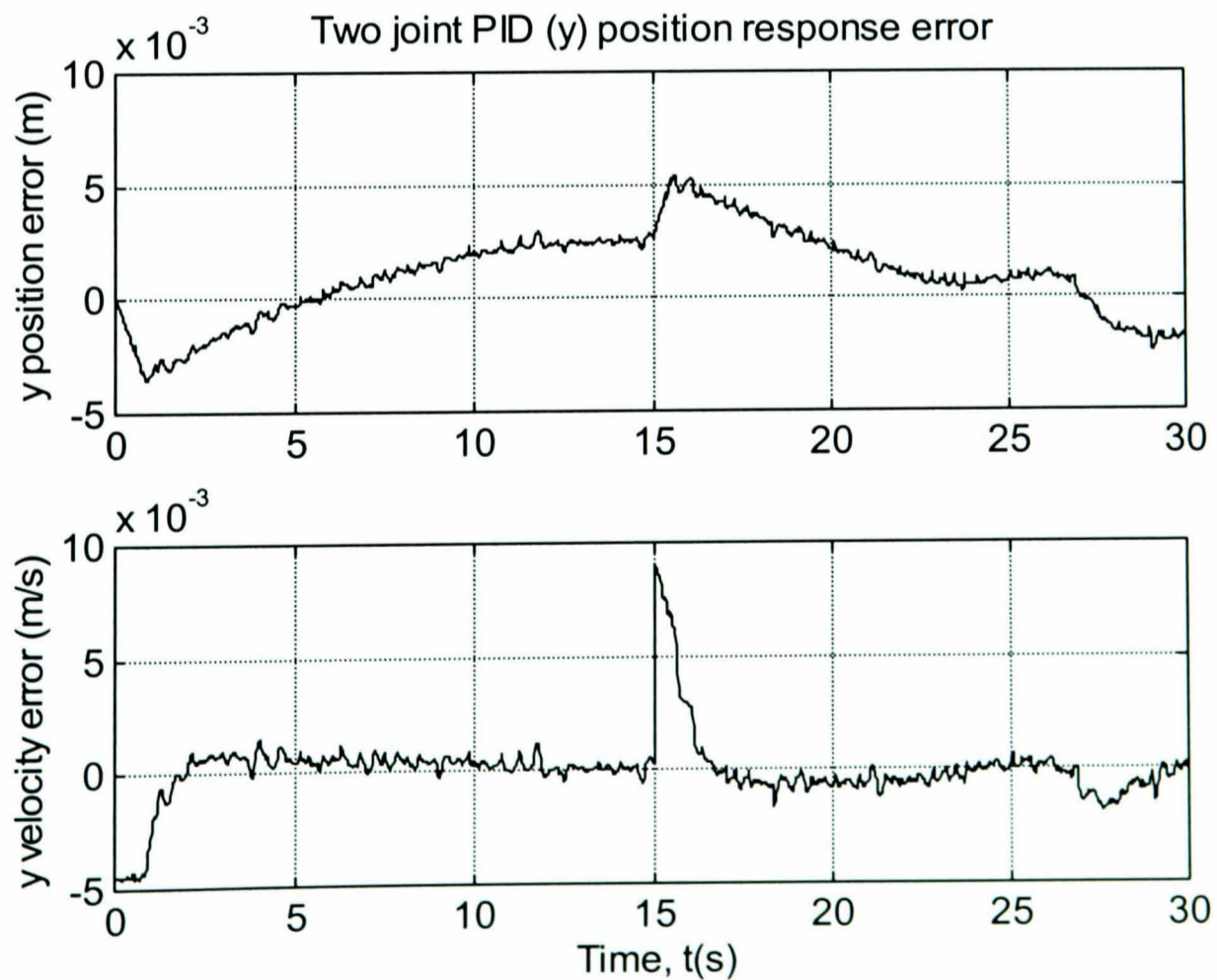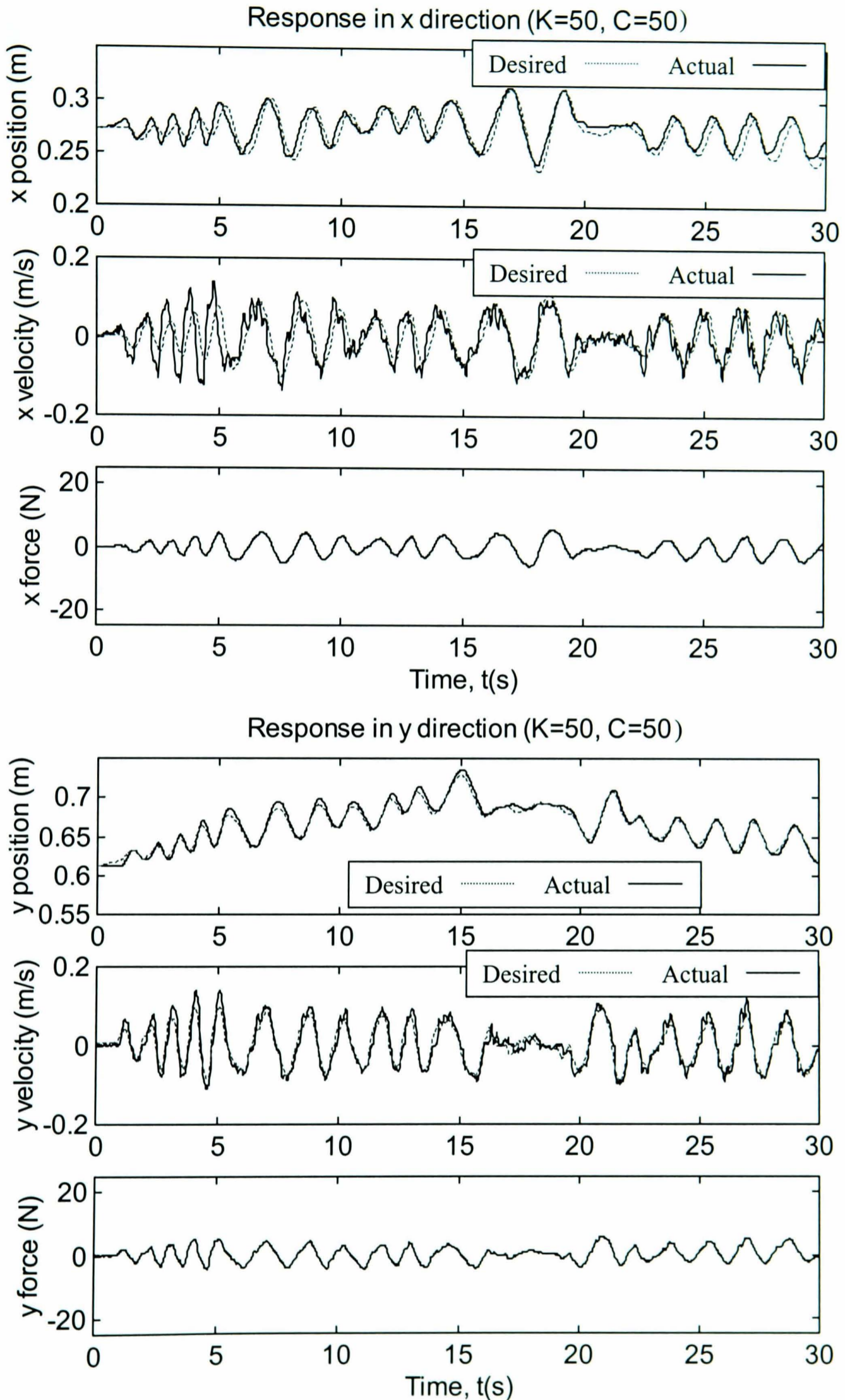**Figure 6. 26** *Two joint PID position response (X)*

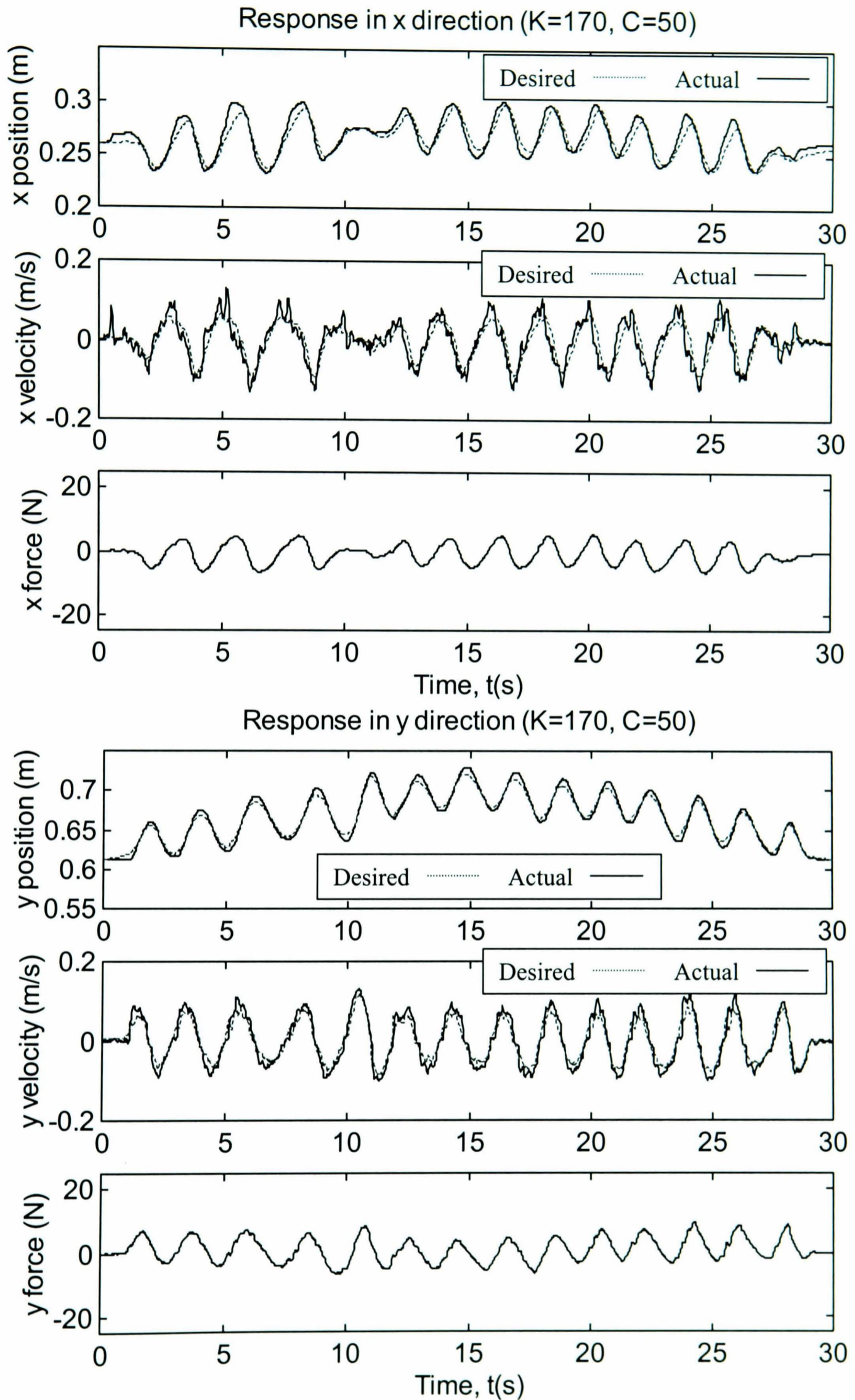**Figure 6. 27** *Two joint PID position response (y)*

Figure 6. 28 *Two joint PID (x) position error*

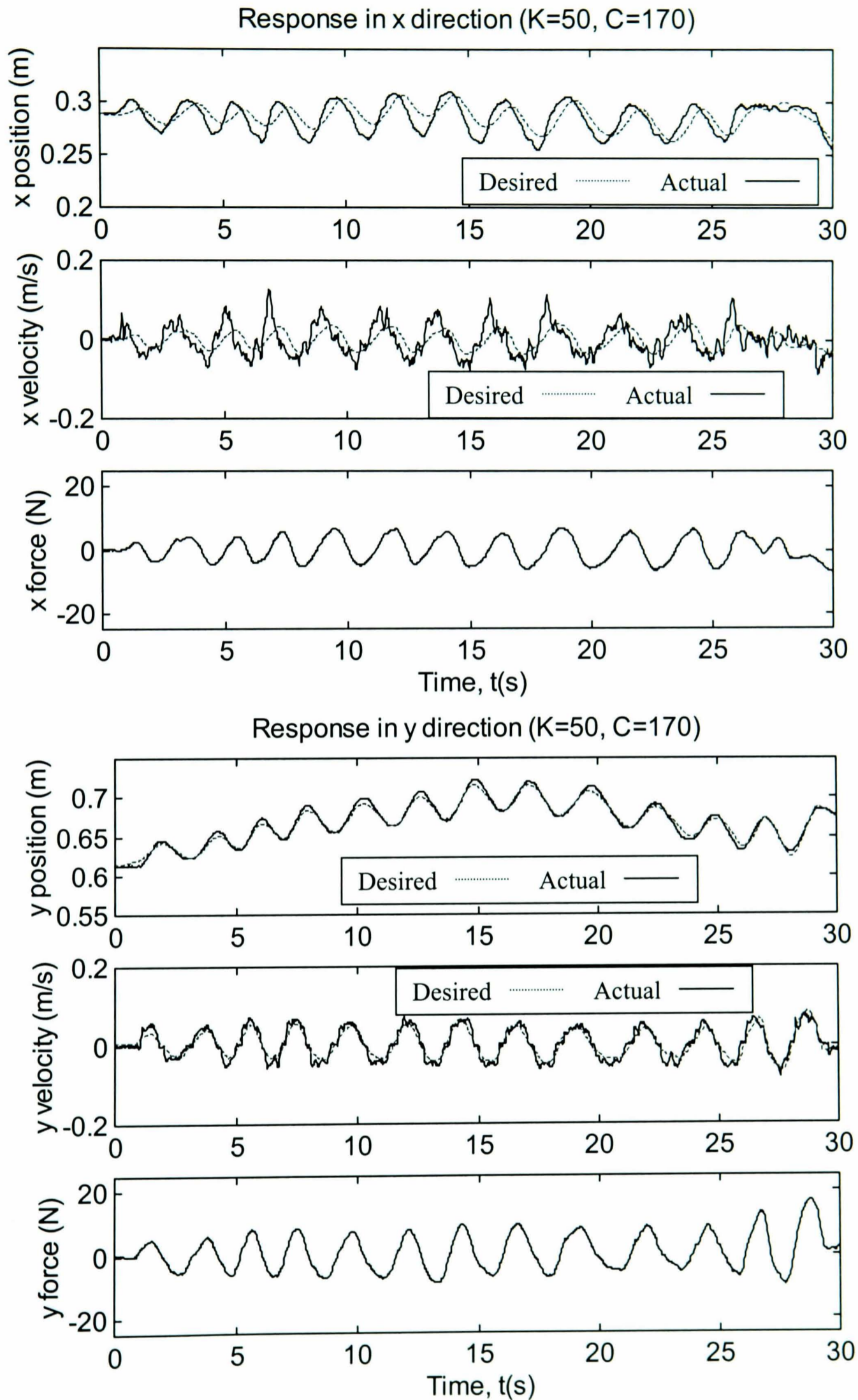**Figure 6. 29** *Two joint PID (y) position error*

Figure 6.30 *Two degree of freedom impedance control (K=50, C=50)*

Figure 6.31 *Two degree of freedom impedance control (K=170, C=50)*

Response in x direction (K=50, C=170)

Response in y direction (K=50, C=170)

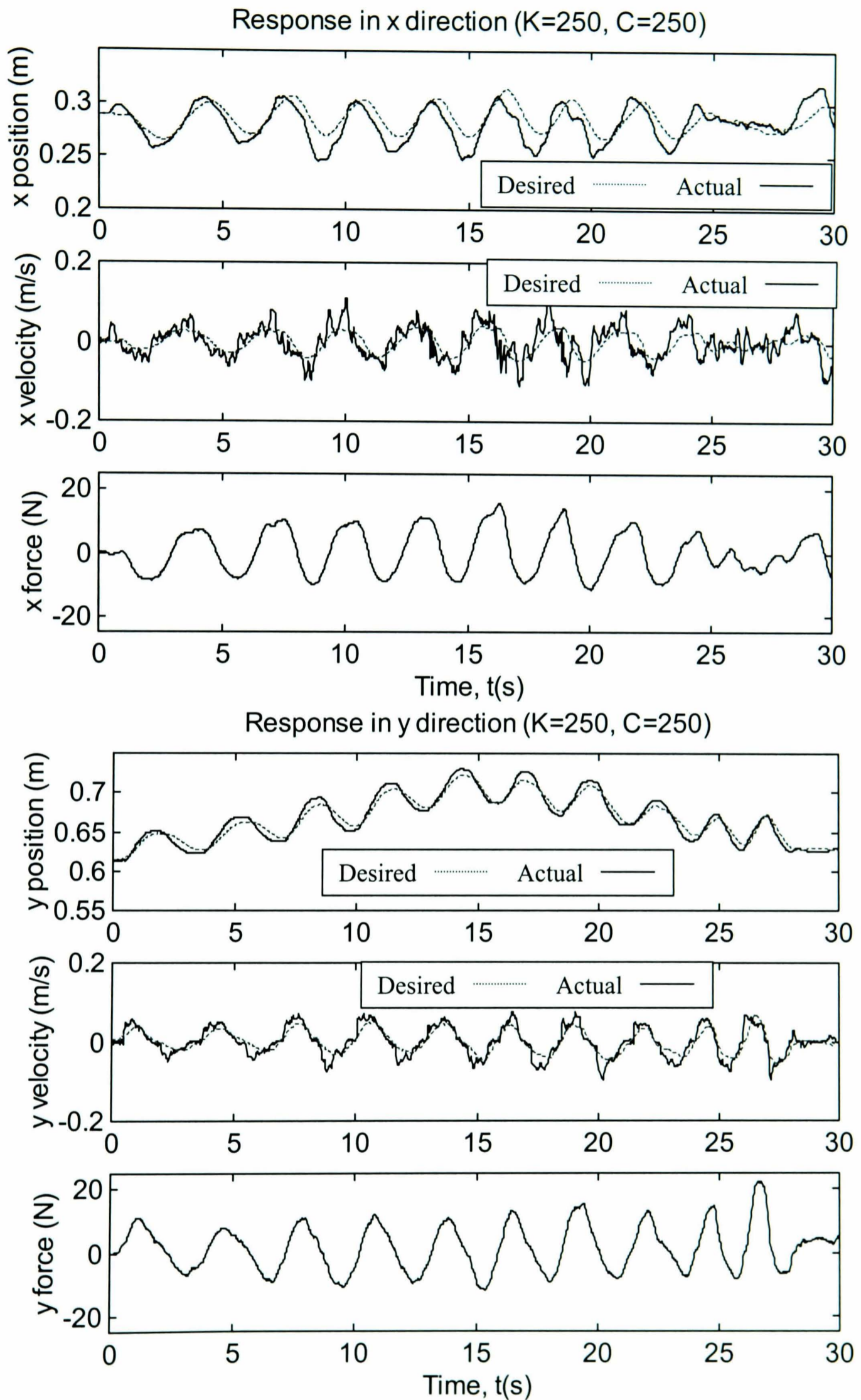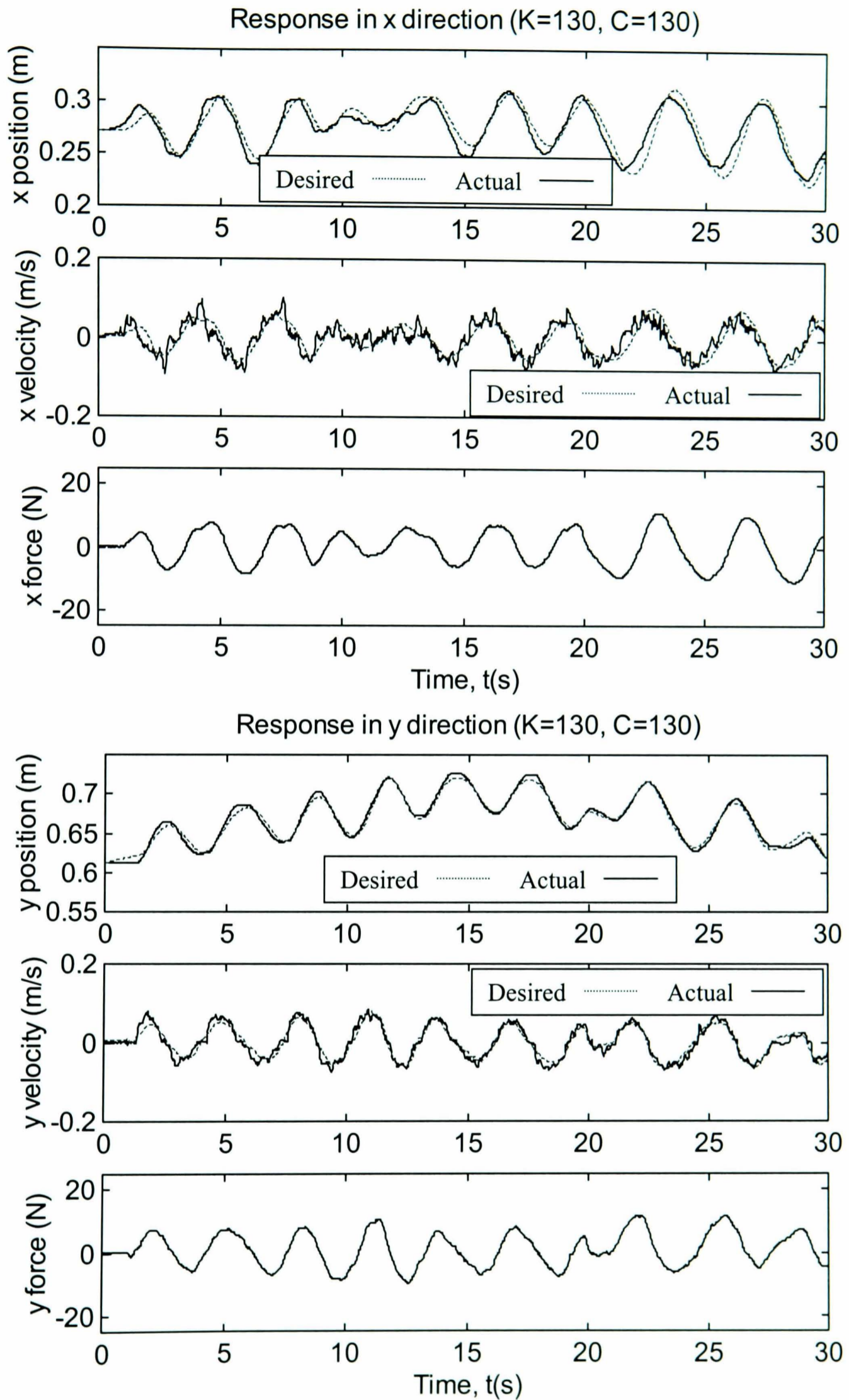***Figure 6.32*** *Two degree of freedom impedance control (K=50, C=170)*

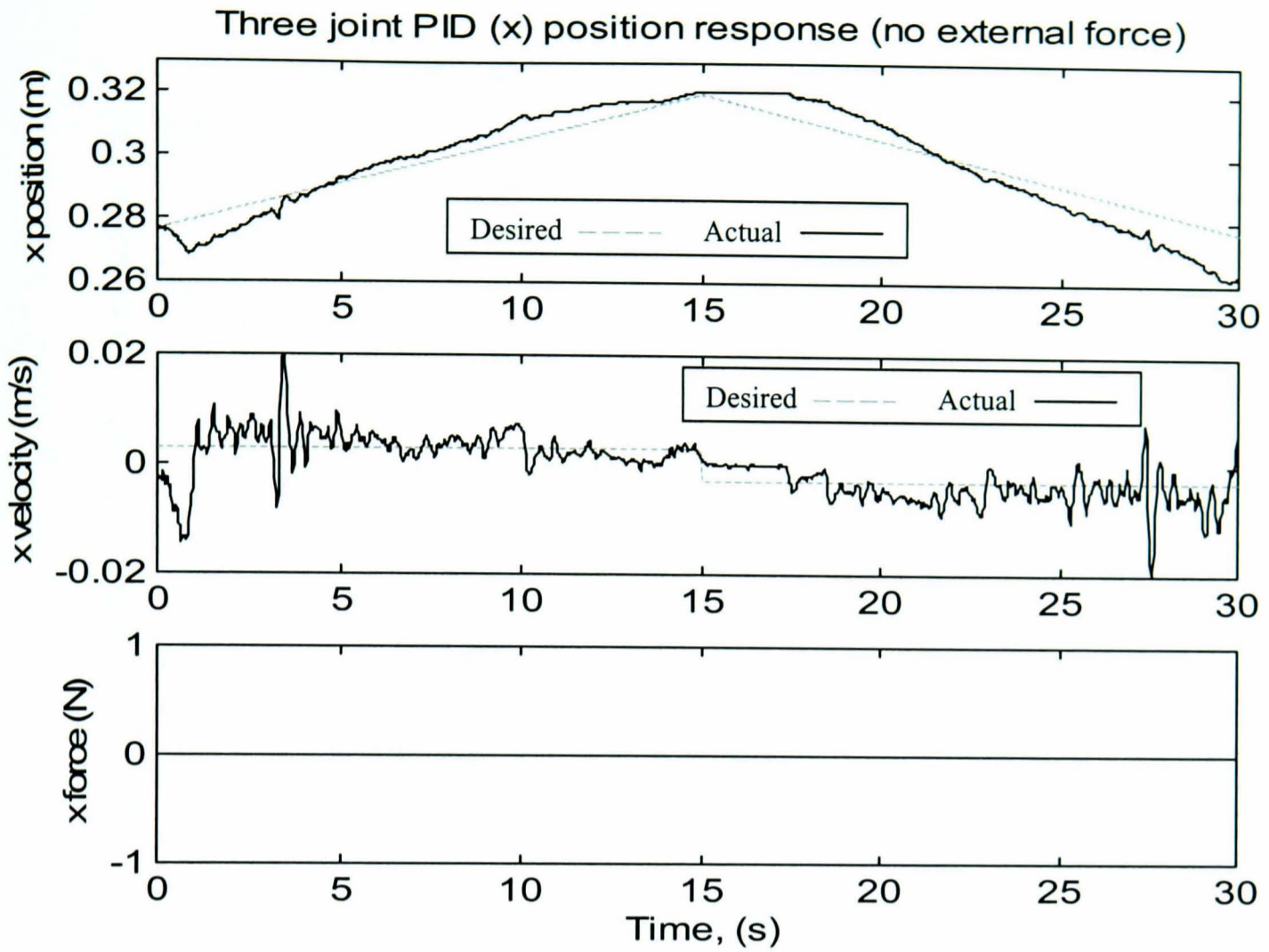**Figure 6.33** *Two degree of freedom impedance control (K=250, C=250)*

Figure 6.34 *Two degree of freedom impedance control (K=130, C=130)*
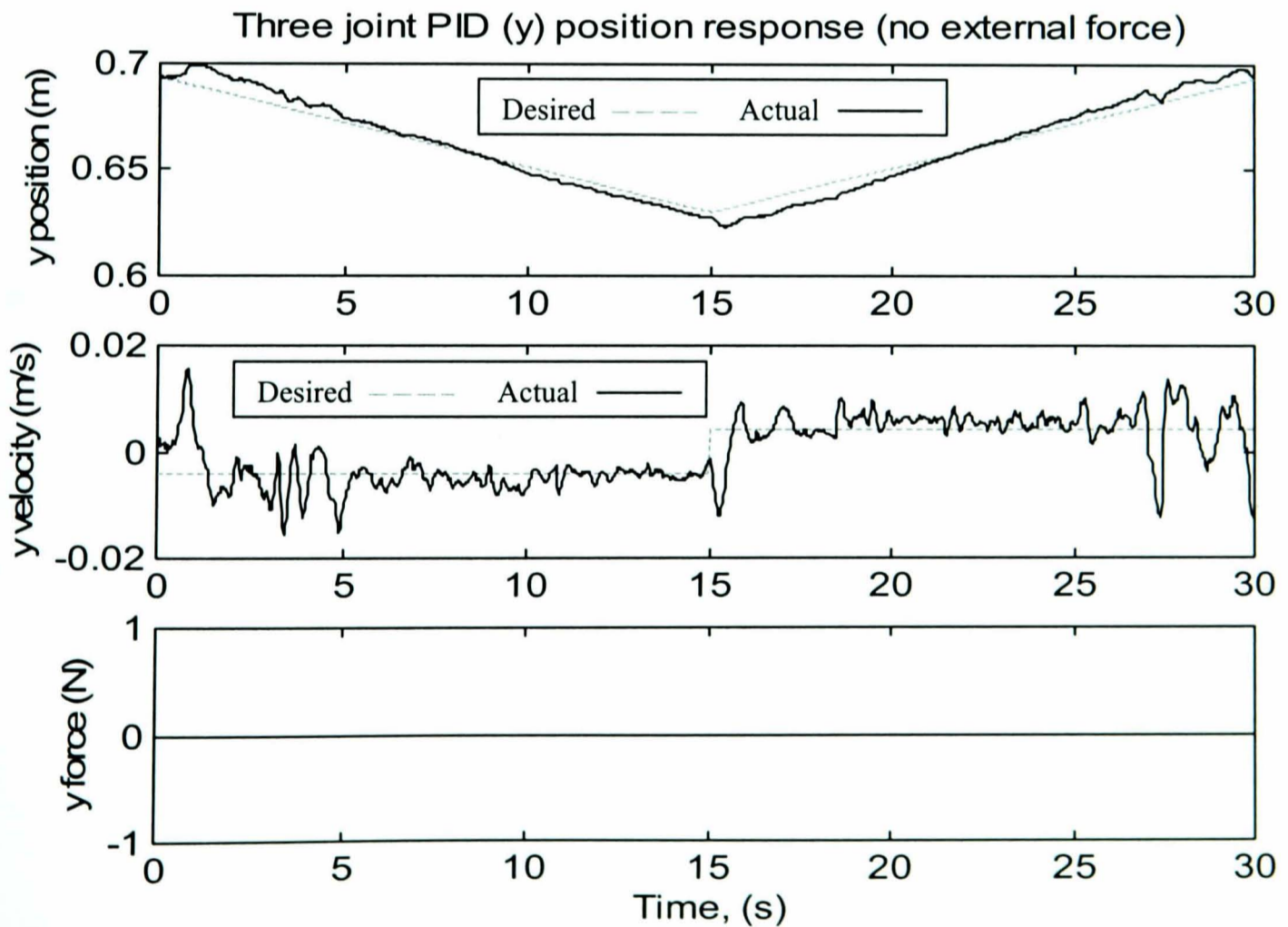
6.8 Three degree-of-freedom impedance control

The controller has been implemented in three degrees of freedom using the inverse kinematics and resolution of forces described earlier. The position response in three degrees of freedom is shown in figures 6.35, 6.36 and 6.37. With the additional degree of freedom the position tracking has slightly degraded in the x and y directions. The z direction is accurately tracked. To assess the performance of the three degree-of-freedom impedance controller, the five sets of impedance characteristics were implemented on the robot. Examining the experimental response for low damping and stiffness parameters (K=50, C=50) figures (6.38 - 6.40), show the response to degrade when compared to the two degree-of-freedom response. In particular, the response in the x direction has significantly degraded. The third degree of freedom is accurately tracked. The response with high stiffness and low damping (K=170, C=50) figures (6.41-6.43) demonstrate the controller performance to degrade in all degrees of freedom. In particular, note the degradation in the performance of the new degree of freedom (z). The excitation force for this response is less consistent than previously, due to the difficulty of manually applying large forces in multiple degrees of freedom.

High damping and low stiffness (K=50, C=170) also results in poor experimental performance (figures 6.44 - 6.46). The velocity responses in the x and z direction are particularly poor. It was noted for the two degree of freedom controller that these parameters result in particularly poor controller performance. High damping and high stiffness (K=250, C=250) figures (6.47- 6.49) result in the poorest response. Both the x and z directions exhibit poor tracking of both position and velocity. These particular parameters require the greatest force to be applied to achieve comparable movement, resulting in the most severe test for both the controller and accuracy of the force sensor.

Finally the response with medium stiffness and damping (K=130, C=130) figures (6.50-6.52) show the x and z response to improve when compared to the high damping and stiffness, however the response is significantly poorer than for the two degrees of freedom.

Three joint PID (x) position response (no external force)

Figure 6.35   Three joint PID (x) position response (no external force)

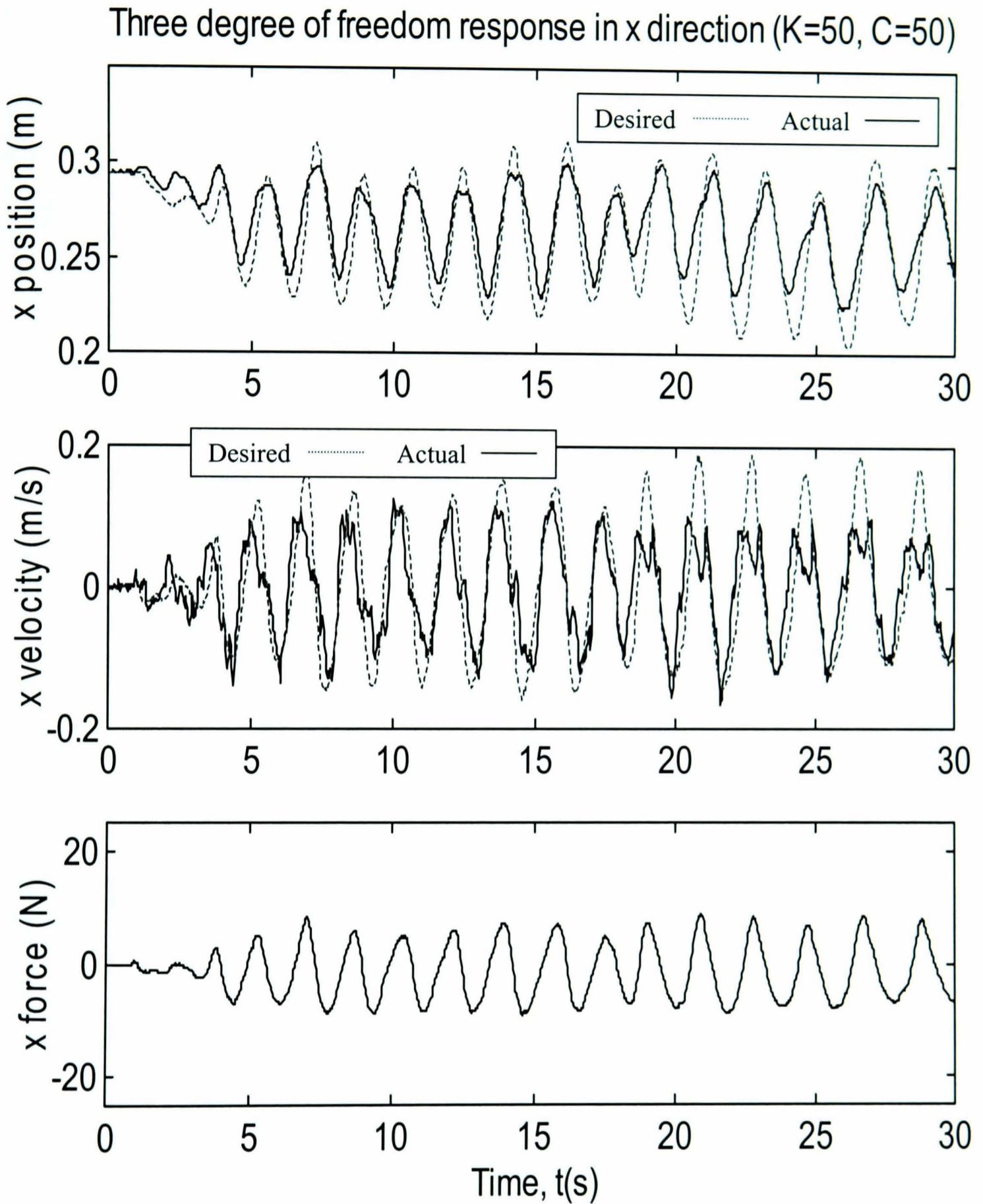**Three joint PID (y) position response (no external force)**

Figure 6.36 Three joint PID (y) position response (no external force)
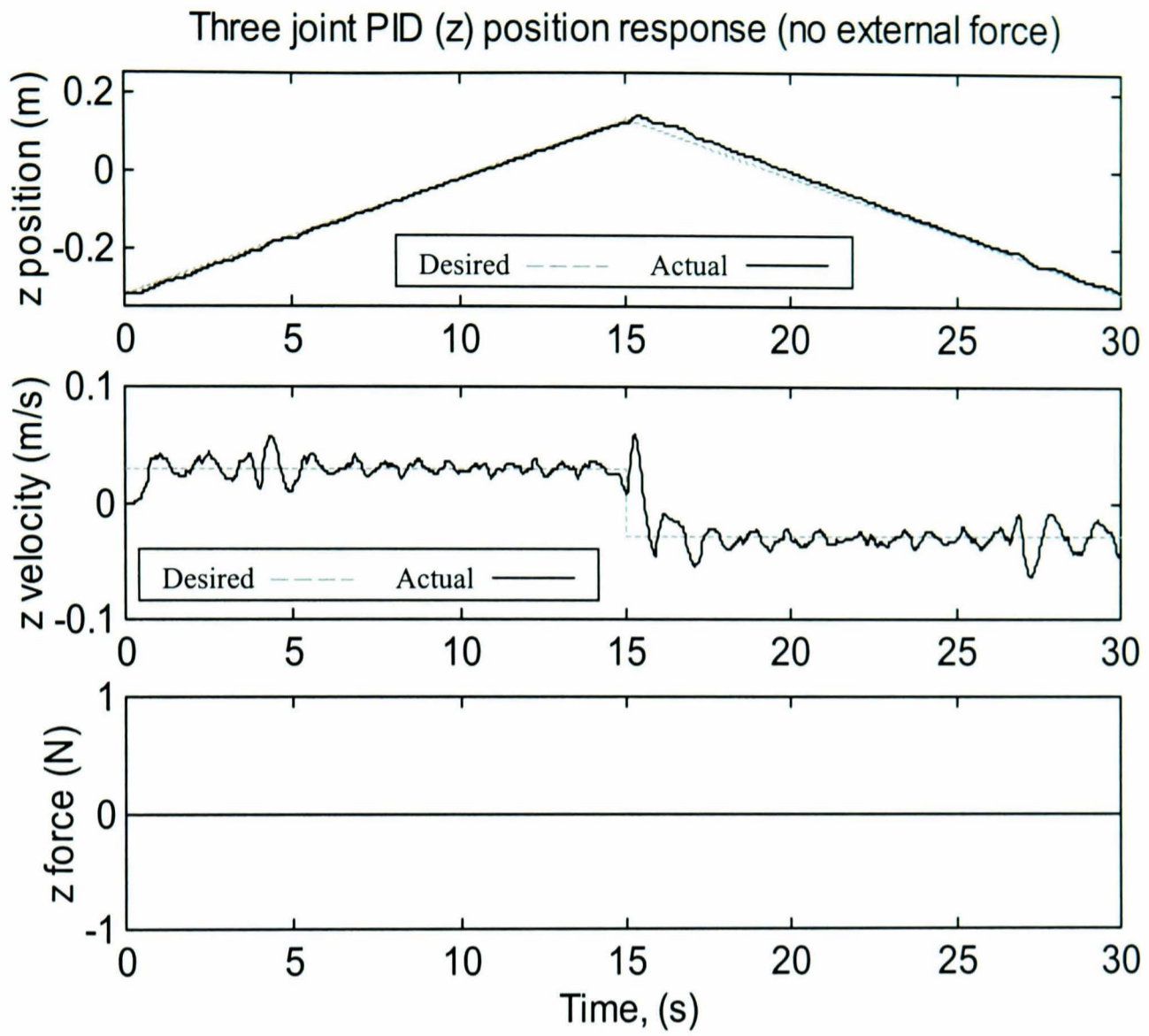
Figure 6.37 Three joint PID (z) position response (no external force)

Figure 6.38 *Three degree of freedom impedance control, x direction (K=50, C=50)*
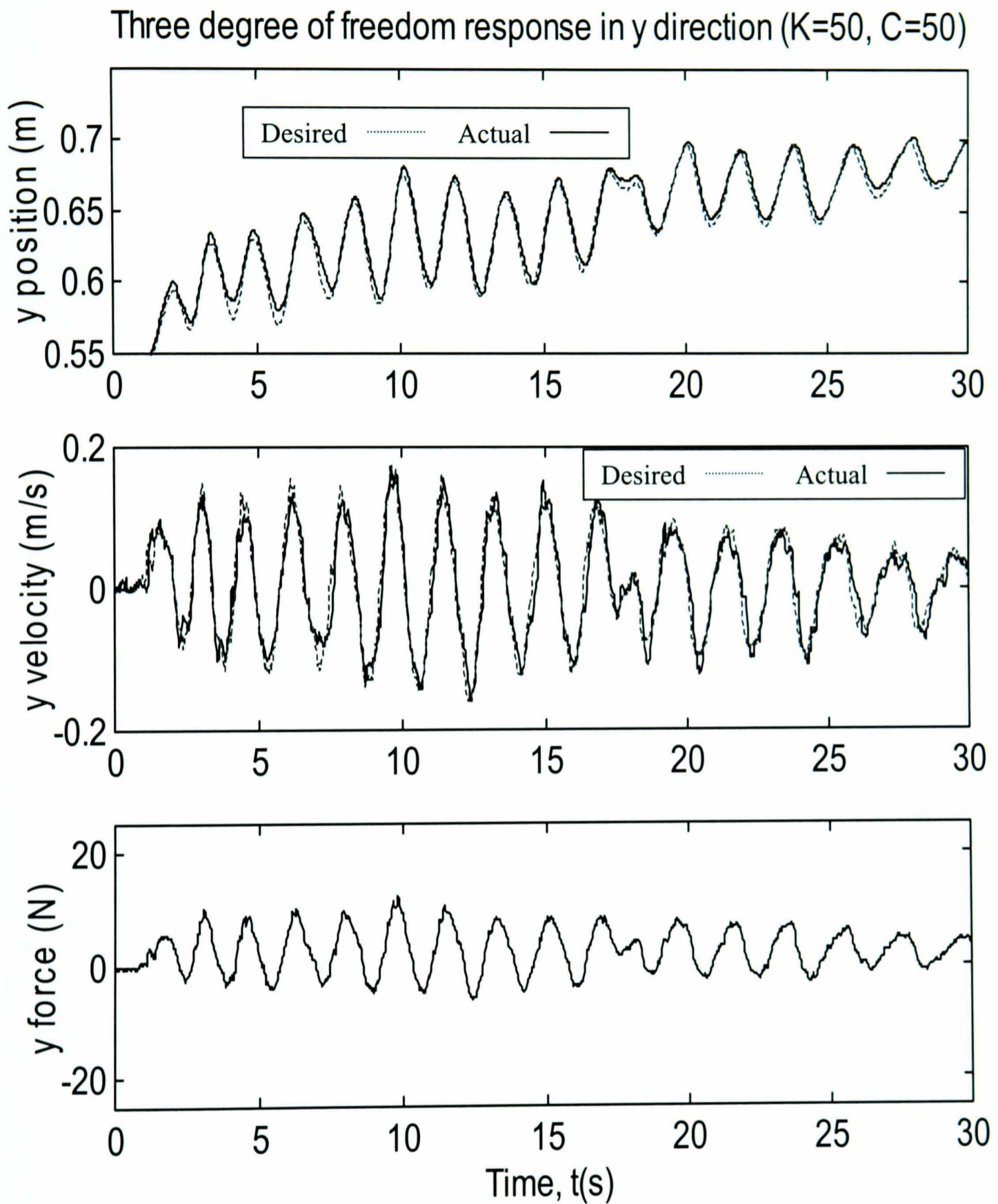
Figure 6.39 *Three degree of freedom impedance control, y direction (K=50, C=50)*

Figure 6.40 *Three degree of freedom impedance control, z direction (K=50, C=50)*

Figure 6.41 *Three degree of freedom impedance control, x direction (K=170, C=50)*

Three degree of freedom response in y direction (K=170, C=50)

Figure 6.42 Three degree of freedom impedance control, y direction (K=170, C=50)

Three degree of freedom response in z direction (K=170, C=50)

Figure 6.43 *Three degree of freedom impedance control, z direction (K=170, C=50)*
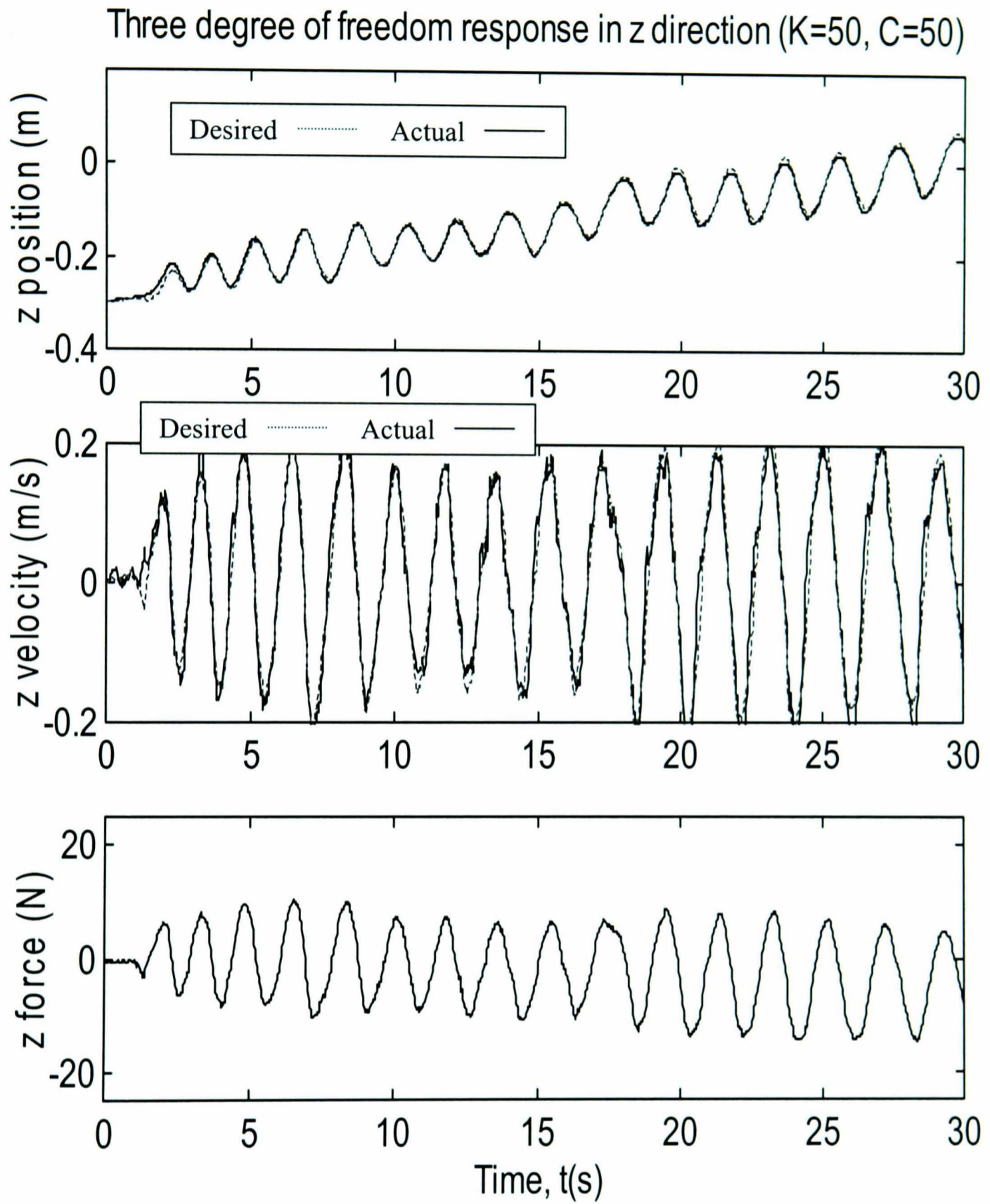
Figure 6.44 *Three degree of freedom impedance control, x direction (K=50, C=170)*

Figure 6.45 *Three degree of freedom impedance control, y direction (K=50, C=170)*

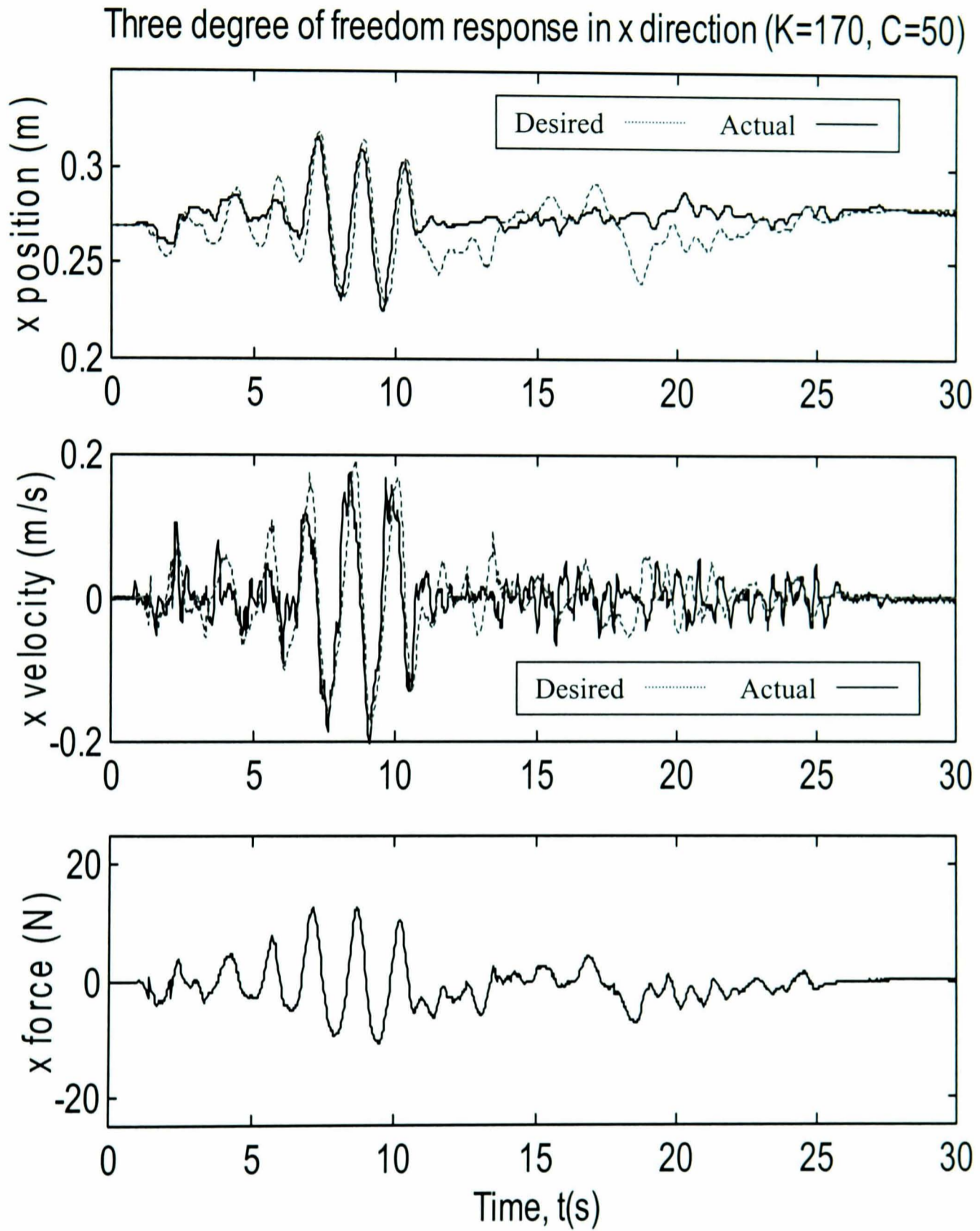## Three degree of freedom response in z direction (K=50, C=170)

Figure 6.46 *Three degree of freedom impedance control, x direction (K=50, C=170)*

Figure 6.47 *Three degree of freedom impedance control, x direction (K=250, C=250)*

Three degree of freedom response in y direction (K=250, C=250)

Figure 6.48 *Three degree of freedom impedance control, y direction (K=250, C=250)*

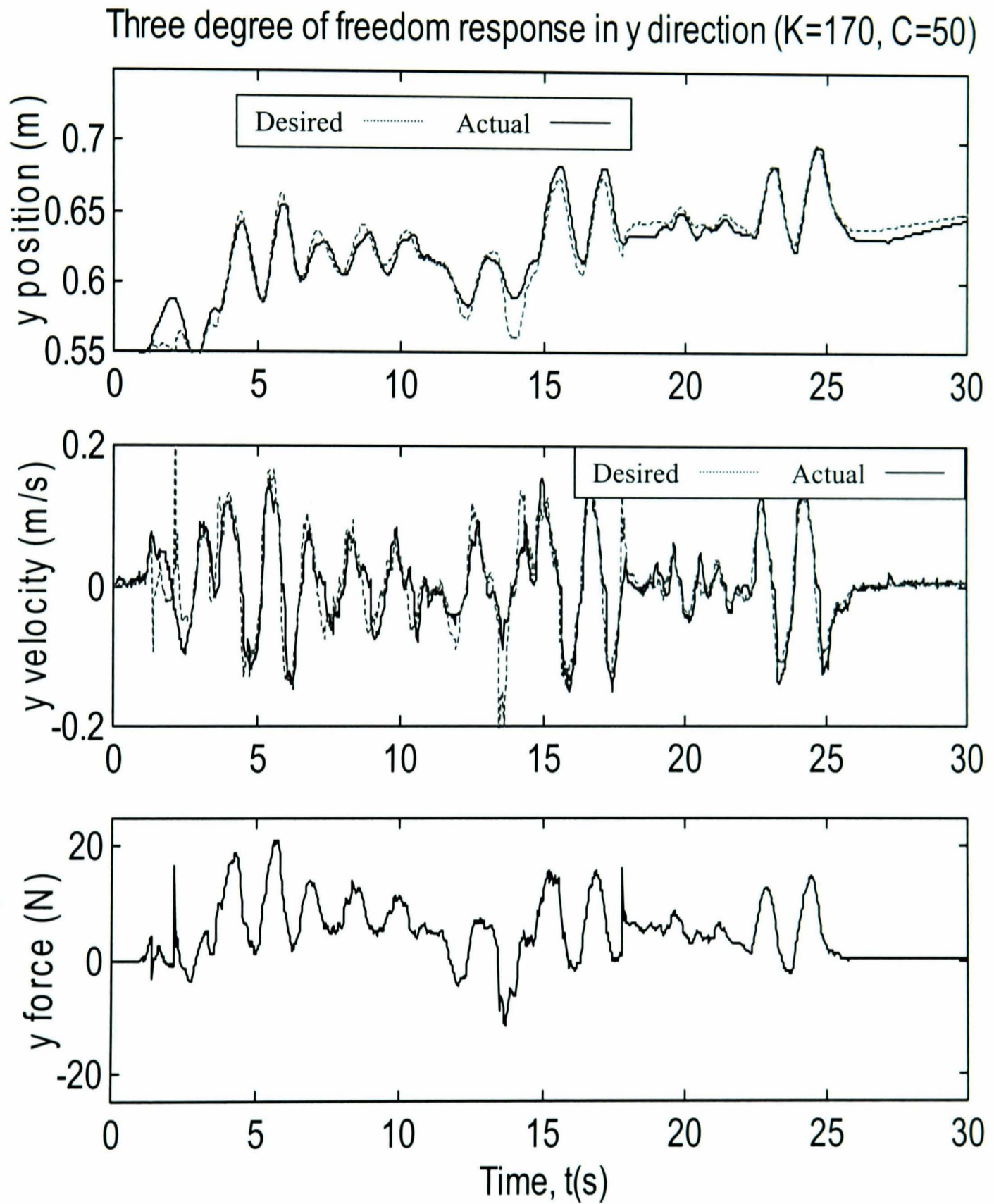**Figure 6.49** *Three degree of freedom impedance control, z direction (K=250, C=250)*
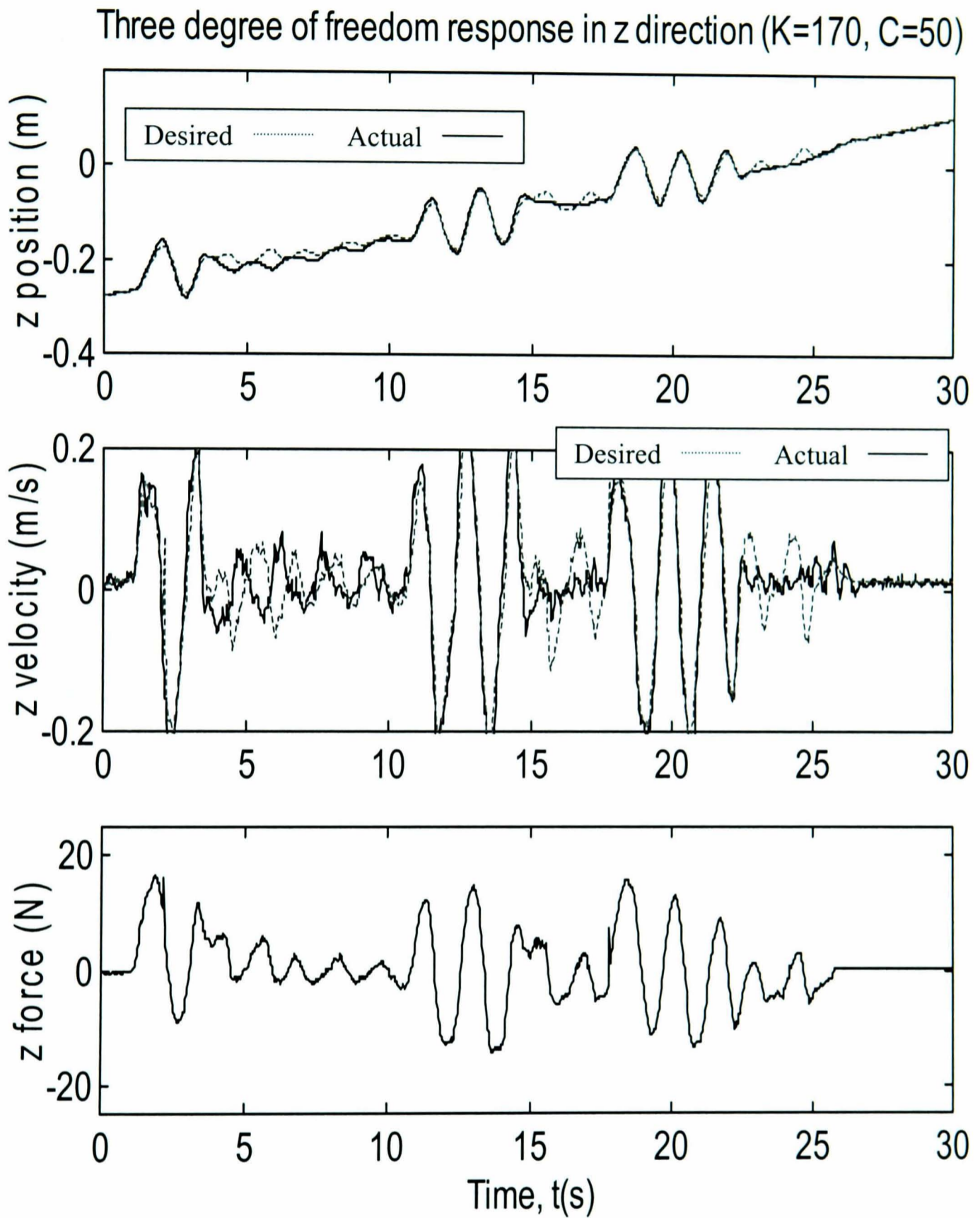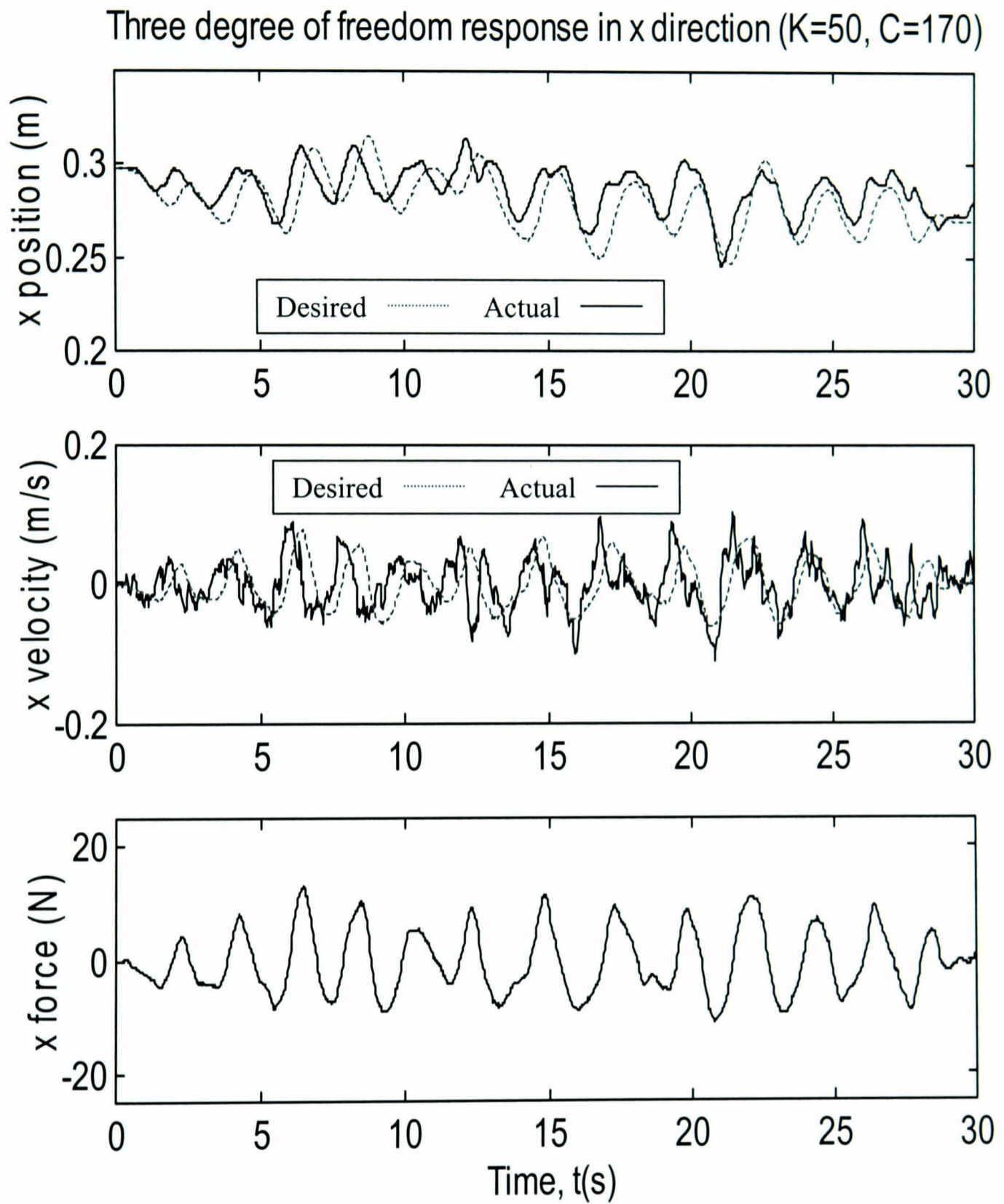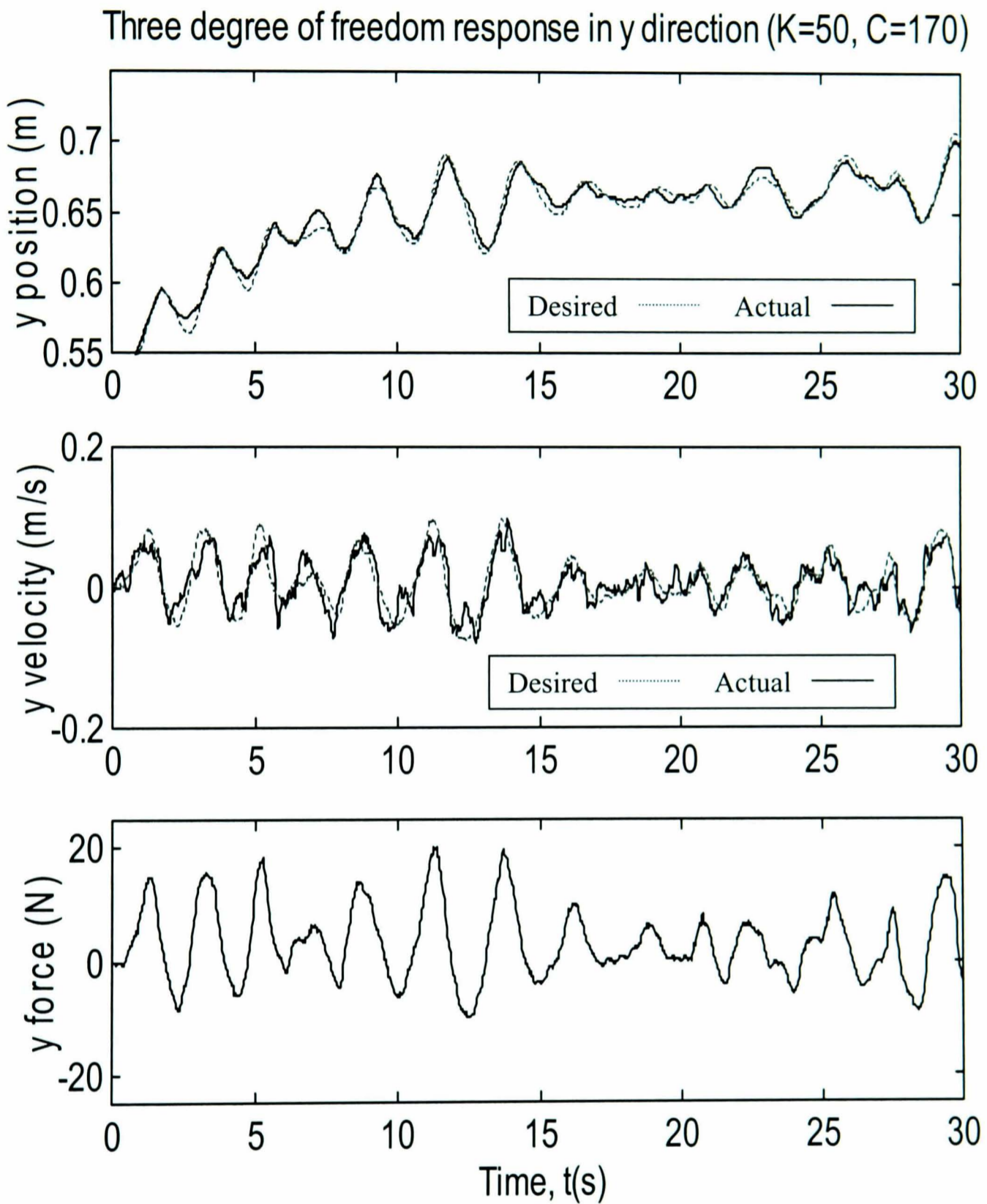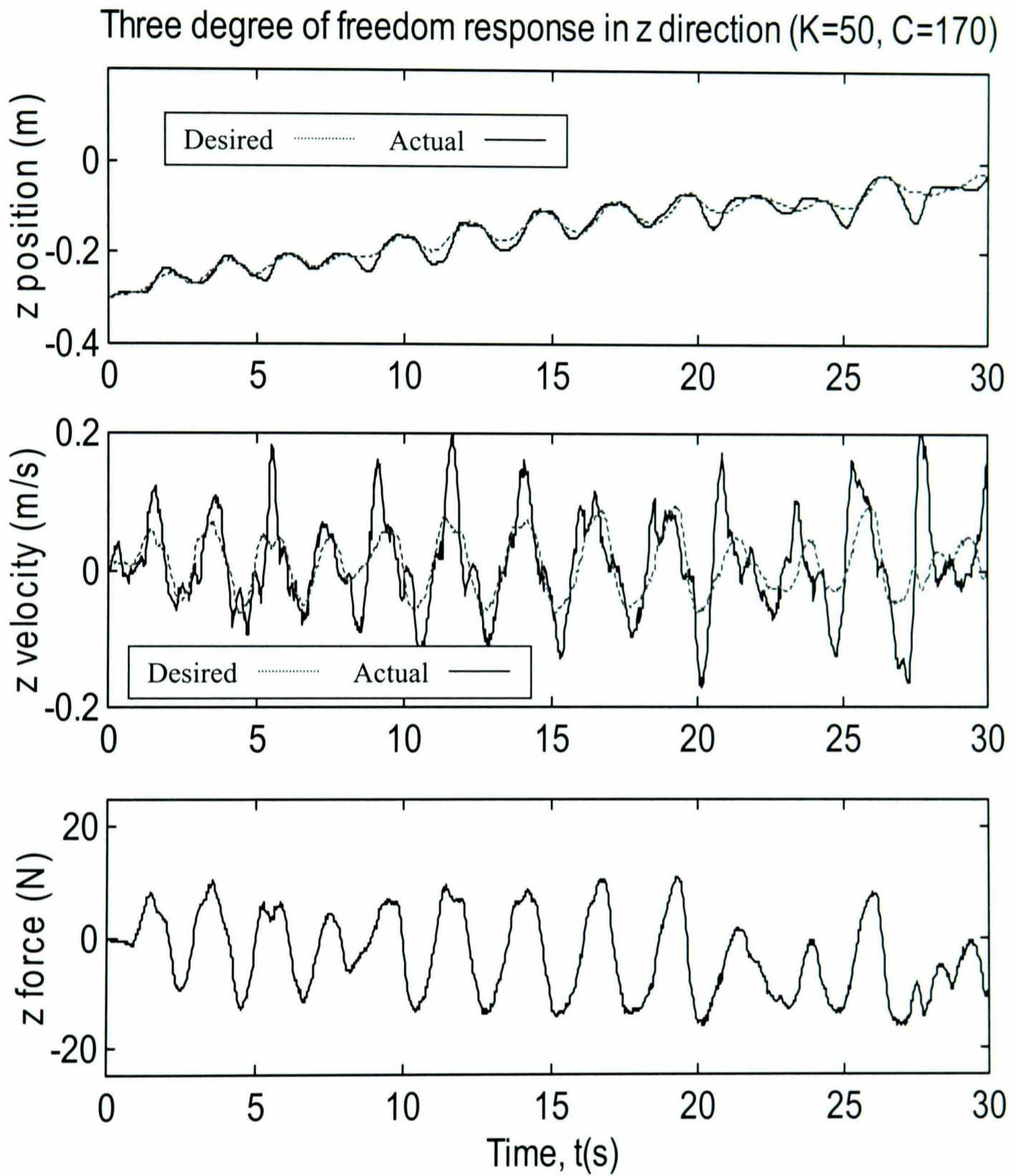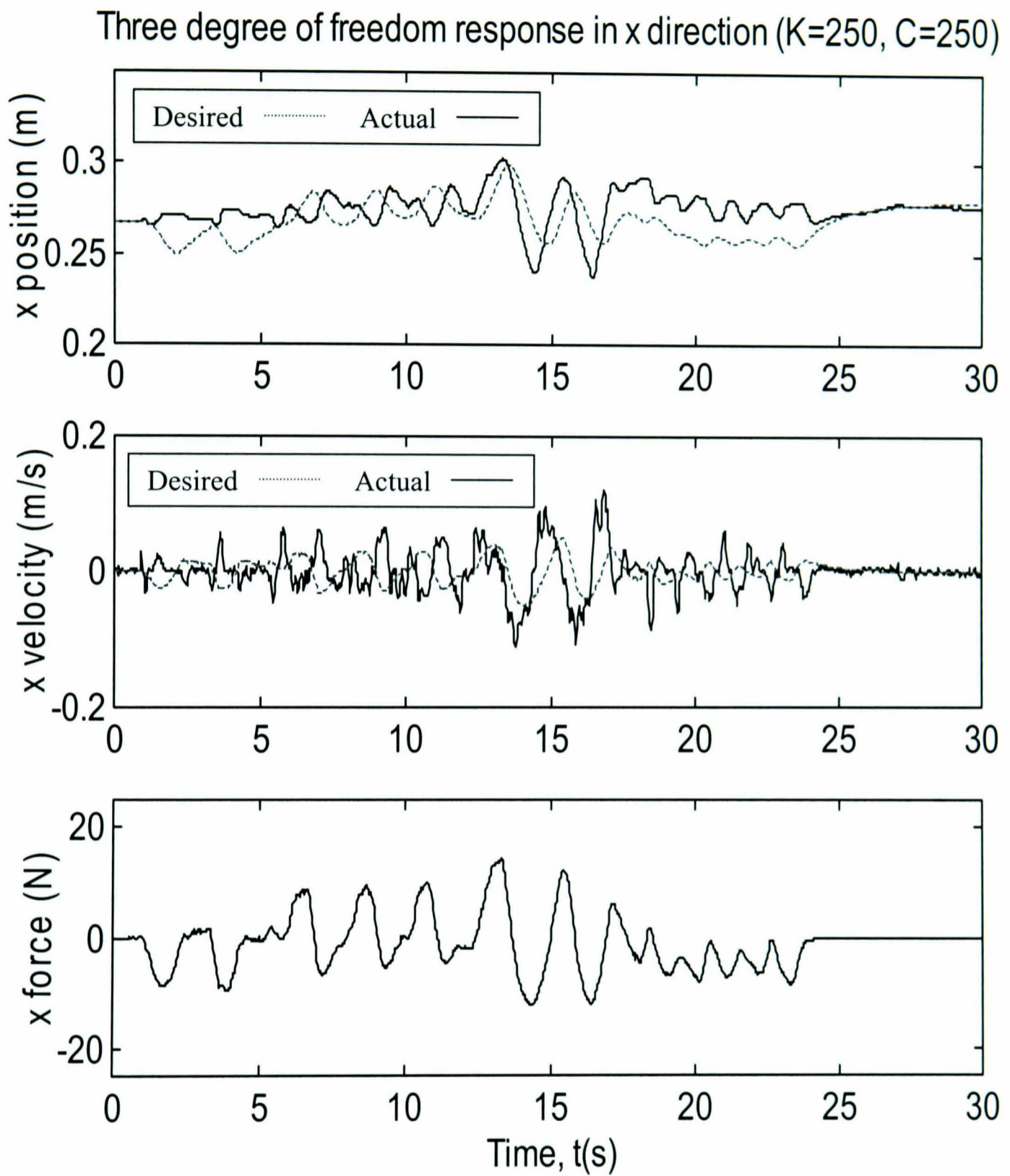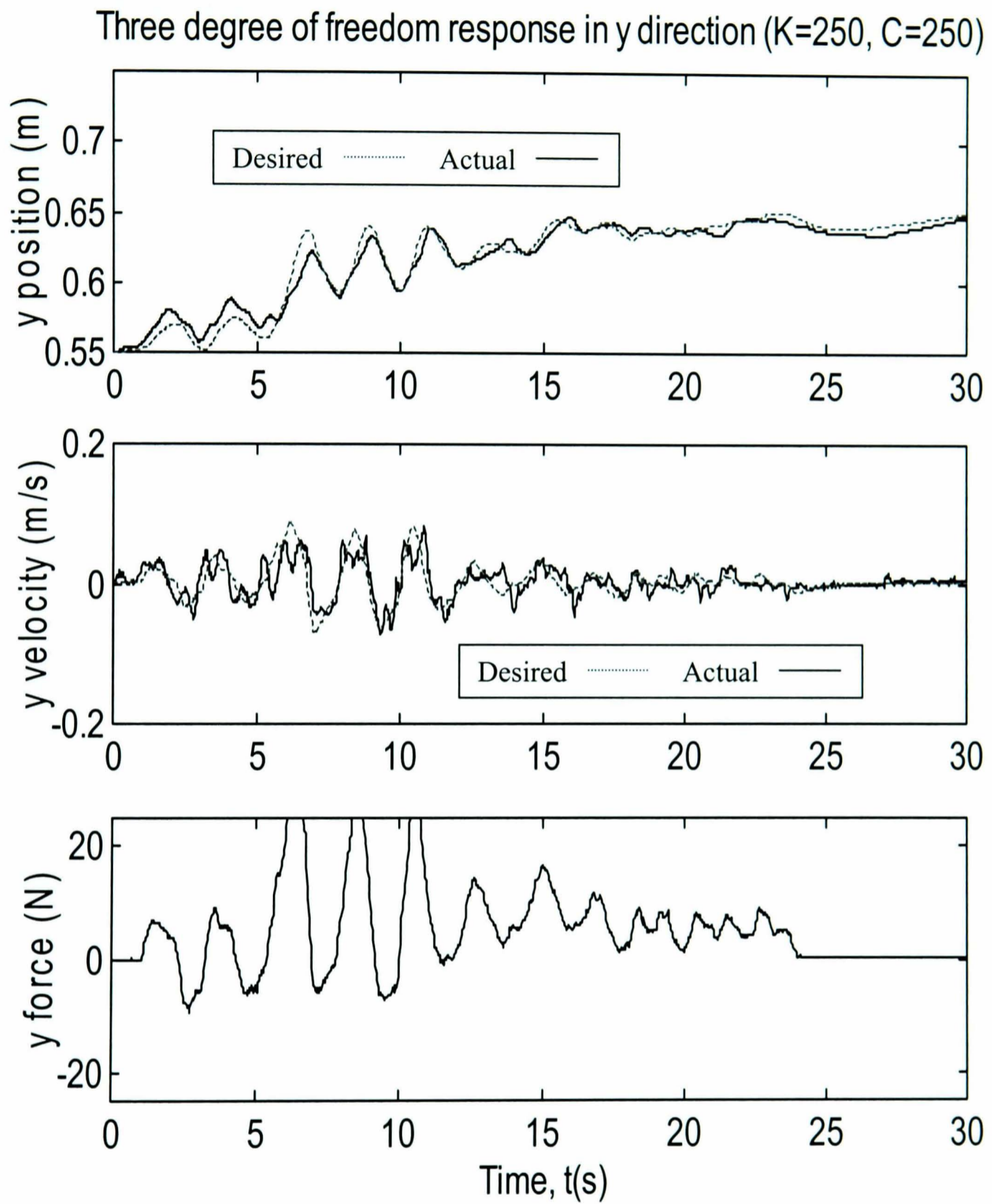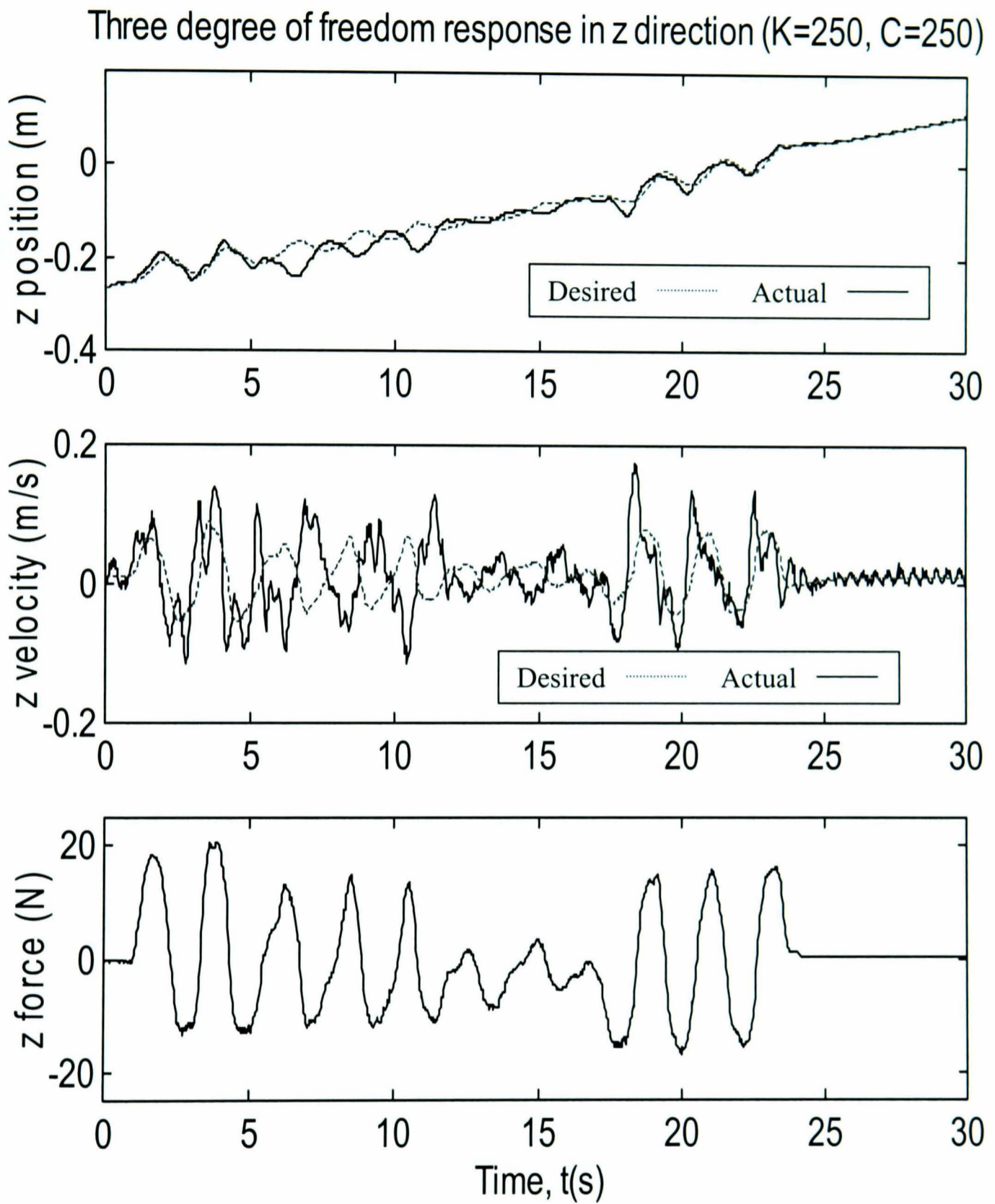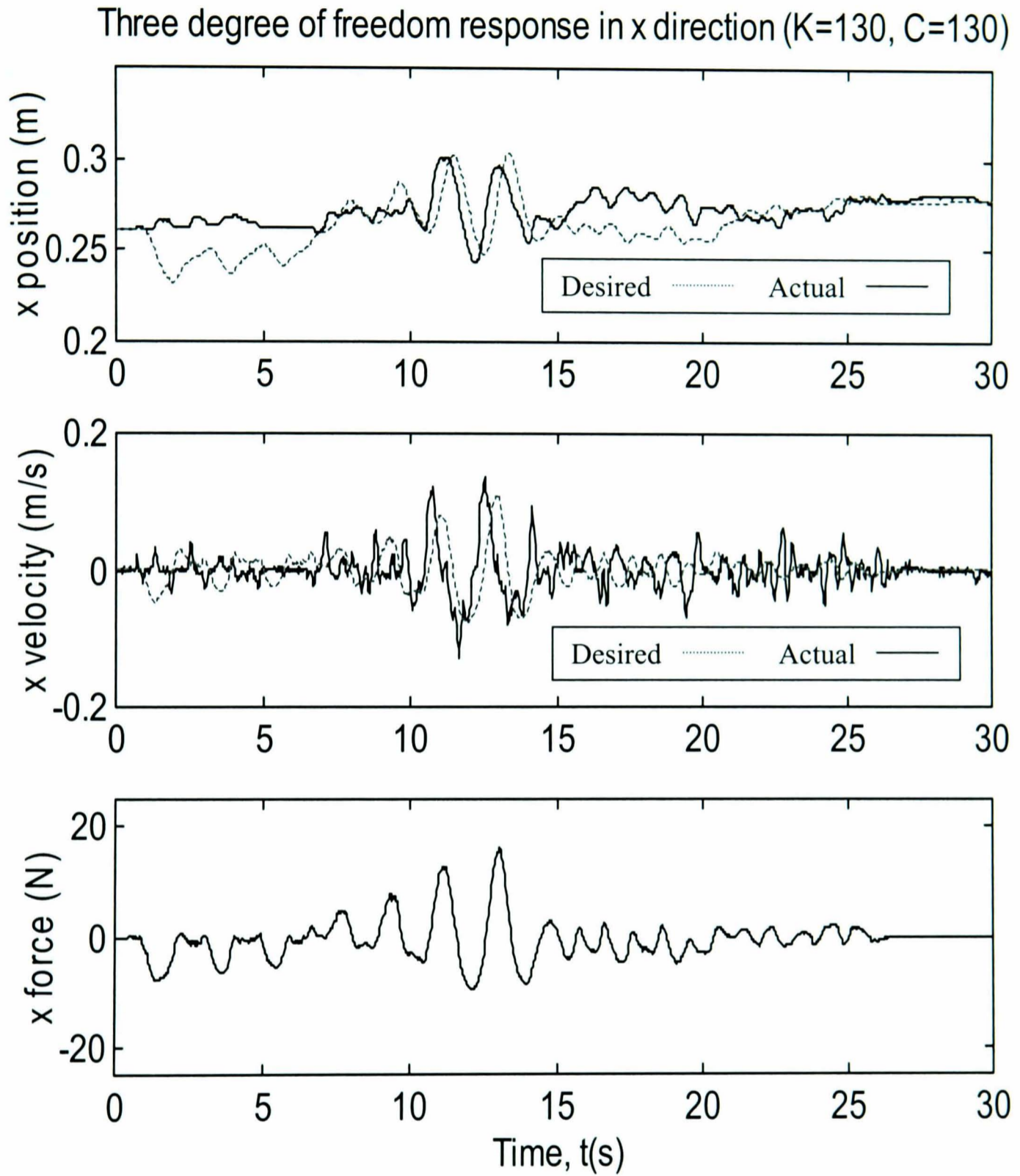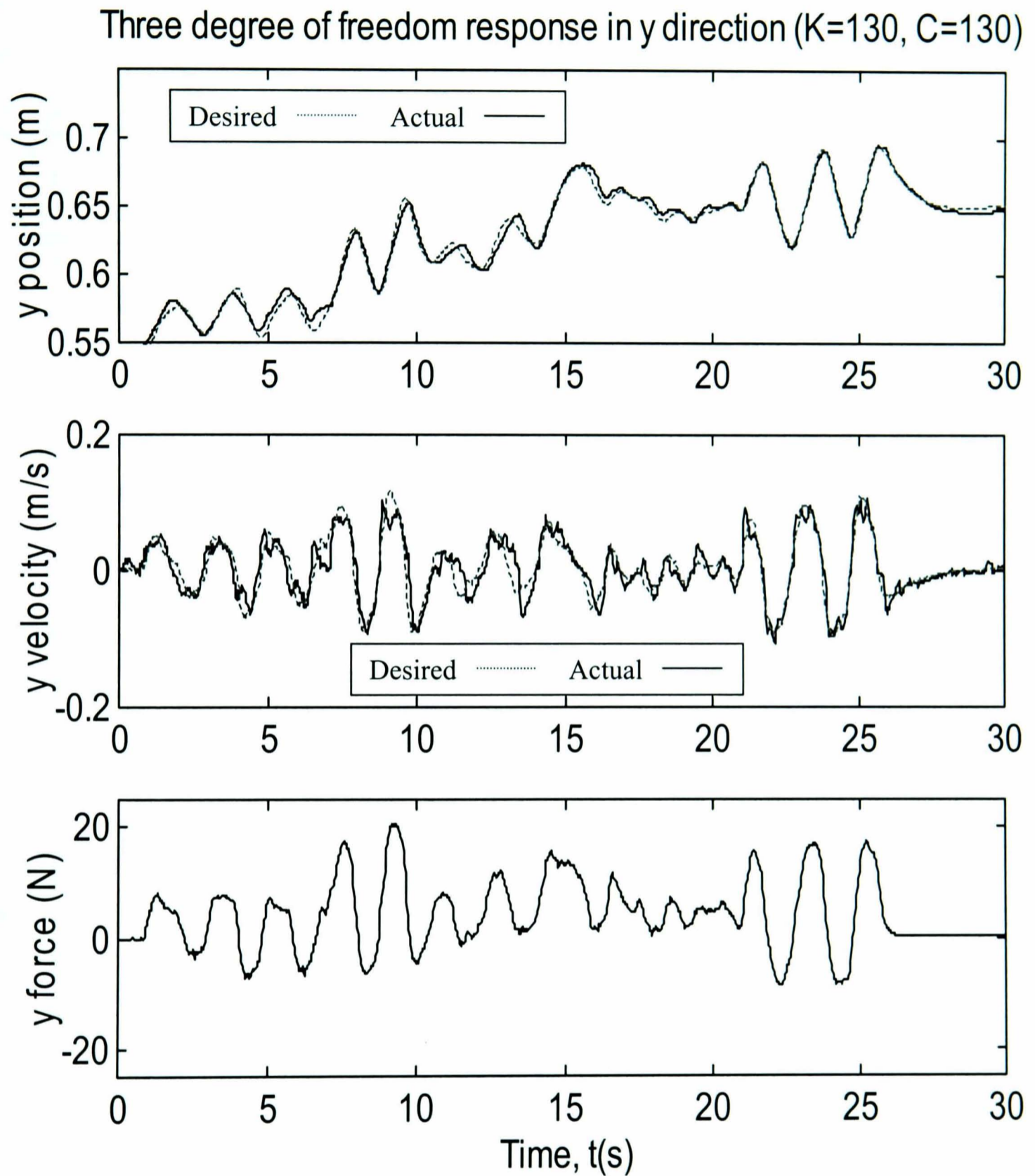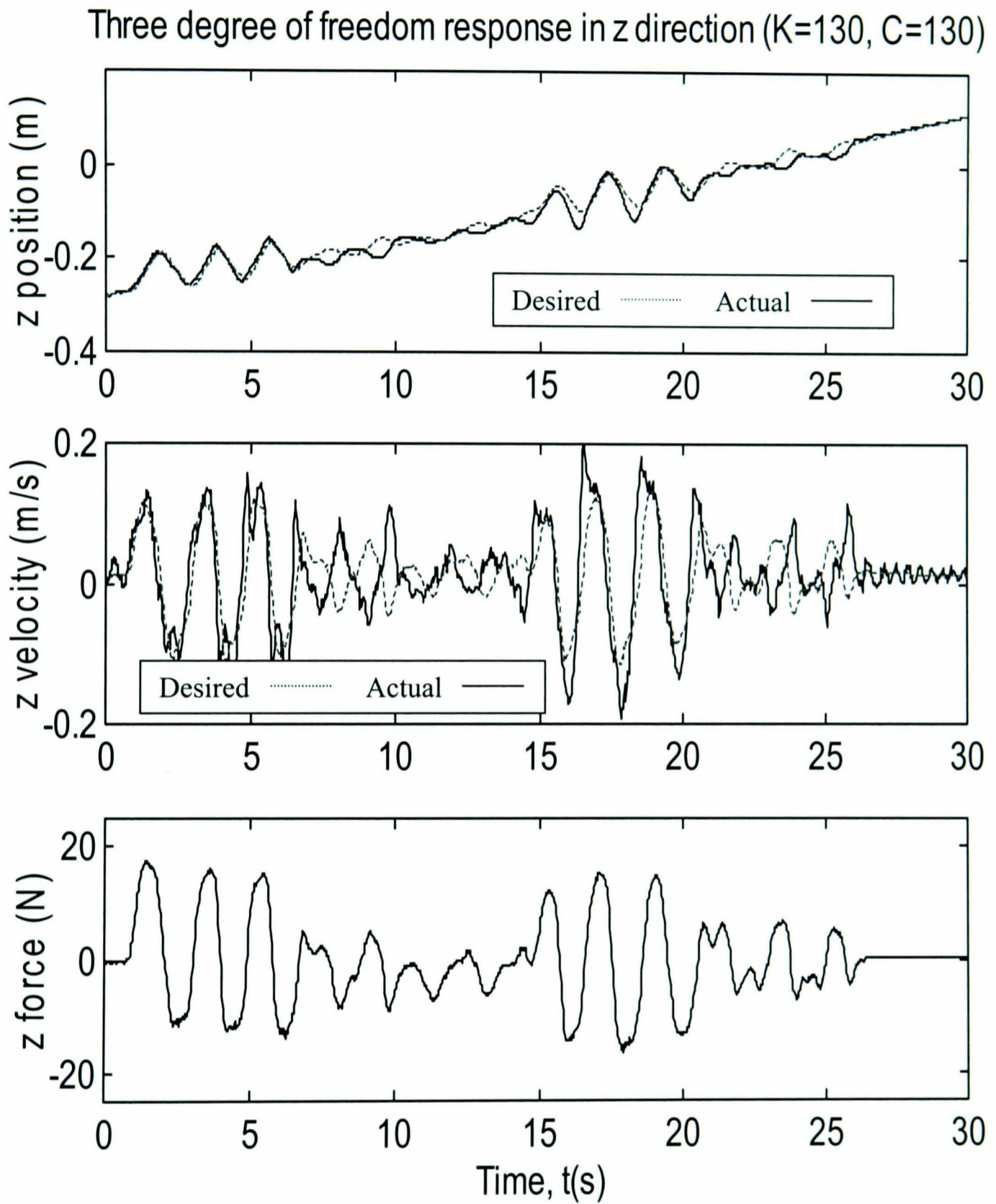
Figure 6.50 *Three degree of freedom impedance control, x direction (K=130, C=130)*

Figure 6.51 *Three degree of freedom impedance control, x direction (K=130, C=130)*

Three degree of freedom response in z direction (K=130, C=130)

Figure 6.52 *Three degree of freedom impedance control, x direction (K=130, C=130)*

6.9 Discussion and conclusions

The difficulty in obtaining accurate force output from pneumatic actuators during motion implies that position based impedance control is the most appropriate for pneumatic systems. Position based impedance control utilises the position controller to smooth the response to non-linear effects such as stiction and air compressibility. However, the use of position based impedance control requires a high gain position controller robust to external forces. The low stiffness and backdrivable nature of pneumatic actuators creates difficulties when designing a controller robust to external force disturbances. Measurement of this external force enables a compensatory force to be generated by the joint actuators. Additional hardware is not required to measure this external force due to the requirement of the impedance controller to measure externally applied forces. The use of this compensatory force does not ensure that the controller is completely robust to external forces, however, the impedance controller requires some movement of the actuator in the direction of the applied force, removing the requirement for instant and exact force compensation. The impedance controller was developed in simulation, expanding on the model developed in chapter 5. The simulation enables quick, safe implementation of controller variations. The simulation could be extended to multiple degrees of freedom to provide further information on the interaction between joints.

Implementation of the impedance controller on a single degree-of-freedom of the pneumatic robot demonstrates appropriate impedance controller behaviour. To implement the impedance controller in multiple degrees-of-freedom requires a multiple degree of freedom force sensor. The accuracy of the simple three degree-of-freedom force sensor is lower than that of the commercial single degree-of-freedom force sensor. Extending the controller to multiple degrees-of-freedom has degraded the controller performance. Other factors such as unmodeled robot dynamics and imperfect gravity compensation have added to this decrease in controller performance.

Concise evaluation of the controller performance for varying impedance characteristics presents extreme difficulty. Ideally, a PRBS (pseudo random binary sequence) would

apply forces to the robot end-point in multiple degrees-of-freedom. The results of this test would be used to generate bode plots of the system response for each degree of freedom. These bode plots could be used to assess the controller linearity, damping and stiffness parameters. Note that it would be necessary to apply forces in multiple directions simultaneously to evaluate any coupling effects between directions. The approach taken here was to apply forces in multiple degrees of freedom to the robot end-point and compare the desired position to the actual position and velocity of the robot. The flaw in this approach is that any errors in force measurement would result in an incorrect desired position alongside an incorrect force balancing output. To minimise the possibility of this occurrence, the calibration of the force sensor was checked periodically.

The controller performance varies with the desired impedance characteristics. High damping and low stiffness resulted in particularly poor controller performance. This is a result of fluid transport delays, leading to a phase lag within the controller response. Phase lags are an inherent part of pneumatic systems, resulting from mass flow saturation transporting fluid. Increasing the diameter of interconnecting pipes or reducing their length are the only means of improving the mass flow transport.

The controller performance degrades with large values of damping and stiffness. This is partly due to the requirement of increased forces to obtain motion for which the controller could be assessed. If, to maintain consistency, these larger forces were applied to low stiffness parameters the joints would undergo excessive movement and strike the end stops.

The overall impedance controller has been successfully implemented in multiple degrees of freedom. The controller can be used for robots interacting with the environment providing limits are set for combination of damping and stiffness parameters implemented. The use of a more accurate multiple degree-of-freedom force sensor should improve the controller response.

Chapter 7

Pole-placement impedance control

The position controller forms the heart of the impedance controller and hence its performance is critical to the overall controller performance. The PID position control strategy is replaced with a pole-placement controller to access the potential improvement in controller response.

7.1 Introduction

An impedance controller has been developed in chapter 6 based upon a PID approach. The impedance controller was shown to provide satisfactory performance for a range of damping and stiffness parameters. Here, a pole-placement approach will be implemented on two joints of the three degree of freedom robot to ascertain any improvement in the impedance controller response. A pole-placement controller has been implemented on the test rig (chapter 3), however, implementing the controller for the angular joints of the robot presents several problems. Firstly, the angle at which the pneumatic cylinder acts against the link is variable, causing the system to exhibit increased non-linearity and secondly, the potentiometers used to measure the link position have a poorer signal to noise ratio than the LVDT due to the relatively small angular displacement of the link. The cylinder action is linearised so force acts perpendicularly to the link. Demand signals then produce consistent force perpendicular to the link regardless of joint angle. To reduce the controller response to noise, a demand filter is implemented within the pole-placement controller.

7.2 Two degree of freedom pole-placement control

Pole-placement control provides a method of controlling the system response by selection of the closed loop poles. The pole-placement controller described in chapter 3 was implemented on an idealised system where the cylinder acts against a gravity load and its position is measured directly. The robot exhibits non-linearity due to the

angle at which the cylinder acts against the joint varying with cylinder angle. Linearisation of joint action is therefore required to implement a linear controller.

7.2.1 Linerisation of joint properties

Examining joint 3, the angle of the pneumatic cylinder acting on the link varies with cylinder angle, causing a non-linear response (figure 7.1). From chapter 6 (equation 6.14) the angle that the pneumatic cylinder acts upon link can be found as:

$$C_3 = a \sin \frac{0.235 . \sin(\theta_3 + \pi/2)}{\sqrt{0.185^2 + 0.235^2 - 2*0.185*0.235*\cos(\theta_3 + \pi/2)}} \qquad (7.1)$$

So the linearised control action perpendicular to the link can be found from.

$$Control_{act} = \frac{Control_{des}}{\sin C_3} \qquad (7.2)$$

where $Control_{act}$ is the input control signal to the cylinder and $Control_{des}$ is the linearised control action.
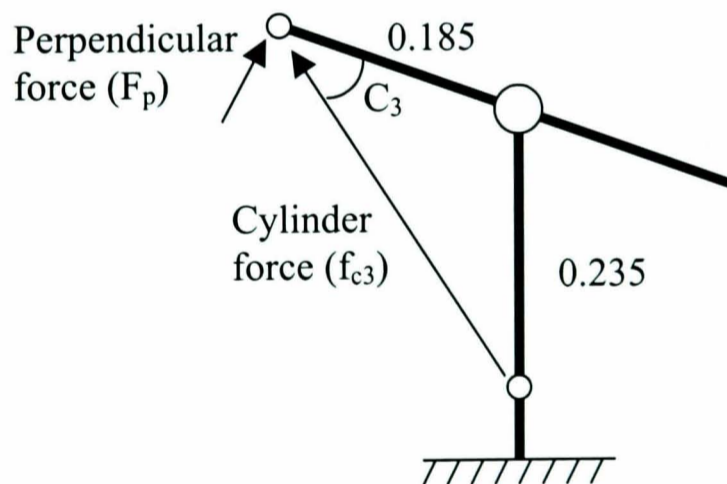
Figure 7.1 *Resolving joint 3 torque*

The control signal into the pneumatic servosystem can be modified so a constant input control signal produces the same link torque regardless of the link angle. The block diagram for linearised PID control is shown in figure 7.2. This linearising element is considered part of the plant, causing the input voltage and output torque to behave in a more linear manner. Including the linearising element amplifies the system gain,

requiring the PID gains to be optimised again. The new optimum controller gains were identified as P=1.39, I =0.0134, D = 0.074. Comparing the linearised and conventional controller illustrates the subtle differences in controller performance (figure 7.3).
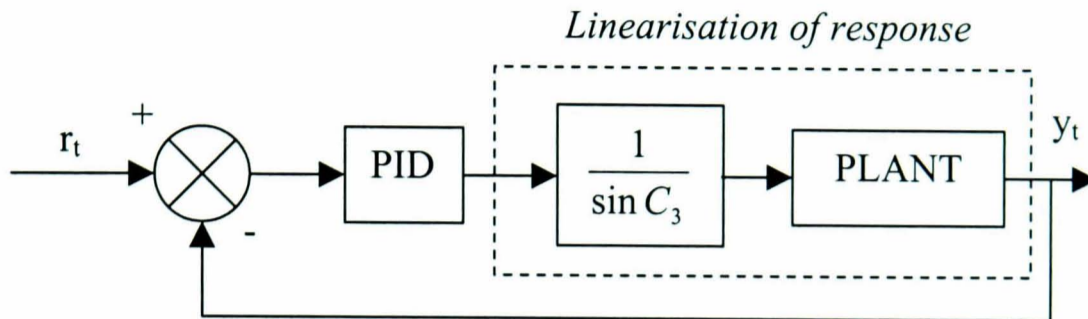
Figure 7.2 *Improving system linearity*
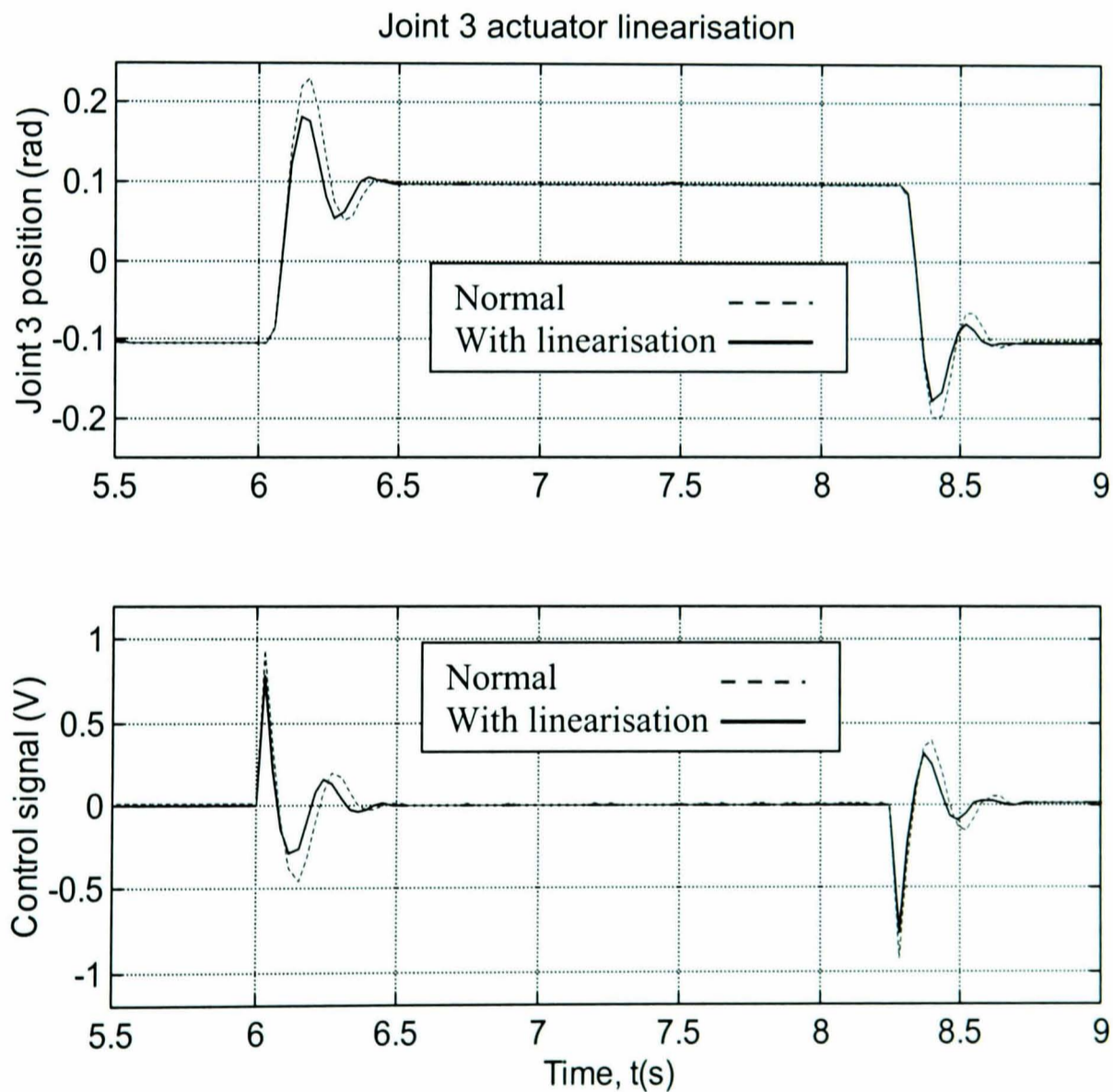
Figure 7.3 *Joint 3 linearised response*

The linearised controller demonstrates improved linearity with the overshoot and oscillation almost identical for the positive and negative steps. It is interesting to note that the overall performance of the controller has improved due to the increased linearity enabling the optimisation strategy to tune the gains with greater accuracy.

7.2.2 Pole-placement control with demand filter

The input/output data of the linear response was used to identify a plant model for pole-placement control as follows:

$$\theta_3 = \frac{B(z)}{A(z)} = \frac{0.0845z^{-2}}{1 - 1.76z^{-1} + 0.76z^{-2}} . u_t \tag{7.3}$$

where θ_3 is the joint angle (rad) and u_t is the control signal (V).

The plant differs from equation 3.14 due the position being measured as an angle rather than percentage displacement.

Due to the susceptibility of the potentiometers to noise, the closed loop poles of the conventional pole-placement controller are required to be slow, severely limiting the performance of the controller. However, it is possible to augment the pole-placement controller with a demand filter to attenuate the controller's response to noise (figure 7.4).
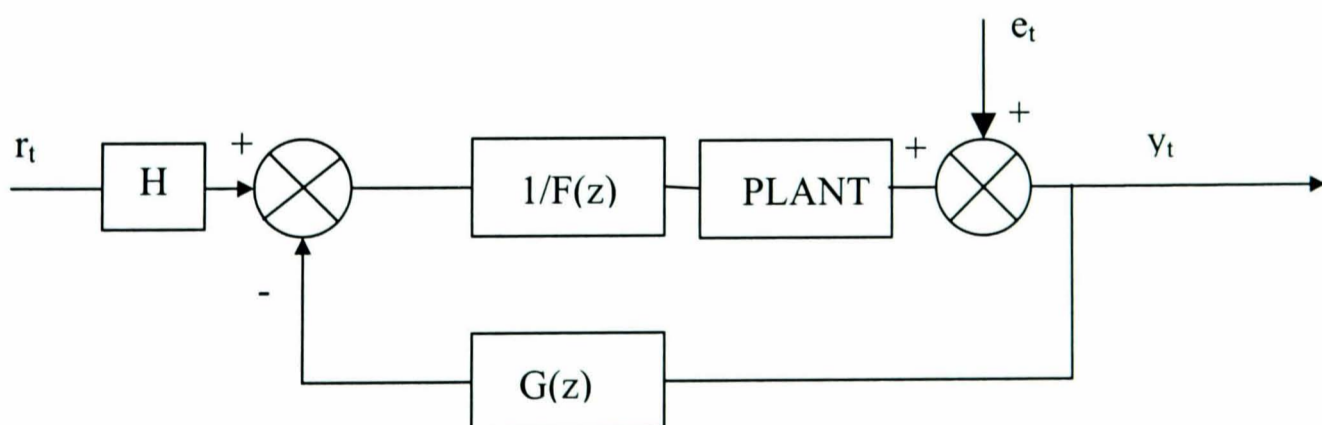
Figure 7.4 *Pole-placement control*

Obtaining a transfer function of the controller in 7.4, demonstrates that the demand filter only appears in the transfer function from noise to output (**Vaughan and Plummer 1990**):

$$y_t = \frac{B(z^{-1})H(z^{-1})}{F(z^{-1})A(z^{-1}) + G(z^{-1})B(z^{-1})} r_t + \frac{F(z^{-1})H(z^{-1})}{F(z^{-1})A(z^{-1}) + G(z^{-1})B(z^{-1})} e_t \qquad (7.4)$$

$F(z^{-1})$ and $G(z^{-1})$ can be chosen to satisfy the following:

$$F(z^{-1})A(z^{-1}) + G(z^{-1})B(z^{-1}) = A_m(z^{-1})H(z^{-1}) \qquad (7.5)$$

Therefore,

$$y_t = \frac{B(z^{-1})}{A_m(z^{-1})} r_t + \frac{F(z^{-1})A(z^{-1})}{A_m(z^{-1})H(z^{-1})} e_t \qquad (7.6)$$

Closed loop poles at $0.3 \pm 0.05i$ result in the standard pole-placement controller responding significantly to measurement noise. Specifying the H filter as a first order low pass filter with a cut off frequency at 6Hz significantly reduces the controller response to measurement noise. Experimental results with and without the demand filter show the response time and overshoot to be consistent, however the steady state response to noise is almost completely removed (figure 7.5). This lack of response to measurement noise is best illustrated by examining the control signal high frequency response for the standard pole-placement controller.

Examining bode plots with and without the demand filter the exact nature of the controllers improved rejection of measurement noise is illustrated (figure 7.6). The high frequency response to noise and disturbances is attenuated.

A similar linearisation process can be performed on the second link of the pneumatic robot. The plant model for this link has been identified as:

$$y_t = \frac{B(z^{-1})}{A(z^{-1})} = \frac{0.02z^{-2}}{1 - 1.94z^{-1} + 0.945z^{-2}} .u_t \qquad (7.7)$$
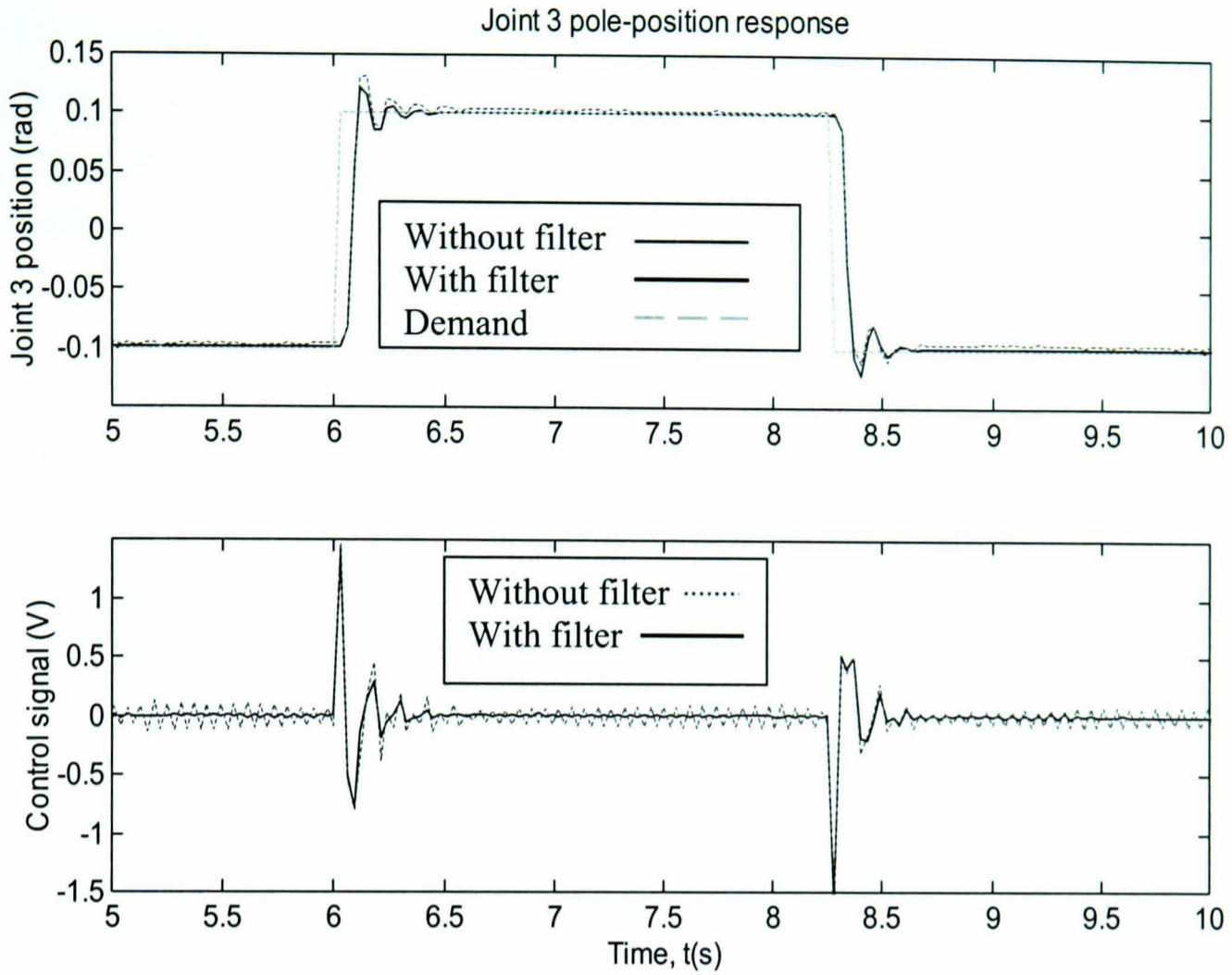
Figure 7.5 *Joint 3 pole-placement response with and without demand filter*
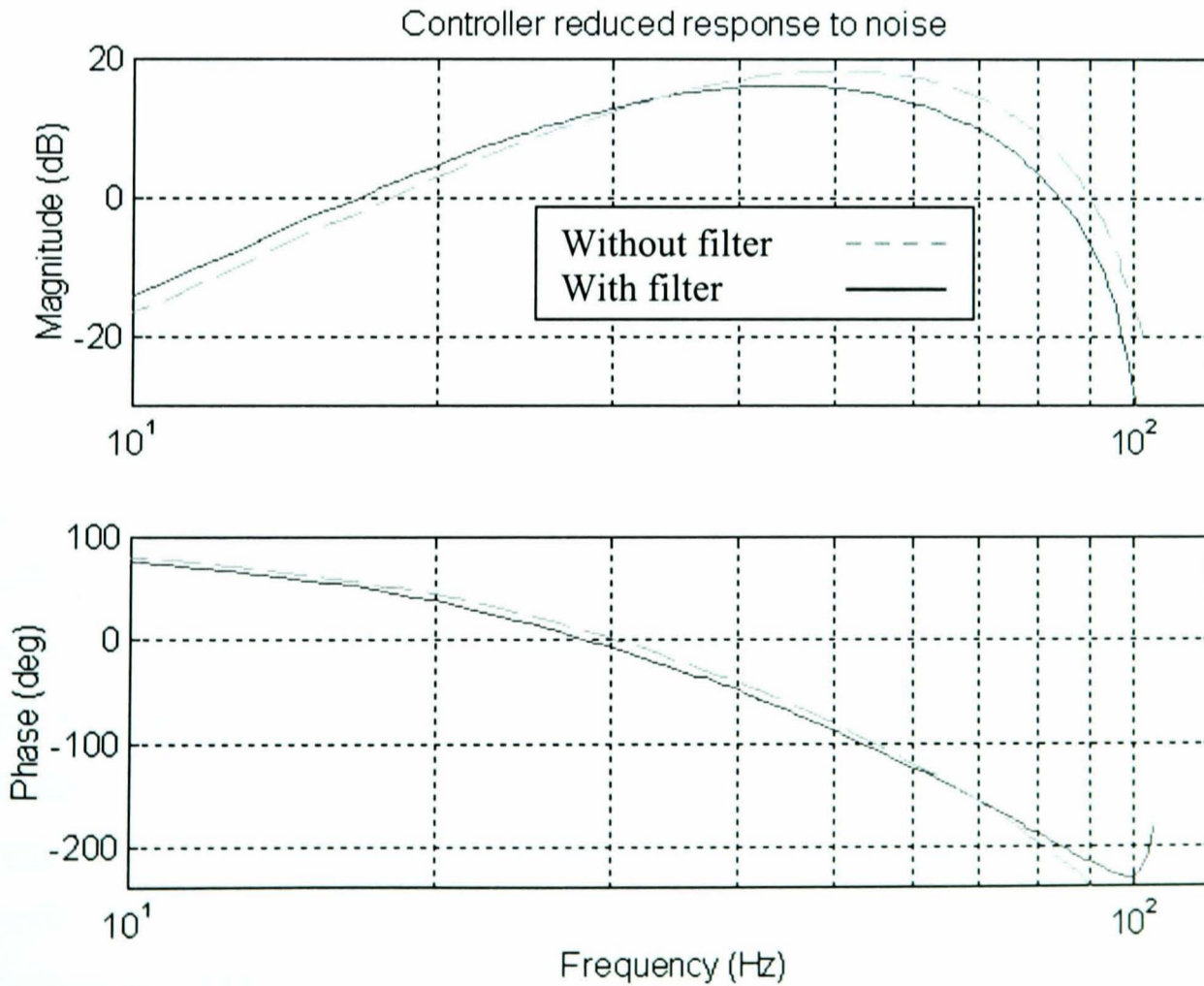
Figure 7.6 *Controller response to noise with H filter*

For closed-loop poles at 0.5±0.1i the closed-loop response with and without the demand filter is shown in figure 7.7. Slower poles were selected to prevent control signal saturation and reduce the controller response to measurement noise. The demand low pass filter has successfully attenuated the controller response to noise.
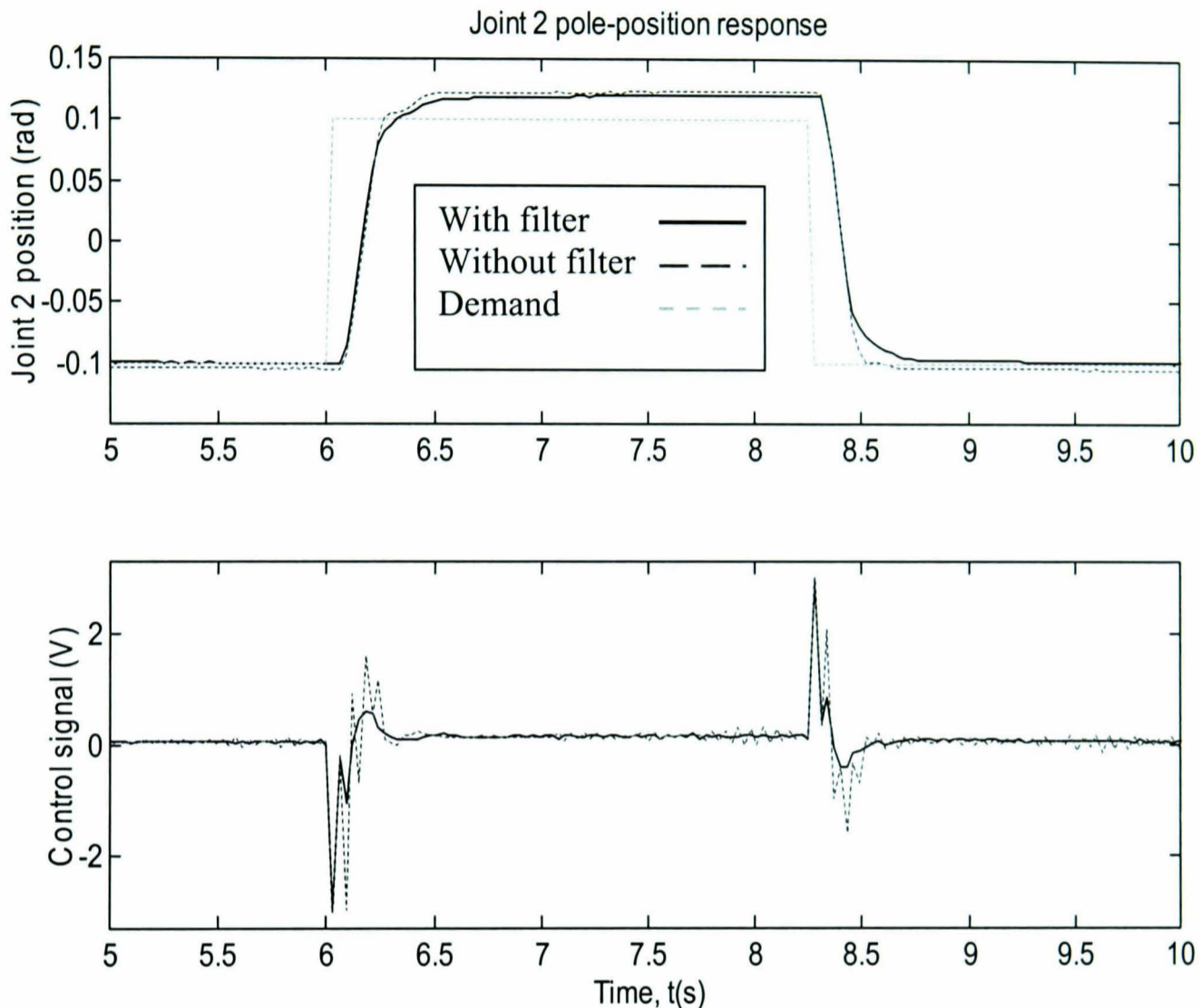
Figure 7.7 *Joint 2 response with and without demand filter*

Comparing the response of the pole-placement joint controllers to the optimised PID controllers the joint 3 response is greatly improved with reduced overshoot and faster settling time. The joint 2 response exhibits reduced overshoot and a slightly faster rise time. Note that the steady state error is still present in the response due to imperfect gravity compensation. The speed of response could be improved by increasing the speed of the system poles, however this would result in output saturation, potentially causing controller instability. A saturation compensated pole-placement controller could allow the pole-placement controller to operate within this saturation region **(Ling et al. 1999)**.

7.2.3   Two degree of freedom pole-placement position response

The two joint space controllers can be combined using inverse kinematics to control the global position of the robot end-point in two degrees of freedom. Two degrees of freedom were sufficient to evaluate the performance of the controller using the multiple degree-of-freedom force sensor.

It is important to note that a single degree-of-freedom pole-placement controller can not be directly compared to the single degree-of-freedom PD impedance controller due to differences in the commercial force sensor and the multiple degree of freedom force sensor used to measure forces on the robot.

The global x and y position responses, without external forces, are shown in figures 7.8 & 7.9. Little improvement in controller performance is evident from the global response when compared to the PID controller. Inspecting the joint angle error for the position response of figures 7.8 & 7.9 better illustrates the pole-placement controller's performance compared to the PID controller for a similar response (figure 7.10). The joint 3 positional error is reduced, however the joint 2 positional error is increased. The poor performance of the joint 2 pole-placement controller is due to the controller closed loop poles set to 0.5±0.1i to prevent controller saturation. Indeed if quicker poles could be specified, using a saturation compensation strategy the response should improve.

7.3   Pole-placement impedance controller

The pole-placement controllers replace the previous PID joint controllers to form a pole-placement impedance control strategy as shown in figure 7.11. The response of the two degree-of-freedom pole-placement controller was assessed using the five sets of impedance characteristics and compared to the two degree of freedom PID impedance controller.

Two joint pole-placement (x) response (no external force)
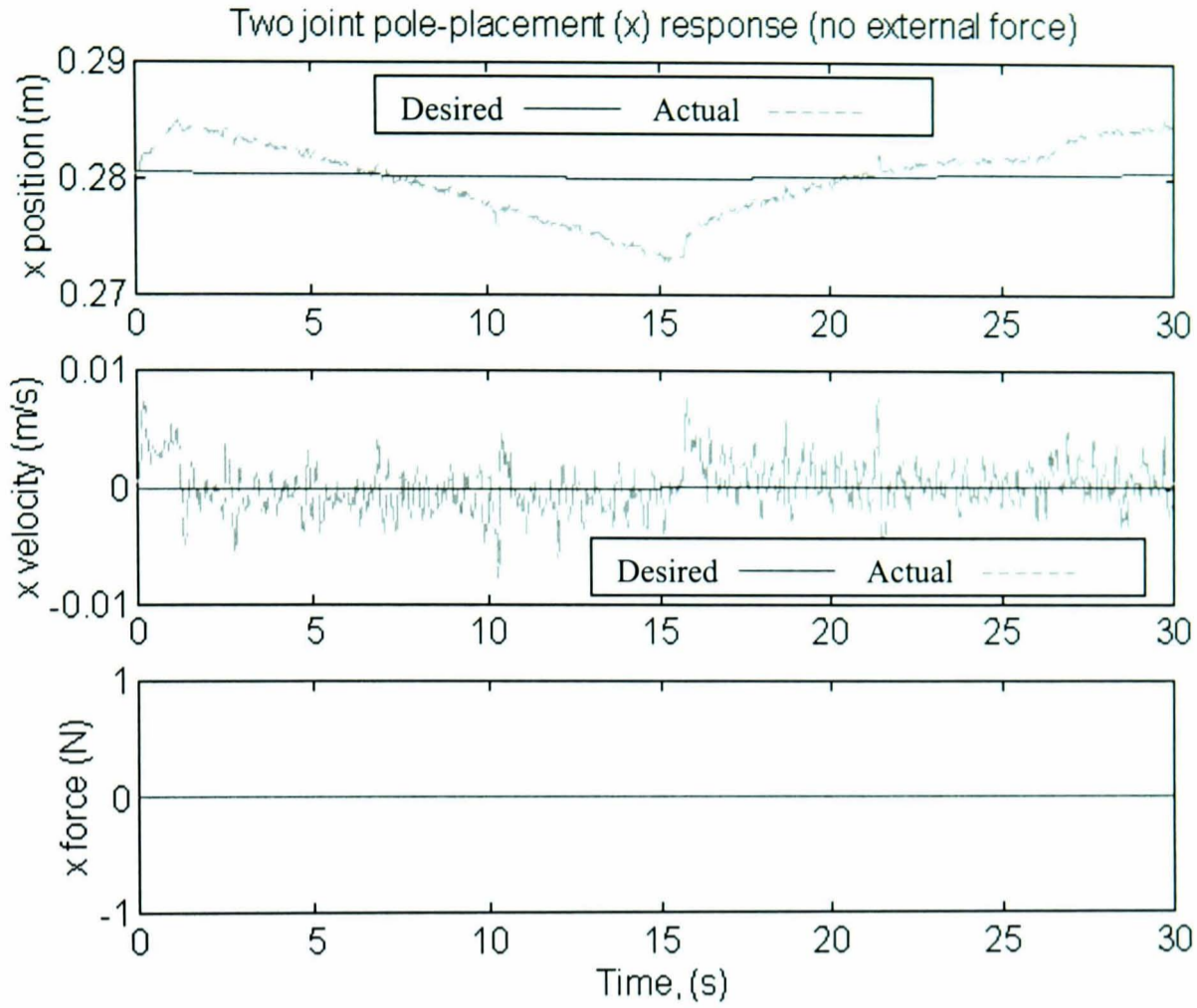
Figure 7.8 *Pole-placement (x) response (no external force)*

Two joint pole-placement (y) position response (no external force)
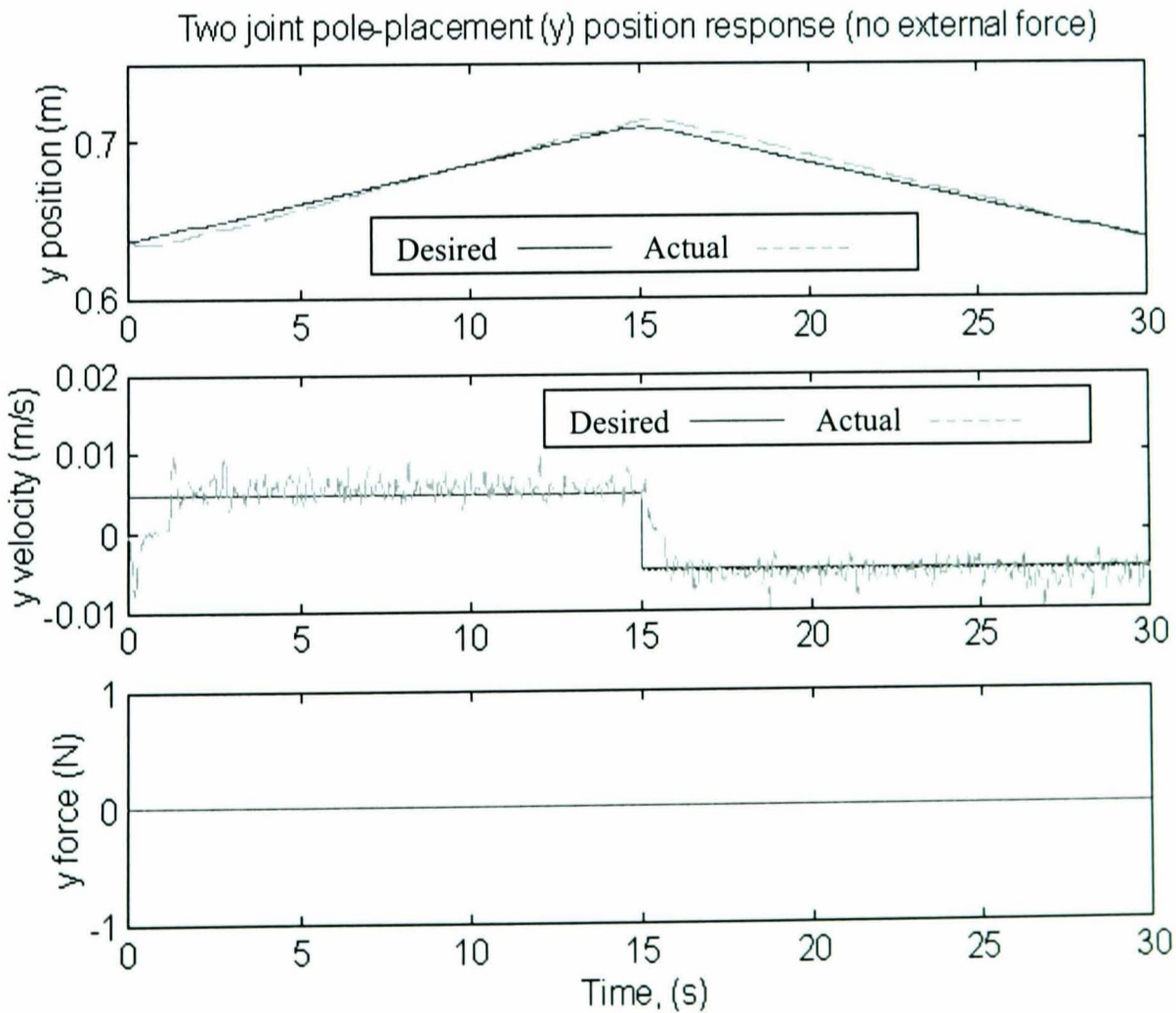
Figure 7.9 *Pole-placement (y) position response(no external force)*

Figure 7.10 *Pole-placement joint space error (no external force)*

Figure 7.11 *Pole-placement impedance controller block diagram*

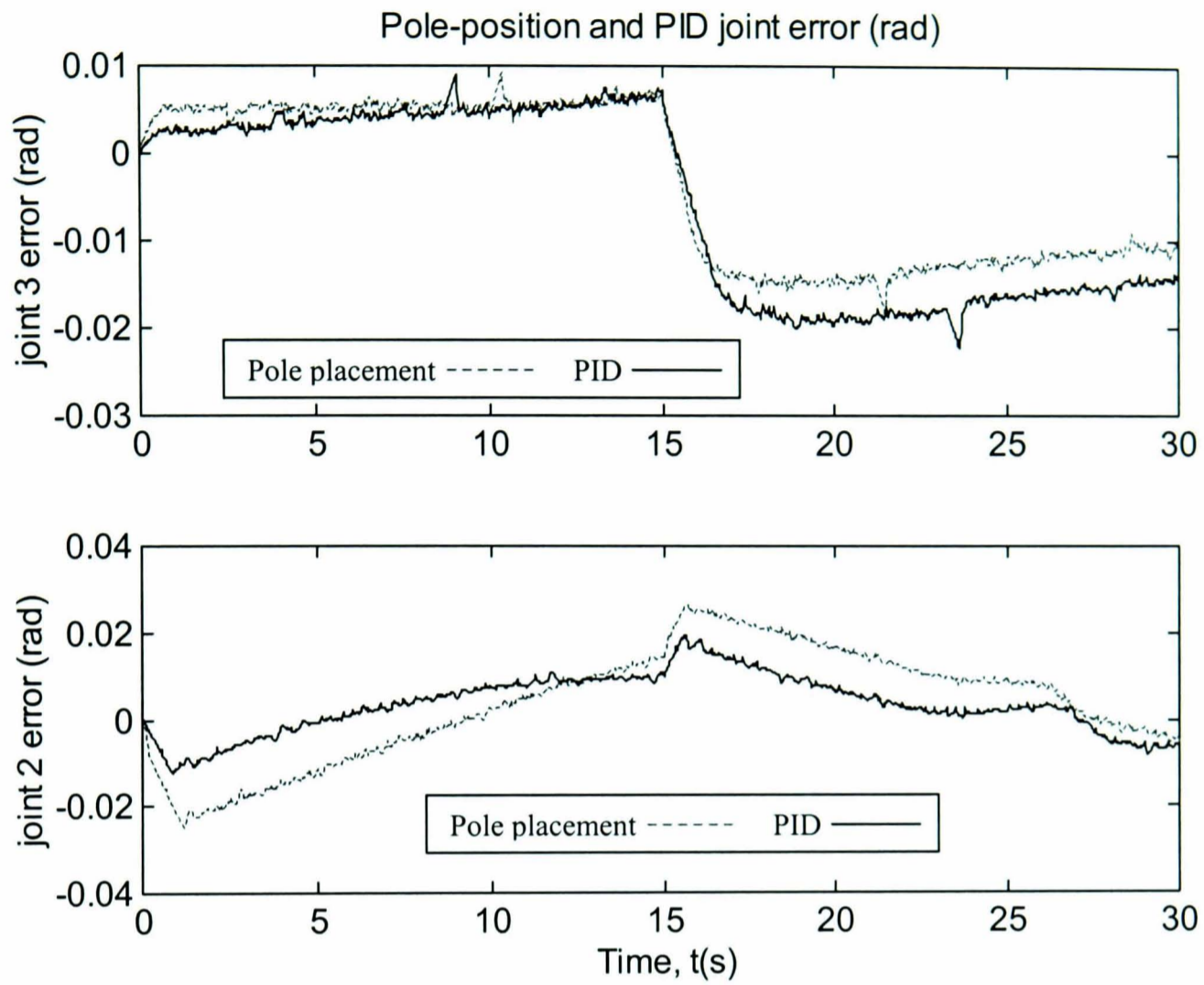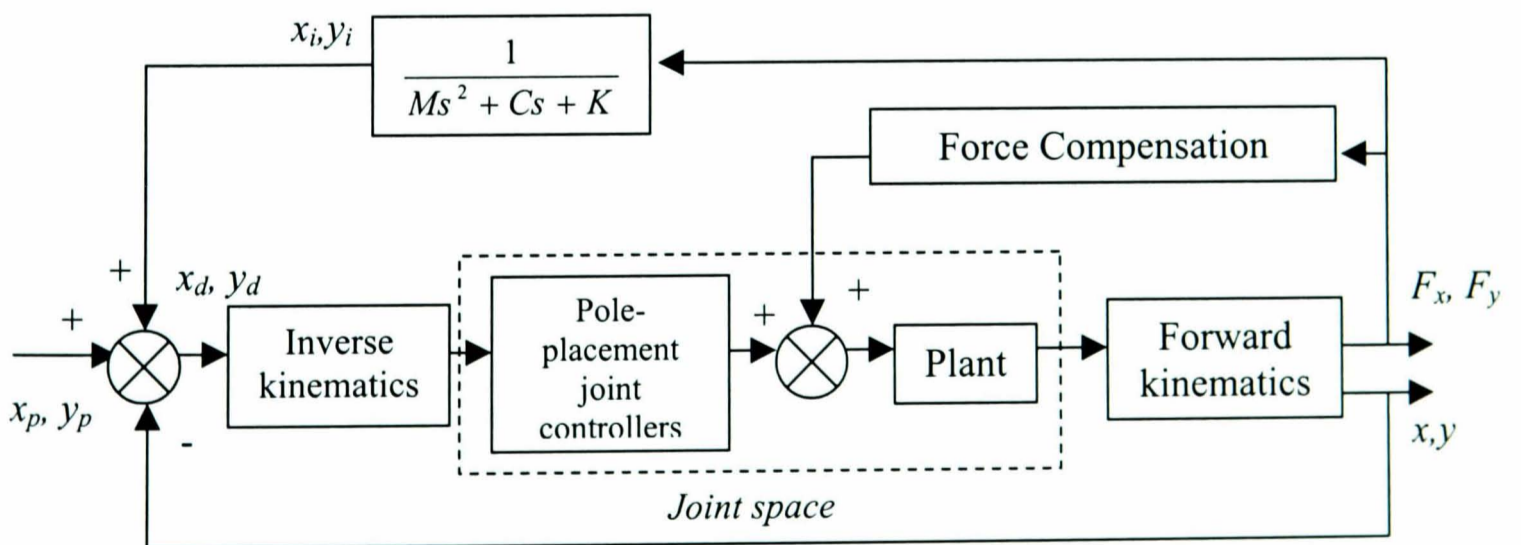The low damping and stiffness parameters (K=50,C=50) experimental response figure 7.12 shows the x and y trajectories to be accurately tracked. The response demonstrates improved velocity tracking particularly in the x direction when compared to the PID response.

The high stiffness and low damping (K=170, C=50) response (figure 7.13) demonstrates accurate velocity tracking, however, the x position response demonstrates poor amplitude tracking. This error in x position tracking can be attributed to the joint 2 control signal being restricted to prevent control signal saturation.

The response with low damping and high stiffness (K=50, C=170) (figure 7.14) demonstrates significant improvement over the PID response, however closer examination shows the velocity tracking to exhibit higher frequency oscillation that the PID response. Indeed, an increase in response vibration is noticeable when attached to the robot.

The high stiffness and high damping (K=250, C=250) response (figure 7.15) demonstrates an improvement in the position tracking, however the high frequency oscillation of the velocity is far greater than for the PID response. Finally, the medium stiffness and damping (K=130, C=130) response tracks the desired position (figure 7.16), again the velocity is shown to be oscillatory.

The pole-placement controller has not demonstrated superior performance when compared to the PID controller. However, if problems such as control signal saturation were solved, it is likely that the pole-placement controller performance would become superior to that of the PID controller.
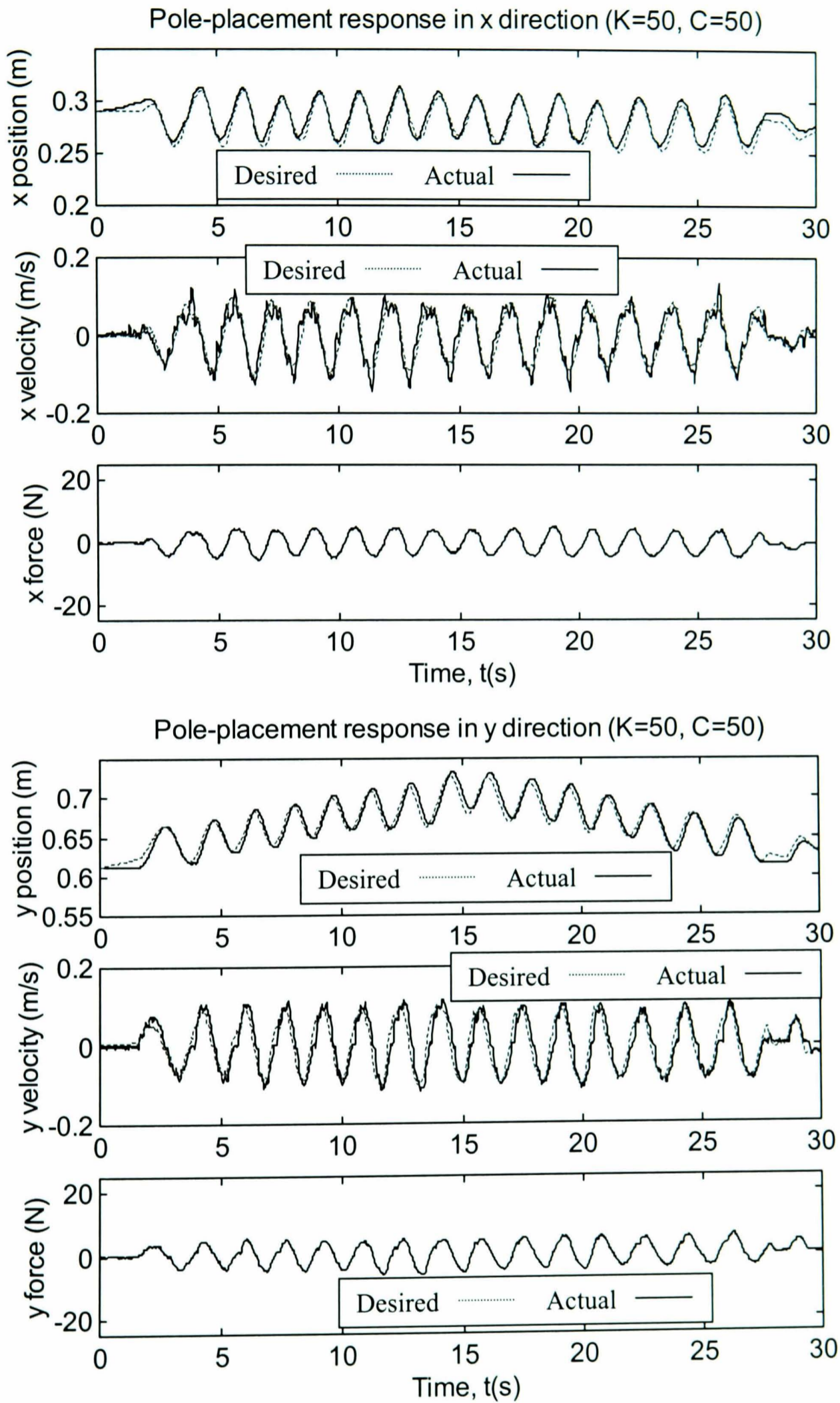
Figure 7.12 *Pole-placement impedance controller (K=50, C=50)*
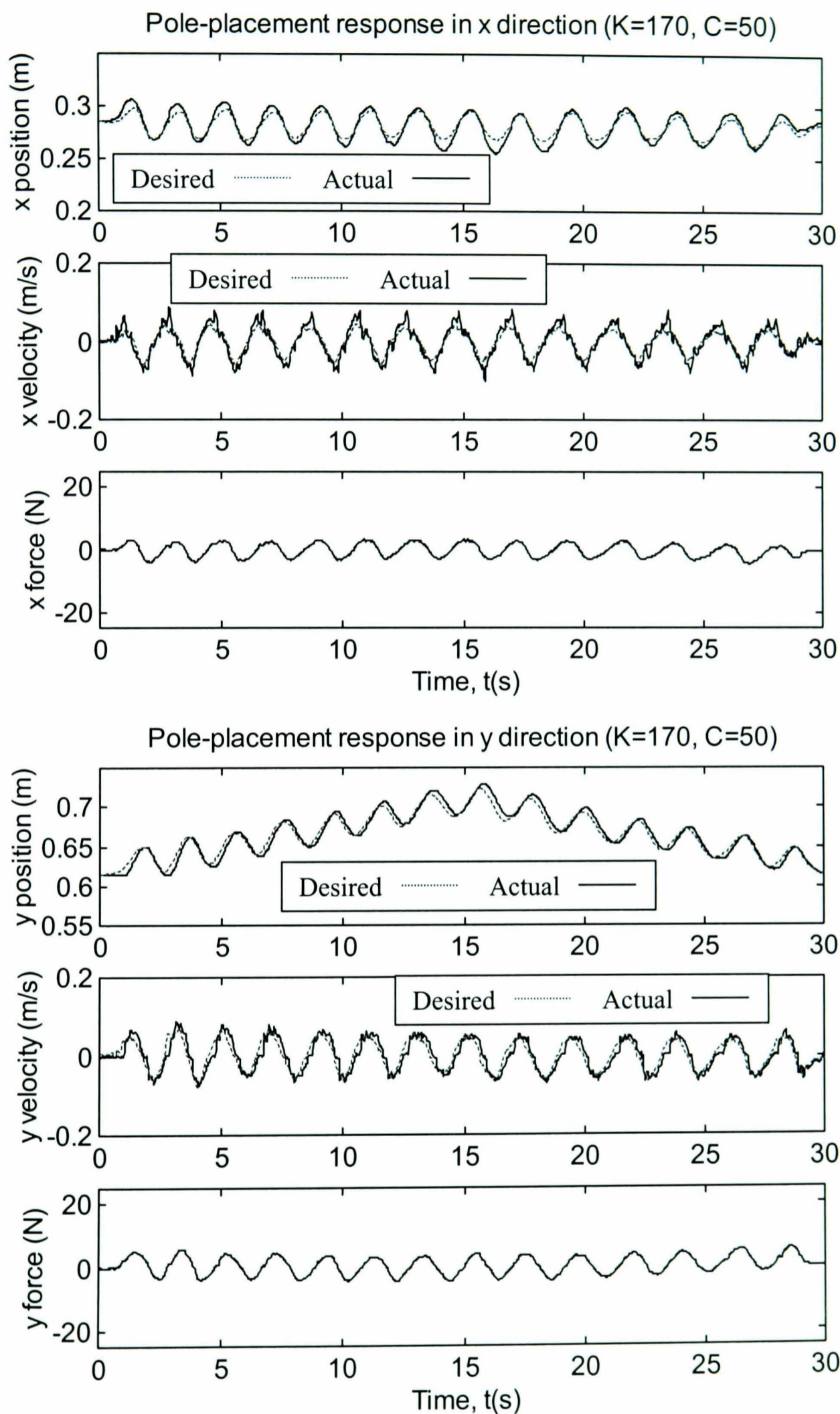
Figure 7.13 *Pole-placement impedance controller (K=170, C=50)*
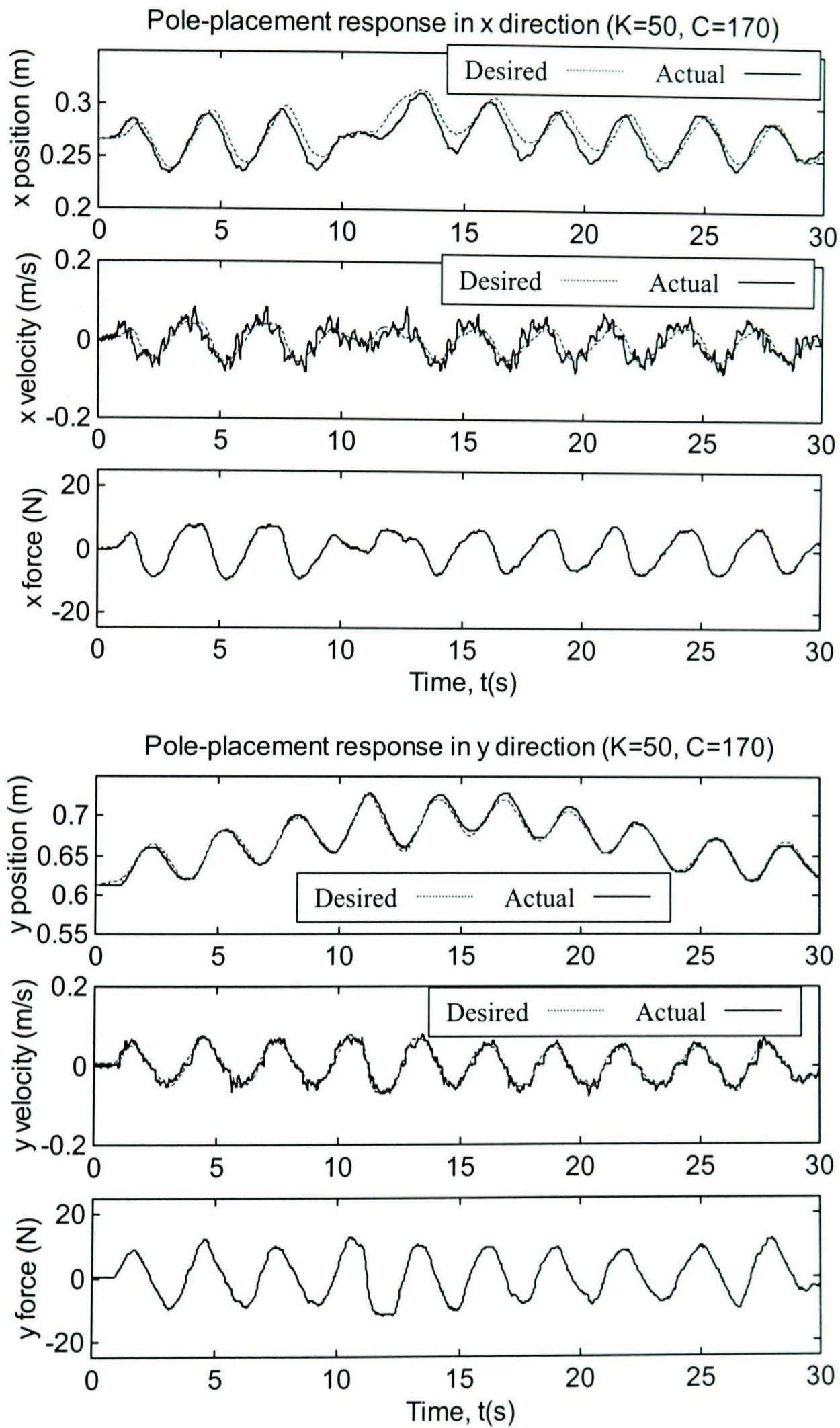
Figure 7.14 *Pole-placement impedance controller (K=50, C=170)*
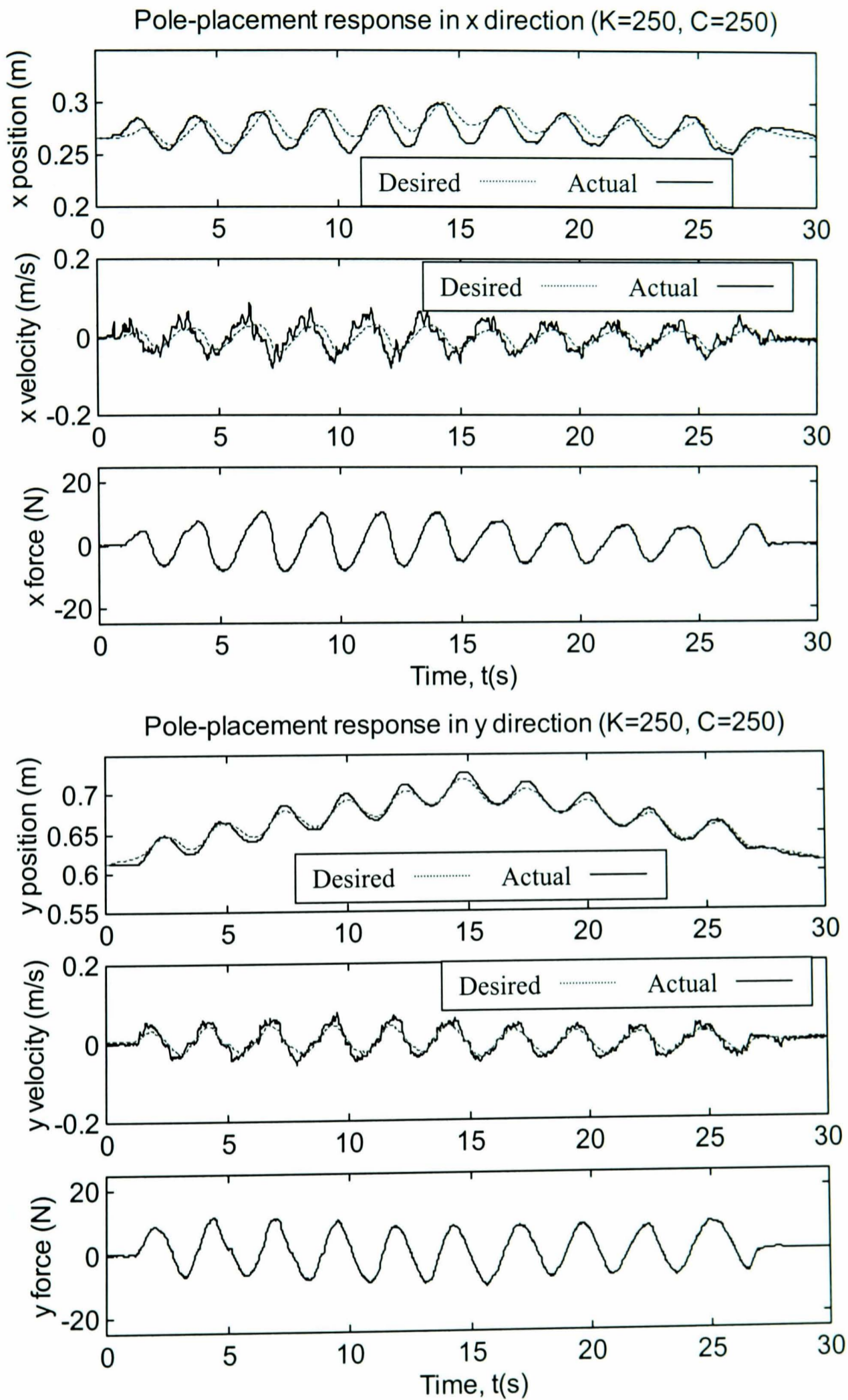
Figure 7.15 *Pole-placement impedance controller (K=250, C=250)*
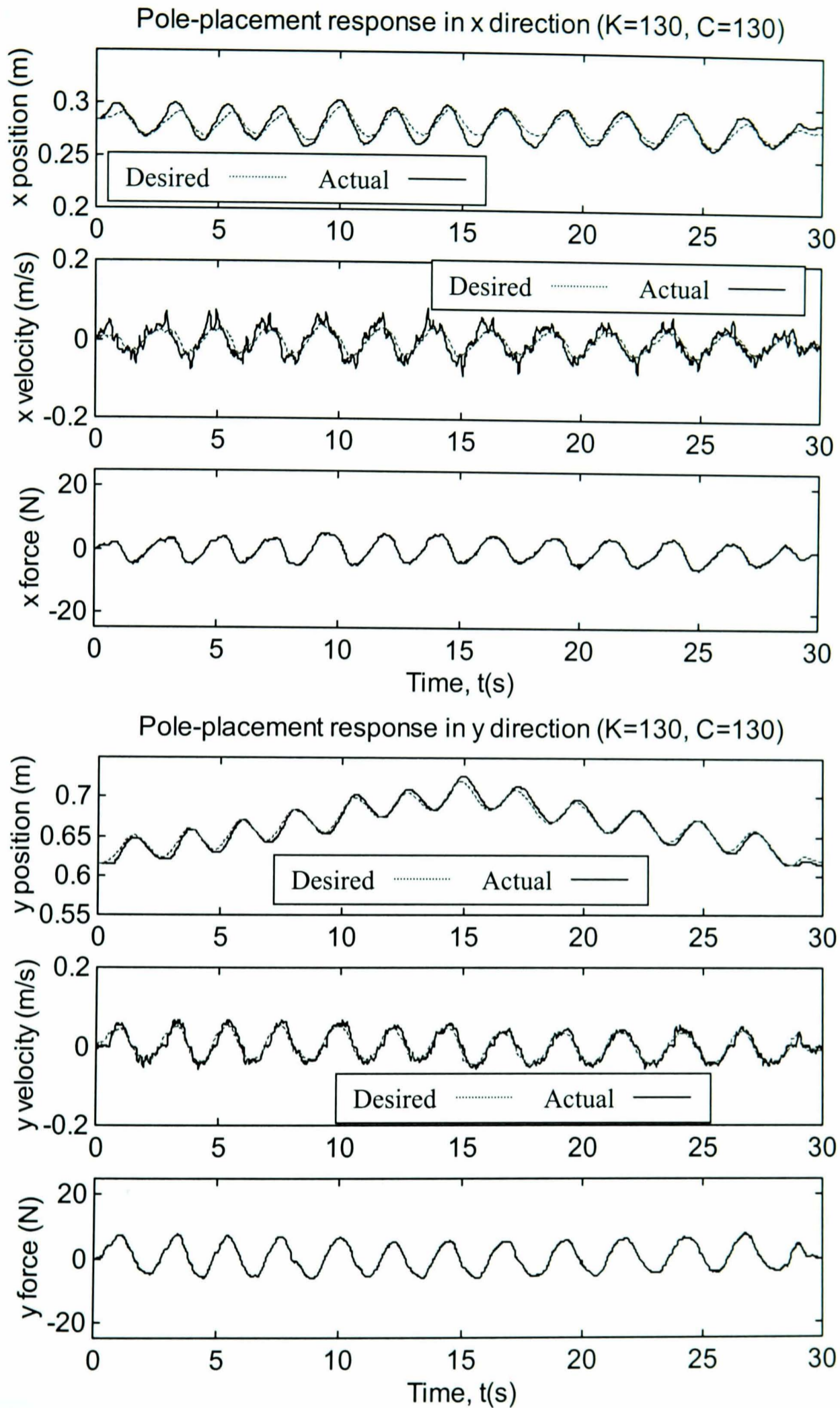
Figure 7.16 *Pole-placement impedance controller (K=130, C=130)*

7.4 Discussion and conclusions

To improve the response obtained from the PID position based impedance controller a pole-placement strategy has been designed. The pole-placement controller replaces the PID controller for the impedance control strategy. However, the design of this pole-placement controller was not as straightforward as for the test rig (chapter 3). The relationship between the line of cylinder action and the robot link varies as with joint angle. This creates non-linearities within the system response. An additional linearising element was required to create a linear plant for which an accurate plant model was then obtained.

The potentiometers that measure the angular displacement of the joint are susceptible to measurement noise. The anti-aliasing filters reduce this noise, however, the measurement noise is still significantly higher than for the LVDT on the test rig. This measurement noise limits the speed of poles that can be implemented on the system. Including a demand filter in the pole-placement controller reduces the controller's response to measurement noise. Experimental results have illustrated the controllers improved performance with the inclusion of this demand filter. Indeed, without the demand filter the robot joints would vibrate as a direct result of high frequency oscillations within the control signal.

The overall performance of the two degree-of-freedom pole-placement position controller was hindered by the second joint. Specifying slow poles for the second joint was necessary to ensure the controller would not experience output saturation and possible instability. A pole-placement saturation compensation strategy such as that described by **Ling et al. (1999)** would improve the controller performance.

Slight improvement of the impedance controller tracking is evident when comparing the pole-placement and PID responses, however, this is at the expense of increased response to noise. The benefits of using the pole-placement control strategy are questionable when compared to the PID controller due to increased complexity and need for an accurate system model. However, is should be noted that the PID gains were chosen through an online optimisation process.

Improvements to the experimental equipment such as increased force output at the second joint through the use of two pneumatic cylinders would prevent controller saturation. Measurement of the cylinder position by mounting linear potentiometers directly to the pneumatic cylinders would improve the measurement of joint angles. If these modifications were performed the use of a pole-placement strategy should improve the controller performance.

Chapter 8

Conclusions and future work

The design and control of a pneumatic physiotherapy robot has been described in this thesis. This chapter details conclusions drawn from the current study and outlined directions for future work.

8.1   Assessment of research objectives

Four research objectives were outlined in chapter one. This section identifies the extent to which they have been fulfilled during this study:

8.1.1   Investigation of actuation systems

The performance and control of modern pneumatic actuation systems has been investigated. The frictional characteristics of modern low friction cylinders were demonstrated to be superior to traditional pneumatic cylinders (chapter 2). Precision position control of the pneumatic servosystem has been demonstrated through implementation of a pole-placement control strategy (chapter 3). The pneumatic servosystem provides acceptable movement characteristics to actuate an upper-limb robotic orthosis device.

8.1.2   Design and construction of experimental device

A pneumatically actuated robot has been designed and fabricated (chapter 2). Experiments have verified that the robot can move the average male's upper limb, through a sufficient movement range to implement upper-limb physiotherapy. Throughout this movement range, the robot is capable of applying forces to assist motion. Measurement of the global end-point position and force are achieved through joint angle measurement and a three degree-of-freedom force sensor.

8.1.3 Application of advanced servo and robot control techniques

Control techniques have been designed and implemented to control position and force. Primarily, an impedance controller (chapter 6) has been developed to control the relationship between position and force at the robot end-point in multiple degrees of freedom. Presently, the accuracy of the force sensor degrades the robot performance. However it is hypothesised that improvements in the measurement of force should greatly improve the controller.

8.1.4 Demonstrate controller using one or two sample patients

The stability of the position based impedance controller has not been proven. Stroke victims would be extremely susceptible to injury should any controller instability be encountered. A rigorous stability analysis would be required before the performance of the device could be evaluated on patients.

A study has been performed to evaluate the robot on able-bodied subjects (appendix D). This study showed the device to have considerable potential as a physiotherapy robot, however, a significant problem was identified with the three degree-of-freedom force sensor. Humans, when attached to the device, had a tendency to apply large torque to the force sensor (figure 8.1).
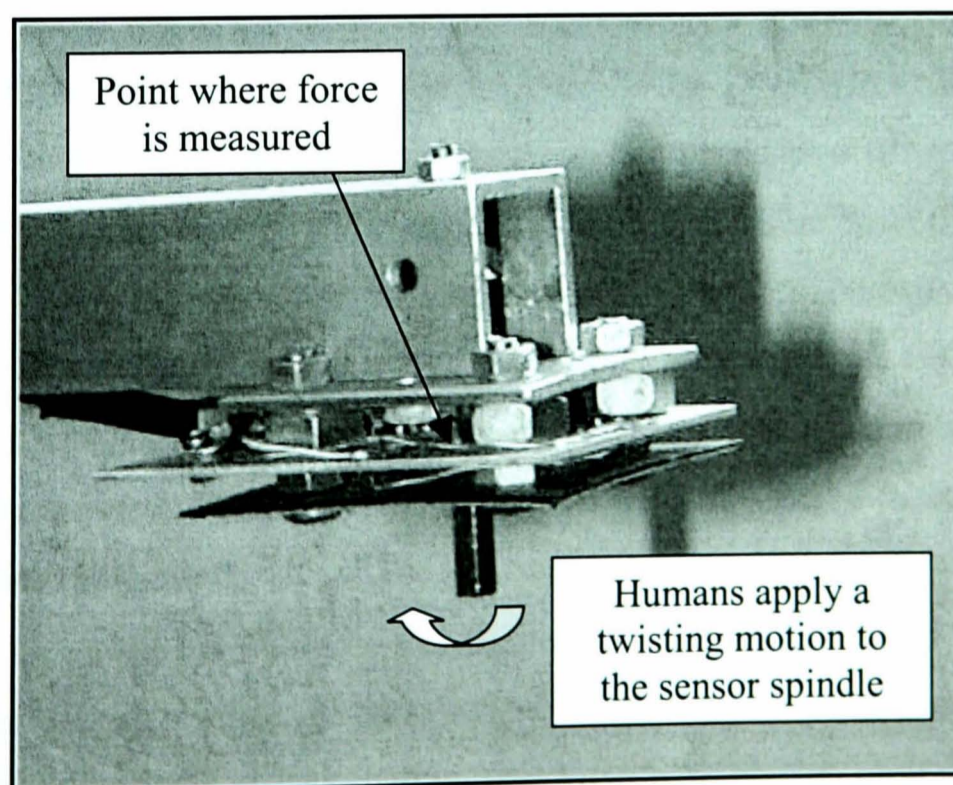
Figure 8.1 Applying torque to force sensor

Inadequacies in the force sensor cause it to measure torque as applied force. The force-balancing element of the impedance controller attempts to counteract these 'ghost' forces, resulting in the robot applying force in undesired directions. This problem causes the robot to be unsuitable for administering physiotherapy in its present form.

8.2 Conclusions

The following conclusions relate to specific elements of the work performed:

8.2.1 Design

- The overall design satisfies the force and position criteria detailed in the design specification (chapter 2). The mounting of the force and position sensor enables forces to be measured at the robot endpoint, however, the orientation of the force sensor varies with joint movement. The robot could have been designed to maintain robot endpoint orientation in the x and y directions, reducing some of the difficulties of accurate force measurement. An example of this alternative arrangement is shown in figure 8.2. However, it should be noted that this considerably increases the design complexity.

- A force sensor has been designed that is capable of measuring forces in three degrees of freedom (chapter 2). The accuracy of the force sensor was poorer than standard commercial sensors, moreover, the force sensor was shown to be susceptible to misreading torque input as force input. The accuracy of the force sensor is not sufficient for it be implemented in applications that interact with humans. However, it is important to remember the simplicity and ease of manufacture of the design compared to the complexity of other researcher's force and torque sensors. The simplicity and cost of the force sensor make it suitable for non-critical applications.

- The robot global position is calculated from individual joint positions that are measured by angular potentiometers. The small rotation that each link undergoes

results in a poor signal-to-noise ratio for angle measurement. The quality of the angular position measurement has restricted the performance of the overall robot (chapter 7).
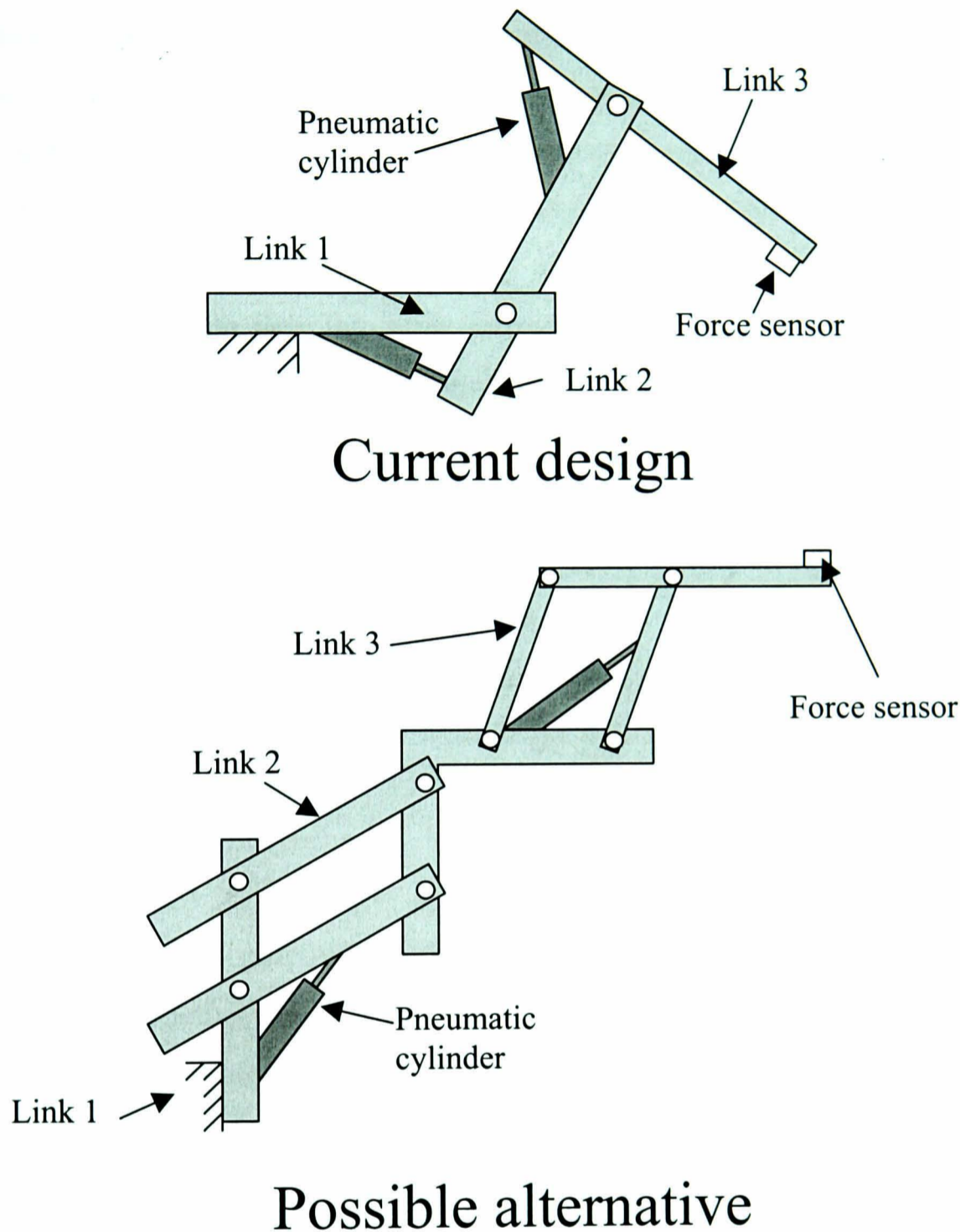
Figure 8.2 Alternative robot configuration

- The use of two electro-pneumatic valves to control one cylinder (chapter 3) provides significant advantages over traditional spool valves, such as independent control of pressures within each chamber. However these valves are significantly more expensive than a single spool valve, increasing the cost of the overall device.

8.2.2 Modelling

• A mathematical model of a single pneumatic valve has been derived and validated by comparison of experimental and simulated results (chapter 5). The valve model, combined with a conventional model of a pneumatic cylinder, resulted in an accurate model of the pneumatic servosystem behaviour. However, a velocity coefficient required experimental identification (chapter 4). This coefficient is likely to consist of predominantly viscous friction, however, it is also likely contain other factors such as friction within the robot links. Experimental data detailing the mass flow into each chamber, along with respective temperature and pressure would provide a further insight into of the composition of this coefficient.

• The modelling section has identified the orifice area of interconnecting pipes as an important consideration when designing pneumatic systems. The orifice area of these pipes can reduce the maximum mass flow rate, delaying the response of the pneumatic servosystem. This is an inherent limitation of pneumatic systems and can only be improved by an increase in the pipe diameter.

8.2.3 Control

• Implementing a pole-placement strategy on a single pneumatic cylinder has demonstrated the potential of modern pneumatic systems to perform precision positioning (chapter 3). The modern pneumatic system exhibits greatly reduced stiction effects when compared to conventional systems. The incorporation of a self-tuning strategy has enabled the controller to behave consistently, however it is unlikely that the pneumatic system is capable of providing equivalent or superior performance when compared to DC motors. It should be remembered, however, that in both the cost and power-to-weight ratio, pneumatic servosystems are significantly superior.

• The performances of the joint space controllers, joint 2 particularly, are influenced by gravity effects acting on the robot links. The robot has gravity compensation masses, at the end of each link, to reduce the influence of gravity on these links.

However, these physical masses cannot provide gravity compensation across the complete range of robot motion. The imperfect gravity compensation of joint 2 results in steady state position error, significantly degrading the robot position response (chapters 6 & 7).

- Impedance control has been identified as the most appropriate force and position control strategy for implementing robotic physiotherapy. Applying the impedance control strategy, to a single link of the robot, resulted in accurate implementation of the force and position relationship (chapter 6). Extending the impedance controller to multiple degrees of freedom has degraded the overall controller performance. Three main factors are likely to be the cause of this degradation; interaction between joints, the accuracy of the force sensor and the performance of the joint 2 controller.

- Modifying the impedance control strategy to implement pole-placement joint controllers has resulted in little controller improvement (chapter 7). Limiting the gain of the second joint controller, to prevent output saturation, adversely effected the performance of the task space controller.

8.3 Future work

This research has provided a starting point for research into pneumatic physiotherapy robots. A great deal of additional research can be performed to improve further research presented here.

8.3.1 Design

- Mounting linear slide potentiometers directly across the pneumatic cylinders would enable accurate measurement of the cylinder piston position. Accurate joint space angles could then be calculated, improving controller performance.

- Use of a commercial force and torque sensor should vastly improve the measurement of forces, hence, improve the impedance controller. Although the robot is not capable of applying controlled torque, measurement of the torque applied by the robot would ensure no harmful torque is applied to the patient.

- The use of two pneumatic cylinders in parallel at joint 2 should prevent any output force saturation. The robot has been designed to allow 2 cylinders to be attached to increase the force output at both joints 1 and 2.

- The cost of the electro-pneumatic valves impacts on the cost of the overall device. It may be possible to replace a single electro-pneumatic valve with a spool valve and pressure sensor. This would require additional control elements, however the cost of the overall device would be significantly reduced.

8.3.2 Control

- The pneumatic actuators could actively compensate for robot link gravity effects. This should improve the performance of the joint space controllers. Remember that it is these gravity effects that cause the steady state error in the joint 2 response. For the joint space actuators to compensate for these effects a force output, dependent on the joint orientation, would be required.

- A rigorous stability analysis of the impedance controller strategy is required before patient testing to ensure controller instability will not occur.

8.3.3 Robotic physiotherapy

- The three degree-of-freedom robot is designed to be attached to a human at the forearm. The robot then applies assistive forces to move the subjects upper-limb. If this approach were taken forces could be exerted on the shoulder joint, which can be extremely vulnerable to excessive forces. A mechanical shoulder brace, to

prevent damaging forces being applied to the shoulder joint, needs to be designed and fabricated before safe clinical evaluation of the device.

- When the desired impedance controller trajectory is accurately tracked, low forces exist between the robot and human. It would be useful to reduce these forces further by implementing a 'dead zone' around the position error (i.e. small errors in position result in no assistive force). Implementation of this dead-zone would require the use of some form of non-linear controller, such as a fuzzy controller.

- Implementing impedance control in three degrees is problematic as no feedback has been developed to indicate the desired position. Some form of three dimensional feedback, either physical or computer generated, needs to be designed and implemented to enable robotic physiotherapy to be administered in three degrees of freedom.

- A clinical trial of the robot implementing physiotherapy in three degrees of freedom could be performed to assess, in more detail, the practical benefits of a pneumatic robotic physiotherapy device.

- Two co-operating three degree-of-freedom robots, one attached to the forearm and one attached to the upper arm, could administer physiotherapy. These robots would enable rehabilitation of the whole upper limb (including the shoulder joint) without the requirement for restrictive shoulder bracing.

References

Anderson R, Spong M. *'Hybrid impedance control of robotic manipulators'*. IEE journal of robotics and automation. Page(s) 549-556, Vol. 4, No. 5, Oct. 1988.

Astrom KJ, Wittenmark B. *'Self-tuning controllers based on pole-zero placement'*. IEE Proceedings (D). Page(s) 120-127, Vol. 127, No.3, May 1980.

Astrom K, Hagglund T. *'PID Controllers: Theory, Design and Tuning'. Instrument society of America'*. 1994. ISBN 1-55617-516-7.

Austin M. *'Robotic upper-limb rehabilitation'*. PhD thesis, University of Leeds, 1999.

Backe W, Ohligschlager O. *'A model of heat transfer in pneumatic chambers'*. Journal of fluid control. Page(s) 61-78, Vol. 20, 1989.

Bamford JM, Sandercock P, Dennis M, Burn J, Warlow C. *'A prospective study of acute cerebrovascular disease in the community: the Oxfordshire Community Stroke Project 1981-1986. Incidence, case fatality rates and overall outcome at one year of cerebral infraction, intracerebral haemorrage and subarachnoid haemorrhage'*. Journal of Neurol, Neurosurgery and Psychiatry. Page(s) 16-22, 1990.

Bekit BW, Seneviratne LD, Althoefer K. *'Fuzzy PID tuning for robot manipulators'*. Proceedings of the 24th annual conference of the IEEE industrial electronics society, IECON '98. Page(s) 2452-2457, Vol 4, 1998.

Ben-Dov D,.Salcudean SE. *'A force controlled pneumatic actuator'*. IEEE transactions on robotics and automation. Vol. 11, No.6, Page(s) 906-911, Dec. 1995.

Ben-Lamine M, Shibata S, Tanaka K, Shimizu A. *'Impedance characteristics of robots considering human emotions'*. JSME International Journal, Series C: Dynamics, Control, Robotics, Design and Manufacturing. Page(s) 309-315, Vol. 40, No. 2, June 1997.

Bilodeau G, Papadopoulos E. *'A model-based impedance control scheme for high-performance hydraulic joints'*. Proceedings of IEEE/RSJ international conference on intelligent robots and systems. Page(s) 1308 –1313, Vol. 2, 1998.

Bobrow JE, Jabbari F. *'Adaptive pneumatic force actuation and position control. Journal of dynamic systems measurement and control'*. Page(s) 26⁻ – 272. Vol. 113 / 267, June 1991.

Bobrow JE, McDonell BW. *'Modelling, Identification and control of a pneumatically actuated, force controllable robot'*. IEEE Transactions on robotics and automation. Page(s) 732 –742, Vol. 14, No. 5, Oct. 1998.

Bradley DA, Dawson D, Burd NC, Loader AJ. *'Mechatronics'*. Chapman and Hall. 1993. ISBN 0-412-58290.

Buckley,MA Platts,RGS Marchese,SS. *'Development of the specification for a motorised upper-limb orthotic system'*. IEE collq digest 1995/107 mechatronic aids for the disabled. Page(s) 1-2, Vol. 107, 1995.

Caldwell DG, Medrano GA, Goodwin M. *'Control of pneumatic muscle actuators. IEEE control systems'*. Page(s) 40-48, Vol. 15, No. 11, 1995.

Chambers. *'Science and technology dictionary'*. W & R Chambers 1991. ISBN 0-550-13239-2

Carignan CR, Smith, JA. *'Manipulator impedance accuracy in position-based impedance control implementations'*. Proceedings of the IEEE international conference robotics and automation. Vol. 2, Page(s): 1216 – 1221, 1994.

Chang YC, Lee CH. *"Robust tracking control for constrained robots actuated by DC motors without velocity measurements"*. Control Theory and Applications, IEE Proceedings. Vol. 146, No. 2, Page(s) 147 –156, March 1999.

Chao L, Yin C. *'The six-component force sensor for measuring the loading of the feet in locomotion'*. Materials and design. Page(s) 237-244, Vol.20, 1999.

Chiavervini S, Sciavicco L. *'The parallel approach to force/position control of robotic manipulators'*. IEEE transactions on robotics and automation. Page(s) 361-373, Vol. 9, No. 4, Aug. 1993.

Choi S, Kim J. *'A fuzzy-sliding mode controller for robust tracking of robotic manipulators'*. Mechatronics. Page(s) 199-216, Vol. 7, No.2, 1997.

Cozens JA. *'Robotic therapy in upper limb rehabilitation'*. Philips Nichols prize paper for original research in rehabilitation, British society of rehabilitation. 1995.

Dolan JM, Friedman B, Nagurka L. *'Dynamic and loaded impedance components in the maintenance of human arm posture'*. IEEE transactions on systems, man and cybernetics. Page(s) 698-709, Vol. 23, No. 3, 1993.

Drankunov S, Hanchin GD, Su WC, Ozguner U. *'Non-linear control of a rodless pneumatic servoactuator, or sliding modes versus coulomb frcition'*. Automatica, Vol. 33, No. 7, Page(s) 1401-1408,1997.

Dunnigan MW, Lane DM, Clegg AC, Edwards I. *'Hybrid position/force control of a hydraulic underwater manipulator'*. IEE proceedings of applied control theory. Page(s) 145 –151, Vol. 143, No. 2, March 1996.

Erlandson RF, Kristy KA, Wu SJ, Debear P, Dijkers M. *'Use of a robotic arm in the rehabilitation of stroke'*. SME technical papers. 1989.

Fagan MJ. *'Finite element analysis'*. Addison Wesley Longman Ltd, 1992. ISBN 0-582-02247-9.

Folk SC, Wang Z, Dransfield PD. *'A digital simulation study of an adaptive controller for a pneumatic cylinder system'*. International journal of computer applications in technology. Page(s) 163-171, Vol. 8. 1995.

Fujiwara A, Katsumata K, Ishida Y. *'Neural network based adaptive I-PD controller for pneumatic cylinder'*. SICE '95. Page(s) 1281-1284, July 1995.

Fujiwara A, Ishida Y. *'An LQI control for pneumatic cylinders with disturbance observer'*. International conference on robotics and manufacturing. Page(s) 19-22, Aug. 1996.

Fujiwara A, Katsumaza K, Ishida Y. *'An LQI control for pneumatic cylinders using multilayer neural networks'*. Journal A. Page(s) 31-37, Vol. 38, No. 2., 1997.

Gaberman M. *'Near Frictionless Air cylinders provide precision pneumatic motion control systems'*. Power conversion and intelligent motion. Page(s) 48-51, Vol.21, No 11, 1995.

Gaikwad S, Dash S, Stein G. *'Auto-tuning PID using loop-shaping ideas'*. Proceedings of the IEEE international conference on control applications. Page(s) 589 –593, Vol. 1, 1999.

Gorce P, Guihard M. *'Joint impedance pneumatic control for multilink systems'*. ASME Journal of dynamic systems, measurement and control. Page(s) 293-297, Vol. 121, June 1999.

Graca RA, Gu YL. *'A Fuzzy learning algorithm for kinematic control of a robotic system'*. Proceedings of the 32nd conference on decision and control. San Antonio. Page(s) 1274-1279, Dec. 1993.

Gross DC, Rattan KS. *'Feedforward MNN controller for pneumatic cylinder trajectory control'*. IEEE international conference on neural networks. Page(s) 794-799, Vol 2, 1997.

Gross DC, Rattan KS. *'An adaptive multilayer neural network for trajectory tracking control of a pneumatic cylinder'*. IEEE International Conference on Systems, Man, and Cybernetics. Page(s) 1662 –1667, Vol. 2 1998.

Guihard M, Gorce P, Fontaine JG, M'Sirdi NK. *'A solution to control the dynamic behaviour of a pneumatic quadruped robot'*. Proceedings of the IEEE international conference on robotics and automation. Page(s) 21-27, May 1995.

Guihard M Gorce P. *'A new way to tackle position/force control for pneumatic robots'*. Proceedings of the IEEE international conference intelligent robots and systems, Osaka. Page(s) 164-168, Vol.2, Nov. 1996.

Guldner J, Carroll JJ, Dawson DM, Qu Z. *'Robust tracking control of rigid-link electrically-driven robots'*. Proceedings of the 31st conference on decision and control. Page(s) 1886-1868, Dec. 1992.

Hamiti K, Voda-besancon A, Roux-Boisson H. *'Position control of a pneumatic actuator under the influence of stiction'*. Control Engineering Practice. Page(s) 1079-1088, Vol. 4, No. 8, 1996.

Hanchin GD, Ozguner U, Drakunov S. *'Nonlinear control of a rodless pneumatic servoactuator'*. IEEE conference on Control Applications. Page(s) 516 – 521, Vol.1, 1992.

Hashimoto T, Ishida Y. *'An adaptive I-PD controller based on frequency domain system identification'*. ISA Transactions. Page(s) 71-78, Vol. 39, Issue 1, Feb. 2000.

Heinrichs B, Sepehri N, Thorton-Trump AB. *'Position-based impedance control of an industrial hydraulic manipulator'*. IEEE control systems magazine (special issue on robotics and automation). Page(s) 46-52, Vol. 17, 1997.

Heinrichs B, Sepehri N. *'Relationship of position-based impedance control to explicit force control: Theory and experiments'*. Proceedings of the American control conference, San Diego. Page(S) 2072-2076, June 1999.

Hogan N. *'Impedance control: An approach to manipulation part I,II,III'*. Journal of dynamic systems, measurements and control. Page(s) 1-24, Vol 107/1, 1985.

Hogan N. *'On the stability of manipulators performing contact tasks'*. IEEE Journal of robotics and automation. Page(s) 677-686, Vol. 4, 1988.

Hogan H, Frebs HI, Sharon A, Charnnarong J. *US Patent 5 466 213*. November 1995.

Homma K, Arai T. *'An upper limb assist system: experiments with arm models'*. Proceedings of the IEEE/RSJ international conference on intelligent robots and systems, Canada. Page(s) 758-63, Oct 1998.

Hsia TC. **'System identification : Theory for the user'**. Prentice Hall. 1977.

Hua Y, Yongxiang L. *'Simulation of speed minimum variance tracking control of pneumatic cylinder with no positioning accumulating error'*. ASME Modelling simulation and control (B). Page(s) 59-64, 1991.

James G, Burley D, Clements D, Dyke P, Searl J, Wright J. *'Modern engineering mathematics'*. Addison-wesley, 1994. ISBN 0-201-18054-5.

Kantowitz BH, Sorkin RD. *'Human factors - understanding people-system relationships'*. Wiley, 1983, ISBN 0-471-0594-X.

Kawamura S, Hayakawa Y, Tami M, Shimizu T. *'A design of motion-support robots for human arms using hexahedron rubber actuators'*. Proceedings of the IEEE/RSJ international conference on intelligent robots and systems, Greenoble. Page(s) 1520-26, Vol. 3, Sept. 1997.

Kawanaka H, Hanada K. *'Many points positioning of pneumatic cylinder for a vertical axis actuator using two degrees of freedom PI control method'*. Proceedings of the 4th international workshop on advanced motion control, Japan. Page(s) 71-74, Vol. 1, March 1996.

Kim G, Kang D, Rhee S. *'Design and fabrication of a six-component force/moment sensor. Sensors and actuators'*. Sensors and Actuators (A), physical, Page(s) 209-220, Vol. 77, 1999.

Kimura T, Hara S, Fujita T, Kagawa T. *'Feedback Linearisation for pneumatic actuator systems with static friction'*. Control Engineering Practice. Page(s) 1385-1394, Vol. 5, No. 10. 1997.

Kobayishi S, Cotsaftis M, Takamori T. *'Robust control of a pneumatic actuators based on impedance matching'*. IEEE international conference on systems man and cybernetics, Vancouver. Page(s) 983-987, Oct. 1995.

Krebs HI, Hogan N, Aisen ML, Volpe BT. *'Robot-aided neuro-rehabilitation'*. IEEE transactions on rehabilitation engineering. Page(s) 75-87. Vol. 6, No. 1, March 1998.

Krebs HI, Hogan N, Volpe BT, Aisen ML, Edelstein L. Diels C. *'Robot -aided neuro-rehabilitation in stroke: three year follow up'*. ICORR '99

international conference on rehabilitation robotics, Stanford. Page(s) 34-41. 1999.

Kumar S. *'Rehabilitation and ergonomics:Complementry disciplines'*. Canadian journal of rehabilitation. Page(s) 99-111, Vol. 3, No. 2, 1989.

Kurigami M, Tanaka K, Shimizug A. *'Multi-rate Indirect MRAC using Delta-operator for pneumatic servo system'*. Proceedings of the IEEE Conference on Decision and Control. Page(s) 39-44, Vol. 1, 1996.

Lai J, Singh R, Menq C. *'Pneumatic pressure and position control using learning law. The journal of fluid control'*. Page(s) 64-88, Vol. 21 Issue 4. 1993.

Lemay MA, Hogan N, Van Dorsten JW. *'Issues in impedance selection and input devices for multijoint powered orthotics'*. Rehabilitation Engineering, IEEE Transactions on. Page(s) 102 -105, Vol. 6, March 1998.

Ling C, Plummer AR. *'Stability and robustness for discrete-time systems, with control signal saturation'*. Proceedings of the institution of mechanical engineers. Vol. 214. Part 1, Page(s) 65-76, 1999.

Linqi H, Wei W, Qingyuan L. *'Dynamics of robotic manipulators with electro-pneumatic proportional/servo balancing system'*. IEEE international conference industrial technology. Page(s) 598 -601, Dec 1994.

Liu S, Bobrow JE. *'An analysis of a pnuematic servo system and it's application to a computer-controlled robot'*. Transactions of ASME Journal of dynamic systems measurements and control. Page(s) 228-235, Vol. 110, Sept 1988.

Lum PS, Reinkensmeyer DJ, Lehman SL. *'Robotic assist devices for bimanual physical therapy: preliminary experiments'*. IEEE transactions on rehabilitation engineering. Page(s) 185 -191, Vol. 13, Sept. 1993.

Lum PS, Burgar CG, Kenney DE, Van-der-loos HFM. *'Quantification of force abnormalities durning passive and active-assisted upper-limb reaching movements in post-stroke hemiparesis'*. IEEE transactions on biomedical engineering. Page(s) 652 -662, Vol. 46, No. 6, June 1999.

Matko D, Kamnik R, Bajd T. *'Adaptive impedance force control of an industrial manipulator'*. Proceedings of the IEEE international symposium on industrial electronics (ISIE'99). Oiscatawa,USA, Page(s) 129-133. 1999.

McComuck W, Schwartz HM. *'An investigation of impedance control for robot manipulators'*. The international journal of robots research. Page(s) 473-489, Vol.12, No. 5, Oct. 1993.

McCormick EJ. *'Human factors engineering'*. McGraw-Hill, Third edition, 1970.

McDonell BW, Bobrow JE. *'Adaptive tracking of an air powered robot actuator'*. Journal of dynamic systems, measurement and control. Page(s) 427-433, Vol. 115, Sep. 1993.

McDonell BW, Bobrow JE. *'Modelling, identification and control of a pneumatically actuated robot'*. Proceedings of the IEEE international conference on robotics and automation. Page(s) 124-129, April 1997.

McDonell BW, Bobrow JE. *'Modelling, identification and control of a pneumatically actuated, force controllable robot'*. IEEE transactions on robotics and automation, Vol. 14, No. 5, Page(s) 732-742, Oct. 1998.

Moore PR, Pu J, Harrison R. *'Progression of servo pneumatic towards advanced applications'*. 5th international fluid power workshop, Bath. Page(s) 346-364, 1992.

Nagai K, Wakanishi I, Hanafusa H, Kawamura S, Makikawa M. *'Development of an 8 dof robotic orthosis for assisting human upper limb motion'*. Proceedings IEEE international conference robotics and automation, Leuven. Page(s) 3486-91, Vol.4, May 1998.

Natale C, Siciliano B, Villani L. *'Robust hybrid force/position control with experiments on an industrial robot'*. Proceedings of ASME international conference on advanced intelligent mechatronics, Atlanta. Page(s) 956-960, Sept. 1999.

Noritsugo T, Takaiwa M. *'Robust positioning control of pneumatic servo system with pressure control loop'*. IEEE International conference on robotics and automation. Page(s) 21-27, May 1995.

Noritsugu T, Yamanaka T. *'Application of Rubber Artificial Muscle Manipulator as a Rehabilitation Robot'*. Proceedings of the 5th IEEE International Workshop on robot and human communication, Japan. Page(s) 112-117, Nov. 1996.

Nouri B, Al-Bender F, Swevers J, Vanherck P, Brussel H. *'Modelling a pneumatic servo positioning system with friction'*. Proceedings of the American control conference, Chicago. Page(s) 1067-1071, June 2000.

Pandian SR, Hayakawa Y, Kanazawa Y, Kawamura S. *'Practical design of a sliding mode controller for pneumatic actuators'*. Proceedings of the Japan/USA symposium on flexible automation, Boston. Page(s) 181-88, Vol 1, July 1996.

Pandian SR, Takemura F, Hayakawa Y, Kawamura S. *'Control performance of an air motor'*. Proceeding 1999 IEEE international conference on Robotics and automation, Detroit. Page(s) 518-524. May 1999.

Paul AK, Mishra JK, Radke MG. *'Reduced order sliding mode control for pneumatic actuator'*. IEEE transactions on control systems technology. Page(s) 271-274, Vol.2, No.3, Sept 1994.

Plummer AR. *'A comparison of linear discrete-time methods for servosystem control'*. Proceedings of the institute of mechanical engineers. Page(s) 281-300, Vol. 211, part 1,1997.

Press WH, Flannery BP, Teukolosky S, Verttering WT. *'Numerical recipes in C, the art of scientific computing'*. Cambridge University press, 1991 ISBN 0-521-35465.

Pu J, Weston RH. *'A new generation of industrial servos for industrial robots'*. Robotica. Page(s) 17-23, Vol. 7, 1989.

Pu J, Wong CB, Moore PR. *'Acceleration characteristics of a servo controlled pneumatic cylinder'*. ASME Fluid power systems and technology. Page(s) 119-130, Vol .3, 1996.

Raibert MH, Craig JJ. *'Hybrid position/force control of manipulators'*. ASME journal of dynamic systems, measurement and control. Page(s) 126-133, Vol. 103, 1981.

Raparelli T, Manuello A, Mazza L. *'Experimental and numerical study of friction in an elastomeric seal for pneumatic cylinders'*. Tribology international. Vol. 30, No. 7, Page(s) 547-552, 1997.

Reinkensmeyer DJ Schmit BD, Rymer WZ [1]. *'Mechatronic assessment of arm impairment after chronic brain injury'*. Proceedings of the symposium on biomechatronics, Enschede. Page(s) 61-65, 1999.

Reinkensmeyer DJ, Dewald J, Rymer W [2]. *'Guidance-based quantification of arm impairment following brain injury: A pilot study'*. IEEE transactions on rehabilitation engineering. Page(s) 1 –11, Vol. 7, No. 1, March 1999.

Richer E, Hurmuzlu Y. *'High performance pneumatic force actuator system: Part I – Non-linear mathematical model'*. Transactions of ASME. Page(s) 416-425, Vol. 122, Sept. 2000.

Salganicoff M, Hersh L. *'Safety issues for kinesthetic interfaces in assistive robotics'*. RESNA '96, Page(s) 137-142, 1996.

Scattareggia S, Buckley MA, Valleggi R, Johnson GR. *'An optimised design of an active orthosis for the shoulder - an iterative approach'*. International conference on rehabilitation robotics (ICORR '97). Page(s) 55-58, April 1997.

Seireg A, Dooner D. *'The kinematic geometry of gearing'.* John wiley and sons inc. 1995. ISBN 0-471-04597-7.

Shaki E, Dayan J, Shohan M. *'Comparison of robot force method. International journal of modelling and simulation'.* Page(s) 173-79, Vol. 18, No. 3, 1998.

Shearer JL. *'Study of pneumatic processes in the continuous control of motion with compressed air I,II'.* Transactions of ASME. Page(s) 233-249, No. 108, Feb. 1956.

Shibata S, Ben-lamine M, Toyohara K, Shimizu A. *'Fuzzy control of vertical pneumatic servo systems using virtual reference'.* JSME international journal. Page(s) 79-84, Series C, Vol. 42, No. 1, 1999.

Shih M, Huang Y. *'Pneumatic servo cylinder positioning control using a self-tuning controller'.* JSME international journal. Page(s) 565-572, Series 2, Vol. 35, No 2, 1992.

Shih M, Tseng S. *'Pneumatic servo cylinder position control by self-tuning PID controller'.* JSME international journal. Page(s) 565-572, Vol. 37, No. 3, 1994.

Shih M, Ma M. *'Position control of a pneumatic cylinder using fuzzy PWM control method'.* Mechatronics. Page(s) 241-253, Vol. 8, 1998.

Siciliano B, Villani L. *'A taxonomy of robot force control strategies'.* EUREL international conference on advanced robotic systems, Manchester. Vol 2, April 2000.

Smiarowski A, Anderson JN. *'Input/output distribution in digital control'.* IEEE system theory. Page(s) 482 –486, 1990.

Song J, Xiaoyan B, Ishida Y. *'An application of MNN trained by MEKA for the position control of pneumatic cylinder'.* International Conference on. neural networks. Page(s) 829 –833, Vol. 2, 1997.

Stanger CA, Anglin C, Harwin W, Romilly D. *'Devices for assisting manipulation: A summary of user task priorities'.* IEEE transactions on rehabilitation engineering. Page(s) 256 –265, Vol. 2, No. 4, Dec. 1994.

Sunderland A, Fletcher D, Bradley L, Tinson D, Hewer RL, Wade DT. *'Enhanced physical therapy for arm function after stroke: a one year follow up study'.* Journal of Neurology, Neurosurgery and psychiatry. Page(s) 856-858, Vol. 57, No.7, 1994.

Surgenor BW, Pieper JK, Wijesuriya ET. *'On the control of pneumatic positioners and the case of the inverted pendulum'*. International Conference on control. Page(s) 1117 –1122, Vol.2, Mar 1991.

Surgenor BW, Wijesuriya ET. *'Experience with an intelligent optimal controller as applied to a high-friction pneumatic actuator'*. ASME Intelligent control systems. Page(s) 93-103, Vol. 45, 1992.

Surgenor BW, Ioranou HN. *'Electic versus pneumatic servo control: A case study with a gantry crane apparatus'*. ASME Winter annual meeting, New Orleans. Page(s) 1-9, Nov. 1993.

Takaiwa M, Noritsugu T. *'Application of pneumatic parallel manipulator as haptic human interface'*. Proceedings ASME international conference On advanced intelligent mechatronics, Atlanta. Page(s) 185-190, Sept. 1999.

Tanaka K, Yamada Y, Shimizu A, Shibata S. *'Multi-rate adaptive pole-placement control for a pneumatic servo system with additive external forces'*. AMC'96 MIE. Page(s) 213-218, 1996.

Tillet ND, Vaughan ND, Bourger A. *'A non-linear model of a rotary pneumatic servo system'*. Proceeding of the Institute of Mechanical Engineers. Page(s) 123-133, Part I, Vol 211, 1997.

Tsai L. *'Robot analysis – the mechanics of serial manipulators'*. John Wiley and sons. 1999. ISBN 0471325937.

Tzafestas C, Sirdi NM, Manamami N. *'Adaptive impedance control applied to a pneumatic legged robot'*. Journal of intelligent and robotic systems. Page(s) 105-129, No. 20, 1997.

Utkin VI, Guldner J, Shi J. *'Sliding mode control in electromechanical systems'*. Taylor & Francis, 1999. ISBN 0748401164.

Vaughan ND, Plummer AR[1]. *'Some issues in pole-placement control of electrohydraulic servo's'*. Fluid power workshop, Bath. Page(s) 6-29, Sep. 1990.

Vaughan ND, Plummer AR[2]. *'Robust adaptive control for hydraulic servo-systems'*. ASME winter annual meeting. Page(s) 2-9, Nov. 1990.

Volpe R Khosla P. *'On the equivalence of second order impedance control and proportional gain explicit force control'*. The international journal of robotics research. Page(s) 574-589, Vol. 14, 1995.

Wang J, Lin-Chen YY. *'Modelling study, validation and robust tracking control of pneumatic cylinder actuator systems'*. UKACC international conference of control 2000, University of Cambridge, 4-7 Sept. 2000.

Wang J, Pu J, Moore P. *'A practical control strategy for servo-pneumatic actuator systems'*. Control Engineering Practice. Page(s) 1483-1488, Vol. 7, Issue 12, Dec. 1999.

Wang Y, Chang M. *'Experimental implementation of decoupling self-organising fuzzy control to a TITO pneumatic position control system'*. JSME international journal (C). Page(s) 535-542, Vol. 42, No. 1, 1999.

Wellstead PE, Sanoff SP. *'Extended self-tuning algorithm'*. International journal of control. Page(s) 433-455, Vol. 34, 1981.

White CJ, Schneifer AM, Brogan W. *'Robotic orthosis for stroke patient rehabilitation'*. Proceedings IEEE 15th annual international conference on engineering in medicine and biology society, San diego. Page(s) 1272-1273 Vol. 15, Oct. 1993.

Xianwen G, Shujiang L, Tianyou C. *'Implicit PID self-tuning controller and its applications'*. International Conference on intelligent processing systems ICIPS '97. Page(s) 670 –674, Vol. 1, 1997.

Xin J, Tsuji H, Sano A. *'Optimal sampling interval for system identification based on decimation and interpolation'*. IEE Proceedings on control theory and applications. Page(s) 15 –22, Vol. 142, Jan. 1995.

Yamamoto T, Kaneda M, Tanaka K. *'A simple explicit self-tuning controller based on pole-assignment scheme and it's applications'*. Proceedings of 21st IEEE international conference industrial electronics control and instrumentation, Orlando. Page(s) 950-55, Vol. 2, Nov. 1995.

Yardley A, Parrini G, Carus D, Thorpe J. *'Development of an upper limb orthotic system'*. International conference on rehabilitation robotics (ICORR '97). Page(s) 59-62, April 1997.

Yin Y, Araki K. *'Modelling analysis of an asymmetric valve-controlled single-acting cylinder of a pneumatic force control system'*. Proceedings of the 37th SICE annual conference, Japan. Page(s) 1099-1104, 1998.

Yu X, Man Z, Wu B. *'Design of fuzzy sliding mode control systems'*. Fuzzy sets and systems 95. Page(s) 296-306, 1998.

Zhuang M, Atherton DP. *'Automatic tuning of optimum PID controllers'*. IEE Proceedings on control theory and applications (D). Page(s) 216 –224, Vol. 140, May 1993.

Appendix A

Robot production drawings

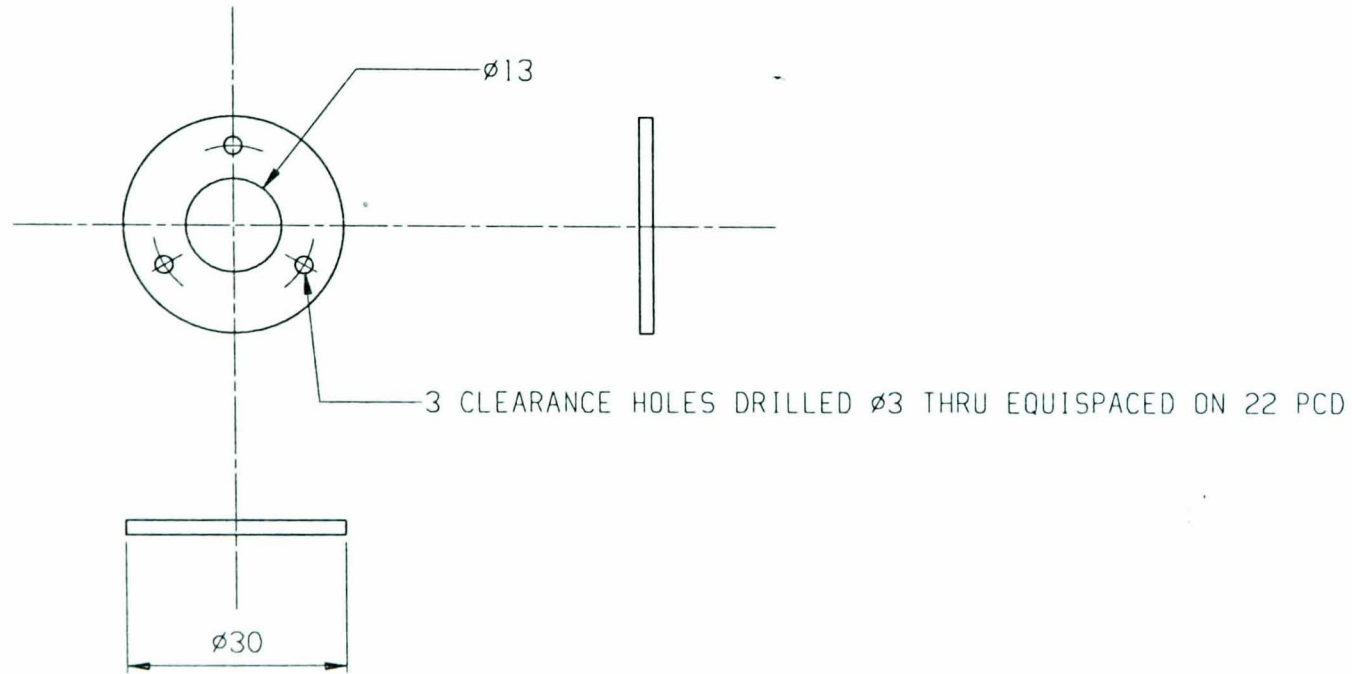*This section contains production drawings to enable fabrication of the three degree-of-freedom robot*

∅ 25.021
  25.000

6 HOLES DRILLED AND TAPPED THRO' M3
EQUISPACED AT 60° ON 34 PCD

2

∅40
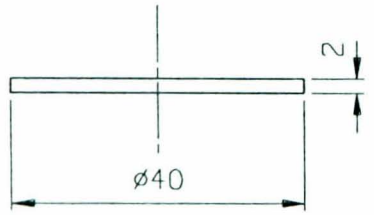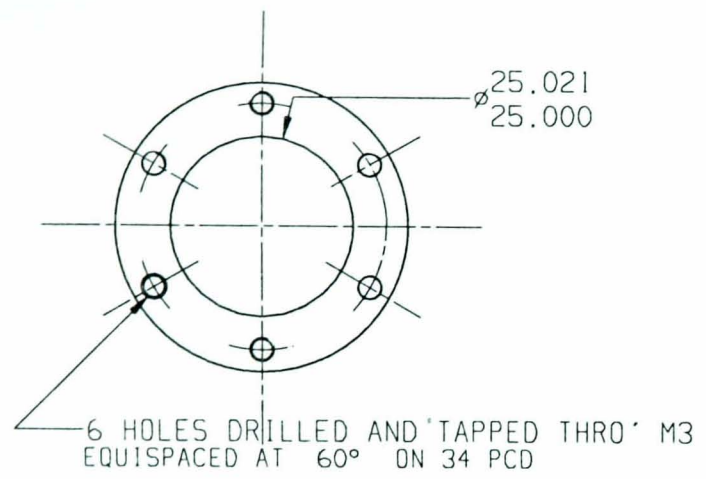
MATERIAL:2mm
ALUMINIUM SHEET

8

24

7

2 CLEARANCE HOLES ∅2.4 THRU

3

6 3

4
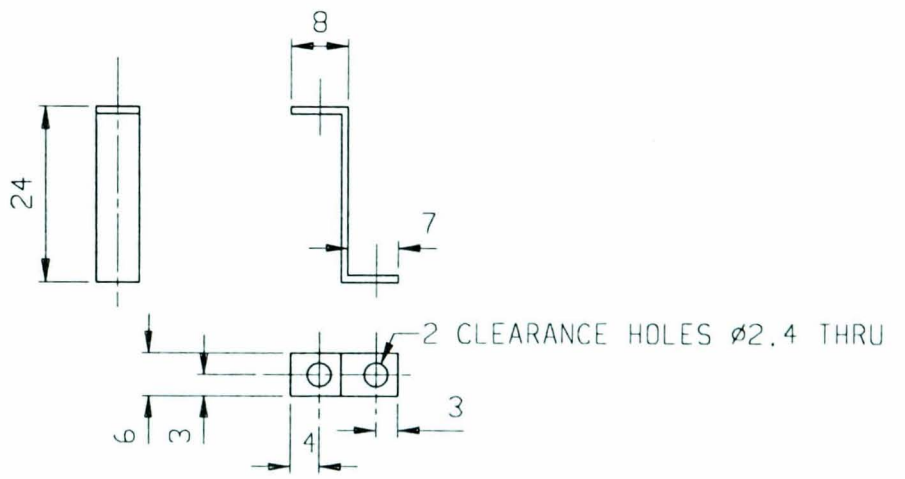
MATERIAL:1mm FOLDED
ALUMINIUM SHEET

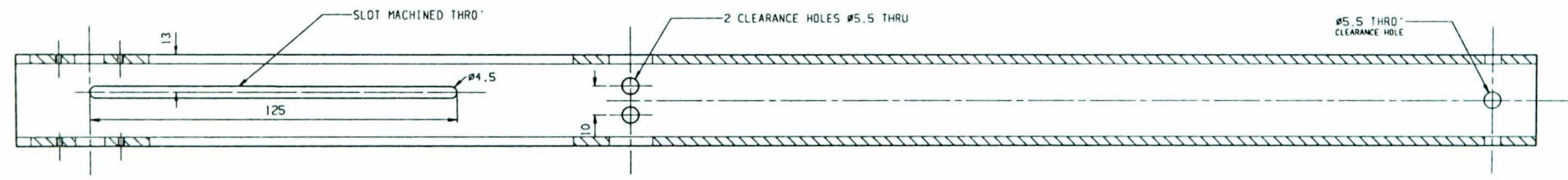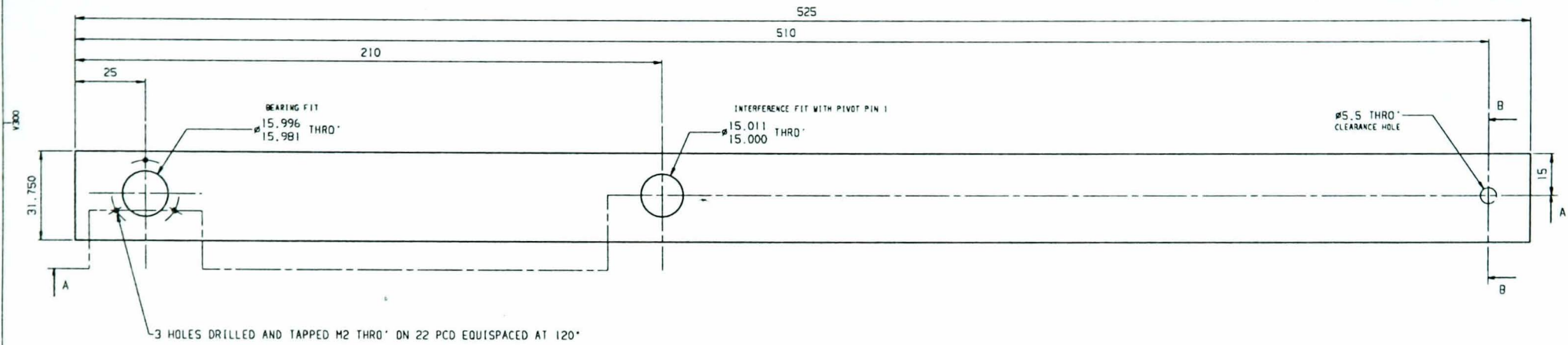| DO NOT SCALE IF IN DOUBT ASK	UNLESS OTHERWISE STATED	1) MACHINE AT ✓ TO 3.2 uM Ra MAX 2) TOLERANCE ON MACHINED DIMENSIONS AS FOLLOWS 0-500 ± 0.2; 500-1000 ± 0.4		LUMED LEEDS UNIVERSITY DEPT. OF MECHANICAL ENGINEERING	DATE 9/11/98	POTENTIOMETER SUPPORTING BRACKET	DRAWN R. RICHARDSON BY
					SCALE 1:1	FILE: POTSUP2	A4 -01

MATERIAL: ALUMINUM
2mm SHEET

Ø13

3 CLEARANCE HOLES DRILLED Ø3 THRU EQUISPACED ON 22 PCD

Ø30

DO NOT SCALE IF IN DOUBT ASK	UNLESS OTHERWISE STATED	1) MACHINE AT ✓ TO 3.2 uM Ra MAX 2) TOLERANCE ON MACHINED DIMENSIONS AS FOLLOWS 0-500 ± 0.2; 500-1000 ± 0.4		LUMED LEEDS UNIVERSITY DEPT. OF MECHANICAL ENGINEERING	DATE 11/9/98	HEAD BEARING COVER 1	DRAWN BY R. RICHARDSON
					SCALE 1 / 1	FILE : HBCOVER1	A4 -02

DRILL AND TAP M5 MINIMUM LENGTH OF ENGAGEMENT 10

7

MATERIAL: ALUMINIUM

ALL CHAMFERS 1mm
AT 45°

40.8

7

4

$\emptyset \begin{array}{c}3.000\\2.994\end{array}$ NOTE: DO NOT CENTER DRILL

$\emptyset \begin{array}{c}10.005\\9.997\end{array}$
BEARING FIT

$\emptyset \begin{array}{c}15.012\\15.001\end{array}$
LINK 1 INTERFERENCE FIT
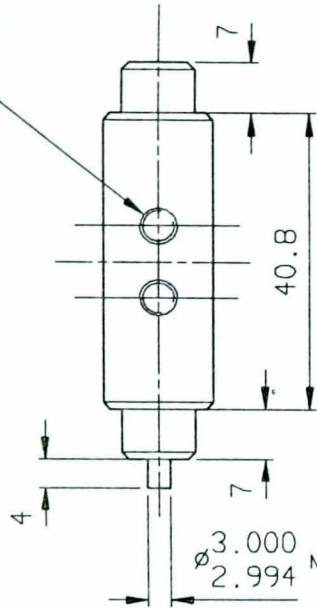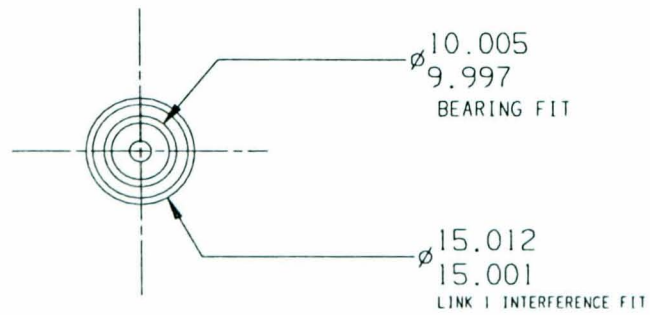
1st PIN

DRILL AND TAP M5 MINIMUM LENGTH OF ENGAGEMENT 10

7

MATERIAL: ALUMINIUM

ALL CHAMFERS 1mm
AT 45°

20

66.2

4

7

$\emptyset \begin{array}{c}3.000\\2.994\end{array}$ NOTE: DO NOT CENTER DRILL

$\emptyset \begin{array}{c}15.012\\15.001\end{array}$
LINK 2 INTERFERENCE FIT

$\emptyset \begin{array}{c}10.005\\9.997\end{array}$
BEARING FIT
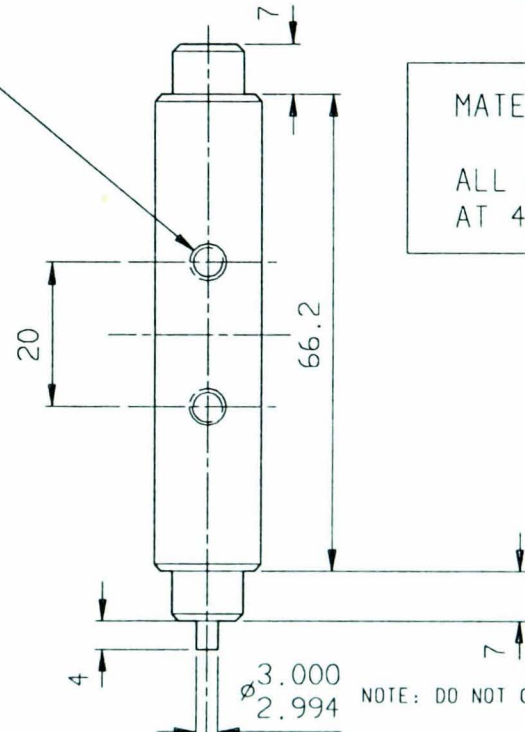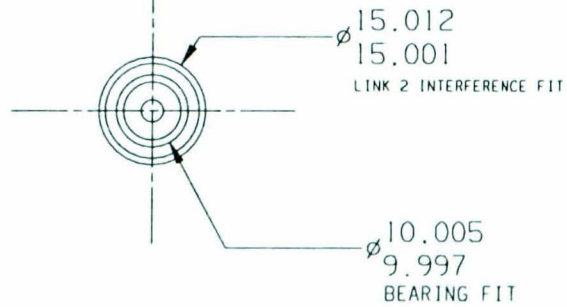
2nd PIN

| DO NOT SCALE IF IN DOUBT ASK | UNLESS OTHERWISE STATED | 1) MACHINE AT ✓ TO 3.2 uM Ra MAX
2) TOLERANCE ON MACHINED DIMENSIONS
AS FOLLOWS 0-500 ± 0.2; 500-1000 ± 0.4 | | LUMED
LEEDS UNIVERSITY
DEPT. OF MECHANICAL ENGINEERING | DATE 22/09/98 | PIVOT POINTS | DRAWN BY R. RICHARDSON |
| | | | | | SCALE 1/1 | FILE : PIVOT | A4 · 05 |

525

510

210

25

BEARING FIT
ø15.996 THRO'
15.981

INTERFERENCE FIT WITH PIVOT PIN 1
ø15.011 THRO'
15.000

ø5.5 THRO'
CLEARANCE HOLE

B

31.750

15

A

A

B

3 HOLES DRILLED AND TAPPED M2 THRO' ON 22 PCD EQUISPACED AT 120°

SLOT MACHINED THRO'

2 CLEARANCE HOLES ø5.5 THRU

ø5.5 THRO'
CLEARANCE HOLE

13

ø4.5

125

10

SECTION A - A
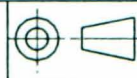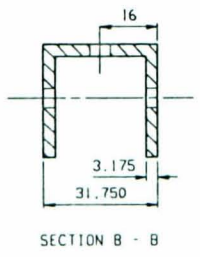
MATERIAL: ALUMINIUM U CHANNEL 1.25" X 1.25" X 0.125"
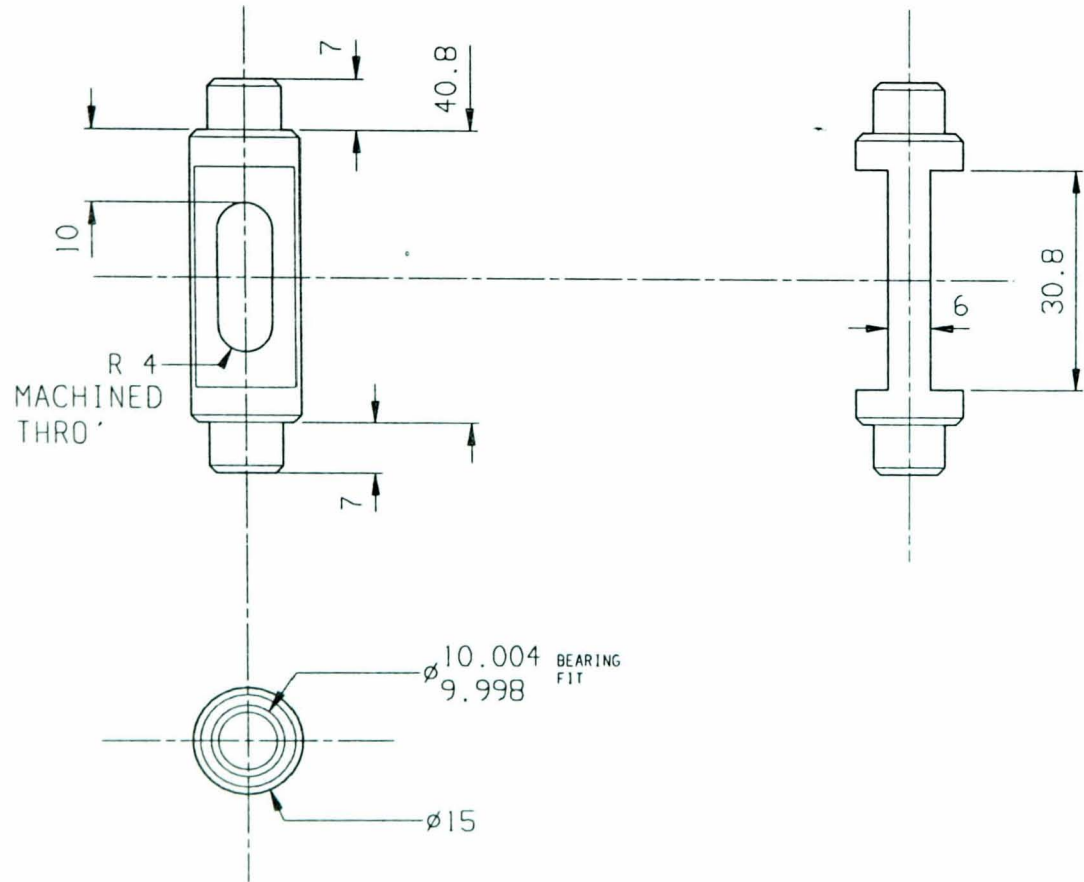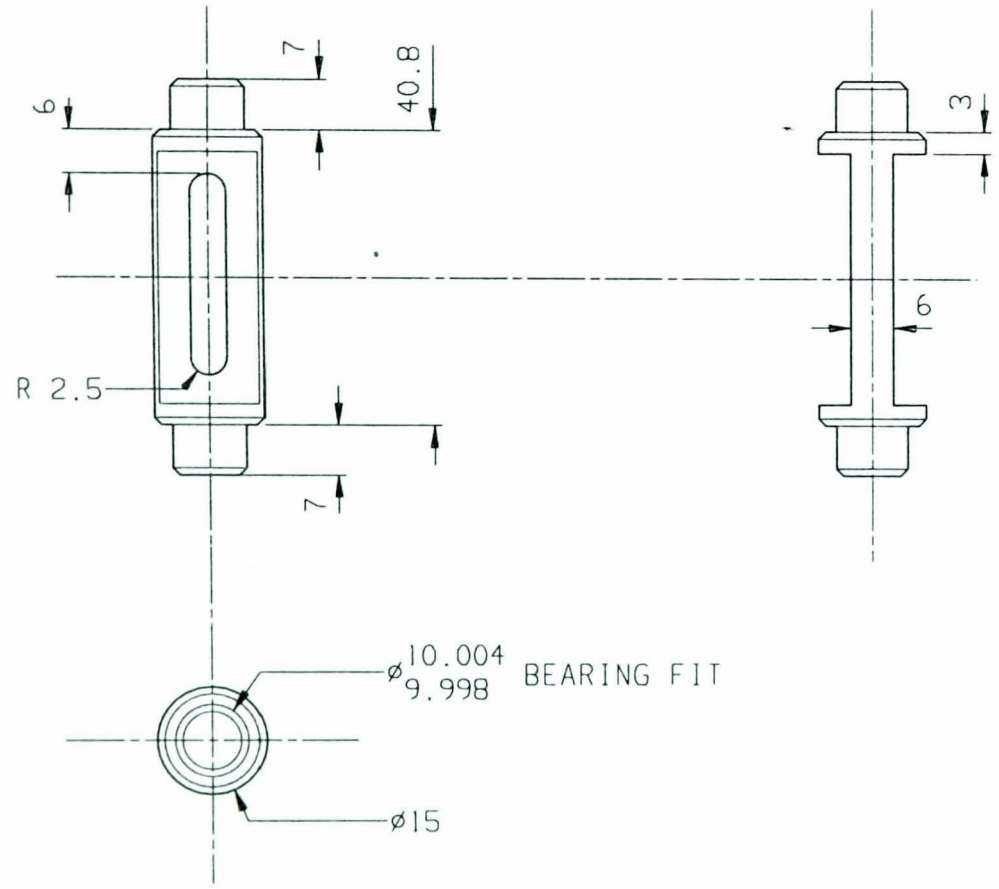
ALL HOLES AND THREADS EXIST ON BOTH UPRIGHTS

16

3.175

31.750

SECTION B - B

DO NOT SCALE. IF IN DOUBT. ASK	UNLESS OTHERWISE STATED	1) DIMENSIONS ARE IN MILLIMETRES 2) MACHINE AT ø' TO 3.2 •• R• MAX 3) REMOVE SHARP EDGES 4) TOLERANCES ON MACHINED DIMENSIONS AS SHOWN	SIZE 0 TO 500 INCL. OVER 500 TO 1000 OVER 1000	TOL. ± 0.2 ± 0.4		LUMED	UNIVERSITY OF LEEDS DEPARTMENT OF MECHANICAL ENGINEERING	DATE	22/09/98	TITLE 3RD LINK OF ROBOTIC ORTHOSIS DEVICE FILE : WLINK1	DRAWN BY	R. RICHARDSON
								SCALE	1/1		DRAWING NUMBER	A2- 06

SECTION B - B
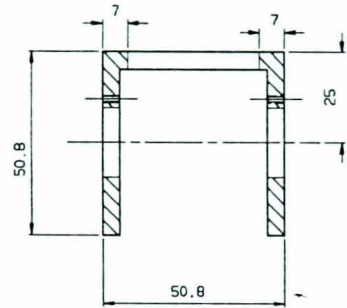
MATERIAL: ALUMINIUM U CHANNEL 2" x 2" x 1/4"

UNLESS OTHERWISE STATED ALL HOLES AND THREADS
EXIST ON BOTH UPRIGHTS

ø18.993 / 18.972 THRO' BEARING FIT

ø18.993 / 18.972 THRO' BEARING FIT

MINIMUM LENGTH OF ENGAGEMENT 4

4 HOLES ø4.5 THRO'

PIVOT PIN 2 INTERFERENCE FIT
ø15.011 / 15.000 THRO'

ø18.993 / 18.972 THRO'
BEARING FIT

3 HOLES DRILLED AND TAPPED THRO' M2 EQUISPACED AT 120° ON 24 PCD
TO SUIT BEARING COVERS

3 HOLES DRILLED AND TAPPED THRO' M2 EQUISPACED AT 120° ON 24 PCD

3 HOLES DRILLED AND TAPPED THRO' M2 EQUISPACED AT 120° ON 24 PCD

3 HOLES DRILLED AND TAPPED M2 EQUISPACED AT 120° ON 50 PCD, 2 OF WHICH THRU
ON THIS SIDE ONLY

SLOT MACHINED THRO'

R2.25
50

2 CLEARANCE HOLES ø5.5 THRU

SECTION A-A

DO NOT SCALE. IF IN DOUBT.	UNLESS OTHERWISE STATED	1) DIMENSIONS ARE IN MILLIMETRES 2) MACHINE AT ø TO 3.2 •• Ra MAX 3) REMOVE SHARP EDGES 4) TOLERANCES ON MACHINED DIMENSIONS AS SHOWN	SIZE	TOL
			0 TO 500 INCL.	± 0.2
ASK			OVER 500 TO 1000	± 0.4
			OVER 1000	

LUMED

UNIVERSITY OF LEEDS
DEPARTMENT OF MECHANICAL ENGINEERING

DATE 11/9/98

SCALE ...

TITLE
2ND LINK OF ROBOTIC ORTHOSIS DEVICE

FILE : LINK2

DRAWN BY   R. RICHARDSON

DRAWING NUMBER   A2 - 07

ø12

7

7

R 2.5
MACHINED THRO'

ø8.004 BEARING
7.998 FIT

23.750

6

6

6

5

5
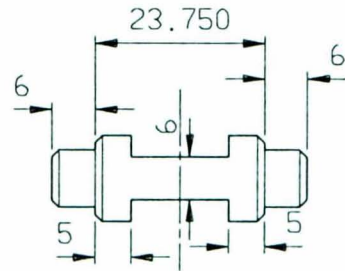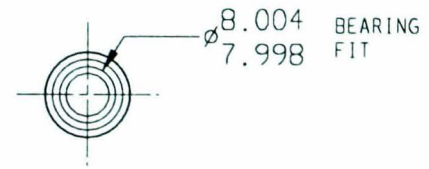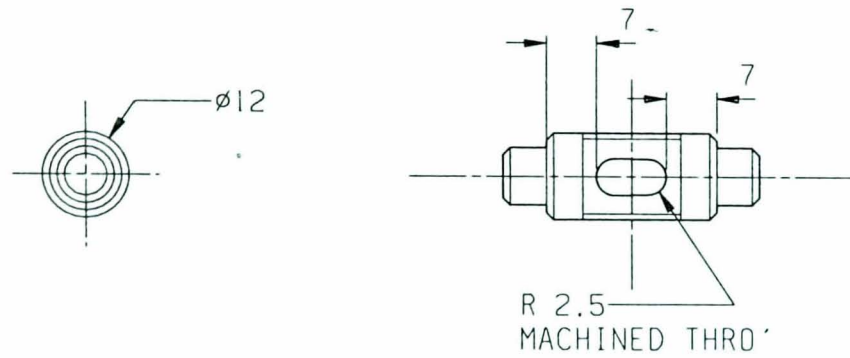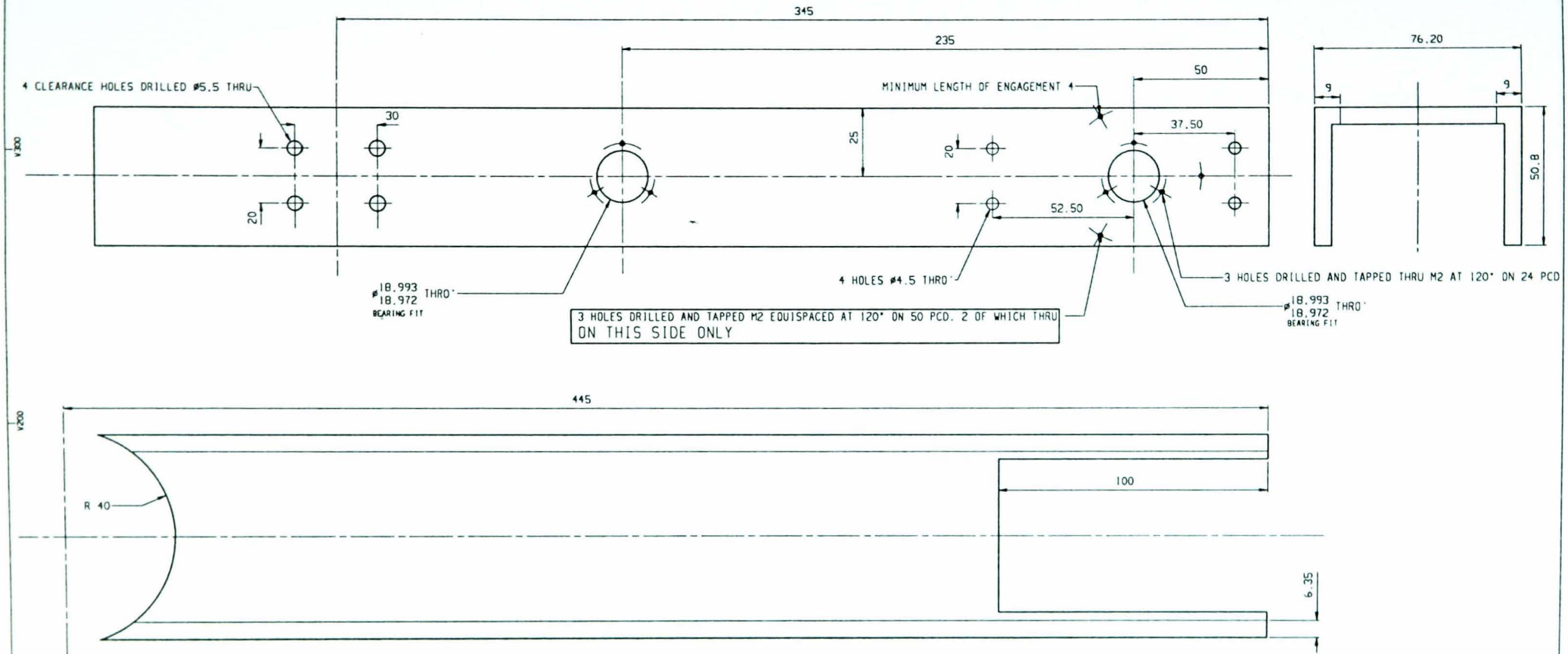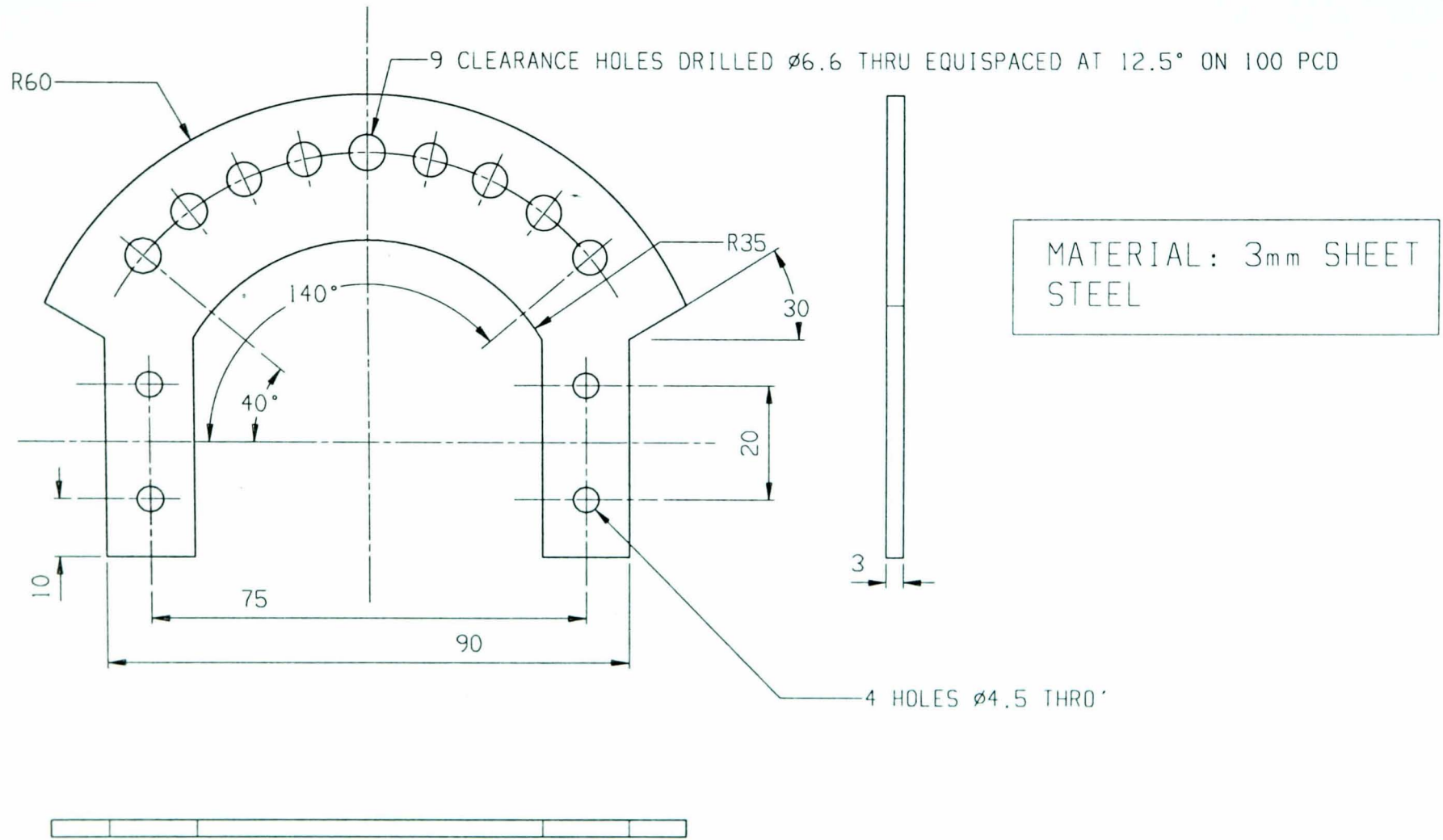
MATERIAL : STEEL

ALL CHAMFERS 1mm AT 45°
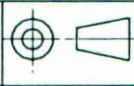
DO NOT SCALE IF IN DOUBT ASK	UNLESS OTHERWISE STATED	1) MACHINE AT ✓ TO 3.2 uM Ra MAX 2) TOLERANCE ON MACHINED DIMENSIONS AS FOLLOWS 0-500 ± 0.2; 500-1000 ± 0.4	⊕ ◁	LUMED LEEDS UNIVERSITY DEPT. OF MECHANICAL ENGINEERING	DATE 22/09/98	TOP SINGLE CYLINDER HOLDER	DRAWN R. RICHARDSON BY
					SCALE 1/1	FILE : STOP	A4 · 08

MATERIAL: STEEL

ALL CHAMFERS 1mm AT 45°

7

40.8

10

R 4
MACHINED
THRO'

7

30.8

6

⌀$^{10.004}_{9.998}$ BEARING FIT

⌀15

DO NOT SCALE IF IN DOUBT ASK	UNLESS OTHERWISE STATED	1) MACHINE AT ✓ TO 3.2 ∪M R∘ MAX 2) TOLERANCE ON MACHINED DIMENSIONS AS FOLLOWS 0-500 ± 0.2; 500-1000 ± 0.4	⊕ ◁	LUMED LEEDS UNIVERSITY DEPT. OF MECHANICAL ENGINEERING	DATE 22/09/98	BOTTOM SINGLE CYLINDER SUPPORT	DRAWN BY R.RICHARDSON
					SCALE 1/1	FILE : SBO1	A4 -09

MATERIAL: STEEL

ALL CHAMFERS 1mm AT 45°

7

40.8

6

3

6

R 2.5

$\phi^{10.004}_{9.998}$ BEARING FIT

ϕ15

DO NOT SCALE IF IN DOUBT ASK	UNLESS OTHERWISE STATED	1) MACHINE AT ✓ TO 3.2 ᴜM R. MAX 2) TOLERANCE ON MACHINED DIMENSIONS AS FOLLOWS 0-500 ± 0.2; 500-1000 ± 0.4		LUMED LEEDS UNIVERSITY DEPT. OF MECHANICAL ENGINEERING	DATE 22/09/98	TOP DOUBLE CYLINDER SUPPORT	DRAWN BY R.RICHARDSON
					SCALE 1/1	FILE : DTOP	A4 -10

MATERIAL: STEEL

ALL CHAMFERS 1mm
AT 45°

R 4 THRO'
MACHINED

⌀10.004 BEARING
⌀9.998 FIT

⌀15

66.2

56.2

7

9

6

7

| DO NOT SCALE IF IN DOUBT ASK | UNLESS OTHERWISE STATED | 1) MACHINE AT ✔ TO 3.2 µM Rₐ MAX 2) TOLERANCE ON MACHINED DIMENSIONS AS FOLLOWS 0-500 ± 0.2; 500-1000 ± 0.4 | | LUMED LEEDS UNIVERSITY DEPT. OF MECHANICAL ENGINEERING | DATE 22/09/98 | DOUBLE CYLINDER BOTTOM SUPPORT | DRAWN BY R. RICHARDSON |
| | | | | | SCALE 1/1 | FILE : DBOT | A4 -11 |

9 CLEARANCE HOLES DRILLED Ø6.6 THRU EQUISPACED AT 12.5° ON 100 PCD

R60

R35

140°

30

40°

20

10

75

90

MATERIAL: 3mm SHEET STEEL

3

4 HOLES Ø4.5 THRO'

| DO NOT SCALE IF IN DOUBT ASK | UNLESS OTHERWISE STATED | 1) MACHINE AT ∇ 10 3.2 uM Ra MAX 2) TOLERANCE ON MACHINED DIMENSIONS AS FOLLOWS 0-500 ± 0.2; 500-1000 ± 0.4 | | LUMED LEEDS UNIVERSITY DEPT. OF MECHANICAL ENGINEERING | DATE 23/09/98 SCALE 1:1 | Motion limiting bracket 1 | DRAWN BY R. RICHARDSON A4 - 13 |

9 CLEARANCE HOLES DRILLED ø9 THRU ON 140 PCD EQUISPACED AT 15°

R 85

R55

30

30

30

10

20

42.50

27.50

10

20

40

105

4 CLEARANCE HOLES DRILLED ø4.5 THRU

20

34

160

MATERIAL: 3mm SHEET STEEL

MATERIAL: ALUMINUM
2mm SHEET

3 CLEARANCE HOLES DRILLED Ø3 THRU EQUISPACED ON 24 PCD

Ø16

2

Ø34

| DO NOT SCALE IF IN DOUBT ASK | UNLESS OTHERWISE STATED | 1) MACHINE AT ✓ TO 3.2 uM Re MAX 2) TOLERANCE ON MACHINED DIMENSIONS AS FOLLOWS 0·500 ± 0.2; 500·1000 ± 0.4 | | LUMED LEEDS UNIVERSITY DEPT. OF MECHANICAL ENGINEERING | DATE 11/9/98 SCALE 1 / 1 | HEAD BEARING COVER 2 FILE : HBCOVER2 | DRAWN R. RICHARDSON BY A4 ·15 |

I LOCATION HOLE ø$\frac{5.008}{5.000}$ 130 PCD 15 DEEP

THREE HOLES TAPPED M5 AT 55° 130 PCD MINIMUM LENGTH OF ENGAGEMENT 20

30°

A

A

ø$\frac{110.022}{110.000}$ LOCATION GROOVE (H6)

ø100

ø160

3 HOLES DRILLED AND TAPPED M5 AT 120° 130 PCD MINIMUM LENGTH OF ENGAGEMENT 15

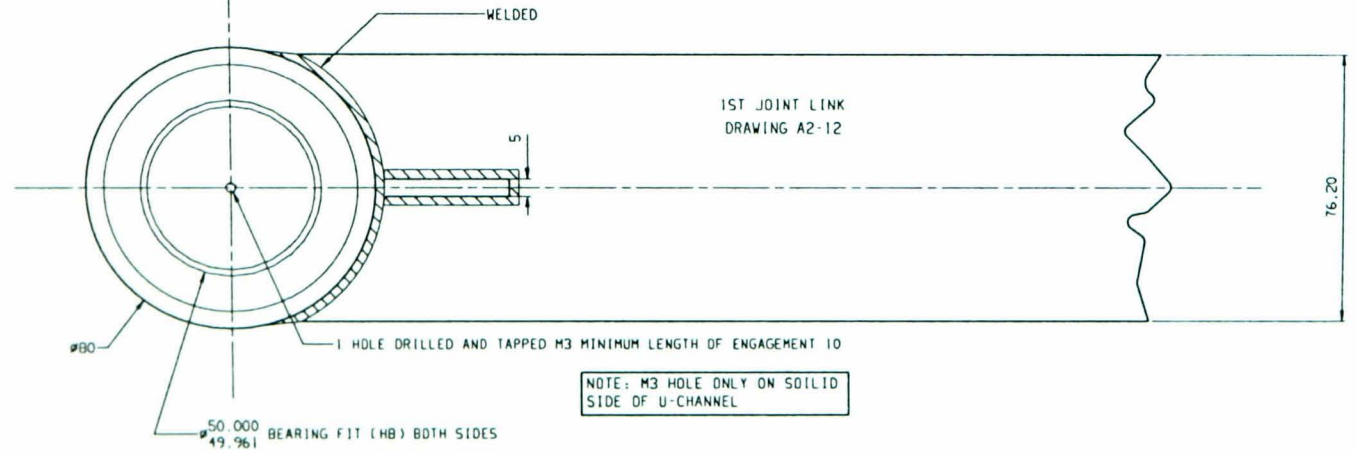ø$\frac{90.054}{90.000}$ BEARING FIT (H8 TOLERANCE)

5.5

5

100

20

25

SECTION A-A

MATERIAL: STEEL BAR DIA 160 (TO BE PURCHASED)
ALL CHAMFERS 2

TO BE MACHINED WITH OTHER SWIVEL
JOINT PARTS TO ENSURE BEARING
ALLIGNMENT AND POSITION OF LOCATING
FEATURES

DO NOT SCALE. IF IN DOUBT. ASK	UNLESS OTHERWISE STATED	1) DIMENSIONS ARE IN MILLIMETRES 2) MACHINE AT ø/ TO 3.2 µm Rɑ MAX 3) REMOVE SHARP EDGES 4) TOLERANCES ON MACHINED DIMENSIONS AS SHOWN	SIZE	TOL	⊕⊲	LUMED	UNIVERSITY OF LEEDS DEPARTMENT OF MECHANICAL ENGINEERING	DATE	20/6/99	TITLE SWIVEL JOINT TOP PART	DRAWN BY	R.RICHARDSON
			0 TO 500 INCL.	± 0.2								
			OVER 500 TO 1000	± 0.4				SCALE	1:1	FILE:TOPSWIV	DRAWING NUMBER	A2- 17
			OVER 1000									

SECTION A-A

MATERIAL: STEEL BAR DIA 160 (TO BE PURCHASED)
ALL CHAMFERS 2

TO BE MACHINED WITH OTHER SWIVEL JOINT PARTS
TO ENSURE BEARING ALLIGNMENT AND POSITION OF
LOCATING FEATURES

TRIANGULAR ELEMENT FOR ADDITIONAL
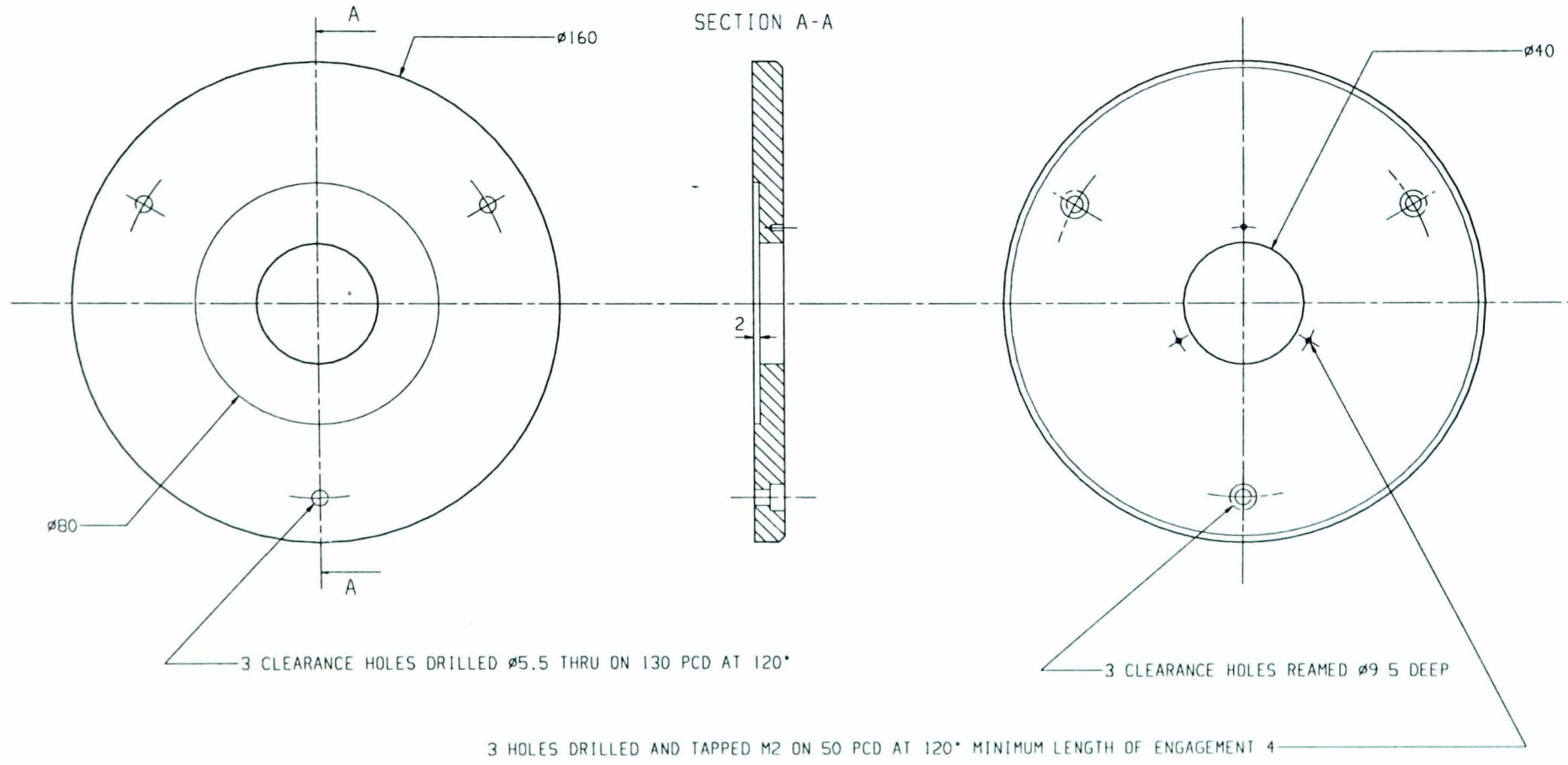STRENGTH, MATERIAL ALUMINIUM

CHAMFER 5

20

15

130

110

40

50.8

MATERIAL: ALUMINIUM BAR DIA. 80

UNLESS OTHERWISE STATED ALL CHAMFERS 2
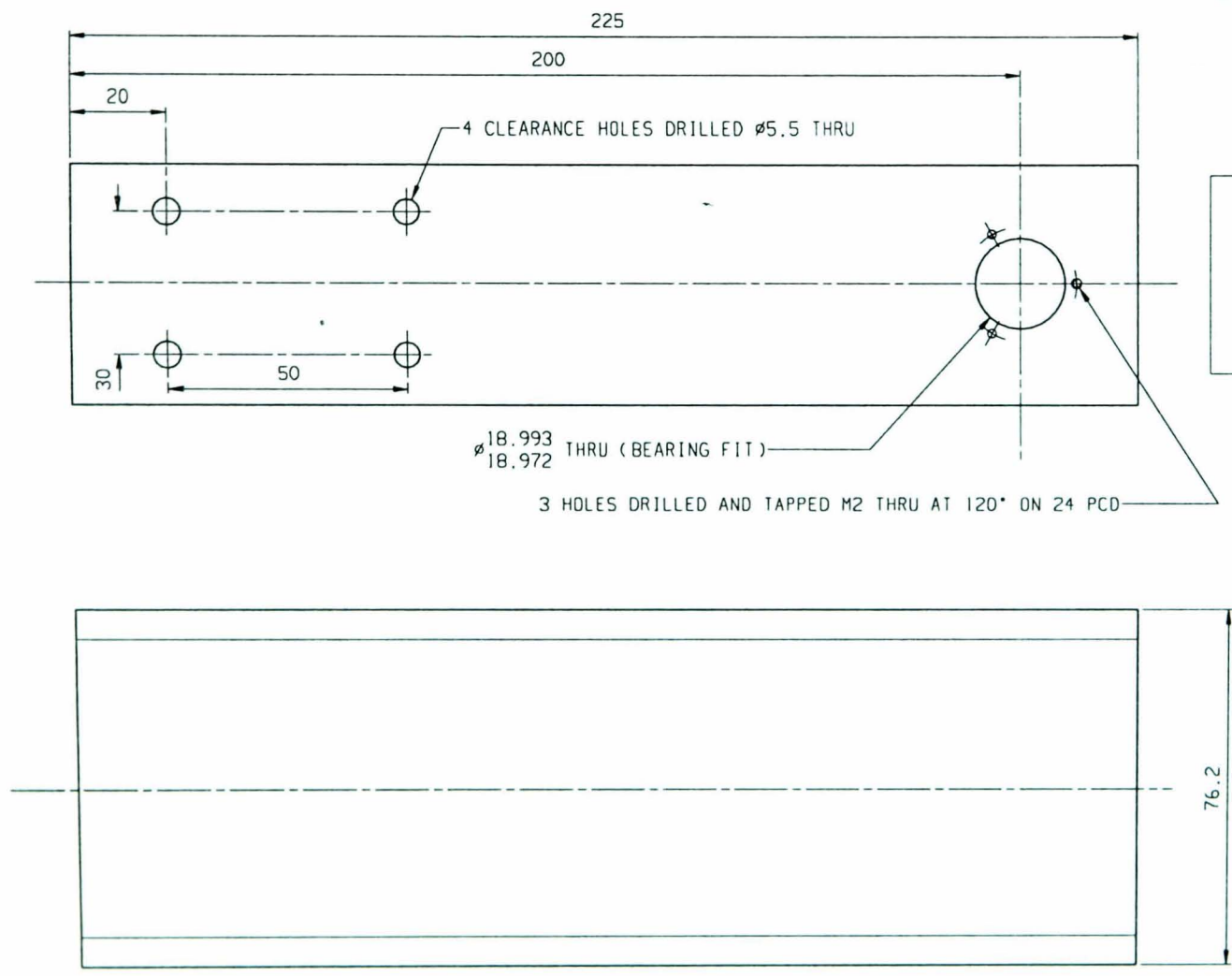
JOINT IS FABRICATED FROM 1ST LINK
AND ALUMINIUM PIN

30

WELDED

1ST JOINT LINK
DRAWING A2-12

5

76.20

Ø80

1 HOLE DRILLED AND TAPPED M3 MINIMUM LENGTH OF ENGAGEMENT 10

NOTE: M3 HOLE ONLY ON SOILID
SIDE OF U-CHANNEL

Ø 50.000
49.961 BEARING FIT (H8) BOTH SIDES

DO NOT SCALE IF IN DOUBT. ASK	UNLESS OTHERWISE STATED	1) DIMENSIONS ARE IN MILLIMETRES 2) MACHINE AT ∜ TO 3.2 ** Rₐ MAX 3) REMOVE SHARP EDGES 4) TOLERANCES ON MACHINED DIMENSIONS AS SHOWN	SIZE	TOL.			
			0 TO 500 INCL.	± 0.2			
			OVER 500 TO 1000	± 0.4			
			OVER 1000				

LUMED UNIVERSITY OF LEEDS
DEPARTMENT OF MECHANICAL ENGINEERING

DATE	22/06/99
SCALE	1:1

TITLE
1st JOINT PIN FABRICATION

DRAWN BY	R.RICHARDSON
DRAWING NUMBER	A2- 19

SECTION A-A

Ø160

Ø80

Ø40

3 CLEARANCE HOLES DRILLED Ø5.5 THRU ON 130 PCD AT 120°

3 CLEARANCE HOLES REAMED Ø9 5 DEEP

3 HOLES DRILLED AND TAPPED M2 ON 50 PCD AT 120° MINIMUM LENGTH OF ENGAGEMENT 4

MATERIAL: STEEL BAR DIA 160 (TO BE BOUGHT IN)
ALL CHAMFERS 2

DO NOT SCALE. IF IN DOUBT. ASK	UNLESS OTHERWISE STATED	1) DIMENSIONS ARE IN MILLIMETRES 2) MACHINE AT ⌀ 10 3 2 .. Ra MAX 3) REMOVE SHARP EDGES 4) TOLERANCES ON MACHINED DIMENSIONS AS SHOWN	SIZE 0 TO 500 INCL. OVER 500 TO 1000 OVER 1000	TOL ± 0.2 ± 0.4	⊕⊲ LUMED	UNIVERSITY OF LEEDS DEPARTMENT OF MECHANICAL ENGINEERING	DATE	3/8/99	TITLE TOP CAP	FILE: TOPCAP	DRAWN BY	R.RICHARDSON
							SCALE	1:1			DRAWING NUMBER	A2- 20

225

200

20

4 CLEARANCE HOLES DRILLED ø5.5 THRU

30

50
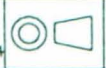
MATERIAL: ALUMINIUM U CHANNEL
3" x 2" x 1/4"

ALL HOLES EXIST ON BOTH
UPRIGHTS

ø$^{18.993}_{18.972}$ THRU (BEARING FIT)
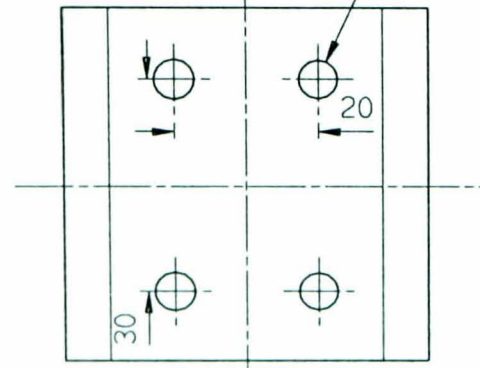
3 HOLES DRILLED AND TAPPED M2 THRU AT 120° ON 24 PCD

76.2

| DO NOT SCALE IF IN DOUBT ASK | UNLESS OTHERWISE STATED | 1) MACHINE AT ✓ TO 3.2 um Ra MAX
 2) TOLERANCE ON MACHINED DIMENSIONS
 AS FOLLOWS: 0-500 ± 0.2; 500-1000 ± 0.4 | | LUMED
 LEEDS UNIVERSITY
 DEPARTMENT OF MECHANICAL ENGINEERING | DATE 5/8/99 | 1.1 JOINT REAR CYLINDER SUPPORT   FILE: ICYLSUPP | DRAWN BY R.RICHARDSON |
| | | | | | SCALE 1/1 | | A3 / 21 |

50.8

50.8

50.8

$\phi \begin{matrix} 18.993 \\ 18.972 \end{matrix}$ THRU (BEARING FIT)

R 25
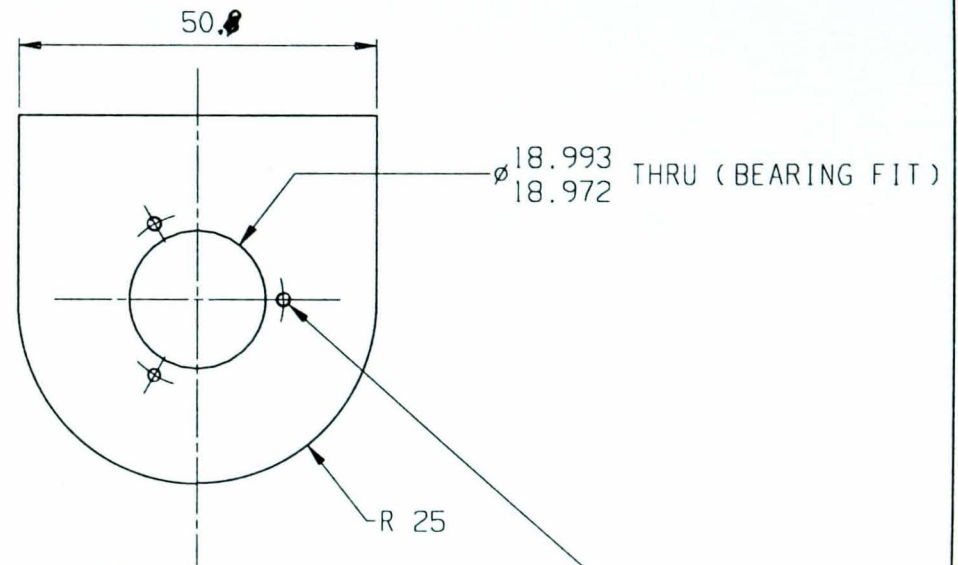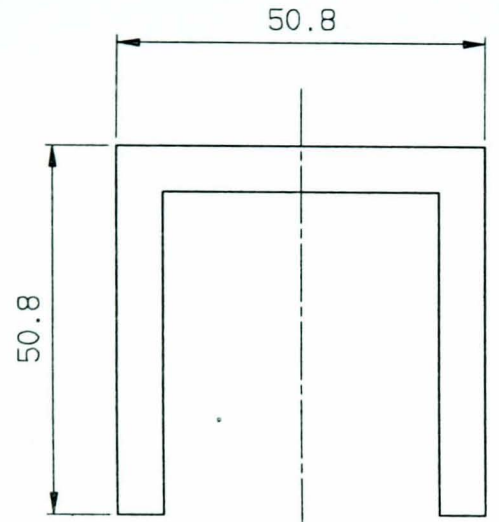
3 HOLES DRILLED AND TAPPED M2 THRU AT 120° ON 24 PCD
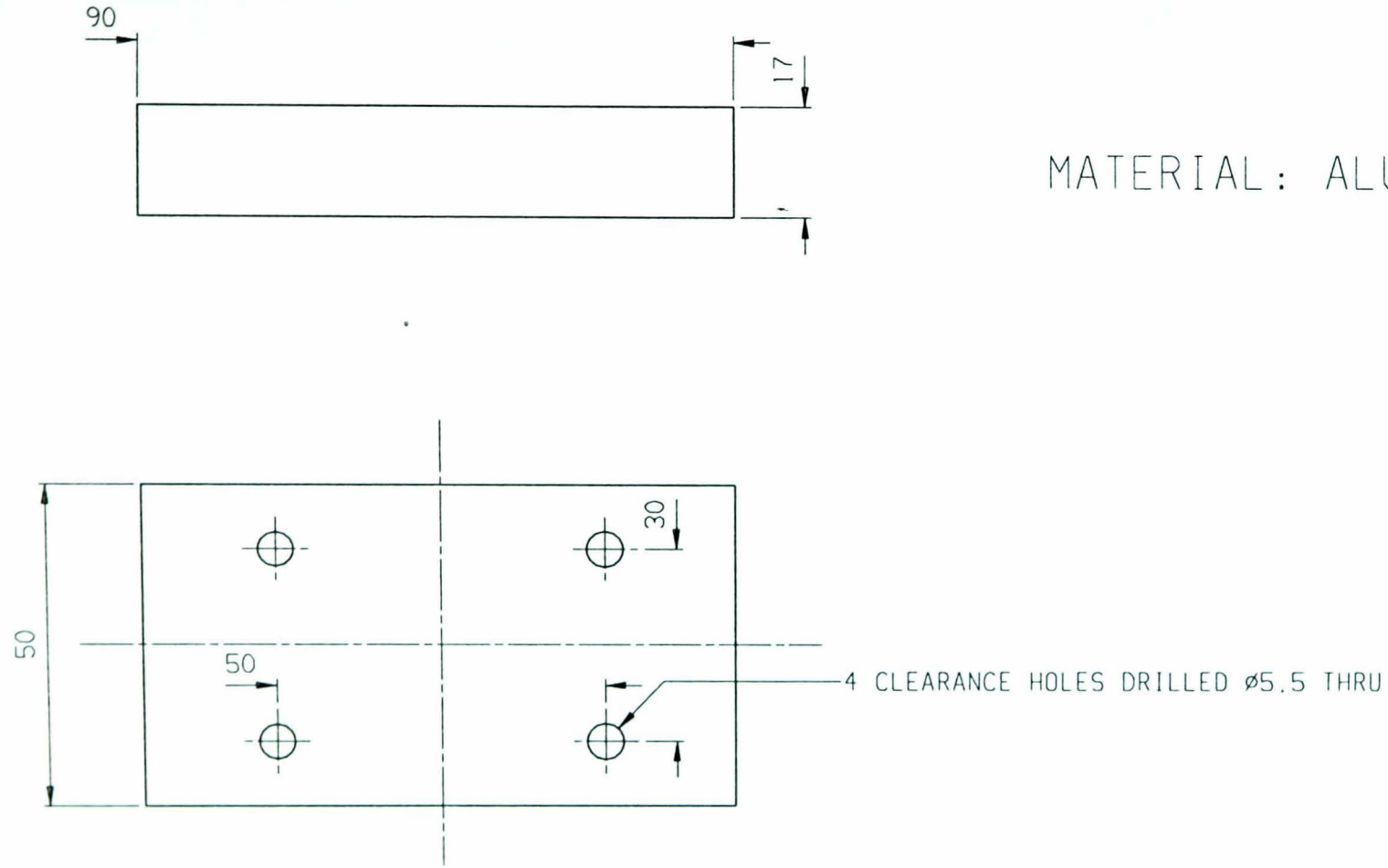
4 CLEARANCE HOLES ø5.5 THRU

20

30

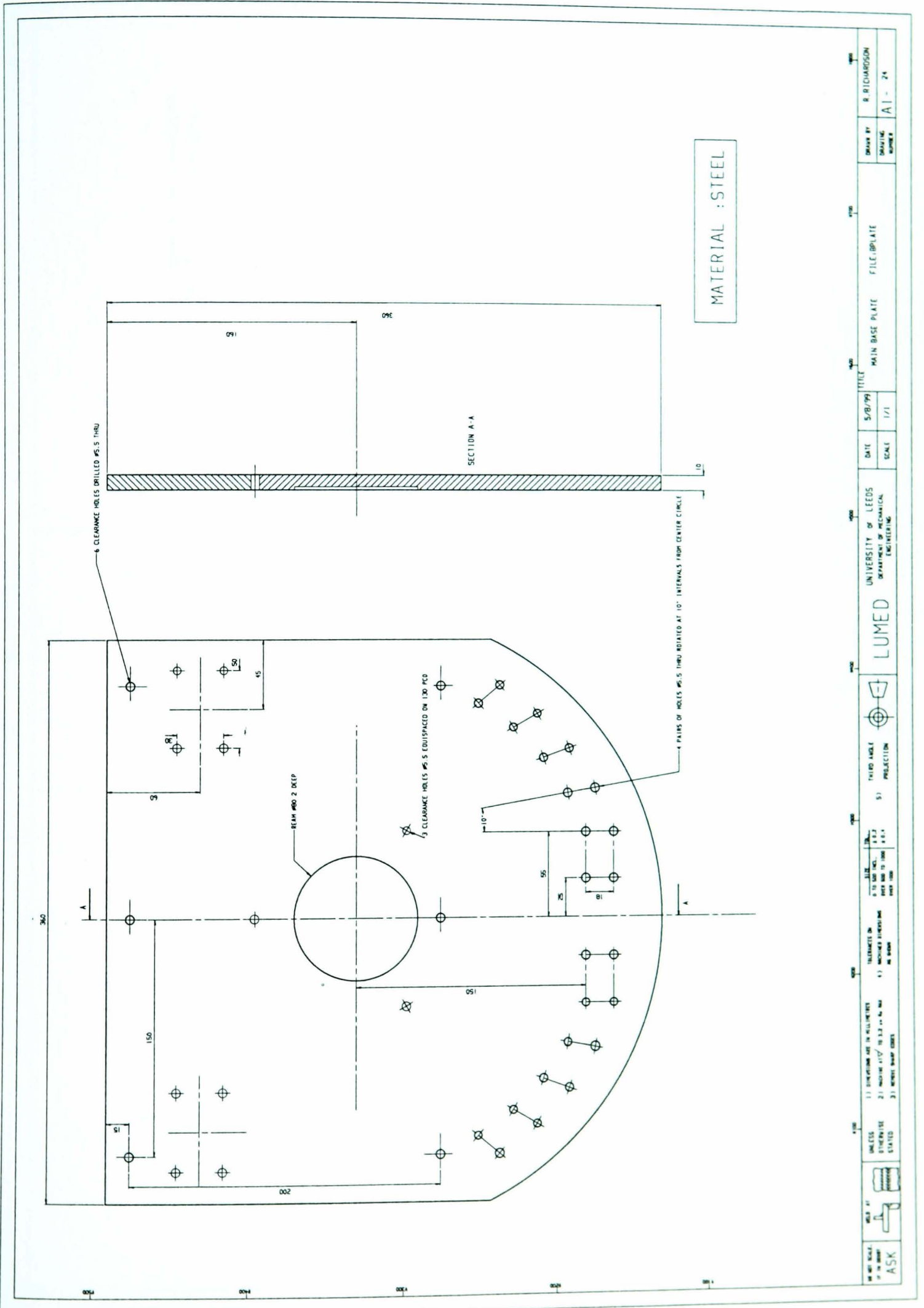MATERIAL: ALUMINIUM U CHANNEL 2"x2"x1/4"

ALL HOLES EXIST ON BOTH UPRIGHTS

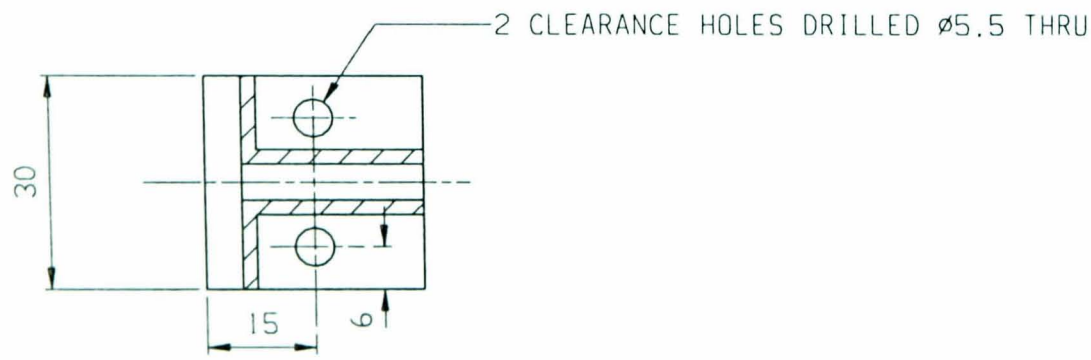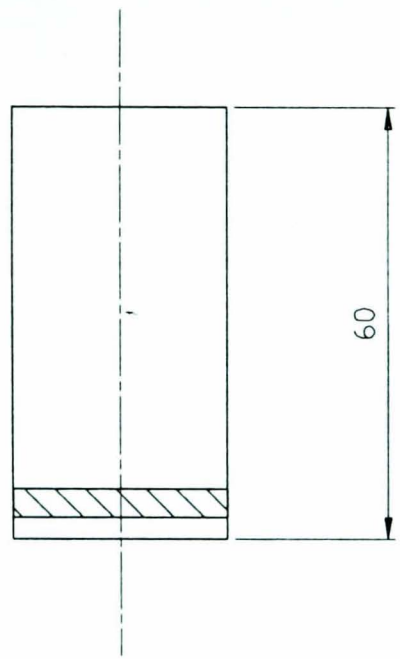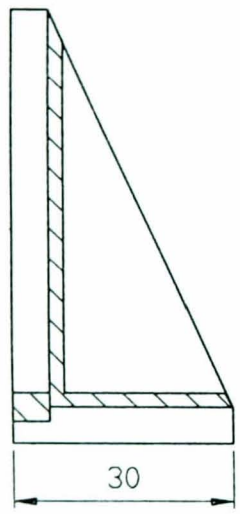| DO NOT SCALE IF IN DOUBT ASK | UNLESS OTHERWISE STATED | 1) MACHINE AT ✓ TO 3.2 µM Rₐ MAX
2) TOLERANCE ON MACHINED DIMENSIONS
AS FOLLOWS 0-500 ⁺₋ 0.2: 500-1000 ⁺₋ 0.4 | | LUMED
LEEDS UNIVERSITY
DEPT. OF MECHANICAL ENGINEERING | DATE 5/8/99
SCALE 1/1 | 1st JOINT FRONT CYLINDER SUPPORT
FILE: 1CYLTOP | DRAWN BY R.RICHARDSON
A4 ·22 |

MATERIAL: ALUMINIUM

90

17

50

50

30

4 CLEARANCE HOLES DRILLED ⌀5.5 THRU

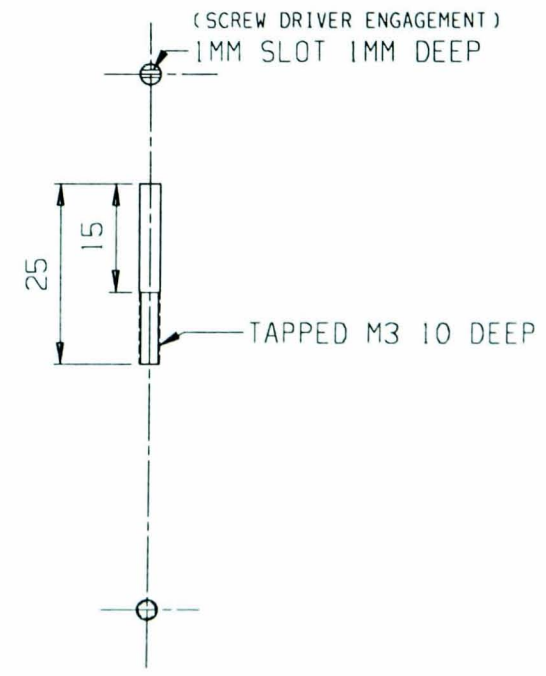| DO NOT SCALE IF IN DOUBT ASK | UNLESS OTHERWISE STATED | 1) MACHINE AT ✓ TO 3.2 ɔM R₀ MAX
2) TOLERANCE ON MACHINED DIMENSIONS
AS FOLLOWS 0-500 ± 0.2; 500-1000 ± 0.4 | | LUMED
LEEDS UNIVERSITY
DEPT. OF MECHANICAL ENGINEERING | DATE 5/8/99 | 1st JOINT REAR SPACER | DRAWN BY R.RICHARDSON |
| | | | | | SCALE 1/1 | FILE: 1SPACE | A4 23 |
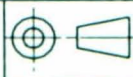
MATERIAL : STEEL

2 CLEARANCE HOLES DRILLED ⌀5.5 THRU

30

60

15

30

15

(SCREW DRIVER ENGAGEMENT)
1MM SLOT 1MM DEEP

25

15

TAPPED M3 10 DEEP

MATERIAL:5mm SHEET STEEL (FABRICATED)
WELD AT HATCHING

| DO NOT SCALE IF IN DOUBT ASK | UNLESS OTHERWISE STATED | 1) MACHINE AT ✓ TO 3.2 uM Ra MAX 2) TOLERANCE ON MACHINED DIMENSIONS AS FOLLOWS 0·500 ± 0.2: 500·1000 ± 0.4 | ⊕ ◁ | LUMED LEEDS UNIVERSITY DEPT. OF MECHANICAL ENGINEERING | DATE 5/8/99 SCALE 1/1 | MOTION LIMITING BRACKET   FILE:1LIMIT 1ST JOINT POTENTIOMETER PIN | DRAWN BY R.RICHARDSON A4 :25 |

MATERIAL: SQUARE STEEL TUBING 30 X 30
FRAME FABRICATED WITH WELDING WHERE REQUIRED
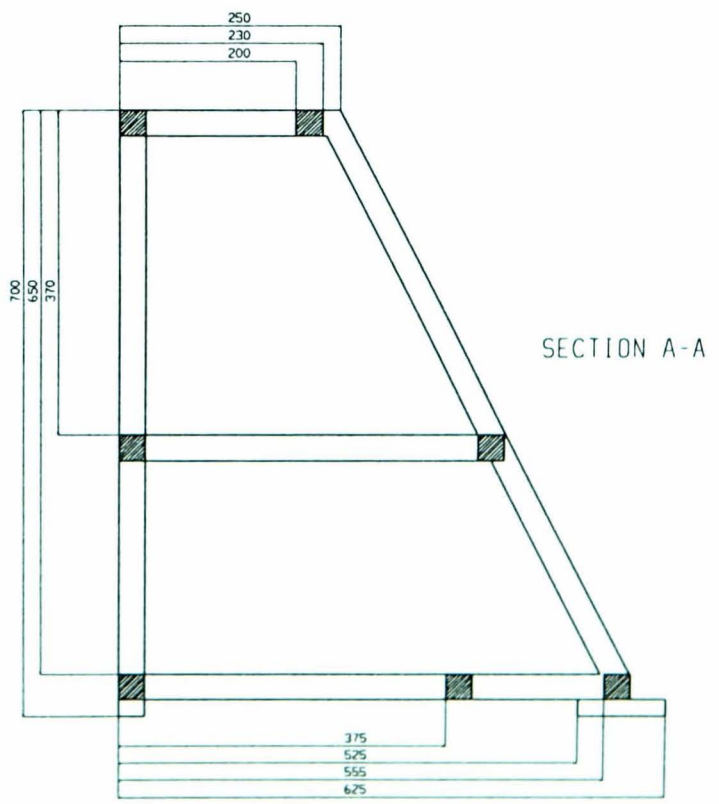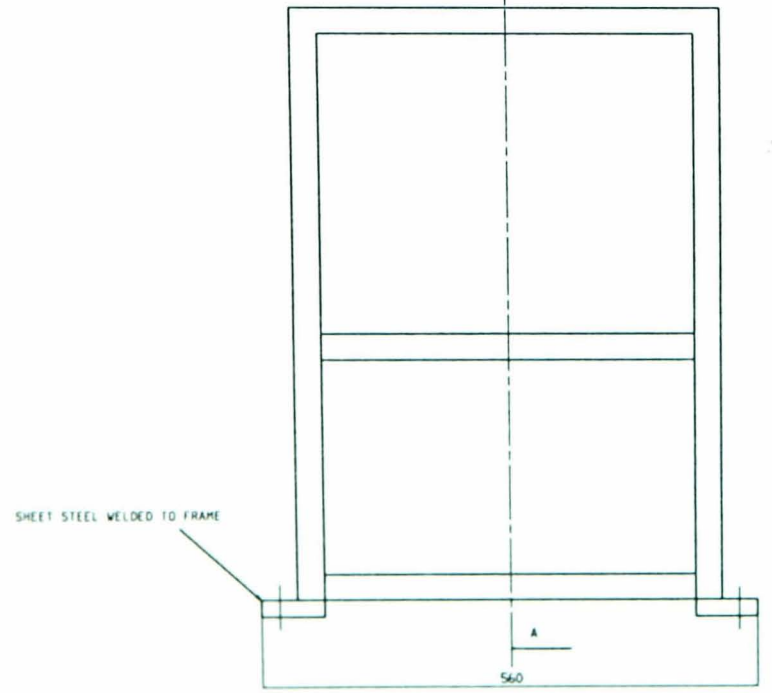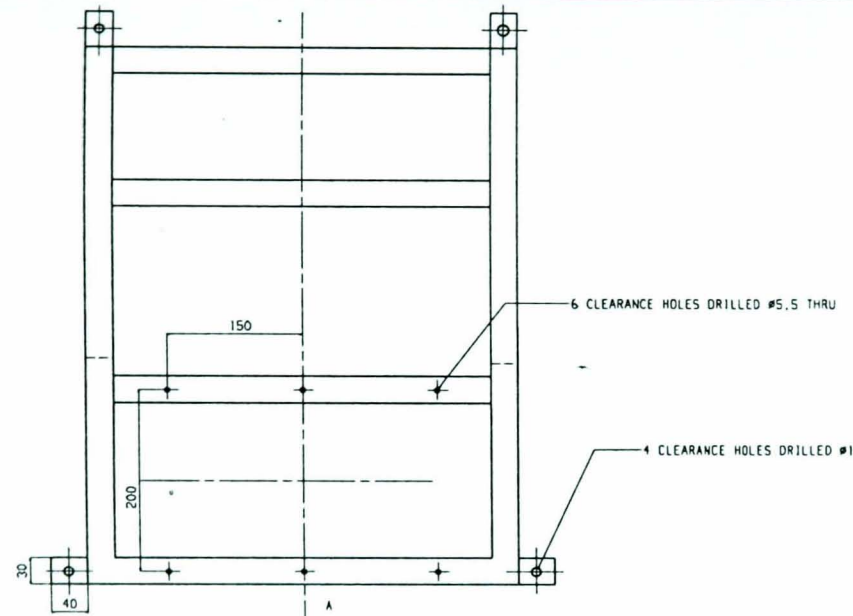
6 CLEARANCE HOLES DRILLED #5.5 THRU

4 CLEARANCE HOLES DRILLED #11 THRU IN CENTERS OF EXPOSED FEET

150

200

30

40

A

250
230
200

700
650
370

SECTION A-A

SHEET STEEL WELDED TO FRAME

A

560

375
525
555
625

LUMED

Appendix B

Papers published

This section contains published work from this thesis.

DEVELOPMENT OF A PHYSIOTHERAPY ROBOT

R.Richardson, M.E.Austin, A.R.Plummer.
School of Mechanical Engineering, University of Leeds, Leeds, LS2 9JT, UK
E-mail: menrr@Leeds.ac.uk

Abstract

Mechatronic systems have the potential to assist in many healthcare tasks which hitherto have been performed manually. One of these tasks is physiotherapy. The aim of this research is to develop a robotic device to provide physiotherapy for patients with upper limb impairments. Where patients cannot exercise unaided, a robot could assist them to undertake their own active exercises between manual physiotherapy or occupational therapy treatments. This assistance would be responsive, i.e. enhance the patient's own efforts rather than impose pre-programmed movements. A study has been completed demonstrating that responsive robotic therapy can help a patient adopt normal movement patterns. The study was concerned with assisting elbow movements. A three degree-of-freedom physiotherapy robot is now under development, using pneumatic actuation and impedance control.

Introduction

Disorder of upper limb movement is common: amongst children, cerebral palsy often involves the upper limbs; amongst adults, upper-limb impairment particularly occurs in multiple sclerosis and stroke patients. For example the annual incidence of stroke is about 2 per 1000 [1]. A survey of 308 new stroke patients has reported upper limb involvement in 86% of cases[2]. Physiotherapy forms a major component of rehabilitation for neurologically disordered subjects. Unfortunately, the therapy is labour intensive and in short supply. This patient group often receives less treatment than prescribed despite the evidence of a dose response relationship [3]. Active physiotherapy supplied by a mechatronic system is capable of providing assistive forces while following an exercise, which has been specified to encourage patient re-learning. Research has shown that responsive mechanical assistance can be applied safely to a human limb. A group at the University of California has developed a device to actively assist subjects to undertake a voluntary bimanual task [4]. The MIT Manus robotic device assists the subjects by applying forces at the hand and wrist [5]. Clinical trials have been safely performed using a force and position control technique known as impedance control.

Single degree of freedom robot

An experimental single degree-of-freedom robotic exerciser has been developed [6]. The forearm is strapped to a lever, which rotates in the horizontal plane; the elbow is aligned with the axis of rotation (fig 1).
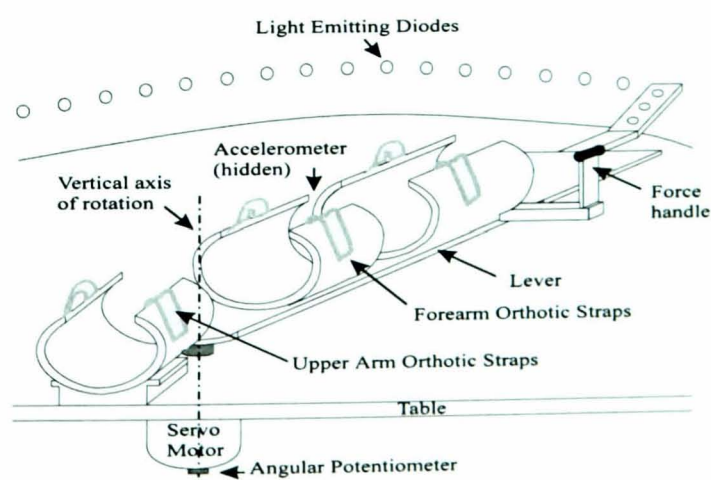

Figure 1. Elbow exerciser

A servomotor driven through a current amplifier is used to drive the lever, with position measured by a potentiometer. A semi-circular array of light emitting diodes (LEDs) around the lever indicates the desired position. A force handle is used to measure forces applied when a physiotherapist assists the movement.

A closed loop lead-lag controller with velocity error feedback is used to assist the patient (Fig. 2). The trajectory achieved by the patient when guided by a physiotherapist is used to generate the reference trajectories for velocity and position. Deadzones are used so that there is an envelope around the reference trajectory in which no assistance is provided. This is important to enable the patient to complete the exercise unaided if possible. This responsive nature of the assistance – i.e only applying torque if required – is central to the robotic physiotherapy concept.
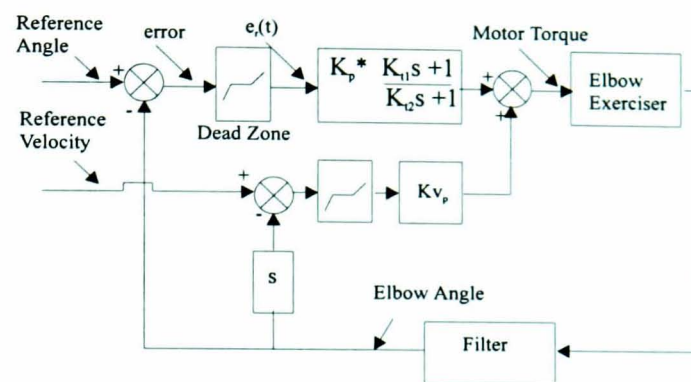

Figure 2 . *Lead lag controller with velocity feedback*

Methodology and results

Post acute stroke subjects with stabilized neurological disorder, limited cognitive problems, and a full range of passive elbow movement were selected for the study. The standard exercise was to undertake ten extension / flexion movements. The data were then spilt into separate extension / flexion movements. The middle eight flexion movements were analyzed. The results presented in this paper are for a 56 year old left side hemiplegic subject. The effected arm has a tone rating of 3 for the flexors and 1 for the extensors using the Ashworth Scale. The MRC power scale ratings are 2 for the flexors and 3 for the extensors. When unassisted the subject's movement was often disjointed and segmented into separate movement attempts (Fig. 3).

With the assistance of a physiotherapist, the subject completed the whole movement in a single continuous controlled manner. During testing, the physiotherapist was asked to assist the movement hand on hand and hand on the force handle. The mean movement trajectory of the middle eight movements for each test was evaluated (Fig. 4).
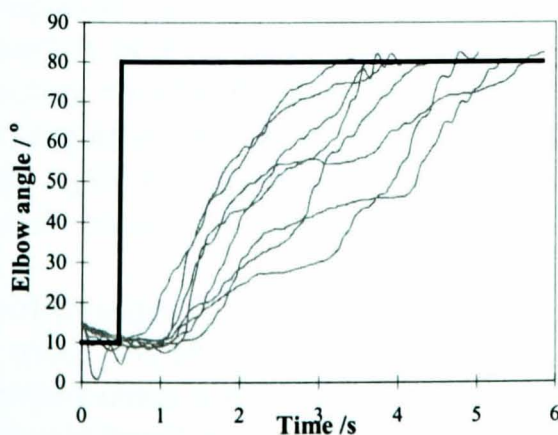

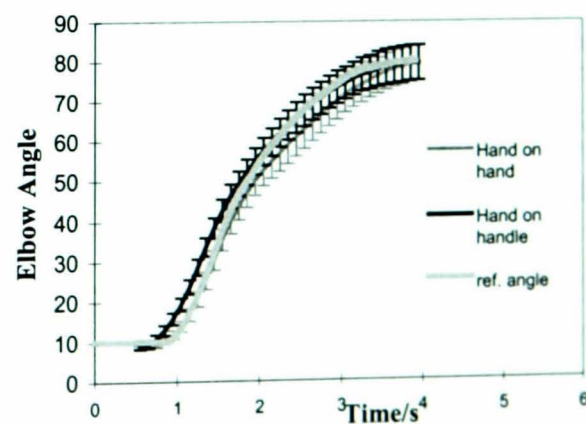Figure 3. *Target (—) and unassisted elbow angle trajectories (—) against time*

Figure 4. *Mean physiotherapist assisted elbow angle trace against time with 95% confidence interval*

The same exercise was performed by a control subject (Fig. 5). It can be noted that the control subject also undertook a smooth continuous movement, however the time required to complete the movement was shorter. Using the coefficients $K_p = 2$, $K_{tl} = 0.5$, $K_{t2}=1$, $K_{vp} = 0.5$, dead zone position $= \pm 5^0$ and dead zone velocity $\pm 10\ ^0/s$ the reference trajectory is the same as that show in figure 4. Physiotherapy was performed using robotic assistance on the same test subject (Fig. 6).
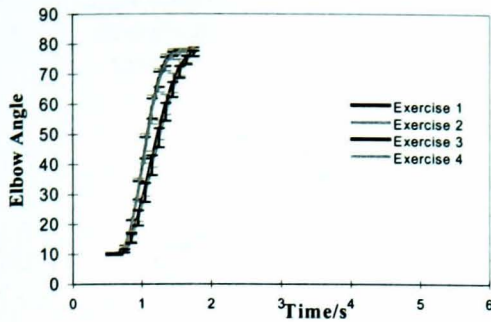

Figure 5 - Mean control subject elbow angle trace against time with 95% confidence limits
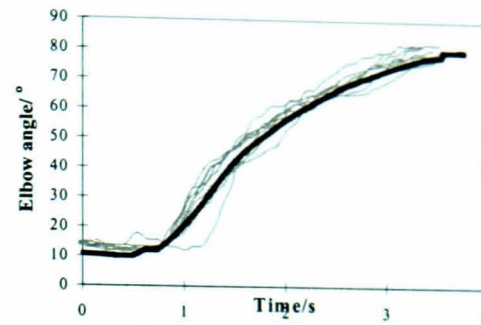
Figure 6 – Motor assisted elbow angle ($—$) and reference angle ($—$) against time for robotic assistance

The results from the controller indicate that the physiotherapist generated reference trajectory was achievable. The resultant patient movement is much more consistent and less ballistic than the unassisted trajectories.

Three degree of freedom robot
Elbow flexion/ extension movements are abstract exercises which are not meaningful to patients. More realistic physiotherapy exercises, such as reach-retrieve, occur in three dimensions. Moreover, many patients with severe disability can perform the gravity-free elbow movement without excessive difficulty. Hence a three degree of freedom robot is under development which can provide assistance during more realistic exercise tasks. Note that work by Stanger et al. [7] in surveying rehabilitation research groups identified that the ability to pick and place objects would provide the greatest advantage for people with upper limb deficiencies. The robot is intended to provide therapy for this type of exercise movement.

Traditionally pneumatic actuators could not be considered for high precision positioning systems due to highly non-linear dynamic properties such as air compressibility and friction effects. Recent developments in low friction pneumatic cylinders, proportional valves and digital control, allow pneumatics to be considered in applications such as this. Pneumatic actuators offer the advantage of high power to weight ratio and low cost while being suitable for medical environments.

The control strategy to be employed on the three degree of freedom robot is based around 'impedance control'. Impedance control allows the system to behave as if it had the properties of a simple mass, spring and damper system. Using this technique a desired trajectory can be implemented with deviation resulting in a compliant assistive force based upon impedance characteristics specified at the beginning of a session. The trajectory would again be determined by manual physiotherapy, and a deadzone would still be required to allow a patient some freedom to perform the task without assistance.

Robot design
The robot prototype is constructed from aluminum U – channel. At each of the pivot points potentiometers are used to obtain positional information. Accelerometers are used for additional feedback to implement impedance control. A six degree of freedom force / moment sensor is to be used to continually monitor any forces applied to the patients arm.

The robot arm is counter balanced so the patient would encounter negligible resistance when there is no pneumatic force (Fig. 7).
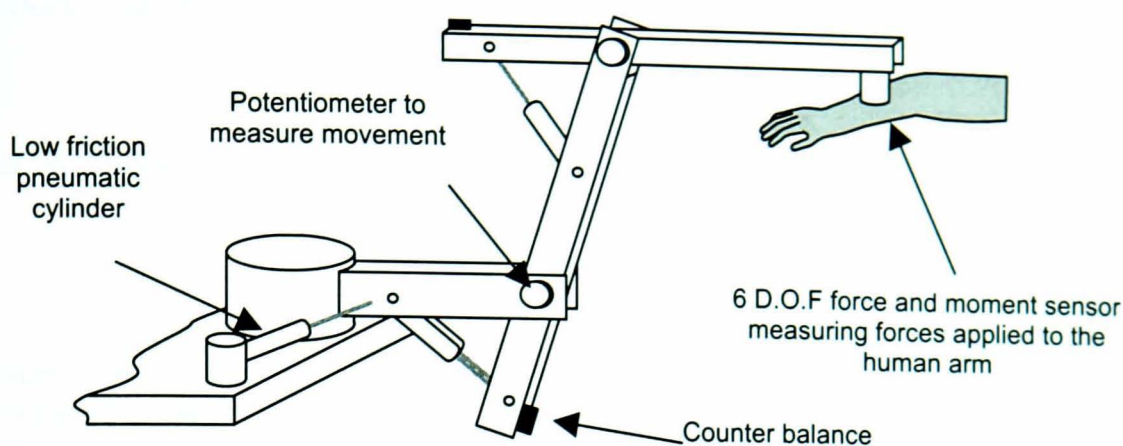

Figure 7. 3 D.O.F robot prototype

Conclusions

The work on the single degree of freedom robot demonstrated that robot physiotherapy could be performed safely and effectively. The single degree of freedom robot has very limited clinical use as exercises are not representative of everyday movement. The three-degree of robot should be able to encourage more normal movement patterns for tasks that patients find less abstract and more motivational. It is hypothesized that encouraging normal movement patterns has therapeutic value.

References

1. Bamford JM, Sandercock P, Dennis M, Burn J and Warlow C "A prospective study of acute cerebrovascular disease in the community: the Oxfordshire Community Stroke Project 1981-1986. Incidence, case fatality rates and overall outcome at one year of cerebral infarction, intracerebral haemorrhage and subarachnoid haemorrhage." *J Neurol Neurosurg Psychiatry* Vol. **54** (1990) pp. 16-22
2. Parker VM, Wade DT and Langton-Hewer R, "Loss of arm function after stroke: measurement, frequency and recovery". *Int Rehab Med* Vol. **8** (1986) pp 69-73
3. Sunderland A; Tinson D, J; Bradley E, L; Flecther, D; Langton Hewer R; Wade,D, 'Enhanced physical therapy improves recovery of arm function after stroke. A randomized controlled trial.' *Jou. of Neurology, Neurosurgery & Psychiatry* Vol. **55** (1992) pp. 530-535
4. Lum PS, Burgar C, & Van der Loos M, 'The uses of a robotic device for post stroke movement therapy' *Proceedings of Intl. Conf. of Rehab. Robotics,* (April 1997) *pp* 107-110.
5. Hogan,N, Krebs,H,I Charnnarong,J; Srikrisha,P & Shardn,A, 'MIT_Manus; A Workstation for Manual Therapy and Training II' *Proceedings of Telemanipulator Technology, SPIE The Intl. Society of Optical Engineering* 1833 Boston (1993), pp 28-34
6. Austin, M.E, Cozens, J.A, Plummer, A.R, Seedhom, B.B.,'Motion control for robotic physiotherapy', MOVIC '98, Zurich, Switzerland, August 25 – 28, Vol **3**, pp1203 - 1206
7. Stanger, C.A, Anglin, C., William, S.H., Romilly, P., 'Devices for assisting manipulation: a summary of users task priorities', IEEE transactions on rehabilitation engineering, Vol. 2 (1994) pp 285-304.

Acknowledgements

Self-tuning control of a low friction pneumatic actuator under the influence of gravity

R.Richardson*, A.R.Plummer[†], M.D.Brown*

*School of Mechanical Engineering, The University of Leeds, UK. Email:menrr@Leeds.ac.uk
[†]Instron Ltd, UK

Abstract

Traditionally the positioning of pneumatic actuators has been limited to movement between pre-set stops or switches. The restricting factors preventing the use of pneumatic cylinders for accurate servo-control arise from highly non-linear dynamic properties such as air compressibility and friction effects, which combine to severely degrade time response and positional accuracy. Many real systems are influenced by external gravity forces, which compound the problem of position control. A self-tuning system incorporating an external force balancing term is proposed using a low friction cylinder. The low friction cylinder is compared to conventional, sealed cylinders to demonstrate the increased performance.

Index terms – Pneumatics, Low friction cylinder, Self-tuning control.

I. INTRODUCTION

Pneumatic systems have been used in industry for many years automating simple industrial tasks. This is largely due to their inherent ability to provide low cost, compact, safe actuation[1]. The control strategies employed on pneumatic cylinders are often simple, with the majority of applications relying on pre-set mechanical stops (bang – bang motion) for their position control. The restricting factors preventing wider use of pneumatic cylinders arise from highly non-linear dynamic properties such as air compressibility and friction effects, which combine to severely degrade time response and positional accuracy[2]. Within the last decade new research initiatives have attempted to use pneumatics in applications that were previously limited to electric motors or hydraulics. The drive behind this research is that the cost advantage can be as high as 10:1. Surgenor and Iordanou[2] have compared pneumatic and electric actuators, and shown that similar performance can be obtained for the example of a gantry crane.

Work is ongoing to enable greater understanding of the physical properties behind pneumatics to enable more appropriate control schemes to be designed. Backe and Ohligschlager[3] analysed the heat transfer behavior in pneumatic chambers, enabling the development of pressures to be described more exactly than in the past. Wong and Moore[4] examined the acceleration characteristics of pneumatic cylinders showing them to behave highly regionally.

Recent developments in low friction pneumatic actuators have been exploited. Ben-Dov and Salcudean[5] used low friction cylinders when developing a pneumatic actuator to accurately apply moderate levels of force. Ishida et al.[6],[7],[8],[9] opted to use low friction actuators in work relating to multi-layer neural networks.

Many control strategies have been employed in an attempt to overcome the non-linearities present in pneumatic systems. Shih and Tseng[10] demonstrated that conventional PID control could be enhanced using a self-tuning strategy. Similar work was performed by Hamiti et al.[11] using a modified form of PI control. The integrator element was modified using a self-tuning strategy to reduce unwanted limit cycles produced by 'stick-slip' effects. McDonell and Bobrow[12] performed adaptive control on a double acting cylinder to drive a rotary joint with an attached arm. Shing and Huang[13] compared the results of conventional PID control with self-tuning pole-placement control for a pneumatic cylinder. The pole-placement controller demonstrated faster response time, less overshoot and improved steady state response especially in the presence of load disturbances.

This present study examines the operation of a low friction pneumatic cylinder under the influence of a constant external force such as a gravity force. Under these conditions, a balancing force must be produced by the control system to counteract this external force. A self-tuning algorithm is proposed to adapt to changeable plant parameters including the balancing force.

Low Friction pneumatic cylinder - Airpot Airpel – Air bearing design	Bore dia: 18mm Stroke: 38mm
Conventional seal cylinder – Lip seal	Bore dia: 20mm Stroke: 80mm
Electro-pneumatic pressure control valves – SMC E– P Hyreg VY1100	Pressure range:0 – 8.8 bar Voltage Range: 1 – 5V
Pressure Transducer RS 249-3959	Pressure Range: 0 – 6 bar Accuracy (%FS) ± 0.1%
Force Transducer RDP 51/1117 - 01	Capacity: 890 N Accuracy (%FS) ± 0.5%
Mass (M)	4.5 kg
LDVT RDP D5/6000	Linear Range: ± 150mm Linearity (%FS) ± 0.2%

Table 1 – Equipment Specifications

II. EXPERIMENTAL APPARATUS

A. Test Rig

Experiments were performed on a test rig (Fig. 1) which enabled the force and displacement of a pneumatic cylinder to be measured. Low friction pneumatic cylinders were used to minimize stiction effects, hence enabling smoother motion to be achieved. This work is part of an ongoing project to develop a physiotherapy robot [14],[15], for which smooth and predictable motion is essential.
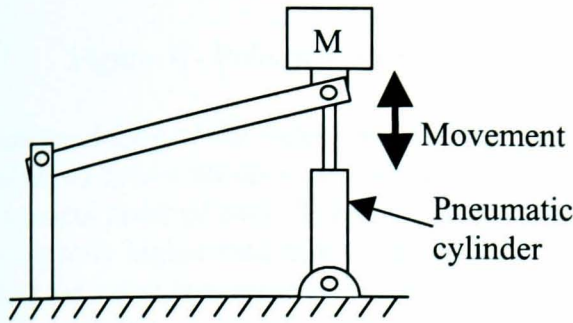

Figure 1 – Pneumatic test rig

The pneumatic cylinder was supplied with air via two electro-pneumatic valves (Fig. 2). This allowed the pressure difference across the cylinder to be altered with software changes alone. A gain of 1.1 was used to increase the pressure P_2 to compensate for differences in piston area.

The position of the pneumatic cylinder was measured using an LVDT attached across the cylinder. A force sensor was attached between the cylinder and load to enable the friction within the cylinder to be estimated. Component specifications are contained in Table 1.
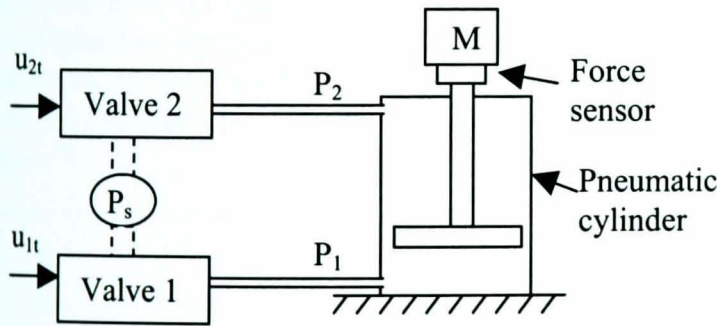

Figure 2 – Supplying air to the cylinder

B. Balance pressure

In order for a zero control signal (u_t) to cause no change in response, it was necessary to create a difference in pressure between P_1 and P_2 to counteract the external force,

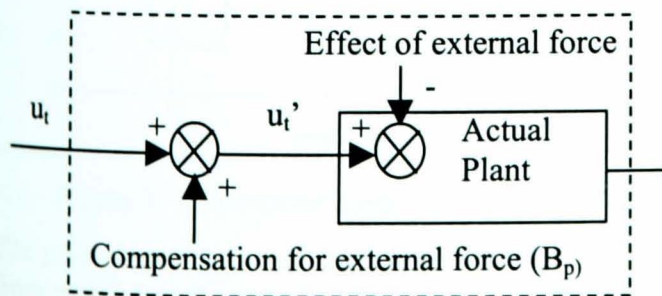

Figure 3. – Considering balance pressure as part of plant

effectively adding a constant value (B_p) to any control signal (Fig. 3). For controller design, the balance signal was considered part of the actual plant.

C. Controlling two valves with one control signal

In order to optimize the speed of airflow to and from the cylinder the valves needed to operate under choked conditions (maximum mass flow rate). For air, choked flow occurs for a pressure ratio less than 0.53.

The pressures P_1 and P_2 were increased by equilibrium pressure (P_{eq}) to operate under these conditions. A control strategy was formulated to control two valves from one control signal. This assumed the two valves to behave identically. The control signal and the balance factor (B_p) were halved, subtracted from the top equilibrium signal and added to the bottom equilibrium signal:

$$u_{1_t} = P_{eq} + \frac{u_t'}{2} \tag{1}$$

$$u_{2_t} = P_{eq} - \frac{u_t'}{2} \tag{2}$$

Where:

$$u_t' = u_t + B_p \tag{3}$$

III. EXPERIMENTAL RESULTS

A. Proportional control

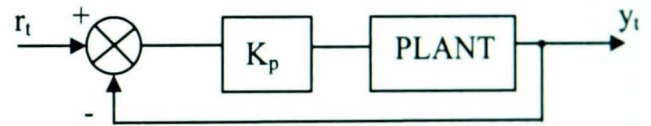Proportional control (Fig. 4) was performed on the pneumatic cylinder.

Figure 4 - Proportional control

Using a proportional gain (K_p) of 2.5 the position response demonstrated the smallest steady state error and fastest response time (Fig. 5). The large overshoot is unacceptable for precision control systems of this nature, so a more advanced control strategy is required.
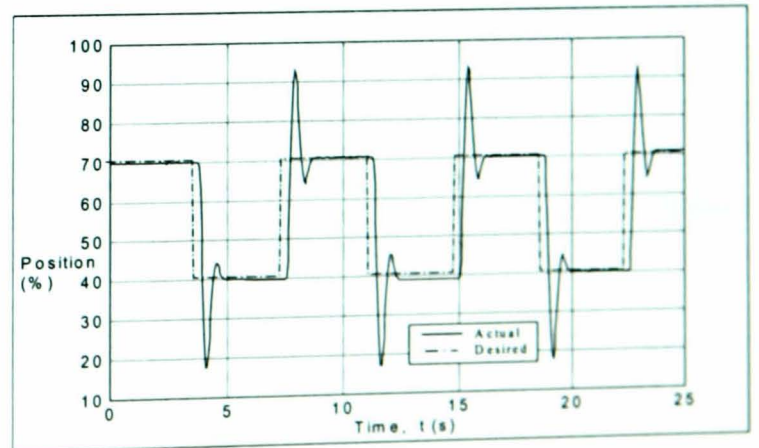

Figure 5 – Proportional control results ($K_p = 2.5$)

B. Pole-placement control

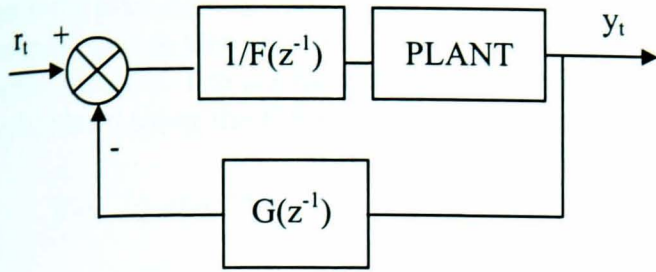Pole-placement is a common form of model-based control using the controller structure shown in figure 6.

Figure 6 - Pole-placement control

Physical modeling of the valves and cylinder have shown the valves to have a model order of three and the cylinder to have a model order of two. The response time of the valves is significantly higher than that of the pneumatic cylinder, enabling the valve dynamics to be simplified to a single gain. The system can then be represented by a second order model. Using data obtained from proportional control, a plant model was calculated using least squares parameter estimation:

$$y_t = \frac{B(z^{-1})}{A(z^{-1})}.u_t \qquad (4)$$

$$A(z^{-1}) = 1 - 1.75z^{-1} + 0.75z^{-2} \qquad (5)$$

$$B(z^{-1}) = 0.0591z^{-2} \qquad (6)$$

Using this plant model the coefficients $F(z^{-1})$ and $G(z^{-1})$ were calculated for specific closed loop poles by solving the diophantine equation[14]. Pole-placement was performed on the pneumatic cylinder using closed-loop pole pairs at $0.4 \pm 0.1i$. The resulting response is shown in figure 7.
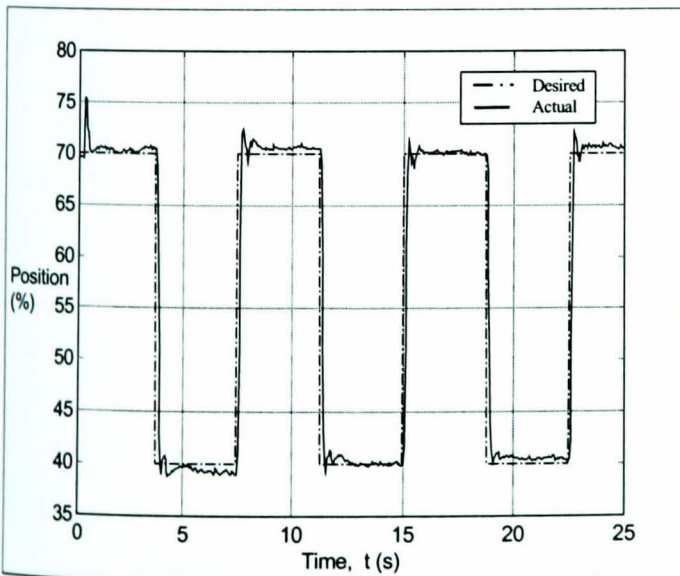

Figure 7 – Pole-placement control results.

The pole-placement results are superior to those obtained from proportional control with reduced overshoot and shorter rise time. These results do not demonstrate the changeable nature of the system (for example due to variations in system temperature) requiring a new plant model to be identified periodically. A self-tuning strategy was adopted to automatically obtain the correct plant model at the commencement of each session.

C. Self-tuning control

It was possible to reduce the number of parameters being estimated by assuming the plant always contains an integrating element[15]:

$$y_t = \frac{b_2 z^{-2}}{(1 - z^{-1})(1 + a_1 z^{-1})}.u_t \qquad (7)$$

It was necessary to incorporate the balance pressure (B_p) into the self-tuning process as it varied between sessions, resulting in three parameters (a_1, b_2, B_p) being estimated. The system including balance signal is shown in figure 8.
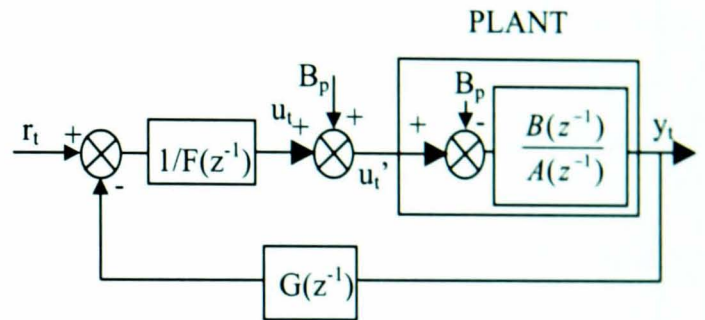

Figure 8 - Pole-placement control with balance pressure

Analyzing the plant to obtain a method of self-tuning the balance pressure:

$$y_t(1 - z^{-1}) = \frac{b_2 z^{-2}}{1 + a_1 z^{-1}}.u_t \qquad (8)$$

For ease of notation

$$y_t' = y_t(1 - z^{-1}) \qquad (9)$$

$$\Rightarrow y_t' = \frac{b_2 z^{-2}}{1 + a_1 z^{-1}}.u_t \qquad (10)$$

Substituting for u_t in (10) using (3)

$$\Rightarrow y_t'(1 + a_1 z^{-1}) = b_2 z^{-2} u_t' - b_2 B_p z^{-2} \qquad (11)$$

A parameter d can be estimated on line

$$d = -b_2 B_p \qquad (12)$$

The time delay (z^{-2}) of d can be ignored since B_p is a constant. Forming the regressor and parameter vectors necessary for recursive least squares self-tuning.

The regressor vector:

$$\underline{\psi}_t = \begin{bmatrix} y_{t-1}' & u_{t-2}' & 1 \end{bmatrix}^\mathsf{T} \qquad (13)$$

The parameter vector:

$$\underline{\hat{\theta}}_t = \begin{bmatrix} -a_1 & b_2 & d \end{bmatrix}^{\mathrm{T}} \qquad (14)$$

The parameter vector is calculated online using standard recursive least squares identification equations [13],[14]. The balance value is then reconstructed from (12) and the plant model from (7). The coefficients $F(z^{-1})$ and $G(z^{-1})$ are recalculated using the following diophantine equation:

$$F(z^{-1})A(z^{-1}) + G(z^{-1})B(z^{-1}) = A_m \qquad (15)$$

Pole placement control can then be performed for the next sample interval using the $F(z^{-1})$ and $G(z^{-1})$ coefficients obtained from (15).
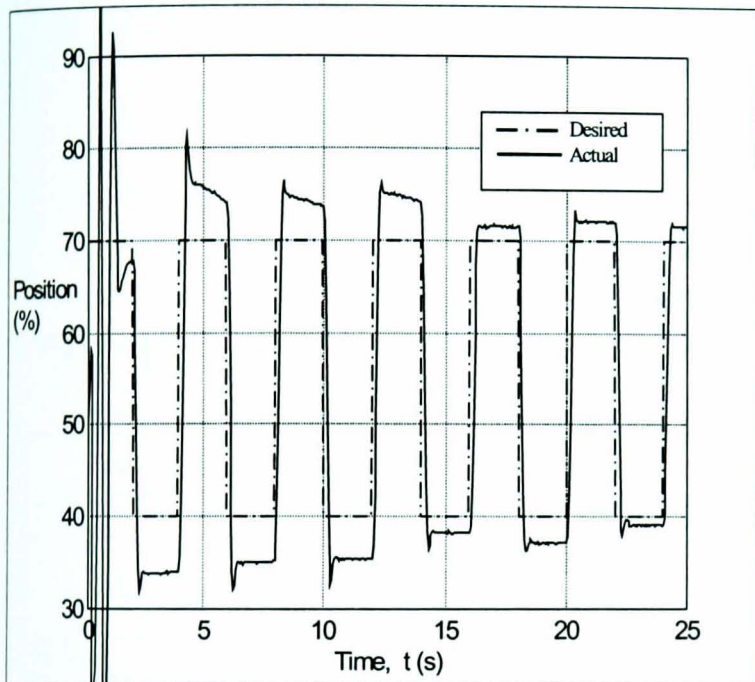

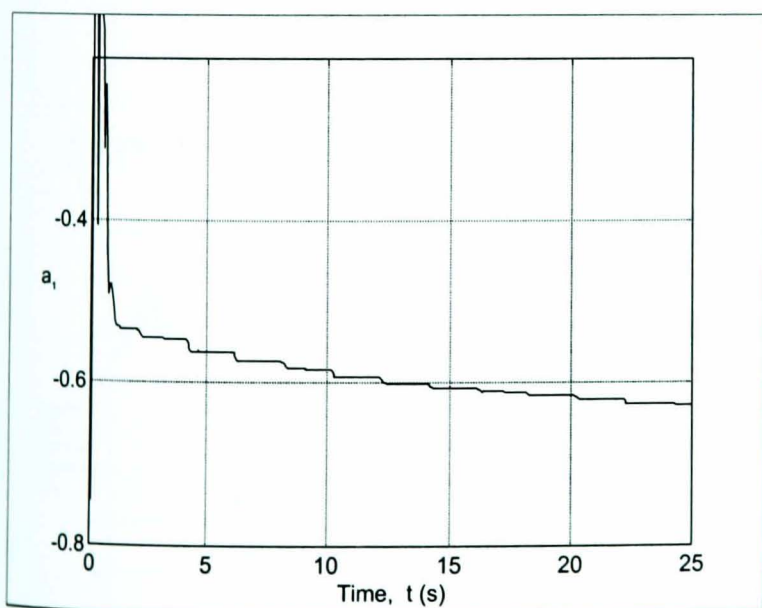Figure 9 – Self-tuning position response

Figure 10 – Self-tuning parameter a_1

The step response of the system is seen to converge appropriately after an initial tuning transient (Fig. 9). The convergence of parameters a_1, b_2 and B_p is shown in figures 10,11 and 12.
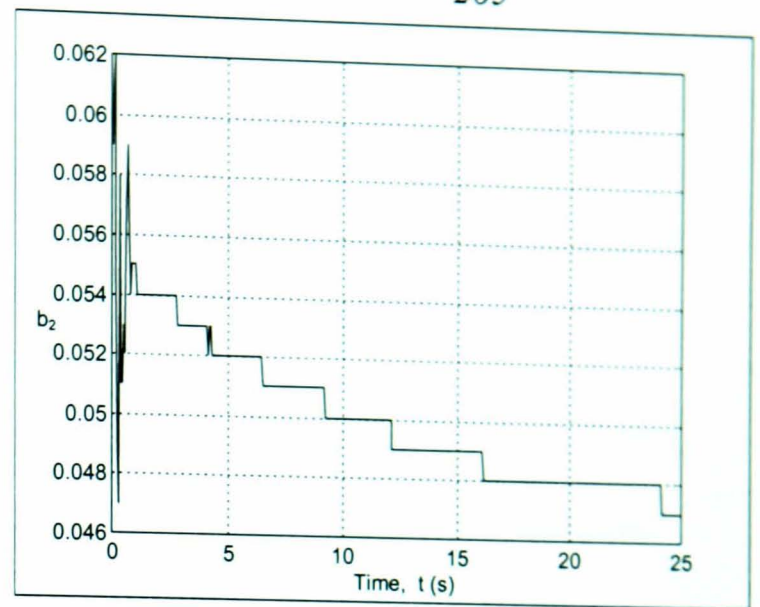

Figure 11 – Self-tuning parameter b_2
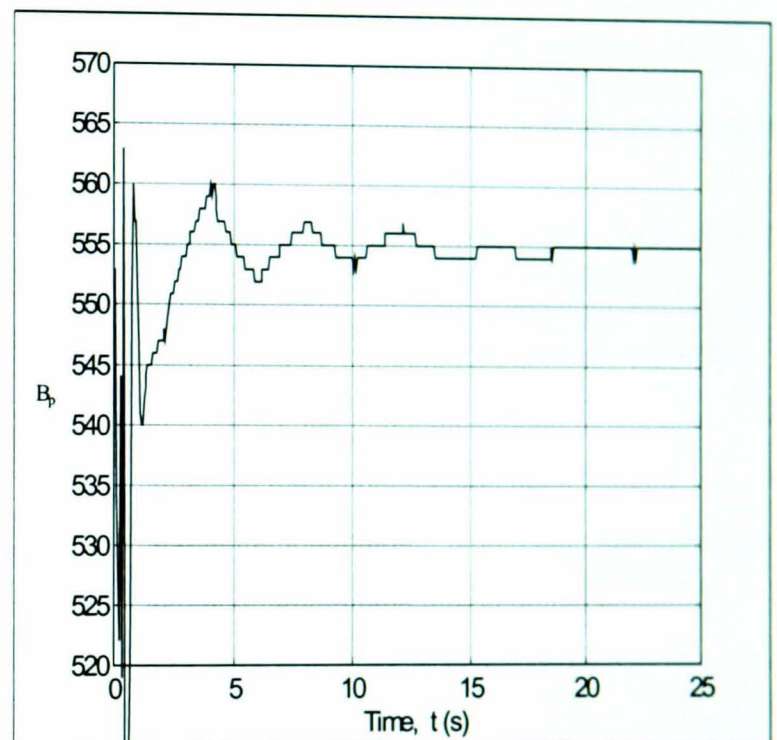
Figure 12 – Self-tuning parameter B_p

IV. ADVANTAGES OF LOW FRICTION CYLINDERS

Low friction pneumatic actuators were used in these control experiments due to their small and predictable friction characteristics. The Airpel Airpot cylinder is a low friction cylinder based on an air bearing design[18]. This design reduces friction and stiction effects compared to modern conventional cylinders. In order to demonstrate the improved performance the frictional forces within the cylinder were calculated by examining the forces due to the pressures P_1 & P_2, and then subtracting the force applied externally by the cylinder (measured by the force sensor). Sine wave demand signals were used as frictional effects are more evident when a slow variation in position is required.

Comparing the position response of the conventional cylinder (Fig. 13) and the Airpel cylinder (Fig. 14) both using pole placement control, a much smoother response is achieved by the Airpel cylinder. Examining the frictional characteristics of the two cylinders indicates the reason for the degradation in response of the conventional cylinder. The conventional cylinder experiences large levels of friction and a stick-slip motion at low speed (Fig. 15), while the magnitude of the Airpel internal friction is much smaller (Fig. 16).
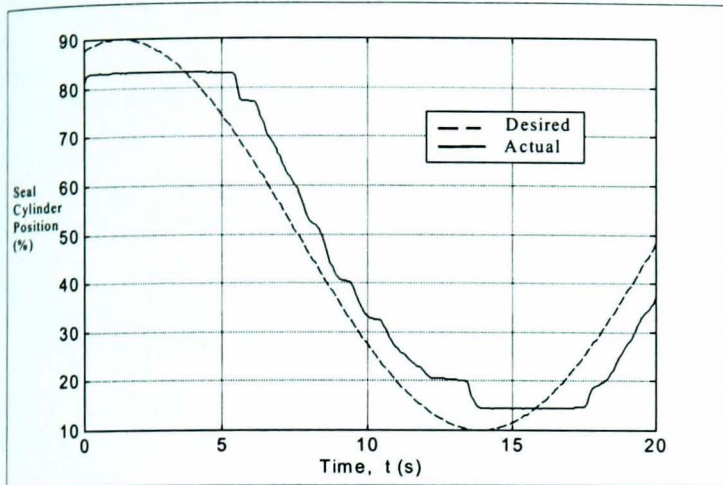

Figure 16 – Airpel friction characteristics

Figure 13 – Conventional cylinder sine wave position response
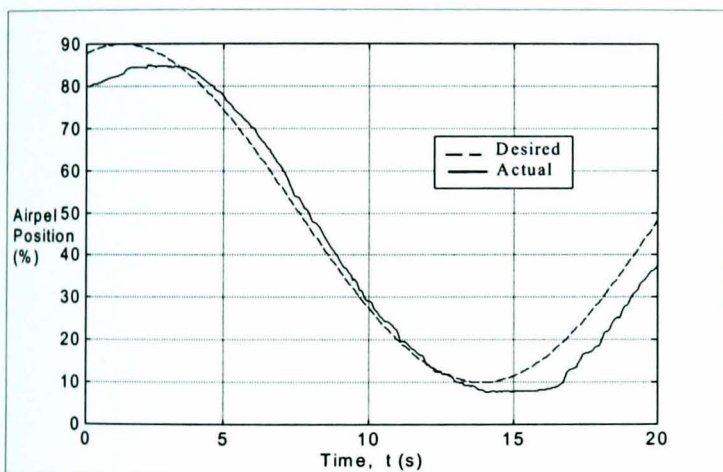
Figure 14 – Airpel sine wave position response

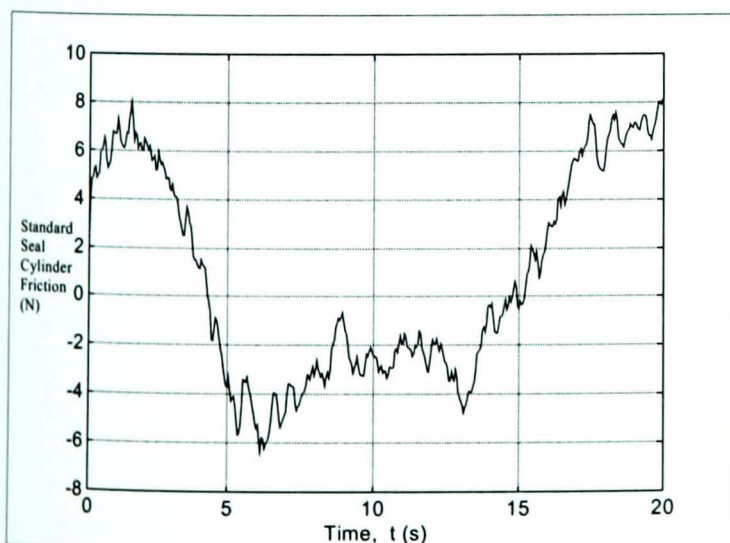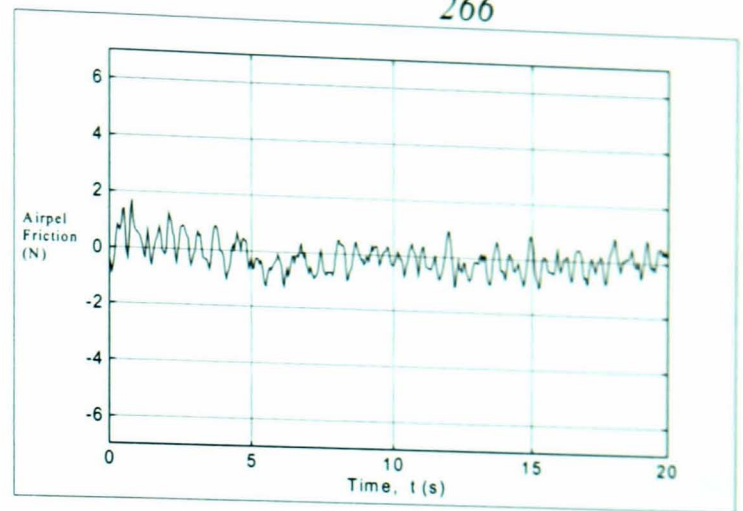## V. CONCLUSIONS

It has been demonstrated that low friction pneumatic cylinders offer real potential for modern precision control systems. The low friction nature enables far greater precision than that obtainable through modern conventional cylinder designs.

The self-tuning strategy shown here provides a method of obtaining correct operating parameters at the start of a session. Identifying an accurate balance pressure is crucial when a constant external force, such as gravity, is present.

VI. REFERENCES

[1]   Moore, P.R Pu, J. Harrison R, "Progression of servo pneumatic towards advanced applications", 5th international fluid power workshop, Bath, UK, pp347-364, 1992.

[2]   Surgenor, B.W Iordanou, H.N, "Electric versus pneumatic servo control: A case study with a gantry crane apparatus", AMSE Winter annual meeting, New Orleans, Louisiana, November 28 - December 3 1993.

[3]   Backe, W., Ohligschlager, O., "A model of heat transfer in pneumatic chambers", Journal of fluid control, Vol 20, part 1, pp61-78, 1989.

[4]   Pu, J., Wong, C. B., Moore, P. R., "Acceleration characteristics of servo controlled pneumatic cylinder", ASME, Fluid power systems and technology, Vol 3, pp119-130, 1996.

[5]   Ben-Dov, D. , Salcudean, S.E, "A force controlled pneumatic actuator", IEEE transactions on robotics and automation, Vol. 11, No 6, pp 906-911, Dec. 1995.

[6]   Ishida Y. , Fujiwara, A. , "An LQI control for pneumatic cylinders with disturbance observer", Proceedings of the IASTED Int. Conf. robotics and manufacturing, Honolulu, Hawaii, USA, August 19-22 1996.

[7]   Ishida Y., Fujiwara, A. , Katsumata, K. , "An LQI control for pneumatic cylinders using multilayer neural networks", Journal A, Vol 38, No. 2, 1997.

[8]   Ishida Y. ,Bao , X. , Song, J. , "An application of MNN trained by MEKA for position control of a pneumatic cylinder" , IEEE international conference on neural networks - Vol 2, pp829-833,1997.

Figure 15– Conventional cylinder friction characteristics

[9]   Ishida, Y., Katsumata, F., Fujiwara, A., "Neural network based adaptive I-PD controller for pneumatic cylinder", SICE '95, July 26-28, Sapporo, pp1281-1284, 1995.

[10]   Shih, M. ,Tseng, S., "Pneumatic servo-cylinder position control by PID-self tuning controller", JSME International Journal, Series C, Vol. 37, No. 3, pp565-572, 1994

[11]   Hamiti, K. , Voda-besancon, A. ,Roux-Boisson, H. "Position control of a pneumatic actuator under the influence of stiction", Control Eng. Practice, Vol. 4, No 8, pp1079-1088, 1996.

[12]   McDonell, B. ,Bobrow, J. , "Adaptive tracking control of an air powered robot actuator", Journal of Dynamic Systems, Measurement, and Control, Vol 115, pp427-433, Sep. 1993.

[13]   Shih, M. , Huang.Y, "Pneumatic servo-cylinder position control using a self-tuning controller", JSME INT. Journal, series 2, Vol.35, No. 2, 1992.

[14]   Austin ME, Cozens JA, Seedhom BB. Motion control for robotic physiotherapy. Movic 98', Switzerland, Vol 3, pp1203-1206, 1998.

[15]   Richardson R, Austin ME, Plummer AR. Development of a physiotherapy robot. Proceedings of the international biomechatronics workshop, Enshede 19-21 April 116-120, 1999.

[16]   Astrom, K., Wittenmark, B., "Computer-Controlled Systems, Theory and Design", pp 165-223, third edition, 1997, ISBN 0-13-314899-8

[17]   Vaughan, N.D , Plummer, A.R , "Robust adaptive control for hydraulic servosystems", ASME winter annual meeting, Dallas, Texas, Nov 25-30, 1990.

[18]   Gabermann M. Near frictionless air cylinders provide precision pneumatic motion control system. Power conversion and intelligent motion, 1995; 21(11):48-51.

Pneumatic impedance control for physiotherapy

R.Richardson*, M.Brown*, A.R.Plummer†

*The University of Leeds, School of Mechanical Engineering, UK.
† Instron Ltd, UK

Abstract—
A simple pneumatic impedance control system is proposed for implementation on a physiotherapy robot. The controller consists of a proportional derivative position controller, feedforward force compensation and impedance filter to modify the desired trajectory. Performance of the proposed controller is demonstrated through simulated and experimental results obtained from a single link of a three-degree of freedom robot intended for physiotherapy. The controller has been shown to accurately respond to position and force demands.

Index terms - Pneumatic, Impedance control, Robotic physiotherapy

I. INTRODUCTION

Many people suffer from debilitating illnesses such as stroke. These patients require physiotherapy to aid towards full or partial recovery of any effected limbs. Robots have the potential to administer physiotherapy with greater consistency than humans while recording patient data that was previously unattainable. Robotic physiotherapy requires consideration of both force and position, wherein a controller guides the patient's limb through a pre-set series of motions, applying forces to assist (not drag) the patient's limb.

Several force and position control schemes have been devised. Chiavernin and Sciavicco [1] proposed a parallel approach to force and position control, where position trajectories are sacrificed due to force demands. For physiotherapy, specifying specific position demands would be difficult, as they would be masked by the dominance of the force loop. Ferretti et al. [2] proposed a hybrid force/position control strategy for robots with multiple degrees of freedom. Force is controlled in constrained directions, while position is controlled in unconstrained directions. With the robot operating in a constrained environment the controller would behave purely as a force controller. Schutter and Brussel [3] used a position control strategy combined with an external force loop

to alter demand position and velocity. An extension to this was devised by Hogan [4] who developed a force /position control strategy, termed 'impedance control', for which the desired force and position are connected through mass, spring and damping characteristics. The controller compromises between force and position demands. This controller was deemed most appropriate for physiotherapy. Indeed, several prototype physiotherapy robots use this technique. Krebs et. al [5] have implemented force based impedance control on a low inertia prototype physiotherapy robot based upon electric motors. Noritsugu and Yamanaka [6] have used position based impedance control on a RAM (Rubber artificial muscle) for a prototype physiotherapy robot, incorporating addition pressure controllers to ensure pressures within the RAM are accurately controlled.

Recent developments in pneumatic actuators and valves allow them to be considered for applications which previously only electric motors were suitable. Using pneumatic actuators to implement impedance control has major benefits. Pneumatic system's inherent low stiffness and direct drive capabilities enable smooth compliant motion, which is difficult to obtain from conventional geared electric motor systems. Moreover, pneumatic actuators can cost up to 10 times less than electric motors, while offering a higher power to weight ratio.

Most impedance controllers are designed around force loops, which make use of the ability of an electric motor to supply torque on demand [5]. Pneumatic and hydraulic actuators could also be used. However, due to factors such as fluid compressibility, stiction and viscous friction, accurate positioning of hydraulic and pneumatic systems is difficult to obtain from a force based control system. Moreover, an accurate model of the system dynamics is required, which can be difficult to obtain [7]. Indeed, Krebs et. al [5] used a low inertia manipulator to reduce the influence of system dynamics. Generally, the inertial dynamics of the manipulator are significant. A position based impedance controller does not require consideration of the system dynamics. Heninrichs et. al [7] proposed a position based impedance controller for an existing

*Corresponding author email: menrr@Leeds.ac.uk

Pneumatic impedance control for physiotherapy

R.Richardson*, M.Brown*, A.R.Plummer†

*The University of Leeds, School of Mechanical Engineering, UK.
† Instron Ltd, UK

Abstract—
A simple pneumatic impedance control system is proposed for implementation on a physiotherapy robot. The controller consists of a proportional derivative position controller, feedforward force compensation and impedance filter to modify the desired trajectory. Performance of the proposed controller is demonstrated through simulated and experimental results obtained from a single link of a three-degree of freedom robot intended for physiotherapy. The controller has been shown to accurately respond to position and force demands.

Index terms - Pneumatic, Impedance control, Robotic physiotherapy

I. INTRODUCTION

Many people suffer from debilitating illnesses such as stroke. These patients require physiotherapy to aid towards full or partial recovery of any effected limbs. Robots have the potential to administer physiotherapy with greater consistency than humans while recording patient data that was previously unattainable. Robotic physiotherapy requires consideration of both force and position, wherein a controller guides the patient's limb through a pre-set series of motions, applying forces to assist (not drag) the patient's limb.

Several force and position control schemes have been devised. Chiavernin and Sciavicco [1] proposed a parallel approach to force and position control, where position trajectories are sacrificed due to force demands. For physiotherapy, specifying specific position demands would be difficult, as they would be masked by the dominance of the force loop. Ferretti et al. [2] proposed a hybrid force/position control strategy for robots with multiple degrees of freedom. Force is controlled in constrained directions, while position is controlled in unconstrained directions. With the robot operating in a constrained environment the controller would behave purely as a force controller. Schutter and Brussel [3] used a position control strategy combined with an external force loop

to alter demand position and velocity. An extension to this was devised by Hogan [4] who developed a force /position control strategy, termed 'impedance control', for which the desired force and position are connected through mass, spring and damping characteristics. The controller compromises between force and position demands. This controller was deemed most appropriate for physiotherapy. Indeed, several prototype physiotherapy robots use this technique. Krebs et. al [5] have implemented force based impedance control on a low inertia prototype physiotherapy robot based upon electric motors. Noritsugu and Yamanaka [6] have used position based impedance control on a RAM (Rubber artificial muscle) for a prototype physiotherapy robot, incorporating addition pressure controllers to ensure pressures within the RAM are accurately controlled.

Recent developments in pneumatic actuators and valves allow them to be considered for applications which previously only electric motors were suitable. Using pneumatic actuators to implement impedance control has major benefits. Pneumatic system's inherent low stiffness and direct drive capabilities enable smooth compliant motion, which is difficult to obtain from conventional geared electric motor systems. Moreover, pneumatic actuators can cost up to 10 times less than electric motors, while offering a higher power to weight ratio.

Most impedance controllers are designed around force loops, which make use of the ability of an electric motor to supply torque on demand [5]. Pneumatic and hydraulic actuators could also be used. However, due to factors such as fluid compressibility, stiction and viscous friction, accurate positioning of hydraulic and pneumatic systems is difficult to obtain from a force based control system. Moreover, an accurate model of the system dynamics is required, which can be difficult to obtain [7]. Indeed, Krebs et. al [5] used a low inertia manipulator to reduce the influence of system dynamics. Generally, the inertial dynamics of the manipulator are significant. A position based impedance controller does not require consideration of the system dynamics. Heninrichs et. al [7] proposed a position based impedance controller for an existing

*Corresponding author email: menrr@Leeds.ac.uk

hydraulic industrial robot, validating their work experimentally. Gorce and Guilhard [8] propose a multi-link, position based impedance controller for implementation on a legged robot. They use an actuator model to predict the torque produced from the pneumatic cylinders. The performance of the controller is demonstrated through simulation.

This paper examines the simulated and experimental results obtained from a simple impedance controller implemented on one degree of a three-degree-of-freedom robot intended to perform physiotherapy. Section 2 describes the experimental equipment and section 3 develops separate force and position control techniques. Section 4 proposes a position based impedance controller from the controllers described in section 3. Simulated and experimental results of the impedance controller are examined in section 5. Finally, section 6 develops the controller for higher degrees of freedom.

II. EXPERIMENTAL EQUIPMENT

Experiments are performed on a single link (Fig. 1) of a three-degree-of-freedom pneumatic robot intended for physiotherapy [9]. A pneumatic cylinder provides torque to rotate the link, while the angular position is measured using a potentiometer. Two electro-pneumatic valves supply air to the pneumatic cylinder. A force sensor measures external forces in the x direction. Previous work has developed a detailed model of the pneumatic system [10]. The system components are outlined in table 1.
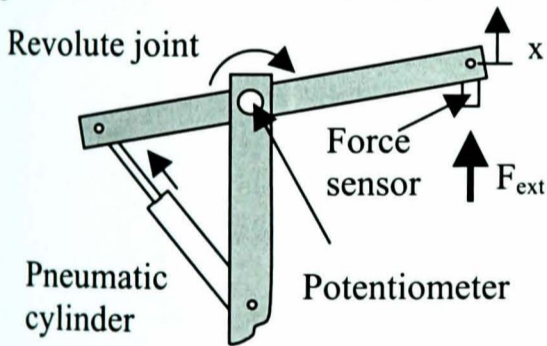

Figure 1 – Single link of physiotherapy robot

Low Friction pneumatic cylinder - Airpot Airpel – Air bearing design	Bore dia: 18mm Stroke: 100mm
Electro-pneumatic pressure control valves – SMC E– P Hyreg VY1100	Pressure range: 0 – 8.8 bar Voltage Range: 1 – 5V
Rotary Potentiometer Novotechnik P2701	Voltage Supply 10V

Table 1 – Equipment Specifications

III. SEPARATE FORCE AND POSITION CONTROL

Position only control of the single link can be implemented using simple proportional derivative (PD) control. PD control uses position error and velocity error gains to attain the desired response.

When implemented experimentally, the PD controller quickly reaches the demand position with a small amount of overshoot (Fig. 2)
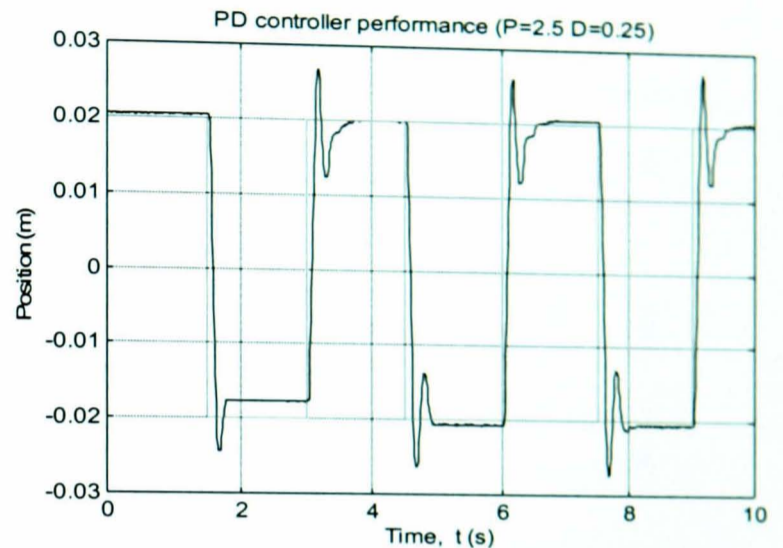

Figure 2 – PD position only response

Force only control, while link movement is prevented, can also be implemented (Fig. 3). Due to the pressure control nature of the electro-pneumatic valves, a constant voltage causes the pneumatic cylinder (position fixed) to output a constant force. This enables open-loop fixed position force control to be performed. (Fig. 4).
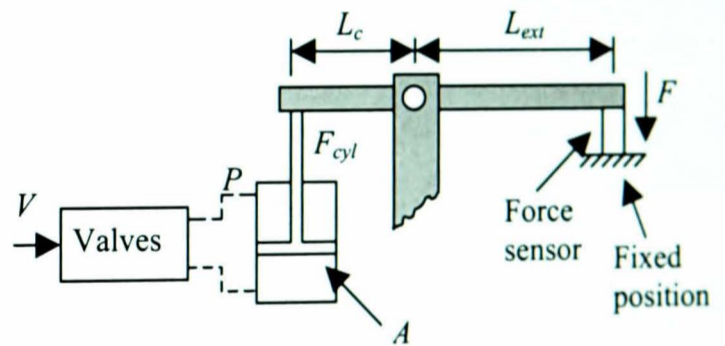

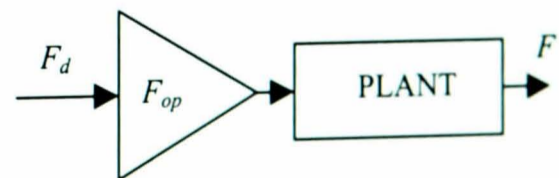Figure 3 – Fixed position force control

Figure 4 – Open loop force control

The desired force (F_d) is scaled by a gain (F_{op}) and fed into the plant, resulting in a force output (F). Examining the cylinder, valves and single link of the

robot enables the appropriate value of F_{op} to be obtained.

Examining the pressure response of the electro-pneumatic valves:

$1V = 2.2e5$ Pa of pressure (P)   (3.1)

The force produced by the cylinder piston due to air pressure from the valves:

$(F_{cyl}) = PA$ (3.2)

As the piston area is known, the force per volt of the pneumatic system can be calculated

$A = 1.98e-4 \Rightarrow 1V = 43.56$ N from F_{cyl} (3.3)

Examining the link dimensions to account for torque:
The ratio L_c/L_{ext} is 0.617, so $1V = 26.83$N at F (3.4)

The force per volt at the force sensor can be calculated to be:

$1N$ at $F = 1/26.83$ V $= 0.0373$ V   (3.5)

So the open-loop force gain is:

$F_{op} = 0.0373$ (3.6)

Experimentally implementing fixed position open-loop force control shows the desired force to be accurately tracked (Fig. 5). The force and position controllers developed here will be combined to form a single force and position control strategy in the next section.
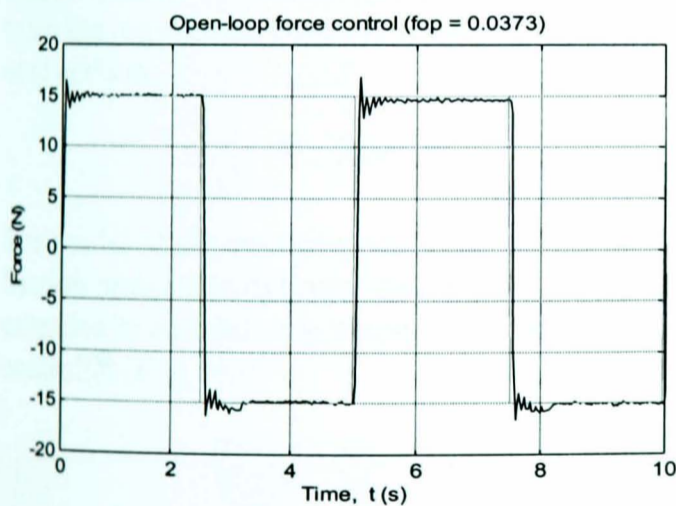

Figure 5 – Open-loop force control ($f_{op} = 0.0373$)

IV. IMPEDANCE CONTROL

Impedance control [4] is a position and force control strategy. The aim of impedance control is to specify the relationship between position and force. Using a position-based impedance controller simplifies the controller design.

For a position based impedance control system (Fig. 6) say x_p = specified position with no force disturbances and x_i = desired change in position due to external force.

The robot responds to external force inputs as if it were a simple mass, spring and damper system. A given external force (F_{ext}) causes a change in position x_i thus:

$$x_i = \frac{F_{ext}}{Ms^2 + Cs + K}$$ (4.1)

Then the overall desired position (x_d) becomes:

$$x_d = x_p + x_i = x_p + \frac{F_{ext}}{Ms^2 + Cs + K}$$ (4.2)
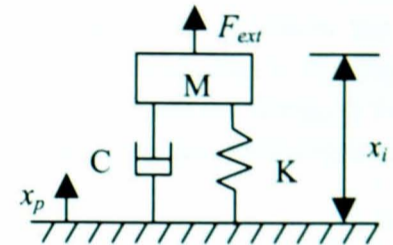
Where:

M = Mass
C = Damping
K = Stiffness

Figure 6 – Free body diagram of impedance system

When no external force is present the system behaves purely as a position controller ($x_i = 0$). If the PD controller was able to reject all force disturbances it would be possible to use a PD position only strategy to implement the desired impedance trajectory (x_d). However, external forces on the link have considerable effect on the PD controller performance. Position control of pneumatic cylinders under the influence of an unknown constant external force has been performed. A self-tuning, constant control signal was used to produce a force to counteract the external force and enable accurate control [11].

The open-loop force controller developed in section 3 is capable of counteracting the influence of the external force.

The external force measured by the force sensor is used to create an equal, but opposite force from the open-loop force controller. This removes the direct effect of the external force on link position. (i.e. link torque resulting from the external force (T_{ext}) is equal, but opposite to the torque applied by the cylinder (T_{cyl}) due to the open-loop force element (fig. 7)). Combining the PD position controller and open-loop force controller creates the final impedance controller (Fig. 8).
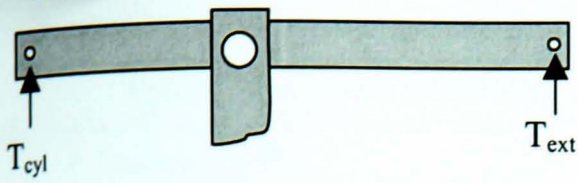
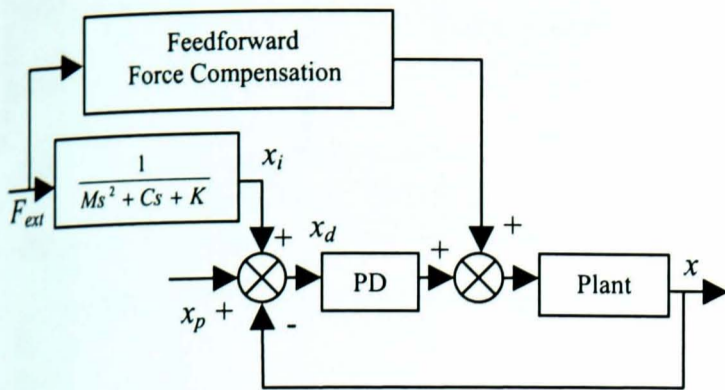Figure 7 – Counteracting the external force

Figure 8 – Impedance Controller block diagram

When implementing the impedance controller for physiotherapy, a patient's limb will be attached to the robot through the force sensor. The patient will be required to follow a desired trajectory (x_p), as implemented by the PD controller. If they experience difficulty in performing this movement their limb will not follow the desired trajectory resulting in a force between the limb and robot. This force alters the position of the robot (through the impedance controller) and provides assistance to the patient's movement. Hence, the level of assistance the robot provides is dependent on the specified impedance characteristics. Simulated and experimental results from the impedance controller are examined in the next section.

V. RESULTS

The model of the electro-pneumatic valves and low friction pneumatic cylinder developed in [10] has been extended to simulate the response of the impedance controller (Fig. 9).
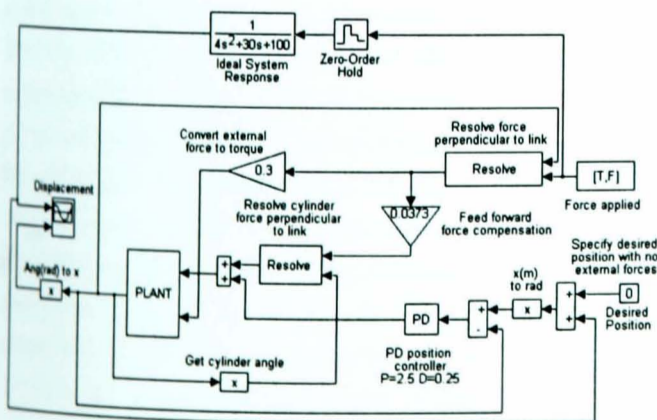

Figure 9 – Impedance controller simulation

The simulation was used to test the impedance controller concept and obtain suitable gains for the PD position controller before implementing experimentally. In order to assess controller performance masses were applied and removed from the end of the robot. With the mass attached, an approximately constant force is applied, regardless of position. This is not representative of physiotherapy where force would be applied gradually, but is an extreme test of controller performance.

The constant force combined with zero desired position (x_p=0) enables the controller performance to be easily assessed. The experimental results were compared to those produced from the simulation (Fig. 10,11,13,14). The results obtained with inertia, damping and stiffness (Fig. 10 & 11) show the experimental and simulated response to closely follow the desired trajectory. For small oscillations the experimental tracking is poor, due to friction within the system.

Examining the voltage output from the PD controller and open-loop force controller (Fig.12) for the response shown in figure 10 illustrates the operation of each element of the impedance controller. The open-loop force controller provides a compensation force to oppose link movement due to the external force. The PD controller's output moves the link along the desired trajectory providing little compensation for the external force, as such its output is much smaller than the force controller.
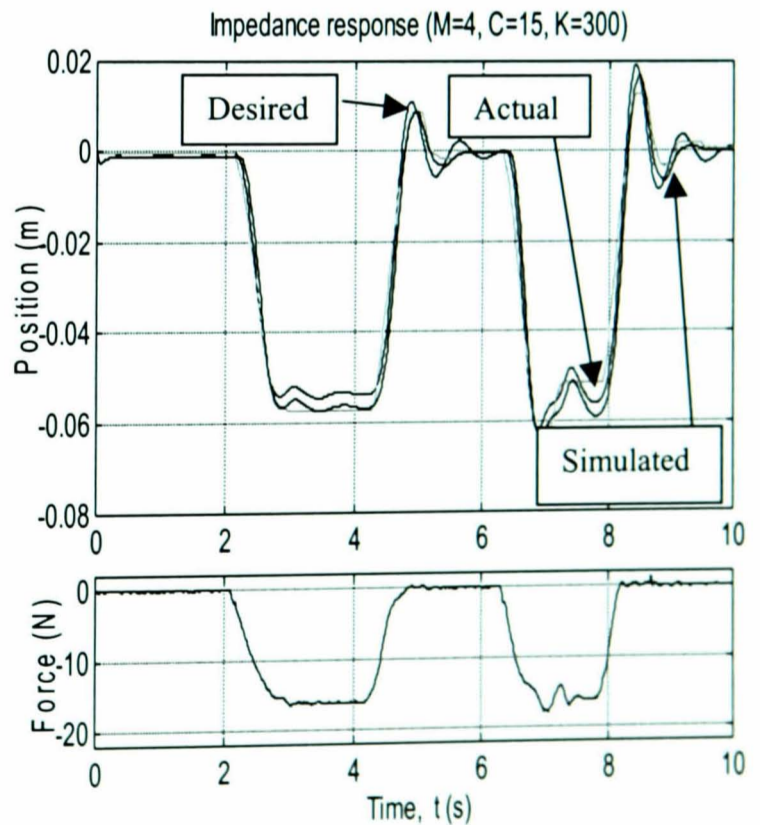

Figure 10 – M=4, C=15, K=300 Impedance response